

Traditional medicine and chronic inflammatory diseases

Edited by

Zheng Xiang, Xiande Ma, Chun Wai Mai and Haitao Wang

Published in

Frontiers in Pharmacology



FRONTIERS EBOOK COPYRIGHT STATEMENT

The copyright in the text of individual articles in this ebook is the property of their respective authors or their respective institutions or funders. The copyright in graphics and images within each article may be subject to copyright of other parties. In both cases this is subject to a license granted to Frontiers.

The compilation of articles constituting this ebook is the property of Frontiers.

Each article within this ebook, and the ebook itself, are published under the most recent version of the Creative Commons CC-BY licence. The version current at the date of publication of this ebook is CC-BY 4.0. If the CC-BY licence is updated, the licence granted by Frontiers is automatically updated to the new version.

When exercising any right under the CC-BY licence, Frontiers must be attributed as the original publisher of the article or ebook, as applicable.

Authors have the responsibility of ensuring that any graphics or other materials which are the property of others may be included in the CC-BY licence, but this should be checked before relying on the CC-BY licence to reproduce those materials. Any copyright notices relating to those materials must be complied with.

Copyright and source acknowledgement notices may not be removed and must be displayed in any copy, derivative work or partial copy which includes the elements in question.

All copyright, and all rights therein, are protected by national and international copyright laws. The above represents a summary only. For further information please read Frontiers' Conditions for Website Use and Copyright Statement, and the applicable CC-BY licence.

ISSN 1664-8714
ISBN 978-2-8325-2397-1
DOI 10.3389/978-2-8325-2397-1

About Frontiers

Frontiers is more than just an open access publisher of scholarly articles: it is a pioneering approach to the world of academia, radically improving the way scholarly research is managed. The grand vision of Frontiers is a world where all people have an equal opportunity to seek, share and generate knowledge. Frontiers provides immediate and permanent online open access to all its publications, but this alone is not enough to realize our grand goals.

Frontiers journal series

The Frontiers journal series is a multi-tier and interdisciplinary set of open-access, online journals, promising a paradigm shift from the current review, selection and dissemination processes in academic publishing. All Frontiers journals are driven by researchers for researchers; therefore, they constitute a service to the scholarly community. At the same time, the *Frontiers journal series* operates on a revolutionary invention, the tiered publishing system, initially addressing specific communities of scholars, and gradually climbing up to broader public understanding, thus serving the interests of the lay society, too.

Dedication to quality

Each Frontiers article is a landmark of the highest quality, thanks to genuinely collaborative interactions between authors and review editors, who include some of the world's best academicians. Research must be certified by peers before entering a stream of knowledge that may eventually reach the public - and shape society; therefore, Frontiers only applies the most rigorous and unbiased reviews. Frontiers revolutionizes research publishing by freely delivering the most outstanding research, evaluated with no bias from both the academic and social point of view. By applying the most advanced information technologies, Frontiers is catapulting scholarly publishing into a new generation.

What are Frontiers Research Topics?

Frontiers Research Topics are very popular trademarks of the *Frontiers journals series*: they are collections of at least ten articles, all centered on a particular subject. With their unique mix of varied contributions from Original Research to Review Articles, Frontiers Research Topics unify the most influential researchers, the latest key findings and historical advances in a hot research area.

Find out more on how to host your own Frontiers Research Topic or contribute to one as an author by contacting the Frontiers editorial office: frontiersin.org/about/contact

Traditional medicine and chronic inflammatory diseases

Topic editors

Zheng Xiang — Liaoning University, China

Xiande Ma — Liaoning University of Traditional Chinese Medicine, China

Chun Wai Mai — UCSI University, Malaysia

Haitao Wang — Center for Cancer Research, National Cancer Institute (NIH),
United States

Citation

Xiang, Z., Ma, X., Mai, C. W., Wang, H., eds. (2023). *Traditional medicine and chronic inflammatory diseases*. Lausanne: Frontiers Media SA.
doi: 10.3389/978-2-8325-2397-1

Table of contents

- 05 **Editorial: Traditional medicine and chronic inflammatory diseases**
Wei Liu, Yang-Cheng Liu and Zheng Xiang
- 08 **Analysis of the absorbed constituents and mechanism of liquidambaris fructus extract on hepatocellular carcinoma**
Shuai Wang, Xin-Xin Yang, Tian-Jiao Li, Lin Zhao, Yong-Rui Bao and Xian-Sheng Meng
- 25 ***Cornus officinalis* prior and post-processing: Regulatory effects on intestinal flora of diabetic nephropathy rats**
Cheng-Guo Ju, Lin Zhu, Wei Wang, Hui Gao, Yu-Bin Xu and Tian-Zhu Jia
- 41 **Transcriptomic analysis of the anti-inflammatory effect of *Cordyceps militaris* extract on acute gouty arthritis**
Chunwei Jiao, Huijia Liang, Li Liu, Shunxian Li, Jiaming Chen and Yizhen Xie
- 52 **Therapeutic effect and metabolomics mechanism of *Patrinia Villosa* (Thunb.) juss on liver injury in rats**
Li-Man Qiao, Hui Zhang, Wei Liu and Dan Lou
- 63 **Effects of *Broussonetia papyrifera* (L.) L'Hér. ex Vent. fruits water extract on hippocampal neurogenesis in the treatment of APP/PS1 transgenic mice**
Yu-hui Yan, Zi-han Huang, Qing-ping Xiong, Yue-wen Song, Si-yang Li, Bao-wei Yang, Lan Sun, Meng-yuan Zhang and Yu Ji
- 78 **Dissolvable hyaluronic acid microneedles loaded with β -Elemene for the treatment of psoriasis**
Chun Wang, Ruiqi Hao, Baowei Peng, Jiang Chang, Shisheng Chen, Yanxin Chen, Xiaohang Yin, Yumei Que, Chen Fan and Yuhong Xu
- 92 ***Asparagus cochinchinensis*: A review of its botany, traditional uses, phytochemistry, pharmacology, and applications**
Meng Wang, Shuang Wang, Wenjing Hu, Zhibin Wang, Bingyou Yang and Haixue Kuang
- 114 ***Channa striatus* in inflammatory conditions: A systematic review**
Vanessa Lin Lin Lee, Brandon Kar Meng Choo, Anwar Norazit, Suzita Mohd Noor and Mohd Farooq Shaikh
- 124 **Pharmacological effects of Bufeijianpi granule on chronic obstructive pulmonary disease and its metabolism in rats**
Xin-Xin Yang, Shuai Wang, Lin-Lin Cui, Tian-Jiao Li, Gang Bai, Yong-Rui Bao and Xian-Sheng Meng
- 141 **Effects of the Radix Ginseng and Semen Ziziphi Spinosae drug pair on the GLU/GABA-GLN metabolic cycle and the intestinal microflora of insomniac rats based on the brain-gut axis**
Tie Qiao, Yuan Wang, Ke Liang, Bingyuan Zheng, Jin Ma, Fangxiao Li, Chi Liu, Mingdan Zhu and Meng Song

- 157 **Effects of *Kalimeris indica* (L.) Sch Bip on colitis-associated colorectal cancer**
Mo-Fei Wang, Hao Li, Jian Cui, Yu-Han Chen and Yong Cui
- 165 **Quercetin 7-rhamnoside protects against alpha-naphthylisothiocyanate (ANIT)-induced in cholestatic hepatitis rats by improving biliary excretion and inhibiting inflammatory responses**
Hong-Liu Jin, Xiao-Jia Liu, Xiao-Ying Feng, Wen-Ting Zhu, Sen-Ling Feng, Li-Ping Cao and Zhong-Wen Yuan
- 176 **Inhibitory effect of main phenolic acid components of *Jacobaea cannabifolia* (Less.) on inflammation caused by PM_{2.5}**
Bao-Li Xu, Yuan-Yuan Wang, Ling-Ling Jiang, Zhen Liu, Ding-Rui Liu, He Zhao, Shi-Liang Li and Xiao-Bo Wang
- 187 **The mechanism of oxymatrine on atopic dermatitis in mice based on SOCS1/JAK-STAT3 pathway**
Xianwei Han, Tianming Ma, Qiang Wang, Chunlin Jin, Yusheng Han, Guijun Liu and Hao Li
- 195 **Sesquiterpene lactones-enriched fractions from *Xanthium mongolicum* Kitag alleviate RA by regulating M1 macrophage polarization via NF- κ B and MAPK signaling pathway**
Jing Han, Jingwen Wang, Yicun Wang, Zhiqi Zhu, Siwang Zhang, Bingrong Wu, Mingsong Meng, Jianning Zhao and Dongsheng Wang



OPEN ACCESS

EDITED BY

Javier Echeverria,
University of Santiago, Chile

REVIEWED BY

Armando Caceres,
Galileo University, Guatemala

*CORRESPONDENCE

Zheng Xiang,
✉ rainbowaftersnow@hotmail.com

RECEIVED 10 April 2023

ACCEPTED 21 April 2023

PUBLISHED 27 April 2023

CITATION

Liu W, Liu Y-C and Xiang Z (2023),
Editorial: Traditional medicine and
chronic inflammatory diseases.
Front. Pharmacol. 14:1202976.
doi: 10.3389/fphar.2023.1202976

COPYRIGHT

© 2023 Liu, Liu and Xiang. This is an
open-access article distributed under the
terms of the [Creative Commons
Attribution License \(CC BY\)](#). The use,
distribution or reproduction in other
forums is permitted, provided the original
author(s) and the copyright owner(s) are
credited and that the original publication
in this journal is cited, in accordance with
accepted academic practice. No use,
distribution or reproduction is permitted
which does not comply with these terms.

Editorial: Traditional medicine and chronic inflammatory diseases

Wei Liu, Yang-Cheng Liu and Zheng Xiang*

School of Pharmaceutical Science, Liaoning University, Shenyang, China

KEYWORDS

traditional medicine, chronic inflammatory diseases, nature product, liver injury, enteritis, arthritis, diabetes nephropathy

Editorial on the Research Topic

Traditional medicine and chronic inflammatory diseases

Inflammatory response is the most common pathological reaction in the human body. If encountering infection and injury, the production of inflammation in the body is usually localized, transient, and belongs to acute inflammation. If inflammatory factors persist and damage tissues, acute inflammation will gradually transform into chronic inflammation. In addition, chronic inflammation can also occur due to the influence of social environment and lifestyle (Furman et al., 2019). Cardiovascular disease, cancer, diabetes, chronic nephritis, nonalcoholic fatty liver disease, autoimmune disease and degenerative disease based on the chronic inflammation seriously threaten human life and health (Straub, 2017; Yang et al., 2020). Since the development of science, people have gradually realized the important harm of chronic inflammation to body tissues. The characteristic of chronic inflammation is that there are often no obvious symptoms between episodes, such as chronic cholecystitis (Wang et al., 2021), chronic pyelonephritis (Tsuji et al., 2007), etc. Chronic inflammation can also occur slowly and insidiously, with no clinical manifestations of acute inflammation. It is common in intracellular viral infections, where the virulence of these pathogens is not strong, but they can cause immune responses. Long term exposure to non-degradable but potentially toxic substances or the effects of persistent autoimmune diseases can also lead to the occurrence of chronic inflammation.

The multiple causes of chronic inflammation lead to a higher incidence in the human body, and because its treatment cycle is longer than acute inflammation, it is crucial to reduce the harmful effects on the human body during the treatment process. Compared to chemical drugs, traditional medical treatment methods have lower side effects. The role of natural products from medicinal plants, medicinal animals, and functional foods in disease treatment is increasingly valued, and the therapeutic effects and mechanisms of traditional medicine on diseases have become a research hotspot. Therefore, the potential of traditional medicine for treating chronic inflammatory diseases needs to be developed. This Research Topic selects traditional medicine and chronic inflammatory diseases as the themes, committed to promoting more meaningful research on the treatment of chronic inflammatory diseases through traditional medicine, exploring more efficient and less side effects treatment methods for chronic inflammatory and improve the relevant theoretical foundation research.

In this Research Topic, a total of 15 articles were published, including two review articles and 13 original research articles. These articles focus on the therapeutic relationships between various traditional medicine drugs and inflammatory diseases, and conduct in-depth research through various research methods such as metabolomics

and microbial genomics. Two review articles focus on the effects of two traditional drugs from plant and animal, respectively, on various inflammations. Wang et al. reviewed the research findings of *Asparagus cochinchinensis* (Lour.) Merr and the progress in botany, traditional use, phytochemistry, pharmacology and application were summarized. Lee et al. reviewed the positive effects of *Channa striatus* on inflammatory conditions such as gastric ulcers, dermatitis, osteoarthritis, and allergic rhinitis. Compared to the widely used non-steroidal anti-inflammatory drugs, the natural ingredient extracted from *Channa striatus* is more user-friendly and can reduce the risk of peptic ulcers, acute renal failure, stroke, and myocardial infarction caused by the use of chemical drugs such as non-steroidal anti-inflammatory drugs.

Three articles focus on inflammation related to liver injury and liver cancer. Due to changes and advancements in lifestyle, liver injury is a very common disease in modern society. Wang et al. revealed the material basis of *Liquidambaris fructus* extract in treating liver cancer cells and demonstrated its effects on inhibiting tumor cell growth, promoting tumor cell apoptosis, reducing inflammatory response, protecting liver cells, and improving the survival status of tumor rats through metabolomics methods. Pathway analysis indicates that the above effects are related to key signaling pathways such as PTEN/PI3K/Akt and fatty acid metabolism. Qiao et al. found that *Patrinia villosa* (Thunb.) Juss has a therapeutic effect on liver injury caused by inflammation, reducing liver tissue structural damage, cytoplasmic vacuolization, cell swelling, and inflammatory cell infiltration. Its therapeutic effect is related to the metabolism of alanine, aspartic acid, and glutamate, as well as the TCA cycle pathway. The research results of Jin et al. suggested that quercetin 7-rhamnoside can treat cholestatic hepatitis by regulating bile acid secretion and reducing inflammation. Two articles focus on skin related inflammatory diseases. The data of Wang et al. indicated that, β -elemene can reduce the expression of inflammatory cytokines secreted by M1-M ϕ and induce apoptosis of psoriasis keratinocytes to suppress inflammation, thereby significantly alleviating the symptoms of the psoriasis mouse model; Han et al. found that oxymatrine can improve skin inflammation symptoms in atopic dermatitis mice by upregulating the expression of cytokine signaling inhibitor 1, inhibiting the activation of JAK-STAT3 pathway, and blocking the activation of T lymphocytes. In addition, two articles focus on traditional medical treatment methods for arthritis; Jiao et al. used the extraction of *Cordyceps militaris* (Linn.) Link to treat gouty arthritis and achieved good results. The extract of *cordyceps militaris* significantly alleviated the inflammatory progression of gouty arthritis and ameliorated the onset of gouty arthritis. The underlying mechanism may be related to triggering the cytokine-cytokine receptor interaction signaling pathway to inhibit the activation of the inflammasome and regulate the immune system. And it regulates the inflammatory response induced by monosodium urate crystals through the genes CCL7, CSF2RB, and IL-1 β . Han et al. used *X. mongolicum* Kitag to treat rheumatoid arthritis, another type of chronic arthritis. The main active ingredient of *X. mongolicum* in the treatment of rheumatoid arthritis is sesquiterpene lactone. Sesquiterpene lactones enriched fraction from *X. mongolicum* may pass NF- κ B and MAPK signaling pathways inhibit

M1 macrophage polarization, thereby exerting their therapeutic effect on rheumatoid arthritis. The inflammatory response in the brain is a more challenging area of onset and is more difficult to effectively treat. Qiao et al. found that Radix Ginseng (the dry root and rhizome of *Panax ginseng* C. A. Meyer) and Semen Ziziphi Spinosae (the dry and mature seed of *Ziziphus jujuba* Mill.var.*spinosa* (Bunge) HuexH.F.Chou) drug pair can improve sleep in insomnia rats by regulating the GLU/GABA-GLN metabolic cycle and gut microbiota. Yan et al. proved that water extract of *Broussonetia Papyrifera* (L.) L'Hér. ex Vent. fruits can enhance the proliferation of neural stem cells and improve neurogenesis, so as to effectively repair the damaged neurons in the hippocampus of APP/PS1 transgenic mice and improve cognitive impairment. Its function is related to the activation of Wnt/ β -catenin signaling pathway. Yang et al. proved that Bufei Jianpi granule, which is a traditional Chinese medicine formulation including *Astragalus mongholicus* Bunge [Fabaceae; *A. mongholicus* radix], *Codonopsis pilosula* (Franch.) Nannf [Campanulaceae; *C. pilosula* radix], *Polygonatum kingianum* Collett & Hemsl [Asparagaceae; *P. kingianum* rhizoma], *Atractylodes macrocephala* Koidz [Asteraceae; *Atractylodes macrocephala* rhizoma], *Poria cocos* (Schw.) Wolf [Poromycetidae; *Poria*], *Fritillaria thunbergii* Miq [Liliaceae; *Fritillariae thunbergii* bulbus], *Pheretima aspergillum* (E. Perrier) [Lumbricidae; *Pheretima*], *Magnolia officinalis* Rehder & E. H. Wilson [Magnoliaceae; *Magnoliae officinalis* cortex], *Citrus reticulata* Blanco [Rutaceae; *Citri reticulatae* pericarpium], *Aster tataricus* L. f [Asteraceae; *Asteris radix et rhizoma*], *Epimedium brevicornu* Maxim [Berberidaceae; *Epimedium folium*], and *Ardisia japonica* (Thunb.) Blume [Primulaceae; *Ardisiae japonicae* herba] at a ratio of 12:6:12:9:9:6:9:6:9:6:6:15, has a pharmacological effect in the treatment of chronic obstructive pulmonary disease, and downregulate the levels of IL-6, IL-8, TNF- α , PGE2, MMP-9, and NO in the serum and bronchoalveolar lavage fluid. Wang et al. focus on the intestinal inflammatory disease. It was found that *K. indica* (L.) Sch Bip could significantly reduce the atypical hyperplasia in colon tissue, and inhibit the expression of proinflammatory factors such as IL-6, TNF, IL-11, IL-7, etc. *Kalimeris indica* could also restore the level of miR-31-5p in mice, and therefore the downstream LATS2 to inhibit the development of colitis-associated colorectal cancer. Ju et al. found that *Cornus officinalis* Torr. ex Dur. may improve the renal injury of diabetic nephropathy rats by blocking the activation of Wnt/ β -catenin signaling pathway, regulating the structural composition of intestinal microorganisms, and ultimately playing a role in renal protection. Xu et al. investigated the inhibitory effect of main phenolic acid components of *J. cannabifolia* (Less.) on inflammation caused by PM2.5. P-hydroxybenzoic acid and p-hydroxyphenylacetic acid from *J. cannabifolia* could attenuated inflammation caused by PM2.5 through suppressing TLRs related signal pathway.

Overall, this Research Topic has received widespread attention and published two review articles jointly written by 11 scientists and 13 original research articles jointly designed and written by 93 scientists. This indicates that the treatment of chronic inflammatory diseases through traditional medicine

has attracted more and more researchers' attention, and its advantages over chemical drug methods are becoming increasingly evident. The articles in this Research Topic cover a variety of inflammatory diseases, including liver injury, skin inflammation, arthritis, brain inflammation, obstructive pulmonary disease, enteritis, and diabetes nephropathy, which expand the research field of traditional medicine in the treatment of inflammatory diseases, and indicate the potential of traditional medicine in the treatment of inflammatory diseases. Developing more mature and effective traditional medical treatment methods for chronic inflammatory diseases is an important research direction that can benefit many patients. Better treatment effects and lower toxic effect and side effect will be an important contribution of traditional medicine to the field of chronic inflammatory diseases.

Author contributions

WL and Y-CL wrote the editorial; ZX conceived and revised the editorial.

References

- Furman, D., Campisi, J., Verdin, E., Carrera-Bastos, P., Targ, S., Franceschi, C., et al. (2019). Chronic inflammation in the etiology of disease across the life span. *Nat. Med.* 25, 1822–1832. doi:10.1038/s41591-019-0675-0
- Straub, R. H. (2017). The brain and immune system prompt energy shortage in chronic inflammation and ageing. *Nat. Rev. Rheumatol.* 13, 743–751. doi:10.1038/nrrheum.2017.172
- Tsuji, T., Ohtake, T., Yonemura, K., Sudoko, H., Komiyama, A., Seki, A., et al. (2007). Chronic pyelonephritis presenting as multiple tumor-like renal lesions. *Intern. Med.* 46, 879–882. doi:10.2169/internalmedicine.46.1885

Acknowledgments

We thank all the authors, reviewers and editors who contributed to this Research Topic.

Conflict of interest

The authors declare that the research was conducted in the absence of any commercial or financial relationships that could be construed as a potential conflict of interest.

Publisher's note

All claims expressed in this article are solely those of the authors and do not necessarily represent those of their affiliated organizations, or those of the publisher, the editors and the reviewers. Any product that may be evaluated in this article, or claim that may be made by its manufacturer, is not guaranteed or endorsed by the publisher.

- Wang, L., Chen, J., Jiang, W., Cen, L., Pan, J., Yu, C., et al. (2021). The relationship between *Helicobacter pylori* infection of the gallbladder and chronic cholecystitis and cholelithiasis: A systematic review and meta-analysis. *Can. J. Gastroenterol. Hepatol.* 6, 8886085. doi:10.1155/2021/8886085

- Yang, Z., Tang, Z., Cao, X., Xie, Q., Hu, C., Zhong, Z., et al. (2020). Controlling chronic low-grade inflammation to improve follicle development and survival. *Am. J. Reprod. Immunol.* 84, e13265. doi:10.1111/aji.13265



OPEN ACCESS

EDITED BY
Zheng Xiang,
Liaoning University, China

REVIEWED BY
Xue Xiao,
Guangdong Pharmaceutical University,
China
Xuemei Fan,
Tsinghua University, China

*CORRESPONDENCE

Yong-Rui Bao,
byr1026@163.com
Xian-Sheng Meng,
mxsvvv@126.com

[†]These authors have contributed equally
to this work and share first authorship

SPECIALTY SECTION

This article was submitted to
Ethnopharmacology,
a section of the journal
Frontiers in Pharmacology

RECEIVED 21 July 2022

ACCEPTED 09 August 2022

PUBLISHED 30 August 2022

CITATION

Wang S, Yang X-X, Li T-J, Zhao L,
Bao Y-R and Meng X-S (2022), Analysis
of the absorbed constituents and
mechanism of liquidambaris fructus
extract on hepatocellular carcinoma.
Front. Pharmacol. 13:999935.
doi: 10.3389/fphar.2022.999935

COPYRIGHT

© 2022 Wang, Yang, Li, Zhao, Bao and
Meng. This is an open-access article
distributed under the terms of the
[Creative Commons Attribution License
\(CC BY\)](https://creativecommons.org/licenses/by/4.0/). The use, distribution or
reproduction in other forums is
permitted, provided the original
author(s) and the copyright owner(s) are
credited and that the original
publication in this journal is cited, in
accordance with accepted academic
practice. No use, distribution or
reproduction is permitted which does
not comply with these terms.

Analysis of the absorbed constituents and mechanism of liquidambaris fructus extract on hepatocellular carcinoma

Shuai Wang^{1,2,3†}, Xin-Xin Yang^{1,2,3†}, Tian-Jiao Li^{1,2,3}, Lin Zhao^{1,2,3},
Yong-Rui Bao^{1,2,3*} and Xian-Sheng Meng^{1,2,3*}

¹College of Pharmacy, Liaoning University of Traditional Chinese Medicine, Dalian, China, ²Liaoning Multi-Dimensional Analysis of Traditional Chinese Medicine Technical Innovation Center, Dalian, China, ³Liaoning Province Modern Chinese Medicine Research Engineering Laboratory, Dalian, China

Background: Hepatocellular carcinoma (HCC) refers to one of the top 10 cancers in terms of morbidity and mortality globally, seriously influencing people's lives. First recorded in Compendium of Materia Medica, liquidambaris fructus (LF) generates definite anti-liver tumor effect. However, its effective substances and mechanism remain to be elucidated.

Methods: Serum pharmacochimistry and UPLC-QTOF-MS technologies were employed to explore the plasma of rats after intragastric administration of liquidambaris fructus extract (LFE) in order to find the active ingredients. Subsequently, DEN-induced rat liver cancer model was established with the purpose of investigating the anti-tumor activity of LFE from physiological, pathological and biochemical aspects. Finally, non-target metabolomics combined with q-PCR and Western blot methods were adopted for revealing the mechanism.

Results: Totally 11 prototype blood transfused ingredients, including imperatorin and phellopterin were detected. LFE presents excellent impact on enhancing the quality of life, prolonging the life cycle, reducing inflammatory reaction, protecting hepatocytes, improving body immunity and killing liver tumor cells. Altogether 82 endogenous differential metabolites were found in metabolomics, suggesting that LFE can treat HCC by acting on key targets of PTEN/PI3K/Akt pathway and fatty acid metabolism. Further research also verified that LFE can upregulate the relative expression levels of PTEN,

Abbreviations: AFP, alpha-fetoprotein; ALT, alanine transaminase; AST, aspartate amino-transferase; BPC, base peak chromatogram; CPM, cyclophosphamide group; DHA, docosahexaenoic acid; EPA, eicosapentaenoic acid; HCC, hepatocellular carcinoma; LCAT, lecithin cholesterol acyltransferase; LF, liquidambaris fructus; LFE, liquidambaris fructus extract; LFEH, LFE high-dose group; LFEL, LFE low-dose group; LPA, lysophosphatidic acid; LPC, lysophosphatidylcholine; Lpcat1, phosphatidylcholine acyltransferase 1; LSD, least significant difference; MPP, Mass Profiler Professional; PC, phosphatidylcholine; PCA, principal component analysis; PIP3, phosphatidylinositol triphosphate; PLA2, phospholipase A2; PLS-DA, partial least squares discriminant analysis; PUFA, polyunsaturated fatty acids; S1P, sphingosine-1-phosphate; SD, Sprague-Dawley; TCM, traditional Chinese medicine; TIC, total ion chromatography; TNF- α , tumor necrosis factor- α ; WHO, World Health Organization.

PDCD4, Caspase 9, Caspase 3, Bax and Bad as well as lower the relative expression levels of PI3K, AKT, VEGFA and Bcl-2.

Conclusion: This study revealed the pharmacodynamic material basis of LFE in the treatment of HCC, and from the perspective of metabolomics proved that the effects of inhibiting the growth of tumor cells, promoting tumor cell apoptosis, reducing inflammatory reaction, protecting hepatocytes, improving the survival state of tumor rats, and prolonging the life cycle are related to its impact on PTEN/PI3K/Akt, fatty acid metabolism and other key signal pathways.

KEYWORDS

liquidambaris fructus, hepatocellular carcinoma, absorbed constituents, pharmacology and efficacy, mechanism of action

Introduction

Cancer is one of the diseases causing great harm to human health. In accordance with the latest report “Global Cancer Statistics 2020” released by the World Health Organization (WHO), the number of new cancer patients in the world in 2020 reached 19.29 million and that of deaths was 9.96 million (Sung et al., 2021). Among them, hepatocellular carcinoma (HCC) is known as the “king of cancer,” which is among the top ten cancers globally in terms of incidence rate and mortality (Bao et al., 2017). Although HCC ranks only the sixth in the global cancer incidence rate ranking (910,000 people, 4.7%), it is characterized by a high mortality rate (830,000 people, 8.3%) due to the fact that it is mostly found in the middle and late stage and has no obvious pain (Nadarevic et al., 2022). At present, in clinical treatment, most patients with liver cancer are discovered to be in the middle and advanced stage, and exhibit abnormal liver function with systemic metastasis, and thus they cannot accept radical surgery. Nevertheless, there are some major problems in the process of radiotherapy and chemotherapy, including poor specificity, strong drug resistance, and large toxic and side effects (Guo et al., 2019). It has always been the primary problem of anti-tumor drug research and development to find a highly specific drug for HCC that can not only prolong the life cycle and guarantee the quality of life, but also assist in the treatment.

In China, Traditional Chinese medicine (TCM) has been adopted for thousands of years, attracting more and more researchers’ attention because of its unique curative effect and great development potential. In addition, the multi-component and multi-target characteristics of TCM can potentially enhance the curative effect while reducing the toxicity and side effects, especially suitable for the treatment of complex diseases (Huang et al., 2020). Liquidambaris fructus (LF), a Traditional Chinese medicine, was first recorded in Compendium of Materia Medica. It is the dried and mature fruit sequence of *Liquidambar formosana* Hance, a plant in the family hamhamica (Qian et al., 2020). It has porous fruit, which goes to the liver and

kidney channels, and has the effect of passing twelve channels. Modern pharmacological studies demonstrate that LF possesses the functions of liver protection, anti-tumor and anti-inflammation (Yang X. X. et al., 2020; Li et al., 2021), and has inhibitory impacts on various tumor cells (Fang and Ji, 2019; Qian et al., 2020), especially liver cancer (Yang Y. P. et al., 2020). In addition, our previous studies have reported that liquidambaris fructus extract (LFE) can hinder cancer cells proliferation, and trigger the cell cycle arrest and apoptosis to exert the anti-tumor role (Yang X. X. et al., 2020; Zhang et al., 2020). And the main chemical components of LFE were identified by chemical separation. However, the active ingredients and precise mechanism underlying remains poorly understood.

Therefore, based on the clear study of the chemical components contained in LFE in the early stage, the current experiment adopts the research method of serum pharmaceutical chemistry and UPLC-QTOF-MS technology for analyzing its absorbed components into the blood, aiming to clarify its active components that play the anti-tumor role (Wang et al., 2021; Xu et al., 2021). Furthermore, the anti-liver cancer effect of LFE was comprehensively evaluated from the changes of physiological, pathological and biochemical indexes. On this basis, non-target metabonomics, q-PCR and Western blot techniques were employed to investigate the key targets and pathways of LFE. Specifically, this study clarified the effective substances, deeply revealed the mechanism of LFE against HCC based on the definite anti-liver tumor effect *in vivo*, aiming to provide a scientific explanation for the clinical application of LFE.

Materials and methods

Chemicals and reagents

Dried mature inflorescences of *Liquidambar formosana* Hance was obtained from Anguo Qimei medicinal materials Co., Ltd. (Anguo, China). MS grade methanol and acetonitrile

were bought from Merck (Darmstadt, Germany). Diethylnitrosamine (DEN) was provided by Sigma (United States). Rat alpha-fetoprotein (AFP) ELISA kit, Rat alanine transaminase (ALT) ELISA kit, Rat aspartate aminotransferase (AST) ELISA kit, Rat tumor necrosis factor- α (TNF- α) ELISA kit were acquired from Shanghai Langdon Biotechnology Co., Ltd. (Shanghai, China).

Animals

Totally ninety healthy male Sprague-Dawley (SD) rats, weighing (200 ± 20) g, were purchased from Liaoning Changsheng Biotechnology Co., Ltd. with the Certificate No. SCXK (Liao) 2015-0001. After 1 week of adaptation in the free feeding and drinking environment, the experiment was performed. In addition, all the experiments were carried out following the approved animal protocols and guidelines proposed by Medicine Ethics Review Committee for animal experiments of Liaoning University of Traditional Chinese Medicine with approval number: 2020YS013(KT)-013-01.

Preparation of liquidambaris fructus extract

LF was air-dried, and extracted with 10 times ethyl acetate under reflux for 1 h. Then, the solvent was recovered, and dried LFE was obtained. The extraction ratio is 3.05%.

Preparation of plasma samples for pharmacochemical analysis

At random, sixteen SD rats were categorized into blank group and administration group, eight rats per group. Besides, the administration group was given 0.27 g/kg/day LFE by gavage (10 times of the clinical dosage, according to crude drug), and the blank group was given the same amount of tertiary water, twice a day for 3 consecutive days. Besides, 12 h before the last administration, fasting and drinking were forbidden. Then, 1 h after the last administration, 1% pentobarbital sodium solution was employed for anesthesia, blood was gathered from hepatic portal vein. After standing at 4°C for 30 min, it was centrifuged at 3,500 rpm for 10 min and plasma was collected. Taking plasma 200 μ l, add 5 times methanol:acetonitrile (1:1, V/V) solvent, vortex shock for 2 min, ultrasonic extract for 1 min, freeze stand at -20°C for 10 min, centrifuge at 12,000 rpm for 15 min at 4°C to precipitate protein. Then, take the supernatant, vacuum centrifuge at 1,200 rpm, add 50 μ l methanol:acetonitrile (1:1, V/V) solvent redissolved, eddy shock for 2 min, ultrasonic extract for 1 min and centrifuge at 12,000 rpm for 10 min at 4°C. Finally, the supernatant was absorbed for analysis.

Chemical components absorbed into rat plasma

In this study, UPLC-QTOF-MS technology was employed to detect the chemical components absorbed into rat plasma. Besides, the plasma samples were explored on an Agilent-1290 UPLC system coupled with the Agilent-6550 QTOF mass spectrometry (Agilent Technologies, Inc., United States). Chromatographic analysis was performed on an Agilent Poroshell 120 column (100 mm \times 4.6 mm, 2.7 μ m) with flow rate 0.8 ml/min, column temperature 30°C, injection volume 3 μ l. In the positive ion mode, the system of 0.1% formic acid aqueous solution (A)-acetonitrile:methanol (95:5) (B) was used, and the gradient elution conditions were 0–5 min, 5%–20% B; 5–60 min, 20%–100% B. While in the negative ion mode, the mobile phase was water (A)-acetonitrile:methanol (95:5) (B) with gradient elution procedure: 0–17 min, 5%–40% B; 17–22 min, 40%–65% B; 22–45 min, 65%–95% B; 45–50 min, 95%–100% B; 50–60 min, 100%–100% B. The MS experiment was performed on a dual spray ion source (Dual AJS ESI) in positive and negative ion modes, with Vcap 4,000 V, Drying Gas Flow 13 L/min, Drying Gas Temp 250°C, Neulizer pressure 45 psig, Sheath Gas Temp 350°C, Sheath Gas Flow 11 L/min, Fragmentor 125 V, and the MS data were collected from m/z 100 to 1,000.

Construction of DEN-induced hepatocellular carcinoma rat model and liquidambaris fructus extract treatment

Rat HCC model was established by DEN induction method. Seventy-four healthy SD rats were randomly classified into blank group ($n = 10$) and model group ($n = 64$). The model group was given 1% DEN solution by gavage at a dose of 70 mg/kg and the blank group was given the same proportion of normal saline once weekly for a total of 14 weeks. After 6 weeks of modeling, the rats in the model group were randomly classified into five groups, including model group ($n = 20$), cyclophosphamide group ($n = 24$) (10 mg/kg/day), LFE low dose group ($n = 10$) (0.27 g/kg/day) and LFE high dose group ($n = 10$) (0.81 g/kg/day). Different doses of liquid were given to each administration group by gavage. The blank group and model group were given equal volumes of normal saline once daily until the 16th weekends.

After the last administration in the 16th week, the mortality rate of each group was calculated. Besides, the remaining rats were sacrificed with 3% pentobarbital. Blood was collected in two parts. Serum was used to detect the contents of AFP, ALT, AST and TNF- α , and plasma was taken for performing metabonomic analysis. Besides, liver, spleen and thymus were excised and weighed to calculate the liver index, spleen index as well as thymus index. The calculation formula is expressed as follows: liver body ratio = (liver weight/body weight) \times 100, thymus

index = (thymus weight/body weight) \times 100, spleen index = (spleen weight/body weight) \times 100. Part of liver tissue was taken out and immersed in fixative solution. Histopathological sections were prepared by HE staining. In addition, electron microscope was used to observe changes in tissue structure, tumor cell density, apoptosis and necrosis degree.

Metabonomics analysis

Non-target metabonomics analysis was performed on the plasma of rats with therapeutic effect of LFE on DEN-induced liver cancer. 200 μ l plasma was mixed with 800 μ l precooled methanol and placed in a vortex for 2 min, which was then centrifuged at 10,000 rpm for 10 min at 4°C. Subsequently, the supernatant was dried with nitrogen and 100 μ l precooled methanol was added before being placed in a vortex for 2 min and centrifuged at 10,000 rpm for 2 min at 4°C. In addition, the supernatant was taken for carrying out UPLC-QTOF-MS analysis.

Agilent Poroshell 120 EC-C18 (2.1 mm \times 100 mm, 1.9 μ m) column was employed to perform chromatographic analysis. Column temperature is 30°C and the flow rate is 0.4 ml/min. The mobile phase is A: 0.1% formic acid-water, B: acetonitrile: methanol = 9:1. Injection volume 2 μ l, while gradient elution: 0–2 min, 3%–3% B; 2–5 min, 3%–10% B; 5–6 min, 10%–55% B; 6–10 min, 55%–80% B; 10–22 min, 80%–95% B; 22–30 min, 95%–100% B; 30–35 min, 100%–100% B. Moreover, positive and negative ion modes were also adopted for mass spectrometry analysis. Other conditions were consistent with blood component analysis, except that the neulizer pressure was 30 psig, m/z range was 100–1,500, and the Vcap of negative ion mode was 3,500 V.

Multivariate data analysis

The plasma metabolism profiles of rats in different groups were normalized through the use of Profinder B.08.00 software including peak detection and peak alignment, and then converted into. Cef files. Subsequently, they were imported into Mass Profiler Professional (MPP) B.14.00 for principal component analysis (PCA), partial least squares discriminant analysis (PLS-DA), T-test analysis and variance analysis. With $p < 0.05$ and Fold change value greater than 2 as the criterion, endogenous differential metabolites were screened. The accurate quality and chemical composition of differential metabolites were obtained using ID Browser function. Then, the above data and fragment spectral data were compared with the standard data in the database to identify the endogenous differential metabolites. Through the biological function analysis of metabolites, the metabolic pathway of LFE to interfere with liver cancer was discovered. In the meanwhile, the mechanism of action of LFE against liver cancer was discussed.

q-PCR analysis

Human HCC SMMC-7721 cells (Wuhan Bode Bioengineering Co., Ltd., Wuhan, China) were routinely cultured in 6-well plates. When the cell density was approximately 70%, LFE containing culture medium with the concentration of 0.5 mg/ml was used for drug intervention. After 36 h, total RNA was extracted from cells with TRIzol (TransGen Biotech, Beijing, China). TransScript First-Strand cDNA Synthesis SuperMix kit (TransGen Biotech, Beijing, China) was employed to synthesize the first strand of cDNA. TransStart Top Green qPCR SuperMix kit (TransGen Biotech, Beijing, China) was performed to amplify the target gene. The whole reflection was conducted on a Real-time Thermal Cycler 5,100 (Thermo Fisher Scientific Inc., Waltham, MA, United States). In addition, the primer sequence of the target genes were presented as follows: PTEN forward primer 5'-TGTAAGCTGGAAAGGGACGA-3' and reverse primer 5'-GGGAATAGTTACTCCCTTTTGTGTC-3', PI3K forward primer 5'-CCA GGGAAATTCTGGGCTCC-3' and reverse primer 5'-TGTATT CAGTTCAATTGCAGAAGGA-3', AKT forward primer 5'-CAGGATGTGGACCAACGTGA-3' and reverse primer 5'-AAGGTGCGTTCGATGACAGT-3', VEGFA forward primer 5'-CTGTCTAATGCCCTGGAGCC-3' and reverse primer 5'-TTAACTCAAGCTGCCTCGCC-3', PDCD4 forward primer 5'-ACCCTGCAGATCCTGATAACT-3' and reverse primer 5'-TCCTTAGTCGCCTTTTTCGCT-3', Bax forward primer 5'-TTGCTTCAGGGTTTCATCC-3' and reverse primer 5'-GAC ACTCGCTCAGCTTCTTG-3', Bcl-2 forward primer 5'-AGT ACCTGAACCGGCACCT-3' and reverse primer 5'-CAGCCA GGAGAAATCAAACA-3', Bad forward primer 5'-CAGACC CGGCAGACAGATGAG-3' and reverse primer 5'-CTCTGG GCTGTGAGGACAAGA-3', Caspase 3 forward primer 5'-TGTTTCATCCAGTCGCTTTG-3' and reverse primer 5'-CATTCTGTTGCCACCTTTCG-3', Caspase 9 forward primer 5'-CAGGCCCATATGATCGAGG-3' and reverse primer 5'-GGCCTGTGCTCTAAGCAG-3', β -actin forward primer 5'-GGGAAATCGTGCCTGACATT-3' and reverse primer 5'-GGA ACCGCTCATTGCCAT-3'. In addition, the fold change in expression was calculated using $2^{-\Delta\Delta CT}$ method.

Western blot analysis

SMMC-7721 cells were pretreated with LFE (0.5 mg/ml) for 36 h. Total protein was extracted and detected with BCA Protein Concentration Determination Kit (Meilun Biotechnology Co., Ltd.). Protein samples were separated by 8%–15% SDS-PAGE (80 V, for 30 min, and then 120 V, for 40 min) and transferred to the PVDF membrane in the transfer buffer at 120 V for 1–3 h. The membranes were blocked with 5% skim milk for 2 h at room temperature and also nurtured overnight at 4°C with primary antibodies against β -actin, PTEN, PI3K, p-PI3K, Akt, p-Akt,

TABLE 1 Prototype blood component of LFE.

No.	Retention time (RT) (min)	Formula	Theoretical mass (m/z)	Measured mass (m/z)	Mass error (ppm)	Identified compounds
1	6.575	C ₁₆ H ₁₄ O ₄	293.0784 [M+Na] ⁺	293.0755[M+Na] ⁺	9.89 [M+Na] ⁺	Imperatorin
2	7.104	C ₁₇ H ₁₆ O ₅	301.1071[M+H] ⁺	301.1063[M+H] ⁺	2.65[M+H] ⁺	Phellopterin
3	16.570	C ₂₉ H ₄₀ O ₄	473.3272[M-H] ⁻	473.3303[M-H] ⁻	-6.54[M-H] ⁻	2-Hydroxy-3-oxo-1,4(5)-oleanadien-28-oic acid
4	23.033	C ₃₀ H ₄₄ O ₅	483.3116[M-H] ⁻	483.3123[M-H] ⁻	-1.44[M-H] ⁻	Lantanoic acid
5	24.025	C ₃₀ H ₄₈ O ₅	487.3429[M-H] ⁻	487.3433[M-H] ⁻	-0.82[M-H] ⁻	Arjunolic acid
6	28.752	C ₃₀ H ₄₆ O ₄	469.3323[M-H] ⁻	469.3331[M-H] ⁻	-1.70[M-H] ⁻	6β-Hydroxyl-3-oxolup-20(29)-en-28-oic acid
7	29.000	C ₃₀ H ₄₄ O ₄	467.3167[M-H] ⁻	467.3165[M-H] ⁻	0.42[M-H] ⁻	Liquidambaric lactone
8	31.650	C ₂₉ H ₄₄ O ₄	457.3312[M+H] ⁺	457.3316[M+H] ⁺	0.87[M+H] ⁺	2α,3β-Dihydroxy-23-demethyloleanol-4(24)-12 (13)-diene-28-carboxylic acid
9	33.661	C ₃₀ H ₄₄ O ₄	467.3167[M-H] ⁻	467.3167[M-H] ⁻	0.00[M-H] ⁻	3,6-Dion-20(29)-lupen-28-oic acid
10	34.975	C ₁₅ H ₂₂ O ₂	235.1693[M+H] ⁺	235.1688[M+H] ⁺	2.12[M+H] ⁺	Sesquichamaenol
11	37.331	C ₃₀ H ₄₆ O ₃	453.3374[M-H] ⁻	453.3387[M-H] ⁻	-2.86[M-H] ⁻	3-Oxo-ursolic acid

VEGFA and Caspase 9 (Proteintech, United States). After being rinsed three times with TBST, membranes were incubated 2 h at room temperature in secondary antibodies and subsequently be visualized with EasySee Western Blot Kit (Beijing Quanshi Gold Biotechnology Co., Ltd., Beijing, China). Finally, the images were quantified using ImageJ software and standardized against β-actin. In addition, three independent assays were performed.

Statistical analysis

SPSS software (version 19.0) was employed to carry out most of the statistical analyses except metabonomics. The data were shown as mean ± SD. Statistical comparisons were explored using one-way analysis of variance (ANOVA) followed by the least significant difference (LSD) test. In addition, the difference was of statistical significance when values of $p < 0.05$, while it indicated very significant when $p < 0.01$.

Results

Chemical components absorbed into rat plasma

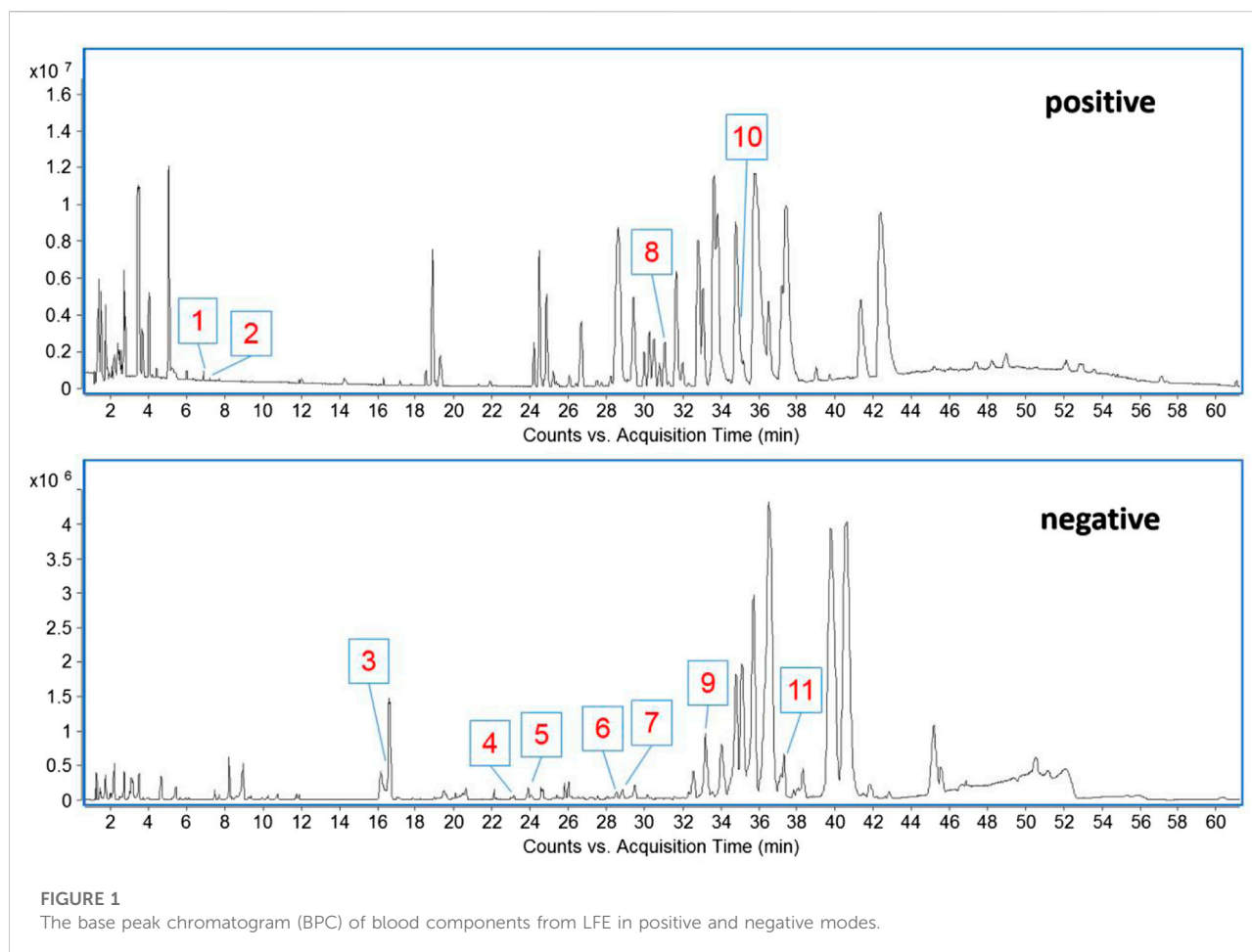
In the early stage, our research group separated and identified the chemical components contained in LFE, and identified totally 30 chemical components (Zhang et al., 2020). In the current work, the chemical components absorbed into rat plasma was further explored, and 11 prototype blood components were found, including phellopterin, 2-hydroxy-3-oxo-1,4(5)-oleanadien-28-oic acid, lantanoic acid and so

on. In addition, eight triterpenoids, two coumarins and one phenolic components were included (Table 1) (Figure 1).

Effect of liquidambaris fructus extract on physiological indexes of hepatocellular carcinoma rats

In 1–6 weeks of modeling, rats in each group exhibited good appetites, which were active and lively with their hair being glossy and dense. After 6–16 weeks of modeling, rats in the model group suffered from anorexia, decreased diet, decreased activity, disordered and dull hair, and the mortality reached up to 50%. Rats in cyclophosphamide group presented less diet, severe depilation, tooth loss, weight loss and other symptoms with the mortality being higher (66.67%). In comparison with the model group, rats in LFE group were in relatively good physical condition and their hair was smooth and tidy with no severe depilation, tooth loss, weight loss and other symptoms. Compared with the model group and cyclophosphamide group, there was no death in LFE high-dose group, and the mortality in low-dose group was lower (10%). Additionally, at week 16, the body weight of rats in the blank group, LFE high-dose and low-dose groups was obviously higher than that in the model group ($p < 0.01$ or $p < 0.05$), while there existed no obvious difference between cyclophosphamide group and model group (Figure 2A). It can be seen that there exists a certain negative correlation between body weight and mortality. And also indicated that LFE could improve the quality of life and prolong the survival time of HCC rats.

The changes of some physiological indexes such as liver index, thymus index and spleen index can be used to assess the efficacy of drugs. The findings of this study demonstrated that the



liver tissue of the model group was congested and inflamed, and its liver index was higher than that of the blank group ($p < 0.01$). Besides, the liver index of LFE high and low dose groups were lower than that of model group ($p < 0.01$), close to that of the cyclophosphamide and blank groups. When the body is cancerous, the immune function is lost, the thymus index decreases, and the spleen index increases. According to the results, compared with the blank group, the thymus index of the model group was smaller and the spleen index was larger, suggesting that the immune function of liver cancer rats was decreased. While there was no difference in thymus index and spleen index between cyclophosphamide group and model group ($p > 0.05$), indicating that although cyclophosphamide improved liver injury, it also reduced the immunity of the body, thus affecting the quality of life of rats. In comparison with the model group, the spleen indexes of LFE groups were smaller ($p < 0.01$) and the thymus indexes were larger ($p < 0.01$ or $p < 0.05$), suggesting that LFE could significantly increase the immune capacity of the body and therefore resist liver cancer, especially at high doses (Figures 2B–D).

Effect of liquidambaris fructus extract on pathological indexes of liver tissue in rats with hepatocellular carcinoma

Based on the appearance, the liver tissue of the blank group was ruddy in color, smooth in surface and soft in texture. The liver tissue of rats in the model group was yellowish in color, and the surface was densely covered with white vesicular tumor including nodules. The nodules were large in volume, and the diameter of some tumors was over 1 mm. The texture was hard. In the low dose group of LFE, the surface of liver tissue was slightly rough and hard, accompanied by a small number of gray white nodules. However, in the high dose group, the surface of liver tissue was smooth, and some small pimple like protrusions appeared on the surface of liver, which was close to the blank group. In addition, the liver tissue of cyclophosphamide group was similar to that of normal group, with smooth surface and slightly dark color (Figure 3A).

According to the pathological section, the liver lobule structure of the blank group rats is complete and clear. In addition, hepatic cord is radially arranged from the central

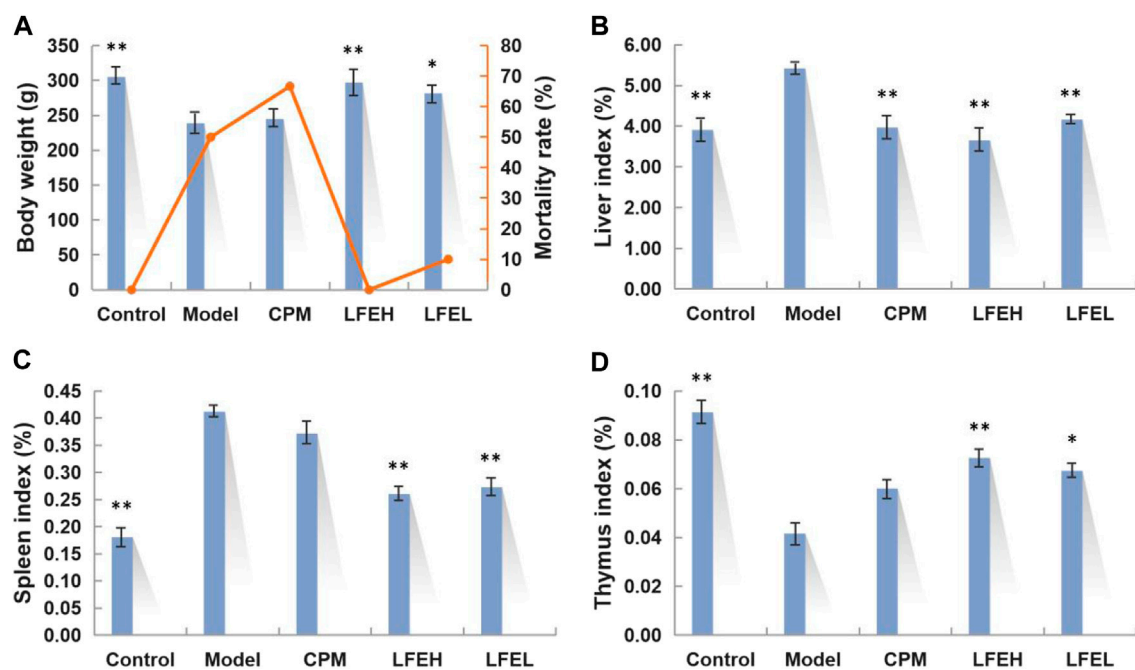


FIGURE 2

Effects of LFE on physiological indexes of HCC rats. (A) Body weight and mortality rate of different groups. (B) Liver index of different groups. (C) Spleen index of different groups. (D) Thymus index of different groups. The findings were denoted to be mean \pm SE. $n = 8$. * $p < 0.05$, ** $p < 0.01$ vs. model group. Control, the blank group; Model, the model group; CPM, the cyclophosphamide group; LFEH, LFE high-dose group; LFEL, LFE low-dose group.

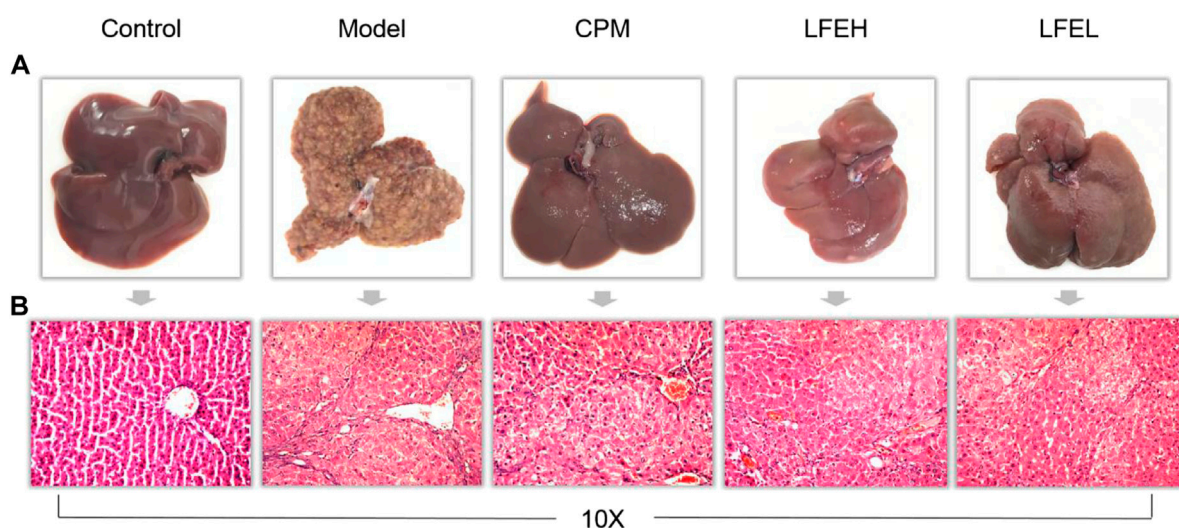


FIGURE 3

Impact of LFE on pathological indexes of liver tissue in rats with HCC. (A) Liver appearance of rats in each group. (B) Liver histopathology of rats in each group. Control, the blank group; Model, the model group; CPM, the cyclophosphamide group; LFEH, LFE high-dose group; LFEL, LFE low-dose group.

vein, the hepatocyte interface is clear, the size is basically the same, the arrangement is neat, the nucleus is large and round, the cytoplasm is uniform, the nucleolus is clear, the liver lobule

structure is very complete, and there exists no significant inflammatory cell invasion. In the model group, the liver cells showed obvious atypical proliferation, increased heterotypic

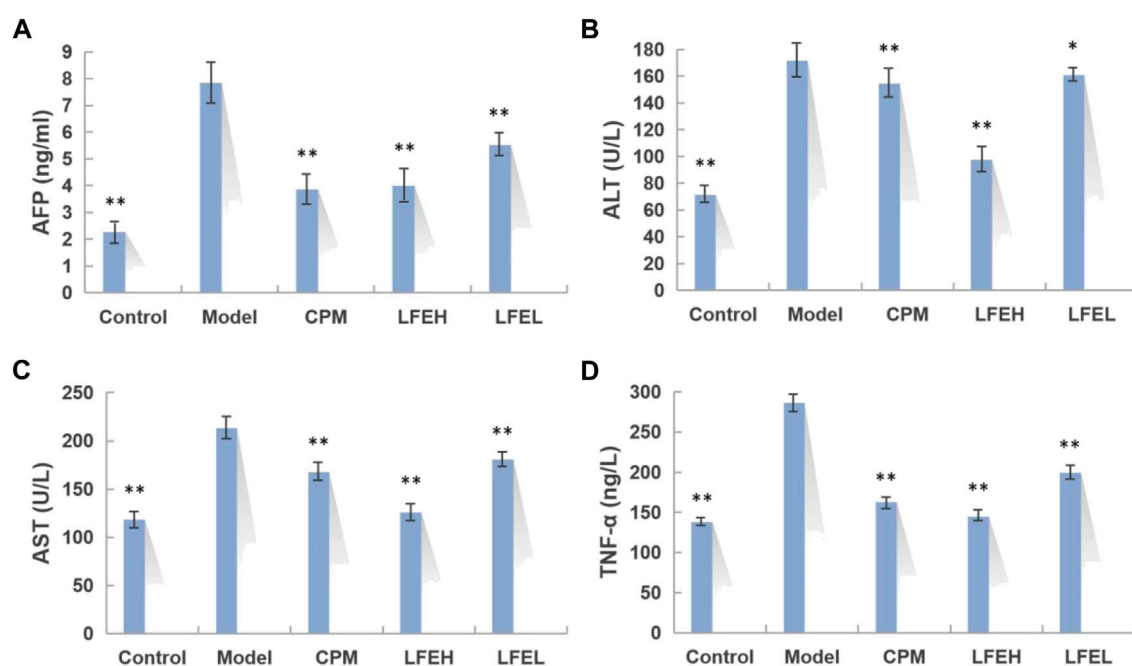


FIGURE 4

Impact of LFE on biochemical indexes of serum in rats with HCC. (A) Content of AFP in each group. (B) Content of ALT in each group. (C) Content of AST in each group. (D) Content of TNF- α in each group. The results were expressed as mean \pm SE. $n = 8$. * $p < 0.05$, ** $p < 0.01$ vs. model group. Control, the blank group; Model, the model group; CPM, the cyclophosphamide group; LFEH, LFE high-dose group; LFEL, LFE low-dose group.

cells, irregular arrangement, deep staining due to nuclear division, hemorrhage, necrosis and inflammatory cell infiltration in some parts. When compared with model group, the hepatocytes of LFE and cyclophosphamide groups were arranged orderly, some hepatocytes were still arranged in a cord shape, the nodules were small and few, and the hepatocytes had less heterogeneous proliferation, which was found to be close to the liver tissue of the blank group. The high dose group of LFE was better than the low dose group, which could alleviate the degree of liver cell damage and have the trend of recovery to normal cells. The results proved that LFE possesses prominent anti-liver tumor effect (Figure 3B).

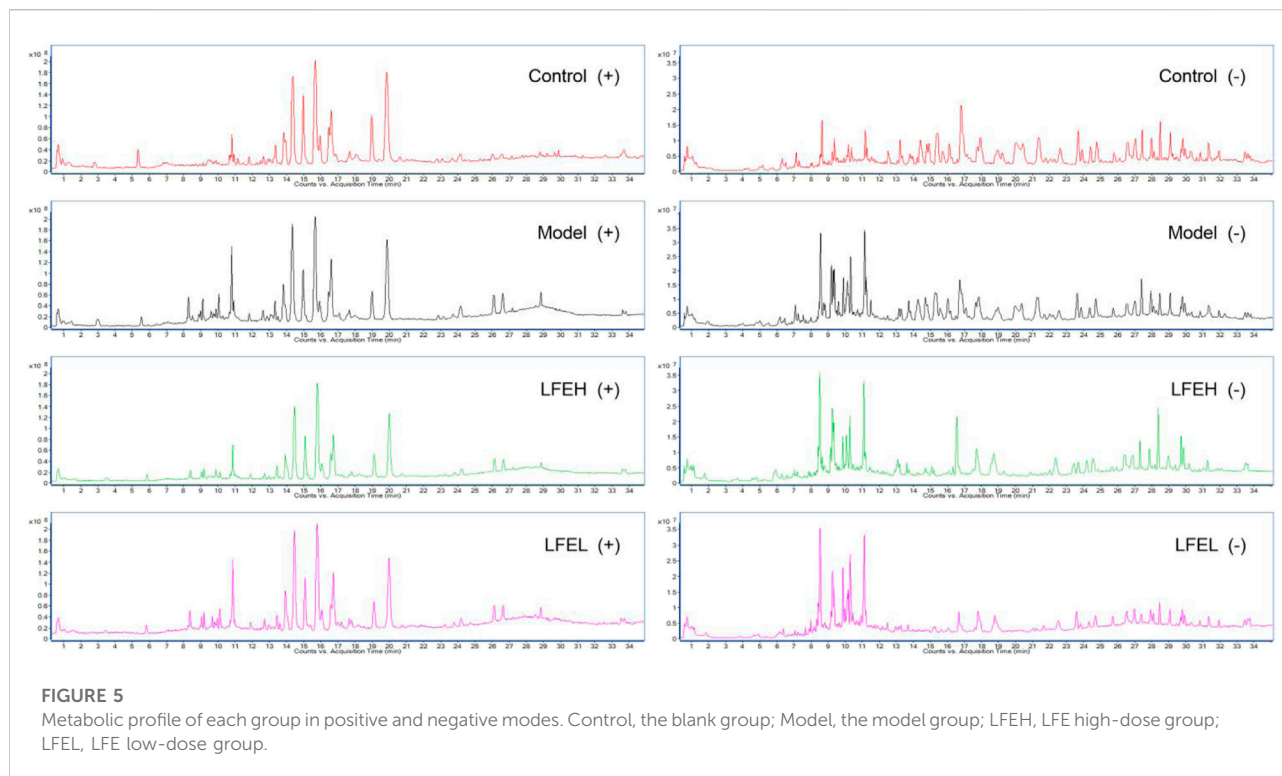
Effect of liquidambaris fructus extract on biochemical indexes of serum in rats with hepatocellular carcinoma

AFP is a tumor biomarker of liver cancer, serum ALT and AST levels are characteristic indexes reflecting liver function, and tumor necrosis factor TNF- α is an important inflammatory factor. The changes of these indicators can also reflect the severity of HCC and the therapeutic effect of drugs from a biochemical point of view. The levels of AFP, ALT, AST, and TNF- α in serum of DEN-induced HCC rats after LFE intervention were determined by ELISA. In

comparison with blank group, the contents of AFP, ALT, AST, and TNF- α in serum of model group were obviously enhanced ($p < 0.01$). However, in comparison with model group, the contents of AFP, ALT, AST, and TNF- α in serum of LFE high-dose group reduced obviously ($p < 0.01$). The levels of AFP, ALT, AST, and TNF- α in LFE low-dose group were also decreased in varying degrees ($p < 0.01$ or $p < 0.05$) (Figures 4A–D). The effect of high dose of LFE on serum AFP content of rats was similar to that of cyclophosphamide, the influences on ALT and AST were better than those of cyclophosphamide, and the impact on TNF- α was also similar to that of cyclophosphamide, slightly better, which indicated that LFE possesses preferable anti-tumor, hepatoprotective and anti-inflammatory effects.

Analysis of metabolic profiles

The metabolic profile of each group was obtained by UPLC-QTOF-MS analysis. The total ion chromatography (TIC) was shown in Figure 5. PCA and PLS-DA analysis results revealed that the points in the group are relatively clustered and have good homogeneity. Better separation can be achieved in the spatial position between each group, and both positive and negative ion modes are far away from the model group, indicating that the metabolites in the body are different (Figures 6A–D).



Identification of endogenous differential metabolites

Based on the significant statistical analysis and the contribution degree of compounds, combined with clinical and biological significance, 82 compounds (59 from positive ion mode, 30 from negative, with 7 both from positive and negative) were preliminarily selected as endogenous differential metabolites. They were identified through the comparison of HMDB, Metlin, KEGG and other databases, as displayed in Tables 2, 3.

Effect on the expression of PI3K-Akt signal pathway related genes

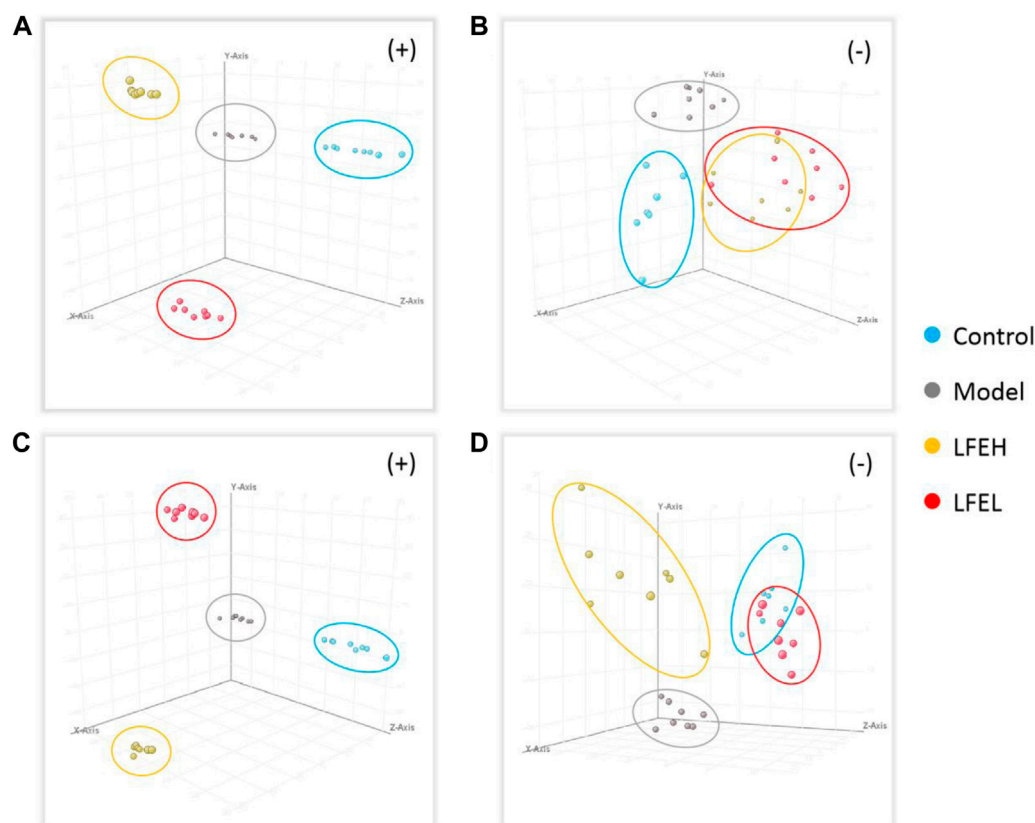
In comparison with the blank group, LFE regulated the mRNA expression levels of PTEN, PI3K, AKT, PDCD4, VEGFA, Caspase 9, Caspase 3, Bcl-2, Bax and Bad in liver cancer cells to different degrees. Among them, the relative expressions of PTEN, PDCD4, Caspase 9, Caspase 3, Bax and Bad genes were upregulated, whereas those of PI3K, AKT, VEGFA and Bcl-2 genes were downregulated (Figures 7A,B).

Effect on the expression of PI3K-Akt signal pathway related proteins

Compared with the blank group, LFE regulated the proteins expression levels of PTEN, PI3K, p-PI3K, Akt, p-Akt, VEGFA and Caspase 9 in liver cancer cells to different degrees. Among them, the relative expressions of PI3K, p-PI3K, Akt, p-Akt and VEGFA proteins presented downregulation ($p < 0.01$), while that of PTEN and Caspase 9 showed upregulation ($p < 0.01$) (Figures 7C,D).

Discussion

Liver cancer refers to one of the top ten cancers globally in terms of incidence rate and mortality (Bao et al., 2017). In addition, it is also the most common malignant tumor in China, which seriously affects people's lives. At present, liver cancer is not sensitive to radiotherapy and chemotherapy drugs, and clinical treatment urgently needs an alternative or auxiliary drug (Guo et al., 2019). Previous studies of our research group have found that LFE exhibits perfect inhibitory impact on liver tumor cells and induces cell cycle arrest and apoptosis (Zhang et al., 2020). On this basis, this work carried out

**FIGURE 6**

PCA and PLS-DA analysis. (A) PCA analysis in positive mode. (B) PCA analysis in negative mode. (C) PLS-DA analysis in positive mode. (D) PLS-DA analysis in negative mode. Control, the blank group; Model, the model group; LFEH, LFE high-dose group; LFEL, LFE low-dose group.

studies on the blood components, pharmacological effects and action mechanism of LFE *in vivo*, with the purpose of further revealing its pharmacodynamic material basis and mechanism of action.

In this study, through the research method of serum pharmacokinetics (Qian et al., 2021), the blood components of rats' plasma after intragastric administration of LFE were analyzed. Meanwhile, 11 prototype components, including imperatorin, phlopterin, arjunolic acid and liquidambaric lactone were found. According to relevant literature reports, imperatorin has the ability to cause Mcl-1 degradation, which then releases Bak and Bax and activates the intrinsic apoptosis pathway, causing multidrug-resistant liver cancer cells to undergo apoptosis (Li et al., 2014). It can reverse the drug resistance in cisplatin-resistant liver cancer cells with cisplatin treatment *in vitro* (Hu et al., 2015). Arjunolic acid possesses anti-inflammatory and anti-tumor cell proliferation activities, and exerts protective effects on liver and kidney toxicity induced by cisplatin (Nehal et al., 2016; Sherif, 2021). Some studies have shown that arjunolic acid possesses nano-sized self-assembly characteristics, is easy to be penetrated

by cancer cells, and is non-toxic to normal cells (Manna et al., 2020). Liquidambaric lactone features anti-angiogenic properties, which can significantly inhibit VEGF-induced proliferation of HUVECs endothelial cells and effectively lower VEGF-induced cell migration (Zhu et al., 2021). 3-Oxo-ursolic acid is cytotoxic to a variety of tumor cells, exhibiting potent cytotoxic activities both in murine and in human cancer cell lines (Min et al., 2000). In addition, phellopterin (Sumiyoshi et al., 2014), 3,6-dion-20(29)-lupen-28-oic acid (Zhang et al., 2020) and others were reported to have varying degrees of antitumor activity. The above studies proved that the monomer components of LFE are certainly the active substances against HCC *in vivo*.

Based on the DEN-induced rat liver cancer model, this study investigated the anti-tumor efficacy of different doses of LFE. After a 4-month experimental cycle, it was found that the survival state of rats in LFE administration groups was significantly better than that in model group. Compared with the mortality of 50% in the model group, there was no death in LFE high-dose administration group, while the mortality of the positive drug cyclophosphamide was 66.67%. Thus, it is demonstrated that

TABLE 2 Endogenous differential metabolites in positive ion mode.

No.	Retention time (RT) (min)	Endogenous differential metabolites	Formula	Measured mass (m/z)	Ion Mode	Trend	
						Control vs. Model	LFEH, LFEL vs. Model
1	0.673	Choline	C ₅ H ₁₄ NO	104.1067	[M+H] ⁺	Down	Down
2	0.689	Carnitine	C ₇ H ₁₅ NO ₃	162.1124	[M+H] ⁺	Up	Up
3	0.716	Valine	C ₅ H ₁₁ NO ₂	118.0859	[M+H] ⁺	Up	Up
4	0.911	Asparagine	C ₄ H ₈ N ₂ O ₃	155.0430	[M+Na] ⁺	Up	Up
5	0.970	Acetylcarnitine	C ₉ H ₁₇ NO ₄	204.1228	[M+H] ⁺	Up	Up
6	1.036	2-Phenylacetamide	C ₈ H ₉ NO	136.0758	[M+H] ⁺	Down	Down
7	1.390	Leucine	C ₆ H ₁₃ NO ₂	132.1017	[M+H] ⁺	Up	Up
8	1.433	Tyrosine	C ₉ H ₁₁ NO ₃	182.0805	[M+H] ⁺	Down	Down
9	1.483	Isoleucine	C ₆ H ₁₃ NO ₂	132.1017	[M+H] ⁺	Up	Up
10	2.971	L-Phenylalanine	C ₉ H ₁₁ NO ₂	166.0861	[M+H] ⁺	Down	Down
11	4.745	Isobutyrylcarnitine	C ₁₁ H ₂₂ NO ₄	232.1528	[M+H] ⁺	Up	Up
12	5.379	Indolelactic acid	C ₁₁ H ₉ NO ₂	188.0714	[M+H] ⁺	Down	Down
13	5.379	Tryptophan	C ₁₁ H ₁₂ N ₂ O ₂	205.0978	[M+H] ⁺	Down	Down
				227.0795	[M+Na] ⁺		
14	6.421	Valerylcarnitine	C ₁₂ H ₂₃ NO ₄	246.1704	[M+H] ⁺	Up	Up
15	6.498	Pivaloylcarnitine	C ₁₂ H ₂₃ NO ₄	246.1694	[M+H] ⁺	Up	Up
16	7.366	Hexanoylcarnitine	C ₁₃ H ₂₅ NO ₄	260.1849	[M+H] ⁺	Up	Up
17	8.809	Octanoylcarnitine	C ₁₅ H ₂₉ NO ₄	288.2156	[M+H] ⁺	Up	Up
18	8.311	Sulfoglycolithocholate	C ₂₆ H ₄₃ NO ₇ S	514.2820	[M+H] ⁺	Down	Down
				536.2643	[M+Na] ⁺		
				478.2607	[M+H-2H ₂ O] ⁺		
				496.2712	[M+H-H ₂ O] ⁺		
19	8.889	Taurallocholic acid	C ₂₆ H ₄₅ NO ₇ S	480.2760	[M+H-2H ₂ O] ⁺	Down	Down
				498.2864	[M+H-H ₂ O] ⁺		
20	8.972	Tauroursocholic acid	C ₂₆ H ₄₅ NO ₇ S	480.2762	[M+H-2H ₂ O] ⁺	Down	Down
				498.2868	[M+H-H ₂ O] ⁺		
				516.2969	[M+H] ⁺		
				538.2791	[M+Na] ⁺		
				560.2628	[M+2Na-H] ⁺		
21	9.584	Tetracosahexaenoic acid	C ₂₄ H ₃₆ O ₂	357.2776	[M+H] ⁺	Down	Down
22	9.782	Glycocholic acid	C ₂₆ H ₄₃ NO ₆	430.2919	[M+H-2H ₂ O] ⁺	Down	Down
				448.3040	[M+H-H ₂ O] ⁺		
				466.3146	[M+H] ⁺		
				488.2973	[M+Na] ⁺		
23	9.881	12-Ketodeoxycholic acid	C ₂₄ H ₃₆ O ₂	373.2727	[M+H-H ₂ O] ⁺	Down	Down
				391.2830	[M+H-H ₂ O] ⁺		
24	10.030	7-Ketodeoxycholic acid	C ₂₄ H ₃₈ O ₅	371.2592	[M+H-2H ₂ O] ⁺	Down	Down
				389.2679	[M+H-H ₂ O] ⁺		
				407.2775	[M+H] ⁺		
				428.2601	[M+Na] ⁺		
25	10.658	Palmitic acid	C ₁₆ H ₃₂ O ₂	274.2737	[M+NH ₄] ⁺	Down	Down
26	10.790	Nutriacholic acid	C ₂₄ H ₃₈ O ₄	355.2624	[M+H-2H ₂ O] ⁺	Down	Down
				373.2730	[M+H-H ₂ O] ⁺		
				391.2827	[M+H] ⁺		
27	10.790	PI(16:0/18:0)	C ₄₃ H ₈₃ O ₁₃ P	839.5623	[M+H] ⁺	Down	Down

(Continued on following page)

TABLE 2 (Continued) Endogenous differential metabolites in positive ion mode.

No.	Retention time (RT) (min)	Endogenous differential metabolites	Formula	Measured mass (m/z)	Ion Mode	Trend	
						Control vs. Model	LFEH, LFEL vs. Model
28	10.906	6,9,12,15,18,21-Tetracosahexaenoic acid	C ₂₄ H ₃₆ O ₂	357.2778	[M+H] ⁺	Down	Down
29	11.154	Glycoursodeoxycholic acid	C ₂₅ H ₄₃ NO ₅	472.3011	[M+Na] ⁺	Down	Down
				450.3188	[M+H] ⁺		
30	11.501	Dodecanoylcarnitine	C ₁₉ H ₃₇ NO ₄	344.2779	[M+H] ⁺	Up	Up
31	11.881	9,10-DHOME	C ₁₈ H ₃₄ O ₄	315.2521	[M+H] ⁺	Down	Down
32	11.948	Leukotriene B	C ₂₀ H ₃₂ O ₄	337.2346	[M+H] ⁺	Down	Down
33	12.295	Sphinganine	C ₁₈ H ₃₉ NO ₂	302.3049	[M+H] ⁺	Down	Down
				324.2860	[M+Na] ⁺		
34	12.460	Sphinganine 1-phosphate	C ₁₈ H ₃₈ NO ₅ P	402.2364	[M+Na] ⁺	Down	Down
				380.2547	[M+H] ⁺		
35	12.625	LysoPC(14:0/0:0)	C ₂₂ H ₄₆ NO ₇ P	490.2892	[M+Na] ⁺	Up	Up
				468.3073	[M+H] ⁺		
36	13.320	LysoPC(16:1(9z)/0:0)	C ₂₄ H ₄₈ NO ₇ P	516.3046	[M+Na] ⁺	Up	Up
				494.3228	[M+H] ⁺		
37	13.683	Tetradecanoylcarnitine	C ₂₁ H ₄₁ NO ₄	394.2913	[M+Na] ⁺	Up	Up
				372.3098	[M+H] ⁺		
38	13.816	LysoPC(18:2(9z,12z))	C ₂₆ H ₅₀ NO ₇ P	542.3206	[M+Na] ⁺	Up	Up
				520.3392	[M+H] ⁺		
39	13.915	LysoPC(20:4(5z,8z,11Z,14Z))	C ₂₈ H ₅₀ NO ₇ P	566.3202	[M+Na] ⁺	Up	Up
				544.3384	[M+H] ⁺		
40	14.345	LysoPC(22:6(4z,7z,10Z,13Z,16Z,19Z))	C ₃₀ H ₅₀ NO ₇ P	566.3202	[M+Na] ⁺	Up	Up
				544.3384	[M+H] ⁺		
41	14.510	Stearidonic acid	C ₁₈ H ₂₈ O ₂	277.2154	[M+H] ⁺	Up	Up
42	14.956	LysoPC(16:0)	C ₂₄ H ₅₀ NO ₇ P	518.3205	[M+Na] ⁺	Up	Up
				496.3398	[M+H] ⁺		
43	15.188	Eicosapentaenoic acid	C ₂₀ H ₃₀ O ₂	303.2307	[M+H] ⁺	Up	Up
44	15.667	LysoPC(0:0/16:0)	C ₂₄ H ₅₀ NO ₇ P	518.3203	[M+Na] ⁺	Up	Up
				496.3403	[M+H] ⁺		
45	15.932	LysoPC(18:1(9z))	C ₂₆ H ₅₂ NO ₇ P	544.3361	[M+Na] ⁺	Up	Up
				522.3540	[M+H] ⁺		
46	16.444	LysoPC(18:1(11z))	C ₂₆ H ₅₂ NO ₇ P	544.3361	[M+Na] ⁺	Up	Up
				522.3545	[M+H] ⁺		
				1,043.7036	[2M+H] ⁺		
47	16.527	PC(14:0/16:0)	C ₃₈ H ₇₆ NO ₈ P	688.5187	[M+H-H ₂ O] ⁺	Up	Up
48	17.139	L-Palmitoylcarnitine	C ₂₃ H ₄₅ NO ₄	400.3404	[M+H] ⁺	Up	Up
49	17.684	LysoPC(20:2(11Z,14Z))	C ₂₈ H ₅₄ NO ₇ P	570.3513	[M+Na] ⁺	Up	Up
				548.3692	[M+H] ⁺		
50	17.684	LysoPE(0:0/20:0)	C ₂₅ H ₅₂ NO ₇ P	532.3374	[M+Na] ⁺	Up	Up
				509.3481	[M+H] ⁺		
51	18.036	2-Hydroxyhexadecanoylcarnitine	C ₂₅ H ₄₇ NO ₄	426.3502	[M+H] ⁺	Up	Up
52	18.660	Docosapentaenoic acid	C ₂₂ H ₃₄ O ₂	331.2629	[M+H] ⁺	Up	Up
53	18.990	LysoPC(18:0)	C ₂₆ H ₅₄ NO ₇ P	546.3513	[M+Na] ⁺	Up	Up
				524.3701	[M+H] ⁺		
54	19.866	LysoPC(0:0/18:0)	C ₂₆ H ₅₄ NO ₇ P	546.3516	[M+Na] ⁺	Up	Up
				524.3714	[M+H] ⁺		

(Continued on following page)

TABLE 2 (Continued) Endogenous differential metabolites in positive ion mode.

No.	Retention time (RT) (min)	Endogenous differential metabolites	Formula	Measured mass (m/z)	Ion Mode	Trend	
						Control vs. Model	LFEH, LFEI vs. Model
55	20.577	LysoPC(20:1(11Z))	C ₂₈ H ₅₆ NO ₇ P	550.3853 572.3669	[M+H] ⁺ [M+Na] ⁺	Up	Up
56	20.941	Stearoylcarnitine	C ₂₅ H ₄₉ NO ₄	428.3712	[M+H] ⁺	Up	Up
57	23.156	Docosahexaenoic acid	C ₂₂ H ₃₂ O ₂	329.2464	[M+H] ⁺	Up	Up
58	23.735	Arachidonic acid	C ₂₀ H ₃₂ O ₂	305.2464	[M+H] ⁺	Down	Down
59	26.573	Cer(d18:0/12:0)	C ₃₀ H ₆₁ NO ₃	484.4714	[M+H] ⁺	Up	Up

LFE has a definite effect on improving the survival cycle in the treatment of HCC. Furthermore, the body weight of rats in LFE high-dose group was also close to the blank group, which was obviously higher than that in model and cyclophosphamide groups. Liver index, spleen index, thymus index and other physiological indicators performed well. The above experimental results proved that LFE can inhibit the abnormal proliferation of liver cells, reduce inflammatory infiltration of liver cells and lower liver body ratio, so as to exert the role of repairing liver function. At the same time, LFE can also increase thymus index, decrease spleen index, and enhance the immune function of liver cancer rats. Thus, it is shown that LFE has a clear role in improving the quality of life in the treatment of HCC. From the perspective of pathological indicators, LFE high-dose group can significantly improve the degree of liver cell injury, with a trend of recovery to normal cells. The levels of liver cancer biomarker AFP, liver injury indicators ALT, AST and pro-inflammatory factor TNF- α in serum of rats treated with LFE were significantly lower than those in model group and close to blank group. It is demonstrated that LFE has definite anti-tumor, hepatoprotective and anti-inflammatory impact on the treatment of HCC. Pharmacological and pharmacodynamic experiments based on DEN-induced rat liver cancer model proved that LFE could prolong the life cycle and improve the quality of life, thus treating liver tumor.

The occurrence and development of HCC refers to a complex multi-step process involving multiple genes and multiple pathways. As one of the most frequently activated signaling pathways in human cancer, the PI3K/Akt signaling pathway mediates almost 50% of malignant tumors. PI3K/Akt signaling pathway plays a pivotal role in intracellular and extracellular signal transduction. As an important regulatory pathway in the development and progression of HCC, PI3K/Akt signaling pathway is closely associated with the proliferation, apoptosis, autophagy, invasion and migration of HCC cells (Martini et al., 2014). In the previous experimental study, the research group found that triterpenoids in LF can regulate the PI3K/Akt signaling pathway to promote the apoptosis of HCC cells (Zhang et al., 2020). In order to further verify the rationality

of the discovered mechanism and explore the in-depth mechanism of LFE in anti-tumor, hepatoprotective, anti-inflammatory and other pharmacological effects, this study adopted non-target metabolomics combined with q-PCR and Western blot technology for investigating the key targets and pathways of LFE.

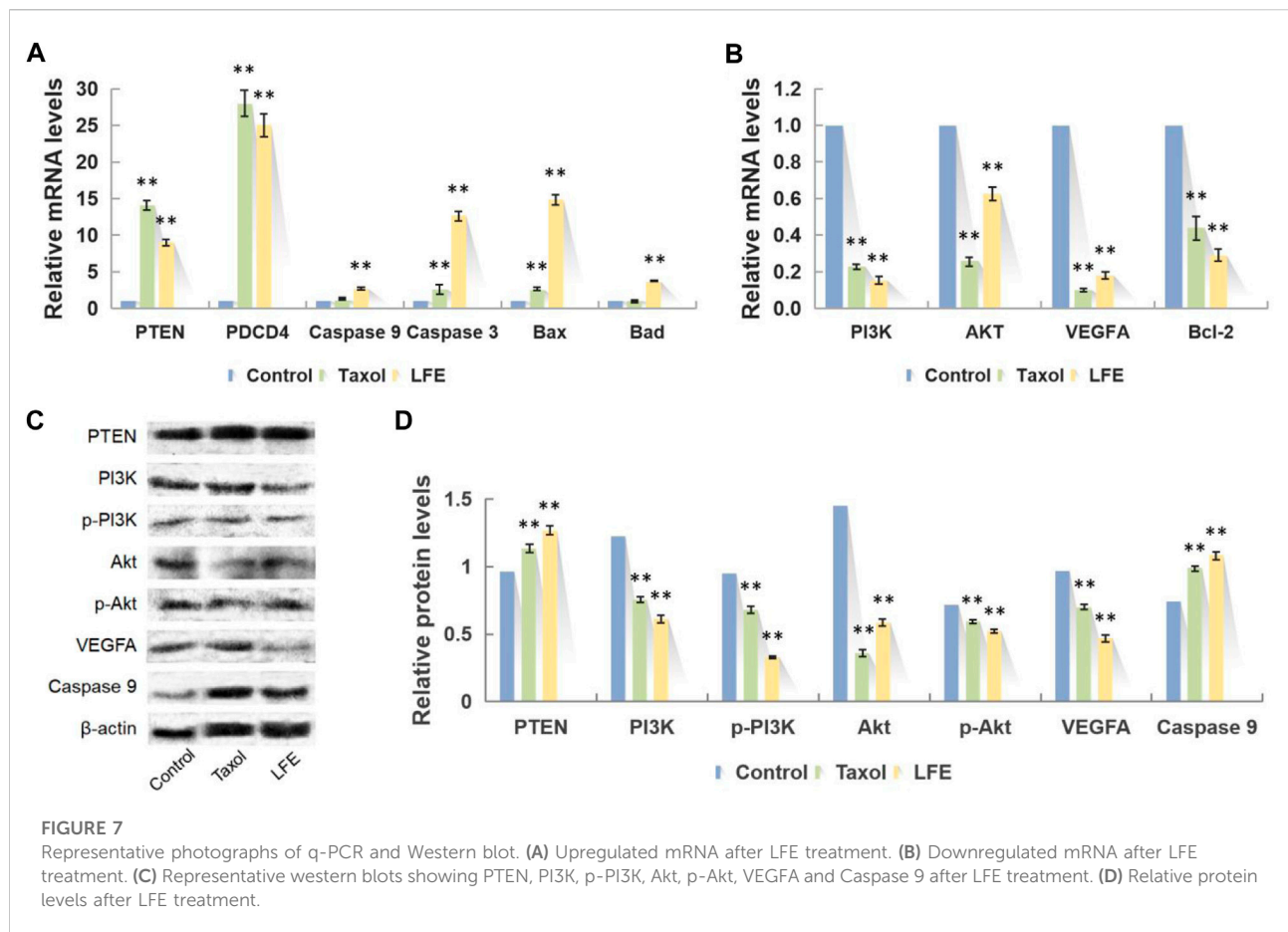
Through the mechanism study of non-target metabolomics, it was found that endogenous lipid metabolites including sphingosine-1-phosphate (S1P), sphingosine 1-phosphate and sphingosine changed, in which S1P has emerged as an important signaling molecule that has been discovered to be involved in many cellular functions (Nagahashi et al., 2015), containing promoting cell proliferation, death, aging, adhesion, migration, angiogenesis and inflammation. These functions are mediated by G protein-coupled S1P receptors, where S1P(1) stimulates cell proliferation through a G(i) mediated signaling pathway including PI3K/Akt and ERK, while S1P(2) mediates cell proliferation through G(12/13)/Rho/Rho kinase/PTEN-dependent Akt inhibition mechanism (Takuwa et al., 2012). In this study, LFE can downregulate the content of S1P in serum of HCC rats, thereby influencing the PTEN/PI3K/Akt signaling pathway. PTEN can inhibit the phosphorylation of the intracellular protein PI3K and downregulate the activity of phosphatidylinositol triphosphate (PIP3), leading to the inhibition of AKT recruitment and phosphorylation on the cell membrane, and affecting the protein proportion on the mitochondrial membrane (Carnero et al., 2008). Bax binds with Bcl-2 to form apoptotic dimer. In addition, it promotes the release of cytochrome C and apoptosis-inducing factors, promotes the occurrence of Caspase cascade reaction, and triggers apoptosis through endogenous pathway. Based on q-PCR and Western blot experiments, it was found that LFE could upregulate PTEN gene and protein expression, inhibit the phosphorylation of anti-apoptotic proteins PI3K and Akt, upregulate the level of Bad gene and downregulate the level of Bcl-2. Meanwhile, it promotes the activation of Caspase 9, the direct target protein downstream of Akt, further activates the downstream Caspase 3 protein, and finally inhibits the proliferation of liver cancer cells and causes apoptosis of liver

TABLE 3 Endogenous differential metabolites in negative ion mode.

No.	Retention time (RT) (min)	Endogenous differential metabolites	Formula	Measured mass (m/z)	Ion mode	Trend	
						Control vs. Model	LFEH, LFEL vs. Model
1	0.564	L-Lysine	C ₆ H ₁₄ N ₂ O ₂	145.0965	[M-H] ⁻	Up	Up
2	1.176	N-Acryloylglycine	C ₅ H ₇ NO ₃	128.0339	[M-H] ⁻	Down	Down
3	4.003	L-Phenylalanine	C ₉ H ₁₁ NO ₂	164.0700	[M-H] ⁻	Down	Down
4	6.846	(R)-3-Hydroxyhexanoic acid	C ₆ H ₁₂ O ₃	131.0695	[M-H] ⁻	Up	Up
5	7.061	p-Cresol sulfate	C ₇ H ₈ O ₄ S	187.0054	[M-H] ⁻	Up	Up
6	8.549	Taurallocholic acid	C ₂₆ H ₄₅ NO ₇ S	512.2692	[M-H] ⁻	Down	Down
7	9.277	Tauroursocholic acid	C ₂₆ H ₄₅ NO ₇ S	514.2809	[M-H] ⁻	Down	Down
8	9.491	Tauroursodeoxycholic acid	C ₂₆ H ₄₅ NO ₆ S	498.2860	[M-H] ⁻	Down	Down
9	11.128	Cholic acid	C ₂₄ H ₄₀ O ₅	815.5652	[2M-H] ⁻	Down	Down
10	11.227	Isohyodeoxycholic acid	C ₂₄ H ₄₀ O ₄	407.2778	[M-H] ⁻	Up	Up
				391.2823	[2M-H] ⁻		
11	11.492	Nutriacholic acid	C ₂₄ H ₃₈ O ₄	783.5737	[M-H] ⁻	Down	Down
				389.2666	[2M-H] ⁻		
12	13.162	Sphingosine 1-phosphate	C ₁₈ H ₃₈ NO ₅ P	779.5423	[M-H] ⁻	Down	Down
				378.2382	[2M-H] ⁻		
13	13.294	Deoxycholic acid	C ₂₄ H ₄₀ O ₄	757.4850	[M-H] ⁻	Down	Down
				391.2817	[2M-H] ⁻		
14	13.707	Chenodeoxycholic acid	C ₂₄ H ₄₀ O ₄	783.5731	M+FA-H	Down	Down
				391.2819	[M-H] ⁻		
				437.2870	[2M-H] ⁻		
15	14.716	LysoPE(20:2(11Z,14Z)/0:0)	C ₂₅ H ₄₈ NO ₇ P	783.5731	[M-H] ⁻	Up	Up
16	14.815	LysoPE(0:0/22:4(7Z,10Z,13Z,16Z))	C ₂₇ H ₄₈ NO ₇ P	504.3055	[M-H] ⁻	Up	Up
17	15.278	LysoPE(0:0/20:2(11Z,14Z))	C ₂₅ H ₄₈ NO ₇ P	528.3048	[M-H] ⁻	Up	Up
18	15.360	LysoPE(22:4(7Z,10Z,13Z,16Z)/0:0)	C ₂₇ H ₄₈ NO ₇ P	504.3057	[M-H] ⁻	Up	Up
19	16.022	LysoPE(18:0/0:0)	C ₂₃ H ₄₈ NO ₇ P	528.3052	[M-H] ⁻	Up	Up
20	16.732	LysoPC(15:0)	C ₂₃ H ₄₈ NO ₇ P	480.3055	[M-H] ⁻	Up	Up
21	16.848	LysoPE(0:0/18:0)	C ₂₃ H ₄₈ NO ₇ P	480.3055	[M-H] ⁻	Up	Up
22	17.658	LysoPE(20:1(11Z)/0:0)	C ₂₅ H ₅₀ NO ₇ P	480.3055	[M-H] ⁻	Up	Up
23	17.791	LysoPE(0:0/20:1(11Z))	C ₂₅ H ₅₀ NO ₇ P	506.3209	[M-H] ⁻	Up	Up
24	20.006	LysoPI(18:0/0:0)	C ₂₇ H ₅₃ O ₁₂ P	506.3209	[M-H] ⁻	Up	Up
25	21.262	LysoPE(20:0/0:0)	C ₂₅ H ₅₂ NO ₇ P	599.3158	[M-H] ⁻	Up	Up
26	21.957	LysoPE(22:1(13Z)/0:0)	C ₂₇ H ₅₄ NO ₇ P	508.3367	[M-H] ⁻	Up	Up
27	22.188	LysoPC(17:0)	C ₂₅ H ₅₂ NO ₇ P	534.3514	[M-H] ⁻	Up	Up
28	22.552	Glycocholic acid	C ₂₆ H ₄₃ NO ₆	508.3367	[M-H] ⁻	Up	Up
29	23.825	Docosahexaenoic acid	C ₂₂ H ₃₂ O ₂	464.3104	[M-H] ⁻	Down	Down
30	24.337	Arachidonic acid	C ₂₀ H ₃₂ O ₂	327.2299	[M-H] ⁻	Down	Down
				303.2301			

cancer cells. In addition, the combination of VEGF and VEGFR1 will also affect Akt signaling pathway, generating tumor cell migration and invasion (Peng et al., 2021). This study found that LFE can downregulate the expression of VEGFA protein, thus inhibiting the angiogenesis of liver tumors and hindering the migration and invasion of tumor cells.

Besides, the differential endogenous substances eicosapentaenoic acid (EPA), docosahexaenoic acid (DHA), docosapentaenoic acid, 6,9,12,15,18,21-tetracosahaxaenoic acid and so on belong to polyunsaturated fatty acids (PUFA). EPA and DHA belong to n-3 polyunsaturated fatty acids, which are vulnerable to free radical attack and eventually lead to the formation of lipid peroxides. However,



the main function of lipid peroxide is to inhibit DNA synthesis, hinder cell division and proliferation, and induce apoptosis (Huang et al., 2016). In this study, the contents of EPA and DHA in plasma of HCC rats treated with LFE were significantly higher than those of model group, providing that LFE can inhibit and block HCC cell cycle and induce apoptosis of HCC cells by increasing the content of unsaturated fatty acids.

Tumors are often accompanied by inflammatory response, and PI3K/Akt pathway also plays an important role in regulating inflammatory response. When PI3K/Akt pathway is activated, activated Akt can enhance the phosphorylation and degradation of NF- κ B inhibitory protein I κ B kinase, then lead to the activation of NF- κ B, further induce the expression of TNF- α and other proinflammatory factors, and eventually lead to inflammatory response (Shi et al., 2016). In this study, the PI3K/Akt pathway was inhibited, the content of proinflammatory factor TNF- α in the blood of rats was decreased, and the content of endogenous differential metabolite arachidonic acid was also significantly lower

than that of the model group, suggesting that LFE could also play an anti-tumor role by reducing inflammation.

Moreover, endogenous differential metabolites, such as LysoPC(14:0/0:0), LysoPC(16:1(9z)/0:0), and LysoPA(19:0/0:0), are related products of fatty acid metabolism. Liver is the main part of lipid metabolism and exerts an important role in maintaining the metabolic balance of blood lipids. The endogenous differential metabolite lysophosphatidylcholine (LPC) generates phosphatidylcholine (PC) under the action of phosphatidylcholine acyltransferase 1 (Lpcat1), PC loses the fatty acid at sn-2 position under the action of phospholipase A2 (PLA2), and generates LPC, which is converted into lysophosphatidic acid (LPA) under the catalysis of hemolytic phospholipase D. When liver cancer occurs in the body, lecithin cholesterol acyltransferase (LCAT) synthesis decreases and the level of Lyso PC in blood lowers significantly (Guri et al., 2017). In this study, compared with the model group, LFE can significantly increase the level of Lyso PCs in rat serum, also increasing LCAT synthesis to protect hepatocytes.

Conclusion

To conclude, LFE possesses definite anti-liver cancer activity in physiology, pathology, biochemistry and other aspects. It can inhibit the growth of tumor cells, promote tumor cell apoptosis, reduce inflammatory reaction, protect hepatocytes, improve body immunity, improve the survival state of tumor rats, and prolong the life cycle. Besides, this study revealed the material basis of LFE, and further demonstrated that most of the above effects were related to the influence of PTEN/PI3K/Akt, fatty acid metabolism and other key signaling pathways from the perspective of metabolomics, which provide a scientific explanation for the clinical application of LFE. However, how the active ingredients are distributed, metabolized, and excreted in the body needs deeply explored, and the influence of LFE on other metabolic pathways will be further verified from the perspective of genes and proteins. These tasks will be the focus of our subsequent studies.

Data availability statement

The original contributions presented in the study are included in the article/supplementary material, further inquiries can be directed to the corresponding authors.

Ethics statement

The animal study was reviewed and approved by the Medicine Ethics Review Committee for animal experiments of Liaoning University of Traditional Chinese Medicine.

References

- Bao, Y. R., Wang, S., Yang, X. X., Li, T. J., Xia, Y. M., and Meng, X. S. (2017). Metabolomic study of the intervention effects of Shuihonghuazi Formula, a Traditional Chinese Medicinal formulae, on hepatocellular carcinoma (HCC) rats using performance HPLC/ESI-TOF-MS. *J. Ethnopharmacol.* 198, 468–478. doi:10.1016/j.jep.2017.01.029
- Carnero, A., Blanco-Aparicio, C., Renner, O., Link, W., and Leal, J. F. (2008). The PTEN/PI3K/AKT signalling pathway in cancer, therapeutic implications. *Curr. Cancer Drug Targets* 8 (3), 187–198. doi:10.2174/156800908784293659
- Fang, H., and Ji, H. (2019). Furanocoumarin A: A novel anticancer agent on human lung cancer A549 cells from fructus liquidambaris. *Anticancer. Agents Med. Chem.* 19 (17), 2091–2096. doi:10.2174/1871520619666191010102526
- Guo, W., Huang, J., Wang, N., Tan, H. Y., Cheung, F., Chen, F., et al. (2019). Integrating network pharmacology and pharmacological evaluation for deciphering the action mechanism of herbal formula zuojin pill in suppressing hepatocellular carcinoma. *Front. Pharmacol.* 10, 1185. doi:10.3389/fphar.2019.01185
- Guri, Y., Colombi, M., Dazert, E., Hindupur, S. K., Roszik, J., Moes, S., et al. (2017). mTORC2 promotes tumorigenesis via lipid synthesis. *Cancer Cell* 32 (6), 807–823.e12. doi:10.1016/j.ccell.2017.11.011
- Hu, J. J., Xu, C. L., Cheng, B. H., Jin, L. X., Li, J., Gong, Y. Q., et al. (2015). Imperatorin acts as a cisplatin sensitizer via downregulating Mcl-1 expression in HCC chemotherapy. *Tumour Biol.* 37 (1), 331–339. doi:10.1007/s13277-015-3591-z
- Huang, J., Guo, W., Cheung, F., Tan, H. Y., Wang, N., and Feng, Y. (2020). Integrating network pharmacology and experimental models to investigate the efficacy of coptidis and scutellaria containing huanglian jiedu decoction on hepatocellular carcinoma. *Am. J. Chin. Med.* 48 (1), 161–182. doi:10.1142/S0192415X20500093
- Huang, Q., Wen, J., Chen, G., Ge, M., Gao, Y., Ye, X., et al. (2016). Omega-3 polyunsaturated fatty acids inhibited tumor growth via preventing the decrease of genomic DNA methylation in colorectal cancer rats. *Nutr. Cancer* 68 (1), 113–119. doi:10.1080/01635581.2016.1115526
- Li, W. X., Qian, P., Guo, Y. T., Gu, L., Jurat, J., Bai, Y., et al. (2021). Myrtenal and β -caryophyllene oxide screened from Liquidambaris Fructus suppress NLRP3 inflammasome components in rheumatoid arthritis. *BMC Complement. Med. Ther.* 21 (1), 242. doi:10.1186/s12906-021-03410-2
- Li, X., Zeng, X. L., Sun, J. G., Li, H., Wu, P., Fung, K. P., et al. (2014). Imperatorin induces Mcl-1 degradation to cooperatively trigger Bax translocation and Bak activation to suppress drug-resistant human hepatoma. *Cancer Lett.* 348, 146–155. doi:10.1016/j.canlet.2014.03.017
- Manna, S., Dey, A., Majumdar, R., Bag, B. G., Ghosh, C., and Roy, S. (2020). Self assembled arjunolic acid acts as a smart weapon against cancer through TNF- α mediated ROS generation. *Heliyon* 6 (2), e03456. doi:10.1016/j.heliyon.2020.e03456
- Martini, M., De Santis, M. C., Braccini, L., Gulluni, F., and Hirsch, E. (2014). PI3K/AKT signaling pathway and cancer: An updated review. *Ann. Med.* 46 (6), 372–383. doi:10.3109/07853890.2014.912836

Author contributions

Study design: SW, Y-RB, and X-SM; Data collection: X-XY and T-JL; Analysis and interpretation: X-XY and LZ; Statistical analysis: SW, X-XY, and Y-RB; Drafting manuscript: SW and X-XY; Revision manuscript: SW, Y-RB, and X-SM. All authors read and approved the final manuscript.

Funding

This study was supported by the 2021 school level Natural Science (key) project of Liaoning University of Traditional Chinese Medicine (2021LZY036 and 2021LZY032).

Conflict of interest

The authors declare that the research was conducted in the absence of any commercial or financial relationships that could be construed as a potential conflict of interest.

Publisher's note

All claims expressed in this article are solely those of the authors and do not necessarily represent those of their affiliated organizations, or those of the publisher, the editors and the reviewers. Any product that may be evaluated in this article, or claim that may be made by its manufacturer, is not guaranteed or endorsed by the publisher.

- Min, B. S., Kim, Y. H., Lee, S. M., Jung, H. J., Lee, J. S., Na, M. K., et al. (2000). Cytotoxic triterpenes from *Crataegus pinnatifida*. *Arch. Pharm. Res.* 23 (2), 155–158. doi:10.1007/BF02975505
- Nadarevic, T., Colli, A., Giljaca, V., Fraquelli, M., Casazza, G., Manzotti, C., et al. (2022). Magnetic resonance imaging for the diagnosis of hepatocellular carcinoma in adults with chronic liver disease. *Cochrane Database Syst. Rev.* 5 (5), CD014798. doi:10.1002/14651858.CD014798.pub2
- Nagahashi, M., Matsuda, Y., Moro, K., Tsuchida, J., Soma, D., Hirose, Y., et al. (2015). DNA damage response and sphingolipid signaling in liver diseases. *Surg. Today* 46 (9), 995–1005. doi:10.1007/s00595-015-1270-8
- Nehal, M. E., Mohamed, A. E., and Mohammed, M. H. A. G. (2016). Renal protective effects of arjunolic acid in a cisplatin-induced nephrotoxicity model. *Cytokine* 77, 26–34. doi:10.1016/j.cyt.2015.10.010
- Peng, C. G., Chen, H. M., Li, Y. W., Yang, H., Qin, P. Z., Ma, B. J., et al. (2021). LRIG3 suppresses angiogenesis by regulating the PI3K/AKT/VEGFA signaling pathway in glioma. *Front. Oncol.* 11, 621154. doi:10.3389/fonc.2021.621154
- Qian, P., Mu, X. T., Su, B., Gao, L., and Zhang, D. F. (2020). Identification of the anti-breast cancer targets of triterpenoids in *Liquidambaris Fructus* and the hints for its traditional applications. *BMC Complement. Med. Ther.* 20 (1), 369. doi:10.1186/s12906-020-03143-8
- Qian, Y. X., Xie, H. M., Zuo, T. T., Li, X., Hu, Y., Wang, H. D., et al. (2021). Ultra-high performance liquid chromatography/ion mobility-quadrupole time-of-flight mass spectrometry and database-driven automatic peak annotation for the rapid profiling and characterization of the multicomponents from *Stephaniae Tetrandrae radix* (Fang-Ji). *World J. Tradit. Chin. Med.* 7, 120–129. doi:10.4103/wjtc.wjtc_56_20
- Sherif, I. O. (2021). Hepatoprotective effect of arjunolic acid against cisplatin-induced hepatotoxicity: Targeting oxidative stress, inflammation, and apoptosis. *J. Biochem. Mol. Toxicol.* 35 (4), e22714. doi:10.1002/jbt.22714
- Shi, Z. M., Han, Y. W., Han, X. H., Zhang, K., Chang, Y. N., Hu, Z. M., et al. (2016). Upstream regulators and downstream effectors of NF- κ B in Alzheimer's disease. *J. Neurol. Sci.* 366, 127–134. doi:10.1016/j.jns.2016.05.022
- Sumiyoshi, M., Sakanaka, M., Taniguchi, M., Baba, K., and Kimura, Y. (2014). Anti-tumor effects of various furocoumarins isolated from the roots, seeds and fruits of *Angelica* and *Cnidium* species under ultraviolet A irradiation. *J. Nat. Med.* 68 (1), 83–94. doi:10.1007/s11418-013-0774-z
- Sung, H., Ferlay, J., Siegel, R. L., Laversanne, M., Soerjomataram, I., Jemal, A., et al. (2021). Global cancer Statistics 2020: GLOBOCAN estimates of incidence and mortality worldwide for 36 cancers in 185 countries. *Ca. Cancer J. Clin.* 71 (3), 209–249. doi:10.3322/caac.21660
- Takuwa, Y., Okamoto, Y., Yoshioka, K., and Takuwa, N. (2012). Sphingosine-1-phosphate signaling in physiology and diseases. *Biofactors* 38 (5), 329–337. doi:10.1002/biof.1030
- Wang, S., Yang, X. X., Wang, W., Zhang, Y. K., Li, T. J., Zhao, L., et al. (2021). Interpretation of the absorbed constituents and pharmacological effect of *Spica Schizonepetae* extract on non-small cell lung cancer. *PLoS One* 16 (3), e0248700. doi:10.1371/journal.pone.0248700
- Xu, F., Zhang, L., Zhao, X., Zhou, Q. L., Liu, G. X., Yang, X. W., et al. (2021). Eleven absorbed constituents and 91 metabolites of *Chuanxiong Rhizoma* decoction in rats. *World J. Tradit. Chin. Med.* 7, 33–46. doi:10.4103/wjtc.wjtc_7_21
- Yang, X. X., Wang, S., Li, T. J., Bao, Y. R., and Meng, X. S. (2020). Study on the anti-tumor efficacy components of *fructus liquidambaris* based on different tumor sites. *Asia-Pacific Tradit. Med.* 16 (10), 76–80. doi:10.11954/ytctty.202010021
- Yang, Y. P., Tasneem, S., Daniyal, M., Zhang, L., Jia, Y. Z., Jian, Y. Q., et al. (2020). Lanostane tetracyclic triterpenoids as important sources for anti-inflammatory drug discovery. *World J. Tradit. Chin. Med.* 6, 229–238. doi:10.4103/wjtc.wjtc_17_20
- Zhang, H. X., Kang, Y., Li, N., Wang, H. F., Bao, Y. R., Li, Y. W., et al. (2020). Triterpenoids from *Liquidambar Fructus* induced cell apoptosis via a PI3K-AKT related signal pathway in SMMC7721 cancer cells. *Phytochemistry* 171, 112228. doi:10.1016/j.phytochem.2019.112228
- Zhu, Y., Guan, Y. J., Chen, Q. Z., Yuan, L. H., Xu, Q. Q., Zhou, M. L., et al. (2021). Pentacyclic Triterpenes from the resin of *Liquidambar formosana* have anti-angiogenic properties. *Phytochemistry* 184, 112676. doi:10.1016/j.phytochem.2021.112676



OPEN ACCESS

EDITED BY
Zheng Xiang,
Liaoning University, China

REVIEWED BY
Jiang Hai,
Heilongjiang University of Chinese
Medicine, China
Qin Wan Huang,
Chengdu University of Traditional
Chinese Medicine, China

*CORRESPONDENCE
Wei Wang,
ww_101737@126.com
Hui Gao,
gaohuitcm@163.com

[†]These authors have contributed equally
to this work and share first authorship

SPECIALTY SECTION
This article was submitted to
Ethnopharmacology,
a section of the journal
Frontiers in Pharmacology

RECEIVED 08 September 2022
ACCEPTED 23 September 2022
PUBLISHED 07 October 2022

CITATION
Ju C-G, Zhu L, Wang W, Gao H, Xu Y-B
and Jia T-Z (2022), *Cornus officinalis*
prior and post-processing: Regulatory
effects on intestinal flora of diabetic
nephropathy rats.
Front. Pharmacol. 13:1039711.
doi: 10.3389/fphar.2022.1039711

COPYRIGHT
© 2022 Ju, Zhu, Wang, Gao, Xu and Jia.
This is an open-access article
distributed under the terms of the
[Creative Commons Attribution License](https://creativecommons.org/licenses/by/4.0/)
(CC BY). The use, distribution or
reproduction in other forums is
permitted, provided the original
author(s) and the copyright owner(s) are
credited and that the original
publication in this journal is cited, in
accordance with accepted academic
practice. No use, distribution or
reproduction is permitted which does
not comply with these terms.

Cornus officinalis prior and post-processing: Regulatory effects on intestinal flora of diabetic nephropathy rats

Cheng-Guo Ju^{1†}, Lin Zhu^{1†}, Wei Wang^{1*}, Hui Gao^{1*}, Yu-Bin Xu²
and Tian-Zhu Jia¹

¹College of Pharmacy, Liaoning University of Traditional Chinese Medicine, Dalian, China, ²Beijing
Jujing Health Technology Group, Beijing, China

Background: Diabetic nephropathy (DN) is one of the most common and serious chronic complications in the clinic. *Cornus officinalis* has the effects of replenishing *qi* and nourishing *yin*, tonifying liver and kidney, and it is one of the main traditional Chinese medicines used clinically to treat diabetes and its complications. However, the effect and mechanism of *Cornus officinalis* before and after processing on intestinal flora of diabetic nephropathy need to be further elucidated.

Methods: SD rats were randomly divided into a blank group (10 rats) and DN groups (70 rats). After 4 weeks of high-sugar and high-fat diet, the DN rat model was established by intraperitoneal injection of streptozotocin. After successful modeling, the rats were randomly divided into DN model group, irbesartan group (1.35 mg·kg⁻¹), *Cornus officinalis* group (281.25 mg·kg⁻¹), wine *Cornus officinalis* group (281.25 mg·kg⁻¹), wine honey *Cornus officinalis* group (281.25 mg·kg⁻¹), auxiliary wine group (10 ml·kg⁻¹), auxiliary wine honey group (10 ml·kg⁻¹). During the observation of the rats' general state, after 6 weeks of continuous administration, the fasting blood glucose of rats in each group was detected, and the kidney index was calculated. The serum creatinine levels, urea nitrogen and 24 h urinary microalbumin were detected by enzyme-linked immunosorbent assay. The expression levels of YKL-40, Wnt4, β -catenin and TGF- β_1 mRNA in renal tissue were detected by fluorescence quantitative PCR. Hematoxylin-eosin staining was used to observe the changes in renal pathological injury in each group; GC-MS detected the changes of short chain fatty acid content. Feces were collected for 16 s high-throughput sequencing to analyze the effects of *Cornus officinalis* on the diversity of intestinal flora in DN before and after processing.

Results: Compared with the blank group, the serum creatinine, urea nitrogen, 24 h urinary microalbumin, kidney index and fasting blood glucose in the DN

Abbreviations: BUN, blood urea nitrogen; DN, Diabetic nephropathy; EI, electron impact ionization; FBG, fasting blood glucose; GC-MS, Gas Chromatography-Mass Spectrometer; HE, Hematoxylin-eosin; KI, kidney index; LDA, linear discriminant analysis; LEfSe, LDA Effect Size; mALB, 24 h urine microalbumin; PCoA, principal coordinate analysis; SCAN, full scanning mode; SCFAs, short chain fatty acids; SIM, selective ion monitoring mode; STZ, streptozotocin; S-Cr, Serum creatinine.

model group were significantly increased ($p < 0.05$). The renal tissue morphology was disordered and a large number of inflammatory cells were infiltrated. The expression of YKL-40, Wnt4, β -catenin and TGF- β_1 mRNA was significantly increased ($p < 0.05$). Compared with the DN model group, the serum creatinine, urea. Nitrogen, 24 h urine microalbumin, kidney index and fasting blood glucose of rats in each administration group were significantly decreased ($p < 0.05$), and the general condition and pathological renal damage of DN rats were improved. The effect of wine honey *Cornus officinalis* was the best, and the expression of YKL-40, Wnt4, β -catenin and TGF- β_1 mRNA was significantly decreased ($p < 0.05$). In each administration group, the improvement of the above indicators in the wine honey *Cornus officinalis* group was significantly better than that in the raw *Cornus officinalis* group and wine *Cornus officinalis* group ($p < 0.05$). There was no significant difference compared with the irbesartan group ($p > 0.05$). Each administration group had a significant callback effect on the content of short-chain fatty acids in rat feces, with increased intestinal beneficial bacteria and decreased pathogenic bacteria. Compared with the blank group, the abundance of Firmicutes in the DN model group increased, the abundance of Bacteroidetes decreased, and the ratio showed an upward trend in the DN model group decreased. Each administration group could improve the relative abundance of the above intestinal flora in the model group to varying degrees.

Conclusion: The processing of *Cornus officinalis* may improve the renal injury of DN rats by blocking the activation of Wnt/ β -catenin signaling pathway, regulating the structural composition of intestinal microorganisms, and ultimately playing a role in renal protection.

KEYWORDS

cornus officinalis, wine *cornus officinalis*, wine honey *cornus officinalis*, DN, Wnt/ β -catenin signaling pathway, intestinal flora

Introduction

Diabetic nephropathy (DN) is one of the most serious and common chronic complications of diabetes mellitus. It is one of the main causes of end-stage renal disease and an important factor in the death of diabetic patients, causing serious harm to human health (Sayed et al., 2012; Yang et al., 2020). So far, the pathogenesis of DN has not been elucidated. Existing research data show that abnormal glucose metabolism, inflammatory response, oxidative stress, endoplasmic reticulum stress, autophagy, and exosomes can cause DN (Shikata and Shikata, 2013; Li et al., 2019). At present, western medicine mainly prevents the occurrence and deterioration of DN by controlling blood pressure, controlling blood lipid and anti-inflammation. Traditional Chinese medicine mainly through oral Chinese medicine, acupuncture, enema treatment, but failed to fully elucidate the pathogenesis of DN and the treatment of specific drugs (Liu et al., 2019; Feng, 2022). Therefore, active prevention and treatment of DN and inhibition of the development of the disease are the main means to avoid renal failure and prolong the life of patients.

Cornus officinalis Siebold & Zucc. Cornaceae. (*Cornus officinalis*), alias *Cornus officinalis*, Shuzao, Shizao, Rouzao, etc., is a plant of *Cornus* genus of *Cornus* family. It is a perennial small tree or shrub. It is traditionally used as a traditional Chinese medicine to remove the dry and mature pulp of the fruit core. It has the effect of tonifying the liver and kidney, astringing the essence and removing the essence. It is mainly used for treating vertigo tinnitus, lumbar and knee pain, impotence and spermatorrhea, internal heat and diabetes (Yang et al., 2016; Lou et al., 2021). Studies have shown that *Cornus officinalis* has anti-tumor, myocardial protection, treatment of diabetes and its complications, hypoglycemic, liver and kidney protection, anti-inflammatory and other pharmacological effects (Jin and Chang, 2015; Zhou et al., 2020). Iridoid glycosides of *Cornus officinalis* is one of the effective components of *Cornus officinalis*. Its characteristic components loganin and morroniside can significantly inhibit the proliferation of renal cortical endothelial cells in DN rats and protect the integrity of endothelium (Yang et al., 2019). Clinical studies have shown that *Cornus officinalis* can effectively improve insulin resistance, reduce blood glucose, and improve the symptoms of diabetic nephropathy. (Park et al., 2013; Qi et al., 2014). Our previous

study found that wine honey processed *Cornus officinalis* can improve the sour taste of *Cornus officinalis*, and the content of iridoid glycosides in traditional wine processed *Cornus officinalis* was significantly reduced. The application of wine honey processed *Cornus officinalis* can increase the content of main iridoid glycosides to varying degrees, but the exact mechanism remains to be further clarified. In this study, DN rat model was induced by high-fat and high-sugar diet combined with intraperitoneal injection of streptozotocin (STZ). The therapeutic mechanism of *Cornus officinalis* before and after processing on DN and its effect on intestinal flora were investigated in order to provide a new experimental basis for the clinical application of *Cornus officinalis* and its processed products.

Materials

Animal

A total of 100 male SD rats, weighing 180–220 g, were provided by Liaoning Changsheng Biotechnology Co., Ltd., with the experimental animal production license number: SCXK (Liaoning) 2020-0001. According to the experimental animal management method of Liaoning University of Traditional Chinese Medicine, at room temperature to the standard feed, free drinking water, sub-cage (8 cages) adaptive feeding 1w for the test. All animals were raised in the SPF animal room of our laboratory and given humanitarian care according to the 3R (Reduction; Replacement; Refinement) principle. Authorized by the Ethics Committee of Liaoning University of Traditional Chinese Medicine.

Drug

Cornus officinalis decoction pieces (place of origin: Xixia, Henan, harvest time: September 2021, identified by Professor Zhang Hui from Liaoning University of Traditional Chinese Medicine as the dried ripe pulp of *Cornus officinalis* Siebold & Zucc. Cornaceae.), yellow wine (Zhejiang Guyue Longshan Shaoxing Wine Co., Ltd., batch number: GB/T 13662), honey (wild mountain nectar, bee farm address: Linyi, Shandong, collection place: Yimeng Mountain Area), irbesartan dispersible tablets (Shuanghe Pharmaceutical Co., Ltd., national drug permit: 6935216804279).

Reagents and instruments

STZ (Dalian Meilun Biotechnology Co., Ltd., Batch No. MB1227), high-fat diet (66.5% conventional feed, 10% lard, 20% sucrose, 2.5% cholesterol, 1% sodium cholate, 7-8 eggs,

appropriate amount of dextrin), acetic acid, propionic acid, butyric acid, isobutyric acid, valeric acid, isovaleric acid, hexanoic acid, 4-methyl valeric acid (Shanghai Yuanye Biotechnology Co., Ltd., Batch No. 64-19-7, 79-09-4, 107-92-6, 79-31-2, 109-52-4, 503-74-2, 142-62-1, 646-07-1). Phosphoric acid (Tianjin Damao Chemical Reagent Factory, Batch No. 20220106), Trizol (Invitrogen life technologies, United States, Batch No. 15596026), horizontal cryopreservation box (Qingdao Haier Electric Appliance Co., Ltd., Batch No. DW-86W100), high-speed refrigerated centrifuge (SIGMA, Germany, Batch No. Sigma3k15), tissue dehydrator (Cherry Blossom, Japan, Batch No. VIP6 AI), embedding machine (Persjje, Batch No. BM450A). Tissue bleaching oven (Paisger, Batch No. PH60). Pathological section machine (Lecia, Batch No. Biocut), panoramic scanner (3DHISTECH, Batch No.: 3DHISTECH P250 FLASH), frozen section machine (Lecia, Batch No. CM 1900), gas chromatography-mass spectrometry, equipped with 7697A headspace sampler and MassHunter Workstation B.07.00 workstation (Agilent, United States, Model: 7890B-5977B). Capillary Column (30 m × 0.25 mm, 0.25 μm, Agilent, United States, Model: DB-WAX). DNA Extraction Kit (MP Biomedicals, United States, Model: FastDNA[®] Spin Kit for Soil), FastPfu Polymerase (TransGen, China, Model: FastPfu Polymerase), AxyPrep DNA Gel Extraction Kit (Axygen, United States, Model: Axygen Biosciences). Serum creatinine (S-Cr), blood urea nitrogen (BUN), 24 h urine microalbumin (mALB) detection kits (Shanghai Kexing Biotechnology Co., Ltd., batch numbers: F40108-A, F40289-A, F8560-A), Gold View dye, Evo M-MLV reverse transcription kit, SYBR[®] Green Pro Taq HS Premix kit (Aikeri Biological Engineering Co., Ltd., batch numbers: A2A1634, AG11711, AG11718). Rapid DNA-Seq Kit (Bioo Scientific, United States, Model: NEXTFLEX), Sequencing Kit (Illumina, United States, Model: MiSeq Reagent Kit v3/ NovaSeq Reagent Kits), Microplate Reader (Biotek, United States, Model: BioTek ELx800), Vortex Mixer (Haimen Kylin-Bell Lab Instrument Manufacturing Co., Ltd., Model: QL-901). Grinder (MP, United States, Model: FastPrep-24 5G), Microfluorimeter (Promega, United States, Model: Quantus TM Fluorometer), Electrophoresis (Beijing Liuyi Instrument Factory, Model: DYY-6C), PCR (ABI, United States, Model: ABI GeneAmp[®] 9700), Sequencing (Illumina, United States, Model: Illumina Miseq).

Methods

Preparation of samples

Preparation of wine *Cornus officinalis*: take the pure *Cornus officinalis*, add an appropriate amount of excipients mixed, airtight, water-sparing stew for 8 h until the excipients are absorbed, take out, dried at 50°C for 4 h, each 600 g *Cornus officinalis* with excipients yellow wine 180 g. Preparation of wine

honeyed *Cornus officinalis*: The *Cornus officinalis* meat was taken, mixed with appropriate amount of excipients, sealed, simmered in water for 6 h until the excipients were exhausted, taken out, dried at 50°C for 5 h, and 210 g (wine: honey = 30: 5) per 600 g of *Cornus officinalis* meat.

Each 600 g sample of *Cornus officinalis* meat, wine *Cornus officinalis* meat and wine honey *Cornus officinalis* meat were accurately weighed and boiled twice with water. The first time, 10 times the amount of water was added, boiled for 1.5 h, and the second time, 8 times the amount of water was added, boiled for 1.5 h. The filtrate was combined twice, and the concentration was concentrated to 0.28125 g·mL⁻¹ by rotary evaporation. The crude product extract of *Cornus officinalis* meat was obtained, packed into glass bottles, sealed and stored at 4°C refrigerator for the experimental cycle.

Modeling, grouping and administration

All rats were adaptively fed for 7 days, and 10 rats with abnormal coat color, spirit and stool were removed in time. The remaining rats were divided into normal group ($n = 10$) and DN group ($n = 80$) by random number table method. The rats in the blank group were fed with normal diet, and those in the DN group were fed with high-sugar and high-fat diet for 4 weeks. After fasting for 12 h, the DN rat model was induced by intraperitoneal injection of STZ 35 mg·kg⁻¹ (prepared immediately, the solvent was citric acid-sodium citrate buffer). The rats in the blank group were given an equal volume of citric acid-sodium citrate buffer by single intraperitoneal injection. After 72 h, blood was taken from the tail vein and the blood glucose was measured by a blood glucose meter. The rats with fasting blood glucose (FBG) ≥ 16.7 mmol·L⁻¹ and urine volume more than doubled were selected as DN rats. The blood glucose of 6 model rats was less than 16.7 mmol·L⁻¹, and 4 rats died during the modeling process, all of which were eliminated. According to the random number table method, 70 successfully modeled rats were divided into DN model group, irbesartan group (1.35 mg·kg⁻¹·d⁻¹), *Cornus officinalis* group (281.25 mg·kg⁻¹·d⁻¹), wine *Cornus officinalis* group (281.25 mg·kg⁻¹·d⁻¹), wine honey *Cornus officinalis* group (281.25 mg·kg⁻¹·d⁻¹), auxiliary wine group (10 ml·kg⁻¹·d⁻¹) and auxiliary wine honey group (10 ml·kg⁻¹·d⁻¹), 10 rats in each group, according to the above drugs and doses, once a day for 6 weeks.

Specimen retention and preservation

Observe the general state of rats. After 6 weeks of administration, blood glucose was measured by tail vein. Metabolic cages were used to collect 24 h urine of rats. During the period of fasting, water was not allowed. The

urine volume of rats in each group was recorded. After centrifugation, the supernatant was taken and frozen at -20°C refrigerator for mAlb determination. Fecal samples of rats in each group were taken by the tail-raising reflex method in a sterile EP tube, frozen in liquid nitrogen, and frozen in a refrigerator at -80°C for the detection of intestinal flora diversity and short-chain fatty acids (SCFAs). The rats were fasted for 12 h before sampling, and the body weight of each group was weighed. After anesthesia with 20% urethane solution by intraperitoneal injection, 5 ml of blood was collected from the abdominal aorta, and the whole blood was collected by the procoagulant tube. After standing for 1 h, the serum was centrifuged (3500 r·min⁻¹, 4°C, 15 min) and frozen for the determination of S-Cr and BUN. The left kidney was weighed and fixed in 4% paraformaldehyde solution, and the right kidney was quickly sub-packed in EP tube. After quick freezing in liquid nitrogen, it was frozen in -80°C ultra-low temperature refrigerator for RT-PCR determination of YKL-40, Wnt4, β -catenin, TGF- β 1 mRNA expression.

General state detection

Observe the reaction, mental status, diet, coat color, urine and stool of rats. The body weight, food intake and water intake of rats were monitored weekly.

Biochemical index detection and kidney index calculation

The serum samples frozen at -80°C were thawed at 4°C refrigerator. The levels of S-Cr, BUN and mALB in rat serum samples were detected by ELISA kit. The experimental steps were carried out strictly according to the kit instructions. The kidney index (KI) is the ratio of kidney mass (mg) to body mass (g).

Pathological observation of kidney tissue

The kidney tissues fixed with 4% paraformaldehyde for more than 48 h were dehydrated with different concentrations of alcohol, embedded in paraffin and sliced. After drying, xylene dewaxing, washing and HE staining, the morphology of kidney tissues in each group was observed under optical microscope.

Expression of YKL-40, Wnt4, β -catenin and TGF- β 1 mRNA

An appropriate amount of frozen kidney tissue samples were taken, homogenized, and total RNA was extracted in

TABLE 1 Genes and their corresponding primer sequences.

Primer name	Primer sequences	Primer length
YKL-40	Upstream: 5'-CTACTACGAGATATGCGACTT-3'	21
	Downstream: 5'-CTGTCTCTCAGGTACTTCAC-3'	21
Wnt4	Upstream: 5'-ATACGCCATCTCTCAGCAGGT-3'	22
	Downstream: 5'-TCACAGCCACACTTCTCCAGAT-3'	22
β -catenin	Upstream: 5'-GTCTGAGGACAAGCCACAGGACTAC-3'	25
	Downstream: 5'-AATGTCCAGTCCGAGATCAGCA-3'	22
TGF- β_1	Upstream: 5'-ATACGCCTGAGTGGCTGTCTTT-3'	22
	Downstream: 5'-AAAGCCCTGTATTCCGTCTCCT-3'	22
β -actin	Upstream: 5'-GGAGATTACTGCCCTGGCTCCTA-3'	23
	Downstream: 5'-GACTCATCGTACTCTGCTTGCTG-3'	24

strict accordance with the instructions of the Trizol kit. RNA concentration was measured, and cDNA was synthesized by reverse transcription kit. According to SYBR Green PCR kit instructions, PCR reaction. PCR cycle reaction conditions: 95°C pre-denaturation 30 s, 95°C denaturation 15 s, 60°C annealing 1 min, 95°C extension 15 s, 40 cycles. The relative expression of the target gene in each sample was calculated by $2^{-\Delta\Delta CT}$ method (CT was the number of cycles). Each sample was repeated 3 times independently. The primer sequence is shown in Table 1.

Detection of SCFAs

Headspace injection conditions

Headspace sampler sample bottle heating temperature: 80°C; quantitative ring heating temperature: 140°C; transmission line heating temperature: 160°C; GC cycle time: 30 min; heating time: 20 min; equilibrium time: 10 min; pressurization time: 0.15 min; injection time: 0.5 min.

Chromatographic and mass spectrometric conditions

Agilent DB-WAX (DB-1MS) chromatographic column (30 m \times 0.25 mm, 0.25 μ m); the injection method is not split; inlet temperature 250°C; ion source temperature 230°C; transmission line temperature 250°C, quadrupole temperature 150°C. The initial temperature of programmed heating was 60°C, and then increased to 120°C at a rate of 30°C·min⁻¹. 5°C·min⁻¹–140°C for 1 min then heated to 150°C at 10°C·min⁻¹ for 1 min; then heated to 160°C at 5°C·min⁻¹ for 1 min; finally, the temperature was raised to 230°C at a rate of 35°C·min⁻¹, and then maintained at 230°C for 5 min. The carrier gas was helium at a flow rate of 1.0 ml·min⁻¹.

Electron impact ionization (EI), 70 eV electron energy, solvent delay 4.5 min, full scan (SCAN) and selected ion monitoring (SIM) modes, scan range 30–200 m·z⁻¹.

Preparation of standard solution

The standard substances of acetic acid, propionic acid, butyric acid, isobutyric acid, isovaleric acid, valeric acid and hexanoic acid were accurately weighed. The mixed standard solution was prepared with ultrapure water, and the mixed working solution with different concentrations was obtained by gradient dilution. Acetic acid 36.69 μ g·mL⁻¹, propionic acid 1.01 μ g·mL⁻¹, isobutyric acid 1.50 μ g·mL⁻¹, butyric acid 16.24 μ g·mL⁻¹, isovaleric acid 1.14 μ g·mL⁻¹, valeric acid 3.00 μ g·mL⁻¹, hexanoic acid 1.10 μ g·mL⁻¹ were prepared in the stock solution.

Determination of short chain fatty acid content in feces of rats in each group

A total of 100 mg sterile feces of rats in each group at the same time point were weighed accurately and placed in a 20 ml headspace injection bottle. Add 50 μ L 0.2% H₃PO₄ solution, containing 4-methylpentanoic acid internal standard solution (0.668 mg·mL⁻¹), fully mixed, quickly sealed, and detected in GC-MS instrument. In order to ensure the true repeatability of the experimental results, the same sample needs to be divided into 6 parts, and the injection is completed one by one. The corresponding SCFAs peak area is calculated, and the concentration of each short-chain fatty acid in the supernatant is calculated according to the standard curve.

Detection of intestinal flora in rats by 16S rRNA high-throughput sequencing

DNA extraction and PCR amplification

The total DNA in feces was extracted according to the DNA extraction kit, and the quality of DNA extraction was detected by 1% agarose gel electrophoresis. NanoDrop2000 was used to determine DNA concentration and purity. The V3-V4 variable region of 16S rRNA gene was amplified by PCR with primers 338F (5'-ACTCCTACGGGAGGGCAGCAG-3') and

806R (5'-GGACTACHVGGGTWTCTAAT-3'). The amplification procedure was as follows: pre-denaturation at 95°C for 3 min, 27 cycles (denaturation at 95°C for 30s, annealing at 55°C for 30 s, extension at 72°C for 30 s), then stable extension at 72°C for 10min, and finally stored at 4°C. Each sample was repeated three times.

Illumina Miseq sequencing

The PCR products of the same sample were mixed and recovered using 2% agarose gel. The recovered products were purified using the AxyPrep DNA Gel Extraction Kit, examined by 2% agarose gel electrophoresis, and quantified using the Quantus™ Fluorometer. Using the NEXTFLEX Rapid DNA-Seq Kit to build the library linker first; using magnetic beads for screening to remove the joint self-connected segment; the library template was enriched by PCR amplification. Finally, the PCR products were recovered by magnetic beads to obtain the library. Sequencing was performed using Illumina's 61 Miseq PE300 platform.

Data processing

Fastp (Chen et al., 2018) software was used to perform quality control on the original sequencing sequence, and FLASH (Magoč and Salzberg, 2011) software was used for splicing: 1) Filter the bases with a tail mass value of less than 20 in the reads, and set a 50 bp window. If the average mass value in the window is less than 20, the back-end bases are removed from the window, and the reads below 50 bp after quality control are filtered to remove the reads containing N bases; 2) According to the overlap relationship between PE reads, the paired reads were merged into a sequence with a minimum overlap length of 10 bp. 3) The maximum allowed mismatch ratio of overlap region of concatenated sequences is 0.2, screening non-conforming sequences; 4) According to the sequence of both ends of the barcode and primers to distinguish between samples, and adjust the direction of the sequence, barcode allows the mismatch is 0, the maximum primer mismatch is 2.

Using UPARSE (Edgar, 2013) software, OTU clustering was performed on the sequence according to 97% similarity and chimeras were removed. RDP classifier (Stackebrandt and Goebel, 1994; Wang et al., 2007) was used to annotate the species classification of each sequence. The Silva 16S rRNA database was compared, and the comparison threshold was set to 70%.

Statistical methods

SPSS 20.0 software was used for statistical analysis. Graphpad Prism 8.0 was used for plotting. The data were expressed as mean ± standard deviation ($\bar{x} \pm s$). The *t* test was used for pairwise comparison, and one-way analysis of variance was used for comparison among multiple groups. $p < 0.05$ indicated that the difference was statistically significant.

Results

Changes of general signs in rats

During the experiment, the rats in the blank group grew well, the fur was bright, the activity was large, the reaction was agile, the eating and excretion were normal, and the body weight gradually increased. The rats in the DN model group, auxiliary wine group, and the auxiliary wine honey group grew significantly slower, had less activity, and drank more, ate more, and urinated more. In the later stage of the experiment, the rats in the DN model group, auxiliary wine group, and the auxiliary wine honey group showed obvious slow response, dull fur, and obvious weight loss. Compared with the DN model group, the rats in the irbesartan group and the wine honey *Cornus officinalis* group were significantly improved in the above aspects. In the later stage of the experiment, the body weight of the DN model group was significantly lower than that of the other groups.

Biochemical indicators level detection

Compared with the blank group, S-Cr, BUN, mALB, KI and FBG in DN model group, auxiliary wine group and auxiliary wine honey group were significantly increased ($p < 0.05$), and the difference was statistically significant. Compared with the DN model group, the S-Cr, BUN, mALB, KI and FBG of the rats in the irbesartan group, the *Cornus officinalis* group, the wine *Cornus officinalis* group and the wine honey *Cornus officinalis* group were significantly decreased ($p < 0.05$). The levels of S-Cr, BUN, mALB, KI and FBG in the wine honey *Cornus officinalis* group were significantly lower than those in the *Cornus officinalis* group and the wine *Cornus officinalis* group ($p < 0.05$). See Figure 1.

Pathological examination of renal tissue of rats in each group

The pathological examination results showed that the blank group rats had normal renal tissue morphology, regular glomerular shape, no hypertrophy or atrophy, normal arrangement of renal tubular epithelial cells, and normal renal interstitial structure. There were obvious pathological changes of DN in the kidney tissue of rats in the DN model group, the auxiliary wine group and the auxiliary wine honey group. The renal tissue structure was disordered, glomerular hypertrophy, mesangial cell proliferation, nodular sclerosis was clearly visible, renal tubular degeneration and atrophy. A large number of vacuoles and swollen cells were seen in the renal tubular epithelial cells. Obvious vacuolar degeneration, partial atrophy, obvious edema of renal, and a large number of inflammatory cell

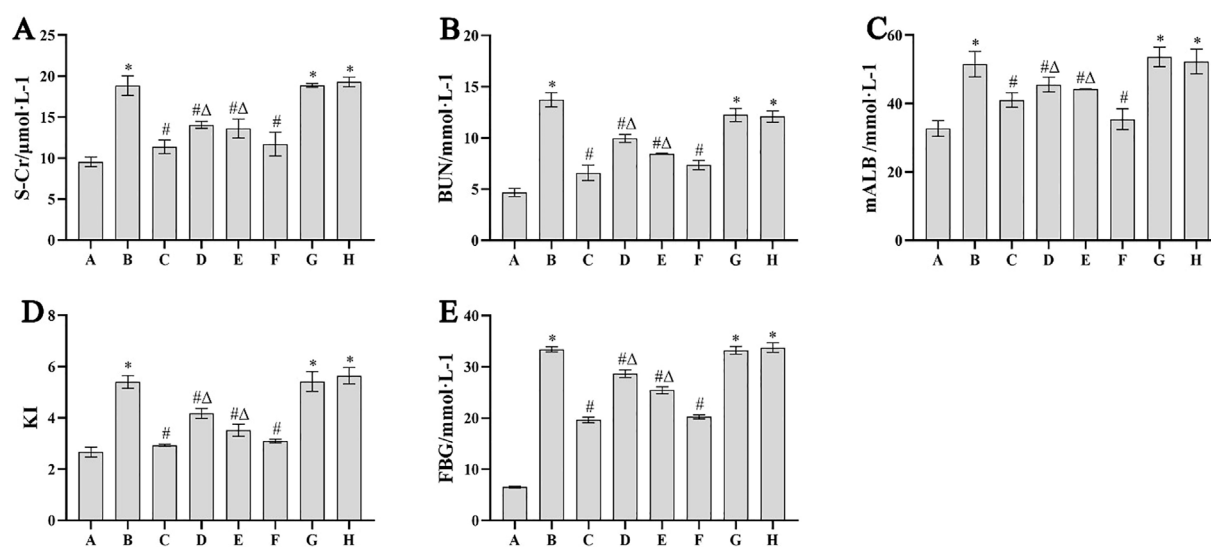


FIGURE 1

Comparison of S-Cr (A), BUN (B), mALB (C), KI (D) and FBG (E) in each group ($n = 10$, $\bar{x} \pm s$). Note: ① A. Blank group B. DN model group C. Irbesartan group D. *Cornus officinalis* group E. Wine *Cornus officinalis* group F. Wine honey *Cornus officinalis* group G. Auxiliary wine group H. Auxiliary wine honey group. ② Compared with the blank group * $p < 0.05$; compared with DN model group # $p < 0.05$; compared with the wine honey group $\Delta p < 0.05$.

infiltration. Compared with the DN model group, the above pathological changes of renal tissue in the *Cornus officinalis* group, the wine *Cornus officinalis* group, the wine honey *Cornus officinalis* group and the irbesartan group were significantly improved, and the glomerular nodule sclerosis and renal interstitial edema were reduced. The most obvious was the degree of pathological inflammatory infiltration, glomerular atrophy, and mesangial proliferation in the wine honey *Cornus officinalis* group. See Figure 2.

Expression of YKL-40, Wnt4, β -catenin and TGF- β_1 mRNA in renal tissue of rats

Compared with the blank group, the expression of YKL-40, Wnt4, β -catenin and TGF- β_1 mRNA in renal tissue of DN model group, auxiliary wine group and auxiliary wine honey group was significantly increased ($p < 0.05$). Compared with DN model group, the expression of YKL-40, Wnt4, β -catenin and TGF- β_1 mRNA in renal tissue of *Cornus officinalis* group, wine *Cornus officinalis* group and wine honey *Cornus officinalis* group was significantly decreased ($p < 0.05$). Compared with the wine honey *Cornus officinalis* group, the expression of YKL-40, Wnt4, β -catenin and TGF- β_1 mRNA in the kidney tissue of the *Cornus officinalis* group and the wine *Cornus officinalis* group was significantly different ($p < 0.05$). See Figure 3.

Results of SCFAs in rats

Compared with the blank group, the contents of seven short-chain fatty acids in the fresh feces of the DN model group, the auxiliary wine group, and the auxiliary wine honey group were significantly reduced ($p < 0.05$). After drug intervention, it was found that the irbesartan group, the wine *Cornus officinalis* group, and the wine honey *Cornus officinalis* group had a significant callback effect on the content of SCFAs in fresh feces. In addition to the significant increase in butyric acid in fresh feces, the *Cornus officinalis* group also had a wide callback effect on the other six SCFAs ($p < 0.05$). Although the range and intensity of SCFAs in each sample were slightly different in each administration group, except for butyric acid in each administration group. They all had significant up-regulation ($p < 0.05$). In short, the wine honey *Cornus officinalis* group had the best regulation effect on the content of 7 kinds of SCFAs (Table 2).

Analysis of differences in intestinal flora of rats at different classification levels

OUT analysis of intergroup species

According to the number of OTUs when the diversity index of the sample is sobs at different sequencing depths, the dilution curve (Figure 4) is drawn. It can be seen that the curve gradually flattens out when the sample is around 30000Reads, indicating

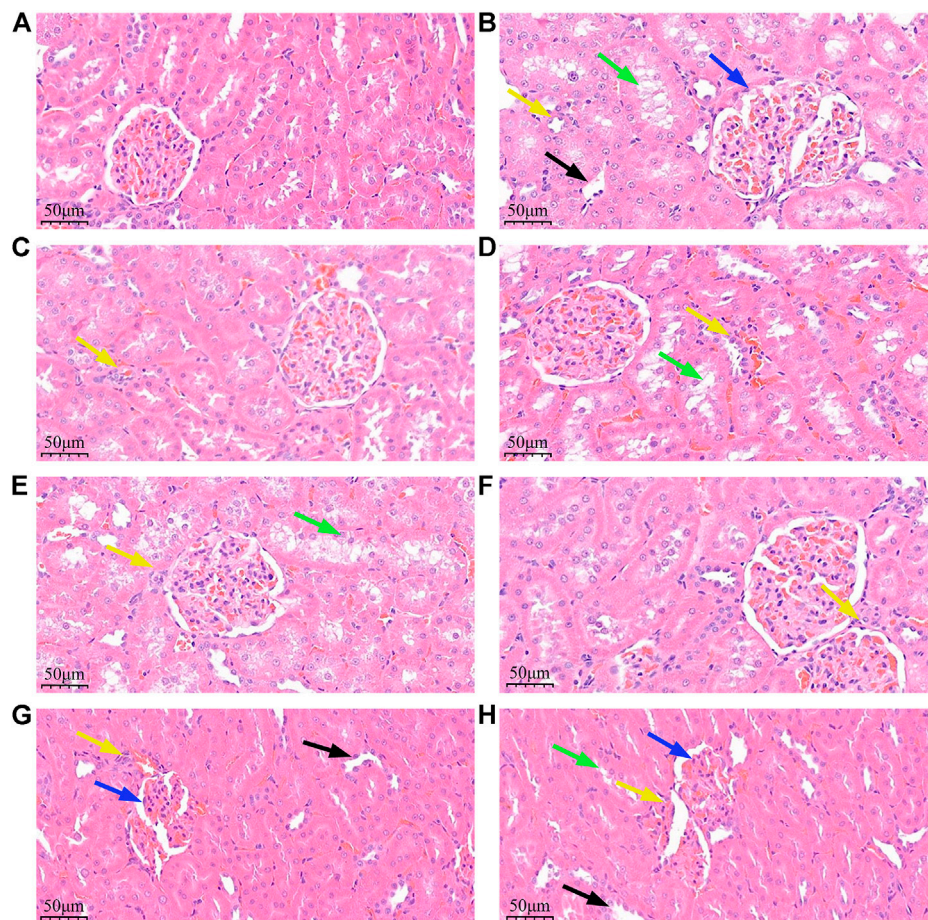


FIGURE 2

Effects of *Cornus officinalis* and its processed products on renal histopathology in DN rats (HE, $\times 400$). Note: ① (A). Blank group (B). DN model group (C). Irbesartan group (D). *Cornus officinalis* group E. Wine *Cornus officinalis* group (F). Wine honey *Cornus officinalis* group (G). Auxiliary wine group (H). Auxiliary wine honey group. ② Blue arrows indicate glomerular deformation, black arrows indicate renal interstitial edema, green arrows indicate renal tubular degeneration and atrophy, and yellow arrows indicate interstitial inflammatory cell infiltration.

that the amount of sequencing data is reasonable. More data will only produce a small number of new species; according to the number of OTUs with Shannon-Wiener diversity index at different sequencing depths, the curve was drawn (Figure 4). It can be seen that the curve gradually tends to be flat when the sample is around 4000Reads, indicating that the amount of sequencing data is large enough to reflect the vast majority of microbial diversity information in the sample.

The Venn diagram was used to count the number of common and unique OTUs in 5 groups of samples, which could directly show the similarity and overlap of OTU composition in different environmental samples. The intestinal flora OTU of each group (Figure 5). There were 22 unique OTUs in the blank group, 19 unique OTUs in the DN model group, 12 unique OTUs in the *Cornus officinalis* group, 26 unique OTUs in the wine *Cornus officinalis* group, and 22 unique OTUs in the wine honey *Cornus officinalis* group. There were 493 OTUs shared by the five groups.

Alpha diversity analysis of intergroup species

Alpha diversity reflects the species diversity within a single sample. It is measured by community abundance index and community diversity index. The community abundance index includes Chao1 and Ace. The larger the index value, the higher the richness of the community. The community diversity index includes Shannon and Simpson. The larger the index value, the higher the species diversity of the sample. The results showed that the richness (Chao1 and Ace) and diversity (Shannon and Simpson) of intestinal flora in the feces of DN model rats were lower than those in the normal group ($p < 0.05$). The richness (Chao1 and Ace) and diversity (Shannon and Simpson) of intestinal flora in the feces of irbesartan group, *Cornus officinalis* group, wine *Cornus officinalis* group and wine honey *Cornus officinalis* group were significantly different from those in the DN model group ($p < 0.05$), close to the blank group. See Table 3.

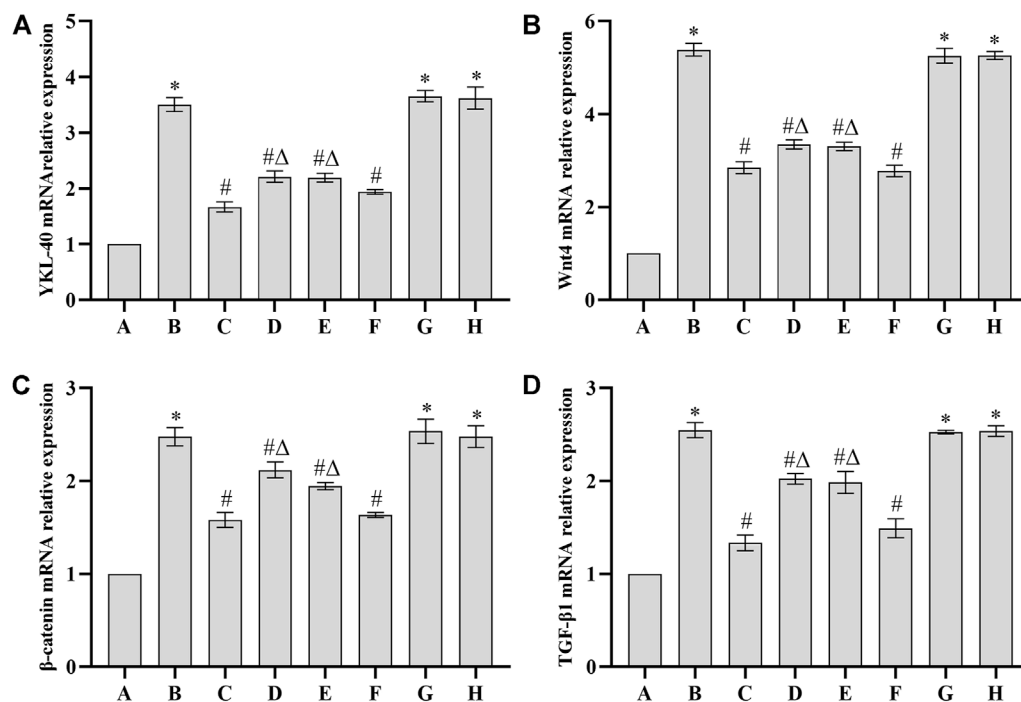


FIGURE 3

Comparison of mRNA expression of YKL-40 (A), Wnt4 (B), β-catenin (C) and TGF-β1 (D) in each group ($n = 10$, $\bar{x} \pm s$). Note: A. Blank group B. DN model group C. Irbesartan group D. *Cornus officinalis* group E. Wine *Cornus officinalis* group F. Wine honey *Cornus officinalis* group G. Auxiliary wine group H. Auxiliary wine honey group.

TABLE 2 Intestinal SCFAs content of rats in each group ($n = 6$, $\bar{x} \pm s$, $\mu\text{g/g}$).

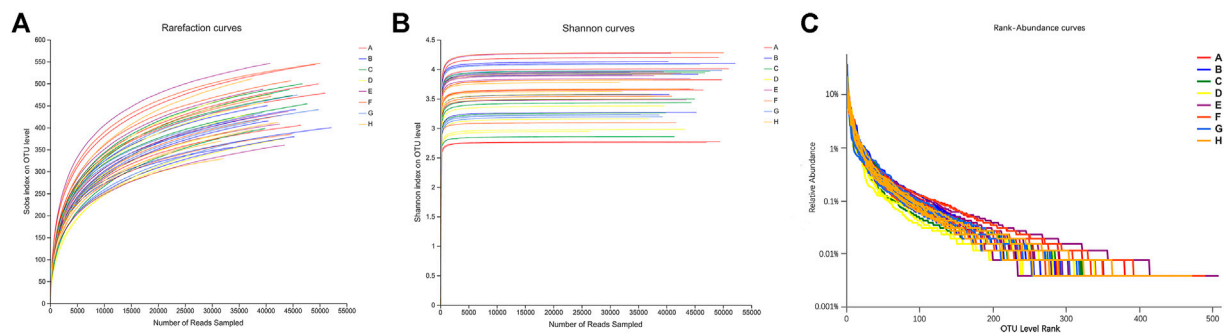
Peer group	Acetic acid	Propionic acid	Isobutyric acid	Butyric acid	Isovaleric acid	Valeric acid	Caproic acid
A	1261.57 \pm 41.70	111.57 \pm 2.56	120.27 \pm 4.86	69.97 \pm 9.39	4.50 \pm 0.98	37.63 \pm 4.76	49.91 \pm 2.32
B	800.85 \pm 71.23*	67.28 \pm 2.62*	68.03 \pm 7.28*	35.72 \pm 8.66*	1.75 \pm 0.48*	23.06 \pm 7.22*	13.68 \pm 1.29*
C	1162.64 \pm 80.62 [#]	103.57 \pm 6.92 [#]	107.70 \pm 4.55 [#]	65.28 \pm 5.91 [#]	3.90 \pm 0.84 [#]	35.03 \pm 7.72 [#]	46.47 \pm 0.78 [#]
D	901.44 \pm 48.42 ^{#Δ}	94.64 \pm 2.66 ^{#Δ}	100.11 \pm 4.39 [#]	38.53 \pm 5.85 ^Δ	2.86 \pm 0.47 ^{#Δ}	29.30 \pm 2.64 [#]	30.22 \pm 1.97 ^{#Δ}
E	1017.26 \pm 73.56 ^{#Δ}	89.32 \pm 3.27 ^{#Δ}	92.08 \pm 5.83 ^{#Δ}	53.20 \pm 7.39 ^{#Δ}	3.00 \pm 0.55 ^{#Δ}	32.97 \pm 3.60 [#]	28.42 \pm 0.70 ^{#Δ}
F	1126.45 \pm 51.19 [#]	108.77 \pm 4.45 [#]	106.04 \pm 3.48 [#]	62.63 \pm 7.71 [#]	3.84 \pm 0.84 [#]	34.75 \pm 3.58 [#]	46.60 \pm 2.09 [#]
G	799.45 \pm 74.81*	67.25 \pm 5.24*	69.81 \pm 8.90*	35.84 \pm 2.56*	2.29 \pm 0.66*	22.54 \pm 2.26*	16.47 \pm 0.52*
H	808.69 \pm 81.10*	69.20 \pm 3.10*	71.92 \pm 9.50*	33.45 \pm 2.27*	2.38 \pm 0.60*	22.36 \pm 7.34*	17.76 \pm 1.06*

Note: ① A. Blank group B. DN, model group C. Irbesartan group D. *Cornus officinalis* group E. Wine *Cornus officinalis* group F. Wine honey *Cornus officinalis* group G. Auxiliary wine group H. Auxiliary wine honey group. ② Compared with normal group * $p < 0.05$; compared with the model group [#] $p < 0.05$; compared with the wine honey group ^Δ $p < 0.05$.

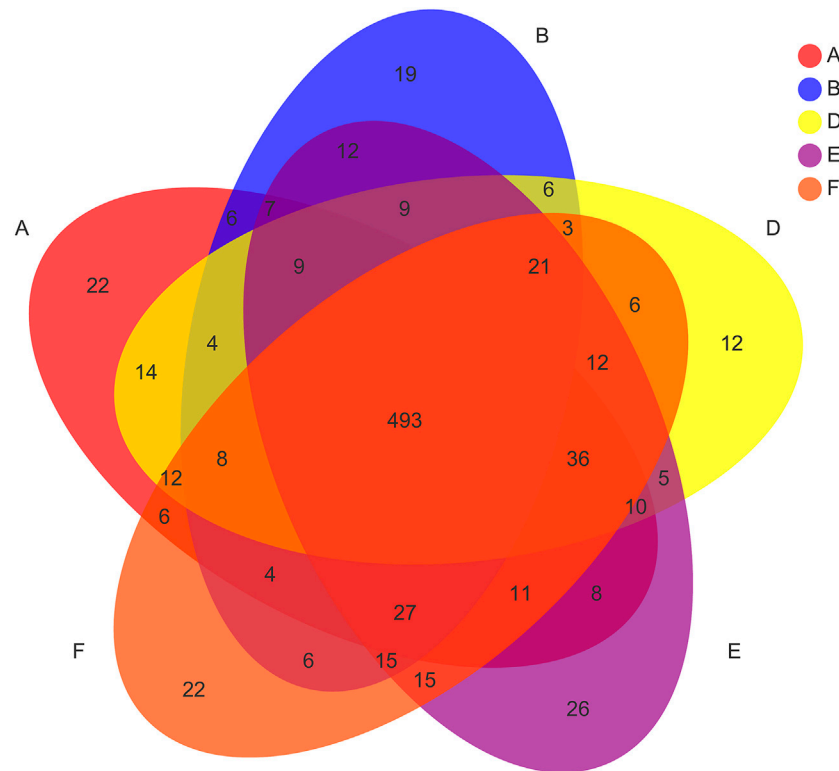
Beat diversity analysis of intergroup species

The principal coordinate analysis (PCoA) is shown in Figure 6, and the results show that the percentages of PCo1 and PCo2 explaining the overall variance are 68.66% and 18.33%, respectively. The blank group and the DN model group were completely separated. Compared with the blank group, the flora structure of the DN model group was significantly different. The sample points of *Cornus officinalis* group, wine *Cornus officinalis* group and wine

honey *Cornus officinalis* group were closer than those of DN model group, and tended to be blank group, indicating that *Cornus officinalis* could affect the intestinal flora composition of DN rats. The sample points of auxiliary wine and auxiliary wine honey group were closer to the DN model group, indicating that auxiliary wine and auxiliary wine honey could not affect the intestinal flora composition of DN rats. Intestinal flora changed significantly in DN state, and *Cornus officinalis* could

**FIGURE 4**

Sequencing Dilution Curve (A), Shannon-Wiener Curve (B) and Rank-Abundance Curve (C) of Intestinal Microflora in Fecal Samples of Rats in Each Group. Note: A. Blank group B. DN model group C. Irbesartan group D. *Cornus officinalis* group E. Wine *Cornus officinalis* group F. Wine honey *Cornus officinalis* group G. Auxiliary wine group H. Auxiliary wine honey group.

**FIGURE 5**

Venn plot of OUT distribution in different treatment groups. Note: A. Blank group B. DN model group C. Irbesartan group D. *Cornus officinalis* group E. Wine *Cornus officinalis* group F. Wine honey *Cornus officinalis* group G. Auxiliary wine group H. Auxiliary wine honey group.

reverse this change before and after processing. The effect of wine honey *Cornus officinalis* was better than that of *Cornus officinalis* and wine *Cornus officinalis*.

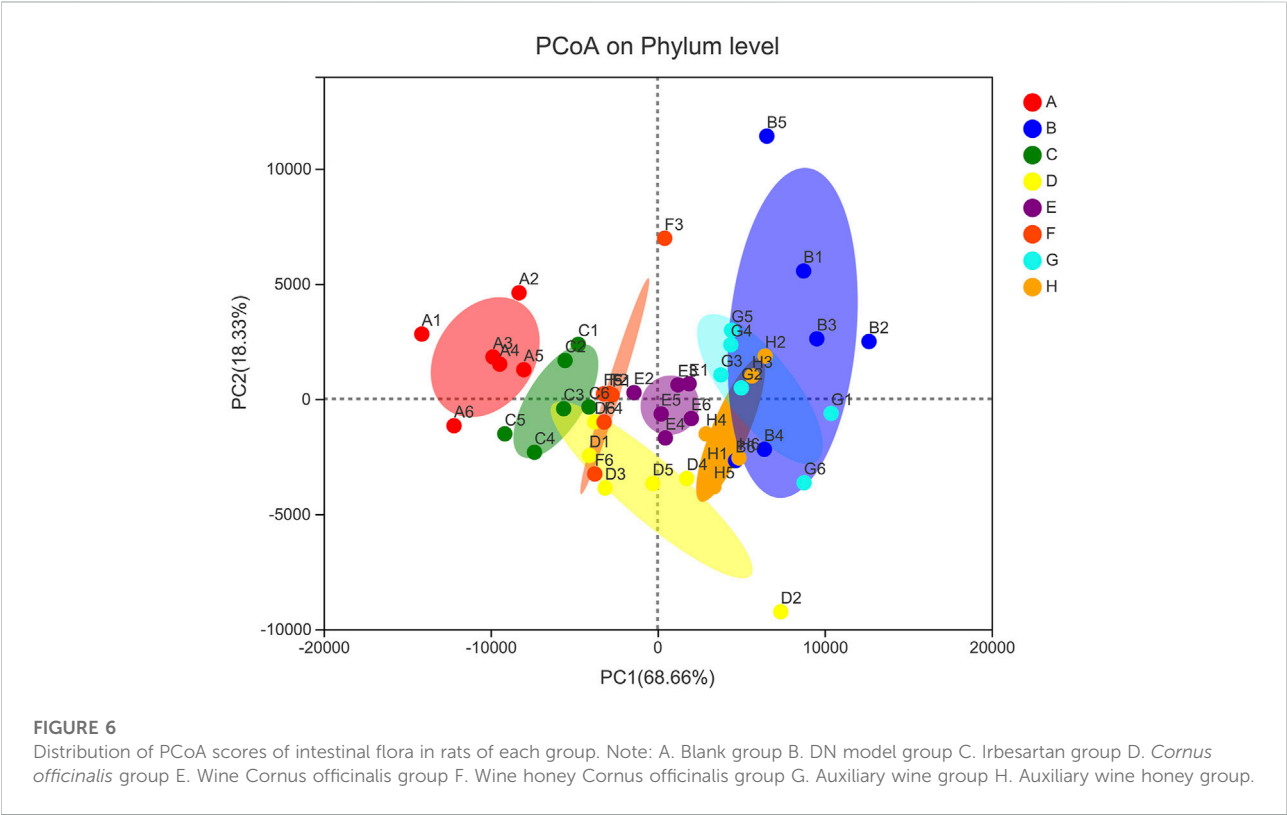
Phylum level analysis of intestinal flora structure

At the level of phylum classification, the composition of the flora in each group of samples is shown in Figure 7A. In the blank

TABLE 3 Effects of *Cornus officinalis* before and after processing on Alpha diversity index of intestinal flora in DN rats ($n = 6$, $\bar{x} \pm s$).

Peer group	Shannon	Simpson	Ace	Chao
A	4.34 ± 0.26	0.16 ± 0.02	595.16 ± 22.19	554.79 ± 25.67
B	2.73 ± 0.37*	0.06 ± 0.02*	361.62 ± 10.08*	325.24 ± 16.60*
C	4.18 ± 0.43#	0.11 ± 0.02#	518.78 ± 22.03#	519.91 ± 26.76#
D	3.78 ± 0.20#	0.08 ± 0.03	417.43 ± 37.08#	455.18 ± 31.12#
E	3.84 ± 0.30#	0.07 ± 0.04	426.09 ± 47.90#	472.91 ± 49.46#
F	3.84 ± 0.33#	0.10 ± 0.02#	421.74 ± 49.67#	516.64 ± 26.65#
G	2.73 ± 0.16*	0.05 ± 0.02*	350.35 ± 27.10*	321.29 ± 13.12*
H	2.75 ± 0.20*	0.06 ± 0.01*	348.90 ± 16.96*	327.96 ± 12.23*

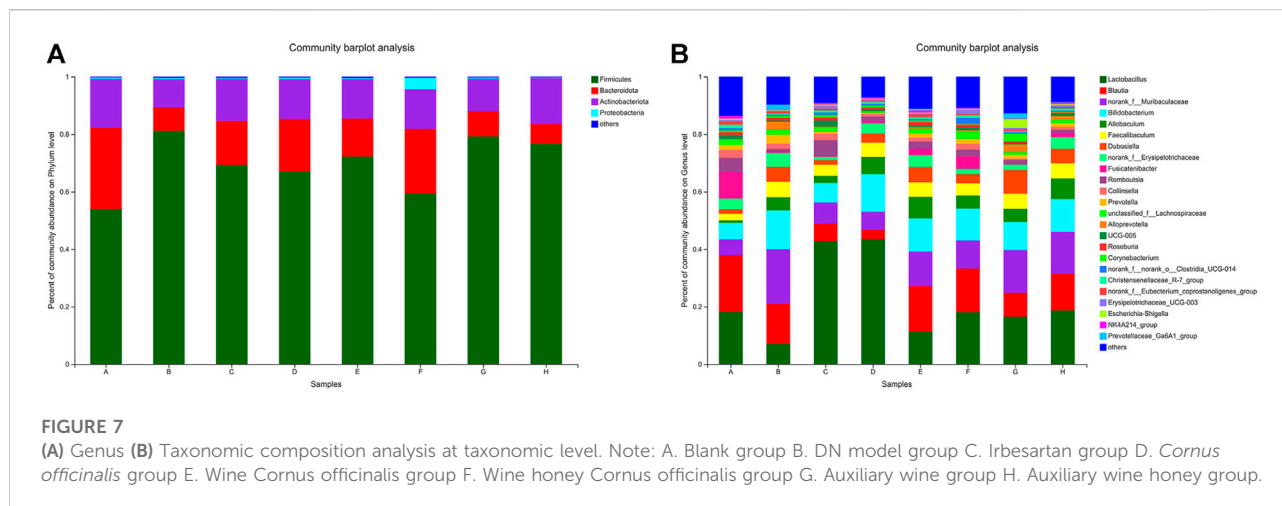
Note: ① A. Blank group B. DN, model group C. Irbesartan group D. *Cornus officinalis* group E. Wine *Cornus officinalis* group F. Wine honey *Cornus officinalis* group G. Auxiliary wine group H. Auxiliary wine honey group. ② Compared with normal group * $p < 0.05$; compared with model group # $p < 0.05$.



group, DN model group and each administration group, the main phylum classification is Firmicutes, Bacteroidetes, Actinobacteriota and Proteobacteria. Among them, Firmicutes has the highest relative abundance, followed by Bacteroidota, and Proteobacteria has the lowest relative abundance. At the genus classification level, see Figure 7B, blank group, DN model group, the relative abundance of each drug group is higher for *Lactobacillus*.

Screening of differential bacteria

Linear discriminant analysis was performed with LEfSe software according to the taxonomic composition of the samples under different grouping conditions to find out the communities or species that had significant differences in sample division. LEfSe analysis has been widely used to find biomarkers with significant differences in abundance between two groups. LEfSe analysis results between each group and the model group are shown in Figure 8.



Compared with the blank group, the DN model group rats' feces in the door, class, order, family, genus classification levels were found on the differential flora. The *c_Bacteroidia*, *p_Bacteroidia* and *o_Bacteroidia* in the feces of the DN model group were significantly higher than those in the blank group, while the dominant bacteria in the feces of the blank group were *c_Clostridia*, *p_Firmicutes*, *g_Lachnospiraceae_FCS020_group*, *g_Butyricococcus*, etc.

Compared with the DN model group, the *g_Lactobacillus*, *f_Lactobacillaceae* and *o_Lactobacillales* in the feces of the irbesartan group were significantly larger than those in the DN model group, while the dominant bacteria in the feces of the DN model group were *o_Bacteroidales*, *c_Bacteroidia*, *p_Bacteroidota*, *f_Muribaculaceae*, etc.

Compared with the DN model group, *c_Bacilli*, *o_Lactobacillales*, *g_Lactobacillus* and *f_Lactobacillaceae* in the feces of rats in the *Cornus officinalis* group were significantly higher than those in the DN model group. The dominant bacteria in feces of DN model group were *c_Bacteroidia*, *p_Bacteroidota*, *o_Bacteroidales*, *f_Muribaculaceae* and so on.

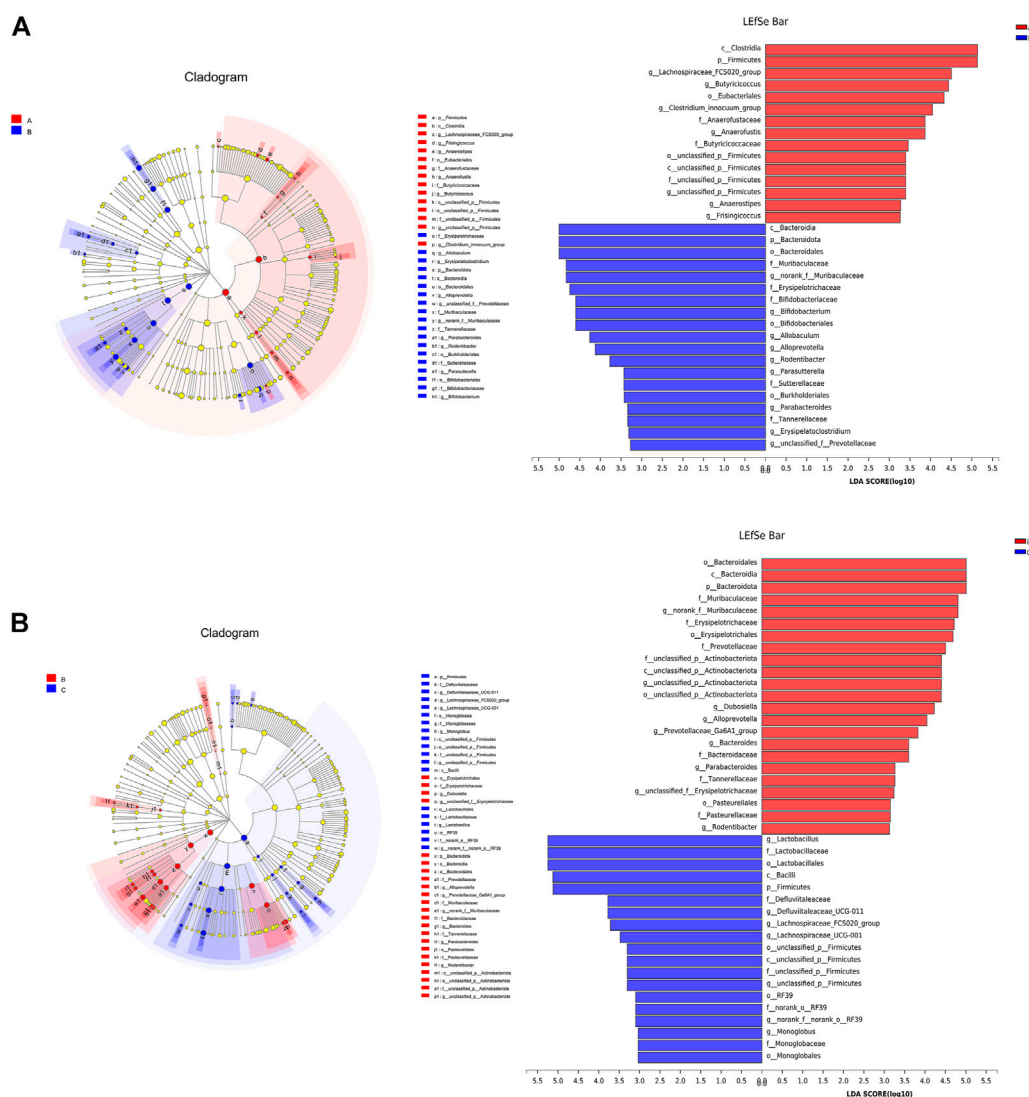
Compared with the DN model group, the *p_Firmicutes*, *g_Family_XIII_p_UDG-001*, *o_unclassified_p_Firmicutes*, *c_unclassified_p_Firmicutes* in the feces of the rats in the wine *Cornus officinalis* group were significantly higher than those in the DN model group; the dominant bacteria in the feces of the DN model group were *c_Bacteroidia*, *p_Bacteroidia*, *o_Bacteroidales*, *f_Muribaculaceae*, etc.

Compared with the DN model group, the *p_Firmicutes* and *g_Butyricococcus* in the feces of the rats in the wine honey *Cornus officinalis* group were significantly larger than those in the model group. The dominant bacteria in feces of DN model group were *c_Bacteroidia*, *p_Bacteroidota*, *o_Bacteroidales*, *f_Muribaculaceae*, *g_norank_f_Muribaculaceae* and so on.

Discussions

Kidney is the most common organ involved in diabetes, DN will eventually develop into end-stage renal disease, affecting the prognosis of patients (Liu et al., 2022). The main clinical pathological changes of DN are glomerular sclerosis and tubulointerstitial fibrosis, and the main manifestations of renal interstitial fibrosis are renal parenchymal cell injury and a large number of extracellular matrix deposition (Guo et al., 2022). Studies have shown that *Cornus officinalis* can inhibit renal tubulointerstitial injury in diabetic rats, improve endoplasmic reticulum stress in mesangial cells, reduce mitochondrial autophagy, reduce renal pathological damage, improve renal fibrosis in DN rats, and inhibit cell proliferation (Lu, 2017; Zhao et al., 2018; Chen et al., 2020). In order to study the effect of *Cornus officinalis* and its processed products on the treatment of DN, this study replicated the DN rat model of streptozotocin model, and treated the DN rats with 281.25 mg/kg *Cornus officinalis*, 281.25 mg/kg wine *Cornus officinalis* and 281.25 mg/kg wine honey *Cornus officinalis*. The results showed that compared with the normal control group, the S-Cr, BUN, mALB and FBG in the model group were significantly increased, while the above indexes were decreased after the intervention of *Cornus officinalis* and its different processed products, and the decrease was obvious in the honey wine *Cornus officinalis* group.

The main pathological changes of DN are glomerulosclerosis and tubulointerstitial fibrosis (Zheng et al., 2022). The results of renal tissue section staining in this experiment suggest that the structure of renal tissue is disordered, glomerular hypertrophy, mesangial cell proliferation, nodular sclerosis is clearly visible, renal tubular degeneration and atrophy, a large number of vacuoles in the cytoplasm of renal tubular epithelial cells and swelling cells are obviously vacuolar degeneration, partial



atrophy, renal interstitial edema and other obvious changes. The detection of the left kidney index of rats in each group also found that the kidney index of the model group was significantly increased, suggesting that the composition of the kidney tissue of the rats was changed. After treatment with each administration group, the left kidney index of the rats decreased, and the wine honey *Cornus officinalis* group decreased most significantly. The above studies showed that after the treatment of *Cornus officinalis* and its processed products, the pathological changes such as renal fibrosis and renal tubular sclerosis in DN rats were alleviated, indicating that *Cornus officinalis* can effectively improve the renal structure and clinical manifestations of DN rats, with the best effect of wine honey *Cornus officinalis*.

The pathogenesis of DN is complex, and Wnt signaling pathway may also be involved in the occurrence and development of kidney disease by regulating the proliferation and apoptosis of glomerular intrinsic cells (Guo and Xu, 2022). The results of this study showed that the expression of YKL-40, Wnt4, β -catenin and TGF- β 1 mRNA in renal tissue of DN rats was significantly increased, suggesting that Wnt/ β -catenin signaling pathway was activated in renal tissue of DN rats. The expression of YKL-40, Wnt4, β -catenin and TGF- β 1 mRNA was significantly decreased after intervention in each administration group, suggesting that *Cornus officinalis* and its processed products may inhibit the development of DN and reduce the pathological changes of renal tissue by inhibiting Wnt/ β -catenin signaling pathway.

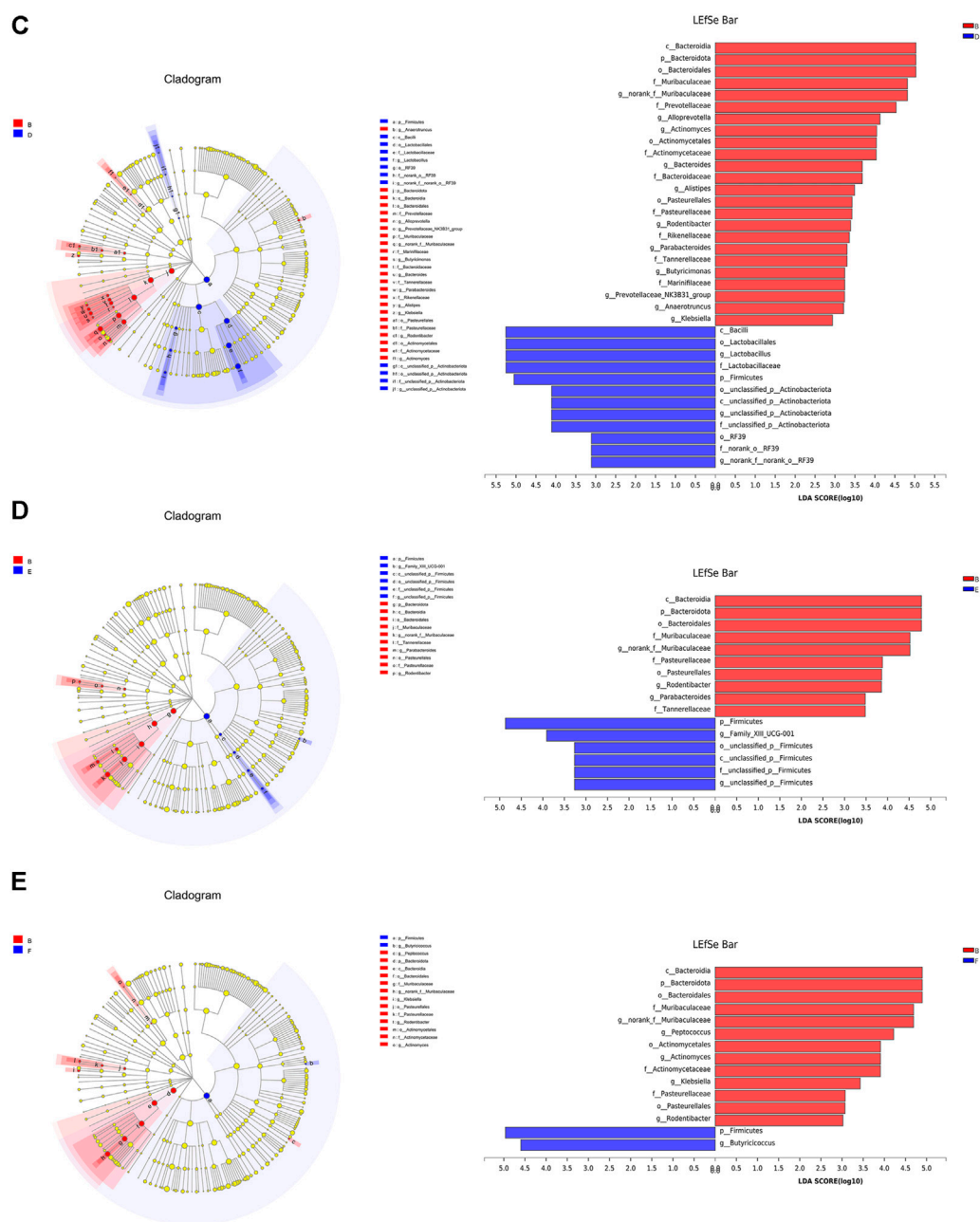


FIGURE 8

Blank group and DN model group (A), DN model group and irbesartan group (B), DN model group and *Cornus officinalis* group (C), DN model group and wine *Cornus officinalis* group (D), DN model group and wine honey *Cornus officinalis* group (E) LefSe difference analysis chart. Note: ① A. Blank group B. DN model group C. Irbesartan group D. *Cornus officinalis* group E. Wine *Cornus officinalis* group F. Wine honey *Cornus officinalis* group G. Auxiliary wine group H. Auxiliary wine honey group. ② Different color nodes represent microbial groups that are significantly enriched in the corresponding groups and have a significant effect on the differences between groups; light yellow nodes indicate microbial groups that have no significant difference in different groups or have no significant effect on the difference between groups. If the number of significantly different species ≤ 50 , the legend position on the right side is shown as a column, if the number of significantly different species > 50 , the legend position on the right side is shown as two columns.

After SCFAs are produced in the intestine and excreted through feces, they can quickly enter the systemic circulatory system and play a very important role in regulating the body's normal physiological

functions (Postler and Ghosh, 2017). It has been reported that propionic acid and butyric acid in SCFAs are important signal transduction molecules that bind to G protein-coupled receptors

and inhibit histone deacetylase activity (McNabney and Henagan, 2017). Compared with the blank group, the content of various short-chain fatty acids in the DN model group was down-regulated, indicating that DN would reduce the content of short-chain fatty acids in rats. After administration, the range and intensity of regulation of each administration group were slightly different, but each administration group except butyric acid, were significantly up-regulated, indicating that each administration group had a better effect to improve the content of short-chain fatty acids in rats. The wine honeyed *Cornus officinalis* group had the best regulating effect on the content of short chain fatty acids in rats.

The results of intestinal flora diversity test showed that compared with the normal group, the flora in the fecal samples of the DN model group changed significantly from phylum to genus level. Although the structure of intestinal flora in fecal samples is similar, the composition ratio between different phyla and genera is quite different. In the fecal samples, the relative abundance of Firmicutes was the highest in the phylum classification level, followed by Bacteroidetes, and the rest also included Actinobacteria and Proteobacteria. At the level of genus classification, *Lactobacillus* had higher relative abundance. In mice and humans, Firmicutes and Bacteroidetes are major components of the level of classification of intestinal flora. Studies have shown that the imbalance of intestinal flora can cause obesity (Qiu et al., 2022), and is related to the proportion of Firmicutes and Bacteroidetes. The higher the proportion, the more obvious the symptoms of obesity (Cheng et al., 2021); studies have also found that the decrease in the ratio is associated with improved glucose levels, reduced fat accumulation, and reduced body weight (Zeng et al., 2016). In the fecal samples of rats in this experiment, compared with the blank group, the abundance of Firmicutes in the DN model group increased, the abundance of Bacteroidetes decreased, and the ratio increased. *Lactobacillus* is a microorganism that lives in the body and benefits the health of the host. It can participate in regulating immunity and insulin resistance, thereby further regulating lipid and glucose metabolism (Yin et al., 2022); studies have also shown that increasing the proportion of *Lactobacillus* can reduce the risk of infection in patients with type 2 diabetes and has a protective effect on blood glucose (Zhou and Xu, 2021). In the fresh fecal samples of rats in this experiment, *Lactobacillus* in the DN model group showed a downward trend.

In summary, *Cornus officinalis* can effectively reduce DN rats 24-h urinary albumin, reduce renal pathological damage. *Cornus officinalis* may play a role in renal protection by anti-oxidation and inhibition of Wnt/ β -catenin signaling pathway, regulating the content of some short-chain fatty acid-producing bacteria to increase the content of short-chain fatty acids in the intestine, and playing the role of energy supply in the body, which is conducive to healthy recovery, increasing beneficial bacteria and reducing pathogenic bacteria. The effect of wine honey *Cornus officinalis* is the best, which is expected to become a therapeutic drug for DN.

The results of this experiment can provide a scientific basis for the rational development and utilization of *Cornus Fructus* after processing.

Data availability statement

The datasets presented in this study can be found in online repositories. The names of the repository/repositories and accession number(s) can be found in the article/Supplementary material.

Ethics statement

The animal study was reviewed and approved by Medicine Ethics Review Committee for animal experiments of Liaoning University of Traditional Chinese Medicine.

Author contributions

Study design: C-GJ and LZ; Analysis and interpretation: C-GJ and LZ; Drafting manuscript: C-GJ and LZ; Statistical analysis: WW and HG; Data collection: WW and HG; Revision manuscript: Y-BX and T-ZJ. All authors read and approved the final manuscript.

Funding

Study on Processing Technology and Product Development of *Fructus officinalis* (2020000000014).

Conflict of interest

Y-BX was employed by the company Beijing Jujing Health Technology Group.

The remaining authors declare that the research was conducted in the absence of any commercial or financial relationships that could be construed as a potential conflict of interest.

Publisher's note

All claims expressed in this article are solely those of the authors and do not necessarily represent those of their affiliated organizations, or those of the publisher, the editors and the reviewers. Any product that may be evaluated in this article, or claim that may be made by its manufacturer, is not guaranteed or endorsed by the publisher.

References

- Chen, S., Zhou, Y., Chen, Y., and Gu, J. (2018). fastp: an ultra-fast all-in-one FASTQ preprocessor. *Bioinformatics* 34 (17), i884–i890. doi:10.1093/bioinformatics/bty560
- Chen, Y., Yan, R., Jia, C. G., and Song, W. Y. (2020). Based on YKL-40 and Wnt/ β -catenin pathway to explore the protective effect of Shanzhuyu granules on diabetic nephropathy. *J. Chin. Med. Mat.* 43 (04), 961–967. doi:10.13863/j.issn1001-4454.2020.04.033
- Cheng, X. Y., Peng, Y. B., Dong, W., Sun, J., Pan, L. H., and Liu, B. (2021). Regulatory mechanism of intestinal flora on type 2 diabetes mellitus. *Chin. J. Microcol.* 33 (12), 1466–1470. doi:10.13381/j.cnki.cjm.202112019
- Edgar, R. C. (2013). UPARSE: Highly accurate OTU sequences from microbial amplicon reads. *Nat. Methods* 10 (10), 996–998. doi:10.1038/nmeth.2604
- Feng, X. (2022). Research on diabetic nephropathy treated by Chinese and Western medicine. *Chin. J. EthoMed. Ethnopharm.* 31 (11), 46–49.
- Guo, J. H., Wei, H., Liang, Z. Z., and He, G. B. (2022). Influencing factors of early diabetic nephropathy in patients with type 2 diabetes mellitus. *Chin. J. Public. Health. Eng.* 21 (01), 99–103. doi:10.19937/j.issn.1671-4199.2022.01.032
- Guo, X., and Xu, C. H. (2022). Research progress on the role of Wnt/ β -catenin signaling pathway in renal fibrosis. *J. Med. Sci. Yanbian. Univ.* 45 (01), 59–62. doi:10.16068/j.1000-1824.2022.01.015
- Jin, Q. X., and Chang, X. Y. (2015). Study on chemical constituents and pharmacological action of cornus. *Chin. J. Clin. Res.* 7 (11), 27–28.
- Li, J. X., Ma, T. T., Nan, Y., and Yuan, L. (2019). Research progress on pathogenesis of diabetic nephropathy. *J. Chin. Nephrol.* 19 (11), 860–864.
- Liu, Y. D., Ma, Z. C., Li, C. C., Lin, Y., Zhang, Y. Q., and Lin, N. (2022). Study on the potential and molecular mechanism of kunxian capsule effectively intervening diabetic nephropathy by correcting 'immune - inflammation' imbalance network. *Acta. Pharm. Sin.* 57 (02), 375–384. doi:10.16438/j.0513-4870.2021-1109
- Liu, Y. D., Meng, X. Y., Cheng, T., Guo, S. M., Ren, Y. P., and Wang, Y. S. (2019). Diabetic nephropathy pathogenesis and treatment of Chinese and Western medicine overview. *West. J. Tradit. Chin. Med.* 32 (07), 134–138.
- Lou, W. F., Zhang, N., and Bu, T. J. (2021). Study on the mechanism of Chinese medicine Cornus officinalis in the treatment of diabetic kidney disease. *J. Chin. Nephrol.* 21 (10), 819–825.
- Lu, X. (2017). Study on mechanism of effective parts and compatibility of rehmanniae radix and cornus officinalis in intervention of diabetic nephropathy. *J. Nanjing. Univ. Tradit. Chin. Med.* doi:10.27253/d.cnki.gnjzu.2017.000008
- Magoč, T., and Salzberg, S. L. (2011). FLASH: Fast length adjustment of short reads to improve genome assemblies. *Bioinformatics* 27 (21), 2957–2963. doi:10.1093/bioinformatics/btr507
- McNabney, S. M., and Henagan, T. M. (2017). Short chain fatty acids in the colon and peripheral tissues: A focus on butyrate, colon cancer, obesity and insulin resistance. *Nutrients* 9 (12), 1348. doi:10.3390/nu9121348
- Park, C. H., Takashi, T., and Yokozawa, T. (2013). Anti-diabetic action of 7-o-galloyl-d-sedoheptulose, a polyphenol from corni fructus, through ameliorating inflammation and inflammation-related oxidative stress in the pancreas of type 2 diabetics. *Biol. Pharm. Bull.* 36 (5), 723–732. doi:10.1248/bpb.b12-00543
- Postler, T. S., and Ghosh, S. (2017). Understanding the holobiont: How microbial metabolites affect human health and shape the immune system. *Cell Metab.* 26 (1), 110–130. doi:10.1016/j.cmet.2017.05.008
- Qi, M. Y., Xie, G. Y., Chen, K., Su, Y. H., Yu, S. Q., and Liu, H. r. (2014). Total triterpene acids, isolated from corni fructus, ameliorate progression of renal damage in streptozotocin-induced diabetic rats. *Chin. J. Integr. Med.* 20 (6), 456–461. doi:10.1007/s11655-013-1532-5
- Qiu, L., Gu, G. Z., Wang, X. Y., Gao, X. J., Yang, W. G., and Xu, D. L. (2022). Regulatory effect of enteromorpha polyphenols on blood lipid metabolism and intestinal flora in obese mice. *J. Nucl. Agric. Sci.* 36 (08), 1638–1647.
- Sayed, A. A. R., Khalifa, M., and Abd el-Latif, F. F. (2012). Fenugreek attenuation of diabetic nephropathy in alloxan-diabetic rats Attenuation of diabetic nephropathy in rats. *J. Physiol. Biochem.* 68 (2), 263–269. doi:10.1007/s13105-011-0139-6
- Shikata, K., and Shikata, K. (2013). Microinflammation in the pathogenesis of diabetic nephropathy. *J. Diabetes Investig.* 4 (2), 142–149. doi:10.1111/jdi.12050
- Stackebrandt, E., and Goebel, B. M. (1994). Taxonomic note: A place for DNA-DNA reassociation and 16S rRNA sequence analysis in the present species definition in bacteriology. *Int. J. Syst. Evol. Microbiol.* 44 (4), 846–849. doi:10.1099/00207713-44-4-846
- Wang, Q., Garrity, G. M., Tiedje, J. M., and Cole, J. R. (2007). Naive bayesian classifier for rapid assignment of rRNA sequences into the new bacterial taxonomy. *Appl. Environ. Microbiol.* 73 (16), 5261–5267. doi:10.1128/AEM.00062-07
- Yang, C. M., Yang, Z. X., and Ma, X. L. (2019). The mechanism of AGEs-RAGE signaling pathway in diabetic nephropathy and the research progress of traditional Chinese medicine. *China J. Chin. Med.* 34 (09), 1864–1868. doi:10.16368/j.issn.1674-8999.2019.09.437
- Yang, K., Bai, Y., Yu, N., Lu, B., Han, G., Yin, C., et al. (2020). Huidouba improved podocyte injury by down-regulating Nox4 expression in rats with diabetic nephropathy. *Front. Pharmacol.* 11, 587995. doi:10.3389/fphar.2020.587995
- Yang, M. M., Yuan, X. X., Zhao, G. Q., Yang, L. M., and Zhang, W. H. (2016). Research progress on chemical constituents and pharmacological effects of cornus officinalis. *J. Chengde. Med. Univ.* 33 (05), 398–400. doi:10.15921/j.cnki.cyx.2016.05.018
- Yin, L., Xia, W. R., Huang, G. X., and Xiao, W. L. (2022). Research progress on the correlation between Chinese medicine - intestinal flora interaction and host metabolic immune homeostasis. *Chin. Tradit. Herb. Drugs.* 53 (08), 2526–2538.
- Zeng, Y. P., Hu, Y., Wu, P., Feng, X. G., Gu, C. Y., and Guo, Y. F. (2016). Analysis of intestinal flora in obese people with type 2 diabetes mellitus. *Lab. Med.* 31 (10), 848–853.
- Zhao, Y. Y., He, N. W., Mu, C. L., and Zhang, X. (2018). Research progress on hypoglycemic effect of iridoid glycosides of cornus officinalis. *Shaanxi. J. Agric. Sci.* 64 (07), 96–104.
- Zheng, T., Wang, H. Y., Chen, Y., Chen, X., Wu, Z. L., Hu, Q. Y., et al. (2022). Src activation aggravates podocyte injury in diabetic nephropathy via suppression of fundc1-mediated mitophagy. *Front. Pharmacol.* 13, 897046. doi:10.3389/fphar.2022.897046
- Zhou, Q., and Xu, J. (2021). Changes of intestinal flora in adolescent patients with type 2 diabetes mellitus with different degrees of abdominal obesity and its relationship with glucose and lipid metabolism and liver fat content. *China J. Tradit. Chin. Med. Pharm.* 11 (13), 13–16.
- Zhou, Y. C., Zhang, L. J., and Zhang, Y. L. (2020). New progress on chemical constituents and pharmacological effects of cornus officinalis. *Inf. Tradit. Chin. Med.* 37 (01), 114–120.



OPEN ACCESS

EDITED BY
Zheng Xiang,
Liaoning University, China

REVIEWED BY
Songül Karakaya,
Atatürk University, Turkey
Meraj Ansari,
National Institute of Pharmaceutical
Education and Research, India

*CORRESPONDENCE

Yizhen Xie,
xyzgdim@sina.com

†These authors have contributed equally
to this work

SPECIALTY SECTION

This article was submitted to
Ethnopharmacology,
a section of the journal
Frontiers in Pharmacology

RECEIVED 02 September 2022
ACCEPTED 26 September 2022
PUBLISHED 14 October 2022

CITATION

Jiao C, Liang H, Liu L, Li S, Chen J and
Xie Y (2022), Transcriptomic analysis of
the anti-inflammatory effect of
Cordyceps militaris extract on acute
gouty arthritis.
Front. Pharmacol. 13:1035101.
doi: 10.3389/fphar.2022.1035101

COPYRIGHT

© 2022 Jiao, Liang, Liu, Li, Chen and Xie.
This is an open-access article
distributed under the terms of the
Creative Commons Attribution License
(CC BY). The use, distribution or
reproduction in other forums is
permitted, provided the original
author(s) and the copyright owner(s) are
credited and that the original
publication in this journal is cited, in
accordance with accepted academic
practice. No use, distribution or
reproduction is permitted which does
not comply with these terms.

Transcriptomic analysis of the anti-inflammatory effect of *Cordyceps militaris* extract on acute gouty arthritis

Chunwei Jiao^{1,2†}, Huijia Liang^{1†}, Li Liu¹, Shunxian Li²,
Jiaming Chen¹ and Yizhen Xie^{1,2*}

¹Guangdong Yuewei Edible Fungi Technology Co. Ltd., Guangzhou, China, ²Guangdong Yuewei Bioscience Co., Ltd., Zhaoqing, China

Background: Gouty arthritis (GA) is a common inflammatory disease that causes pain due to the deposition of monosodium urate (MSU) crystals into joints and surrounding tissues. Anti-inflammatory drugs have significant clinical anti-inflammatory and analgesic effects, but they have many side effects. *Cordyceps militaris* is an edible and medicinal fungus, and its extract (CME) has good anti-inflammatory and analgesic effects. This study aimed to investigate the anti-inflammatory effect of CME on GA and its underlying mechanism.

Methods: The effect of CME on the expression of related inflammatory factors and histopathological changes in the MSU-induced acute inflammatory gout model in rats was studied by ELISA and HE, and its anti-inflammatory mechanism was analyzed by transcriptome combined with RT-qPCR.

Results: CME significantly improved gait scores and joint swelling in GA rats, and reduced MSU-induced inflammatory cell infiltration. CME inhibited MSU-induced inflammatory responses by reducing the levels of pro-inflammatory factors TNF- α , IL-1 β , IL-6, and Caspase-1 and increasing the anti-inflammatory factor IL-10. Transcriptome analysis showed that CME significantly altered inflammation-related cytokine pathways, and identified four major genes involved in regulation of inflammation, CCL7, CSF2RB, LIF, and IL-1 β . In addition, RT-qPCR was performed to verify these differential genes.

Conclusion: CME significantly alleviated the inflammatory progression of GA and ameliorated the onset of GA. The underlying mechanism may be related to triggering the cytokine-cytokine receptor interaction signaling pathway to inhibit the activation of the inflammasome and regulate the immune system. And it regulates the inflammatory response induced by MSU crystals through the genes CCL7, CSF2RB, and IL-1 β .

KEYWORDS

gouty arthritis, inflammation, *Cordyceps militaris* extract, monosodium urate, transcriptomics

1 Introduction

Gout, a chronic disease of monosodium urate (MSU) crystal deposition, typically presents as acute inflammatory arthritis of the deposited crystals, progressing to more frequent attacks involving multiple joints and severe pain (Dalbeth et al., 2021). The most common symptoms include swelling, redness, pain, and joint fever (Rowczenio et al., 2017). Neglecting treatment can lead to an increased prevalence of other comorbidities, such as hypertension, diabetes, chronic kidney disease, and cardiovascular disease (Dalbeth et al., 2016). The initial treatment of gout aims to relieve the acute inflammation and pain of gout first, and then treat chronic gout to prevent recurring attacks. Therefore, acute gouty arthritis (GA), as the first clinical symptom, is the key to the treatment of gout. In addition, its main pathogenesis is that pathogenic crystals (MSUs) stimulate toll-like receptors (TLRs) and NOD-like receptor family pyrin domain-containing-3 (NLRP3) inflammasomes, which recruit monocytes, macrophages and cells such as synovial cells to release inflammatory factors through NALP3 inflammasome activity, leading to autoimmune disorders that promote inflammatory progression and tissue destruction (Dalbeth et al., 2021). The inflammasome is a key signaling platform for inflammatory responses, and active inflammasomes induce caspase-1 enzymatic activity, leading to inflammatory cell death and the maturation and secretion of inflammatory cytokines IL-1 β and IL-18 (Spel and Martinon, 2020). IL-1 β is a key inflammatory mediator that induces GA, stimulates NF- κ B via TLR4 and TLR2, promotes inflammasome assembly, and regulates inflammatory cytokines (IL-1 β , IL-6, IL-10, and TNF- α) (Martinon et al., 2006; Busso and So, 2010; Amaral et al., 2012; Andrés et al., 2015). To achieve anti-inflammatory and analgesic effects, the clinical treatment of acute GA currently relies primarily on nonsteroidal anti-inflammatory drugs, colchicine, and glucocorticoids (Dalbeth et al., 2016; Dalbeth et al., 2021). However, the long-term high-dose use of these drugs has limitations such as toxicity and side effects (Jayaprakash et al., 2007; Eleftheriou et al., 2008; Richette and Bardin, 2008). Among them, colchicine, the first-line treatment for gout, has toxic and side effects such as severe bone marrow suppression, renal failure, alopecia, disseminated intravascular coagulation, liver necrosis, diarrhea, seizures, and death (Roberts et al., 1987; Gottlieb et al., 2022). Therefore, there is an urgent need to develop new drugs that are safer and more effective in the treatment of GA.

Fungi have become a research hotspot in the field of edible medicine, with Phase I, II, and III clinical trials and widespread success in Asia for the treatment of various cancers and other diseases (Dubey et al., 2019; Panda and Luyten, 2022). *Cordyceps militaris* (L) Fr., belonging to Family *Cordycipitaceae*, Order *Hypocreales*, genus *Cordyceps*, class *Sordariomycetes*, Phylum *Ascomycota*, Kingdom *Fungi*, is an important edible and medicinal fungus which is parasitic on the cocoons and pupae

of Lepidoptera larvae and is widely distributed all over the world (Sung et al., 2007; Singh et al., 2009). It has various biological activities such as anti-inflammatory, antioxidant, anti-aging, anti-tumor, and anti-proliferation (Liu et al., 1997; Nan et al., 2001; Zhan et al., 2006; Ji et al., 2009; Choi et al., 2014). And it is rich in various active chemicals such as cordycepin, adenosine, cordyceps polysaccharide, etc., which have the functions of enhancing immunity, lowering blood lipids, and anti-tumor (Wang and Zhang, 2021). Due to similar chemical characteristics and medicinal properties, *Cordyceps militaris* is increasingly used and considered as a substitute for *Cordyceps sinensis* (Chen et al., 2018; Zhang et al., 2019). *Cordyceps militaris* is sweet in taste, neutral in nature, beneficial to the lungs and kidneys, replenishes the essence, stops bleeding and resolves phlegm. It has been used for hundreds of years as a tonic in Chinese folk to treat impotence and assist in anti-cancer. Due to the great potential of natural products to develop new drugs, we chose *Cordyceps militaris* as a material for the treatment of acute gouty arthritis, based on its main component's anti-inflammatory advantage through the NLRP3 inflammasome, and it has been used as a traditional herbal medicine to nourish the liver and kidney (Choi et al., 2014; Das et al., 2020; Yang et al., 2020). In addition, the liver and kidneys play important roles in uric acid reabsorption and metabolism. Gout is clinically characterized by hyperuricemia and urate crystal deposition, predisposing to the characteristic acute arthritis. At present, our team has carried out research on the treatment of hyperuricemia with *Cordyceps militaris* extract (CME) (Yong et al., 2016; Yong et al., 2018). Therefore, the main purpose of this study was to determine the effect and underlying mechanism of CME on MSU-induced acute gouty arthritis.

2 Materials and methods

2.1 Reagents and materials

Cordyceps militaris was provided by Hong Hao Biotechnology Co., Ltd., (Jiangmen, China). Cordycepin was purchased from Refensi Biotechnology Co., Ltd., (Chengdu, China). Colchicine was obtained from Sigma Chemical Co., (St. Louis, MO, United States). IL-1 β , IL-6, IL-10, TNF- α , and CAS-1ELISA kits were purchased from Jiang Lai Biotechnology Co., Ltd., (Shanghai, China). Decalcification solution, hematoxylin and eosin were purchased from Sevier Biotechnology Co., Ltd., (Wuhan, China). TRIzol reagent was purchased from Thermo Fisher Scientific (Carlsbad, CA, United States). circRNAs and miRNAs, miRcute Plus miRNA First-Strand cDNA Kit and miRcute Plus miRNA qPCR Kit were provided by Tiangen Biochemical Technology Co., Ltd., (Beijing, China). The mRNA, GoScript™ Reverse Transcription Mix Kit, and GoTaq® qPCR Master Mix Kit were provided by American Promega Biotechnology Co., Ltd., Acetonitrile of HPLC grade

was obtained from Merck (Darmstadt, Hesse, Germany). Pure water for HPLC was obtained from an ultrapure water system machine (PureLab, United States).

2.2 Preparation of CME

Cordyceps militaris was extracted twice with water at a solid-to-liquid ratio (1:10) at 100°C for 1 h–1.5 h. The vacuum concentration temperature is 45°C ± 5°C, the vacuum degree is −0.090 Mpa~−0.095 Mpa, and it is concentrated to 12% ± 2% of Baileys. Dry at an inlet air temperature of 165°C–170°C and an outlet air temperature of 85°C–90°C. The resulting concentrate was purified on an macroporous resin (AB-8) column, first eluted with a 4% basic solution at a flow rate of 200 L/h, and then loaded onto an AB-8 resin column (φ20 × 180 cm × 2), the sample was loaded and washed with water at a flow rate of 2BV/h, then eluted with 10% ethanol at a flow rate of 2BV/h. Pump the alcohol cleaning solution to the single-effect concentrator, the concentration temperature is 45°C ± 5°C, the vacuum degree is −0.090 Mpa~−0.095 Mpa, and the concentration degree is 15%–20% of the berry degree. The above-mentioned *Cordyceps* concentrate is spray-dried, the air inlet temperature is 165°C–170°C, the outlet air temperature is 85°C–90°C, the moisture content of the product is controlled to be ≤ 7%, and the concentration of soluble solids is 2%. The content of cordycepin in CME was 1% by high performance liquid chromatography.

2.3 Models and treatment

All experiments were conducted according to the “Guiding Principles for the Care and Use of Laboratory Animals”, and all procedures were reviewed and approved by Ethics Committee of Institute of Microbiology, Guangdong Academy of Sciences (approval number: GT-IACUC202106101).

Male Sprague-Dawley rats (5–6 weeks old, 200 ± 10 g) were purchased from Guangdong Medical Laboratory Animal Center (Certificate of Quality: SCXK-2018-0002). All rats were housed in a temperature-controlled room at 22°C ± 2°C, with 55% ± 10% relative humidity and a 12 h light–dark cycle. They were allowed food and water ad libitum for the duration of the study. After 1 week of adaptive feeding, rats were randomly divided into 4 groups, with 10 rats in each group: the gout group (Gout, 25 mg/ml MSU), CME-low group (CME-low, 0.135 g/kg/d), CME-high group (CME-high, 0.54 g/kg/d), colchicine group (Colchicine, 0.8 mg/kg) and control group (Control, distilled water). MSU was suspended in sterile phosphate-buffered saline and injected into the ankle joint after anesthesia in rats to model acute gouty arthritis. The establishment of this model is consistent with the method reported in previous study (Fan et al., 2021). In addition, this model has a high incidence of arthritis, peaking within 12 h, and spontaneous remission after 5–6 days,

which completely simulates the pathogenesis of clinical acute gouty arthritis in humans (Coderre and Wall, 1987; Pineda et al., 2015).

The control and gout groups were given an equivalent volume of distilled water, and the CME group was given CME by intragastric administration for 9 consecutive days. After administration on day 10, all groups, except the control group, were given injection of 25 mg/ml MSU solution to the right ankle joint to induce acute gout model. Subsequently, the colchicine group was given 0.8 mg/kg colchicine-water solution. All animals were sacrificed at the end of the experiment. Serum was collected for enzyme-linked immunosorbent assay (ELISA). The ankle and foot joints were taken for histopathological analysis. The synovial fluid was removed from the ankle joints for transcriptomic analysis and quantitative real-time polymerase chain reaction (qRT-PCR).

2.4 Anti-inflammatory effect *in vivo*

2.4.1 Joint swelling

The formation of ankle edema is one of the main symptoms in the evaluation of acute gout symptoms. We measured the ankle circumference at 0.5 mm below the ankle joint before and 2 h, 4 h, 6 h, 8 h, 10 h, and 24 h after MSU injection. Each measurement was repeated three times to obtain an average. The degree of ankle swelling (ASD) was calculated as follows: ASD (%) = [Ankle circumference after injection (mm) - ankle circumference before injection (mm)] / [Ankle circumference before injection (mm)] × 100%. Meanwhile, the ankle temperatures of these rats were measured with precision thermometers.

2.4.2 Functional disorder evaluation

The evaluation standard of the dysfunction index refers to the method of scoring system (Coderre and Wall, 1987). Grade 0 dysfunction index evaluation: normal gait, all four feet are evenly on the ground; grade 1: left foot relaxed, toes open, mild lameness; grade 2: left hind foot bent, toes are touched on the ground, obviously lame; grade 3: left hind foot is completely off the land.

2.4.3 ELISA

Blood samples were collected from the abdominal aorta 24 h after the MSU injection. The serum was separated for measurement of IL-1β, IL-6, IL-10, TNF-α, Caspase-1 using an ELISA kit according to its instructions.

2.4.4 Histopathological analysis

The joint tissue was immersed in 4% paraformaldehyde and soaked in decalcification solution for 3 days. Then the tissue was fixed with a wax block and sliced, stained with hematoxylin and eosin (HE) solution after preparation, and the pathological changes of the joint were observed by light microscope.

2.5 Transcriptome of ankle joint

Total RNA was extracted from three randomly selected right joint tissue samples using TRIzol reagent. Libraries were identified and quantified by PCR amplification of enriched library fragments using an Agilent 2100 Bioanalyzer. Based on the Illumina HiSeq sequencing platform (Personalbio, Shanghai, China), the libraries were paired-end sequenced using Next-Generation Sequencing (NGS). After data filtering and quality assessment, the RNA-Seq data were compared with the reference genome with reference to the Ensembl database (<http://www.ensembl.org/>). The read count value for each gene was compared as the raw expression of the gene using HTSeq, and expression was normalized using TPM. mRNA expression level determined by FPKM > 1. Analysis of differential expression was performed using DESeq R ($|\log_2 \text{FoldChange}| > 1$, p value < 0.05). To gain insight into phenotypic changes, Gene Ontology (GO) and Kyoto Encyclopedia of Genes and Genomes (KEGG) functional and pathway enrichment analyses were performed by Metascape (<http://metascape.org>). GO covers three aspects, which describe the Molecular Function of genes, Cellular Component and Biological Process involved respectively. Go feature enrichment of differentially expressed genes (DEGs) and enriched pathways considered statistically significant were all defined by adjusted $p < 0.05$.

2.6 Quantitative real-time polymerase chain reaction analysis

Right joint tissue from the MSU rat model was used for total RNA extraction according to the manufacturer's instructions for TRIzol. Total RNA was used to check quality and integrity shortly after reverse transcription to cDNA by real-time qPCR on the ABI 7500 PCR system (Applied Biosystems, CA, United States). For circRNAs and miRNAs, the miRcute Plus miRNA First-Strand cDNA Kit and the miRcute Plus miRNA qPCR Kit were used. PCR conditions were 95°C for 15 min, followed by 40 cycles of 94°C for 20 s and 60°C for 34 s. For mRNA, GoScript™ Reverse Transcription Mix Kit and GoTaq® qPCR Master Mix Kit were used. PCR conditions were 95°C for 10 min, followed by 40 cycles of 95°C for 15 s and 60°C for 30 s.

2.7 Statistical analysis

All statistical analyses were performed using the GraphPad Prism software 8.0 program. Measurement data is presented as mean ± standard deviation, and the repeatability of each experiment is greater than or equal to 3. Normally distributed data were compared between multiple groups using one-way analysis of variance (ANOVA), and repeated measures and two-way ANOVA were used to analyze functional disorder

evaluation, ASD and ankle temperatures, $p < 0.05$ was considered statistically significant.

3 Results

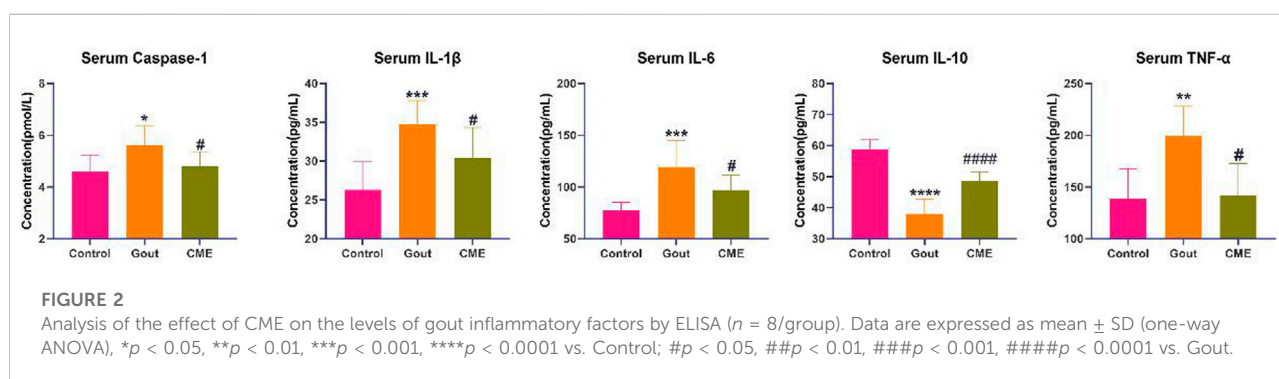
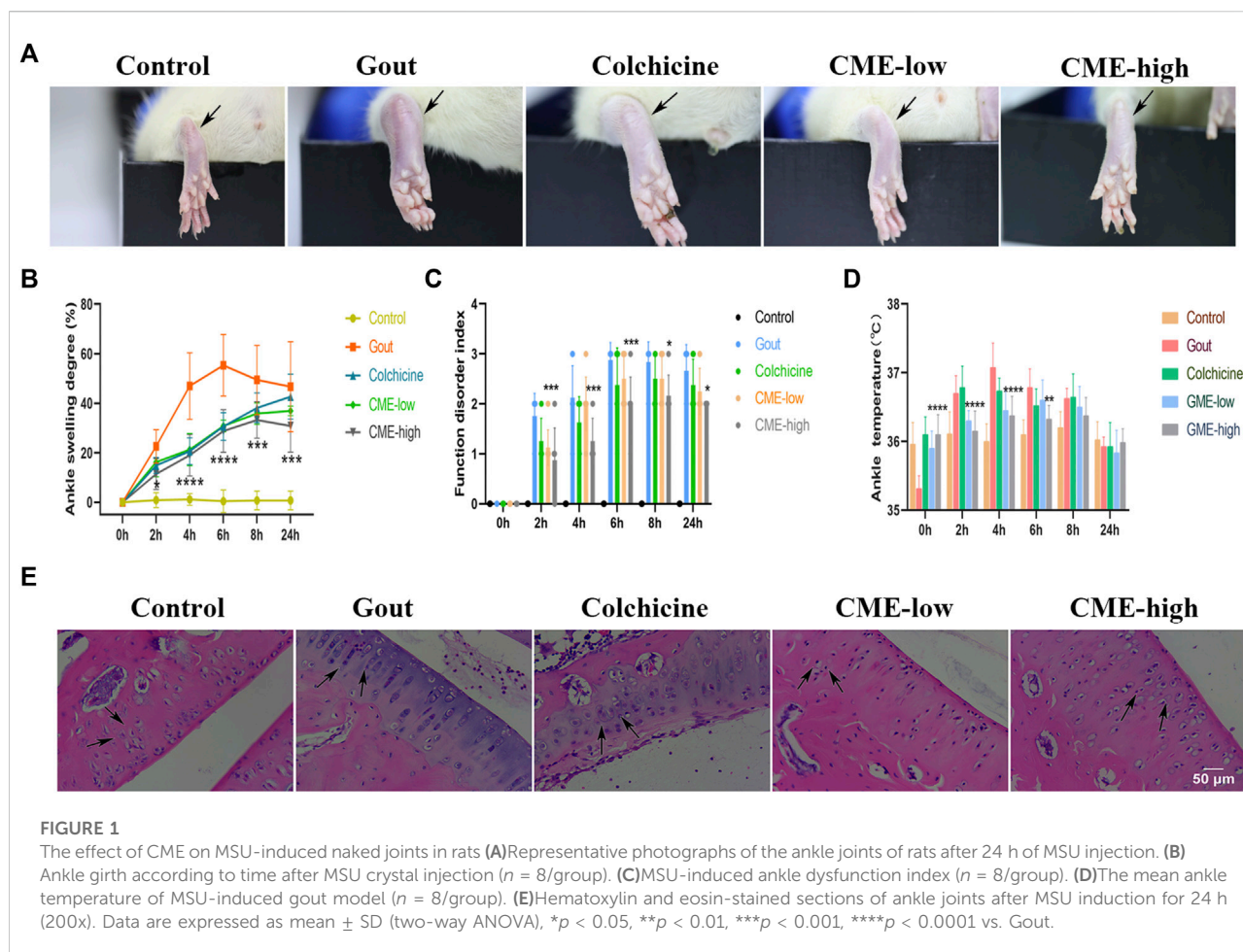
3.1 CME inhibits the onset of acute gout in rats

Pain, stiffness, swelling, and inflammation in the joints and periarticular areas are the most common symptoms of MSU. To assess the recovery of these symptoms by CME, we found that the degree of heat, redness and swelling in the hind paws of the rats varied significantly between groups 24 h after MSU injection (Figure 1A). At the 6th hour, the gout group had the highest ASD, indicating that the swelling of the ankle joints was the most severe, showing a sharp increase from 0 to 6 h and a slow decline after 6 h–24 h (Figure 1B). However, at 0 h–6 h, compared with the gout group, the CME-high group significantly inhibited edema formation, restored foot function, and reduced redness and fever ($p < 0.01$), and compared with the colchicine group, the CME -high group had more effective prevention of gout flares in the short term (Figures 1B–D). These results suggest that CME ameliorates MSU crystal-induced acute gouty arthritis symptoms.

After 24 h, we selected rat ankles for sectioning and HE staining to study the tissue inflammatory state (Figure 1E). In the control group, the synovial tissue structure was clear, the cell morphology was normal, and there was no inflammatory cell infiltration. In the gout group, the density of interstitial cells increased, the infiltration of inflammatory cells was severe, and the synovial vacuolar hyperplasia was observed. However, these pathological changes were significantly reduced in both the CME-low and CME-high groups compared with the gout group. Especially after the treatment of CME-high group, the HE staining in the tissue synovium was more consistent with that of the control group. These results suggest that CME can effectively inhibit the inflammatory cell infiltration of MSU in naked rat joints and slow down the progression of synovial inflammation.

3.2 CME modulates inflammation in acute gout in rats

By analyzing the effect of CME on GA in rats, it was found that the CME-high group had the best effect on GA. Therefore, the control group (Control), the gout group (Gout), and the CME-high group (CME) were used for subsequent specific mechanism analysis. MSU-induced acute GA triggers an inflammatory response by producing inflammatory mediators, which increases cytokine levels in tissues around



the ankle joint. ELISA analysis (Figure 2) showed that the gout group significantly up-regulated the levels of IL-1 β , Caspase-1, IL-6 and TNF- α , and significantly decreased the levels of IL-10, which were induced by MSU ($p < 0.05$). Compared with the gout group, the CME-high group significantly modulated the levels of these inflammatory factors ($p < 0.05$).

3.3 Effects of CME on the global transcriptomic profile of naked joints

With an expression level of FPKM > 1 , 12,872 genes were successfully mapped and identified from RNA-Seq. The differential genes between the gout, control and CME groups

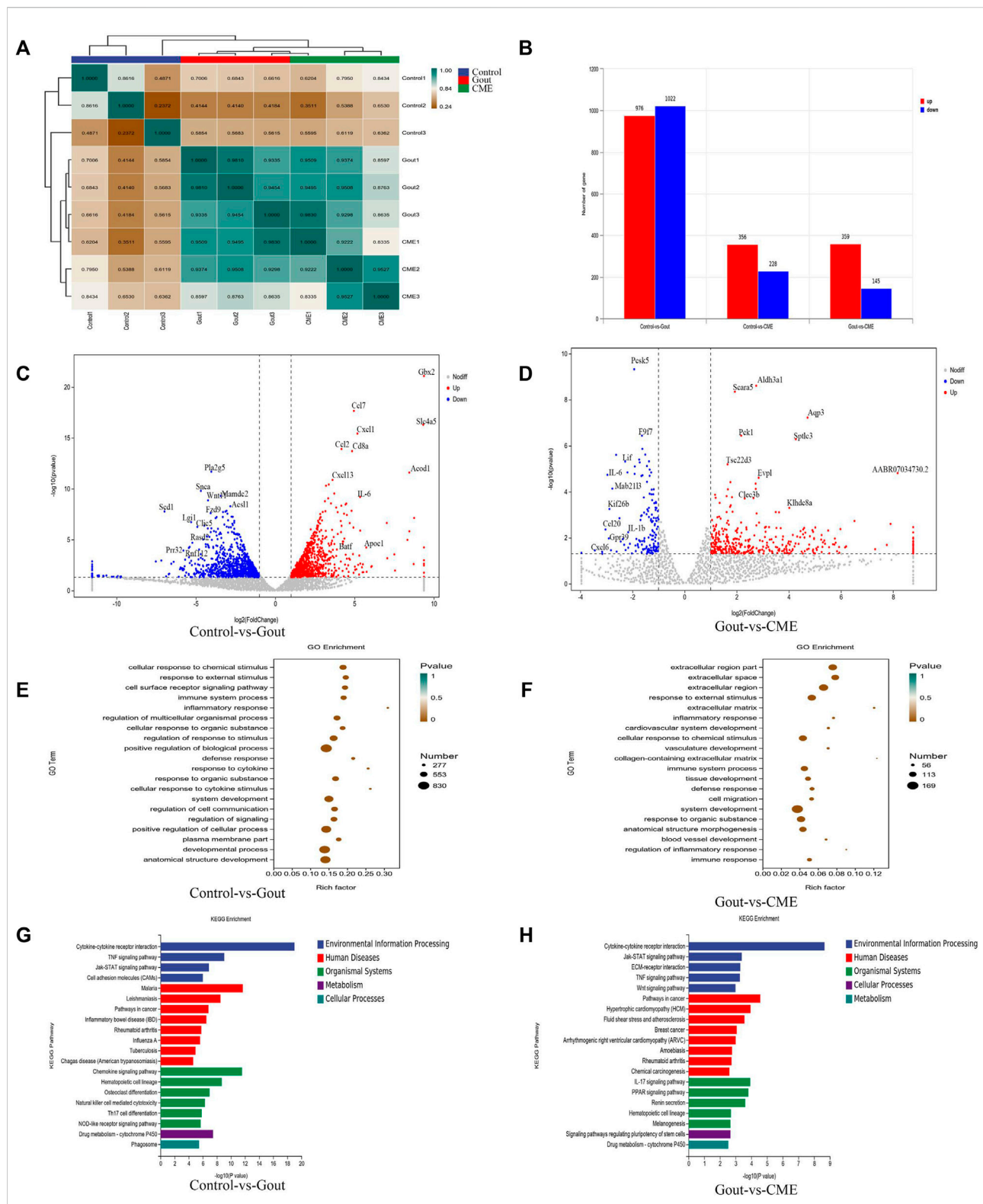


FIGURE 3

Effects of CME on the transcriptomic profile of MSU-induced acute gout. (A) Correlation heat map of differential genes between groups (B) Statistics of differential expression results (C) Volcano plot of differential genes between control and gout groups ($n = 3/\text{group}$) (D) Volcano plot of differential genes between CME and gout groups ($n = 3/\text{group}$) (E) Control and gout groups GO enrichment analysis (F) GO enrichment analysis of CME and gout group (G) KEGG enrichment analysis of control and gout group (H) KEGG enrichment analysis of CME and gout group.

are clustered together, with yellow colors representing significant correlations (between-group value < 0.8) and green representing low correlations. The heatmap showed that the differentially expressed genes were significantly separated between the CME group and the control group (Figure 3A).

We finally obtained a total of 1998 genes identified as DEGs in the control group VS gout group, of which 976 were up-regulated and 1,022 were down-regulated. A total of 504 genes were identified as DEGs in the CME group VS gout group, of which 359 were up-regulated and 145 were down-regulated. In the control group VS CME group, a total of 584 genes were identified as DEGs, of which 356 were up-regulated and 228 were down-regulated (Figure 3B). DESeq R analysis was performed on the condition that $|\log_2 \text{FoldChange}| > 1$, p value < 0.05 , and the differential gene expression changes among the three groups were screened out. The genes CCL7, IL-6, GBX2, CXCL1, CD8A, CCL2, CXCL13, and SLC4A5, ACOD1 were significantly up-regulated in the control and gout groups. However, the genes PLA2G5, SNCA, WNT11, MADC2, SCD1, LGI1, CLIC5, RASD2, FZD9, and ACS11 was significantly downregulated in the control and gout groups (Figure 3C). After CME treatment, gout group genes AQP3, SPTLC3, PCK1, ALDH3A1, SCARA5, EVPL, TSC22D3, CLEC3B, KLHDC8A, and AABR07034730.2 were significantly up-regulated, gout group genes PCSK5, F9F7, LIF, IL-6, MAB21L3, KIF26B, CCL20, IL-1 β , CXCL6 and GPR39 were significantly down regulated (Figure 3D). The functions of the top 20 DEGs were analyzed based on the GO database and annotated with GO terms. The results showed that cellular response to chemical stimulus, response to external stimulus, cell surface receptor signaling pathway, immune system process, inflammatory response and regulation of multicellular organismal process were strongly expressed in biological processes; plasma membrane part, membrane microdomain and cell surface were dominant in cellular components; protein binding, cytokine binding and cytokine receptor activity were the main molecular functions (Figures 3E,F).

Through differential gene expression analysis of KEGG-enriched pathways, we concluded that in MSU-induced rats, the effect of CME on GA was significantly enriched mainly in the signaling pathway of cytokine-cytokine receptor interaction (p value < 0.05). Followed by chemokine signaling pathway, TNF signaling pathway, cancer pathway, IL-17 signaling pathway, rheumatoid arthritis, drug metabolism-cytochrome P450, inflammatory bowel disease (IBD) and cell adhesion molecule (CAM) enriched in signaling pathways (Figures 3G,H).

3.4 Confirmation of gene expression by RT-qPCR

Focusing on the aforementioned GO terms and KEGG-enriched pathways, CME treatment of GA is closely related to the cytokine-

cytokine receptor interaction signaling pathway. For further study, four down-regulated DEGs in the cytokine-cytokine receptor interaction pathway were randomly selected for RT-qPCR validation, including CCL7, CSF2RB, LIF, and IL-1 β . The results of RT-qPCR showed that the expressions of CCL7, CSF2RB and IL-1 β were significantly up-regulated in the gout group compared with the control group ($p < 0.05$). However, the expressions of 4 genes were significantly decreased after CME treatment compared with the gout group ($p < 0.05$) (Figures 4A,B). Therefore, the transcriptome sequencing data were consistent with the RT-qPCR gene results, indicating that the RT-qPCR results demonstrate the reliability of RNA-Seq data for gene expression profiling.

4 Discussion

Inflammation is one of the main causes of gout, because MSU crystals interact with cells, recruit a large number of infiltrating neutrophils, synovial cells, and tissue macrophages, resulting in immune system disorders, and the recruitment of immune cells leads to the production of inflammatory factors (Martin et al., 2009; Dinesh and RASOOL, 2017). In addition, clinical studies have shown that gout is prone to other complications, and the common link between these diseases is the presence of sterile inflammation (Pillinger et al., 2010; Ichikawa et al., 2011; Rahimi-Sakak et al., 2019). If inflammation is not treated promptly, a long-term immune program can have systemic consequences, leading to chronic inflammation and tissue damage (Cab  u et al., 2020). Therefore, the anti-inflammatory effect plays a very important role in the treatment of gout. GA is an acute reaction triggered by MSU, which is one of the prominent clinical features of gout (Ragab et al., 2017). The GA attack is the pathogenic inflammatory response caused by MSU, during which IL-1 β , IL-6, IL-10, TNF- α , Caspase-1 were all involved in the development of inducing and expanding inflammation (Das et al., 2020; Galozzi et al., 2021; Makoni and Nichols, 2021). NLRP3 and IL-1 β have been identified as risk factors for gout, and it has been clinically confirmed that high levels of NLRP3, Caspase-1, IL-1 β and IL-6 have been detected in serum and synovial fluid of patients (Son et al., 2013; Cavalcanti et al., 2016). Therefore, the expression of these proteins is an important factor affecting the onset of GA.

The biologically active compounds of *Cordyceps militaris* (total extracts, polysaccharides, and cordycepin) have significant immunomodulatory effects and can be used to treat tumors, allergies, viral infections, and as immunosuppressants for delayed-type hypersensitivity reactions (Lee et al., 2020). Among them, cordycepin has a protective effect on inflammatory damage in various diseases including acute lung injury, asthma, rheumatoid arthritis, Parkinson's disease, hepatitis and atopic dermatitis (Tan et al., 2020). Cordycepin fights inflammation by regulating the release of IL-1 β from the NLRP3 inflammasome (Yang et al., 2020). Studies have demonstrated that MSU crystals activate the NLRP3 inflammasome and release IL-1 β to play a central role in

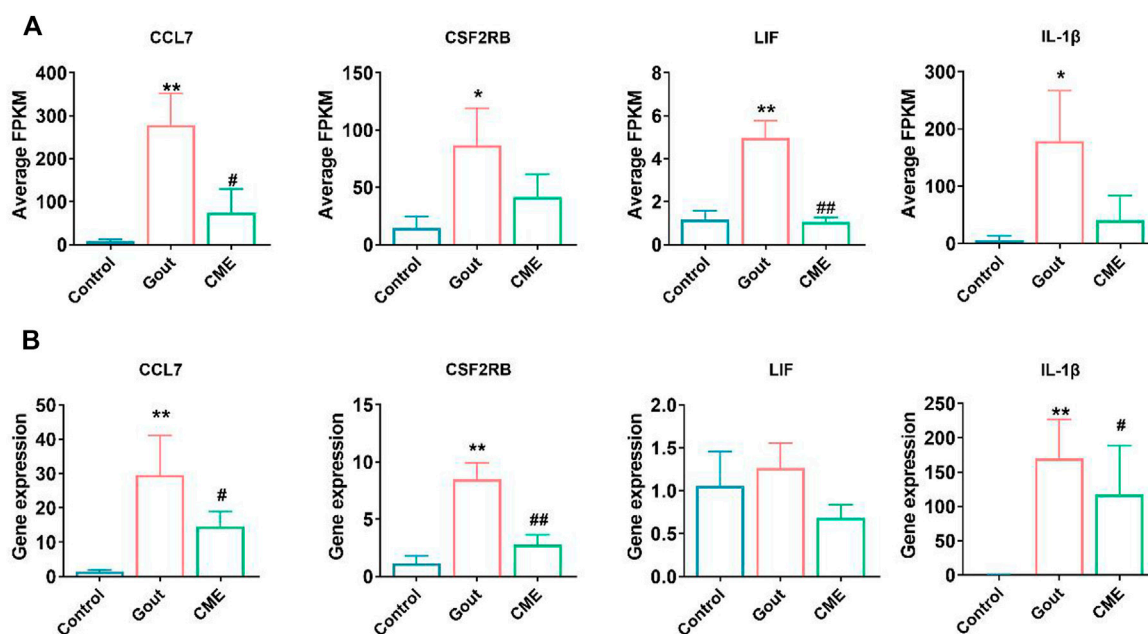


FIGURE 4

Comparison of relative expression levels between RNA-Seq and RT-qPCR results. (A) Detection of expression of four differential genes from RNA-Seq ($n = 3/\text{group}$). (B) Detection of expression of four differential genes by RT-qPCR ($n = 3/\text{group}$). Data are expressed as mean \pm SD (one-way ANOVA), * $p < 0.05$, ** $p < 0.01$ vs. Control; # $p < 0.05$, ## $p < 0.01$ vs. Gout.

the initiation of gout attacks (Dalbeth et al., 2021). Therefore, We mainly extract and isolate *Cordyceps militaris* extract, with cordycepin as the main active compound (Hu et al., 2015). Simultaneously, MSU-induced GA rat experiments were carried out to prove that CME (containing polysaccharide and cordycepin) effectively reduced the levels of IL-1 β , IL-6, TNF- α and Caspase-1 pro-inflammatory factors and increased IL-10 anti-inflammatory factors in GA rats. Combined with the pathological changes of rat HE-stained joints, it was proved that CME significantly alleviated the inflammatory process. Furthermore, our results showed that CME can relieve joint swelling and fever in the short term, and the effect of restoring foot function was significantly better than that of colchicine. Overall, CME has great potential for the treatment of acute GA caused by MSU.

However, components of CME are complex, and the mechanism of treating GA is difficult to explain. Therefore, we used transcriptomics to elucidate the potential mechanism of action of CME in the treatment of GA. Our study concluded that the GO enrichment analysis of DEGs mainly involved immune system processes and inflammatory responses, and the KEGG analysis of DEGs identified several signaling pathways of inflammation-related cytokines, mainly including TNF signaling pathway, cancer pathway, IL-17 signaling pathway and rheumatoid arthritis. The present study demonstrated that these pathways were involved in the inflammasome-induced inflammatory response, which in turn leads to gout, indicating that the transcriptomic analysis of this study is consistent with previous findings (Latz and Duewell, 2018;

Wree et al., 2018; Shin et al., 2019; Zhen and Zhang, 2019; Spel and Martinon, 2020). It was further found that the pathway after CME treatment in the KEGG analysis and the pathway of gout disease are involved in many of the same pathways to play their role, and the most influential one is the cytokine-cytokine-receptor interaction signaling pathway. To further dissect the mechanism of CME's anti-inflammatory effect on GA, we analyzed DEGs belonging to the cytokine-cytokine-receptor interaction signaling pathway. These four DEGs (CCL7, CSF2RB, LIF, and IL-1 β) were verified by RT-qPCR to promote the production and activation of inflammatory cytokines.

Inflammasomes aim for restoration of damage by initiating immune responses and repair mechanisms. When the activation of the inflammasome platform is unbalanced, its inflammatory effects can lead to arthritis (Spel and Martinon, 2020). We know that crystalline sodium urate is a damage-related molecule that can stimulate innate immune pathways and induce acute inflammatory responses, and the "inflammasome" is a core factor in activating inflammatory events (Martinon et al., 2002; Dinarello, 2019). Decreased levels of IL-1 β inhibit msu-induced activation of NLRP3 inflammatory vesicles, impede maturation and secretion of inflammatory cytokines, thereby reducing the recruitment of neutrophils and other cells and regulating immune disorders (Liu-Bryan et al., 2005; Bauernfeind et al., 2009). LIF is a pleiotropic cytokine that modulates autoimmune responses by increasing T-cell numbers and neutrophil accumulation, and disrupts the balance of inflammasome platform activation by stimulating the release of cytokines from multiple cells,

whose inflammatory effects lead to gout (Schainberg et al., 1988; Villiger et al., 1993; Janssens et al., 2015; Davis et al., 2018). LIF is induced in response to inflammatory stimuli of macrophages and switches macrophages from a pro-inflammatory phenotype to an anti-inflammatory phenotype. Further study LIF inhibits interferon gamma and granulocyte-macrophage colony stimulating factor (GM-CSF)-induced activation of STAT1 and STAT5 in macrophages, and inhibits macrophage motility through STAT3 and matrix metalloproteinase 9 (MMP9) (Hamelin-Morrisette et al., 2020). These pathways are mediated by ROS (Meier et al., 2017; Walter et al., 2020). MSU in turn activates NLRP3 inflammasome activity through ROS to produce IL-1 β (Tschopp and Schroder, 2010). Our data showed that the transcript levels of CCL7, CSF2RB, LIF and IL-1 β in MSU-induced GA rats were higher than those in normal rats, while the expression levels of these genes were significantly decreased after CME treatment. And RT-qPCR experiments verified the transcriptomic analysis. Therefore, we speculate that CME plays an important protective role in the regulation of inflammasome homeostasis during MSU-induced ventilation.

Inflammasomes are more commonly found in cells of myeloid origin, such as monocytes, macrophages, neutrophils, and dendritic cells. CCL7 is a chemokine that attracts monocytes and eosinophils, promotes the recruitment of many innate immune cell types, and thus mediates many inflammatory responses (Ben-Baruch et al., 1995). It is a chemokine that attracts monocytes and eosinophils and binds to CCR1, CCR2 and CCR3. Eosinophils are typical effector cells of allergic inflammation, and CCR3 mediates their migration to different chemokines to inflammation (Uguccioni et al., 1997). CCR2 potently regulates the recruitment of monocytes to sites of inflammation (Tsou et al., 2007). The CSF2RB is the common signaling subunit of the cytokine receptors for IL-3, IL-5, and GM-CSF (Croxford et al., 2015). It mediates IL-3, IL-5 and GM-CSF through cell surface receptors to stimulate eosinophil production, function and survival, thereby affecting inflammatory diseases (Begley et al., 1986; Lopez et al., 1986; Lopez et al., 1988; Rothenberg et al., 1988). Our results showed that CME treatment reduced the expression of inflammation-related genes and improved the inflammatory state of the joints of GA rats through the combination of cytokines and cytokines. In summary, CME treatment can effectively inhibit the inflammatory response of GA and modulate the interaction of inflammatory cytokines through CCL7, CSF2RB and IL-1 β . Compared with colchicine and non-steroidal anti-inflammatory drugs (NSAIDs), which have clinical side effects, CME it has the potential for further development. In addition, our study demonstrated for the first time the anti-inflammatory and analgesic effects of *Cordyceps militaris* on acute gouty arthritis, providing pioneering evidence for gout treatment.

5 Conclusion

In conclusion, the effect of CME in relieving acute GA has been confirmed, and its molecular mechanism may mainly involve the

cytokine-cytokine receptor interaction signaling pathway based on transcriptomic analysis and regulate inflammation through the levels of CCL7, CSF2RB and IL-1 β reaction.

Data availability statement

The data that support the findings of this study are available from the corresponding author, CJ, upon reasonable request.

Author contributions

The experiment was completed with the help of multiple authors. YX conceived and designed the work; YX and CJ coordinated technical support and funding; LL and HL performed the experiments and collected the samples; HL and LL acquired, analyzed, and interpreted the data; JC and SL participated in data collection and analysis. CJ, HL, and LL wrote the manuscript. All authors read and approved the final manuscript.

Funding

This work was supported by the International Scientific and Technological Cooperation Project of Guangzhou Development Zone(2020GH07) and Funding of Introducing Innovation and Entrepreneurship Team Project in Zhaoqing High-tech Zone(2019ZHQ10).

Acknowledgments

We gratefully thank all colleagues who participated in this experiment.

Conflict of interest

The authors declare that the research was conducted in the absence of any commercial or financial relationships that could be construed as a potential conflict of interest.

Publisher's note

All claims expressed in this article are solely those of the authors and do not necessarily represent those of their affiliated organizations, or those of the publisher, the editors and the reviewers. Any product that may be evaluated in this article, or claim that may be made by its manufacturer, is not guaranteed or endorsed by the publisher.

References

- Amaral, F. A., Costa, V. V., Tavares, L. D., Sachs, D., Coelho, F. M., Fagundes, C. T., et al. (2012). NLRP3 inflammasome-mediated neutrophil recruitment and hypernociception depend on leukotriene B(4) in a murine model of gout. *Arthritis Rheum.* 64 (2), 474–484. doi:10.1002/art.33355
- Andrés, M., Francés, R., and Pascual, E. (2015). SAT0328 uric acid enhances monosodium urate induced pro-inflammatory response in gouty patients: A basic and translational research study. *Ann. Rheum. Dis.* 74 (2), 777.2–8. doi:10.1136/annrheumdis-2015-eular.1958
- Bauernfeind, F. G., Horvath, G., Stutz, A., Alnemri, E. S., MacDonald, K., Speert, D., et al. (2009). Cutting edge: NF-kappaB activating pattern recognition and cytokine receptors license NLRP3 inflammasome activation by regulating NLRP3 expression. *J. Immunol.* 183 (2), 787–791. doi:10.4049/jimmunol.0901363
- Begley, C. G., Lopez, A. F., Nicola, N. A., Warren, D. J., Vadas, M. A., Sanderson, C. J., et al. (1986). Purified colony-stimulating factors enhance the survival of human neutrophils and eosinophils *in vitro*: A rapid and sensitive microassay for colony-stimulating factors. *Blood* 68 (1), 162–166. doi:10.1182/blood.v68.1.162.162
- Ben-Baruch, A., Xu, L., Young, P. R., Bengali, K., Oppenheim, J. J., and Wang, J. M. (1995). Monocyte chemoattractant protein-3 (MCP3) interacts with multiple leukocyte receptors. C-C CKR1, a receptor for macrophage inflammatory protein-1 alpha/Rantes, is also a functional receptor for MCP3. *J. Biol. Chem.* 270 (38), 22123–22128. doi:10.1074/jbc.270.38.22123
- Busso, N., and So, A. (2010). Mechanisms of inflammation in gout. *Arthritis Res. Ther.* 12 (2), 206. doi:10.1186/ar2952
- Cabău, G., Crișan, T. O., KlüCK, V., Popp, R. A., and Joosten, L. A. B. (2020). Urate-induced immune programming: Consequences for gouty arthritis and hyperuricemia. *Immunol. Rev.* 294 (1), 92–105. doi:10.1111/imr.12833
- Cavalcanti, N. G., Marques, C. D., Lins, E. L. T. U., Pereira, M. C., Rego, M. J. B. d. M., Duarte, A. L. B. P., et al. (2016). Cytokine profile in gout: Inflammation driven by IL-6 and IL-18? [J]. *Immunol. Invest.* 45 (5), 383–395. doi:10.3109/08820139.2016.1153651
- Chen, L., Liu, Y., Guo, Q., Zheng, Q., and Zhang, W. (2018). Metabolomic comparison between wild *Ophiocordyceps sinensis* and artificial cultured *Cordyceps militaris*. *Biomed. Chromatogr.* 32, e4279. doi:10.1002/bmc.4279
- Choi, H. N., Jang, Y. H., Kim, M. J., Seo, M. J., Kang, B. W., Jeong, Y. K., et al. (2014). *Cordyceps militaris* alleviates non-alcoholic fatty liver disease in ob/ob mice. *Nutr. Res. Pract.* 8 (2), 172–176. doi:10.4162/nrp.2014.8.2.172
- Coderre, T. J., and Wall, P. D. (1987). Ankle joint urate arthritis (AJUA) in rats: An alternative animal model of arthritis to that produced by Freund's adjuvant. *Pain* 28 (3), 379–393. doi:10.1016/0304-3959(87)90072-8
- Croxford, A. L., Lanzinger, M., Hartmann, F. J., Schreiner, B., Mair, F., Pelczar, P., et al. (2015). The cytokine GM-CSF drives the inflammatory signature of CCR2+ monocytes and licenses autoimmunity. *Immunity* 43 (3), 502–514. doi:10.1016/j.immuni.2015.08.010
- Dalbeth, N., Gosling, A. L., Gaffo, A., and Abhishek, A. (2021). Gout. *Lancet (London, Engl.)* 397 (10287), 1843–1855. doi:10.1016/S0140-6736(21)00569-9
- Dalbeth, N., Merriman, T. R., and Stamp, L. K. (2016). Gout. *Lancet (London, Engl.)* 388 (10055), 2039–2052. doi:10.1016/S0140-6736(16)00346-9
- Das, G., Shin, H. S., Leyva-Gómez, G., Gutierrez-Grijalva, E. P., Heredia, J. B., Nissapatorn, V., et al. (2020). Plants of the genus *Terminalia*: An insight on its biological potentials, pre-clinical and clinical studies. *Front. Pharmacol.* 11, 561248. doi:10.3389/fphar.2020.561248
- Davis, S. M., Collier, L. A., Winford, E. D., Leonardo, C. C., Ajmo, C. T., Foran, E. A., et al. (2018). Leukemia inhibitory factor modulates the peripheral immune response in a rat model of emergent large vessel occlusion. *J. Neuroinflammation* 15 (1), 288. doi:10.1186/s12974-018-1326-y
- Dinarello, C. A. (2019). The IL-1 family of cytokines and receptors in rheumatic diseases. *Nat. Rev. Rheumatol.* 15 (10), 612–632. doi:10.1038/s41584-019-0277-8
- Dinesh, P., and Rasool, M. (2017). Berberine, an isoquinoline alkaloid suppresses TXNIP mediated NLRP3 inflammasome activation in MSU crystal stimulated RAW 264.7 macrophages through the upregulation of Nrf2 transcription factor and alleviates MSU crystal induced inflammation in rats. *Int. Immunopharmacol.* 44, 26–37. doi:10.1016/j.intimp.2016.12.031
- Dubey, S. K., Chaturvedi, V. K., Mishra, D., Bajpeyee, A., Tiwari, A., and Singh, M. P. (2019). Role of edible mushroom as a potent therapeutics for the diabetes and obesity. *3 Biotech.* 9 (12), 450. doi:10.1007/s13205-019-1982-3
- Eleftheriou, G., Baci, G., Fiocchi, R., and Sebastiano, R. (2008). Colchicine-induced toxicity in a heart transplant patient with chronic renal failure. *Clin. Toxicol.* 46 (9), 827–830. doi:10.1080/15563650701779703
- Fan, W., Chen, S., Wu, X., Zhu, J., and Li, J. (2021). Resveratrol relieves gouty arthritis by promoting mitophagy to inhibit activation of NLRP3 inflammasomes. *J. Inflamm. Res.* 14, 3523–3536. doi:10.2147/JIR.S320912
- Galozzi, P., Bindoli, S., Doria, A., Oliviero, F., and Sfriso, P. (2021). Autoinflammatory features in gouty arthritis. *J. Clin. Med.* 10 (9), 1880. doi:10.3390/jcm10091880
- Gottlieb, M., Rabah, W., and Long, B. (2022). Colchicine for acute gout. *Acad. Emerg. Med.* 29 (3), 387–388. doi:10.1111/acem.14425
- Hamelin-Morrisette, J., Dallagi, A., Girouard, J., Ravelojaona, M., Oufqir, Y., Vaillancourt, C., et al. (2020). Leukemia inhibitory factor regulates the activation of inflammatory signals in macrophages and trophoblast cells. *Mol. Immunol.* 120, 32–42. doi:10.1016/j.molimm.2020.01.021
- Hu, H., Xiao, L., Zheng, B., Wei, X., Ellis, A., and Liu, Y. M. (2015). Identification of chemical markers in *Cordyceps sinensis* by HPLC-MS/MS. *Anal. Bioanal. Chem.* 407 (26), 8059–8066. doi:10.1007/s00216-015-8978-6
- Ichikawa, N., Taniguchi, A., Urano, W., Nakajima, A., and Yamanaka, H. (2011). Comorbidities in patients with gout. *Nucleosides Nucleic Acids* 30 (12), 1045–1050. doi:10.1080/15257770.2011.596499
- Janssens, K., Van Den Haute, C., Baekelandt, V., Lucas, S., van Horsen, J., Somers, V., et al. (2015). Leukemia inhibitory factor tips the immune balance towards regulatory T cells in multiple sclerosis. *Brain Behav. Immun.* 45, 180–188. doi:10.1016/j.bbi.2014.11.010
- Jayaprakash, V., Ansell, G., and Galler, D. (2007). Colchicine overdose: The devil is in the detail. *N. Z. Med. J.* 120 (1248), U2402.
- Ji, D. B., Ye, J., Li, C. L., Wang, Y. H., Zhao, J., and Cai, S. Q. (2009). Antiaging effect of *Cordyceps sinensis* extract. *Phytother. Res.* 23 (1), 116–122. doi:10.1002/ptr.2576
- Latz, E., and Duewell, P. (2018). NLRP3 inflammasome activation in inflammaging. *Semin. Immunol.* 40, 61–73. doi:10.1016/j.smim.2018.09.001
- Lee, C. T., Huang, K. S., Shaw, J. F., Chen, J. R., Kuo, W. S., Shen, G., et al. (2020). Trends in the immunomodulatory effects of *Cordyceps militaris*: Total extracts, polysaccharides and cordycepin. *Front. Pharmacol.* 11, 575704. doi:10.3389/fphar.2020.575704
- Liu, J., Yang, S., Yang, X., Chen, Z., and Li, J. (1997). Anticarcinogenic effect and hormonal effect of *Cordyceps militaris* Link. *Zhongguo Zhong yao za zhi = Zhongguo zhongyao zazhi = China J. Chin. materia medica* 22 (2), 111–113. inside back cover.
- Liu-Bryan, R., Scott, P., Sydlaske, A., Rose, D. M., and Terkeltaub, R. (2005). Innate immunity conferred by Toll-like receptors 2 and 4 and myeloid differentiation factor 88 expression is pivotal to monosodium urate monohydrate crystal-induced inflammation. *Arthritis Rheum.* 52 (9), 2936–2946. doi:10.1002/art.21238
- Lopez, A. F., Sanderson, C. J., Gamble, J. R., Campbell, H. D., Young, I. G., and Vadas, M. A. (1988). Recombinant human interleukin 5 is a selective activator of human eosinophil function. *J. Exp. Med.* 167 (1), 219–224. doi:10.1084/jem.167.1.219
- Lopez, A. F., Williamson, D. J., Gamble, J. R., Begley, C. G., Harlan, J. M., Klebanoff, S. J., et al. (1986). Recombinant human granulocyte-macrophage colony-stimulating factor stimulates *in vitro* mature human neutrophil and eosinophil function, surface receptor expression, and survival. *J. Clin. Invest.* 78 (5), 1220–1228. doi:10.1172/JCI112705
- Makoni, N. J., and Nichols, M. R. (2021). The intricate biophysical puzzle of caspase-1 activation [J]. *Archives Biochem. biophysics* 699, 108753.
- Martin, W. J., Walton, M., and Harper, J. (2009). Resident macrophages initiating and driving inflammation in a monosodium urate monohydrate crystal-induced murine peritoneal model of acute gout. *Arthritis Rheum.* 60 (1), 281–289. doi:10.1002/art.24185
- Martinon, F., Burns, K., and Tschopp, J. (2002). The inflammasome: A molecular platform triggering activation of inflammatory caspases and processing of proIL-beta. *Mol. Cell* 10 (2), 417–426. doi:10.1016/s1097-2765(02)00599-3
- Martinon, F., Pétrilli, V., Mayor, A., Tardivel, A., and Tschopp, J. (2006). Gout-associated uric acid crystals activate the NALP3 inflammasome. *Nature* 440 (7081), 237–241. doi:10.1038/nature04516
- Meier, J. A., Hyun, M., Cantwell, M., Raza, A., Mertens, C., Raj, V., et al. (2017). Stress-induced dynamic regulation of mitochondrial STAT3 and its association with cyclophilin D reduce mitochondrial ROS production. *Sci. Signal.* 10 (472), eaag2588. doi:10.1126/scisignal.aag2588
- Nan, J. X., Park, E. J., Yang, B. K., Song, C. H., Ko, G., and Sohn, D. H. (2001). Antifibrotic effect of extracellular biopolymer from submerged mycelial cultures of *Cordyceps militaris* on liver fibrosis induced by bile duct ligation and scission in rats. *Arch. Pharm. Res.* 24 (4), 327–332. doi:10.1007/BF02975101
- Panda, S. K., and Luyten, W. (2022). Medicinal mushrooms: Clinical perspective and challenges. *Drug Discov. Today* 27 (2), 636–651. doi:10.1016/j.drudis.2021.11.017
- Pillinger, M. H., Goldfarb, D. S., and Keenan, R. T. (2010). Gout and its comorbidities. *Bull. NYU Hosp. Jt. Dis.* 68 (3), 199–203.

- Pineda, C., Fuentes-Gómez, A. J., Hernández-Díaz, C., Zamudio-Cuevas, Y., Fernández-Torres, J., López-Macay, A., et al. (2015). Animal model of acute gout reproduces the inflammatory and ultrasonographic joint changes of human gout. *Arthritis Res. Ther.* 17 (1), 37. doi:10.1186/s13075-015-0550-4
- Ragab, G., Elshahaly, M., and Bardin, T. (2017). Gout: An old disease in new perspective - a review. *J. Adv. Res.* 8 (5), 495–511. doi:10.1016/j.jare.2017.04.008
- Rahimi-Sakak, F., Maroofi, M., Rahmani, J., Bellissimo, N., and Hekmatdoost, A. (2019). Serum uric acid and risk of cardiovascular mortality: A systematic review and dose-response meta-analysis of cohort studies of over a million participants. *BMC Cardiovasc. Disord.* 19 (1), 218. doi:10.1186/s12872-019-1215-z
- Richette, P., and Bardin, T. (2008). Should prednisolone be first-line therapy for acute gout? [J]. *Lancet (London, Engl.)* 372 (9646), 1301–1302. ; author reply -2. doi:10.1016/S0140-6736(08)61548-2
- Roberts, W. N., Liang, M. H., and Stern, S. H. (1987). Colchicine in acute gout: Reassessment of risks and benefits [J]. *Jama* 257 (14), 1920–1922. doi:10.1001/jama.1987.03390140090033
- Rothenberg, M. E., Owen, W. F., JR., Silberstein, D. S., Woods, J., Soberman, R. J., Austen, K. F., et al. (1988). Human eosinophils have prolonged survival, enhanced functional properties, and become hypodense when exposed to human interleukin 3. *J. Clin. Invest.* 81 (6), 1986–1992. doi:10.1172/JCI113547
- Rowczenio, D. M., Gomes, S. M., Aróstegui, J. I., Mensa-Vilaro, A., Omoyinmi, E., Trojer, H., et al. (2017). Late-onset cryopyrin-associated periodic syndromes caused by somatic NLRP3 mosaicism-UK single center experience. *Front. Immunol.* 8, 1410. doi:10.3389/fimmu.2017.01410
- Schainberg, H., Borish, L., and Rocklin, R. E. (1988). Potentiation of neutrophil aggregation by human leukocyte inhibitory factor. *Inflammation* 12 (3), 203–211. doi:10.1007/BF00920072
- Shin, M., Cho, S., Kim, T. H., Park, S., Jeon, B. Y., Jeong, H., et al. (2019). Inflammasomes and autoimmune and rheumatic diseases: A comprehensive review. *J. Autoimmun.* 103, 102299. doi:10.1016/j.jaut.2019.06.010
- Singh, R., Negi, P. S., and Ahmed, Z. (2009). Genetic variability assessment in medicinal caterpillar fungi *Cordyceps* spp. (ascomycetes) in central himalayas. *Int. J. Med. Mushrooms* 11 (2), 185–189. doi:10.1615/intjmedmushr.v11.i2.70
- Son, C.-N., Bang, S.-Y., Kim, J. H., Choi, C. B., Kim, T. H., and Jun, J. B. (2013). Caspase-1 level in synovial fluid is high in patients with spondyloarthropathy but not in patients with gout. *J. Korean Med. Sci.* 28 (9), 1289–1292. doi:10.3346/jkms.2013.28.9.1289
- Spel, L., and Martinon, F. (2020). Inflammasomes contributing to inflammation in arthritis. *Immunol. Rev.* 294 (1), 48–62. doi:10.1111/imr.12839
- Sung, G. H., Hywel-Jones, N. L., Sung, J. M., Luangsa-Ard, J. J., Shrestha, B., and Spatafora, J. W. (2007). Phylogenetic classification of *Cordyceps* and the clavicipitaceous fungi. *Stud. Mycol.* 57, 5–59. doi:10.3114/sim.2007.57.01
- Tan, L., Song, X., and Ren, Y. (2020). Anti-inflammatory effects of cordycepin: A review [J]. *Phytotherapy Res. PTR* 2020, 1–14. doi:10.1002/ptr.6890
- Tschopp, J., and Schroder, K. (2010). NLRP3 inflammasome activation: The convergence of multiple signalling pathways on ROS production? [J]. *Nat. Rev. Immunol.* 10 (3), 210–215. doi:10.1038/nri2725
- Tsou, C. L., Peters, W., Si, Y., Slaymaker, S., Aslanian, A. M., Weisberg, S. P., et al. (2007). Critical roles for CCR2 and MCP-3 in monocyte mobilization from bone marrow and recruitment to inflammatory sites. *J. Clin. Invest.* 117 (4), 902–909. doi:10.1172/JCI29919
- Uguccioni, M., Mackay, C. R., Ochensberger, B., Loetscher, P., RhiS, S., LaRosa, G. J., et al. (1997). High expression of the chemokine receptor CCR3 in human blood basophils. Role in activation by eotaxin, MCP-4, and other chemokines. *J. Clin. Invest.* 100 (5), 1137–1143. doi:10.1172/JCI119624
- Villiger, P. M., Geng, Y., and Lotz, M. (1993). Induction of cytokine expression by leukemia inhibitory factor. *J. Clin. Invest.* 91 (4), 1575–1581. doi:10.1172/JCI116363
- Walter, L., Canup, B., Pujada, A., Bui, T. A., Arbasi, B., Laroui, H., et al. (2020). Matrix metalloproteinase 9 (MMP9) limits reactive oxygen species (ROS) accumulation and DNA damage in colitis-associated cancer. *Cell Death Dis.* 11 (9), 767. doi:10.1038/s41419-020-02959-z
- Wang, Y., and Zhang, H. (2021). Advances in the extraction, purification, structural-property relationships and bioactive molecular mechanism of flammulina velutipes polysaccharides: A review. *Int. J. Biol. Macromol.* 167, 528–538. doi:10.1016/j.ijbiomac.2020.11.208
- Wree, A., McGeough, M. D., Inzaugarat, M. E., Eguchi, A., Schuster, S., Johnson, C. D., et al. (2018). NLRP3 inflammasome driven liver injury and fibrosis: Roles of IL-17 and TNF in mice. *Hepatology* 67 (2), 736–749. doi:10.1002/hep.29523
- Yang, J., Zhou, Y., and Shi, J. (2020). Cordycepin protects against acute pancreatitis by modulating NF-κB and NLRP3 inflammasome activation via AMPK. *Life Sci.* 251, 117645. doi:10.1016/j.lfs.2020.117645
- Yong, T., Chen, S., Xie, Y., Chen, D., Su, J., Shuai, O., et al. (2018). Cordycepin, a characteristic bioactive constituent in cordyceps militaris, ameliorates hyperuricemia through URAT1 in hyperuricemic mice. *Front. Microbiol.* 9 (58), 1410. doi:10.3389/fmicb.2018.00058
- Yong, T., Zhang, M., Chen, D., Shuai, O., Chen, S., Su, J., et al. (2016). Actions of water extract from *Cordyceps militaris* in hyperuricemic mice induced by potassium oxonate combined with hypoxanthine. *J. Ethnopharmacol.* 194, 403–411. doi:10.1016/j.jep.2016.10.001
- Zhan, Y., Dong, C.-H., and Yao, Y.-J. (2006). Antioxidant activities of aqueous extract from cultivated fruit-bodies of *Cordyceps militaris* (L.) link *in vitro*. *J. Integr. Plant Biol.* 48 (11), 1365–1370. doi:10.1111/j.1744-7909.2006.00345.x
- Zhang, J., Wen, C., Duan, Y., Zhang, H., and Ma, H. (2019). Advance in cordyceps militaris (linn) link polysaccharides: Isolation, structure, and bioactivities: A review. *Int. J. Biol. Macromol.* 132, 906–914. doi:10.1016/j.ijbiomac.2019.04.020
- Zhen, Y., and Zhang, H. (2019). NLRP3 inflammasome and inflammatory bowel disease. *Front. Immunol.* 10, 276. doi:10.3389/fimmu.2019.00276



OPEN ACCESS

EDITED BY

Xiande Ma,
Liaoning University of Traditional
Chinese Medicine, China

REVIEWED BY

Yanwu Li,
Guangzhou University of Chinese
Medicine, China
Senling Feng,
Third Affiliated Hospital of Guangzhou
Medical University, China

*CORRESPONDENCE

Wei Liu,
liuweiolina@163.com
Dan Lou,
loudan81@163.com

SPECIALTY SECTION

This article was submitted to
Ethnopharmacology,
a section of the journal
Frontiers in Pharmacology

RECEIVED 30 September 2022

ACCEPTED 11 October 2022

PUBLISHED 21 October 2022

CITATION

Qiao L-M, Zhang H, Liu W and Lou D
(2022), Therapeutic effect and
metabolomics mechanism of *Patrinia
Villosa* (Thunb.) juss on liver injury in rats.
Front. Pharmacol. 13:1058587.
doi: 10.3389/fphar.2022.1058587

COPYRIGHT

© 2022 Qiao, Zhang, Liu and Lou. This is
an open-access article distributed
under the terms of the [Creative
Commons Attribution License \(CC BY\)](#).
The use, distribution or reproduction in
other forums is permitted, provided the
original author(s) and the copyright
owner(s) are credited and that the
original publication in this journal is
cited, in accordance with accepted
academic practice. No use, distribution
or reproduction is permitted which does
not comply with these terms.

Therapeutic effect and metabolomics mechanism of *Patrinia Villosa* (Thunb.) juss on liver injury in rats

Li-Man Qiao¹, Hui Zhang¹, Wei Liu^{2*} and Dan Lou^{1*}

¹The Second Affiliated Hospital and Yuying Children's Hospital of Wenzhou Medical University, Wenzhou, China, ²School of Pharmaceutical Science, Liaoning University, Shenyang, China

Patrinia villosa (Thunb.) Juss (P.V) is widely used in the treatment of chronic diseases, such as appendicitis, enteritis and gynecological inflammation. Modern research indicated that the herb has pharmacological effect on liver injury caused by inflammation, but the metabolomics mechanism is not clear. For the purpose of discovering the therapeutic effect and metabolomic mechanism of P.V on liver injury, 40 Sprague-Dawley (SD) rats were divided into normal group, model group, and P.V groups (0.98, 1.97, and 2.96 g/kg). The model group and P.V groups were injected intraperitoneally with 40% CCl₄ (v/v, olive oil) to establish liver injury model. After administration of P.V for seven consecutive days. Therapeutic effect of P.V on liver injury rats were analyzed. P.V could decrease serum alanine aminotransferase (ALT) and aspartate aminotransferase (AST) levels of liver injury rats as a dose-dependent manner. Compared with the model group, the pathological analysis of liver tissue of P.V groups exhibit significant decrease tendency of hepatic tissue structure destruction, cytoplasmic vacuolation, cellular swelling, and inflammatory cell infiltration as a dose-dependent manner. 82 endogenous metabolites in rat serum and liver were analyzed by Ultra-high performance liquid chromatography tandem mass spectrometry (UPLC-MS/MS). 14 metabolites in serum and 26 metabolites in liver were significantly different between the P.V group (2.96 g/kg) and the model group. Metabolic pathway analysis revealed that the main pathway including alanine, aspartate and glutamate metabolism, and TCA cycle were significantly altered. It is suggested that P.V can alleviate CCl₄ induced liver injury, and its effect on metabolites may be an important mechanism of action.

KEYWORDS

Patrinia villosa (Thunb.) juss, liver injury, inflammation, metabolism, UPLC-MS

1 Introduction

The liver is an important metabolic organ of the human body. It mainly has the physiological functions of storing glycogen, decomposing blood sugar, and participating in the metabolism of protein, fat, vitamins and hormones (Wu et al., 2017a). The liver not only regulates metabolism, but also has the function of detoxification, phagocytosis and defense against foreign toxic substances (Mega et al., 2021; Qian et al., 2021). The extensive application of toxic chemicals, drugs, alcohol, dietary supplements and food additives may cause liver injury (Yang et al., 2017). Liver cell injury will cause inflammatory reaction, oxidative stress, fat-like changes, and then a series of pathological changes such as liver cell necrosis, apoptosis and fibrosis (Navarro et al., 2017; Kong et al., 2021).

Liver injury progresses to the stage of liver failure, which has clinical manifestations such as fatigue, anorexia, abdominal fullness and loose stools (Wang et al., 2021). It is often delayed due to insufficient attention, and severe cases can even cause liver failure and endanger life (Jaeschke et al., 2012). Poor prognosis after liver injury have always been a problem in the medical community (Khemichian et al., 2021). In modern medicine, symptomatic treatment is often used clinically to treat liver injury (Navarro et al., 2017). At the same time of treatment, it lacks comprehensive consideration of systemic pathological state, which will cause harm to the body (Sun et al., 2014).

Patrinia villosa (Thunb.) Juss (P.V) is a traditional Chinese medicine which is commonly used in the treatment of chronic inflammation diseases, such as intestinal carbuncle, pulmonary carbuncle, dysentery, postpartum petechial abdominal pain, and carbuncle (Huang et al., 2022). Modern medical research has found that the herb has various pharmacological activities such as anti-inflammatory, sedative and hypnotic, anti-viral, anti-tumor, liver-protecting, and immunity-enhancing actions (Zheng et al., 2012; Li et al., 2016; Sheng et al., 2019), but its mechanism of liver-protection action has not been reported.

Chemical investigation indicated that saponins, flavonoids, coumarins, cycloethenes terpenoids, lignans, and volatile oils are the main active ingredients of P.V (Peng et al., 2005; Xiang et al., 2016; Xin-Jia et al., 2016; Yang et al., 2016). P.V can inhibit the hepatitis virus, improve liver function, and promote hepatocyte regeneration and bile secretion (Liao et al., 2012; Dai et al., 2013). Previous study indicated apigenin in P.V could inhibit hepatocellular carcinoma cell growth by CyclinD1/CDK4 regulation via p38 MAPK-p21 signaling (Li et al., 2016). In this study, the therapeutic effect of P.V on liver injury was studied, and the metabolic mechanism was analyzed by UPLC-MS/MS.

2 Materials and methods

2.1 Materials and reagents

Patrinia villosa (Thunb.) Juss was obtained from Xinqi Traditional Chinese Medicine Pellets Co., Ltd (Hebei, China), and the herb was identified by Dr. Jian Wu from Harbin University of Commerce. A voucher specimen (No. PVJ20130821) was deposited at the Pharmacognosy Laboratory of Liaoning University. L-tryptophan (Try), L-kynurenine (Kyn), Oxidized glutathione (GSSG), N-phenylacetyl glycine (N-Phe), 5-hydroxytryptophan (5-HTP), L-leucine (Leu), 5-HT, cholic acid (CA), and Glutathione (GSH) were obtained from Dalian Melon Biology Technology Co., N-Ethylmaleimide (NEM) and formic acid were purchased from Sigma-Aldrich Chemical Co., PBS buffer was obtained from Hyclone Chemical Co., Internal standard (L-phenylalanine-*d*₅, *d*₅-Phe) was obtained from Cambridge isotope laboratories. All standard stock solutions were stored at -40 °C before use. Methanol and acetonitrile were purchased from ACS Chemical Co.

2.2 Preparation of *Patrinia villosa* (Thunb.) Juss extract

960 g of P.V was refluxed with 9.6 L of distilled water for 1.5 h, before being cooled, the supernatant was filtered and concentrated under reduced pressure gave extract residue of 90.29 g. Samples were stored at 4°C in a refrigerator before use.

2.3 Animals and treatments

A total of 40 male Sprague-Dawley rats, weighing about 200 ± 20 g, were divided into five groups (*n* = 8) including normal group, model group and P.V groups with three dosages (0.98, 1.97, and 2.96 g/kg). After 2 weeks of adaptive feeding, the P.V groups and model group were injected intraperitoneally with 40% CCl₄ (v/v, olive oil) at the dose 2 ml/kg (Wang et al., 2021). P.V groups were intragastric administered once daily for 7 days, the normal group and model group were intragastric administered with the same volume of saline once daily for 7 days. All the rats were anesthetized with sodium pentobarbital intraperitoneally 2 h after administration on the seventh day and blood samples were collected from the abdominal aorta and exposed to laparotomy. Blood was collected in a non-anticoagulant tube, and serum was collected after centrifugation at 3,500 rpm and 4 °C for 10 min. Rat livers were washed with normal saline after routine sampling and then fixed in formalin solution for the preparation of pathological sections of liver tissue. The

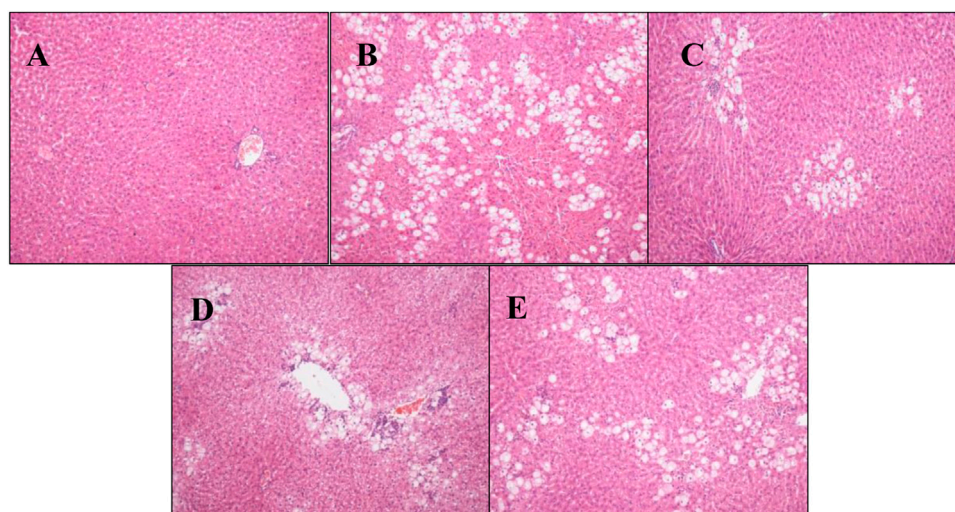


FIGURE 1
Pathological analysis results of rat liver tissue (H-E staining, $\times 100$) (A) Blank group (B) Model group (C) P.V group (2.96 g/kg) (D) P.V group (1.97 g/kg) (E) P.V group (0.98 g/kg).

histopathological changes in the rat livers were observed by microscope after HE staining.

2.4 Metabolic analysis

Metabolic analysis was performed according to the previous report with minor modification (Wang et al., 2022). In this study, 82 endogenous metabolites involved in oxidative stress, inflammation, amino acid metabolism, purine metabolism, the tricarboxylic acid cycle, glycolysis, and lipid metabolism were selected as targets.

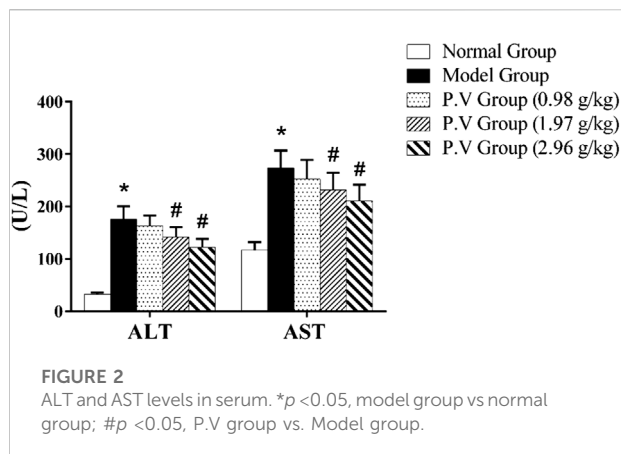
For the preparation of stripped serum, 1.8 g of activated carbon powder was added to 30 ml of rat serum. After mixing in a shaker for 2 h, the mixture was centrifuged at 13,500 rpm for 20 min at 4°C. The supernatant was collected and filtered with Millipore express PES membranes (Merck Millipore, Ltd.) in order of 5, 1.2, 0.45 and 0.22 μm , respectively, to prepare the stripped serum samples.

For the preparation of standard solutions, L-tryptophan (Try), L-kynurenine (Kyn), oxidized glutathione (GSSG), N-phenylacetylglutamine (N-Phe), 5-hydroxytryptophan (5-HTP), L-leucine (Leu), 5-HT and cholic acid (CA) were dissolved in methanol and prepared to a final concentration of 1 mg/ml. Glutathione (GSH) was dissolved in 10 mM of NEM PBS buffer to a final concentration of 0.5 mg/ml. All standard stock solutions were stored at -40°C and protected from light. L-phenylalanine- d_5 (d_5 -Phe) was used as the internal standard, and a 10 ng/ml stock solution was prepared in methanol and stored at -40°C. The components were mixed, and distilled water was used to prepare

standard curve solutions and diluted with 50% methanol-water to prepare a series of standard solutions. Because of the degradability of the GSH component, to ensure its quantitative assay accuracy and its component stability, GSH was derivatized with the reaction of NEM and GSH at an NEM concentration of 50 mM (Carretero et al., 2014; Younossi et al., 2016; Wang et al., 2022).

200 μL of PBS solution containing 10 mM of NEM and 1,200 μL of methanol (containing 10 ng/ml of d_5 -Phe) was added to 200 μL of serum in the tube and incubated at -20°C for 20 min. After vortex mixing, centrifugation was performed at 13,500 rpm and 4°C for 15 min 1,000 μL of supernatant were collected and blown dry by nitrogen to obtain samples. Samples were reconstituted with 50 μL of 5% acetonitrile (ACN) in water and centrifuged at 13,500 rpm and 4°C for 15 min. Then, 30 μL of the supernatant was pipetted into a sample tube for metabolic analysis.

0.2 g of liver tissue was weighted precisely, and 10 times the volume of normal saline were added in a centrifuge tube and homogenized, then the samples were centrifuged at 12,000 rpm for 15 min 100 μL of PBS solution containing 10 mM of NEM and 800 μL of methanol (containing 10 ng/ml of d_5 -Phe) was added to 100 μL of supernatant in the tube and incubated at -20°C for 20 min. After vortex mixing, centrifugation was performed at 13,500 rpm and 4°C for 15 min 800 μL of supernatant were collected and blown dry by nitrogen to obtain samples. Samples were reconstituted with 50 μL of 5% acetonitrile (ACN) in water and centrifuged at 13,500 rpm and 4°C for 15 min. Then, 30 μL of the supernatant was pipetted into a sample tube for metabolic analysis.



Metabolic analysis was performed on an AB4000Q TRAP LC/MS/MS mass spectrometer with deuterated internal standards (IS) (Phe- d_5) as the internal standard. The column used was Waters X Bridge™ BEH C18 2.5 μ m, 3.0 \times 100 mm. Positive and negative ions were quantified and semi-quantified using an ESI ion source detector. UPLC was performed using 0.1% formic acid-water (A) and acetonitrile (B) as elution systems. The gradient separation conditions were 0–2 min, 5% (B); 2–5 min, 5–50% (B); 5–6 min, 50% (B); 6–17 min, 50–95% (B); 17–18 min, and 95%–5% (B). The injection volume was 10 μ L and flow rate was 0.3 ml/min. Sample detecting were in an MRM mode with positive and negative model. Curtain gas (CUR): 10; collision gas (CAD): Medium; ion spray voltage: The Ion Spray voltage: ± 4500 V; Temperature: 450°C; ion source gas (GS1): 40; ion source gas (GS2): 40.

2.4.1 Methodology validation

Methodology validation was conducted in accordance with the “Guidance for Industry-Bio analysis Method Validation” (Food and Drug Administration, September 2013) issued by the United States Food and Drug Administration. A mixed standard solution of GSH, L-tryptophan, L-kynurenine, GSSG, N-phenylacetylglutamine, 5-HTP, L-leucine, 5-HT, and cholic acid

was prepared and diluted successively to prepare two solutions at each concentration. The standard curve was calculated by the ratio of the peak area of the sample to the area of the internal standard sample, and the least-squares method with 1/x weight were used to fit the linear regression equation of the standard curve.

2.4.2 Precision and accuracy assay

The assay precision of the UPLC-MS method was analyzed using quality control (QC) samples, and the QC samples were assayed using untreated rat serum to determine the intraday and interday precision.

High, medium and low concentration QC samples were prepared by adding standard solutions of L-tryptophan, L-kynurenine, GSSG, N-phenylacetylglutamine, 5-HTP, L-leucine, 5-HT, cholic acid, and GSH-NEM to stripped plasma. The stability of the method was evaluated by calculating the sample concentration according to the sample test content calculation method.

2.4.3 Data analysis

The MS analysis was performed by the software of Analyst (1.6.4). The standard curve method was used to measure the ratio of the peak area (Area ratio) of the sample to the internal standard. The least-squares method with 1/x weight was used to fit the standard curve linear regression equation. For test metabolites where no standard exists, a semi-quantitative analysis was performed to evaluate the change trend of the same test component based on the ratio of the peak area of the test sample to the area of the internal standard.

2.4.4 Metabolic pathway analysis

Pattern discrimination analysis was performed on each group of relevant data using the principal component analysis (PCA) method with SIMCA-P software. Based on the differential metabolites, serum metabolite profiles were analyzed using the The Human Metabolome Database (HMDB) and Kyoto

TABLE 1 Calibration curves of the nine metabolites.

Metabolites	Calibration curve	R ²	Linearity range
GSH	$Y = 0.0001X - 0.0065$	0.9995	100–10000 ng/ml
GSSG	$Y = 0.0022X + 0.3209$	0.9981	200–20000 ng/ml
L-Leucine	$Y = 0.0279X + 2.4351$	0.9983	100–10000 ng/ml
L-Kynurenine	$Y = 0.0347 X + 0.0147$	0.9980	5–500 ng/ml
L-Tryptophan	$Y = 0.0017 X + 0.8435$	0.9921	600–60000 ng/ml
5-HTP	$Y = 0.0891X - 0.0088$	0.9919	0.2–20 ng/ml
Cholic acid	$Y = 0.00005 X - 0.0009$	0.9932	40–4000 ng/ml
5-HT	$Y = 0.0505 X + 0.001$	0.9986	0.8–80 ng/ml
N-phenylacetylglutamine	$Y = 0.0154X + 4.1334$	0.9932	250–25000 ng/ml

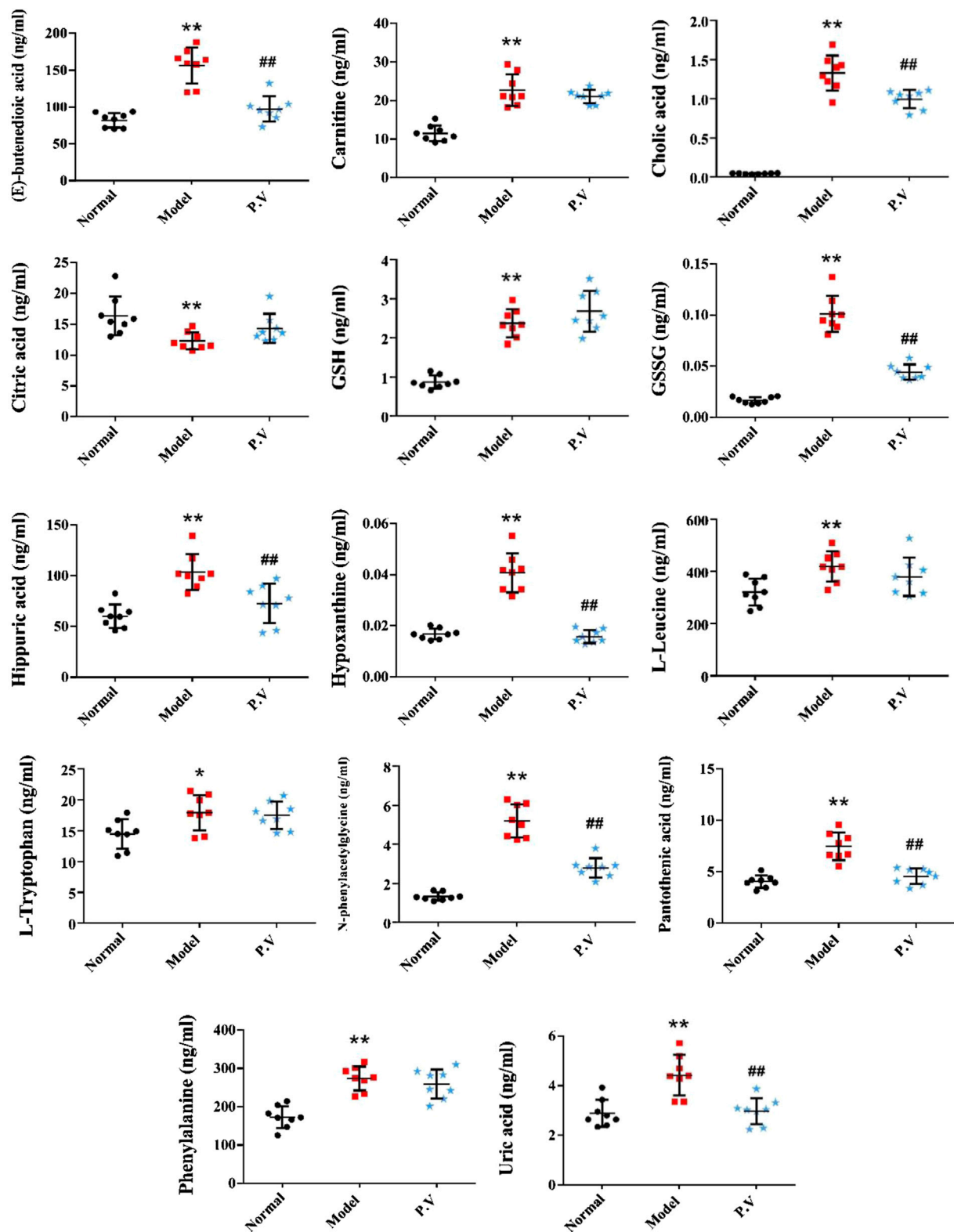
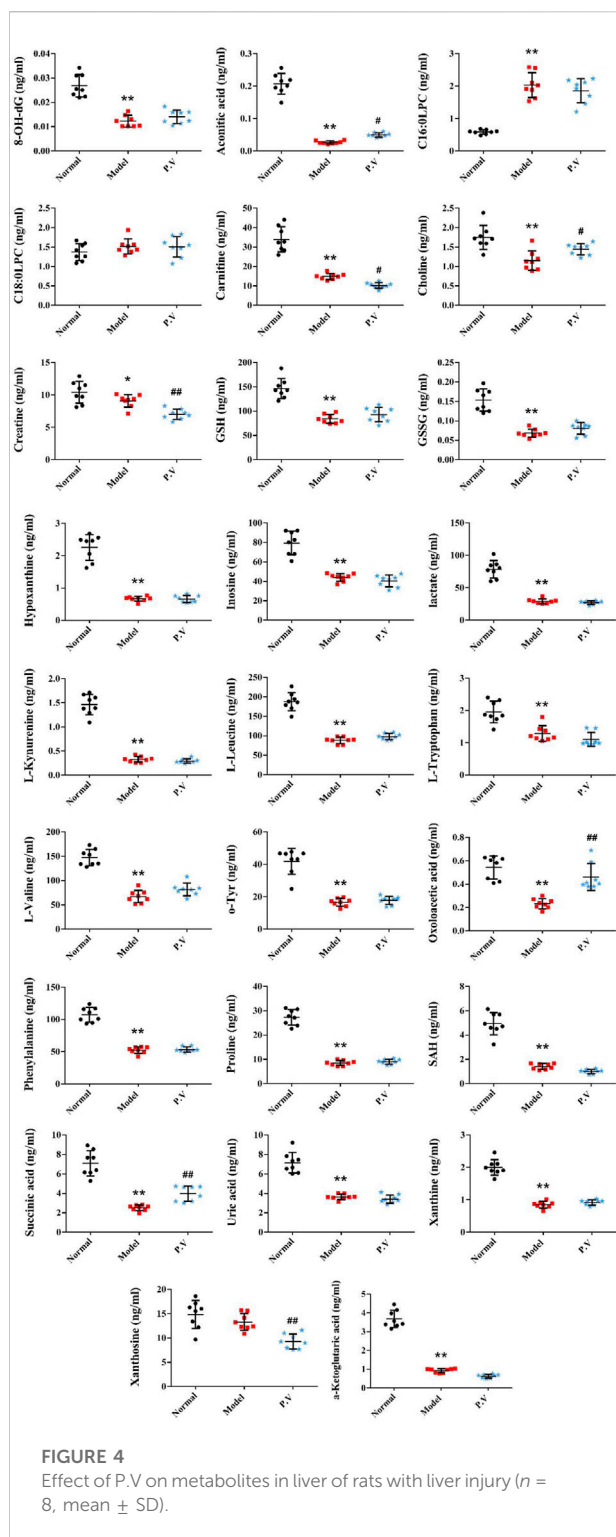


FIGURE 3
Effect of P.V. on metabolites in serum of rats with liver injury ($n = 8$, mean \pm SD).



Encyclopedia of Genes and Genomes (KEGG)-related metabolomics databases to identify the metabolic pathways associated with the prevention of CCl_4 -induced liver injury in rats.

2.5 Statistics analysis

The statistical analysis was performed using SPSS 17.0. ALT, AST, and the metabolites contents were described by means and standard deviations (Mean \pm SD). ALT and AST levels were compared between groups by t-tests. $p < 0.05$ was taken as a statistically significant.

3 Results

3.1 Protect effect of P.V on liver injury

3.1.1 Histopathological analysis

In terms of the gross anatomical appearance, the adhesion condition of the liver to peritoneum and intestine was severe in the model group, no adhesion condition was found in the normal group, and the adhesion degree was lower in the P.V groups.

Pathological analysis of rat liver tissue sections showed that the structure of rat liver tissues in the normal group was intact and clear, the cell morphology was regular, and no necrosis and inflammatory cell infiltration were observed. In the model group, the liver tissue structure was severely damaged, the cells were swollen and denatured, cytoplasmic vacuolation was observed, and inflammatory cell infiltration was observed to different degrees. Compared with the model group, hepatic tissue structure destruction, cytoplasmic vacuolation, and cellular swelling significantly decreased, and inflammatory cell infiltration decreased, in the P.V groups. The injury level tended to decrease as the dose dependant manner (Figure 1), which was consistent with the changes in ALT and AST levels.

3.1.2 ALT and AST in serum

Compared with the normal group, the levels of ALT and AST in the model group were significantly higher ($p < 0.01$), indicating that the model of CCl_4 -induced liver injury was successful. The levels of ALT and AST in P.V groups decreased compared with those in the model group as a dose-dependent manner, indicating that P.V could reduce the levels of ALT and AST in the serum of rats with liver injury to a different extent and play a liver-protective role in liver injury (Figure 2).

3.2 Metabolic analysis

3.2.1 Linearity

The linear regression equation of the standard curve was fitted using the least-squares method and $1/x$ weighting, using the concentration of the metabolites as the horizontal coordinate and the ratio of the peak area of the detected component to the internal standard component as the vertical coordinate (Table 1).

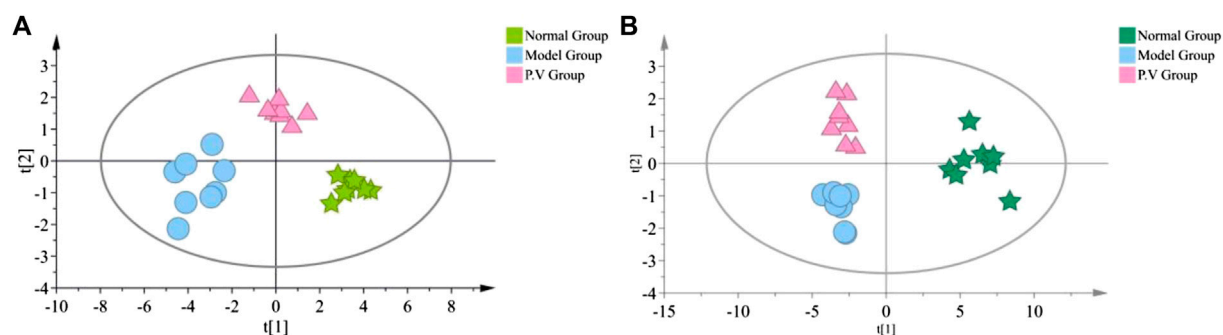


FIGURE 5
PCA analysis of metabolites (A) Serum (B) liver.

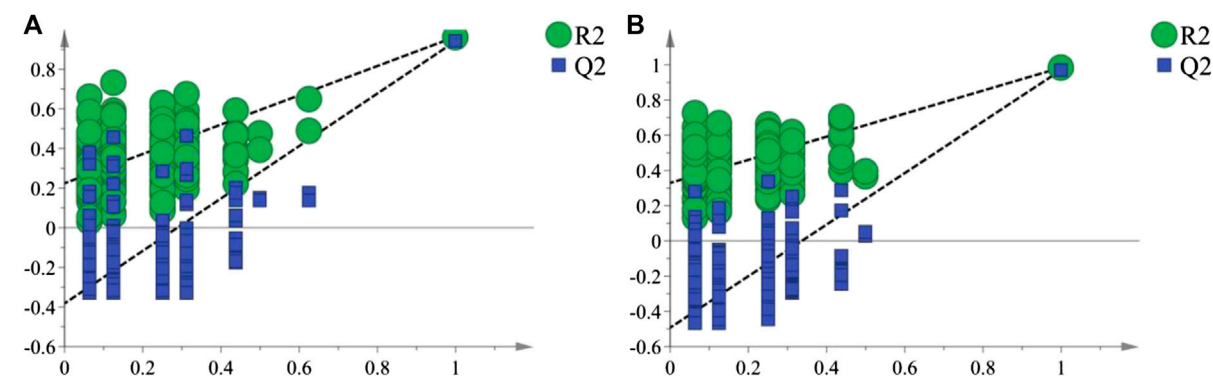


FIGURE 6
P-test analysis of the metabolites (A) Serum (B) liver.

3.2.2 Accuracy and precision

The results indicate that the accuracy and precision of the method was appropriate for all study samples. Precision analysis of GSH, GSSG, L-Leu, L-Try, L-Kyn, 5-HTP, cholic acid, 5-HT, and N-phenylacetyl glycine indicated that the intra-day precision of each metabolite ranged from 2.35% to 4.19%, and the inter-day precision ranged from 2.76% to 4.82%. All the values of these parameters were less than 5% which had satisfactory results within the acceptable criteria.

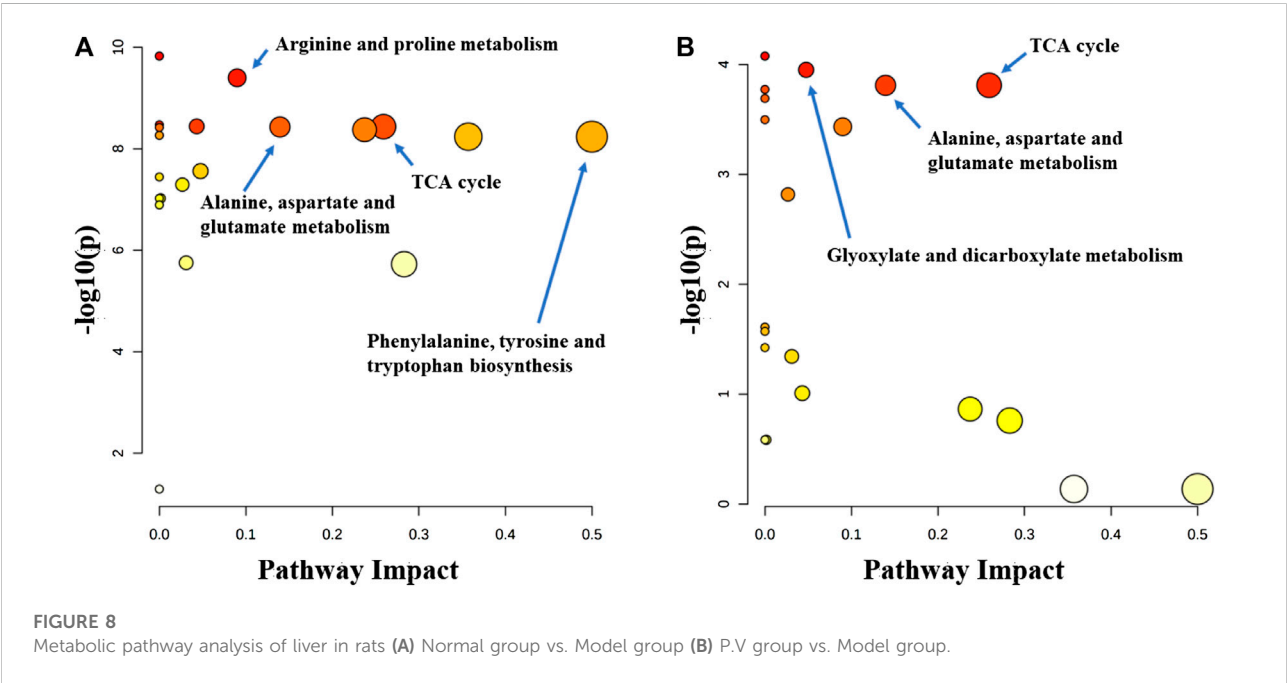
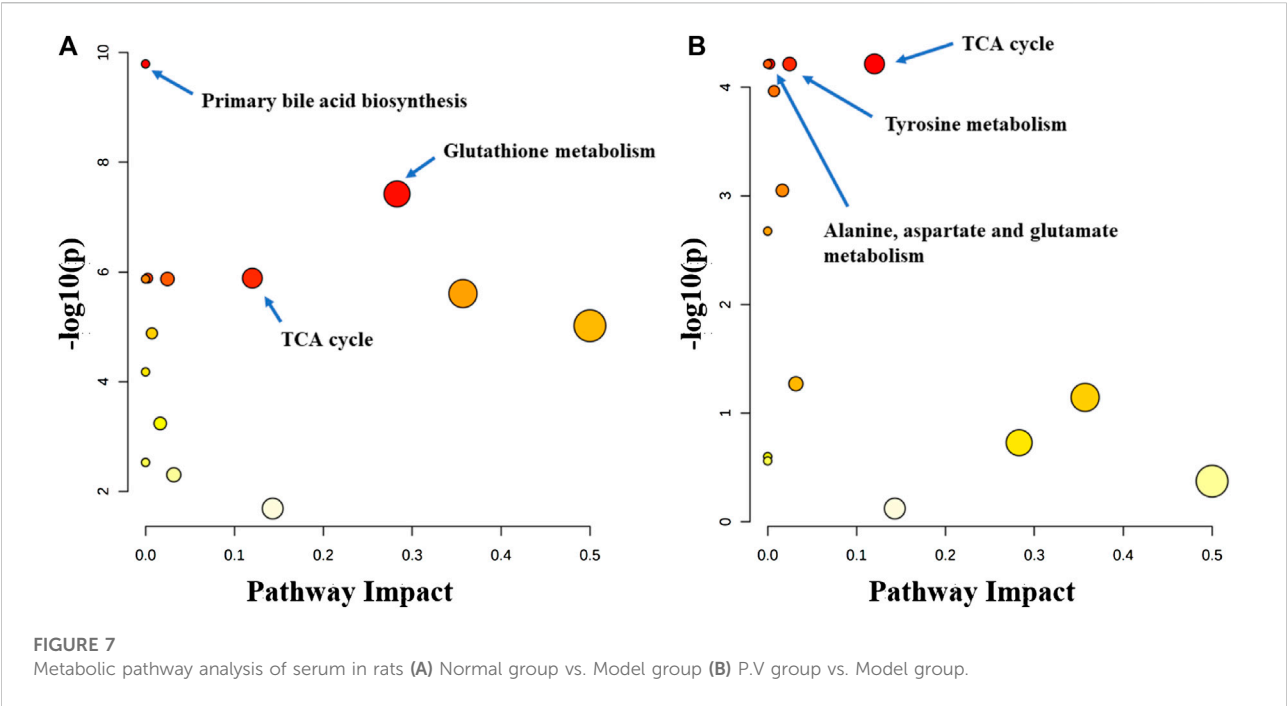
3.2.3 UPLC-MS/MS analysis

On the basis of establishing a stable and reliable method for the determination of metabolites by UPLC-MS/MS, 82 metabolites were simultaneously determined in normal group, model group, and P.V group (2.96 g/kg). We then compared the differences of 14 metabolites in serum (Figure 3) and 26 metabolites in liver (Figure 4) between the groups by combining the chromatograms with the relative standard deviation (RSD%) of the content of each component

within the same group, which was less than 30%. The results indicated that there were significant changes in metabolites in the serum samples of the model group, and there were multiple related differential metabolites that could be differentiated between the normal group and the model group. The GSH/GSSG ratio decreased significantly in the model group compared with that in normal group, which was consistent with the decrease in the antioxidant capacity in the model group. The levels of phenylalanine and citric acid in the model group were significantly lower than those in the normal group, and the levels of phenylalanine and citric acid in the model group recovered to the level of the normal group after treatment. The levels of L-leucine, cholic acid, N-phenylacetyl glycine, hippuric acid, carnitine, and hypoxanthine in the model group were significantly higher than those in the normal group.

3.2.4 Pathway analysis

As shown in the PCA analysis (Figure 5), the serum samples (Figure 5A) and liver samples (Figure 5B) of the



normal group and model group were distributed in different regions and far away from each other, and the same group showed an obvious aggregation trend, indicating the

difference in metabolite content between the normal group and model group. This further confirmed the success of the model of liver injury and also suggested that P.V could

significantly adjust the biomarker content in the serum and liver of rats with liver injury, causing an obvious change in the metabolic network. P-test analysis also showed that the different components tested were replaced to ensure that there was no overfitting in the between-group separation models (Figure 6).

Metabolic pathway analysis indicated that primary bile acid biosynthesis, glutathione metabolism, and TCA cycle were the most important metabolic pathway affected in the serum of the normal group vs. model group (Figure 7A). The alanine, aspartate and glutamate metabolism, TCA cycle, and tyrosine metabolism pathways were significantly affected by the administration of the P.V (Figure 7B). While in the liver tissue, arginine and proline metabolism, TCA cycle, alanine, aspartate and glutamate metabolism, Phenylalanine, tyrosine and tryptophan biosynthesis were the most important metabolic pathway affected in the normal group vs. model group (Figure 8A). Alanine, aspartate and glutamate metabolism, TCA cycle, glyoxylate and dicarboxylate metabolism pathways were significantly affected by the administration of P.V (Figure 8B).

4 Discussion

In this study, the liver injury induced by CCl_4 was improved by P.V. Further, the elevation of serum ALT and AST in the rat model was reversed, the liver histological damage was alleviated to a certain extent, and the effect showed a dose-dependent manner. 82 molecules related to oxidative stress, inflammation, amino acid metabolism, purine metabolism, tricarboxylic acid cycle, glycolysis, and lipid metabolism were analyzed. It was found that 14 metabolites in serum and 26 metabolites in liver showed significant changes, of which appeared to be key different metabolizers.

It is well known that despite having different etiologies, liver injuries are frequently associated with excessive oxidative stress. Liver function is protected by enhancing the activity of the endogenous antioxidant defense system (Wang et al., 2017). Glutathione has two active forms, reduced and oxidized. GSH is an important scavenger to protect against oxidative stress in the liver. A decreased GSH/GSSG ratio is used as the index of oxidative stress. In this study, the serum GSH/GSSG values in the model group (23.7) were significantly decreased compared with those in the normal group (51.2), which is in accordance with the state of abrupt decrease of antioxidant capacity in the rat model of liver injury. The GSH/GSSG value in the P.V group (60.1) was similar to that in the normal group, suggesting that P.V could repair the liver injury by reducing the level of oxidative stress in the hepatocytes.

Nucleoside is the major component of nucleic acid, while hypoxanthine is a metabolite of nucleoside and is an important alkaloid purine. AMP first generates hypoxanthine, which is oxidized to xanthine under the action of xanthine oxidase and ultimately decomposes to form uric acid, which is excreted in the urine. This pathway is an important metabolic pathway in the body, and gout is a clinical condition caused by abnormal uric acid metabolism. In this study, the increase of hypoxanthine content in the serum of model rats is considered to be related to a decrease in xanthine oxidase activity and the hindrance of hypoxanthine oxidation.

The TCA cycle is a common pathway for the metabolism of the three major nutrients: sugar, fat and amino acids. Citric acid is the key intermediate product of the TCA cycle, and oxaloacetic acid and acetyl-CoA are the important regulatory points of the TCA cycle. In this study, citric acid levels in serum were significantly reduced in the model group, presumably due to impairment of the TCA cycle process in rat hepatocytes (Li et al., 2014; Wu et al., 2017b), partial recovery of the TCA cycle, and increased citric acid levels after treatment.

Amino acid metabolism can be used to synthesize specific proteins, peptides, and nitrogen-containing compounds, either through decarboxylation by deamination, transamination, and catabolism of ammonia, or by the release of energy through citric acid cycling. Therefore, these changes in amino acid metabolism may elicit important signaling events within hepatocytes. Our results suggest that P.V can cause metabolic abnormalities of amino acid. L-Leucine is one of the eight essential amino acids in the human body. It has been reported that CCl_4 can cause decreases in leucine, glutamine/glutathione, and betaine contents, presumably due to inhibition of the expression of these amino acid synthesis genes (Li et al., 2014). Phenylacetylglutamine could be involved in the metabolism of intestinal microorganisms. It has been suggested that the level of phenylacetylglutamine in the urine of CCl_4 liver injury model rats decreased (Wu et al., 2017b). In this study, the level of N-phenylacetylglutamine in the serum of the model group increased and the level of acetylglutamine in the P.V group decreased. We presume that this was related to the decrease in urinary excretion and the increase in the serum concentration in the model rats.

In this study, the therapeutic effect of P.V on liver injury was assayed. P.V could decrease the hepatic tissue structure destruction, cytoplasmic vacuolation, cellular swelling, and inflammatory cell infiltration obviously. And it could decrease ALT and AST levels in rats suffered liver injury as a dose dependant manner. Metabolic mechanism analysis revealed that P.V could treat liver injury by regulating alanine, aspartate and glutamate metabolism, and TCA cycle.

Data availability statement

The raw data supporting the conclusions of this article will be made available by the authors, without undue reservation.

Ethics statement

The animal study was reviewed and approved by Institutional Animal Ethics Committee of Liaoning University.

Author contributions

WL and DL were responsible for overall supervision. L-MQ was responsible for experiments and data collection. HZ analysed data. L-MQ and WL wrote the manuscript. All authors read and approved the final manuscript.

References

- Carretero, A., León, Z., García-Cañaveras, J. C., Zaragoza, A., Gómez-Lechón, M. J., Donato, M. T., et al. (2014). *In vitro/in vivo* screening of oxidative homeostasis and damage to DNA, protein, and lipids using UPLC/MS-MS. *Anal. Bioanal. Chem.* 406 (22), 5465–5476. doi:10.1007/s00216-014-7983-5
- Dai, Y., Tu, F. J., Yao, Z. H., Ding, B., Xu, W., Qiu, X. H., et al. (2013). Rapid identification of chemical constituents in traditional Chinese medicine fufang preparation xianling gubao capsule by LC-linear ion trap/Orbitrap mass spectrometry. *Am. J. Chin. Med.* 41 (5), 1181–1198. doi:10.1142/S0192415X13500808
- Huang, L. Y., Sun, Y. Z., Chen, Q. Q., Bai, X. L., Du, T. T., Xu, H. T., et al. (2022). New compounds from *Patrinia villosa* Juss. and their anti-inflammatory activities. *Nat. Prod. Res.* 2022, 1–9. doi:10.1080/14786419.2022.2035382
- Jaesckhe, H., McGill, M. R., and Ramachandran, A. (2012). Oxidant stress, mitochondria, and cell death mechanisms in drug-induced liver injury: Lessons learned from acetaminophen hepatotoxicity. *Drug Metab. Rev.* 44 (1), 88–106. doi:10.3109/03602532.2011.602688
- Khemichian, S., Francoz, C., Durand, F., Karvellas, C. J., and Nadim, M. K. (2021). Hepatorenal syndrome. *Crit. Care Clin.* 37 (2), 321–334. doi:10.1016/j.ccc.2020.11.011
- Kong, M., Dong, W., Zhu, Y., Fan, Z., Miao, X., Guo, Y., et al. (2021). Redox-sensitive activation of CCL₇ by BRG₁ in hepatocytes during liver injury. *Redox Biol.* 46, 102079. doi:10.1016/j.redox.2021.102079
- Li, X., Zhang, F., Wang, D., Li, Z., Qin, X., and Du, G. (2014). NMR-based metabolomic and quantitative real-time PCR in the profiling of metabolic changes in carbon tetrachloride-induced rat liver injury. *J. Pharm. Biomed. Anal.* 89, 42–49. doi:10.1016/j.jpba.2013.10.023
- Li, Y., Cheng, X., Chen, C., Huijuan, W., Zhao, H., Liu, W., et al. (2016). Apigenin, a flavonoid constituent derived from *P. villosa*, inhibits hepatocellular carcinoma cell growth by CyclinD1/CDK4 regulation via p38 MAPK-p21 signaling. *Pathol. Res. Pract.* 216 (1), 152701. doi:10.1016/j.prrp.2019.152701
- Liao, J. C., Deng, J. S., Chiu, C. S., Huang, S. S., Hou, W. C., Lin, W. C., et al. (2012). Chemical compositions, anti-inflammatory, antiproliferative and radical-scavenging activities of *Actinidia callosa* var. *ephippoides*. *Am. J. Chin. Med.* 40 (5), 1047–1062. doi:10.1142/S0192415X12500772
- Mega, A., Marzi, L., Kob, M., Piccin, A., and Floreani, A. (2021). Food and nutrition in the pathogenesis of liver damage. *Nutrients* 13 (4), 1326. doi:10.3390/nu13041326
- Navarro, V., Khan, I., Björnsson, E., Seeff, L. B., Serrano, J., and Hoofnagle, J. H. (2017). Liver injury from herbal and dietary supplements. *Hepatology* 65 (1), 363–373. doi:10.1002/hep.28813
- Peng, J., Fan, G., and Wu, Y. (2005). Studies on chemical constituents of *Patrinia villosa* Juss. *Zhong Yao Cai* 28 (10), 883.
- Qian, H., Chao, X., Williams, J., Fulte, S., Li, T., Yang, L., et al. (2021). Autophagy in liver diseases: A review. *Mol. Asp. Med.* 82, 100973. doi:10.1016/j.mam.2021.100973
- Sheng, L., Yang, Y., Zhang, Y., and Li, N. (2019). Chemical constituents of *Patrinia heterophylla* Bunge and selective cytotoxicity against six human tumor cells. *J. Ethnopharmacol.* 236, 129–135. doi:10.1016/j.jep.2019.03.005
- Sun, T. F., Wang, P., and Zhang, C. L. (2014). Research progress on Chinese medicine treatment of liver injury. *J. Pharm. Res.* 33 (12), 715–717. doi:10.13506/j.cnki.jpr.2014.12.013
- Wang, J., Wang, X., Ma, X., Xu, B., Chen, L., Chen, C., et al. (2022). Therapeutic effect of *Patrinia villosa* on TNBS-induced ulcerative colitis via metabolism, vitamin D receptor and NF- κ B signaling pathways. *J. Ethnopharmacol.* 288, 114989. doi:10.1016/j.jep.2022.114989
- Wang, M. F., Zhao, S. S., Thapa, D. M., Song, Y. L., and Xiang, Z. (2021). Metabolomics of Fuzi-Gancao in CCl₄ induced acute liver injury and its regulatory effect on bile acid profile in rats. *World J. Gastroenterol.* 27 (40), 6888–6907. doi:10.3748/wjg.v27.i40.6888
- Wang, M. Y., Srinivasan, M., Dasari, S., Narvekar, P., Samy, A., Dontaraju, V. S., et al. (2017). Antioxidant activity of yichun blue honeysuckle (YBHS) berry counteracts CCl₄-Induced toxicity in liver injury model of mice. *Antioxidants (Basel)* 6 (3), 50. doi:10.3390/antiox6030050
- Wu, F., Zheng, H., Yang, Z. T., Cheng, B., Wu, J. X., Liu, X. W., et al. (2017a). Urinary metabolomics study of the hepatoprotective effects of total alkaloids from *Corydalis saxicola* Bunting on carbon tetrachloride-induced chronic hepatotoxicity in rats using ¹H NMR analysis. *J. Pharm. Biomed. Anal.* 140, 199–209. doi:10.1016/j.jpba.2017.03.031
- Wu, H. T., Zhang, G., Huang, L. S., Pang, H. Y., Zhang, N., Chen, Y. P., et al. (2017b2017). Hepatoprotective effect of polyphenol-enriched fraction from *Folium microcos* on oxidative stress and apoptosis in acetaminophen-induced liver injury in mice. *Oxid. Med. Cell. Longev.* 2017, 3631565. doi:10.1155/2017/3631565
- Xiang, Z., Chen, N., Xu, Y., Wu, J., Liu, Y. J., Tan, C., et al. (2016). New flavonoid from *Patrinia villosa*. *Pharm. Biol.* 54 (7), 1219–1222. doi:10.3109/13880209.2015.1064449

Funding

This study was supported by Wenzhou Science and Technology Bureau Project (Y20210220).

Conflict of interest

The authors declare that the research was conducted in the absence of any commercial or financial relationships that could be construed as a potential conflict of interest.

Publisher's note

All claims expressed in this article are solely those of the authors and do not necessarily represent those of their affiliated organizations, or those of the publisher, the editors and the reviewers. Any product that may be evaluated in this article, or claim that may be made by its manufacturer, is not guaranteed or endorsed by the publisher.

Xin-Jia, Y., Wei, L., Ying, Z., Ning, C., Ying, X., Jian, W., et al. (2016). A new biphenyl neolignan from leaves of *Patrinia villosa* (thunb.) Juss. *Pharmacogn. Mag.* 12 (45), 1–3. doi:10.4103/0973-1296.175988

Yang, Y. F., Ma, H. M., Chen, G., Wang, H. F., Xiang, Z., Feng, Q. M., et al. (2016). A new sesquiterpene lactone glycoside and a new quinic acid methyl ester from *Patrinia villosa*. *J. Asian Nat. Prod. Res.* 18 (10), 945–951. doi:10.1080/10286020.2016.1173678

Yang, Y., He, Q., Wang, H., Hu, X., Luo, Y., Liang, G., et al. (2017). The protection of meloxicam against chronic aluminium overload-induced liver injury in rats. *Oncotarget* 8 (14), 23448. doi:10.18632/oncotarget.15588

Younossi, Z. M., Koenig, A. B., Abdelatif, D., Fazel, Y., Henry, L., and Wymer, M. (2016). Global epidemiology of nonalcoholic fatty liver disease-Meta-analytic assessment of prevalence, incidence, and outcomes. *Hepatology* 64 (1), 73–84. doi:10.1002/hep.28431

Zheng, Y., Jin, Y., Zhu, H. B., Xu, S. T., Xia, Y. X., and Huang, Y. (2012). The anti-inflammatory and anti-nociceptive activities of *Patrinia villosa* and its mechanism on the proinflammatory cytokines of rats with pelvic inflammation. *Afr. J. Tradit. Complement. Altern. Med.* 9 (3), 295–302. doi:10.4314/ajtcam.v9i3.1



OPEN ACCESS

EDITED BY
Zheng Xiang,
Liaoning University, China

REVIEWED BY
Qiang Meng,
Dalian Medical University, China
Haibo Xu,
Chengdu University of Traditional
Chinese Medicine, China

*CORRESPONDENCE

Yu-hui Yan,
ctyanyh@163.com

SPECIALTY SECTION
This article was submitted to
Ethnopharmacology,
a section of the journal
Frontiers in Pharmacology

RECEIVED 29 September 2022

ACCEPTED 18 October 2022

PUBLISHED 26 October 2022

CITATION

Yan Y-h, Huang Z-h, Xiong Q-p,
Song Y-w, Li S-y, Yang B-w, Sun L,
Zhang M-y and Ji Y (2022), Effects of
Broussonetia papyrifera (L.) L'Hér. ex
Vent. fruits water extract on
hippocampal neurogenesis in the
treatment of APP/PS1 transgenic mice.
Front. Pharmacol. 13:1056614.
doi: 10.3389/fphar.2022.1056614

COPYRIGHT

© 2022 Yan, Huang, Xiong, Song, Li,
Yang, Sun, Zhang and Ji. This is an open-
access article distributed under the
terms of the [Creative Commons
Attribution License \(CC BY\)](https://creativecommons.org/licenses/by/4.0/). The use,
distribution or reproduction in other
forums is permitted, provided the
original author(s) and the copyright
owner(s) are credited and that the
original publication in this journal is
cited, in accordance with accepted
academic practice. No use, distribution
or reproduction is permitted which does
not comply with these terms.

Effects of *Broussonetia papyrifera* (L.) L'Hér. ex Vent. fruits water extract on hippocampal neurogenesis in the treatment of APP/PS1 transgenic mice

Yu-hui Yan^{1*}, Zi-han Huang^{1,2}, Qing-ping Xiong³,
Yue-wen Song¹, Si-yang Li¹, Bao-wei Yang¹, Lan Sun¹,
Meng-yuan Zhang¹ and Yu Ji¹

¹School of Pharmacy, Jiangsu Food & Pharmaceutical Science College, Huai'an, Jiangsu, China,

²School of Food Science and Engineering, Jiangsu Ocean University, Lianyungang, Jiangsu, China,

³Jiangsu Key Laboratory of Regional Resource Exploitation and Medicinal Research, Huaiyin Institute of Technology, Huai'an, Jiangsu, China

Background: Adult neurogenesis plays an important role in repairing damaged neurons and improving cognitive impairment in Alzheimer's disease (AD). *B. Papyrifera* (L.) L'Hér. ex Vent. fruits (BL), a traditional Chinese medicine for tonifying the kidney, has been reported to improve cognitive function in AD mice, but the underlying mechanisms have not been clearly illuminated. This study aimed to provide an overview of the differential compounds in the brain of APP/PS1 mice after BL water extract (BLWE) treatment through metabolomics technology and to elucidate whether the therapeutic effect and mechanism are through the enhancement of neurogenesis.

Methods: APP/PS1 transgenic mice were treated with different doses of BLWE. After 6 weeks of intragastric injection, the therapeutic effects of BLWE on APP/PS1 transgenic mice were determined by the Morris water maze test, immunohistochemistry, hematoxylin & eosin and Nissl staining, enzyme-linked immunosorbent assay and terminal deoxynucleotidyl transferase dUTP nick end labeling staining. Subsequently, metabolomics technology was used to analyze the regulatory effect of BLWE on differential compounds in the brain of APP/PS1 mice, and on this basis, its molecular mechanism of BLWE was screened. Finally, the protein expression of the Wnt/ β -catenin signaling pathway was detected by Western blotting.

Results: After BLWE treatment, the learning and memory function of APP/PS1 mice were significantly improved, which was related to the increase in the number of Nestin⁺/BrdU⁺ and NeuN⁺/BrdU⁺ cells, and the decrease in the number of apoptotic cells in the hippocampus. BLWE treatment could also up-regulate the expression of synapse-associated proteins. Moreover, BLWE could modulate endogenous metabolic compounds in the brains of AD mice, including N-acetyl-aspartate, glutamine, etc. Furthermore, BLWE inhibited

the phosphorylation of Tyr216-GSK-3 β and β -catenin protein while increased CyclinD₁ protein expression.

Conclusion: We demonstrated that BLWE can enhance neural stem cells proliferation and improve neurogenesis, thereby efficiently repairing damaged neurons in the hippocampus and ameliorating cognitive impairment in APP/PS1 transgenic mice. The mechanism is at least partly through activating the Wnt/ β -catenin signaling pathway.

KEYWORDS

Broussonetia papyrifera (L.) L'Hér. ex Vent. fruits water extract (BLWE), Alzheimer's disease, neurogenesis, metabolomics, wnt/ β -catenin signaling pathway

Introduction

Alzheimer's disease (AD) is a common neurodegenerative disorder that affects the elderly. As the population ages, the prevalence of AD is rising, which represents a substantial threat to the health of older people. Among the pathological characteristics of AD is the aberrant amyloid beta peptide (A β) deposition in the brain, which may promote neuroinflammatory responses, leading to a high number of synaptic losses and neuronal death in the brain. Consequently, AD patients will lose their capacities for learning and memorization (Golde et al., 2018; Uddin et al., 2020; de Almeida et al., 2022; Shakir and Dugger, 2022). Drugs continue to play a significant role in the treatment of AD, with acetylcholinesterase inhibitors and N-methyl-D-aspartate receptor antagonists being two of the most used types of medications for this condition (Liang et al., 2022). However, these medications may only alleviate the symptoms of certain patients but cannot effectively compensate the loss of neurons in the brain (Schott et al., 2019). Consequently, there is an urgent need for novel treatment strategies.

Neural stem cells (NSCs) are self-renewing cell populations that have the ability to differentiate into neurons, astrocytes, and oligodendrocytes (Jaberi et al., 2021). NSCs transplantation is regarded to be a successful treatment option for AD. However, the inflammatory microenvironment in the AD patients brains is not favorable to the survival of transplanted NSCs, therefore the therapeutic benefit is limited (Llorens-Bobadilla and Martin-Villalba, 2017). It has been hypothesized through previous research that the adult mammalian brain lacks regenerative repair capabilities. The following studies, however, demonstrate that neurogenesis does occur in the adult central nervous system (CNS), allowing for the treatment of CNS degenerative diseases and the repair of CNS injuries (Gage, 2019; Hanspal and Gillotin, 2022). Stimulating the proliferation of endogenous NSCs is considered as a practical way for CNS disease treatment, including AD and other neurodegenerative diseases. Certain traditional Chinese medicinal herbs and their extracts or active compounds have the abilities to modulate the biological characteristics of NSCs and enhance neurogenesis (Chen et al., 2019b). Kong et al. (2015) reported that osthole, an active compound derived from *Angelica*

biserrata, can promote neurogenesis in the hippocampus of APP/PS1 transgenic mice. This resulted in an improvement in the mice's cognitive performance. The active substance Astragaloside VI, derived from *Radix Astragalus*, promotes the proliferation of NSCs and neurogenesis in a model of transient cerebral ischemia injury, thereby improving the restoration of neurological function in rats with post-ischemic stroke (Chen et al., 2019a).

Broussonetia papyrifera (L.) L'Hér. ex Vent. fruits (BL) is a kind of Chinese herbal medicine distributed in most parts of China. Recent studies have revealed that BL extracts have a wide range of pharmacological effects, some of which include boosting the immune system, lowering blood lipids, anti-oxidation, and offering protection against drug-induced liver injury (Pang et al., 2014; Zhang et al., 2020). In addition, recent pharmacological studies have shown that BL extracts have neuroprotective actions on improving cognitive function in AD mouse model and chronic cerebral hypoperfusion rat model (Liu et al., 2020; Li Y. H. et al., 2021). However, it is unknown whether BL water extract (BLWE) can stimulate the growth of endogenous NSCs.

The proliferation, differentiation of NSCs, and neuronal apoptosis are closely related to the Wnt/ β -catenin signaling pathway (Yu et al., 2017). Recent studies showed that the expression of glycogen synthase kinase-3 β (GSK-3 β) and β -catenin, two key molecules of the Wnt/ β -catenin signaling pathway, were shown to be significantly different in normal mice and AD model mice (Sun et al., 2019; Menet et al., 2020). However, it is unknown if BLWE could increase the proliferation of endogenous NSCs and whether the Wnt/ β -catenin signaling pathway is involved in this process. In this study, we aimed to assess the effects of BLWE on the neurogenesis of AD mice and to investigate underlying mechanism.

Materials and methods

Animals, drug preparation, and administration

BL was purchased from Kangmei Pharmaceutical Co., Ltd. (Guangdong, China). The voucher specimens were identified by

Professor Tian-min Wang, who is working at Liaoning University of Traditional Chinese Medicine, then put in Jiangsu Food & Pharmaceutical Science College for storage (No. JSFPC20191207-01, Huai'an, China). BL (90 g) was soaked in deionized water (900 ml) for 1 h, then heated to boil at 100°C, and maintained in micro-boiling state for 1 h by a thermostat electric heating mantle (DZTW, Shanghai Lichen, China). The extracted solution was collected, and the dregs of a decoction was continued to be extracted twice according the same method, combine the three extracts to obtain the BLWE. After that, the BLWE was concentrated, freeze-dried, and its yielding capacity was calculated by three repeated experiments. The extraction yield of BL was calculated to be 8.48%. 5-Bromo-2-deoxyuridine (BrdU, Sigma Chemical Company, St. Louis, MO, United States) was prepared with deionized to a final concentration of 10 mg/mL and then deposited at 4°C.

APP_{swe}/PS1_{ΔE9} transgenic (Tg) mice were purchased from Beijing HFK Bioscience Co., Ltd. (Beijing, China), which can overexpress mutated human APP and PS1 (APP_{swe}/PS1_{ΔE9}) genes and simulate the pathological features of AD patients. Usually, cognitive impairment can be observed in 7-month-old Tg mice, and Aβ deposits can be detected in the hippocampus and cortex of 10-month-old Tg mice (Zhang et al., 2021). In this study, 9-month-old Tg mice were used and divided into model group, BLWE low dose (L-dose) group, and BLWE high dose (H-dose) group. The dose of mouse was converted according to the dose of human body, that is, 0.15g/kg for BLWE L-dose group and 0.30g/kg for BLWE H-dose group. We treat APP/PS1 mice according to the 'Guidelines for the Care and Use of Laboratory Animals published by the Shanghai Science and Technology Press of China in 2012. The BLWE groups received different doses of BLWE intragastric treatment once daily for 6 weeks. The model group was given an equal volume of deionized water for 6 weeks, and wild-type C57BL/6 mice at the same age were used as the control group. Three days before the end of the administration, mice were injected with BrdU (50 mg/kg, i. p.) twice a day to label proliferative cells.

Morris water maze test

Six weeks after administration, the learning and memory abilities of mice were evaluated by the MWM test. The MWM includes a circular pool with a black inner wall, a diameter of 120 cm and a height of 60 cm, a camera, and automatic image acquisition and analysis system. The pool was divided into four quadrants in which a 10 cm diameter platform was placed as an escape platform. Add water (25°C) until the water surface is 2 cm higher than the platform. The swimming paths of mice were captured with the camera, and the images were collected and analysed to assess their spatial acquisition and memory abilities.

The operation details could be reviewed from our previous research (Yan et al., 2018).

Immunohistochemistry

After the MWM experiment, the mice were anesthetized by i. p. with pentobarbital sodium (40 mg/kg), and fixed in the supine position. The brains were taken after cardiac perfusion, placed in the precooled paraformaldehyde solution, and fixed for 4–6 h. A rotary microtome (RM2235, Leica, Germany) was used to prepare paraffin sections (4 μm).

Sections were transparented twice in xylene solution for 15 min each time and then dehydrated by 70%, 80%, and 90% alcohol solution. The sections were placed in 0.01 mol/L sodium citrate buffer (pH = 6.0), heated to boiling in a microwave oven, and the process repeated three times for 5min each time. After permeabilizing the sections with 3% hydrogen peroxide 0.1% Triton X-100 for 30 min, the sections were blocked with 5% bovine serum albumin (BSA) solution for 1 h, then add the primary antibody diluent (rat-anti-Nestin; mouse anti-NeuN; mouse anti-synapsin-1 (SYN-1); mouse anti-Aβ₁₋₄₂, all diluted 200 times, Millipore, Billerica, MA, United States) at 4°C overnight. Then add Cy3-or HRP- labeled secondary antibody diluent (1:250, Jackson ImmunoResearch Lab, West Grove, PA, United States) in the dark for 60 min at room temperature. 4, 6-diamidino-2-phenylindole (DAPI, Sigma-Aldrich, St. Louis, MO, United States) or DAB chromogenic solution was added to each section for 5–15 min, respectively. After washing with PBS, add an anti-fluorescence quencher to mount the slides, observe and take pictures under a fluorescence microscope. As it does in the previous reports (Li H. et al., 2021; Xiao et al., 2021), we use ImageJ software to scan the fluorescence intensity of each field to measure the expression level.

Enzyme-linked immunosorbent assays

The mouse brain tissue was added to cold normal saline (NS) to prepare 10% homogenates and then centrifuged for 10 min at 3,000/min. The levels of synaptophysin (SYP), postsynaptic density-95 (PSD-95), interleukin-6 (IL-6), IL-1β and tumor necrosis factor-α (TNF-α) in the supernatant were evaluated by ELISA kit (Wuhan Elite Biotechnology Co., Ltd. Wuhan, China) according to the kit instructions. Add 100 μL of supernatant to a 96-well plate and incubate at 37°C for 90 min. 100 μL biotinylated antibody working solution was added immediately after discarding the liquid and then incubated at 37°C for 60 min. Discard the liquid and wash 3 times, then add horseradish peroxidase-conjugated (HRP, Genview, United States) enzyme conjugate working solution 100 μL to each well, incubate at 37°C for 30 min, and then discard the liquid and wash 5 times. Add 90 μL of substrate solution to each well in

dark conditions and incubate at 37°C for 15 min. The absorbance of each well at 450 nm was detected using a microplate spectrophotometer immediately after adding 50 μ L of stop solution.

Hematoxylin and eosin and nissl staining

To evaluate the morphological changes of neurons and brain damage in mice, H&E and Nissl staining were performed as previously described (Su et al., 2019; Wang et al., 2019). Briefly, brain sections were dehydrated by 70%, 80%, and 90% alcohol solution and then stained with hematoxylin. Put the slices into 1% hydrochloric acid alcohol solution to fade until the color turns red. After being washed until the color returned blue, the sections incubated with 0.5% ammonia hydroxide and followed by dying with eosin for 5 s, permeabilized with dimethylbenzene after dehydration, and then sealed with neutral gum. For Nissl staining, the brain sections were stained with Cresyl violet after being degreased with different concentrations of alcohol solution (Xiao et al., 2021).

Terminal deoxynucleotidyl transferase dUTP nick end labeling assay

TUNEL assay can detect apoptotic DNA strand breaks in cell nuclei. The above brain sections were fixed with 4% paraformaldehyde and then permeabilized with 0.1% Triton X-100. After being washed with PBS, they were incubated with PE buffer for 1 h at 37°C and counterstained the nuclear with DAPI. Use an inverted fluorescence microscope to take pictures of brain sections and use ImageJ software to count the TUNEL-positive cells.

Metabolomics analysis

Using Ultimate 3,000 liquid chromatograph (LC) combined with Q Exactive mass spectrometer (MS, Thermo), we performed metabolomics to investigate the mechanism by which BLWE ameliorates cognitive impairment by promoting nerve regeneration in APP/PS1 mice. A portion of mouse brain tissue is stored at -80°C for 24 h. After thawing, accurately weighed 50 mg and homogenized with 80% cold aqueous methanol 800 μ L for 90 s, then vortex and shake to mix well. Ultrasonic extraction at 4°C for 30 min, stand at -20°C for 1 h, vortex for 30 s, and then stand at 4°C for 0.5 h. After centrifugation (4°C, 12,000 rpm, 15 min), transfer all supernatant to a new centrifuge tube and let them stand at -20°C for 1 h, then centrifuged again under the above conditions. Pipette 200 μ L of the supernatant, add 5 μ L of internal standard dichlorophenylalanine (140 $\mu\text{g/mL}$) and transfer to a sample vial for LC-MS analysis.

The chromatographic column for LC-MS is ACQUITY UPLC HSS T3 column (100 mm \times 2.1 mm \times 1.8 μm) and was

carried out in positive ion mode. The column temperature was 40°C, and a flow rate of 0.3 ml/min was used in this study. 0.05% formic acid aqueous solution and acetonitrile solution were used as mobile phase A and mobile phase B, respectively. Inject 4 μ L sample at the injection temperature of 4°C for determination. The heater temperature of MS was 300°C, following 45 arb sheath gas flow rate, 15 arb auxiliary gas flow rate, and 1arb exhaust gas flow rate. The electrospray voltage and capillary temperatures were 3.0 KV and 350°C, respectively.

The original data underwent peak alignment, retention time correction, and peak area extraction. The identification of the metabolite structure adopts accurate mass matching (<30 ppm) and secondary spectrum matching and searches the Human Metabolome Database (HMDB). Then use autoscaling or UV method to normalize the data. Use MetaboAnalysis tool suite, SIMCA-P software (Umetrics AB, Umea, Sweden), and Kyoto Encyclopedia of Genes and Genomes (KEGG) databases for multi-dimensional statistical analysis and single-dimensional statistical analysis, including principal component analysis (PCA), partial least squares discriminant analysis (PLS-DA), Students' t-test, multiple variation analysis, and pathway enrichment analysis (Ji et al., 2018).

Western blot analysis

WB analysis was performed according to the method in the literature (Yan et al., 2017; Xiao et al., 2022). Briefly, after the brain tissue of each mouse was weighed, Lysis Buffer, a protease inhibitor, a phosphatase inhibitor, and PMSF were added in sequence according to the manufacturer's instructions (R&D, Emeryville, CA, United States) to extract the total protein. 8% SDS-PAGE was formulated to fractionate the protein and then transferred it onto PVDF membranes. After transfer, the PVDF membrane was washed with TBST and then blocked with 5% BSA. The membrane was probed with primary antibodies for 18 h at 4°C as follows: rabbit polyclonal antibody against t-GSK-3 β , t- β -catenin, p- β -catenin (1:1000, Cell signaling, United States), mouse polyclonal antibody against p-Tyr216-GSK-3 β , CyclinD₁ and GAPDH (1:1000, Santa Cruz, United States). After washing three times, the membrane was put into HRP-labeled anti-rabbit or anti-mouse secondary antibodies and incubated at room temperature for 1 h. The proteins were visualized with Electrochemiluminescence (ECL) WB detection reagents (Millipore, Billerica, MA, United States) and then analyzed using ImageJ software.

Statistical analysis

All experiments were repeated at least 3 times, and data were expressed as means \pm SD. The differences among multiple groups were analysed by one-way analysis of variance (ANOVA)

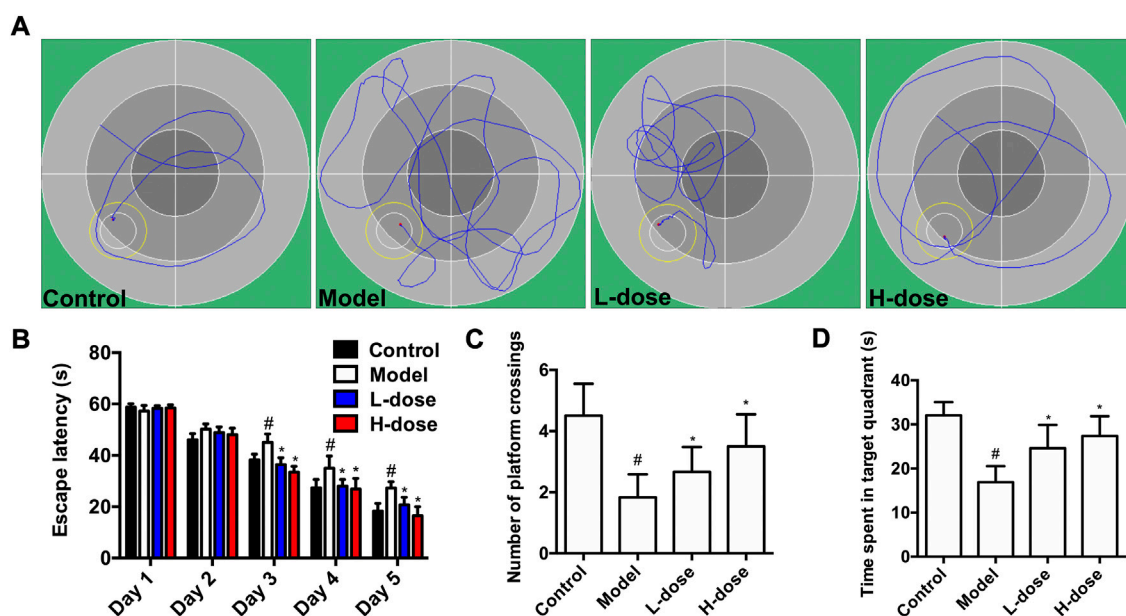


FIGURE 1

BLWE improved learning and memory ability in APP/PS1 mice. Representative individual swimming trajectory diagram in the water maze trial of each group (at day 5) (A). Comparison of escape latency in different groups of mice in place navigation test (B). Comparison of the number of platform crossings in each group in the space exploration experiment (C). Comparison of the time spent in target quadrant of each group in the space exploration experiment (D). # $p < 0.05$ vs. the control group; * $p < 0.05$ vs. the model group. Values were expressed as the mean \pm SD ($n = 6$ per group).

followed by Tukey's post-hoc test. The statistical significance between the two groups was analysed by two-way ANOVA followed by Bonferroni post-hoc test. The above analysis was performed using the SPSS version 13.0 statistics software, and $p < 0.05$ was considered statistically significant.

Results

BLWE improved cognitive impairment in APP/PS1 mice

A water maze test was first performed to explore the improvement effect of BLWE on the learning and memory abilities of AD mice. The representative swimming trajectory diagram of each group is shown in Figure 1A. The place navigation test results showed that, with the extension of training time, the escape latency of mice in each group gradually shortened, and there were clearly differences among each group after 4 days of training. At day 5, the mice in the control group had the shortest escape latency at 18.32 s, while those in the model group had the longest escape latency at 27.33 s, and there was a significant difference between the two groups ($p < 0.05$, Figure 1B). Meanwhile, after the mice were treated with low and high doses of BLWE, their escape latency

was significantly shortened to 20.85 s and 16.57 s compared with the model group, respectively ($p < 0.05$, Figure 1B).

Subsequently, the spatial probe test was performed to detect the maintenance of memory function. As shown in Figure 1C, the average number of platform crossings in the model group was 1.83, significantly different from that in the control group ($p < 0.05$). However, the average number of platform crossings was increased considerably after BLWE treatment (2.67 in the BLWE L-dose group and 3.50 in the BLWE H-dose group); both were statistically significant compared with the model group ($p < 0.05$). In addition, the swimming times of mice in the target quadrant in the BLWE group were significantly prolonged than that in the model group (16.90 s in the model group vs. 24.62 s in the BLWE L-dose group and 27.40 s in the BLWE H-dose group, $p < 0.05$, Figure 1D). The above results indicated that BLWE treatment could enhance both the learning and memory function of APP/PS1 mice.

BLWE attenuated the deposition of A β and inflammatory response in APP/PS1 mice

After the MWM test, immunohistochemistry stained the A β burden in the brains of mice in each group. The results revealed that there was no A β plaque deposition in the control group,

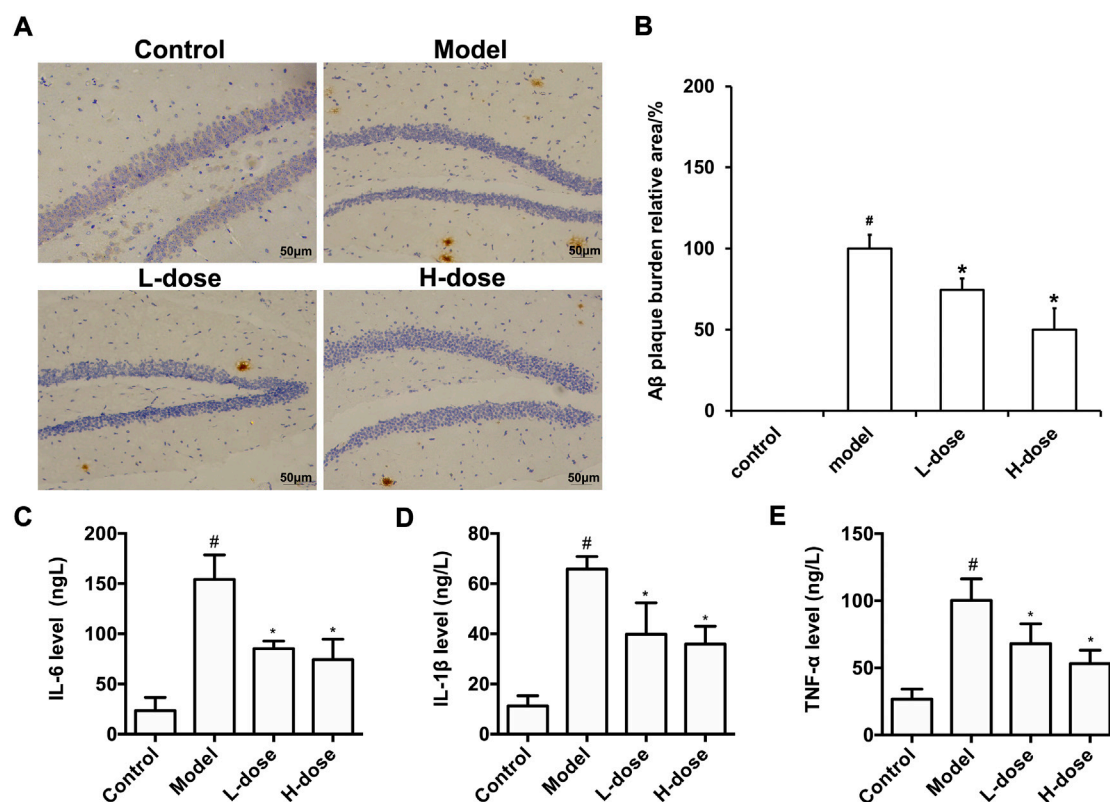


FIGURE 2

BLWE attenuated the deposition of A β and inflammatory response in APP/PS1 mice. A β immunoreactive plaques in the hippocampus was immunostained with anti-A β monoclonal antibody (A). Scale bar = 50 μ m. ImageJ analyzed the percentage area of A β -immunoreactive plaques of each group (B). Detection of IL-6 (C), IL-1 β (D) and TNF- α (E) levels in brain tissue of mice in each group by ELISA kit. [#] $p < 0.05$ vs. the control group; ^{*} $p < 0.05$ vs. the model group. Values are expressed as the mean \pm SD ($n = 6$ per group).

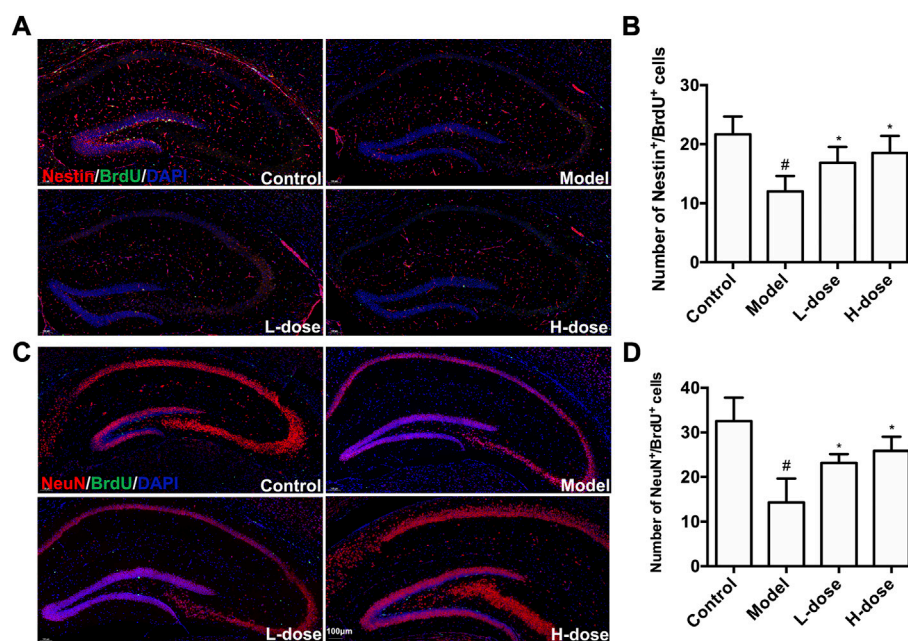
while obvious brownish-yellow deposition of A β plaques of different sizes and diffusely distributed could be observed in the brain of the model group (Figure 2A). Compared with the model group, BLWE treatment significantly reduced the A β plaque positive area in the brain, which was the most significant reduction in the BLWE H-dose group (Figure 2B, $p < 0.05$).

The abnormal deposition of A β can activate microglia in the brain, thus promoting the release of inflammatory factors, such as TNF- α , IL-1 β , and IL-6. The released inflammatory factors will cause inflammation response in the brain, accelerate the formation of senile plaques due to nerve fiber tangles, and further worsen the course of AD. In order to evaluate the effect of BLWE on the inflammatory reaction in the brain of AD mice, the levels of IL-6, IL-1 β , and TNF- α in the whole brain tissue were analyzed by an ELISA kit. The results exhibited that the levels of IL-6, IL-1 β , and TNF- α were increased significantly in the brain of the model group, and after BLWE treatment, the levels of these inflammatory factors were significantly reduced, indicating that BLWE can inhibit the inflammatory reaction in the brain (Figures 2C–E, $p < 0.05$).

BLWE promoted endogenous NSCs proliferation and increased the number of newborn neurons in APP/PS1 mice

Proliferating NSCs were labeled with Nestin⁺/BrdU⁺ to test and verify the effect of BLWE on neurogenesis. As shown in Figure 3A,B, the Nestin⁺/BrdU⁺ cells in the model group were only 12.00 ± 2.61 , which was significantly reduced compared with 21.67 ± 3.01 in the control group ($p < 0.05$). At the same time, we observed that both BLWE L-dose and H-dose treatment can significantly increase the number of Nestin⁺/BrdU⁺ cells in the brains of AD mice (16.83 ± 2.71 cells in the L-dose group and 18.50 ± 2.88 cells in the H-dose group vs. the model group, $p < 0.05$). These results indicate that BLWE can enhance the proliferation of endogenous NSCs in APP/PS1 mouse brains.

Next, we further explored whether BLWE treatment can increase the number of newborn neurons in APP/PS1 mice. Immunostaining against NeuN was used to label neurons, and BrdU was used to label proliferative cells. It can be observed in Figure 3C,D significantly fewer NeuN⁺/BrdU⁺ cells were detected in the model group (14.33 ± 5.32 cells) than that in the control

**FIGURE 3**

BLWE enhanced endogenous NSCs proliferation and differentiates into neurons in APP/PS1 mice. Mice were treated with different dose of BLWE or deionized water for 6 weeks and were injected with BrdU twice a day to label proliferative cells. Proliferating NSCs were labeled with antibodies against Nestin (red) and BrdU (green), respectively (A). ImageJ software counted Nestin/BrdU positive cells in each group (B). Newborn neurons were labeled with antibodies against NeuN (red) and BrdU (green), respectively (C). ImageJ software counted NeuN/BrdU positive cells in each group (D). The nucleus is counterstained with DAPI (blue). Scale bar = 100 μ m in A and C. [#] $p < 0.05$ vs. the control group; ^{*} $p < 0.05$ vs. the model group. Values are expressed as the mean \pm SD ($n = 6$ per group).

group (32.50 ± 5.22 , $p < 0.05$). In contrast, in both BLWE L-dose and BLWE H-dose groups, the number of NeuN⁺/BrdU⁺ cells increased significantly (14.33 ± 5.32 cells in the model group vs. 23.17 ± 1.94 cells in the BLWE L-dose group and 25.83 ± 3.19 cells in the BLWE H-dose group, $p < 0.05$). These findings indicated that BLWE treatments promote the proliferating NSCs differentiating into new neurons in the brain of APP/PS1 mice.

BLWE increased the expression of synapse-associated protein in APP/PS1 mice

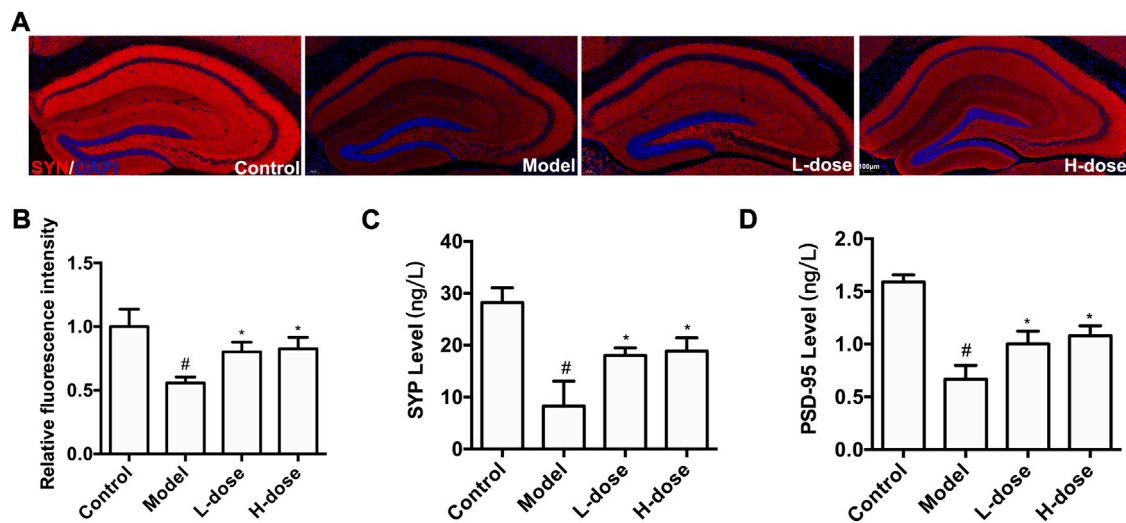
Furthermore, to determine whether new neurons can establish synaptic connections, we used immunostaining and ELISA methods to detect three important protein markers, including SYN-1, SYP, and PSD-95, which were associated with regulating synaptic plasticity and synaptic transmission (Luo et al., 2019; Muhammad et al., 2019). The fluorescence of SYN-1 in each group was shown in Figure 4A, and the expression was quantitatively analyzed using ImageJ software. Compared with the control group, the SYN-1 protein expression was significantly reduced in the model group ($p < 0.05$,

Figure 4B). Nonetheless, BLWE therapy effectively restored the expression of the SYN-1 protein ($p < 0.05$ vs. the model group, Figure 4B).

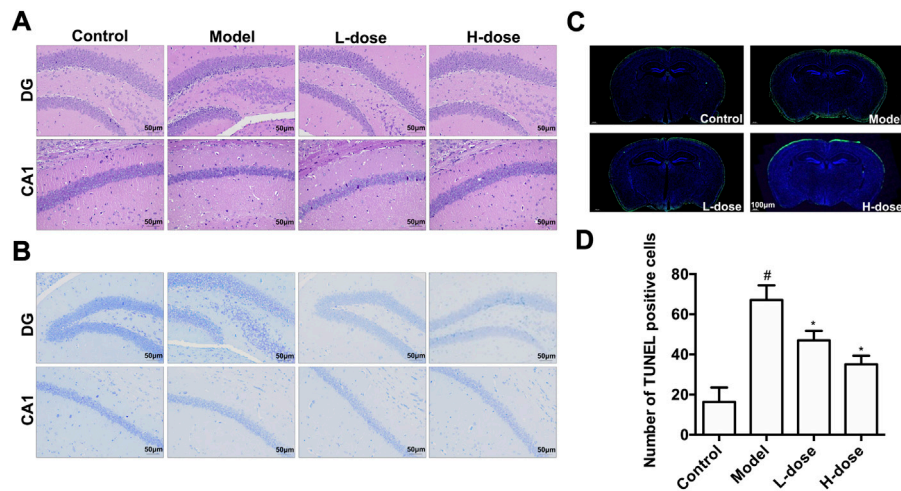
Subsequently, ELISA method was used to detect the level of PSD-95 and SYP. Results in our study demonstrated that compared with the control group, these two proteins significantly decreased in the model group ($p < 0.05$, Figure 4C,D), which could be reversed significantly by BLWE treatment ($p < 0.05$, vs. the model group, Figure 4C,D). These results indicate that BLWE can improve the expression of synapse-related proteins, which is beneficial to the repair of nerve function.

BLWE inhibited neuron pathological damage and neuronal apoptosis in APP/PS1 mice

We used H&E, Nissl staining, and TUNEL assays to detect neuron pathological damage and apoptosis. In the control group, H&E staining revealed no significant neuronal pathological damage in the hippocampus, DG, and CA1 regions. In contrast, the model group has shrunken neurons, condensed nuclei, and blood cell congestion. Even while neuronal

**FIGURE 4**

BLWE up-regulated the expression of synapse-associated proteins in APP/PS1 mice. Immunocytochemistry staining for SYN-1 (red) and DAPI (blue) in the brain of each group (A). Scale bar = 100 μ m. Quantification of the SYN-1 immunofluorescence intensity by ImageJ software (B). Quantification the concentration of SYP (C) and PSD-95 (D) by ELISA kit. [#] $p < 0.05$ vs. the control group; ^{*} $p < 0.05$ vs. the model group. Values are expressed as the mean \pm SD ($n = 6$ per group).

**FIGURE 5**

BLWE reversed neuron pathological damage and neuronal apoptosis in APP/PS1 mice. H&E staining of hippocampus DG and CA1 areas (A). Scale bar = 50 μ m. Nissl staining of hippocampus DG and CA1 areas (B). Scale bar = 50 μ m. TUNEL staining of hippocampus DG and CA1 areas (C). Scale bar = 100 μ m. ImageJ software for quantitative counting of apoptotic cells (D). [#] $p < 0.05$ vs. the control group; ^{*} $p < 0.05$ vs. the model group. Values are expressed as the mean \pm SD ($n = 6$ per group).

pathological damage was also observed in the two BLWE-treated groups, it was less severe than in the model group (Figure 5A). Nissl staining was subsequently conducted to elucidate the extent of neuron loss in the brain of APP/PS1 mice. The results indicated that in the control group, the hippocampus, DG,

and CA1 area cells were neatly arranged, and the Nissl bodies were tigroid or dotted, while the Nissl bodies in the model group were blurred and the cell bodies were shrunken. After treatment with different doses of BLWE, a significant improvement in cell morphology can be observed (Figure 5B).

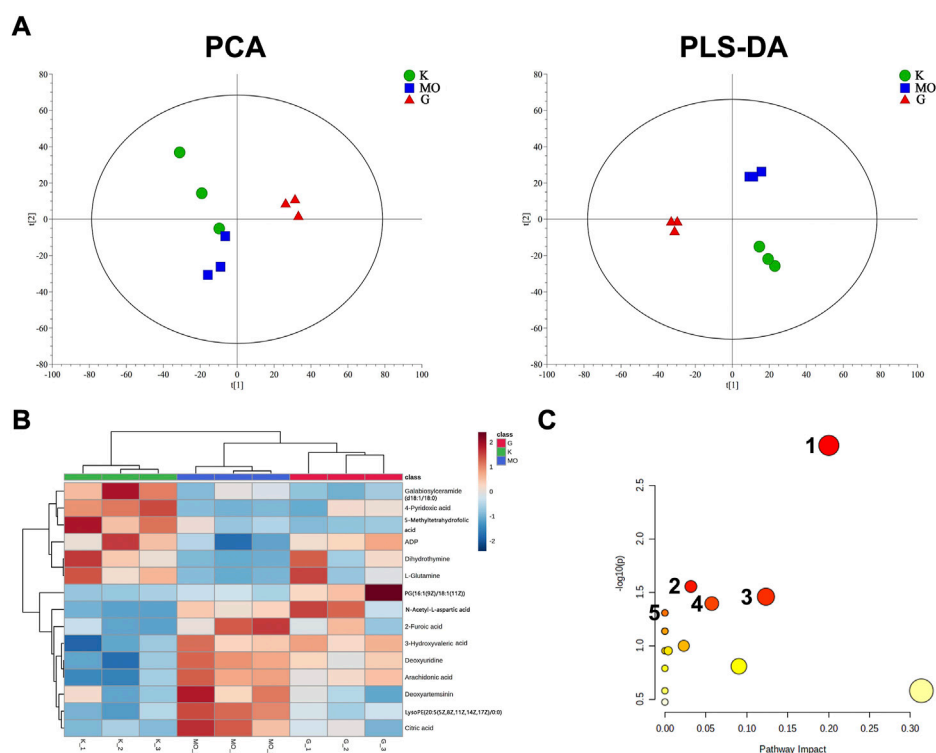


FIGURE 6

BLWE regulated different metabolites in the brain of APP/PS1 mice. Analysis of PCA and PLS-DA in brain tissue of mice. K denotes the control group; MO denotes the model group and G denotes the BLWE H-dose group (A). Thermal map analysis of differential biomarkers. Metabolites marked in red represent up-regulated metabolites, while those marked in blue represent down-regulated metabolites. Differential metabolites were displayed in each row, and single samples were listed in each column (B). $n = 3$ per group. Overview of BLWE-regulated metabolic pathways. 1, 2, 3, 4, and 5 refer to the alanine, aspartate and glutamate metabolism pathway, glyoxylate, and dicarboxylate metabolism pathway, glycerophospholipid metabolism pathway, pyrimidine metabolism pathway and D-glutamine and D-glutamate metabolism pathway, respectively (C).

Moreover, we utilized the TUNEL assay to explore the improvement of neuronal apoptosis by BLWE. As shown in Figure 5C, the green fluorescent staining is TUNEL positive cells. Using ImageJ quantitative analysis, it was shown that the number of TUNEL-positive cells in the control group was only 16.33 ± 2.20 cells, while it was significantly increased to 67.17 ± 7.25 cells in the model group ($p < 0.05$, Figure 5D). Nevertheless, the number of TUNEL-positive cells was decreased in the two BLWE groups (47.01 ± 4.77 cells in the BLWE L-dose group and 35.08 ± 4.34 cells in the BLWE H-dose group), which were significantly different from the model group ($p < 0.05$, Figure 5D), indicating that BLWE could extenuate neuronal apoptosis in APP/PS1 mice.

Metabolomics analysis of BLWE in AD treatment

Metabolomics analysis was performed to illustrate the mechanism of anti-AD of BLWE. The results of PCA and

PLS-DA analysis showed that the samples of each group have high aggregation, and the three groups K (control group), MO (model group), and G (the BLWE H-dose group), can be distinguished by the PLS-DA analysis (Figure 6A). The control group, model group, and BLWE H-dose group can be basically divided, indicating that there are certain differences in metabolism among the three groups. As shown in Table 1, 13 different compounds were screened by KEGG database. Subsequently, the heat map results showed that the metabolites in the brain tissue of mice had significant changes after BLWE treatment. Compared with the model group, eight metabolites, including N-acetyl-aspartate (NAA), glutamine, lactoseceramide, 4-pyridoxic acid, 5-methyltetrahydrofolic acid, ADP, dihydrothymine, and phosphatidylglycerol were increased, and five metabolites including citric acid, 2-furoic acid, deoxyuridine, arachidonic acid, and phosphatidylethanolamine were decreased (Figure 6B). Using the MetaboAnalyst 3.0 software, we conducted an in-depth analysis of the 13 differentially identified compounds to screen out the compounds that are related to the pathogenesis

TABLE 1 Differential metabolites screen by KEGG.

	M1.VIP [5]	M/Z	HMDB	Name	KEGG ID
1	1.54186	192.02678	HMDB0000094	Citric acid	C00158
2	1.4793	174.0396	HMDB0000812	N-Acetyl-L-aspartic acid	C01042
3	1.47922	182.0449	HMDB0000017	4-Pyridoxic acid	C00847
4	1.30564	745.50262	HMDB0010574	Phosphatidylglycerol	C00344
5	1.44032	303.2327	HMDB0001043	Arachidonic acid	C00219
6	1.44016	227.0665	HMDB0000012	Deoxyuridine	C00526
7	1.39829	145.0606	HMDB0000641	L-Glutamine	C00064
8	1.35857	127.05	HMDB0000079	Dihydrothymine	C00906
9	1.34534	458.1668	HMDB0001396	5-Methyltetrahydrofolic acid	C00440
10	1.32724	888.6236	HMDB0004866	lactosylceramide	C01290
11	1.46154	498.26245	HMDB0005779	Phosphatidylethanolamine	C00350
12	1.29828	111.0074	HMDB0000617	2-Furoic acid	C01546
13	1.2915	426.0218	HMDB0001341	ADP	C00008

of AD and that BLWE can regulate. Results showed that there were 14 metabolic pathways that BLWE might regulate. Sorted according to the degree of correlation, the top five influences were Alanine, aspartate and glutamate metabolism, Glyoxylate and dicarboxylate metabolism, Glycerophospholipid metabolism, Pyrimidine metabolism, D-glutamine and D-glutamate metabolism (Figure 6C).

To further screen the most likely intervening signaling pathways of BLWE, we imported the differential metabolites into the KEGG database for query, matching, and finally found that the affected signaling pathways included Wnt, MAPK, RAS, etc. The Wnt signaling pathway might be the most relevant pathway for BLWE treatment of AD, as most differential biomarkers were associated with it.

BLWE enhanced neurogenesis in a Wnt signaling-dependent way

It is generally accepted that the activation of the Wnt/ β -catenin signaling pathway affects neurogenesis (Kriska et al., 2021). To further investigate the mechanism of BLWE promoting neurogenesis in the treatment of AD, we analyzed the expression of proteins such as t-GSK-3 β , p-Tyr216-GSK-3 β , t- β -catenin, p- β -catenin, and CyclinD₁, which were related to the Wnt/ β -catenin signaling pathway (Figure 7A,B). Results showed that compared with the control group, the expression of p-Tyr216-GSK-3 β , p-Tyr216-GSK-3 β /t-GSK-3 β , p- β -catenin, and p- β -catenin/t- β -catenin were markedly increased, while the expression of CyclinD₁ was decreased in the model group ($p < 0.001$, Figure 7B). However, the expression of these above proteins can be reversed by BLWE treatment in which

the levels of p-Tyr216-GSK-3 β , p-Tyr216-GSK-3 β /t-GSK-3 β , p- β -catenin, and p- β -catenin/t- β -catenin were all down-regulated except the CyclinD₁ level that was up-regulated significantly ($p < 0.01$, $p < 0.05$, Figure 7B). In addition, there was no significant difference in the protein expression of t-GSK-3 β and t- β -catenin among all groups. From the above results, we could conclude that BLWE enhanced neurogenesis through the Wnt/ β -catenin signaling pathway.

Discussion

Combined with pharmacological and metabolomics technology, this study examined the effects and molecular mechanism of BLWE in promoting endogenous NSCs proliferation and regenerative repair for AD treatment. Results confirmed that BLWE treatment for 6 weeks could activate endogenous NSCs proliferation, promote their differentiation into neurons, and establish synaptic networks, as well as reduce neuron pathological damage and neuronal apoptosis in the hippocampus, thereby enhancing the cognitive function of AD mice.

AD is a complex neurodegenerative disease characterized by A β deposits, high tau protein phosphorylation, and neurofibrillary tangles in the cerebral cortex and hippocampus. The persistent inflammation and oxidative stress damage around the brain lesion lead to a large number of neuronal ulcerations and losses. The patient exhibited memory loss, cognitive and behavioral disorders, and eventually lost self-care abilities. At present, therapeutic drugs for AD can only compensate for the neurotransmitter that is lacking due to the loss of a large number of neurons but cannot directly supplement

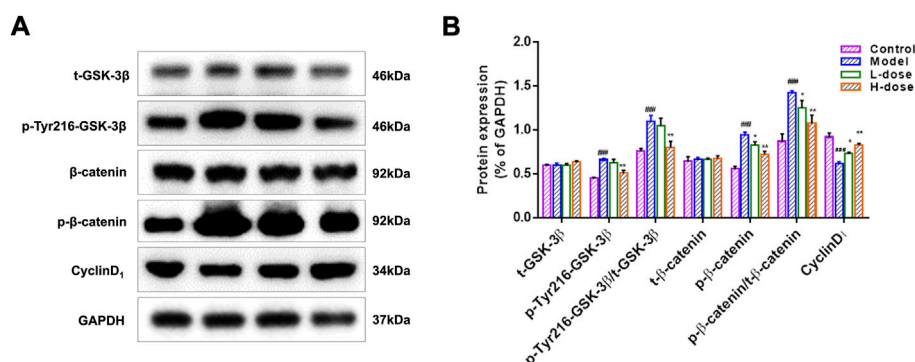


FIGURE 7

BLWE activated the expression of Wnt/ β -catenin signaling pathway-associated proteins in APP/PS1 mice. Protein expression of t-GSK-3 β , p-Tyr216-GSK-3 β , t- β -catenin, and p- β -catenin in the mice brain measured by WB. GAPDH served as control (A). ImageJ software to quantify protein expression and normalized with GAPDH internal control (B). $^{###}p < 0.001$ vs. the control group; $^{*}p < 0.05$, $^{**}p < 0.01$ vs. the model group. Values are expressed as the mean \pm SD ($n = 6$ per group).

the neuron. Therefore, they can only partially alleviate the symptoms of mild and moderate AD patients and have serious side effects, which cannot fundamentally control the natural course of AD (Schott et al., 2019). Most mammals, including humans, have NSCs survive in the subventricular zone (SVZ) and the subgranular zone (SGZ) throughout their lives. After proliferation, the NSCs in the SGZ migrate to the granular layer of the hippocampus, and ulnar gyrus, differentiate into mature neurons and integrate their functions into the neural circuit, thereby making up for the missing neurons in the lesion. This is essential for maintaining the normal function of the hippocampus, such as the learning and memory functions (Gage, 2019; Ou et al., 2022).

We first performed MWM tests to determine the cognitive function in mice. The results indicated that the 6-week treatment of BLWE could shorten the escape latency, increase the number of plate crossings, and prolong the swimming time in the target quadrant to enhance the cognitive function of AD mice (Figures 1A–D). Secondly, we detected $A\beta_{1-42}$ burden to explore whether BLWE can improve the typical pathological features of AD mice and found that $A\beta_{1-42}$ deposition in the brains of mice treated with BLWE was significantly reduced (Figure 2). Further, we separately detected the number of Nestin⁺/BrdU⁺ and NeuN⁺/BrdU⁺ cells, the expression of synapse-related proteins to determine whether neurogenesis increases after treating with BLWE. Results show that, compared to the model group, the number of Nestin⁺/BrdU⁺ and NeuN⁺/BrdU⁺ cells increased significantly in the BLWE group (Figures 3A–D), indicating that BLWE could facilitate the proliferation of endogenous NSCs in the brains of AD mice and promote them to differentiate into neurons. In the process of neuron development, the formation of synaptic connections is the basis for the function of the CNS and a key step for the

development of memory. SYN-1 and SYP are specific proteins located in the presynaptic membrane, which are mainly responsible for regulating the release of neurotransmitters in synaptic vesicles, thereby participating in the transmission of chemical information. PSD-95 is the main scaffold protein located in the post-protruding membrane and plays an important role in the synaptic structure and functional plasticity, and then participates in the stability and development of the synapse (Liu et al., 2018; Royero et al., 2020; Yang et al., 2022). Our results also showed the levels of SYN-1, SYP, and PSD-95 in the model group were down regulated, while BLWE could up-regulate the level of the above synaptic proteins (Figure 4). It demonstrated that BLWE could improve synaptic plasticity, which was one of the reasons why it enhanced the cognitive function of AD mice. More importantly, through the results of H&E, Nissl, and TUNEL staining, we found that BLWE can significantly reduce the neuropathological damage caused by AD, as well as reduce neuronal cell necrosis and apoptosis (Figures 5A–D). In summary, the above experimental results were strong evidence to prove that BLWE promotes neurogenesis, thereby treating AD.

Using metabolomics technology to identify differential metabolites and analyze the metabolic pathways has important guiding significance for exploring the drug's mechanism. Gong et al. (2015) found and identified 19 biomarkers in AD model mice induced by intracerebral injection of $A\beta_{1-42}$ by UHPLC-TOF/MS method, including proline, valine, tryptophan, LPC, plant sphingosine, and fatty acids, etc. Some scholars found that the metabolism of NAA, choline and inositol in the brain tissue of AD patients differs from that of healthy patients, and the results have certain specificity (Glodzick et al., 2015; Lin et al., 2018; Kirov et al., 2021). In our study, we used the LC-MS method to analyze the brain tissue of mice and found

13 metabolites were changed significantly, including NAA, glutamine, lactosceramide, 4-pyridoxic acid, 5-methyltetrahydrofolic acid, ADP, dihydrothymine, and phosphatidylglycerol, etc. NAA is mainly concentrated in neurons, and its decrease usually represents neurons' loss, injury, and functional defects. Most studies revealed an increase in NAA in the treatment of AD with cholinesterase inhibitors (Paslakis et al., 2014). Glutamine is the most abundant amino acid in cerebrospinal fluid and is essential for a variety of central nervous system processes, such as depression, pain, and cognitive function. Studies indicate that a drastically decreased glutamine level in the brain may be one of the diagnostic criteria for early AD patients. (Huang et al., 2017). Our research also revealed that the changes of these two important metabolites in the brains of AD mice are similar to those of AD patients. More importantly, these two metabolites can be significantly up-regulated after treatment with BLWE, which may be the main reason for improving neurological function.

By analyzing different metabolites, we determined the metabolic pathways that BLWE might affect, and then used the KEGG database to identify the signaling pathways that may also be influenced. Our results show that the Wnt signaling pathway is the most relevant to the effect of BLWE in the treatment of AD patients. The canonical Wnt signaling pathway was considered closely related to the occurrence, development, and deterioration of neurodegenerative diseases such as AD and PD (Tapia-Rojas and Inestrosa, 2018; Wu et al., 2018). Notably, neurogenesis in the hippocampus was significantly reduced when Wnt signaling was blocked (Casse et al., 2018). In the Wnt/ β -catenin pathway, β -catenin is an important cytoplasmic central effector, and GSK-3 β is an important negative regulator which could participate in the phosphorylation of β -catenin. Tyr216 is the excitatory phosphorylation site of GSK-3 β protein. When the expression of p-Tyr216-GSK-3 β decreases, the activity of GSK-3 β is inhibited, which can inhibit the phosphorylation of β -catenin, hence increasing the activity of β -catenin, augment the transduction of Wnt signal and then initiate the transcription of downstream CyclinD₁ (Zeng et al., 2019). CyclinD₁ is one of the important factors downstream of the Wnt/ β -catenin signaling pathway, which is related to the process of neurodegenerative diseases such as AD and PD. Researches have shown that activating the Wnt/ β -catenin signaling pathway can initiate CyclinD₁ transcription, and the increased expression of CyclinD₁ can promote the activation of the pathway (Liu et al., 2021). Our results found that the expression of p-Tyr216-GSK-3 β and p- β -catenin, the ratio of p-Tyr216-GSK-3 β /GSK-3 β and p- β -catenin/ β -catenin in the brain of AD mice all increased significantly. However, these proteins were significantly downregulated by BLWE. These results indicated that the GSK-3 β protein was activated, and the transduction of the

Wnt signal was weakened in AD mice but can be reversed by BLWE treatment. Meanwhile, we also found that the expression of CyclinD₁ protein was decreased significantly in the AD mice but increased after BLWE treatment. CyclinD₁ a regulator of cyclin dependent kinases (CDKs), plays an important role in promoting cell proliferation and is a key molecule in regulating neurons from G₀ to G₁. Current study suggested that the therapeutic effect of BLWE in promoting neurogenesis in the treatment of AD may be achieved by initiating CyclinD₁ transcription and then activating the Wnt/ β -catenin signaling pathway.

In addition, we also focused on the astrocyte-mediated glutamate-glutamine cycle (GGC), which can support the metabolic demands and neurotransmitter transmission of neurons, promote the establishment of synaptic connections between neurons and form neural networks (Tani et al., 2014; Sidoryk-Wegrzynowicz and Struzynska, 2019). NAA and glutamine are precisely the key substances in GGC. Based on this, we speculate that the BLWE can promote neurogenesis, and treatment of AD may also be related to astrocytes, which will be the key point to our further research in the future.

Conclusion

The present study evaluated the effects of BLWE in promoting neurogenesis in the treatment of AD and used metabolomics technology to screen different metabolites, and then accurately analyzed its mechanism. BLWE can promote the regeneration of neurons in the brain and establish synaptic connections. These effects may be achieved by activating the Wnt/ β -catenin signaling pathway. These findings provide an experimental foundation for the application of BLWE in TCM clinical treatment of AD.

Data availability statement

The original contributions presented in the study are included in the article/Supplementary Material, further inquiries can be directed to the corresponding author.

Ethics statement

The animal study was reviewed and approved by the Experimental Animal Ethics Committee of Jiangsu Food & Pharmaceutical Science College.

Author contributions

Study design: Y-HY, Q-PX; Data collection: Y-HY, Y-WS, Z-HH, and YJ; Analysis and interpretation: Y-HY, S-YL, and

B-WY; Statistical analysis: M-YZ and LS; Drafting manuscript: Y-HY and Q-PX; Revision manuscript: Y-HY and Y-WS. All authors read and approved the final manuscript.

Funding

This work was supported by the National Natural Science Foundation of China (grant number 82104422); Natural Science Foundation of Huai'an City (Grant numbers HAB201915, HAB202067); Natural Science Foundation of the Universities of Jiangsu Province (grant numbers 21KJA360006, 20KJA360007, and 21KJB360012); High-end Training Program for Teacher Professional Leaders in Higher Vocational Colleges in Jiangsu Province (Grant number 2022TDFX004); and "Huai Shang Elite" project [grant number (2020)19].

References

- Casse, F., Richetin, K., and Toni, N. (2018). Astrocytes' contribution to adult neurogenesis in physiology and alzheimer's disease. *Front. Cell. Neurosci.* 12, 432. doi:10.3389/fncel.2018.00432
- Chen, X., Chen, H. S., Peng, C., and Shen, J. G. (2019b). Active compounds and molecular targets of Chinese herbal medicine for neurogenesis in stroke treatment: Implication for cross talk between Traditional Chinese Medicine and biomedical sciences. *World J. Tradit. Chin. Med.* 5, 104–115. doi:10.4103/wjtcn.wjtcn_14_19
- Chen, X., Wu, H., Chen, H., Wang, Q., Xie, X. J., and Shen, J. (2019a). Astragaloside VI promotes neural stem cell proliferation and enhances neurological function recovery in transient cerebral ischemic injury via activating EGFR/MAPK signaling Cascades. *Mol. Neurobiol.* 56 (4), 3053–3067. doi:10.1007/s12035-018-1294-3
- de Almeida, E. J. R., Ibrahim, H. J., Chitolina Schetinger, M. R., de Andrade, C. M., and Cardoso, A. M. (2022). Modulation of inflammatory mediators and microglial activation through physical exercise in alzheimer's and Parkinson's diseases. *Neurochem. Res.* 47, 3221–3240. doi:10.1007/s11064-022-03713-x
- Gage, F. H. (2019). Adult neurogenesis in mammals. *Science* 364 (6443), 827–828. doi:10.1126/science.aav6885
- Glodzik, L., Sollberger, M., Gass, A., Gokhale, A., Rusinek, H., Babb, J. S., et al. (2015). Global N-acetylaspartate in normal subjects, mild cognitive impairment and Alzheimer's disease patients. *J. Alzheimers Dis.* 43 (3), 939–947. doi:10.3233/JAD-140609
- Golde, T. E., DeKosky, S. T., and Galasko, D. (2018). Alzheimer's disease: The right drug, the right time. *Science* 362 (6420), 1250–1251. doi:10.1126/science.aau0437
- Gong, Y., Liu, Y., Zhou, L., Di, X., Li, W., Li, Q., et al. (2015). A UHPLC-TOF/MS method based metabonomic study of total ginsenosides effects on Alzheimer disease mouse model. *J. Pharm. Biomed. Anal.* 115, 174–182. doi:10.1016/j.jpba.2015.07.007
- Hanspal, M. A., and Gillotin, S. (2022). A new age in understanding adult hippocampal neurogenesis in Alzheimer's disease. *Neural Regen. Res.* 17 (12), 2615–2618. doi:10.4103/1673-5374.339472
- Huang, D., Liu, D., Yin, J., Qian, T., Shrestha, S., and Ni, H. (2017). Erratum to: Glutamate-glutamine and GABA in brain of normal aged and patients with cognitive impairment. *Eur. Radiol.* 27 (7), 2706–2707. doi:10.1007/s00330-017-4753-8
- Jaberi, R., Mirsadeghi, S., and Kiani, S. (2021). *In vitro* characterization of subventricular zone isolated neural stem cells, from adult monkey and rat brain. *Mol. Biol. Rep.* 48 (2), 1311–1321. doi:10.1007/s11033-021-06201-7
- Ji, H., Liu, Y., He, F., An, R., and Du, Z. (2018). LC-MS based urinary metabolomics study of the intervention effect of aloe-emodin on hyperlipidemia rats. *J. Pharm. Biomed. Anal.* 156, 104–115. doi:10.1016/j.jpba.2018.04.015
- KirovII, Sollberger, M., Davitz, M. S., Glodzik, L., Soher, B. J., Babb, J. S., et al. (2021). Global brain volume and N-acetyl-aspartate decline over seven decades of

Conflict of interest

The authors declare that the research was conducted in the absence of any commercial or financial relationships that could be construed as a potential conflict of interest.

Publisher's note

All claims expressed in this article are solely those of the authors and do not necessarily represent those of their affiliated organizations, or those of the publisher, the editors and the reviewers. Any product that may be evaluated in this article, or claim that may be made by its manufacturer, is not guaranteed or endorsed by the publisher.

normal aging. *Neurobiol. Aging* 98, 42–51. doi:10.1016/j.neurobiolaging.2020.10.024

Kong, L., Hu, Y., Yao, Y., Jiao, Y., Li, S., and Yang, J. (2015). The Coumarin derivative osthole stimulates adult neural stem cells, promotes neurogenesis in the Hippocampus, and ameliorates cognitive impairment in APP/PS1 transgenic mice. *Biol. Pharm. Bull.* 38 (9), 1290–1301. doi:10.1248/bpb.b15-00142

Kriska, J., Janeckova, L., Kirdajova, D., Honsa, P., Knotek, T., Dzamba, D., et al. (2021). Wnt/ β -Catenin signaling promotes differentiation of ischemia-activated adult neural stem/progenitor cells to neuronal precursors. *Front. Neurosci.* 15, 628983. doi:10.3389/fnins.2021.628983

Li, H., Lei, T., Zhang, J., Yan, Y., Wang, N., Song, C., et al. (2021a). Longan (*Dimocarpus longan* Lour.) Aril ameliorates cognitive impairment in AD mice induced by combination of D-gal/AlCl₃ and an irregular diet via RAS/MEK/ERK signaling pathway. *J. Ethnopharmacol.* 267, 113612. doi:10.1016/j.jep.2020.113612

Li, Y. H., Jin, Y., Wang, X. S., Chen, X. L., Chen, H. B., Xu, J., et al. (2021b). Neuroprotective effect of fructus broussonetiae on APP/PS1 mice via upregulation of AKT/ β -Catenin signaling. *Chin. J. Integr. Med.* 27 (2), 115–124. doi:10.1007/s11655-019-3178-4

Liang, Z., Li, X., Luo, X., Luo, H., Chen, Y., Cai, M., et al. (2022). The Aptamer Ob2, a novel AChE inhibitor, restores cognitive deficits and alleviates amyloidogenesis in 5xFAD transgenic mice. *Mol. Ther. Nucleic Acids* 28, 114–123. doi:10.1016/j.omtn.2022.02.018

Lin, R., Li, L., Zhang, Y., Huang, S., Chen, S., Shi, J., et al. (2018). Electroacupuncture ameliorate learning and memory by improving N-acetylaspartate and glutamate metabolism in APP/PS1 mice. *Biol. Res.* 51 (1), 21. doi:10.1186/s40659-018-0166-7

Liu, P., Wang, L. Y., Wang, Y. Q., Wang, R. L., Li, F. F., Zhang, S., et al. (2020). The Chinese herb Fructus Broussonetiae aids learning and memory in chronic cerebral hypoperfusion by reducing proinflammatory microglia activation in rats. *J. Integr. Neurosci.* 19 (1), 21–29. doi:10.31083/j.jin.2020.01.1213

Liu, X., Wang, K., Wei, X., Xie, T., Lv, B., Zhou, Q., et al. (2021). Interaction of NF- κ B and wnt/ β -catenin signaling pathways in alzheimer's disease and potential active drug treatments. *Neurochem. Res.* 46 (4), 711–731. doi:10.1007/s11064-021-03227-y

Liu, Y., Zhang, Y., Zheng, X., Fang, T., Yang, X., Luo, X., et al. (2018). Galantamine improves cognition, hippocampal inflammation, and synaptic plasticity impairments induced by lipopolysaccharide in mice. *J. Neuroinflammation* 15 (1), 112. doi:10.1186/s12974-018-1141-5

Llorens-Bobadilla, E., and Martin-Villalba, A. (2017). Adult NSC diversity and plasticity: The role of the niche. *Curr. Opin. Neurobiol.* 42, 68–74. doi:10.1016/j.conb.2016.11.008

Luo, H., Xiang, Y., Qu, X., Liu, H., Liu, C., Li, G., et al. (2019). Apelin-13 suppresses neuroinflammation against cognitive deficit in a streptozotocin-induced rat model of alzheimer's disease through activation of BDNF-TrkB signaling pathway. *Front. Pharmacol.* 10, 395. doi:10.3389/fphar.2019.00395

- Menet, R., Lecordier, S., and ElAli, A. (2020). Wnt pathway: An emerging player in vascular and traumatic mediated brain injuries. *Front. Physiol.* 11, 565667. doi:10.3389/fphys.2020.565667
- Muhammad, T., Ali, T., Ikram, M., Khan, A., Alam, S. I., and Kim, M. O. (2019). Melatonin rescue oxidative stress-mediated neuroinflammation/neurodegeneration and memory impairment in scopolamine-induced amnesia mice model. *J. Neuroimmune Pharmacol.* 14 (2), 278–294. doi:10.1007/s11481-018-9824-3
- Ou, Y., Zhou, M., Che, M., Gong, H., Wu, G., Peng, J., et al. (2022). Adult neurogenesis of the median eminence contributes to structural reconstruction and recovery of body fluid metabolism in hypothalamic self-repair after pituitary stalk lesion. *Cell. Mol. Life Sci.* 79 (8), 458. doi:10.1007/s00018-022-04457-1
- Pang, S. Q., Wang, G. Q., Lin, J. S., Diao, Y., and Xu, R. A. (2014). Cytotoxic activity of the alkaloids from *Broussonetia papyrifera* fruits. *Pharm. Biol.* 52 (10), 1315–1319. doi:10.3109/13880209.2014.891139
- Paslakis, G., Traber, F., Roberz, J., Block, W., and Jessen, F. (2014). N-acetyl-aspartate (NAA) as a correlate of pharmacological treatment in psychiatric disorders: A systematic review. *Eur. Neuropsychopharmacol.* 24 (10), 1659–1675. doi:10.1016/j.euroneuro.2014.06.004
- Royero, P. X., Higa, G. S. V., Kostecki, D. S., Dos Santos, B. A., Almeida, C., Andrade, K. A., et al. (2020). Ryanodine receptors drive neuronal loss and regulate synaptic proteins during epileptogenesis. *Exp. Neurol.* 327, 113213. doi:10.1016/j.expneurol.2020.113213
- Schott, J. M., Aisen, P. S., Cummings, J. L., Howard, R. J., and Fox, N. C. (2019). Unsuccessful trials of therapies for Alzheimer's disease. *Lancet* 393 (10166), 29. doi:10.1016/S0140-6736(18)31896-8
- Shakir, M. N., and Dugger, B. N. (2022). Advances in deep neuropathological phenotyping of alzheimer disease: Past, present, and future. *J. Neuropathol. Exp. Neurol.* 81 (1), 2–15. doi:10.1093/jnen/nlab122
- Sidoryk-Wegrzynowicz, M., and Struzynska, L. (2019). Astroglial contribution to tau-dependent neurodegeneration. *Biochem. J.* 476 (22), 3493–3504. doi:10.1042/BCJ20190506
- Su, Y. T., Guo, Y. B., Cheng, Y. P., Zhang, X., Xie, X. P., Chang, Y. M., et al. (2019). Hyperbaric oxygen treatment ameliorates hearing loss and auditory cortex injury in noise exposed mice by repressing local Ceramide accumulation. *Int. J. Mol. Sci.* 20 (19), E4675. doi:10.3390/ijms20194675
- Sun, S., Zhu, X. J., Huang, H., Guo, W., Tang, T., Xie, B., et al. (2019). WNT signaling represses astrogliogenesis via Ngn2-dependent direct suppression of astrocyte gene expression. *Glia* 67 (7), 1333–1343. doi:10.1002/glia.23608
- Tani, H., Dulla, C. G., Farzampour, Z., Taylor-Weiner, A., Huguenard, J. R., and Reimer, R. J. (2014). A local glutamate-glutamine cycle sustains synaptic excitatory transmitter release. *Neuron* 81 (4), 888–900. doi:10.1016/j.neuron.2013.12.026
- Tapia-Rojas, C., and Inestrosa, N. C. (2018). Loss of canonical Wnt signaling is involved in the pathogenesis of Alzheimer's disease. *Neural Regen. Res.* 13 (10), 1705–1710. doi:10.4103/1673-5374.238606
- Uddin, M. S., Kabir, M. T., Tewari, D., Mamun, A. A., Mathew, B., Aleya, L., et al. (2020). Revisiting the role of brain and peripheral A β in the pathogenesis of Alzheimer's disease. *J. Neurol. Sci.* 416, 116974. doi:10.1016/j.jns.2020.116974
- Wang, L., Song, L. F., Chen, X. Y., Ma, Y. L., Suo, J. F., Shi, J. H., et al. (2019). MiR-181b inhibits P38/JNK signaling pathway to attenuate autophagy and apoptosis in juvenile rats with kainic acid-induced epilepsy via targeting TLR4. *CNS Neurosci. Ther.* 25 (1), 112–122. doi:10.1111/cns.12991
- Wu, D. M., Han, X. R., Wen, X., Wang, S., Fan, S. H., Zhuang, J., et al. (2018). Salidroside protection against oxidative stress injury through the wnt/ β -catenin signaling pathway in rats with Parkinson's disease. *Cell. Physiol. Biochem.* 46 (5), 1793–1806. doi:10.1159/000489365
- Xiao, H. H., Chen, J. C., Li, H., Li, R. H., Wang, H. B., Song, H. P., et al. (2022). Icarisid II rescues cognitive dysfunction via activation of Wnt/ β -catenin signaling pathway promoting hippocampal neurogenesis in APP/PS1 transgenic mice. *Phytother. Res.* 36 (5), 2095–2108. doi:10.1002/ptr.7430
- Xiao, H., Wang, Y., Wu, Y., Li, H., Liang, X., Lin, Y., et al. (2021). Osthole ameliorates cognitive impairments via augmenting neuronal population in APP/PS1 transgenic mice. *Neurosci. Res.* 164, 33–45. doi:10.1016/j.neures.2020.04.001
- Yan, Y. H., Li, S. H., Li, H. Y., Lin, Y., and Yang, J. X. (2017). Osthole protects bone marrow-derived neural stem cells from oxidative damage through PI3K/Akt-1 pathway. *Neurochem. Res.* 42 (2), 398–405. doi:10.1007/s11064-016-2082-y
- Yan, Y., Kong, L., Xia, Y., Liang, W., Wang, L., Song, J., et al. (2018). Osthole promotes endogenous neural stem cell proliferation and improved neurological function through Notch signaling pathway in mice acute mechanical brain injury. *Brain Behav. Immun.* 67, 118–129. doi:10.1016/j.bbi.2017.08.011
- Yang, G. Z., Gao, Q. C., Li, W. R., Cai, H. Y., Zhao, H. M., Wang, J. J., et al. (2022). (D-Ser2) oxyntomodulin recovers hippocampal synaptic structure and theta rhythm in Alzheimer's disease transgenic mice. *Neural Regen. Res.* 17 (9), 2072–2078. doi:10.4103/1673-5374.335168
- Yu, N., Zhu, K. J., Ma, S. J., Tang, H., and Tan, X. N. (2017). The total flavonoids of *Clerodendrum bungei* suppress A549 cells proliferation, migration, and invasion by impacting Wnt/ β -Catenin signaling. *World J. Tradit. Chin. Med.* 3, 15–20. doi:10.4103/wjtc.wjtc_m18_17
- Zeng, Q., Long, Z., Feng, M., Zhao, Y., Luo, S., Wang, K., et al. (2019). Valproic acid stimulates hippocampal neurogenesis via activating the wnt/ β -catenin signaling pathway in the APP/PS1/nestin-GFP triple transgenic mouse model of alzheimer's disease. *Front. Aging Neurosci.* 11, 62. doi:10.3389/fnagi.2019.00062
- Zhang, H., Su, Y., Sun, Z., Chen, M., Han, Y., Li, Y., et al. (2021). Ginsenoside Rg1 alleviates A β deposition by inhibiting NADPH oxidase 2 activation in APP/PS1 mice. *J. Ginseng Res.* 45 (6), 665–675. doi:10.1016/j.jgr.2021.03.003
- Zhang, Y., Biao, Y., Chu, X., Hao, L., Shi, C., Liu, Y., et al. (2020). Protective effect of Chushizi (*Fructus Broussonetiae*) on acetaminophen-induced rat hepatitis by inhibiting the Toll-like receptor 3/c-Jun N-terminal kinase/c-jun/c-fos/janus protein tyrosine kinase/activators of transcription 3 pathway. *J. Tradit. Chin. Med.* 40 (6), 965–973. doi:10.19852/j.cnki.jtcm.2020.06.008

Glossary

AD Alzheimer's disease

A β amyloid beta peptide

NMDA N-methyl-D-aspartic acid

AchE acetylcholinesterase

NSCs neural stem cells

CNS central nervous system

APP/PS1 amyloid beta precursor protein/presenilin-1

Tg transgenic

BL *Broussonetia papyrifera* (L.) L'Hér. ex Vent. fruits

BLWE *Broussonetia papyrifera* (L.) L'Hér. ex Vent. fruits water extract

GSK-3 β glycogen synthase kinase-3 β

BrdU 5-Bromo-2-deoxyuridine

MWM Morris water maze

NeuN neuronal nuclei

BSA bovine serum albumin

SYN synapsin

SYP synaptophysin

PSD-95 postsynaptic density protein 95

ELISA Enzyme-linked immunosorbent assay

SDS sodium dodecyl sulfate

H&E hematoxylin and eosin

PBS phosphate buffered saline

TUNEL terminal deoxynucleotidyl transferase dUTP nick end labeling

DAPI 4,6-diamidino-2-phenylindole

NS normal saline

HRP horseradish peroxidase conjugated

ECL electrochemiluminescence

LC liquid chromatograph

MS mass spectrometer

PVDF polyvinylidene fluoride

HMDB Human Metabolome Database

KEGG Kyoto Encyclopedia of Genes and Genomes

PCA principal component analysis

PLS-DA partial least squares discriminant analysis

OPLS-DA orthogonal partial least squares

SVZ subventricular zone

SGZ subgranular zone

TCM Traditional Chinese medicine.



OPEN ACCESS

EDITED BY
Zheng Xiang,
Liaoning University, China

REVIEWED BY
Zeyu Chen,
Tongji University, China
Jianmin Chen,
Putian University, China

*CORRESPONDENCE
Chen Fan,
fanchenbiomedicals@ucas.ac.cn
Yuhong Xu,
yhxu@ dali.edu.cn

†These authors have contributed equally
to this work

SPECIALTY SECTION
This article was submitted to
Ethnopharmacology,
a section of the journal
Frontiers in Pharmacology

RECEIVED 11 October 2022
ACCEPTED 10 November 2022
PUBLISHED 18 November 2022

CITATION
Wang C, Hao R, Peng B, Chang J,
Chen S, Chen Y, Yin X, Que Y, Fan C and
Xu Y (2022), Dissolvable hyaluronic acid
microneedles loaded with β -Elemene
for the treatment of psoriasis.
Front. Pharmacol. 13:1067051.
doi: 10.3389/fphar.2022.1067051

COPYRIGHT
© 2022 Wang, Hao, Peng, Chang, Chen,
Chen, Yin, Que, Fan and Xu. This is an
open-access article distributed under
the terms of the [Creative Commons
Attribution License \(CC BY\)](#). The use,
distribution or reproduction in other
forums is permitted, provided the
original author(s) and the copyright
owner(s) are credited and that the
original publication in this journal is
cited, in accordance with accepted
academic practice. No use, distribution
or reproduction is permitted which does
not comply with these terms.

Dissolvable hyaluronic acid microneedles loaded with β -Elemene for the treatment of psoriasis

Chun Wang^{1,2,3}, Ruiqi Hao^{2,3}, Baowei Peng¹, Jiang Chang^{2,3},
Shisheng Chen⁴, Yanxin Chen^{2,3}, Xiaohang Yin^{2,3}, Yumei Que^{2,3},
Chen Fan^{2,3*†} and Yuhong Xu^{1*†}

¹College of Pharmaceutical Science, Dali University, Dali, China, ²Joint Centre of Translational Medicine, The First Affiliated Hospital of Wenzhou Medical University, Wenzhou, China, ³Wenzhou Institute, University of Chinese Academy of Sciences, Wenzhou, China, ⁴Department of Dermatology, The Second Affiliated Hospital and Yuying Children's Hospital of Wenzhou Medical University, Wenzhou, China

The pathology of psoriasis involves the over-proliferation of keratinocytes, exaggerated inflammation of keratinocytes, and infiltration of inflammatory cells such as macrophages (M ϕ), etc. The therapeutic outcomes of current treatment targeting one single pathological process are less than satisfactory. Based on their diverse biological activities, natural products offer a potential solution to this problem. In this study, we investigated the effects of β -Elemene (ELE) on both psoriatic keratinocytes and M1-type M ϕ (M1-M ϕ) *in vitro*. Hyaluronic acid (HA) microneedles loaded with ELE (HA-ELE-MN) were also fabricated and tested for the treatment of psoriasis *in vivo* using an imiquimod (IMQ)-induced psoriatic mice model. Our data suggest that ELE induces apoptosis and inhibits inflammation of psoriatic keratinocytes. In addition, ELE attenuates the expression of inflammatory cytokines secreted from M1-M ϕ , thus indirectly inhibiting the inflammation of keratinocytes. Furthermore, HA-ELE-MN has been found to significantly alleviate symptoms in an IMQ-induced psoriatic mice model by inducing keratinocytes apoptosis, suppressing keratinocytes proliferation, and inhibiting M1-M ϕ infiltration. Taken together, this study demonstrates that ELE can be used for the treatment of psoriasis by targeting both keratinocytes and M1-M ϕ , which provides a potential novel reagent for psoriasis treatment.

KEYWORDS

β -Elemene, Psoriasis, Microneedles, apoptosis, inflammation

1 Introduction

Psoriasis is a chronic inflammatory skin disease in clinic, it has been reported that more than 120 million people suffer from psoriasis worldwide (Greb et al., 2016). It not only causes physical damage such as pain and itching (Dubertret et al., 2010) but also has a great negative impact on the mental health of the patients (Boehncke and Schon, 2015). In

addition, studies also found that psoriatic patients have significantly increased risks of other chronic and serious complications, including psoriatic arthritis, metabolic syndrome, cardiovascular diseases, *etc.* (Barker Jonathan, 2007; Nestle et al., 2009). To date, the exact pathogenesis of psoriasis is still not fully understood. The over-proliferation and exaggerated inflammation of keratinocytes are the main pathological features of psoriasis (Zhou et al., 2022). Except for the environmental and genetic factors, excessive aggregation of inflammatory cytokines caused by the infiltration of various inflammatory cells is one of the main causes of the over-proliferation and inflammation of keratinocytes. For example, studies have found that the number of CD68⁺ M1-Mø is significantly elevated in psoriasis skin, indicating that infiltration of M1-Mø plays an essential role in psoriasis (Kim et al., 2019). Further study revealed that infiltration of M1-Mø leads to an increased expression of various inflammatory cytokines such as tumor necrosis factor- α (TNF- α), interleukin-1 (IL-1), IL-6, IL-12, IL-23, and Interferon γ (IFN- γ). These inflammatory cytokines further stimulate keratinocytes proliferation and inflammation, thus leading to the onset of psoriasis.

Although there are various therapies for psoriasis in clinic, their therapeutic effects are limited and often cause various side effects. For example, methotrexate is a commonly used psoriasis drug by inducing apoptosis in keratinocytes (Elango et al., 2017), however, it has strong hepatotoxicity. Light therapy is also frequently used for the treatment of severe psoriasis by triggering keratinocytes apoptosis, while it causes erythema, itching, blistering, and photoaging (Armstrong and Read, 2020). In addition, corticosteroids have been demonstrated to relieve psoriasis by suppressing inflammation, but it is only suitable for mild psoriasis. The long-term use of corticosteroids results in skin atrophy, telangiectasia, and skin striae (Armstrong and Read, 2020). In recent years, various biologics targeting specific inflammatory cytokines, such as IL-17A inhibitors, TNF- α inhibitors, IL-23 inhibitors, *etc.*, have also been shown to be effective in treating psoriasis. However, side effects such as upper respiratory tract infections are observed after their clinical use (Armstrong and Read, 2020; Diotallevi et al., 2022). Therefore, the therapeutic effects of treatment targeting one single pathological process of psoriasis are unsatisfactory. With the increased understanding of the roles of inflammatory cells in psoriasis, recent studies also explored the possibility of treating psoriasis by regulating inflammatory cells such as Mø, however, the therapeutic effects need to be further evaluated (Tao et al., 2022). To improve the therapeutic effects, other studies also used combination therapies. For example, Wang et al. (2022) explored a chemo-photodynamic strategy using the combination of methotrexate and 5-aminolevulinic acid, which has been shown to effectively alleviate psoriasis by inducing apoptosis and inhibiting inflammation simultaneously (Wang et al., 2022). Although combination therapies have been found to generate better therapeutic outcomes, they make the

pharmacological mechanisms more elusive, and the safety of these combination therapies needs to be further evaluated (Nakamura and Koo, 2020).

Natural products offer a potential solution to the above issue, as they often possess diverse biological activities, allowing the use of one molecule to simultaneously regulate multiple pathological processes. By analyzing the literature, we found that ELE holds both apoptosis-inducing and inflammation-inhibiting properties. For example, ELE has been shown to induce apoptosis in various tumor cell lines including hepatocellular carcinoma cell lines (Wu et al., 2016), Osteosarcoma MG 63 and U2OS cell lines (Ding et al., 2018), and human non-small lung cancer A549 cell lines (Liu et al., 2012). In addition, Hu et al. (2020) found that ELE significantly inhibits the inflammatory responses in mouse skin tumor tissues (Hu et al., 2020). Han et al. (2021) reported that ELE attenuates the elevated expression of IL-1 in Lipopolysaccharides (LPS)-stimulated Mø, suggesting the inflammation-inhibiting ability of ELE by regulating Mø (Han et al., 2021). Based on the bioactivities of ELE, we therefore hypothesized that ELE induces apoptosis in psoriatic keratinocytes and inhibits inflammation in both psoriatic keratinocytes and M1-Mø, thus can be used for the treatment of psoriasis.

Since the epidermis layer of psoriatic skin is significantly thicker than that in normal skin, the effective delivery of drugs is therefore another key point for psoriasis treatment. To date, most of the anti-psoriasis drugs are topically applied to the lesion by plasters, however, the poor drug delivery efficiency causes limited therapeutic effects (Qu et al., 2022). Particularly for natural products, although promising therapeutic effects can be observed in *vitro* studies, the therapeutic outcomes *in vivo* are often significantly reduced due to their unstable physicochemical properties, poor solubility, and low bioavailability. The emergence of microneedle (MN) technology offers a potential solution to this problem. Compared to traditional formulations, MN delivery significantly increases the drug concentration at the site of the lesion. In addition, MN transdermal delivery technique has been demonstrated to minimize systemic toxicity, sense of pain, and tissue invasion (Qu et al., 2022).

In this study reported herein, we investigated the effects of ELE on both psoriatic keratinocytes and M1-Mø. In addition, how ELE directly affects keratinocytes *via* the regulation of M1-Mø was also detected. Furthermore, the therapeutic effects of HA-ELE-MN were validated using an IMQ-induced psoriatic mice model.

2 Materials and methods

2.1 Experimental reagents

ELE was purchased from Macklin (Shanghai, China) and dissolved in DMSO to make a stock solution at 10 mM. IMQ was

purchased from Med-Shine Pharmaceutical (Sichuan, China). TNF- α , IL-1 α , IL-17, IL-22, and oncostatin-M (OSM) were purchased from Beyotime (Shanghai, China) and mixed together to make an M5 solution at 2.5 ng/ml based on the previously published method (Gao et al., 2020). LPS was purchased from Sigma (Shanghai, China) and dissolved in the cell culture medium to make a 10 ng/ml stock solution. Recombinant mouse IFN- γ was purchased from Novoprotein (Suzhou, China) and dissolved in sterile water to obtain a 10 ng/ml stock solution.

2.2 Cell culture

Human keratinocytes (HaCaT), dermal fibroblasts (HFF-1), and mouse M ϕ (RAW264.7) cell lines were purchased from American type culture collection (ATCC) and cultured in high glucose Dulbecco's Modified Eagle's Medium (DMEM) containing 10% fetal bovine serum (FBS) and 1% penicillin-streptomycin. Cells were maintained at 37 °C in an incubator with 5% CO₂.

2.3 Cell viability

Effects of ELE on the viability of keratinocytes, fibroblasts, and M5-stimulated keratinocytes were measured using Cell Counting Kit (CCK-8; Yeasen Biotechnology, Shanghai, China). Briefly, the cells were seeded in a 96-well plate at 5000 cells/well for 24 h. Then different concentrations (50 and 100 μ M) of ELE were applied to the cells for 72 h. To detect the effect of ELE on M5-stimulated keratinocytes, cells were seeded in a 96-well plate at 5000 cells/well for 24 h. Then the cells were further treated with ELE (100 μ M) mixed with M5 (2.5 ng/ml) for 72 h. A group containing M5 only was also included as a control. Cell viability was measured by reading the absorbance at 450 nm after incubated with CCK-8 reagents for 1 h.

2.4 Cell apoptosis

Cell apoptosis triggered by ELE in M5-stimulated keratinocytes was detected using a TUNEL apoptosis assay kit (Beyotime). Briefly, keratinocytes (2 \times 10⁴ cells/well) were seeded in a 48-well plate for 24 h and then treated with M5 mixed with ELE as described above. After exposure for 48 h, the cells were fixed and permeabilized using reagents provided in the assay kit. The cells were then further incubated with a biotin-labeled solution for 60 min followed by Streptavidin-HRP for another 30 min. Apoptotic cells were visualized using an Olympus CKX53 microscope (Olympus, Japan) after incubation with DAB chromogenic solution.

2.5 RT-PCR

Keratinocytes (2 \times 10⁴ cells/well) were seeded in a 48-well plate for 24 h, then the cells were treated with M5 mixed with ELE as described above for 48 h. For the M ϕ study, the cells were first resuspended in a medium containing LPS (100 ng/ml), IFN- γ (20 ng/ml), and ELE (100 μ M), respectively. The cells (2 \times 10⁵ cells/well) were then further seeded in a 48-well plate for 48 h. To identify the effects of ELE-pretreated M1-M ϕ , M ϕ was cultured in a medium containing LPS/IFN- γ or LPS/IFN- γ /ELE for 24 h. The medium was then discarded and replaced with fresh medium (without LPS/IFN- γ and ELE) for another 24 h. The conditioned medium (CM) was eventually collected and placed in dishes pre-seeded with keratinocytes for 48 h. Total RNA was extracted using MolPure Cell/Tissue miRNA Kit (Yeast Biotechnology). The first strand cDNA was synthesized using Hifair11st Strand cDNA Synthesis SuperMix for qPCR (Yeast Biotechnology). qRT-PCR was performed using SYBR green reagent in an LightCycler 480 II (Roche, Swiss). Primers of targeted genes are listed in Table 1 below:

2.6 HA-ELE-MN preparation

Polydimethylsiloxane (PDMS) mold was purchased from Taizhou Microchip Pharmaceutical Technology (Taizhou, China). The parameters of the PDMS mold are: needle length = 1 mm, bottom dimension = 0.45 mm * 0.45 mm, number of arrays = 15 * 15, and groove depth = 16 mm * 16 mm. HA powder was dissolved in deionized water to make a 7% (w/v) HA solution, and then the ELE stock solution (10 mM) was mixed with 7% HA solution at different ratios for MN containing different amounts of ELE. The HA-ELE mixtures were then poured into a PDMS mold, centrifuged at 4000 rpm for 5 min, and eventually dried in a fume hood at room temperature for 2 days. ELE-HA-MN was obtained by peeling off the PDMS mold and stocked at room temperature for future use.

2.7 Mechanical performance of HA-ELE-MN

As described above, the ELE stock solution was mixed with 7% HA solution at ratios of 1:250, 1:50, and 1:10 to make the concentration of ELE in ELE-HA-MN at 40, 200, and 1000 μ M, respectively. The mechanical property of HA-ELE-MN was tested using Electronic universal Material Testing Machine (Instron 5944). In brief, MNs were placed on the metal platform with tips facing upwards. The cylindrical probe sensor was set to move down at the speed of 1 mm/s to compress the MNs. Force and displacement data were recorded and eventually processed into a force-displacement curve.

TABLE 1 Primers used in RT-PCR.

Protein Name	Corresponding Gene Name	Primer Sequences
For keratinocytes		
GAPDH	<i>GAPDH</i>	F: 5'-CAGGAGAGTGTTTCCTCGTCC-3' R: 5'-TTTGCCGTGAGTGGAGTCAT-3'
IL-1 α	<i>IL1A</i>	F: 5'-CATGTCAAATTTCACTGCTTCATCC-3' R: 5'-GTCTCTGAATCAGAAATCCTTCTATC-3'
IL-1 β	<i>IL1B</i>	F: 5'-ATGATGGCTTATTACAGTGGCAA-3' R: 5'-GTCGGAGATTCGTAGCTGGA-3'
IL-6	<i>IL6</i>	F: 5'-TCCCACGAAATCCAGGATGC-3' R: 5'-GGATGTTTCAGGTTGACCATCAC-3'
IL-8	<i>IL8</i>	F: 5'-ACTGAGAGTGATTGAGAGTGGAC-3' R: 5'-AACCTCTGCACCCAGTTTTC-3'
Keratin 6	<i>KRT6</i>	F: 5'-GGGTTTCAGTGCCAACTCAG-3' R: 5'-CCAGGCCATACAGACTGCGG-3'
Filaggrin	<i>FLG</i>	F: 5'-TTTCGTGTTTGTCTGCTTGC-3' R: 5'-CTGGACACTCAGGTTCCCAT-3'
For M ϕ		
GAPDH	<i>Gapdh</i>	F: 5'-CAGGAGAGTGTTTCCTCGTCC-3' R: 5'-TTTGCCGTGAGTGGAGTCAT-3'
TNF- α	<i>Tnf</i>	F: 5'-TAGCCACGTCGTAGCAAAC-3' R: 5'-GCAGCCTTGTCCTTGAAGA-3'
IL-1 α	<i>Il1a</i>	F: 5'-GTCGGGAGGAGACGACTCTAA-3' R: 5'-GTTTCTGGCACTCCTTCAGC-3'
IL-12A	<i>Il12a</i>	F: 5'-TGTTCAATCACGCTACCTCC-3' R: 5'-TGGTCTTCAGCAGGTTTCGG-3'

2.8 In vivo penetration of HA-ELE-MN

ELE-HA-MN (ELE concentration at 1 mM) was inserted into the back skin of normal BALB/c mice and IMQ-induced psoriasis BALB/c mice for 1 min, respectively. The skin was then removed from the mice, fixed with 4% paraformaldehyde, embedded, sectioned, and stained with Hematoxylin and Eosin. Penetration of skin was recorded using an Olympus CKX53 microscope (Olympus).

2.9 In vivo dissolution of HA-ELE-MN

ELE-HA-MN (ELE concentration at 1 mM) was inserted into the back skin of BALB/c mice for 0, 3, 5, and 10 min, respectively. The MNs were then peeled off and cut into strips. The dissolution of the tips was captured using an Olympus SZ61 microscope (Olympus).

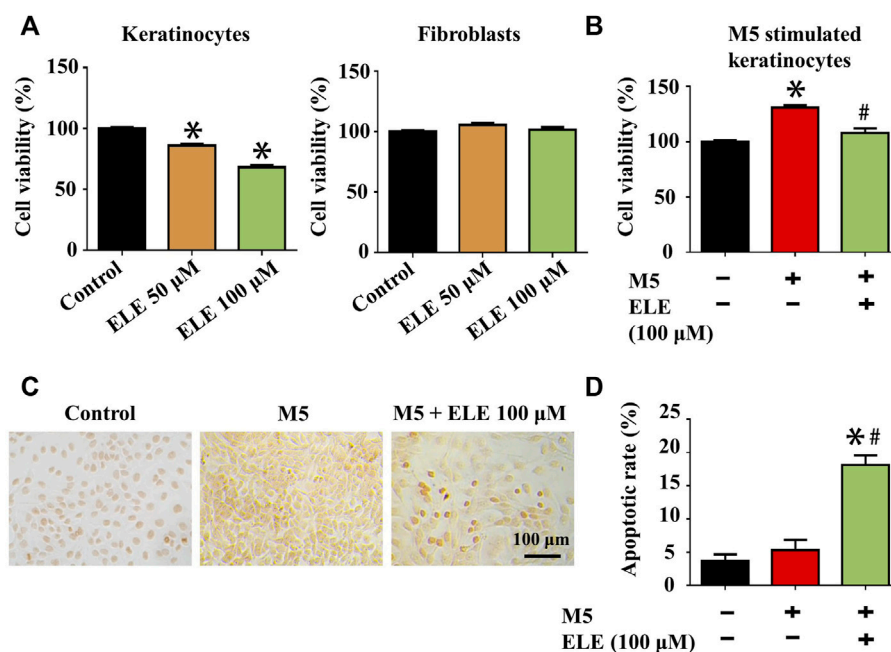
2.10 IMQ-induced psoriasis mouse model establishment and treatment

The hair on the back skin of BALB/c mice (male, 8 weeks) was removed using a razor. After isoflurane inhalation

anesthesia, the mice received topical treatment of 70 mg 5% IMQ cream on the back skin every morning for 7 days. Psoriasis-like symptoms including erythema and scales could be observed 3 days later. From then, HA-MN, HA-ELE-MN (1mM), and ELE Vaseline cream (1 mM) were applied every night for 4 days. Images of back skin were recorded every morning for the assessment of the psoriasis area and severity index (PASI). Parameters of PASI, including erythema, scales, and infiltration, were scored as follows: 0 (none), 1 (mild), 2 (moderate), 3 (severe), and 4 (very severe). These three parameter scores were then summed to obtain a total score that reflects the severity of inflammation in mice back. After stimulated with IMQ for 7 days along with the treatment of ELE for 4 days, the mice were sacrificed to obtain skin tissues for further analysis.

2.11 Histological analysis

The skin samples collected from the sacrificed mice were fixed with paraformaldehyde, dehydrated with graded alcohol, embedded in paraffin, and sectioned (thickness = 8 μ m). Sections were then deparaffinized and rehydrated with xylene and graded

**FIGURE 1**

(A) Effects of ELE on the viability of keratinocytes and fibroblasts at 72 h. (B) Effects of ELE on the viability of M5-stimulated keratinocytes at 72 h. (C) ELE-induced apoptosis cells (dark brown) detected in M5-stimulated keratinocytes using TUNEL assay. (D) Quantitative analysis of TUNEL assay. * $p < 0.05$ versus control, # $p < 0.05$ versus M5. Error bars indicate SEM ($n = 3$).

alcohol. Hematoxylin and Eosin (H&E) staining were performed to evaluate the thickness of the skin samples; TUNEL assay was used to identify the apoptotic cells in the skin samples; and immunohistochemical staining of ki67 and CD86 (1:150 dilution, Beyotime) was applied to detect the proliferation of cells and inflammation in the skin samples.

2.12 Statistical analysis

Statistical analysis was carried out using IBM SPSS software (version 20). Results were shown as means \pm standard error of the mean (SEM). Differences between groups were by one-way ANOVA followed significant and p -value less than 0.05 was considered as statistically significant.

3 Results

3.1 ELE reduces cell viability and induces apoptosis in M5-stimulated keratinocytes

Effects of ELE on the viability of keratinocytes and fibroblasts were evaluated using CCK-8 assay. As shown in Figure 1A, ELE at 50 and 100 μ M significantly attenuated keratinocytes viability by $14.08 \pm 1.4\%$ and $31.83 \pm 1.63\%$, respectively. However, no

inhibitory effects of ELE on fibroblasts were observed at the same concentrations, indicating that ELE is able to specifically inhibit the viability of keratinocytes. To further explore how ELE affects psoriatic keratinocytes *in vitro*, the effects of ELE on M5-stimulated keratinocytes were also investigated based on the previously published method (Gao et al., 2020). As illustrated in Figure 1B and C, ELE was found to inhibit cell viability and induce apoptosis in M5-stimulated keratinocytes. Quantitative analysis (Figure 1D) showed that ELE at 100 μ M triggered $18.11 \pm 0.49\%$ of cells undergoing apoptosis. Taken together, these data suggest that ELE specifically reduces the viability of keratinocytes without affecting the viability of dermal fibroblasts. In addition, ELE inhibits cell viability and induces apoptosis in psoriatic keratinocytes *in vitro*.

3.2 ELE-induced gene changes in M5-stimulated keratinocytes

As shown in Figure 2, ELE was found to significantly attenuate M5-triggered up-regulation of *IL1A* (encoding IL-1 α), *IL1B* (encoding IL-1 β), *IL6* (encoding IL-6), and *IL8* (encoding IL-8). In addition, ELE also attenuated the M5-induced expression of *KRT6* (encoding keratin 6). Furthermore, M5 significantly reduced the expression of *FLG* (encoding filaggrin) in keratinocytes, while ELE improved the

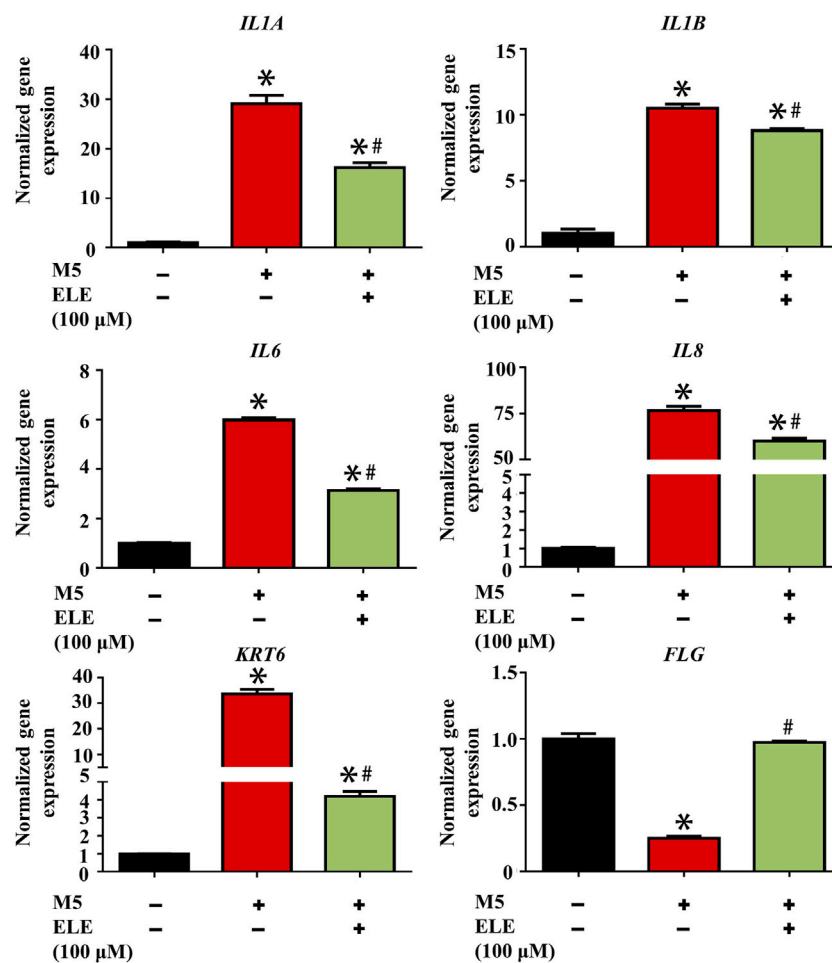


FIGURE 2

Effects of ELE on the expression of psoriasis-related genes in M5-stimulated keratinocytes. * $p < 0.05$ versus control, # $p < 0.05$ versus M5. Error bars indicate SEM ($n = 3$).

expression of FLG in M5-stimulated keratinocytes. Taken together, these data suggest that ELE inhibits M5-stimulated inflammation and proliferation in keratinocytes. It also protects the M5-induced damages to the barrier function of keratinocytes.

3.3 ELE indirectly attenuates keratinocytes inflammation by mediating M1-Mø

Elevated expression of M1-Mø is another key characteristic of psoriasis, it has been found that various inflammatory cytokines such as ILs and TNF- α secreted by M1-Mø contribute to psoriasis by triggering inflammation in keratinocytes (Kamata and Tada, 2022). We therefore stimulated Mø using LPS/INF- γ to obtain M1-Mø *in vitro* and then examined the effects of ELE on the gene expression

of key inflammatory cytokines in M1-Mø. As shown in Figure 3A, ELE significantly down-regulated the expression of *Tnf* (encoding TNF- α), *Il1a* (encoding IL-1 α), and *Il12a* (encoding IL-12A) in M1-Mø. In addition, we also investigated how the ELE-pretreated M1-Mø indirectly affects keratinocytes (Figure 3B). As demonstrated in Figure 3C, CM collected from M1-Mø significantly enhanced the expression of *IL1A* and *KRT6* in keratinocytes, while the expression of these two genes was significantly down-regulated after exposure to the ELE-pretreated M1-Mø CM. Although no up-regulation of *IL1B* was detected in keratinocytes treated with M1-Mø CM, ELE-pretreated M1-Mø CM significantly reduced the expression of *IL1B* in keratinocytes. These data indicate that ELE indirectly attenuates keratinocyte inflammation by inhibiting inflammatory cytokines released from M1-Mø.

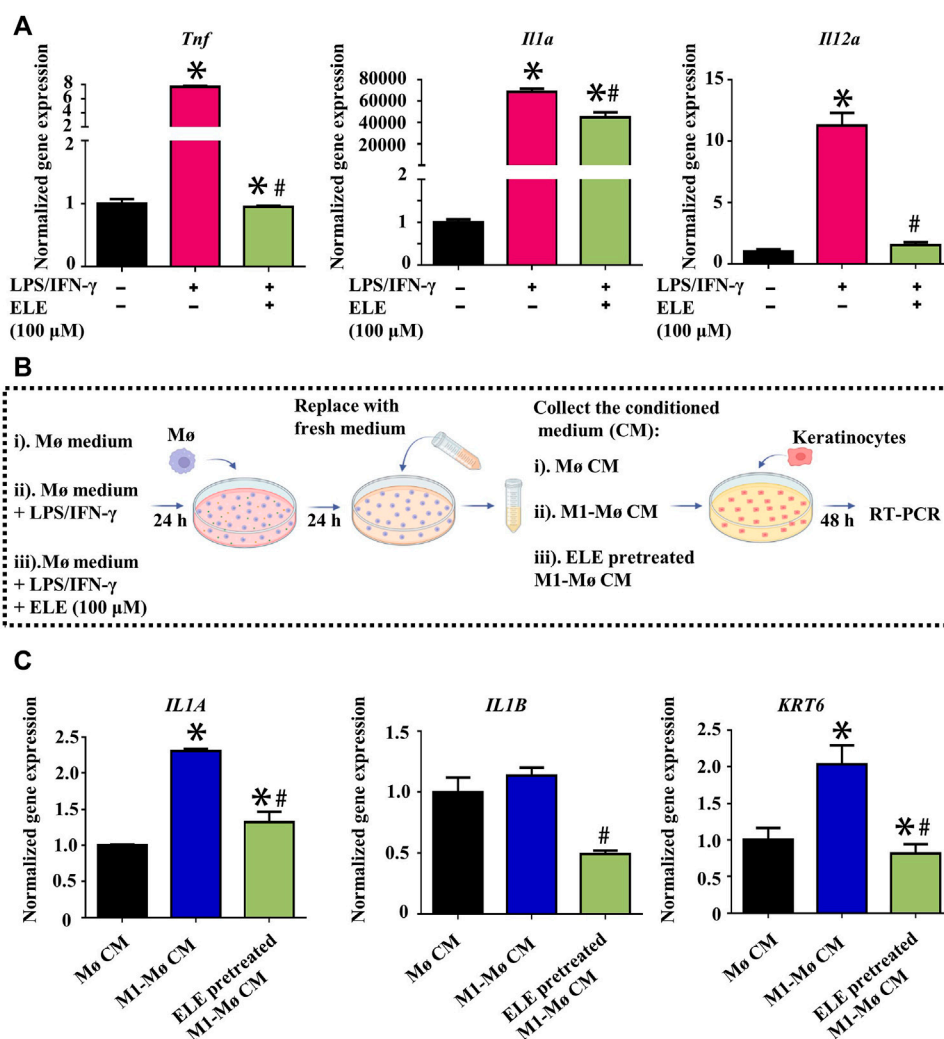


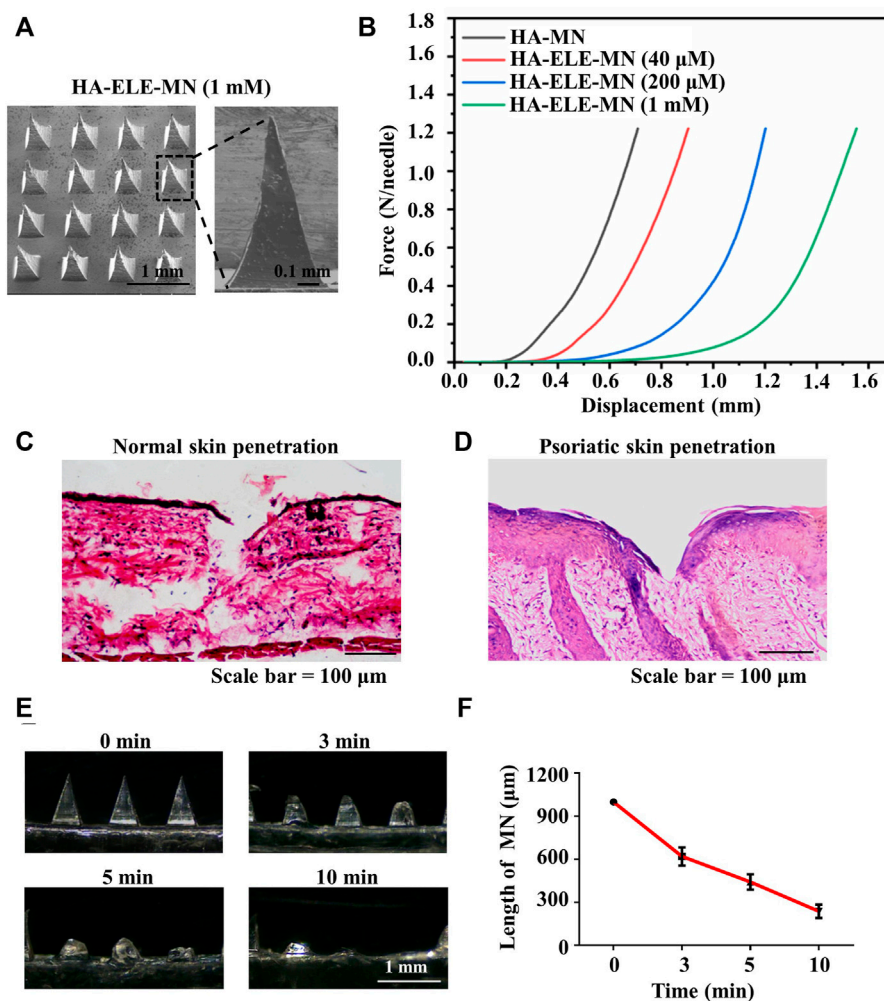
FIGURE 3

(A) Effects of ELE on the expression of *Tnf*, *Il1a*, and *Il12a* in M1-M ϕ . (B) Scheme illustration of the effects of M ϕ CM on keratinocytes. (C) Effects of M1-M ϕ and ELE-pretreated M1-M ϕ CM on the expression of *IL1A*, *IL1B*, and *KRT6* in keratinocytes. * $p < 0.05$ versus control, # $p < 0.05$ versus LPS/IFN- γ or M1-M ϕ CM. Error bars indicate SEM ($n = 3$).

3.4 Characterization of HA-ELE-MN

As illustrated in Figure 4A, the needle arrays were intact and consecutive, and each single needle showed a triangular pyramidal shape. As demonstrated in Figure 4B, the stiffness of HA-ELE-MN dropped with the increase in ELE concentration, however, HA-ELE-MN at the highest ELE concentration (1 mM) was still strong enough to withstand a force of more than 1.2 N/needle without fracture. Previous studies reported that the minimum force required for skin penetration was less than 0.1 N/needle (Zhu et al., 2017), indicating that the HA-ELE-MN is capable to penetrate the skin. To further confirm this, we tested the penetrating ability of HA-ELE-MN (1 mM) on the back skin of BALB/c mice using H&E staining. As shown in

Figure 4C, the HA-ELE-MN (1mM) successfully broke the epidermis and reached the dermis. Given that psoriasis skin normally has a thicker epidermis compared to normal skin, therefore the same test on the back skin of IMQ-induced psoriasis BALB/c mice was also performed. As can be seen in Figure 4D broken epidermis was observed in psoriasis skin after treated with HA-ELE-MN (1mM), indicating the HA-ELE-MN (1mM) is able to penetrate the psoriasis skin as well. Dissolution of HA-ELE-MN *in vivo* was tested by applying the HA-ELE-MN (1mM) on the back skin of BALB/c mice for 3, 5, and 10 min, respectively. As proved in Figure 4E and F, the needles containing ELE almost totally dissolved in the skin tissue within 10 min, indicating the fast drug release capability of the HA-ELE-MN (1mM).

**FIGURE 4**

Characterizations of HA-ELE-MN (1mM). (A) Morphology of HA-ELE-MN (1mM) recorded using SEM. (B) Force-displacement curves of HA-ELE-MNs containing different concentrations of ELE. (C) H&E staining of normal back skin of BALB/c mice after application of HA-ELE-MN (1mM). (D) H&E staining of psoriasis skin of IMQ-induced psoriasis BALB/c mice after application of HA-ELE-MN (1mM). (E) Dissolution of HA-ELE-MN (1mM) in the skin of BALB/c mice. (F) Quantitative analysis of the speed of *in vivo* drug release by measuring the change of needle length.

3.5 HA-ELE-MN alleviates symptoms in IMQ-induced psoriasis model

The therapeutic effects of HA-ELE-MN (1mM) were evaluated using PASI scores on an IMQ-induced psoriasis model. As can be seen in Figure 5B, symptoms including erythema, scaling, and infiltration were found to be alleviated in ELE cream (1mM), HA-MN, and HA-ELE-MN (1mM) groups compared to the IMQ group. HA-ELE-MN (1mM) showed better therapeutic outcomes compared to the HA-MN and ELE cream (1mM) groups. Based on the PASI scores, the scales (Figure 5C) were significantly reduced in HA-ELE-MN (1mM) treated group compared to the IMQ group on day 6 and 7. Erythema (Figure 5D) on the back skin was significantly

alleviated in HA-ELE-MN (1mM) treated group compared to the IMQ group on day 5, 6, and 7. ELE cream (1mM) was also found to attenuate the erythema compared to the IMQ group on day 7. Reduced infiltration (Figure 5E) was detected on day 5 in the HA-MN and HA-ELE-MN (1mM) groups, while attenuated infiltration was observed in the ELE cream (1mM) and HA-ELE-MN (1mM) group on day 6 compared to the IMQ group. Significantly down-regulated infiltration was found in HA-MN, ELE cream (1mM), and HA-ELE-MN (1mM) groups at day 7 compared to the IMQ group. Taken together, the total PASI scores shown in Figure 5F suggest that both ELE cream (1mM) and HA-ELE-MN (1mM) possess therapeutic effects on psoriasis, and HA-ELE-MN (1mM) generates better therapeutic outcomes compared to ELE cream (1mM).

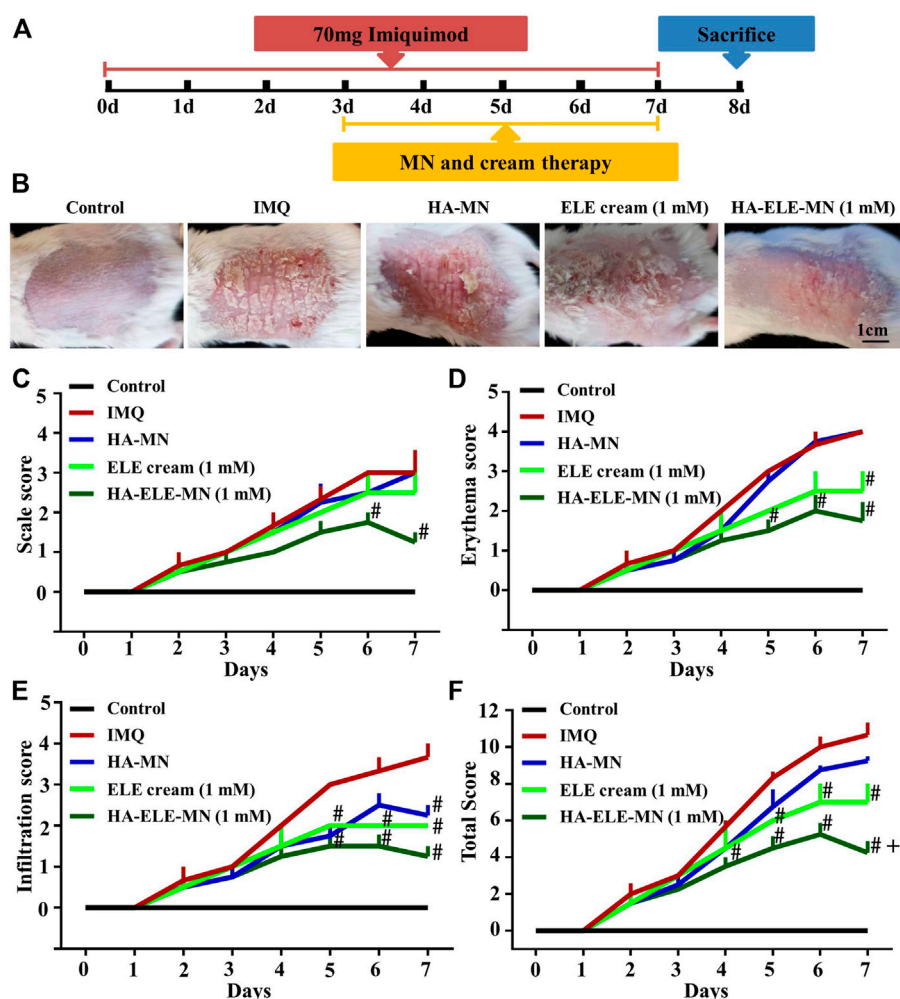


FIGURE 5

Mitigation of IMQ-induced psoriasis after exposure to HA-ELE-MN (1mM). (A) Schematic illustration of HA-ELE-MN (1mM) for the treatment of IMQ-induced psoriasis. (B) Representative photographs captured on day 7 (treated with IMQ for 7 days and exposed to ELE cream (1mM), HA-MN, and HA-ELE-MN (1mM) for 4 days). (C–E) PASI scores of scales, erythema, and infiltration. (F) Total PASI scores by pooling scales, erythema, and infiltration together. # $p < 0.05$ versus IMQ, + $p < 0.05$ versus ELE cream (1mM). Error bars indicate SEM ($n = 3$).

3.6 HA-ELE-MN reduces epidermal thickness, induces apoptosis, inhibits cell proliferation, and attenuates M1-M ϕ infiltration in the IMQ-psoriasis model

H&E staining was performed to assess the effects of HA-ELE-MN (1mM) on the epidermal thickness in the IMQ-induced psoriasis model (Figure 6A and E). It can be seen that HA-MN containing no ELE had no effect on the epidermal thickness compared to the IMQ group, however, both ELE cream (1mM) and HA-ELE-MN (1mM) groups significantly reduced the epidermal thickness compared to the IMQ group. In addition, the epidermal thickness in HA-ELE-MN (1mM) treated group was found to be significantly thinner than that in the ELE cream

(1mM) group, suggesting a better therapeutic outcome by delivering ELE using MN.

TUNEL assay was performed to identify the apoptotic cells triggered by HA-ELE-MN (1mM) *in vivo*. As exhibited in Figure 6B and F, an increased number of apoptotic cells was observed in the ELE cream (1mM) group compared to the IMQ and HA-MN groups, however, no statistical differences were obtained in the quantitative analysis, suggesting the apoptosis-inducing ability of ELE is limited by the formulation. In contrast, a significantly increased number of apoptotic cells was detected in the HA-ELE-MN (1mM) group compared to all other groups.

In addition, increased expression of ki67 in the epidermis reflects enhanced proliferation of keratinocytes. It can be seen in Figure 6C and G that the expression of ki67 was significantly

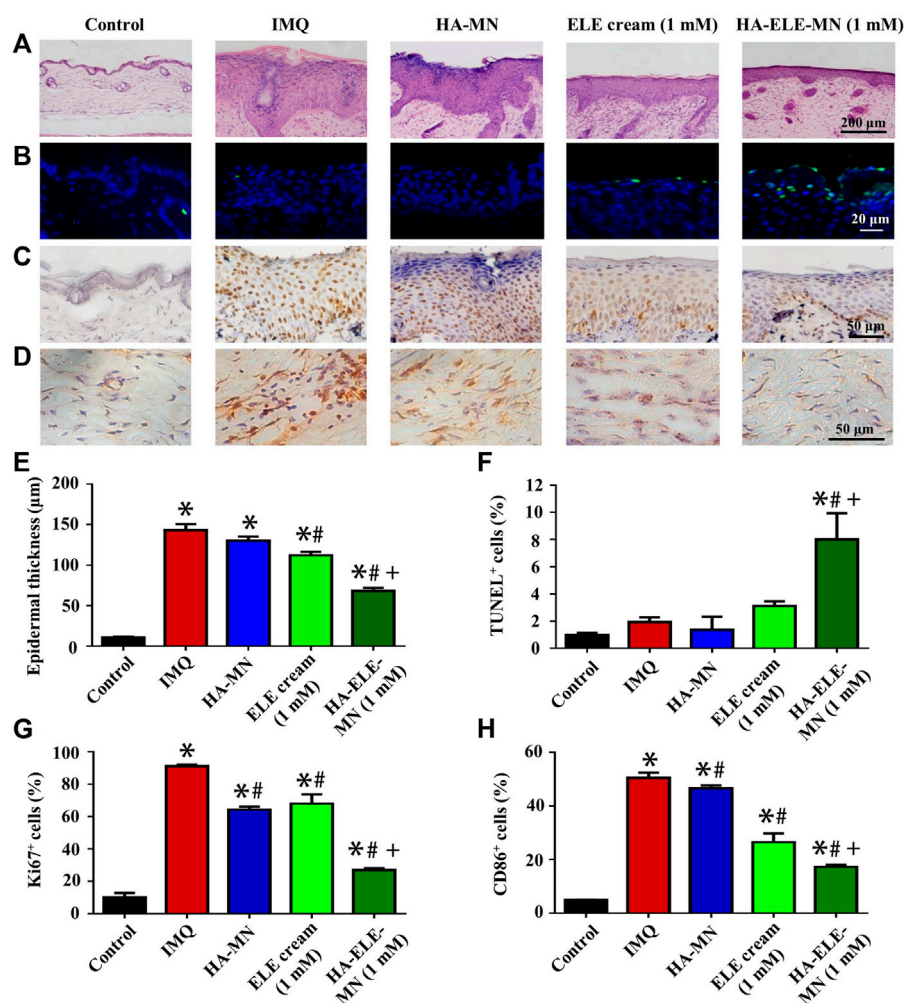


FIGURE 6

Histopathological analysis of skin samples in IMQ-induced psoriasis model after treated with HA-ELE-MN (1mM). (A) H&E staining for the assessment of epidermal thickness. (B) TUNEL staining. Green indicates apoptotic cells, blue indicates cell nucleus. (C–D) Immunohistochemical staining of ki67 and CD86. (E–H) Quantitative analysis of the epidermal thickness, TUNEL positive (apoptotic) cells, ki67⁺, and CD86⁺ cells. **p* < 0.05 versus control, #*p* < 0.05 versus IMQ, +*p* < 0.05 versus ELE cream. Error bars indicate SEM (*n* = 3).

down-regulated after treated with HA-MN, ELE cream (1mM), and HA-ELE-MN (1mM) compared to the IMQ group. HA-ELE-MN (1mM) group showed higher inhibitory effects on the expression of ki67 compared to the ELE cream (1mM) group.

Furthermore, the effects of HA-ELE-MN (1mM) on the infiltration of M1-Mø in the dermis were examined by detecting CD86⁺ cells (Figure 6D and H), as CD86 is one of the commonly used biomarkers for M1-Mø. It can be seen that the number of CD86⁺ cells was significantly attenuated in HA-MN, ELE cream (1mM), and HA-ELE-MN (1mM) groups compared to the IMQ group. HA-ELE-MN (1mM) group exhibited higher inhibitory effects on the number of CD86⁺ cells compared to the ELE cream (1mM) group.

Taken together, these data demonstrate that ELE delivered using MN has better therapeutic effects compared to the cream formulation. The therapeutic effects of HA-ELE-MN (1mM) result from the apoptosis-inducing, proliferation-inhibiting, and inflammation-relieving properties of ELE.

4 Discussion

Psoriasis is a chronic inflammatory disease that involves the participation of keratinocytes, Mø, and other inflammatory cells (Dainichi et al., 2018). Although there are various therapies targeting different pathological processes of psoriasis, none of them have achieved satisfactory outcomes. Based on the

biological activities of ELE, we proposed a psoriasis treatment strategy of using one single molecule to simultaneously regulate both keratinocytes and M1-Mø. Our results showed that ELE is able to alleviate psoriasis by simultaneously inducing apoptosis in keratinocytes, inhibiting keratinocytes inflammation, and suppressing the expression of inflammatory cytokines secreted by M1-Mø.

Inducing apoptosis in keratinocytes is one of the most important modalities for psoriasis treatment. The major issue of current apoptosis-inducing treatments, such as methotrexate and phototherapy, is their toxicity. It is therefore important to minimize the toxicity while maintaining the apoptosis-inducing ability. ELE has been previously reported to induce apoptosis in various cancer cell lines, including SiHa cervical squamous carcinoma cells and NCI-H1975 human lung adenocarcinoma cells (Wang et al., 2018; Wang et al., 2021). Due to its excellent biosafety, ELE injection and ELE oral emulsion have been approved as one of the Class II antitumor drugs (Zhai et al., 2018). However, the effects of ELE on psoriasis keratinocytes have not been investigated. In this study, we first examined the effects of ELE on keratinocytes as well as fibroblasts. The results showed that ELE at concentrations below 100 μ M significantly inhibits the viability of keratinocytes without affecting fibroblast viability, indicating that ELE has low toxicity. To further investigate the role of ELE on psoriasis keratinocytes, we constructed an *in vitro* psoriasis model using M5-stimulated keratinocytes and detected the effects of ELE on these cells. Our data showed that ELE significantly inhibits cell viability and induces apoptosis in M5-stimulated keratinocytes. Data from animal experiments also indicated that HA-ELE-MN (1mM) inhibits keratinocytes proliferation (ki67⁺) and induces keratinocytes apoptosis (TUNEL⁺) in the IMQ-induced psoriatic mice model. These results demonstrate that ELE alleviates psoriasis by inducing apoptosis of keratinocytes.

In addition, the exaggerated inflammation in keratinocytes is another key reason for psoriasis (Ni and Lai, 2020). Studies have demonstrated that suppression of keratinocyte inflammation significantly alleviates psoriasis (Zuo et al., 2022). Previous studies have reported that ELE down-regulates the expression of TNF- α and IL-6 in 7,12-dimethylbenz(a)anthracene (DMBA)/12-O-tetradecanoylphorbol-13-acetate (TPA)-induced inflammation in mouse skin, indicating the potential anti-inflammatory activity of ELE (Hu et al., 2020). However, the effects of ELE on the inflammation of psoriatic keratinocytes have not been validated. It has been proven that the over-expression of interleukins in keratinocytes is associated with psoriasis, and inhibiting the expression of interleukins significantly relieves psoriasis (Tsai and Tsai, 2017). We therefore examined the effects of ELE on the inflammation of M5-stimulated keratinocytes. Our results showed that ELE significantly inhibits the expression of *IL1A*, *IL1B*, *IL6*, and *IL8* in M5-stimulated keratinocytes, demonstrating that ELE suppresses the inflammatory responses of psoriasis

keratinocytes by attenuating the expression of various interleukins. Interestingly, we also found that ELE is able to decrease the expression of *KRT6* and promote the expression of *FLG* in M5-stimulated keratinocytes. It has been proven that the up-regulation of keratin 6/16/17 stimulates the proliferation, adhesion, and migration of keratinocytes (Zhang et al., 2019). In addition, previous studies also found that psoriasis is often accompanied by a decreased expression of *FLG*, suggesting that impaired epidermal barrier function is associated with psoriasis (Gutowska-Owsiak et al., 2012). Therefore, our results not only demonstrate that ELE possesses anti-inflammatory effects on psoriatic keratinocytes by attenuating the expression of interleukins, but also inhibits psoriatic keratinocytes proliferation by down-regulating *KRT6* and helps to maintain the barrier function of keratinocytes by stimulating the expression of *FLG*.

Furthermore, the infiltration of M1-Mø is another key characteristic of psoriasis. Previous studies have shown that the infiltration of M1-Mø greatly elevates the expression of inflammatory cytokines such as interleukins and TNF- α , which triggers psoriasis by stimulating the proliferation and inflammation of keratinocytes (Kamata and Tada, 2022). To date, little is known about the regulatory effects of ELE on Mø. A recent study reported that ELE inhibits the over-expression of IL-1 in LPS-stimulated Mø, suggesting the regulatory roles of ELE on M1-Mø (An et al., 2017). However, whether the regulatory effects of ELE on Mø help to relieve psoriasis is unknown. Our results showed that ELE significantly attenuates the expression of *Tnf*, *Il1a*, and *Il12a* in M1-Mø. Data from animal experiments also showed that HA-ELE-MN (1mM) significantly reduces the number of CD86⁺ cells in the dermis. These results demonstrated that ELE inhibits the infiltration and the expression of key inflammatory cytokines of M1-Mø. In addition, to further reveal how ELE alleviates psoriasis *via* the regulation of M1-Mø, we also examined the effects of ELE-pretreated M1-Mø CM on keratinocytes. Our results showed that ELE-pretreated M1-Mø CM significantly reduces the expression of *IL1A*, *IL1B*, and *KRT6* in keratinocytes, suggesting that ELE also indirectly inhibits the inflammation and proliferation of keratinocytes by regulating M1-Mø.

As mentioned above, inducing apoptosis in keratinocytes, inhibiting keratinocyte inflammation, or suppressing the expression of inflammatory cytokines from M1-Mø is able to alleviate psoriasis, however, therapies targeting one single pathological process fail to generate satisfactory outcomes. To address this, other studies also explored combination therapies for the treatment of psoriasis. For example, An et al. (2017) investigated a combination strategy using methotrexate and acitretin, in which methotrexate triggers apoptosis in keratinocytes while acitretin inhibits the infiltration of inflammatory cells. The results showed that this combination strategy generates better therapeutic outcomes compared to the application of methotrexate or acitretin alone (An et al., 2017). Similarly, Gold et al. (2021) explored the combination of calcipotriol and betamethasone dipropionate foam for psoriasis treatment and found that the

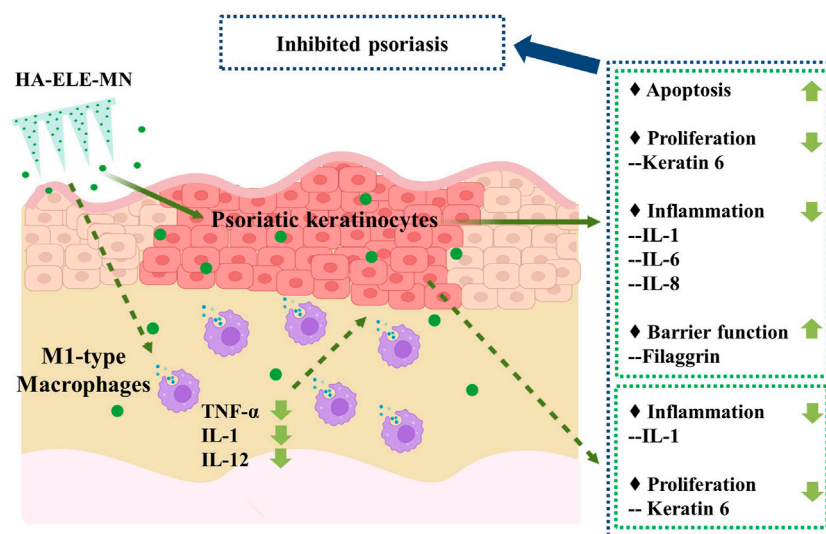


FIGURE 7

Potential mechanisms of ELE on psoriasis treatment. ELE directly induces apoptosis in psoriatic keratinocytes and inhibits psoriatic keratinocyte inflammation by down-regulating the expression of IL-1, IL-6, and IL-8. ELE may also reduce psoriatic keratinocyte proliferation by decreasing the expression of keratin 6 and help to maintain the barrier function of keratinocytes by stimulating the expression of filaggrin. In addition, ELE attenuates the expression of TNF- α , IL-1, and IL-12 in M1-M ϕ , which indirectly suppresses the inflammation and proliferation of psoriatic keratinocytes by attenuating the expression of IL-1 and keratin 6.

therapeutic effects are significantly improved compared to the application of calcipotriol or betamethasone dipropionate alone (Stein Gold et al., 2021). Although these combination therapies have been demonstrated to provide better therapeutic outcomes than monotherapy, it makes the pharmacological mechanisms more complicated and the side effects are harder to be predicted. Based on the diverse biological activities of ELE, we proposed a psoriasis treatment strategy by using one molecule to simultaneously regulate keratinocytes and M ϕ . Our results demonstrated that ELE not only directly induces apoptosis and inhibits inflammation in psoriatic keratinocytes, but also indirectly attenuates keratinocytes inflammation and proliferation by suppressing the expression of key inflammatory cytokines secreted from M1-M ϕ . These findings confirm the feasibility of our proposed strategy for psoriasis treatment.

Given that the epidermis of psoriatic skin is dramatically enhanced compared to normal skin, it is therefore important to guarantee effective drug delivery for psoriasis treatment. Recent studies have shown that the use of MN technology for the delivery of anti-psoriasis drugs is a promising research direction (Shravanth et al., 2021). Based on its excellent biocompatibility, HA is widely used in the design of MNs. For example, Du et al. (2019) prepared an HA-MN loaded with methotrexate and found that this HA-methotrexate-MN generates better therapeutic effects on psoriasis compared to the oral application of methotrexate (Du et al., 2019). Based on this, we fabricated an HA-MN loaded with ELE and tested

its therapeutic effects on psoriasis treatment using an IMQ-induced psoriatic mice model. Our results showed that HA-ELE-MN (1mM) generates better therapeutic outcomes compared to the ELE cream (1mM). These findings once again demonstrate the advantages of MN technology for psoriasis treatment.

5 Conclusion

In conclusion, this study, for the first time, explored the direct effects of ELE on psoriasis keratinocytes and whether ELE indirectly affects keratinocytes *via* the regulation of M1-M ϕ . Based on the activities of ELE in triggering apoptosis in psoriatic keratinocytes, inhibiting psoriatic keratinocytes inflammation, and suppressing the expression of inflammatory cytokines from M1-M ϕ , we proposed a psoriasis treatment strategy by using one single molecule to simultaneously regulate multiple pathological processes (Figure 7) and validated its feasibility using an IMQ-induced psoriatic mice model. Data generated from this study not only provide a potential novel anti-psoriasis drug but also offer new insights into the future design of anti-psoriasis drugs.

Data availability statement

The raw data supporting the conclusion of this article will be made available by the authors, without undue reservation.

Ethics statement

The animal study was reviewed and approved by Wenzhou Institute, University of Chinese Academy of Sciences.

Author contributions

CF, BP, JC, and YX designed the research; CW, RH, SC, YC, XY, and YQ performed the experiments; CW, RH, and CF analyzed the data; CW, RH, JC, and CF wrote the paper.

Funding

This work has been supported by National Natural Science Foundation of China (Grant No. 32101067), the seed grants from Wenzhou Institute, University of Chinese Academy of Sciences (WIUCASQD2021029 and WIUCASQD2020013), the funding from First Affiliated Hospital of Wenzhou Medical University, and the Program for University Talents and Team of Science and Technology in Yunnan Province (#202105AE160010).

References

- An, J., Zhang, D., Wu, J., Li, J., Teng, X., Gao, X., et al. (2017). The acitretin and methotrexate combination therapy for psoriasis vulgaris achieves higher effectiveness and less liver fibrosis. *Pharmacol. Res.* 121, 158–168. doi:10.1016/j.phrs.2017.04.014
- Armstrong, A. W., and Read, C. (2020). Pathophysiology, clinical presentation, and treatment of psoriasis: A review. *JAMA* 323 (19), 1945–1960. doi:10.1001/jama.2020.4006
- Boehncke, W. H., and Schon, M. P. (2015). *Lancet* 386 (9997), 983–994. doi:10.1016/S01406736(14)61909-7
- Dainichi, T., Kitoh, A., Otsuka, A., Nakajima, S., Nomura, T., Kaplan, D. H., et al. (2018). The epithelial immune microenvironment (EIME) in atopic dermatitis and psoriasis. *Nat. Immunol.* 19 (12), 1286–1298. doi:10.1038/s41590-018-0256-2
- Ding, L., Zhang, G., Hou, Y., Chen, J., and Yin, Y. (2018). Elemene inhibits osteosarcoma growth by suppressing the renin-angiotensin system signaling pathway. *Mol. Med. Rep.* 17 (1), 1022–1030. doi:10.3892/mmr.2017.7965
- Diotallevi, F., Paolinelli, M., Radi, G., and Offidani, A. (2022). Latest combination therapies in psoriasis: Narrative review of the literature. *Dermatol. Ther.* 35 (10), e15759. doi:10.1111/dth.15759
- Du, H., Liu, P., Zhu, J., Lan, J., Li, Y., Zhang, L., et al. (2019). Hyaluronic acid-based dissolving microneedle patch loaded with methotrexate for improved treatment of psoriasis. *ACS Appl. Mat. Interfaces* 11 (46), 43588–43598. doi:10.1021/acsami.9b15668
- Dubertret, L., Mrowietz, U., Ranki, A., Van De Kerkhof, P. C. M., Chimenti, S., Lotti, T., et al. (2010). European patient perspectives on the impact of psoriasis: The EUROPSO patient membership survey. *Br. J. Dermatol.* 155 (4), 729–736. doi:10.1111/j.1365-2133.2006.07405.x
- Elango, T., Thirupathi, A., Subramanian, S., Ethiraj, P., Dayalan, H., and Gnanaraj, P. (2017). Methotrexate treatment provokes apoptosis of proliferating keratinocyte in psoriasis patients. *Clin. Exp. Med.* 17 (3), 371–381. doi:10.1007/s10238-016-0431-4
- Gao, J., Chen, F., Fang, H., Mi, J., Qi, Q., and Yang, M. (2020). Daphnetin inhibits proliferation and inflammatory response in human HaCaT keratinocytes and ameliorates imiquimod-induced psoriasis-like skin lesion in mice. *Biol. Res.* 53 (1), 48. doi:10.1186/s40659-020-00316-0
- Greb, J., Goldminz, A., Elder, J., Lebwohl, M., Gladman, D., Wu, J., et al. (2016). Psoriasis. *Nat. Rev. Dis. Prim.* 2, 16082. doi:10.1038/nrdp.2016.82
- Gutowska-Owsiak, D., Schaupp, A. L., Salimi, M., Selvakumar, T. A., McPherson, T., Taylor, S., et al. (2012). IL-17 downregulates filaggrin and affects keratinocyte expression of genes associated with cellular adhesion. *Exp. Dermatol.* 21 (2), 104–110. doi:10.1111/j.1600-0625.2011.01412.x
- Han, B., Wang, T., Xue, Z., Wen, T., Lu, L., Meng, J., et al. (2021). Elemene nanoemulsion inhibits metastasis of breast cancer by ROS scavenging. *Int. J. Nanomedicine* 16, 6035–6048. doi:10.2147/ijn.S327094
- Hu, X., Wang, L., Zhang, L., and Zhang, T. (2020). β -Elemene inhibits 7 12-dimethylbenz(a)anthracene/12-O-tetradecanoylphorbol-13-acetate-induced skin tumorigenesis through suppression of NF- κ B-associated signaling events in the mouse skin model. *J. Biochem. Mol. Toxicol.* 34 (10), e22550. doi:10.1002/jbt.22550
- BarkerJonathan, N. (2007). Pathogenesis and clinical features of psoriasis. *Lancet* 370, 263–271. doi:10.1016/s0140-6736(07)61128-3
- Kamata, M., and Tada, Y. (2022). Dendritic cells and macrophages in the pathogenesis of psoriasis. *Front. Immunol.* 13, 941071. doi:10.3389/fimmu.2022.941071
- Kim, H. J., Jang, J., Lee, E.-H., Jung, S., Roh, J. Y., and Jung, Y. (2019). Decreased expression of response gene to complement 32 in psoriasis and its association with reduced M2 macrophage polarization. *J. Dermatol.* 46 (2), 166–168. doi:10.1111/1346-8138.14733
- Liu, J., Hu, X., Jin, B., Qu, X., Hou, K., and Liu, Y. (2012). β -Elemene induces apoptosis as well as protective autophagy in human non-small-cell lung cancer A549 cells. *J. Pharm. Pharmacol.* 64 (1), 146–153. doi:10.1111/j.20427158.2011.01371.x
- Nakamura, M., and Koo, J. (2020). Safety considerations with combination therapies for psoriasis. *Expert Opin. Drug Saf.* 19 (4), 489–498. doi:10.1080/14740338.2020.1722640
- Nestle, F. O., Kaplan, D. H., and Barker, J. (2009). *N. Engl. J. Med.* 361 (5), 496–509. doi:10.1056/nejmra804595
- Ni, X., and Lai, Y. (2020). Keratinocyte: A trigger or an executor of psoriasis? *J. Leukoc. Biol.* 108 (2), 485–491. doi:10.1002/JLB.5MR0120-439R
- Qu, F., Geng, R., Liu, Y., and Zhu, J. (2022). Advanced nanocarrier- and microneedle-based transdermal drug delivery strategies for skin diseases treatment. *Theranostics* 12 (7), 3372–3406. doi:10.7150/thno.69999

Acknowledgments

We thank Dr Chen Yang for the help on microneedle preparation and Dr. Yiren Jiao for the help on histology analysis. We also thank Scientific Research Center of Wenzhou Medical University for consultation and instrument availability that supported this work.

Conflict of interest

The authors declare that the research was conducted in the absence of any commercial or financial relationships that could be construed as a potential conflict of interest.

Publisher's note

All claims expressed in this article are solely those of the authors and do not necessarily represent those of their affiliated organizations, or those of the publisher, the editors and the reviewers. Any product that may be evaluated in this article, or claim that may be made by its manufacturer, is not guaranteed or endorsed by the publisher.

- Shravanth, S. H., Osmani, R. A. M., Anupama, V. P., Rahamathulla, M., and Gangadharappa, H. V. (2021). Microneedles-based drug delivery for the treatment of psoriasis. *J. Drug Deliv. Sci. Technol.* 64, 102668. doi:10.1016/j.jddst.2021.102668
- Stein Gold, L., Paul, C., and Romiti, R. (2021). Efficacy and safety of fixed-dose combination calcipotriol/betamethasone dipropionate foam for the treatment of psoriasis. *J. Eur. Acad. Dermatol. Venereol.* 35 (S1), 10–19. doi:10.1111/jdv.17028
- Tao, T., Chen, Y., Lai, B., Wang, J., Wang, W., Xiao, W., et al. (2022). Shikonin combined with methotrexate regulate macrophage polarization to treat psoriasis. *Bioengineered* 13 (4), 11146–11155. doi:10.1080/21655979.2022.2062090
- Tsai, Y.-C., and Tsai, T.-F. (2017). Anti-interleukin and interleukin therapies for psoriasis: Current evidence and clinical usefulness. *Ther. Adv. Musculoskelet. Dis.* 9 (11), 277–294. doi:10.1177/1759720x17735756
- Wang, J., Xu, C., Chen, Y., Shao, L., Li, T., Fan, X., et al. (2021). β -elemene enhances the antitumor activity of erlotinib by inducing apoptosis through AMPK and MAPK pathways in TKI-resistant H1975 lung cancer cells. *J. Cancer* 12 (8), 2285–2294. doi:10.7150/jca.53382
- Wang, L., Zhao, Y., Wu, Q., Guan, Y., and Wu, X. (2018). Therapeutic effects of β -elemene via attenuation of the Wnt/ β -catenin signaling pathway in cervical cancer cells. *Mol. Med. Rep.* 17 (3), 4299–4306. doi:10.3892/mmr.2018.8455
- Wang, Y., Fu, S., Lu, Y., Lai, R., Liu, Z., Luo, W., et al. (2022). Chitosan/hyaluronan nanogels co-delivering methotrexate and 5-aminolevulinic acid: A combined chemo-photodynamic therapy for psoriasis. *Carbohydr. Polym.* 277, 118819. doi:10.1016/j.carbpol.2021.118819
- Wu, B., Jiang, Y., Zhu, F., Sun, D., and Huang, H. (2016). Demethylation effects of elemene on the GSTP1 gene in HCC cell line QGY7703. *Oncol. Lett.* 11 (4), 2545–2551. doi:10.3892/ol.2016.4243
- Zhai, B., Zeng, Y., Zeng, Z., Zhang, N., Li, C., Zeng, Y., et al. (2018). Drug delivery systems for elemene, its main active ingredient β -elemene, and its derivatives in cancer therapy. *Int. J. Nanomedicine* 13, 6279–6296. doi:10.2147/ijn.s174527
- Zhang, X., Yin, M., and Zhang, L.-j. (2019). Keratin 6, 16 and 17—critical barrier alarmin molecules in skin wounds and psoriasis. *Cells* 8 (8), 807. doi:10.3390/cells8080807
- Zhou, X., Chen, Y., Cui, L., Shi, Y., and Guo, C. (2022). Advances in the pathogenesis of psoriasis: From keratinocyte perspective. *Cell Death Dis.* 13 (1), 81. doi:10.1038/s41419-022-04523-3
- Zhu, D. D., Chen, B. Z., He, M. C., and Guo, X. D. (2017). Structural optimization of rapidly separating microneedles for efficient drug delivery. *J. Ind. Eng. Chem.* 51, 178–184. doi:10.1016/j.jiec.2017.02.030
- Zuo, Y., Dai, L., Li, L., Huang, Y., Liu, X., Liu, X., et al. (2022). ANGPTL4 regulates psoriasis via modulating hyperproliferation and inflammation of keratinocytes. *Front. Pharmacol.* 13, 850967. doi:10.3389/fphar.2022.850967



OPEN ACCESS

EDITED BY

Zheng Xiang,
Liaoning University, China

REVIEWED BY

Xingbin Yin,
Beijing University of Chinese Medicine,
China
Zijia Zhang,
Shanghai University of Traditional
Chinese Medicine, China
Changfu Wang,
Guangdong Pharmaceutical University,
China

*CORRESPONDENCE

Haixue Kuang,
hxkuang@hljucm.net

SPECIALTY SECTION

This article was submitted to
Ethnopharmacology,
a section of the journal
Frontiers in Pharmacology

RECEIVED 13 October 2022

ACCEPTED 15 November 2022

PUBLISHED 30 November 2022

CITATION

Wang M, Wang S, Hu W, Wang Z, Yang B
and Kuang H (2022), *Asparagus
cochinchinensis*: A review of its botany,
traditional uses, phytochemistry,
pharmacology, and applications.
Front. Pharmacol. 13:1068858.
doi: 10.3389/fphar.2022.1068858

COPYRIGHT

© 2022 Wang, Wang, Hu, Wang, Yang
and Kuang. This is an open-access
article distributed under the terms of the
Creative Commons Attribution License
(CC BY). The use, distribution or
reproduction in other forums is
permitted, provided the original
author(s) and the copyright owner(s) are
credited and that the original
publication in this journal is cited, in
accordance with accepted academic
practice. No use, distribution or
reproduction is permitted which does
not comply with these terms.

Asparagus cochinchinensis: A review of its botany, traditional uses, phytochemistry, pharmacology, and applications

Meng Wang, Shuang Wang, Wenjing Hu, Zhibin Wang,
Bingyou Yang and Haixue Kuang*

Key Laboratory of Basic and Application Research of Beiyao (Heilongjiang University of Chinese Medicine), Ministry of Education, Heilongjiang University of Chinese Medicine, Harbin, China

Asparagus cochinchinensis (Lour.) Merr. (*A. cochinchinensis*) is a traditional herbal medicine that is used to treat constipation, fever, pneumonia, stomachache, tracheitis, rhinitis, cataract, acne, urticaria. More than 90 compounds have been identified from different structural types in *A. cochinchinensis*, including steroidal saponins, C₂₁-steroides, lignans, polysaccharides, amino acids, etc. These bioactive ingredients make *A. cochinchinensis* remarkable for its pharmacological effects on anti-asthma, anti-inflammatory, anti-oxidation, anti-tumor, improving Alzheimer's disease, neuroprotection, gut health-promoting and so on. Moreover, *A. cochinchinensis* also plays an important role in food, health product, cosmetic, and other fields. This review focused on the research publications of *A. cochinchinensis* and aimed to summarize the advances in the botany, traditional uses, phytochemistry, pharmacology, and applications which will provide reference for the further studies and applications of *A. cochinchinensis*.

KEYWORDS

Asparagus cochinchinensis (Lour.) Merr, traditional uses, phytochemistry, pharmacology, applications

Introduction

A. cochinchinensis is belonging to the genus *Asparagus* in the family *Liliaceae*, it is widely distributed in temperate and tropical regions, including China, Japan, Korea, and Vietnam. (Kubota et al., 2012; Pegiou et al., 2019; Pahwa et al., 2022). *A. cochinchinensis* is one of the most frequently used traditional herbal medicines, with documented cases of its clinical therapeutic effect in many countries. (Sheng, 2022a; Wong et al., 2022). *A. cochinchinensis* first appeared as a traditional Chinese medicine (TCM) in the earliest Chinese medicinal classic work Shennong's Classic of Materia Medica (written more than 2000 years ago during the Han Dynasty), it has a long history of medicinal use and its medicinal value has been proved by clinical experience. It was included in the Pharmacopoeia of the People's Republic of China 1977 edition as a clinical TCM in

common use for the first time, and was continuously included until the latest 2020 edition. Dried roots are the main medicinal parts of *A. cochinchinensis*, it has been commonly used either alone or in combination with other herbal medicines to treat asthma, cough, constipation, thrombosis and inflammatory disease in China for centuries. Many classic formulas containing *A. cochinchinensis* have been widely used in clinic and have made important contributions to the health of people in China and other traditional medicinal systems in Asia. In addition to its medicinal value, *A. cochinchinensis* has various commercial applications in health products, food, and cosmetics (Safriani et al., 2022). It is commonly used as a food or nutritional supplement (Siand et al., 2015), cosmetics with whitening and anti-aging effects, and even used as a raw material for fermentation and winemaking (Kim et al., 2017; Topolska et al., 2021). Therefore, its huge potential and broad development prospects are worth exploring.

In the past few decades, *A. cochinchinensis* has attracted widespread attention as an important herbal medicine. Significant progress on isolation and identification of active constituents in *A. cochinchinensis* have been made in relevant researches. So far, more than 90 components have been isolated and identified. They mainly include steroidal saponins, C₂₁-steroids, lignans, polysaccharides, and amino acids. At present, *A. cochinchinensis* has a variety of pharmacological effects and has curative effects in the treatment of asthma, tumor, Alzheimer's disease, gut diseases, inflammatory diseases (Lee et al., 2009; Lei et al., 2016; Choi et al., 2019; Zhang R. S. et al., 2021). Besides that, medicinal prescription research also has revealed that it functions synergistically in combination with various herbal medicines (Weiyang et al., 2006; Jung et al., 2014). With the in-depth exploration of TCM the exploitation and utilization of traditional herbal medicine in the prevention and treatment of various diseases are steadily increasing.

With the current scientific and technological advances and the increasing international recognition of traditional herbal medicine in recent years, research on *A. cochinchinensis* has made significant progress. However, to the best of our knowledge, there is no review on *A. cochinchinensis*. It is particularly important and necessary to collate a review on *A. cochinchinensis* progress in recent years. This is the first review on up to date of *A. cochinchinensis* research developments in the fields of botany, traditional uses, phytochemistry, pharmacology, and applications. It provides an accurate overview of *A. cochinchinensis* research and identifies deficiencies in present studies, proposing further research targets. The authors expect this review to encourage further research into the pharmacological effects and mechanisms associated with *A. cochinchinensis* therapeutic effects and to provide a broader vision and new inspiration for research in current and potential applications of *A. cochinchinensis*.

Botany

A. cochinchinensis is a climbing perennial plant, which has the structural characteristics of pale green stalks, sickle-shaped leaves, pale green axillary flowers, red fruits, and the branches angular or narrowly winged. It usually grows on slopes, roadsides, underwoods, valleys, or wastelands, below 1750 m *A. cochinchinensis* is usually harvested in autumn and winter, cleaned silt, removed fibrous root, retained tuberous root, boiled in boiling water for 15 min, then peeled and cored, further dried to obtain the medicinal part of *A. cochinchinensis*. According to the online records of China's flora (<http://www.cn-flora.ac.cn/index.html>), the medicinal part of *A. cochinchinensis* is fusiform, with a swelling in the middle or near the end, which is 3–5 cm long and 1–2 cm thick. *A. cochinchinensis*'s stem is smooth, often curved or twisted, up to 1–2 m long. *A. cochinchinensis*'s leafy branches are usually clustered every 3, which are flat or slightly acute triangular due to the keel shape of the midvein, slightly falcate, 0.5–8 cm long, and 1–2 mm wide. Its inflorescence usually has two axillary flowers with alternate petals. The pedicel is 2–6 mm long. The joint is generally located in the middle, the perianth is 2.5–3 mm long, and the female flowers are similar in size to the male flowers. The flowering and fruiting period is generally from May to October. When the fruit matures, it becomes red, with a diameter of 6–7 mm, with only one seed per fruit, as shown in Figure 1.

Traditional uses

A. cochinchinensis has a long history of ethnopharmacological use and is characterized by bitter in taste and cold in nature. Since ancient times, researchers continuously explore and exploited TCM practices (Zhang X. et al., 2021; Wang et al., 2021). Dating back more than 1700 years of history, *A. cochinchinensis* was first documented in Shennong's Classic of Materia Medica (Dong Han Dynasty, 25–220 A.D.), which is the earliest classic on TCM. Later, it was listed in many other well-known works on Chinese herb, including "Ming Yi Bie Lu" (Wei and Jin Dynasty, 220–420 A.D.), "Yao Xing Lun" (Tang Dynasty, 618–907 A.D.). In the folk culture, it is often used as a treatment cough, constipation, fever, pneumonia, stomachache, tracheitis, rhinitis, cataract, acne, urticaria and other diseases. In different countries, *A. cochinchinensis* has different therapeutic effects. It can be combined with other herb medicines to achieve a greater therapeutic effect. In Korea, extracts of formulations composed of *A. cochinchinensis* and other herbs were shown to have the effect of treating thrombosis (Chang et al., 2005; Lee et al., 2019). In China, the classic prescription composed of *A. cochinchinensis* (Qisheng pill) contains 114 chemical compounds were identified, including diosgenin, Methyl protodioscin, and ferroic acid, total saponin etc., which can inhibit the occurrence of inflammation, regulate intestinal dysfunction and improve the effect of Alzheimer disease (Xiong et al., 2022). At the same time, the herb formula water decoction composed of *A. cochinchinensis* can treatment of intestinal



FIGURE 1

A. cochinchinensis plant morphology. (A) The above-ground portion, (B) Flower, (C) Fruits, (D) The underground part, (E) Medicinal part.

diseases, especially alleviate allergic airway inflammation and treat asthma (Luo et al., 2020). This also reflects the different therapeutic effects of *A. cochinchinensis* in traditional use and the broad application prospects in the future. Therefore, its clinical efficacy and function still need to be further explored.

Phytochemistry

In the past few decades, *A. cochinchinensis* have been investigated from a phytochemical perspective. The literature indicates the presence of multiple chemical compounds, predominantly steroidal saponin, C_{21} -steroids, amino acids, lignan, and polysaccharides. To date, more than 90 compounds have been isolated and identified from *A. cochinchinensis*. These compounds are summarized in Tables 1 and Table 2, and their structures are shown in Figure 2, and Figure 3, and Figure 4.

Steroidal saponins

Steroidal saponins are the major chemical components in *A. cochinchinensis* (Lee et al., 2015). Thus far, 71 steroidal saponins (1–71) have been isolated from *A. cochinchinensis* in Table 2. Steroid saponins are mainly composed of steroidal saponins and sugar condensation. They are classified into spirostanol saponins, isospirostanol saponins, pseudospirostanol saponins and furostanol saponins based on the aglycone component differences. Aglycones are composed of six rings, of which the rutil rings are

usually connected in a spiroketal form. The sugar moieties in the ordinary steroidal saponins are attached to the hydroxyl groups at C_3 . In a word, the structural diversity of different compounds is more reflected in the kind, length of each monosaccharide, the type of glycoside bond at the C_3 position, and the position of the substituent.

C_{21} -steroides

C_{21} -steroides are steroid derivatives with 21 carbon atoms and are one of the key compounds in *A. cochinchinensis*. C_{21} steroids are mostly hydroxyl derivatives with pregnane or its isomers as the basic skeleton. According to the skeleton type, they can be divided into four types, of which 72–79 (Jian et al., 2013; Liu et al., 2021; Zhu et al., 2021) are typical C_{21} -steroides in Figure 3. In addition, there are many hydroxyl and carbonyl groups on the C_{21} -steroid mother nucleus, and most of the carbonyl groups are at C_{20} .

Amino acids

Four kinds of amino acids were isolated from *A. cochinchinensis* 80–83 (Choi et al., 2019), and their structures are shown in Figure 4. Amino acids are compounds containing both amino and carboxyl groups. In terms of their structure, amino acids are derivatives of carboxylic acid molecules in which amino groups replace the hydrogen in the alkyl group. According to the relative number of amino and carboxyl groups in amino acid molecules, amino acids can be divided into neutral, acidic and basic.

TABLE 1 Chemical compounds isolated from *A. cochinchinensis*.

Number	Chemical composition	Extraction solvent	Molecular formula	Molecular weight	Reference
Steroidal Saponin					
1	Dioscin	MeOH	C ₄₅ H ₇₂ O ₁₆	869.0436	Lee et al. (2015)
2	Prosapogenin B	70% EtOH	C ₃₉ H ₆₂ O ₁₂	722.9024	Liu et al. (2021)
3	(23R, 24R, 25S)-spirost-5-ene-3 β ,23,24-triol-3-O- α -L-rhamnopyranosyl-(1 \rightarrow 2)-[α -L-rhamnopyranosyl-(1 \rightarrow 4)]- β -D-glucopyranoside	70% EtOH	C ₄₅ H ₇₂ O ₁₈	901.0424	Liu et al. (2021)
4	(24S,25S)-spirost-5-ene-3 β ,24-diol-3-O- α -L-rhamnopyranosyl-(1 \rightarrow 2)-[α -L-rhamnopyranosyl-(1 \rightarrow 4)]- β -D-glucopyranoside	70% EtOH	C ₄₅ H ₇₂ O ₁₇	885.0430	Liu et al. (2021)
5	Methylprotodioscin	MeOH	C ₅₂ H ₈₆ O ₂₂	1063.2260	Liang et al. (1988)
6	(25S)-26-O- β -D-glucopyranosyl-5 β -furost-20(22)-en-3 β ,15 β ,26-triol-3-O-[α -L-rhamnopyranosyl-(1-4)]- β -D-glucopyranoside	75% EtOH	C ₄₅ H ₇₄ O ₁₇	887.0589	Shen et al. (2011)
7	Aspacochioside C	75% EtOH; Water	C ₄₅ H ₇₅ O ₁₇	888.0705	Shen et al., 2011 Kim et al. (2021)
8	3-O-[α -L-rhamnopyranosyl(1 \rightarrow 4)- β -D-glucopyranosyl]- (25S) -5 β -spirostan-3 β -ol	70% MeOH	C ₃₉ H ₆₄ O ₁₂	724.9183	Zhu et al. (2021)
9	Asparacoside	MeOH	C ₄₉ H ₈₀ O ₂₁	1005.1469	Zhang et al. (2004)
10	Nicotianoside B	70% MeOH	C ₃₉ H ₆₄ O ₁₂	724.9183	Zhu et al. (2021)
11	Immunoside	70% MeOH	-	-	Zhu et al. (2021)
12	Shatavarin IV	70% MeOH	-	-	Zhu et al. (2021)
13	(25S)-5 β -spirostan-3 β -ol-3-O- α -L-rhamnopyranoside	70% MeOH	C ₃₃ H ₅₄ O ₇	562.7777	Zhu et al. (2014)
14	(25S)-5 β -spirostan-3 β -ol-3-O- β -D-glucopyranoside	70% MeOH	C ₃₃ H ₅₄ O ₈	578.7771	Zhu et al. (2014)
15	(23S,25R)-23-hydroxyspirost-5-en-3 β -yl-O- α -L-rhamnopyranosyl-(1 \rightarrow 4)- β -D-glucopyranoside	70% EtOH	C ₃₉ H ₆₂ O ₁₃	738.9018	Liu et al. (2021)
16	Dioseptemloside F	70% EtOH	C ₃₉ H ₆₂ O ₁₃	738.9018	Liu et al. (2021)
17	Pseudoprotoneodioscin	75%EtOH; Water	C ₅₁ H ₈₂ O ₂₁	1031.1842	Shen et al., 2011
18	26-O- β -D-glucopyranosyl-(25R)-furost-5-ene-3 β ,22 α ,26-triol 3-O-(1-4)- β -D-glucopyranosyl- α -L-rhamnopyranosyl-(1-2)-[α -L-rhamnopyranosyl-(1-4)]- β -D-glucopyranoside	Water	C ₅₇ H ₉₄ O ₂₇	1211.3401	Zhang et al. (2021b)
19	Protodioscin	Water; 90% EtOH	C ₅₁ H ₈₄ O ₂₂	1049.1995	Kim et al. (2021) Zhang et al. (2021b)
20	15-hydroxypseudoprotodioscin	Water	C ₅₁ H ₈₂ O ₂₂	1047.1836	Kim et al. (2021)
21	Dioscoreside H	90% EtOH	C ₅₁ H ₈₂ O ₂₂	1047.1836	Zhang et al. (2021b)
22	Pseudoprotodioscin	Water	C ₅₁ H ₈₂ O ₂₁	1031.1842	Liang et al. (1988)
23	(25R)-26-O- β -D-glucopyranosyl-3 β ,20 α ,26-trihydroxyfurostan-5,22-diene-3-O- α -L-rhamnopyranosyl-(1 \rightarrow 2)-[α -L-rhamnopyranosyl-(1 \rightarrow 4)]-O- β -D-glucopyranoside	90% EtOH	-	-	Zhang et al. (2021b)
24	3-O- α -L-rhamnopyranosyl(1 \rightarrow 4)-[β -D-glucopyranosyl(1 \rightarrow 2)]- β -D-glucopyranosyl-26-O- β -D-glucopyranosyl-(25R)-5 β -furostane-3 β ,22 α ,26-triol	75% EtOH	C ₅₁ H ₈₆ O ₂₃	1067.2147	Jian et al. (2013)
25	3-O- β -D-xylopyranosyl(1 \rightarrow 4)-[β -D-glucopyranosyl(1 \rightarrow 2)]- β -D-glucopyranosyl-26-O- β -D-glucopyranosyl-(25S)-5 β -furostane-3 β ,22 α ,26-triol	75% EtOH	C ₅₀ H ₈₄ O ₂₃	1053.1882	Jian et al. (2013)
26	3-O- β -D-glucopyranosyl(1 \rightarrow 2)- β -D-glucopyranosyl-26-O- β -D-glucopyranosyl-(25S)-5 β -furostane-3 β ,22 α ,26-triol	75% EtOH	C ₄₅ H ₇₆ O ₁₉	921.0735	Jian et al. (2013)
27	3-O- α -L-rhamnopyranosyl (1 \rightarrow 4)-[β -D-xylopyranosyl(1 \rightarrow 2)]- β -D-glucopyranosyl-26-O- β -D-glucopyranosyl-(25S)-5 β -furostane-3 β ,22 α ,26-triol	60% EtOH	C ₅₀ H ₈₄ O ₂₂	1037.1888	Pang et al. (2021)

(Continued on following page)

TABLE 1 (Continued) Chemical compounds isolated from *A. cochinchinensis*.

Number	Chemical composition	Extraction solvent	Molecular formula	Molecular weight	Reference
28	(25S)-26-O- β -D-glucopyranosyl-5 β -furostan-3 β ,22 α ,26-triol-3-O- α -L-rhamnopyranosyl-(1 \rightarrow 4)- β -D-glucopyranoside	70% MeOH	C ₄₅ H ₇₆ O ₁₈	905.0741	Zhu et al. (2014)
29	(25S)-26-O- β -D-glucopyranosyl-5 β -furostan-3 β , 22 α , 26-triol-3-O- β -D-glucopyranoside	70% MeOH	C ₃₉ H ₆₆ O ₁₄	758.9329	Zhu et al. (2014)
30	(25S)-5 β -12-one-spirost-3 β -ol-3-O- β -D-glucopyranoside	60% EtOH	C ₃₃ H ₅₂ O ₉	592.7606	Pang et al. (2021)
31	26-O- β -D-glucopyranosyl-(25S)-5 β -12-one-furost-3 β ,26-diol-3-O- α -L-rhamnopyranosyl-(1 \rightarrow 2)-[β -D-xylopyranosyl-(1 \rightarrow 4)]- β -D-glucopyranoside	60% EtOH	C ₅₀ H ₈₂ O ₂₃	1051.1723	Pang et al. (2021)
32	(25S)-26-O- β -D-glucopyranosyl-5 β -furostan-3 β ,22 α ,26-triol-12-one-3-O- β -D-glucopyranoside	60% EtOH	C ₃₉ H ₆₄ O ₁₅	772.9165	Pang et al. (2021)
33	26-O- β -D-glucopyranosyl-(25S)- $\Delta^{5(6)}$ -12-one-furost-3 β ,26-diol-3-O- α -L-rhamnopyranosyl-(1 \rightarrow 2)-[β -D-xylopyranosyl-(1 \rightarrow 4)]- β -D-glucopyranoside	60% EtOH	C ₅₀ H ₈₀ O ₂₃	1049.1564	Pang et al. (2021)
34	26-O- β -D-glucopyranosyl-(25S)- $\Delta^{5(6)}$ -12-one-furost-3 β ,26-diol-3-O- α -L-rhamnopyranosyl-(1 \rightarrow 2)-[α -L-rhamnopyranosyl-(1 \rightarrow 4)]- β -D-glucopyranoside	60% EtOH	C ₅₁ H ₈₂ O ₂₃	1063.1830	Pang et al. (2021)
35	(25S)-26-O- β -D-glucopyranosyl-22 α -methoxy-5 β -furostan-3 β ,26-diol-12-one-3-O- β -D-glucopyranoside	70% MeOH	C ₄₀ H ₆₆ O ₁₅	786.9430	Zhu et al. (2014)
36	26-O- β -D-glucopyranosyl-(25S)-5 β -furost-3 β ,12 α ,26-triol-3-O- α -L-rhamnopyranosyl-(1 \rightarrow 2)-[α -L-rhamnopyranosyl-(1 \rightarrow 4)]- β -D-glucopyranoside	60% EtOH	C ₃₉ H ₆₆ O ₁₅	774.9323	Pang et al. (2021)
37	Officinalisin II	60% EtOH	-	-	Pang et al. (2021)
38	(25S)-officinalisin-I	60% EtOH	C ₄₅ H ₇₆ O ₁₉	921.0735	Pang et al. (2021)
39	(25S)-26-O- β -D-glucopyranosyl-5 β -furostan-3 β ,22 α ,26-triol	70% MeOH	C ₃₃ H ₅₆ O ₉	596.7923	Zhu et al. (2014)
40	Pallidifloside I	60% EtOH	C ₅₀ H ₈₂ O ₂₂	1035.1729	Pang et al. (2021)
41	3-O-[bis- α -L-rhamnopyranosyl-(1 \rightarrow 2and1 \rightarrow 4)- β -D-glucopyranosyl-25R-furost-5-ene-3 β ,22 α ,26-triol]	70% EtOH	C ₄₅ H ₇₄ O ₁₇	887.0589	Liu et al. (2021)
42	3-O-[[α -L-rhamnopyranosyl-(1 \rightarrow 4)] β -D-glucopyranosyl]-26-O-[β -D-glucopyranosyl]-(25S)-5 β -furost-20(22)-en-3 β ,26-diol	EtOH	C ₄₅ H ₇₄ O ₁₇	887.0589	Shi et al. (2004)
43	3-O- β -D-xylopyranosyl(1 \rightarrow 4)-[β -D-glucopyranosyl(1 \rightarrow 2)]- β -D-glucopyranosyl-26-O- β -D-glucopyranosyl-(25R)-5 β -furostane-3 β ,22 α ,26-triol	75% EtOH	-	-	Jian et al. (2013)
44	3-O-[[α -L-rhamnopyranosyl-(1 \rightarrow 4)] β -D-glucopyranosyl]-26-O-[β -D-glucopyranosyl]-(25S)-5 β -furostane-3 β ,22 α ,26-triol	Water; EtOH	C ₄₅ H ₇₆ O ₁₈	905.0741	Shi et al. (2004)
45	Chamaedroside E	Water	C ₄₅ H ₇₆ O ₁₉	921.0735	Kim et al. (2021)
46	Furospirost-5-ene-3 β ,6 α ,23 α -triol-3-O- α -L-rhamnopyranosyl-(1 \rightarrow 4)- β -D-glucopyranoside	70% MeOH	C ₄₀ H ₆₄ O ₁₄	768.9278	Liu et al. (2021)
47	16 β ,22,23-trihydroxycholest-5-ene-3 β -yl-O- α -L-rhamnopyranosyl-(1 \rightarrow 4)- β -D-glucopyranoside	70% MeOH	C ₃₉ H ₆₆ O ₁₃	742.9335	Liu et al. (2021)
48	(24S,25R)-spirost-5-ene-3 β ,24-diol-3-O- α -L-rhamnopyranosyl-(1 \rightarrow 2)-[α -L-rhamnopyranosyl-(1 \rightarrow 4)]- β -D-glucopyranoside	70% MeOH	C ₄₅ H ₇₂ O ₁₇	884.0430	Liu et al. (2021)
49	(24S,25S)-spirost-5-ene-3 β ,24-diol-3-O- α -L-rhamnopyranosyl-(1 \rightarrow 4)- β -D-glucopyranoside	70% EtOH	C ₃₉ H ₆₂ O ₁₃	738.9018	Liu et al. (2021)
50	(23S,24R,5S)-23,24-dihydroxyspirost-5-en-3 β -yl-O- α -L-rhamnopyranosyl-(1 \rightarrow 4)- β -D-glucopyranoside	70% EtOH	C ₃₉ H ₆₂ O ₁₄	754.9012	Liu et al. (2021)
51	Smilagenin-3-O- α -L-rhamnopyranosyl-(1 \rightarrow 4)- β -D-glucopyranoside	70% EtOH	C ₃₉ H ₆₄ O ₁₂	724.9183	Liu et al. (2021)
52	3-O-[[β -D-glucopyranosyl-(1 \rightarrow 2)]- α -L-rhamnopyranosyl-(1 \rightarrow 4)]- β -D-glucopyranosyl]-(25R)-5 β -spirostan-3 β -ol	70% EtOH	C ₄₅ H ₇₄ O ₁₇	887.0589	Liu et al. (2021)
53		70% EtOH	-	-	Liu et al. (2021)

(Continued on following page)

TABLE 1 (Continued) Chemical compounds isolated from *A. cochinchinensis*.

Number	Chemical composition	Extraction solvent	Molecular formula	Molecular weight	Reference
	(25R)-26-[(β -D-glucopyranosyl) oxy]-22 α -methoxyfurost-5-en-3 β -yl-O- α -L-rhamnopyranosyl-(1 \rightarrow 4)- β -D-glucopyranoside				
54	Pseuprotodioscin	70% EtOH	-	-	Liu et al. (2021)
55	Dioscin F	70% EtOH	C ₃₉ H ₆₀ O ₁₃	736.8859	Liu et al. (2021)
56	Dioscin E	70% EtOH	C ₃₉ H ₆₂ O ₁₂	722.9024	Liu et al. (2021)
57	3-O-[α -L-rhamnopyranosyl-(1 \rightarrow 4)- β -D-glucopyranosyl]-26-O- β -D-glucopyranosyl-20, 22-seco-25R-furoene-20, 22-dione-3 β , 26-diol	70% EtOH	C ₄₅ H ₇₄ O ₁₉	919.0577	Liu et al. (2021)
58	(23S, 24R, 25R)-spirost-5-ene-3 β ,23,24-triol-3-O- α -L-rhamnopyranosyl-(1 \rightarrow 2)-[α -L-rhamnopyranosyl-(1 \rightarrow 4)- β -D-glucopyranoside	70% EtOH	C ₄₅ H ₇₂ O ₁₈	901.0424	Liu et al. (2021)
59	(23R, 25S)-spirost-5-ene-3 β , 23-diol-3-O- α -L-rhamnopyranosyl-(1 \rightarrow 2)-[α -L-rhamnopyranosyl-(1 \rightarrow 4)- β -D-glucopyranoside	70% EtOH	C ₄₅ H ₇₂ O ₁₇	885.0430	Liu et al. (2021)
60	Dumoside	70% EtOH	C ₄₀ H ₆₂ O ₁₆	798.9107	Liu et al. (2021)
61	Asparacosins A	MeOH	C ₂₇ H ₄₀ O ₅	444.6035	Zhang et al. (2004)
62	Asparacosins B	MeOH	C ₂₉ H ₄₆ O ₆	490.6719	Zhang et al. (2004)
63	26-O- β -D-glucopyranosyl-(25R)-5 β -furost-3 β ,26-diol-3-O- α -L-rhamnopyranosyl-(1 \rightarrow 2)-[β -D-xylcopyranosyl-(1 \rightarrow 4)- β -D-glucopyranoside	60% EtOH	C ₅₀ H ₈₄ O ₂₂	1037.1888	Pang et al. (2021)
64	25- <i>epi</i> -officialisnin II	60% EtOH	-	-	Pang et al. (2021)
65	Disporoside C	60% EtOH	C ₄₅ H ₇₆ O ₁₉	921.0735	Pang et al. (2021)
66	26-O- β -D-glucopyranosyl-(25R)-5 β -furost-3 β ,26-diol-3-O- α -L-rhamnopyranosyl-(1 \rightarrow 2)-[β -D-xylcopyranosyl-(1 \rightarrow 4)-[α -L-rhamnopyranosyl-(1 \rightarrow 6)]- β -D-glucopyranoside	60% EtOH	C ₅₆ H ₉₄ O ₂₇	1199.3294	Pang et al. (2021)
67	26-O- β -D-glucopyranosyl-(25R)-5 β -furost-3 β ,26-diol-3-O- α -L-rhamnopyranosyl-(1 \rightarrow 2)-[α -L-rhamnopyranosyl-(1 \rightarrow 4)]-[α -L-rhamnopyranosyl-(1 \rightarrow 6)]- β -D-glucopyranoside	60% EtOH	C ₅₇ H ₉₆ O ₂₇	1213.3560	Pang et al. (2021)
68	3-O-[[α -L-rhamnopyranosyl-(1 \rightarrow 4)] [β -D-glucopyranosyl]]-26-O-[[β -D-glucopyranosyl]-22 α -methoxy-(25S)-5 β -furostane-3 β ,26-diol	EtOH	C ₄₆ H ₇₉ O ₁₈	904.1131	Shi et al. (2004)
69	Protoneodioscin	60% EtOH	-	-	Pang et al. (2021)
70	3-O-[α -L-rhamnopyranosyl-(1 \rightarrow 4) β -D-glucopyranosyl]-26-O-(β -D-glucopyranosyl) -(25R)-furosta-5,20-diene, -3 β ,26-diol	Water	-	-	Liang et al., 1988 Liu et al. (2021)
71	5 β -pregn-20-ene-3,16-diol-22-one 3-O- α -L-rhmnoypyranosyl-(1 \rightarrow 2)- β -D-glucopyranoside	70% MeOH	C ₃₄ H ₅₂ O ₁₂	652.7695	Zhu et al. (2021)
C ²¹ -steroids					
72	3-O- β -D-xylopyranosyl(1 \rightarrow 4)-[β -D-glucopyranosyl(1 \rightarrow 2)]- β -Dglucopyranosyl-5 β -pregna-16-ene-3 β -ol-20-one	75% EtOH	C ₃₈ H ₆₀ O ₁₆	772.8734	Jian et al. (2013)
73	3-O- α -L-rhamnopyranosyl (1 \rightarrow 4)- [β -D-glucopyranosyl (1 \rightarrow 2)]- β -D-glucopyranosyl-5 β -pregna-16-ene-3 β -ol-20-one	75% EtOH	C ₃₃ H ₅₂ O ₁₂	640.7588	Jian et al. (2013)
74	3-O- β -D-glucopyranosyl (1 \rightarrow 2)- β -D-glucopyranosyl-5 β -pregna-16-ene-3 β -ol-20-one	75% EtOH	C ₃₃ H ₅₂ O ₁₂	640.7588	Jian et al. (2013)
75	(3 β ,5 β)-pregn-16(17)-en-3-ol-20-one 3-O- α -L-rhmnoypyranosyl-(1 \rightarrow 4)- β -D-glucopyranoside	70% MeOH	C ₃₃ H ₅₂ O ₁₁	624.7594	Zhu et al. (2021)
76	(3 β ,5 β)-pregn-16(17)-en-3-ol-20-one 3-O- α -L-rhmnoypyranosyl-(1 \rightarrow 2)- β -D-glucopyranoside	70% MeOH	C ₃₃ H ₅₂ O ₁₁	624.7594	Zhu et al. (2021)
77	(3 β ,5 β)-pregn-16(17)-en-3-ol-20-one 3-O- α -L-arabinopyranosyl-(1 \rightarrow 4)- β -D-glucopyranoside	70% MeOH	C ₂₀ H ₅₀ O ₁₁	466.6040	Zhu et al. (2021)
78	(3 β ,5 β)-pregn-16(17)-en-3-ol-20-one 3-O- α -L-arabipyranosyl-(1 \rightarrow 4)- β -D-glucopyranosyl-(1 \rightarrow 2)- β -D-glucopyranosid	70% MeOH	C ₃₈ H ₆₀ O ₁₆	772.8734	Zhu et al. (2021)
79	3 β -[(O- α -L-rhamnopyranosyl-(1 \rightarrow 4)- β -D-glucopyranosyl)oxy]pregna-5,16-dien-20-one	70% EtOH	C ₃₃ H ₅₀ O ₁₁	622.7435	Liu et al. (2021)

(Continued on following page)

TABLE 1 (Continued) Chemical compounds isolated from *A. cochinchinensis*.

Number	Chemical composition	Extraction solvent	Molecular formula	Molecular weight	Reference
Amino acid					
80	Alanine	Water	C ₃ H ₇ NO ₂	89.0932	Choi et al., 2019
81	Glycine	Water	C ₂ H ₅ NO ₂	75.0666	Choi et al., 2019
82	Methionine	Water	C ₅ H ₁₁ NO ₂ S	149.2113	Choi et al., 2019
83	Tryptophan	Water	C ₁₁ H ₁₂ N ₂ O ₂	204.2252	Choi et al., 2019
Lignan					
84	Iso-agatharesinol	70% EtOH	C ₁₇ H ₁₈ O ₄	286.3224	Li et al. (2012)
85	Iso-agatharesinoside	70% EtOH	C ₂₃ H ₂₈ O ₉	448.4630	Li et al. (2012)
Others					
86	1-[4-hydroxyphenoxy]-5-[3-methoxy-4-hydroxyphenyl] pent-2-en-3-yne	MeOH	C ₁₈ H ₁₆ O ₄	296.3172	Zhang et al. (2004)
87	Asparenydiol	MeOH	C ₁₇ H ₁₃ O ₃	265.2839	Zhang et al. (2004)
88	3'-hydroxy-4'-methoxy-4'-dehydroxynyasol	MeOH	C ₁₈ H ₁₈ O ₃	282.3337	Zhang et al. (2004)
89	Nyasol	MeOH	C ₁₇ H ₁₆ O ₂	252.3077	Zhang et al. (2004)
90	3''-methoxynyasol	MeOH	C ₁₇ H ₁₆ O ₃	268.3071	Zhang et al. (2004)
91	1,3-bis-di-p-hydroxyphenyl-4-penten-1-one	MeOH	C ₁₇ H ₁₆ O ₃	268.3071	Zhang et al. (2004)
92	Trans-coniferyl alcohol	MeOH	C ₁₀ H ₁₂ O ₃	180.2005	Zhang et al. (2004)
93	Acrylamide	Water	C ₃ H ₅ NO	71.0779	Shi et al. (2009)

Lignans

Lignans are a kind of natural compounds synthesized by the polymerization of two-molecular phenylpropanoid derivatives, most of which are free, and a few are glycosides bound to a sugar. At present, a small concentration of lignans 84–85 (Li et al., 2012) was identified from *A. cochinchinensis*. Compared with other compounds, lignans have less structure. Therefore, future efforts should be made to isolate and characterize lignans in *A. cochinchinensis*.

Polysaccharides

In recent years, plant polysaccharides have attracted high research interest due to their unique biological activity and natural origin, with great potential to protect human health. Many natural products are is rich in polysaccharide resources, especially medicinal plant polysaccharides, with long application history and broad development prospects. *A. cochinchinensis* polysaccharides are mainly comprised of Man, Rha, Glc, Gal, Ara, Xyl, Fru, GlcUA, and GalUA, as shown in Table 3.

Other compounds

In addition to the five major phytochemical compound classes mentioned above, other bioactive constituents have also been isolated from *A. cochinchinensis* (Zhang et al., 2004; Shi et al., 2009). These include 1-[4-hydroxyphenoxy]-5-[3-methoxy-4-hydroxyphenyl] pent-2-en-3-yne (86), asparenydiol (87),3'-hydroxy-4'-methoxy-4'dehydroxynyasol (88), Nyasol(89), 3''-methoxynyasol(90), 1,3-bis-di-p-hydroxyphenyl-4-penten-1-one(91), trans-coniferyl alcohol(92), Acrylamide(93). The above findings illustrate the wide chemical composition of *A. cochinchinensis*, which is of immense future research value.

Pharmacological activities

A. cochinchinensis exerts various pharmacological activities, including anti-asthma, anti-inflammation, anti-oxidant, anti-tumor, anti-depressant, neuroprotective, improve Alzheimer's disease and gut diseases. To illustrate the nature of the active

TABLE 2 The structures of steroidal saponins in *A. cochinchinensis*.

NO	Structure					
	Mother nucleus	R ₁	R ₂	R ₃	R ₄	R ₅
1	I	α-L-Rha (1→2)-[α-L-Rha (1→4)]-β-D-Glc	H	H	H	H
2	I	α-L-Rha (1→4)-β-D-Glc	H	H	H	H
3	I	α-L-Rha (1→2)-[α-L-Rha (1→4)]-β-D-Glc	H	H	OH	OH
4	I	α-L-Rha (1→2)-[α-L-Rha (1→4)]-β-D-Glc	H	H	H	OH
5	II	α-L-Rha (1→2)- [α-L-Rha (1→4)]-β-D-Glc	H	H	OCH ₃	β-D-Glc
6	III	α-L-Rha (1→4)-β-D-Glc	OH	H	H	β-D-Glc
7	III	α-L-Rha (1→4)-β-D-Glc	H	H	H	β-D-Glc
8	IV	α-L-Rha (1→4)-β-D-Glc	H	H	H	H
9	IV	β-D-Glc(1→2)-[α-L-Ara(1→4)]-[α-L-Ara(1→6)]-β-D-Glc	H	H	H	H
10	IV	α-L-Rha (1→2)-β-D-Glc	H	H	H	H
11	IV	α-L-Rha(1→2)-[α-L-Rha(1→4)]-β-D-Glc	H	H	H	H
12	IV	β-D-Glc(1→2)-[α-L-Rha(1→4)]-β-D-Glc	H	H	H	H
13	IV	α-L-Rha	H	H	H	H
14	IV	β-D-Glc	H	H	H	H
15	V	α-L-Rha (1→4)-β-D-Glc	H	H	OH	H
16	V	α-L-Rha (1→4)-β-D-Glc	α-H,β-OH	H	H	H
17	VI	α-L-Rha(1→2)-[β-D-Glc(1→4)]-β-D-Glc	H	H	H	β-D-Glc
18	VII	α-L-Rha(1→2)-[β-D-Glc(1→4)-α-L-Rha(1→4)]-β-D-Glc	H	H	OH	β-D-Glc
19	VII	α-L-Rha(1→2)-[α-L-Rha(1→4)]-β-D-Glc	H	H	OH	β-D-Glc
20	VIII	α-L-Rha(1→2)-[α-L-Rha(1→4)]-β-D-Glc	OH	H	H	β-D-Glc
21	VIII	α-L-Rha(1→2)-[α-L-Rha(1→4)]-β-D-Glc	H	H	OH	β-D-Glc
22	VIII	α-L-Rha(1→2)-[α-L-Rha(1→4)]-β-D-Glc	H	H	H	β-D-Glc
23	IX	α-L-Rha(1→2)-[α-L-Rha(1→4)]-β-D-Glc	H	H	H	β-D-Glc
24	X	β-D-Glc(1→2)-β-D-Glc	H	H	OCH ₃	β-D-Glc
25	X	α-L-Rha (1→4)-β-D-Glc	H	O	OH	β-D-Glc
26	X	β-D-Glc(1→2)-[α-L-Rha(1→4)]-β-D-Glc	H	H	OH	β-D-Glc
27	X	β-D-Xyl(1→2)-[α-L-Rha(1→4)]-β-D-Glc	H	H	OH	β-D-Glc
28	X	α-L-Rha (1→4)-β-D-Glc	H	H	OH	β-D-Glc
29	X	β-D-Glc	H	H	OH	β-D-Glc
30	XI	β-D-Glc	H	H	H	H
31	XII	α-L-Rha(1→2)-[β-D-Xyl(1→4)]-β-D-Glc	H	H	OH	β-D-Glc
32	XII	β-D-Glc	H	H	H	β-D-Glc
33	XIII	α-L-Rha(1→2)-[β-D-Xyl(1→4)]-β-D-Glc	H	H	OH	β-D-Glc
34	XIII	α-L-Rha(1→2)-[α-L-Rha(1→4)]-β-D-Glc	H	H	OH	β-D-Glc
35	XIII	β-D-Glc	H	H	OCH ₃	β-D-Glc
36	XIV	β-D-Glc	H	OH	OH	β-D-Glc
37	XIV	β-D-Glc(1→2)-[β-D-Xyl(1→4)]-β-D-Glc	H	H	OH	β-D-Glc
38	XIV	β-D-Glc(1→2)-β-D-Glc	H	H	OH	β-D-Glc
39	XIV	H	H	H	OH	β-D-Glc
40	XV	α-L-Rha(1→2)-[β-D-Xyl(1→4)]-β-D-Glc	H	H	OH	β-D-Glc
41	XV	α-L-Rha(1→2)-[α-L-Rha(1→4)]-β-D-Glc	H	H	OH	β-D-Glc
42	XVI	α-L-Rha (1→4)-β-D-Glc	H	H	H	β-D-Glc
43	XVII	β-D-Glc(1→2)-[β-D-Xyl(1→4)]-β-D-Glc	H	OH	CH ₃	β-D-Glc
44	XVII	α-L-Rha(1→4)-β-D-Glc	H	OH	β-methyl	β-D-Glc
45	XVII	β-D-Glc(1→4)-β-D-Glc	H	OH	α-methyl	β-D-Glc
46	XVIII	α-L-Rha (1→4)-β-D-Glc	OH	H	OH	H

(Continued on following page)

TABLE 2 (Continued) The structures of steroidal saponins in *A. cochinchinensis*.

NO	Structure					
	Mother nucleus	R ₁	R ₂	R ₃	R ₄	R ₅
47	XIX	α-L-Rha (1→4)-β-D-Glc	H	OH	OH	OH
48	XX	α-L-Rha(1→2)-[α-L-Rha(1→4)]-β-D-Glc	H	H	H	OH
49	XXI	α-L-Rha (1→4)-β-D-Glc	H	H	H	OH
50	XXI	α-L-Rha (1→4)-β-D-Glc	H	H	OH	OH
51	XXII	α-L-Rha (1→4)-β-D-Glc	H	H	H	H
52	XXII	β-D-Glc(1→2)-[α-L-Rha(1→4)]-β-D-Glc	H	H	H	H
53	XXIII	β-D-Glc(1→4)-β-D-Glc	H	H	OCH ₃	β-D-Glc
54	XXIV	α-L-Rha(1→2)-[α-L-Rha(1→4)]-β-D-Glc	H	H	H	β-D-Glc
55	XXV	α-L-Rha (1→4)-β-D-Glc	H	H	H	H
56	XXVI	α-L-Rha (1→4)-β-D-Glc	H	H	H	H
57	XXVII	α-L-Rha (1→4)-β-D-Glc	H	H	H	β-D-Glc
58	XXVIII	α-L-Rha(1→2)-[α-L-Rha(1→4)]-β-D-Glc	H	H	OH	OH
59	XXVIII	α-L-Rha(1→2)-[α-L-Rha(1→4)]-β-D-Glc	H	H	OH	H
60	XXIX	α-L-Rha(1→2)-[α-L-Rha(1→4)]-β-D-Glc	H	H	H	H
61	XXX	OH	OH	H	H	H
62	XXXI	H	OH	H	H	H
63	XXXII	α-L-Rha(1→2)-[β-D-Xyl(1→4)]-β-D-Glc	H	H	OH	β-D-Glc
64	XXXII	β-D-Glc(1→2)-[β-D-Xyl(1→4)]-β-D-Glc	H	H	OH	β-D-Glc
65	XXXII	β-D-Glc(1→2)-β-D-Glc	H	H	OH	β-D-Glc
66	XXXII	β-D-Glc(1→2)-[β-D-Xyl(1→4)]-[α-L-Rha(1→6)]-β-D-Glc	H	H	OH	β-D-Glc
67	XXXII	β-D-Glc(1→2)-[α-L-Rha(1→4)]-[α-L-Rha(1→6)]-β-D-Glc	H	H	OH	β-D-Glc
68	XXXIII	α-L-Rha (1→4)-β-D-Glc	H	OCH ₃	H	β-D-Glc
69	XXXIV	α-L-Rha(1→2)-[α-L-Rha(1→4)]-β-D-Glc	H	H	OH	β-D-Glc
70	XXXV	α-L-Rha (1→4)-β-D-Glc	H	H	CH ₃	β-D-Glc
71	XXXVI	α-L-Rha (1→2)-β-D-Glc	H	H	H	H

compounds of *A. cochinchinensis*, the pharmacological effects and potential mechanisms of this plant on the basis of different types of extracts and compounds were summarized in Table 4. A simplified diagram of its pharmacological effects is presented in Figure 5.

Anti-asthma

Asthma is a common chronic and stubborn respiratory disease, clinically presenting with cough, chest tightness, wheezing, and shortness of breath (Papi et al., 2018). Non-timely treatment will lead to a series of secondary diseases, such as chronic obstructive pulmonary disease and heart failure, which can become life-threatening (Schoettler and Strek, 2020; Miller et al., 2021). At the same time, it also added a serious financial burden to the family (López-Tiro et al., 2022). Therefore, researchers found that the butanol extract of *A. cochinchinensis* roots, when fermented with *Weissella cibaria* (BAfW), was found to inhibit the

development of asthma development through various potential mechanisms. Choi et al., 2018 alterations in key parameters were measured in ovalbumin (OVA)-challenged Balb/c mice treated with different BAFW dose regimens at three different time points. The results show that when the dosage of *A. cochinchinensis* fermentation extract was 500 mg, the number of immune cells, OVA-specific immunoglobulin E (Ig E) level, thickness of respiratory enzyme and mucus score decreased significantly in mice, and these parameters could be maintained for 48 h (Choi et al., 2018b). At the same time, researchers explored biomarkers for asthma in OVA-induced asthma mice. The extract of *A. cochinchinensis* was administered to the model mice at a low concentration of 250 mg/kg and a high concentration of 500 mg/kg, respectively. The changes in their metabolites were observed after administration. The results showed that the immune cells, Ig E serum concentration, the respiratory epithelium's thickness, and inflammatory cell infiltration in the airway in mice treated with *A. cochinchinensis* extract recovered significantly. Notably, when assessing the endogenous metabolites, only alanine, glycine,

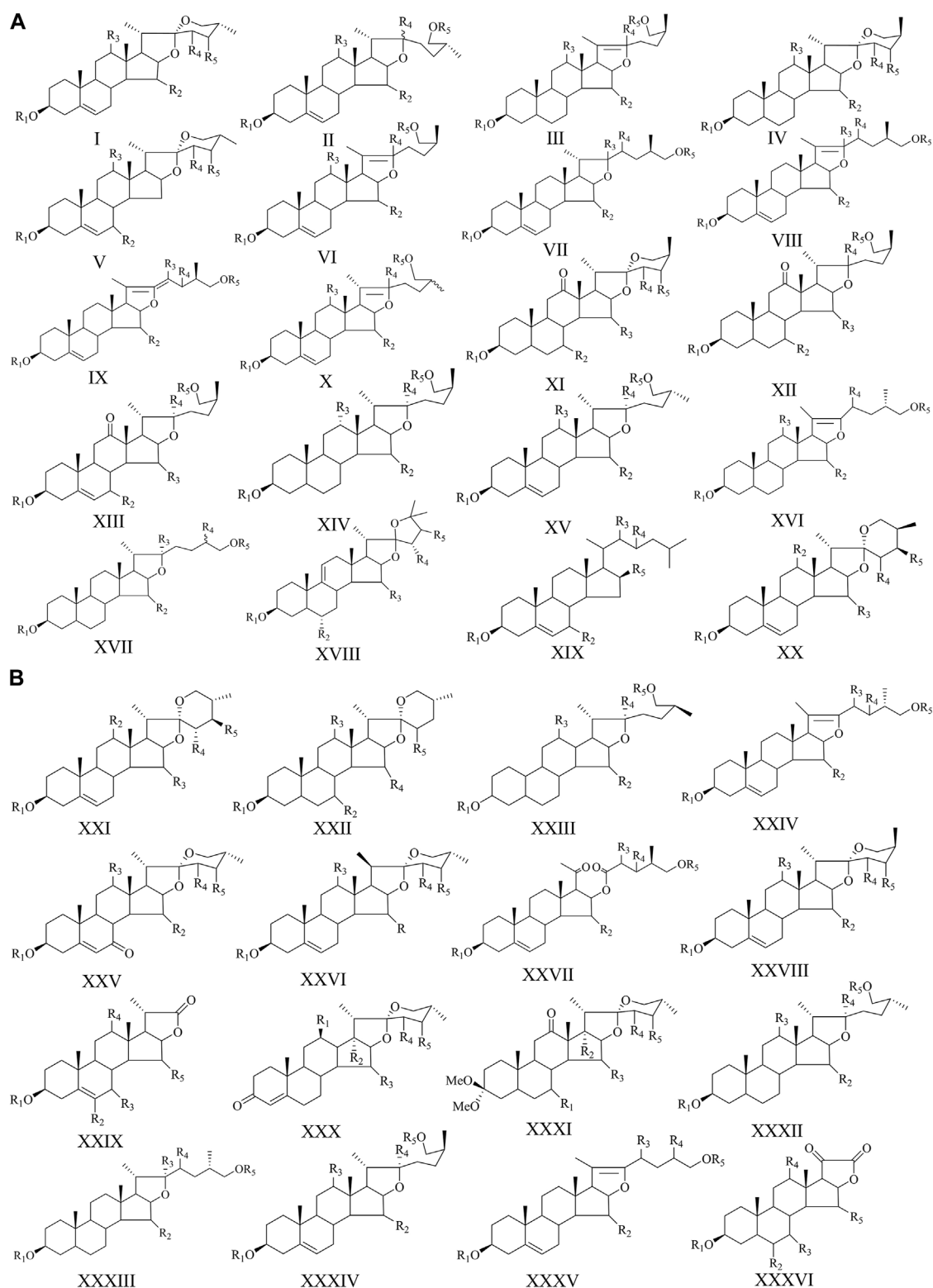


FIGURE 2

The structures of steroidal saponins (1–71) in *A. cochinchinensis*.

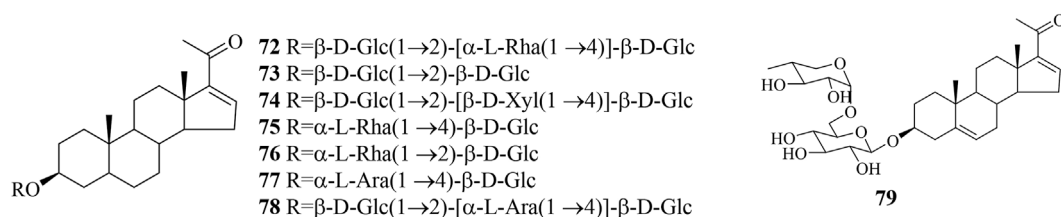


FIGURE 3

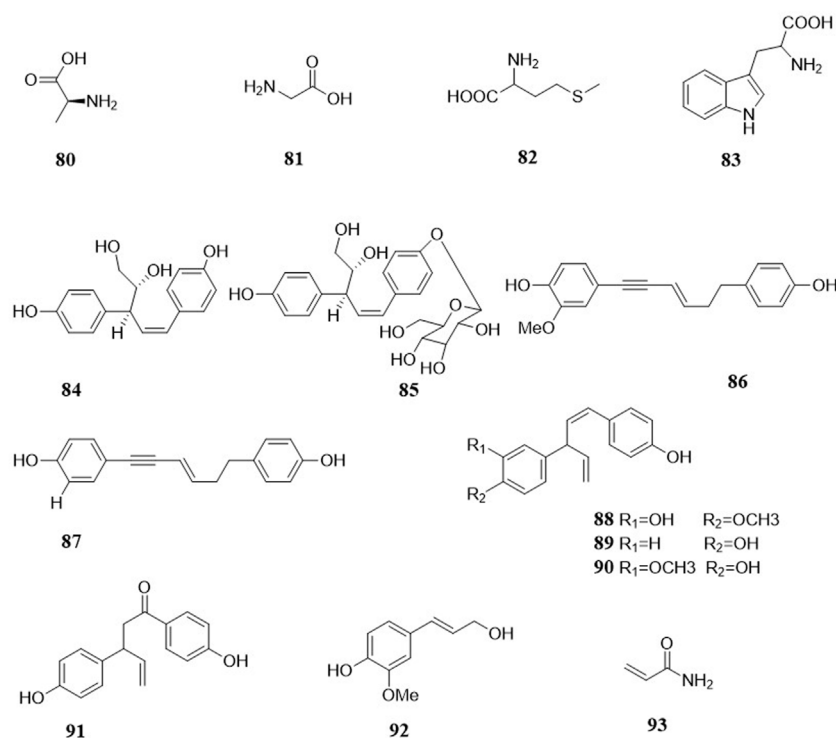
The structures of C_{21} -steroidals in *A. cochinchinensis*.

FIGURE 4

The structures of amino acids, lignans, and other compounds in *A. cochinchinensis*.

methionine, and tryptophan were significantly recovered after *A. cochinchinensis* extract treatment, compared with the control group. Therefore, these four metabolites can be used as biomarkers to predict the anti-asthmatic effects (Choi et al., 2019). Moreover, the *A. cochinchinensis* fermentation extract was shown for the first time to accelerate the recovery from chronic asthma. It prevented airway inflammation and remodeling by restoring the cholinergic regulation of structural cells and inflammatory cells in chronic asthma models. Thus, it can further potentiate the effects of asthma treatments (Choi et al., 2018a). Furthermore, *in vitro* and *in vivo* experiments have been conducted to explore the effects of total saponins in *A.*

cochinchinensis extract on asthma. Lipopolysaccharide (LPS)-activated RAW264.7 cells and OVA-induced mice asthma were treated with saponins-rich *A. cochinchinensis* extract, respectively. The result showed that the concentration of nitric oxide (NO) and mRNA levels of and cyclooxygenase-2 (COX-2) and inducible nitric oxide synthase (iNOS) were significantly decreased in the SEAC/LPS-treated RAW264.7 cells compared with the vehicle/LPS-treated RAW264.7 cells. At the same time, the number of immune cells, infiltration of inflammatory cells and bronchial thickness decreased, meanwhile the levels of interleukin 4 (IL-4), interleukin 13 (IL-13) decreased significantly under the

TABLE 3 Composition and analysis of polysaccharides in *A. cochinchinensis*.

No	Name	Extraction	Analytical method	Analytical condition	Monosaccharide composition	Molecular weight (Da)	Main structure	Reference
1	ACNP	distilled water refluxed (6h)	HPLC	Sugar-pack TM column (6.5 mm × 300 mm, 10 μm) and ELSD (evaporative light scattering detector); distilled water; 0.4 ml/min; column temperature 30°C	Fru, Glc	2690	2,1-β-D-Fruf residues, ending with a (1→2) bonded α-D-Glcp	Sun et al. (2020)
			GC-MS		93.3: 6.7(area %)			
2	Radix Asparagi polysaccharide	deionized water refluxed (4.5h)	CZE	40 mM sodium tetraborate buffer (pH 10.1); hydrodynamic injection (10 cm × 4 s); 14 kV	Xyl, Ara, Glc, Rha, Man, Gal, GlcUA, GalUA	-	-	Chen et al. (2015)

treatment of *A. cochinchinensis* extract (Sung et al., 2017). In general, *A. cochinchinensis* extracts can inhibit airway inflammation and remodeling, providing an important natural medicine option for the treatment of asthma.

Anti-inflammatory

Inflammation commonly occurs due to the modern lifestyle, and its complications can detrimentally affect people’s health (Yeung et al., 2018; McInnes and Gravallesse, 2021). Numerous studies have proved that *A. cochinchinensis* has anti-inflammatory effect. Previous research by Kim et al., 1998 showed that *A. cochinchinensis* could inhibit tumor necrosis factor-α (TNF-α) secretion by inhibiting interleukin 1 (IL-1) secretion and that *A. cochinchinensis* extracts had anti-inflammatory activity in the central nervous system (Kim et al., 1998). Another study showed that the ethanol extract of *A. cochinchinensis* inhibited acute and chronic inflammation. When the extract was administered at a 200 mg/kg dose, the symptoms of 12-o-tetradecanoyl-phorbol-13-acetate (TPA)-induced mice ear were significantly alleviated. In addition, the skin thickness and tissue weight, inflammatory cytokine production, neutrophil-mediated myeloperoxidase (MPO) activity and histopathological parameters were significantly decreased (Lee et al., 2009). Furthermore, researchers have found that the ethyl acetate extract of *A. cochinchinensis* was shown to inhibits skin inflammation. In this study, phthalic anhydride (PA) -induced skin inflammation mice were used to identify the effects of *A. cochinchinensis* ethyl acetate extract on inflammation. The results suggest that ethyl acetate extract of *A. cochinchinensis* significantly reduced the concentration of Ig E, the surface thickness and number of infiltrating mast cells, and ethyl acetate extract played a key role in the treatment process (Sung et al., 2016). Using *in vitro* cell experiments, the

researchers showed that the *A. cochinchinensis* ethyl acetate extract could inhibit the LPS stimulated RAW264.7 cell NO production, COX-2 expression, reactive oxygen species (ROS) production, and the inflammatory cytokine cell cycle (Lee et al., 2017). Thus, the above research findings provide strong evidence that *A. cochinchinensis* extracts may have important medicinal properties for treating specific skin inflammatory diseases. Surprisingly, after fermentation with BAfW, compounds such as protodioscin were significantly enhanced. In addition, a significant suppression was observed in the expression of key members of the iNOS-mediated COX-2 induction pathway and the phosphorylation of mitogen-activated protein kinases. These observations point to the ability to inhibit inflammatory reaction occurrence (Lee et al., 2015). Furthermore, studies have shown that the compound methyl protodioscin in *A. cochinchinensis* can inhibit the production of pro-inflammatory factors such as interleukin 16 (IL-16), interleukin 8 (IL-8) and TNF-α in lung tissue, suggesting that the compound has therapeutic value for airway inflammatory diseases (Lee et al., 2017a). Additionally, through *in vitro* cell experiments, the researchers took LPS-induced microglia cell as the study model. They were found that the ethanol extract of *A. cochinchinensis* at 1.0 μg mL⁻¹ could significantly inhibit the production of NO in microglia cell induced by LPS, so as to play an anti-inflammatory role (Jian et al., 2013). All in all, all these studies have emphasized the potential of *A. cochinchinensis* extract to inhibit inflammatory reactions.

Anti-oxidant

Anti-oxidants have always played a vital role in people’s health (Milisav et al., 2018; Martemucci et al., 2022). Studies have recently confirmed the anti-oxidant effect of *A. cochinchinensis*

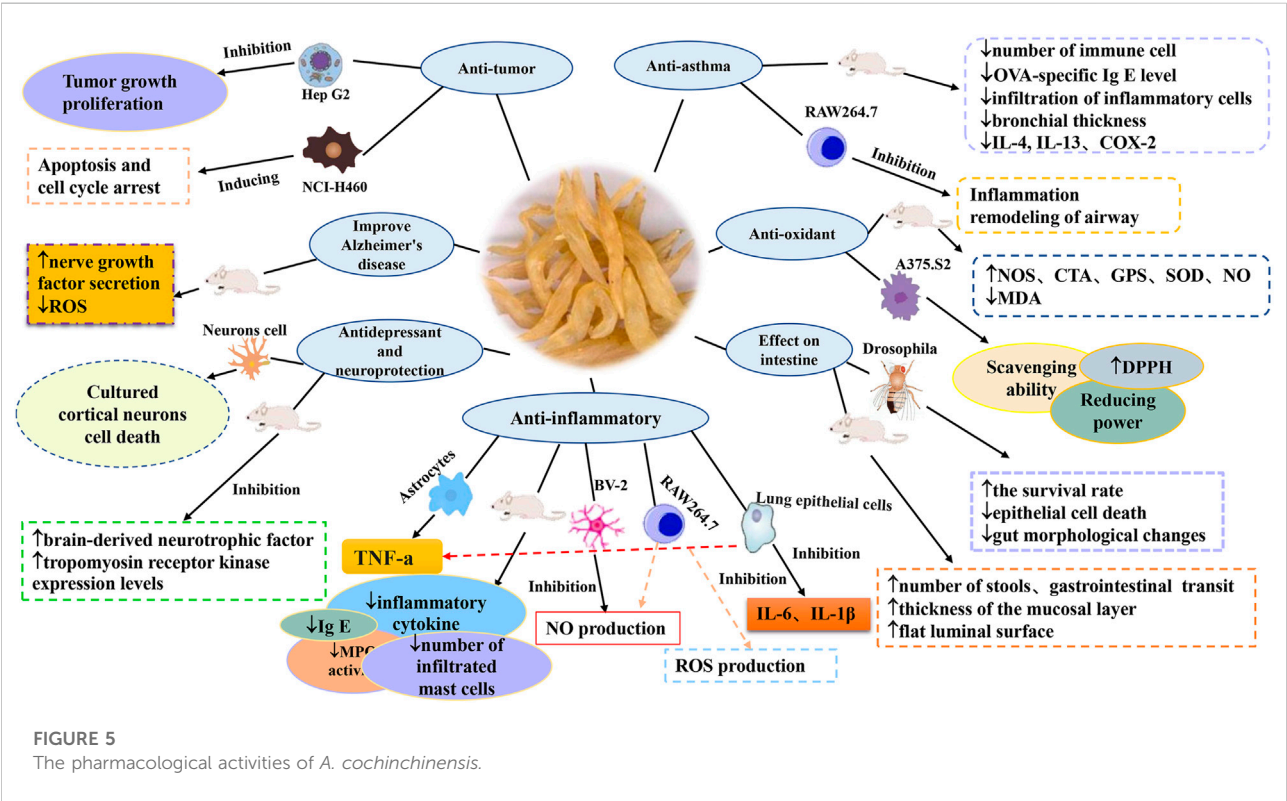
TABLE 4 Summary of pharmacological activities of *A. cochinchinensis* extracts/compounds.

Pharmacological activities	Extracts/Compounds	Models	Results/Mechanisms	Dosages	References
Anti-asthma	Water extract (2.5 h)	Mice (OVA-induced)	↓Number of immune cells, ↓OVA-specific Ig E level, ↓thickness of respiratory epithelium and mucus score	500 mg·kg ⁻¹	Choi et al. (2018b)
	Water extract	Mice (OVA-induced)	Prevent inflammation and remodeling of airway	250 and 500 mg·kg ⁻¹	Choi et al. (2019)
	Water extract (2.5 h)	Mice (OVA-induced)	↓Infiltration of inflammatory cells and bronchial thickness; ↓number of macrophages and eosinophils, ↓concentration of OVA-specific Ig E, and expression of Th2 cytokines	250 and 500 mg·kg ⁻¹	Choi et al. (2018a)
	Total saponin	Mice (OVA-induced); RAW264.7 cells (LPS-activated)	↓Number of immune cells, ↓infiltration of inflammatory cells, ↓bronchial thickness, ↓IL-4, IL-13 and COX-2	250 and 500 mg·kg ⁻¹ ; 200 µg·mL ⁻¹	Sung et al. (2017)
Anti-inflammatory	Distilled water extract (70°C for 5 h)	Astrocytes (stimulated with SP and LPS)	Inhibit TNF-α secretion by inhibiting IL-1 secretion	10 ¹ –10 ³ µg·mL ⁻¹	Kim et al. (1998)
	70% EtOH extract (three times, with 2 h reflux)	Mice (TPA-induced)	↓Skin thickness and tissue weight, ↓inflammatory cytokine production, ↓neutrophil-mediated MPO activity	200 mg·kg ⁻¹	Lee et al. (2009)
	Ethyl acetate extract (three times, with 2 h reflux)	Mice (IL-4/Luc/CNS-1 Tg)	↓Immunoglobulin E concentration, ↓epidermis thickness, ↓number of infiltrated mast cells	200 and 400 mg·kg ⁻¹	Sung et al. (2016)
	Ethyl acetate extract (50°C for 24 h)	RAW264.7 cells (LPS-activated)	Inhibition of NO production, COX-2 expression, ROS production, differential regulation of inflammatory cytokines cell cycle	100 and 200 µg·mL ⁻¹	Lee et al. (2017b)
	Methyl Protodioscin	Lung epithelial cells; Mice (airway inflammation)	Inhibited the production of proinflammatory cytokines IL-6, TNF-α, IL-1β in lung tissue	10–100 µM	Lee et al. (2015)
	Butanol extract (three times)	RAW264.7 macrophage cells (LPS-stimulated)	Inhibition of proinflammatory cytokine expression	100 and 200 µg·mL ⁻¹	Lee et al. (2017b)
	75% EtOH (three times, 3 h at 70°C)	BV-2 microglial cells (LPS-induced)	Inhibition of NO production	1.0 µg·mL ⁻¹	Jian et al. (2013)
Anti-oxidant	Water extract (three times)	Mice (D-galactose-induced aging)	↑NOS, CAT, SOD activities, ↑NO content, ↓MDA content	0.7 g·mL ⁻¹	Lei et al. (2017)
	Water extract (three times)	Mice (D-galactose-induced aging)	↑NOS, CAT, SDA activities and the NO content; ↑expressions of NOS, ↑SOD and GPX	0.7 g·mL ⁻¹	Lei et al. (2016)
	25% ethyl acetate extract (three times, 40°C for 2 h)	CCD-966SK cell; A375.S2 cell	↑Scavenging ability, reducing power, ↑anti-tyrosinase activity of DPPH	100–1000 mg·L ⁻¹	Wang et al. (2019)
	Water extract (1 h three times)	Mice (D-Galactose)	↑Spleen index and the SOD activity; ↓MDA content	2.66 g·kg ⁻¹	Xiong et al. (2011)
Anti-tumor	90% EtOH extract (80°C for 3 h)	Hep G2 cells, Hep 3B cell, LO 2 cell; mice (Tumor-Bearing)	Inhibit tumor growth and proliferation	200 mg·kg ⁻¹	Zhang et al. (2021b)
	70% EtOH extract (refluxing three times, 2 hours each time)	NCI-H460 cell	Inducing apoptosis and cell cycle arrest; inhibition of lung cancer cell proliferation	10, 50 and 100 µM	Liu et al. (2021)
	Water extract (decoction 3 h)	Hep G2 cells	Inhibited the TNF-α-induced apoptosis of Hep G2 cells	1–100 mg·mL ⁻¹	Koo et al. (2000)
Antidepressant and neuroprotection	Water extract (100°C for 2 h)	Mice (Ovariectomized)	↑Brain-derived neurotrophic factor	1000 and 2000 mg·kg ⁻¹	Kim et al. (2020)
	MeOH extract (5 days)	Cortical neurons cell	↑Tropomyosin receptor kinase expression levels Inhibited H2O2-induced cell death in cultured cortical neurons		Jalsrai et al. (2016)

(Continued on following page)

TABLE 4 (Continued) Summary of pharmacological activities of *A. cochinchinensis* extracts/compounds.

Pharmacological activities	Extracts/Compounds	Models	Results/Mechanisms	Dosages	References
Treat intestinal related diseases	Water extract (3 h, repeated twice)	Mice <i>Drosophila</i>	↑The survival rate; ↓epithelial cell death; attenuated metal ion-induced gut morphological changes	0.01, 0.50 and 1.00 μM; 100 and 200 mg·kg ⁻¹	Zhang et al. (2016)
	Saponin (24 h at 50°C)	Mice (loperamide-induced constipation)	↑Number of stools and gastrointestinal transit, ↑thickness of the mucosal layer, ↑flat luminal surface, ↑number of paneth cells, ↑lipid droplets	1000 mg·kg ⁻¹	Kim et al. (2019)
Improve Alzheimer's disease	Water extract (121°C for 45 min)	Mice	↑Nerve growth factor secretion; ↓intracellular ROS	100 mg·kg ⁻¹	Lee et al. (2018)



extract. *A. cochinchinensis* is shown to significantly increase the activities of anti-oxidant enzymes such as superoxide dismutase (SOD), catalase (CAT), nitric oxide synthase (NOS), NO, and glutathione peroxidase (GPX). Liver and kidney hematoxylin and eosin stain sections revealed that D-galactose could cause serious injury, and *A. cochinchinensis* treatment improved immunity and

substantially protected the liver and kidney from oxidative damage in aging mice (Lei et al., 2016). In a similar experiment, compared with the Vitamin C (Vc) positive control group, 0.7 mg·mL⁻¹ aqueous root extract of *A. cochinchinensis* had similar 1,1-Diphenyl-2-picrylhydrazyl (DPPH) and 3-ethylbenzothiazoline-6-sulfonic (ABTS⁺)

scavenging activities, but significantly increased superoxide anion ($p < 0.05$) and OH scavenging activities ($p < 0.01$), which suggested strong radical scavenging ability of the aqueous root extract *in vitro* (Lei et al., 2017). At the same time, the researchers took D-galactose -induced mice as the research object and administered intraperitoneal injection (0.2 ml/20g) to mice for 15 days to make them senile, and further explored the effect of *A. cochinchinensis* extract on aging mice. The study found that through the detection of mice spleen and plasma, *A. cochinchinensis* extract could increase the spleen index and the SOD activity, reduces malondialdehyde (MDA) content, inhibits oxidation and slows down aging (Xiong et al., 2011). Additionally, 2,2-diphenyl-1-picrylhydrazine (DPPH) plays an indispensable role in antioxidant process. In a recent study, the fermented *A. cochinchinensis* root extract's effects on melanogenic factor levels in human epidermal melanocytes (HEMs) and its anti-tyrosinase activity were analyzed and compared with the unfermented extract. The results showed that the scavenging ability, reducing power, and anti-tyrosinase activity of DPPH in the fermented extract were significantly increased (Wang et al., 2019). Therefore, *A. cochinchinensis* can be used as a natural antioxidant, with broad development and application prospects in the future.

Anti-tumor

The prevention and treatment of malignant tumors and cancer is a major challenge faced in our modern societies (Liu and Dong, 2021; DiMaio et al., 2022; Mao et al., 2022). With the development of molecular biology and pharmacology, *A. cochinchinensis* has attracted increasing attention from domestic and foreign medical scholars working in the cancer field. Through *in vitro* and *in vivo* experiments, *A. cochinchinensis* extracts were mainly internalized into tumor cells through phagocytosis, but once they entered the blood, tumor cells would be quickly cleared, further inhibiting the growth and proliferation of tumor cells (Zhang R. S. et al., 2021). Another study found that the compound 3-O-[[β -D-glucopyranosyl-(1 \rightarrow 2)]-[α -L-rhamnopyranosyl-(1 \rightarrow 4)]- β -D-glucopyranosyl]-(25R)-5 β -spirostan-3 β -ol mainly exerted its effect on inhibiting the proliferation of human large cell lung cancer cells (NCI-H460) by inducing apoptosis and cell cycle arrest, with an IC_{50} value of 1.39 μ M (Liu et al., 2021). Besides that, the extract of *A. cochinchinensis* (1–100 mg/ml) dose-dependently not only inhibited the EtOH-induced tumor necrosis TNF- α secretion but also inhibited the EtOH and TNF- α -induced cytotoxicity. In addition, the extract of *A. cochinchinensis* inhibited the TNF- α -induced apoptosis of Hep G2 cells. Therefore, the above results suggest that *A. cochinchinensis* may prevent the EtOH-induced cytotoxicity by inhibiting the apoptosis of Hep G2 cells (Koo et al., 2000). These

studies will provide a reference for further in-depth clinical application of *A. cochinchinensis* in cancer treatment.

Anti-depressant and neuroprotection

The risk of depression has greatly increased due to the enormous mental and physical stress people face due to modern, fast-paced lifestyles (Martins and S., 2018; Angeloni and Vauzour, 2019; Payne et al., 2022). The researchers ovariectomized rats and exposed them to a chronic stress reaction state for 4 weeks. They additionally administered *A. cochinchinensis* extract (1000 and 2000 mg/kg) to observe mental state alterations of the menopausal rats. The results showed that the expression of brain-derived neurotrophic factor (BDNF) and its main receptor tropomyosin receptor kinase B (TrkB) increased in rats. Thus, *A. cochinchinensis* extract could potentially exert anti-depressant effects (Kim et al., 2020). In addition, another study showed that the *A. cochinchinensis* extract, activating phosphatase 2 (Shp-2), ERK1/2, and Akt signaling pathways, could directly affect treating depression and nerve protection (Jalsrai et al., 2016). The pathogenesis of Alzheimer's disease is unclear, but neuroprotection is shown in different studies to prevent and alleviate it. Lee et al., 2018 study showed that phenols, saponins and protodiosgenin in *A. cochinchinensis* extracts induced enhanced nerve growth factor secretion and decreased intracellular ROS in neurons and microglia cell lines, inhibiting the activity of acetylcholinesterase, thereby improving Alzheimer's disease (Lee et al., 2018). This study provides novel directions for developing new drugs from *A. cochinchinensis*, and, more importantly, offers new insights into the treatment of Alzheimer's disease.

Effects on the gut

Maintaining a normal gut and digestive tract function is one of the key elements to maintaining good health (Sommer et al., 2017; Fassarella et al., 2021; Nathan et al., 2021). Studies have shown that *A. cochinchinensis* extract can treat gut damage caused by metal ions. To evaluate such *A. cochinchinensis* extract effects, the metal ions *Drosophila* model was used. The results showed that *A. cochinchinensis* extract can improve the survival rate of *Drosophila melanogaster*, reduce the mortality of intestinal epithelial cells, and reduce the intestinal damage caused by metal ions (Zhang L. et al., 2021). At the same time, Kim et al., 2019 found that saponins can increase stool frequency, gastrointestinal transit, mucosal layer thickness, flat luminal surface, and the number of paneth cells, thus playing a role in the treating constipation. Improvements were also observed in the levels of acetylcholine esterase activity, the phosphorylation of myosin light chains, and the expression of muscarinic

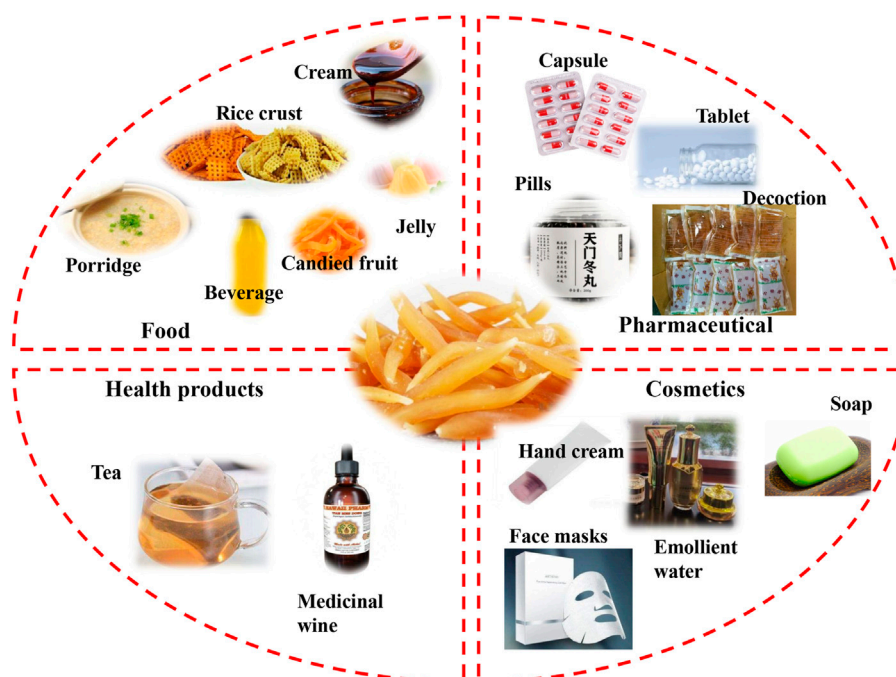


FIGURE 6

The applications of *A. cochinchinensis* in pharmaceutical, food, health products, and cosmetics.

acetylcholine receptors M2/M3 (Kim et al., 2019). This study provides strong evidence for *A. cochinchinensis* applications in treating certain gut-related diseases. However, another study showed that polysaccharides in *A. cochinchinensis* have a role in gut flora regulation. The impact of inulin-type fructan on gut microbiota was investigated by *in vitro* mediation with human fecal cultures. The results showed that inulin-type fructan was digested by gut microbiota, while the pH value in the *A. cochinchinensis* neutral polysaccharide (ACNP) fecal culture was greatly decreased. The total short-chain fatty acids, acetic, propionic, i-valeric, and n-valeric acids were significantly increased (Sun et al., 2020). Collectively, inulin-type fructan was shown to regulate gut microbiota beneficially (Vandeputte et al., 2017; Tao et al., 2021). Thus, it has the potential to be used as a dietary supplement or drug to improve health.

Other activities

As *A. cochinchinensis* is widely used as a traditional herbal medicine with high medicinal value, its safety profile is very important. A recent study evaluated the hepatotoxicity and nephrotoxicity of *A. cochinchinensis* toward the livers and kidneys in ICR mice. Female and male ICR mice were orally administered with 150 mg/kg, 300 mg/kg, and 600 mg/kg *A. cochinchinensis* extract for 14 days, respectively, and the

changes in relevant markers (organ weight, urine composition, liver pathology, and kidney pathology) were observed. The results showed that Female and male ICR mice were orally administered with 150 mg/kg, 300 mg/kg, and 600 mg/kg *A. cochinchinensis* extract for 14 days, respectively, and the changes in relevant markers (organ weight, urine composition, liver pathology, and kidney pathology) were observed (Sung et al., 2017a). Therefore, the saponins in the *A. cochinchinensis* extract have no specific liver and kidney toxicity, reinforcing the excellent safety profile of *A. cochinchinensis*.

Applications

A. cochinchinensis embodies not only significant medicinal value in the field of TCM but also shows distinctive application value in the fields of pharmaceuticals, health care products, food, cosmetics, and others. These applications are summarized in Figure 6, and *A. cochinchinensis* patents in pharmaceuticals, foods, health products and cosmetics are listed in Table 5.

As mentioned above, *A. cochinchinensis* contains numerous active compounds having many promising effects *in vitro* and *in vivo*, indicating their great potential to for pharmaceutical applications (Ren et al., 2021). The pharmaceutical properties

TABLE 5 The patents for *A. cochinchinensis*.

NO	Patent name	Approval number
Pharmaceutical		
1	Traditional Chinese medicine pill for treating internal injury cough	CN104013932B
2	A traditional Chinese medicine for treating old cough	CN103611141B
3	Chinese medicine for clearing lung in children	CN103550594B
4	Application and preparation method of pharyngitis tablet	CN103656415B
5	A drug and capsule for constipation	CN103948780B
6	A traditional Chinese medicine preparation for rapid cough relief	CN103028057B
7	A Chinese herbal compound for the treatment of jaundice hepatitis and cholecystitis	CN103349748B
8	A Chinese medicine combination for anti-aging and its preparation method	CN194370700B
9	A pharmaceutical composition for treating juvenile white hair loss	CN103690798B
Food		
10	<i>Radix asparagi</i> and <i>platycodon grandiflorum</i> healthcare rice crust	CN103652639B
11	<i>Rehmannia-radix asparagi</i> beverage and preparation method thereof	CN102150912B
12	A preparation method of health jelly with algae flavor	CN103621855B
Health product		
13	A medicinal wine for lowering blood pressure, blood sugar and blood lipid	CN103860903B
14	A traditional Chinese medicine health wine and its preparation method	CN103013795B
15	A longevity medicinal wine and its preparation method	CN104784474B
16	A health tea for preventing diabetes	CN102935186B
Cosmetic		
17	<i>A. cochinchinensis</i> whitening compound soap	CN103361213B
18	Beauty antibacterial soap	CN103589537B
19	A plant combination for delaying skin aging and its preparation method	CN103550511B
20	A Traditional Chinese Medicine Composition for increasing skin moisture and its preparation method	CN101322800B
Others		
21	A compound additive for cigarette and its preparation method and application	CN103549652B
22	A chrysanthemum scented snuff	CN103005679B
23	<i>A.cochinchinensis</i> immune adjuvant and influenza vaccine containing the adjuvant	CN101926995B

of *A. cochinchinensis* were recorded well in ancient Chinese medical literature. Nowadays, *A. cochinchinensis* has a wide range of clinical applications in the respiratory, digestive, urinary system, with diverse uses. Clinically, *A. cochinchinensis* is often used to treat respiratory diseases such as cough, asthma, and lung cancer. *A. cochinchinensis* can be used alone, in combination with other pharmaceuticals, or for external use (Hong et al., 2000; Liu et al., 2015). Health care products are becoming highly popular as people pay increasing attention to their physical health (Tabatabai and Sellmeyer, 2021). *A. cochinchinensis* through self-fermentation or fermentation with other Chinese herbal medicines, is marketed form of functional medicinal wine (Kim et al., 2017; Wuyts et al., 2020). It contributes to lowering blood pressure, blood sugar, and blood lipid, so it is highly sought after by middle-aged and elderly people (Sikand et al., 2015). Moreover, there are functional teas with health-promoting properties (Fu et al., 2018). *A. cochinchinensis* is also widely used in the food and culinary field. In the folk, people usually use *A. cochinchinensis* is

used as the main raw material to cook porridge or paste, used to relieve cough, expectorant, tonsillitis, dry throat, sore throat, hemoptysis, and treat constipation. It is also processed into *A. cochinchinensis* candied fruit, that is popular, especially among young people. Certain modern *A. cochinchinensis* foods products have been patented, such as *Radix asparagi* and *platycodon grandiflorum* healthcare rice crust, *Rehmannia-radix asparagi* beverage and health jelly with algae flavor. Recent studies have shown that long-term consumption of *A. cochinchinensis* as a traditional edible plant can inhibit the production of pro-inflammatory cytokines interleukin-1 beta (IL-1 β) and TNF- α , thereby treating various immune-related diseases (Safriani et al., 2022). Despite the currently limited research on *A. cochinchinensis* food products, *A. cochinchinensis* has great potential applications and novel future products in the food field. Interestingly, the extract obtained from fermented *A. cochinchinensis* is also used as a whitening facial mask and whitening soap, with increasing sales, as it can inhibit the formation of tyrosinase and melanin (Sakuma et al., 1999;

Pillaiyar et al., 2017). At the same time, patents granted on *A. cochinchinensis* show that it has beneficial properties for improving skin aging, skin whitening, reducing skin wrinkles, and moisturizing, among others. Therefore, the potential of further *A. cochinchinensis* commercial applications in the cosmetics industry should be sought after with increased research efforts.

Conclusions and perspectives

In this paper, we review the botany, traditional uses, phytochemistry, applications, and pharmacology activities of *A. cochinchinensis* according to ancient classics and modern researches, and it will provide a new insight for future exploration of *A. cochinchinensis*. The root of *A. cochinchinensis* has been widely used to treat cough, fever, pneumonia, stomachache, tracheitis, rhinitis, cataract, acne and urticaria. Meanwhile, the root of *A. cochinchinensis* has a predominant therapeutic effect in diseases such as asthma, constipation, pneumonia. Interestingly, *A. cochinchinensis* exerts multiple functions as medicine, food, and cosmetics, which has been widely used as whitening or healthcare product. Up to now, more than 90 compounds have been isolated and identified from *A. cochinchinensis*. Among these constituents, steroidal saponins represent the main active ingredients. It is expected that more compounds of these categories will be discovered in the future studies. In addition, researches have shown that both extracts and active components of *A. cochinchinensis* possess a wide range of pharmacological activities, including anti-asthma, anti-inflammatory, anti-oxidation, anti-tumor, improving Alzheimer's disease, nerve protection, gut health-promoting and so on. These modern pharmacological studies supported most traditional uses of *A. cochinchinensis* as an indispensable TCM.

However, gaps still exist in the systematic research on *A. cochinchinensis*. Firstly, reported studies have shown that the main chemical components of *A. cochinchinensis* is steroidal saponins. While other chemical constituents such as polysaccharides, lignans and amino acids extracted and isolated from *A. cochinchinensis* are very few compared with steroidal saponins. More chemical constituents must be obtained to explore the relationship between compounds and pharmacological effects in depth. Therefore, new separation and analysis techniques should be developed and implemented to analyze and determine *A. cochinchinensis* chemical composition comprehensively. Secondly, quality standards have not been adequately set. Since *A. cochinchinensis* has a wide variety and is easily confused with other varieties, it is very necessary to establish a complete set of quality standards to distinguish these products. This will also contribute to better-protecting people's health and safety. Thus, it is crucial to establish the *A. cochinchinensis* quality analytical

standards and find the appropriate markers to implement such quality control. At the same time, it is also necessary to conduct systematic and in-depth research on the toxicology of *A. cochinchinensis* to improve the safety profile of its clinical use. Thirdly, the main part of *A. cochinchinensis* used for medicinal compound extraction is its dried root, and the other parts are discarded. However, the resources of roots are relatively rare compared to the resources of leaves and fruits. In the future, in-depth research should be conducted on the leaves and fruits of *A. cochinchinensis*, to explore their value so that the plant can be fully utilized. This reduces the waste of plant resources and might contribute to the development of new drugs, as novel compounds might be discovered in other plant parts. Therefore, we should solve the existing problems as soon as possible, so that the future development of *A. cochinchinensis* will be better.

In addition, in order to further elucidate the mechanism of *A. cochinchinensis* in treating diseases, it is essential to establish the internal relationship between chemical components and their pharmacological activities. Pharmacokinetic studies of *A. cochinchinensis* can also be conducted to try to elucidate its changes including absorption, distribution, metabolism and excretion. This will further elucidate the complex relationship between chemical components and clinical effects to reveal potential mechanism of action. At the same time, *A. cochinchinensis* can also be used as food and nutritional supplement. People become more aware of their health, edible Chinese herbal medicines with health-promoting and therapeutic effects are becoming very popular. On this basis, in-depth research should be conducted in the fields of *A. cochinchinensis* health products, food, and cosmetics, which may have broader prospects for future development, providing new idea for *A. cochinchinensis* research.

To sum up, the root of *A. cochinchinensis* is an important edible medicinal herb with extensive pharmacological activities and great values in medicine, food, and cosmetics. However, more in-depth and comprehensive studies on clinical utility are needed to determine its safety and availability. Until now, multiple compounds have been discovered in *A. cochinchinensis*, but what we have done is far from enough. Furthermore, the precise molecular mechanisms of these active ingredients in some diseases still worth further study. Consequently, systematic studies on phytochemistry and bioactivities of *A. cochinchinensis* will undoubtedly be the key direction of future research. This review should provide an important reference for the development and application of *A. cochinchinensis*. Siand et al., 2015, Sheng, 2022b.

Author contributions

MW and HK proposed the framework of this paper. SW and ZW drafted the manuscript. SW and WH make tables and

figures. BY provided some helpful suggestions in this paper. All authors read and approved the final manuscript.

Funding

This work was supported by the National Natural Science Foundation of China (No.81803686), Supporting Project of National Natural Science Foundation (No.2018PP01), University Nursing Program for Young Scholars with Creative Talents in Heilongjiang Province (No.UNPYSCT-2020225), Special Fund Project of Post doctor in Heilongjiang Province (LBH-Q20180), Chief Scientist of Qi-Huang Project of National Traditional Chinese Medicine Inheritance and Innovation “One Hundred Million” Talent Project ([2021] No.7), Heilongjiang Touyan Innovation Team Program ([2019] No.5).

References

- Angeloni, C., and Vauzour, D. (2019). Natural products and neuroprotection. *Int. J. Mol. Sci.* 20 (22), 5570. doi:10.3390/ijms20225570
- Chang, G. T., Min, S. Y., Kim, J. H., Kim, S. H., Kim, J. K., and Kim, C. H. (2005). Anti-thrombotic activity of Korean herbal medicine, Dae-Jo-Whan and its herbs. *Vasc. Pharmacol.* 43 (4), 283–288. doi:10.1016/j.vph.2005.08.014
- Chen, J., Yang, F., Guo, H., Wu, F., and Wang, X. (2015). Optimized hydrolysis and analysis of *Radix Asparagi* polysaccharide monosaccharide composition by capillary zone electrophoresis. *J. Sep. Sci.* 38 (13), 2327–2331. doi:10.1002/jssc.201500120
- Choi, J. Y., Kim, J. E., Park, J. J., Lee, M. R., Song, B. R., Park, J. W., et al. (2018a). The anti-inflammatory effects of fermented herbal roots of *Asparagus cochinchinensis* in an ovalbumin-induced asthma model. *J. Clin. Med.* 7 (10), 377. doi:10.3390/jcm7100377
- Choi, J. Y., Kim, S. H., Kim, J. E., Park, J. W., Kang, M. J., Choi, H. J., et al. (2019). Four amino acids as serum biomarkers for anti-asthma effects in the ovalbumin-induced asthma mouse model treated with extract of *Asparagus cochinchinensis*. *Lab. Anim. Res.* 35 (1), 32–10. doi:10.1186/s42826-019-0033-x
- Choi, J. Y., Park, J. W., Kim, J. E., Park, J. J., Lee, M. R., Song, B. R., et al. (2018b). Dose dependence and durability of the therapeutic effects of *Asparagus cochinchinensis* fermented extract in an ovalbumin-challenged asthma model. *Lab. Anim. Res.* 34 (3), 101–110. doi:10.5625/lar.2018.34.3.101
- DiMaio, D., Emu, B., Goodman, A. L., Mothes, W., and Justice, A. (2022). Cancer microbiology. *J. Natl. Cancer Inst.* 114 (5), 651–663. doi:10.1093/jnci/djab212
- Fassarella, M., Blaak, E. E., Penders, J., Nauta, A., Smidt, H., and Zoetendal, E. G. (2021). Gut microbiome stability and resilience: Elucidating the response to perturbations in order to modulate gut health. *Gut* 70 (3), 595–605. doi:10.1136/gutjnl-2020-321747
- Fu, Y., Yang, J. C., Cunningham, A. B., Towns, A. M., Zhang, Y., Yang, H. Y., et al. (2018). A billion cups: The diversity, traditional uses, safety issues and potential of Chinese herbal teas. *J. Ethnopharmacol.* 222, 217–228. doi:10.1016/j.jep.2018.04.026
- Hong, S. J., Fong, J. C., and Hwang, J. H. (2000). Effects of crude drugs on glucose uptake in 3T3-L1 adipocytes. *Kaohsiung J. Med. Sci.* 16 (9), 445–451.
- Jalsrai, A., Numakawa, T., Kunugi, H., Dieterich, D. C., Becker, A., and Becker, A. (2016). The neuroprotective effects and possible mechanism of action of a methanol extract from *Asparagus cochinchinensis*: *In vitro* and *in vivo* studies. *Neuroscience* 322, 452–463. doi:10.1016/j.neuroscience.2016.02.065
- Jian, R., Zeng, K. W., Li, J., Li, N., Jiang, Y., and Tu, P. (2013). Anti-neuroinflammatory constituents from *Asparagus cochinchinensis*. *Fitoterapia* 84, 80–84. doi:10.1016/j.fitote.2012.10.011
- Jung, K. H., Choi, H. L., Park, S., Lee, G., Kim, M., Min, J. K., et al. (2014). The effects of the standardized herbal formula PM014 on pulmonary inflammation and airway responsiveness in a murine model of cockroach allergen-induced asthma. *J. Ethnopharmacol.* 155 (1), 113–122. doi:10.1016/j.jep.2014.04.029
- Kim, H., Lee, E., Lim, T., Jung, J., and Lyu, Y. (1998). Inhibitory effect of *Asparagus cochinchinensis* on tumor necrosis factor- α secretion from astrocytes. *Int. J. Immunopharmacol.* 20 (4–5), 153–162. doi:10.1016/s0192-0561(98)00022-8
- Kim, H. R., Lee, Y. J., Kim, T. W., Lim, R. N., Hwang, D. Y., Moffat, J. J., et al. (2020). *Asparagus cochinchinensis* extract ameliorates menopausal depression in ovariectomized rats under chronic unpredictable mild stress. *BMC Complement. Med. Ther.* 20 (1), 325. doi:10.1186/s12906-020-03121-0
- Kim, J. E., Park, J. W., Kang, M. J., Choi, H. J., Bae, S. J., Choi, Y. S., et al. (2019). Anti-inflammatory response and muscarinic cholinergic regulation during the laxative effect of *Asparagus cochinchinensis* in loperamide-induced constipation of SD rats. *Int. J. Mol. Sci.* 20 (4), 946. doi:10.3390/ijms20040946
- Kim, J. Y., Choi, H. Y., Kim, H. M., Choi, J. H., and Jang, D. S. (2021). A novel cytotoxic steroidal saponin from the roots of *Asparagus cochinchinensis*. *Plants* 10 (10), 2067. doi:10.3390/plants10102067
- Kim, M., Kim, W. B., Koo, K. Y., Kim, B. R., Kim, D., Lee, S., et al. (2017). Optimal fermentation conditions of hyaluronidase inhibition activity on *Asparagus cochinchinensis* merrill by *Weissella cibaria*. *J. Microbiol. Biotechnol.* 27 (4), 701–708. doi:10.4014/jmb.1611.11051
- Koo, H. N., Jeong, H. J., Choi, J. Y., Choi, S. D., Choi, T. J., Cheon, Y. S., et al. (2000). Inhibition of tumor necrosis factor- α -induced apoptosis by *Asparagus cochinchinensis* in Hep G2 cells. *J. Ethnopharmacol.* 73 (1–2), 137–143. doi:10.1016/s0378-8741(00)00287-7
- Kubota, S., Konno, I., and Kanno, A. (2012). Molecular phylogeny of the genus *Asparagus* (Asparagaceae) explains interspecific crossability between the garden asparagus (*A. officinalis*) and other *Asparagus* species. TAG. Theoretical and applied genetics. *Theor. Appl. Genet.* 124 (2), 345–354. doi:10.1007/s00122-011-1709-2
- Lee, D. Y., Choo, B. K., Yoon, T., Cheon, M. S., Lee, H. W., Lee, A. Y., et al. (2009). Anti-inflammatory effects of *Asparagus cochinchinensis* extract in acute and chronic cutaneous inflammation. *J. Ethnopharmacol.* 121 (1), 28–34. doi:10.1016/j.jep.2008.07.006
- Lee, H. A., Kim, J. E., Sung, J. E., Yun, W. B., Kim, D. S., Lee, H. S., et al. (2018). *Asparagus cochinchinensis* stimulates release of nerve growth factor and abrogates oxidative stress in the Tg2576 model for Alzheimer's disease. *BMC Complement. Altern. Med.* 18 (1), 125. doi:10.1186/s12906-017-1775-3
- Lee, H. A., Koh, E. K., Sung, J. E., Kim, J. E., Song, S. H., Kim, D. S., et al. (2017b). Ethyl acetate extract from *Asparagus cochinchinensis* exerts anti-inflammatory effects in LPS-stimulated RAW264.7 macrophage cells by regulating COX-2/iNOS, inflammatory cytokine expression, MAP kinase pathways, the cell cycle and anti-oxidant activity. *Mol. Med. Rep.* 15 (4), 1613–1623. doi:10.3892/mmr.2017.6166
- Lee, H. A., Song, B. R., Kim, H. R., Kim, J. E., Yun, W. B., Park, J. J., et al. (2017a). Butanol extracts of *Asparagus cochinchinensis* fermented with *Weissella cibaria* inhibit iNOS-mediated COX-2 induction pathway and inflammatory cytokines in LPS-stimulated RAW264.7 macrophage cells. *Exp. Ther. Med.* 14 (5), 4986–4994. doi:10.3892/etm.2017.5200
- Lee, H. J., Park, J. S., Yoon, Y. P., Shin, Y. J., Lee, S. K., Kim, Y. S., et al. (2015). Dioscin and methylprotodioscin isolated from the root of *Asparagus cochinchinensis* suppressed the gene expression and production of airway

Conflict of interest

The authors declare that the research was conducted in the absence of any commercial or financial relationships that could be construed as a potential conflict of interest.

Publisher's note

All claims expressed in this article are solely those of the authors and do not necessarily represent those of their affiliated organizations, or those of the publisher, the editors and the reviewers. Any product that may be evaluated in this article, or claim that may be made by its manufacturer, is not guaranteed or endorsed by the publisher.

- MUC5AC mucin induced by phorbol ester and growth factor. *Phytomedicine* 22 (5), 568–572. doi:10.1016/j.phymed.2015.03.009
- Lee, J. H., Lim, H. J., Lee, C. W., Son, K. H., Son, J. K., Lee, S. K., et al. (2015). Evidence-based complementary and alternative medicine, *Methyl protodioscin from the roots of Asparagus cochinchinensis attenuates airway inflammation by inhibiting cytokine production*. *CAM*, 2015, 640846, doi:10.1155/2015/640846
- Lee, S. R., Park, H. S., Kim, B. Y., Lee, J. H., Fan, Q., Gaskin, J. F., et al. (2019). An unexpected genetic diversity pattern and a complex demographic history of a rare medicinal herb, Chinese asparagus (*Asparagus cochinchinensis*) in Korea. *Sci. Rep.* 9 (1), 9757. doi:10.1038/s41598-019-46275-9
- Lei, L., Chen, Y., Ou, L., Xu, Y., and Yu, X. (2017). Aqueous root extract of *Asparagus cochinchinensis* (Lour.) Merr. Has antioxidant activity in D-galactose-induced aging mice. *BMC Complement. Altern. Med.* 17 (1), 469. doi:10.1186/s12906-017-1975-x
- Lei, L., Ou, L., and Yu, X. (2016). The antioxidant effect of *Asparagus cochinchinensis* (Lour.) Merr. shoot in D-galactose induced mice aging model and *in vitro*. *J. Chin. Med. Assoc.* 79 (4), 205–211. doi:10.1016/j.jcma.2015.06.023
- Li, X. N., Chu, C., Cheng, D. P., Tong, S. Q., and Yan, J. Z. (2012). Norlignans from *Asparagus cochinchinensis*. *Nat. Prod. Commun.* 7 (10), 1357–1358.
- Liang, Z. Z., Aquino, R., De Simone, F., Dini, A., Schettino, O., and Pizzi, C. (1988). Oligofurostanosides from *Asparagus cochinchinensis*. *Planta Med.* 54 (04), 344–346. doi:10.1055/s-2006-962453
- Liu, B., Li, B., Zhou, D., Wen, X., Wang, Y., Chen, G., et al. (2021). Steroidal saponins with cytotoxic effects from the rhizomes of *Asparagus cochinchinensis*. *Bioorg. Chem.* 115, 105237. doi:10.1016/j.bioorg.2021.105237
- Liu, H., and Dong, Z. (2021). Cancer etiology and prevention principle: "1 + X. *Cancer Res.* 81 (21), 5377–5395. doi:10.1158/0008-5472.CAN-21-1862
- Liu, H., Zheng, Y. F., Li, C. Y., Zheng, Y. Y., Wang, D. Q., Wu, Z., et al. (2015). Discovery of anti-inflammatory ingredients in Chinese herbal formula kouyanqing granule based on relevance analysis between chemical characters and biological effects. *Sci. Rep.* 5, 18080. doi:10.1038/srep18080
- López-Tiro, J., Contreras-Contreras, A., Rodríguez-Arellano, M. E., and Costa-Urrutia, P. (2022). Economic burden of severe asthma treatment: A real-life study. *World Allergy Organ. J.* 15 (7), 100662. doi:10.1016/j.waojou.2022.100662
- Luo, Z., Xu, W., Zhang, Y., Di, L., and Shan, J. (2020). A review of saponin intervention in metabolic syndrome suggests further study on intestinal microbiota. *Pharmacol. Res.* 160, 105088. doi:10.1016/j.phrs.2020.105088
- Mao, J. J., Pillai, G. G., Andrade, C. J., Ligibel, J. A., Basu, P., Cohen, L., et al. (2022). Integrative oncology: Addressing the global challenges of cancer prevention and treatment. *Ca. Cancer J. Clin.* 72 (2), 144–164. doi:10.3322/caac.21706
- Martemucci, G., Portincasa, P., Di Ciaula, A., Mariano, M., Centonze, V., and D'Alessandro, A. G. (2022). Oxidative stress, aging, antioxidant supplementation and their impact on human health: An overview. *Mech. Ageing Dev.* 206, 111707. doi:10.1016/j.mad.2022.111707
- Martins, J., and S. B. (2018). Phytochemistry and pharmacology of anti-depressant medicinal plants: A review. *Biomed. Pharmacother.* 104, 343–365. doi:10.1016/j.biopha.2018.05.044
- McInnes, I. B., and Gravalles, E. M. (2021). Immune-mediated inflammatory disease therapeutics: Past, present and future. *Nat. Rev. Immunol.* 21 (10), 680–686. doi:10.1038/s41577-021-00603-1
- Milšav, I., Ribarič, S., and Poljsak, B. (2018). Antioxidant vitamins and ageing. *Subcell. Biochem.* 90, 1–23. doi:10.1007/978-981-13-2835-0_1
- Miller, R. L., Grayson, M. H., and Strothman, K. (2021). Advances in asthma: New understandings of asthma's natural history, risk factors, underlying mechanisms, and clinical management. *J. Allergy Clin. Immunol.* 148 (6), 1430–1441. doi:10.1016/j.jaci.2021.10.001
- Nathan, N. N., Philpott, D. J., and Girardin, S. E. (2021). The intestinal microbiota: From health to disease, and back. *Microbes Infect.* 23 (6–7), 104849. doi:10.1016/j.micinf.2021.104849
- Pahwa, P., Singh, T., and Goel, R. K. (2022). Anticonvulsant effect of *Asparagus racemosus* Willd. In a mouse model of catamenial epilepsy. *Neurochem. Res.* 47 (2), 422–433. doi:10.1007/s11064-021-03455-2
- Pang, X., Gao, L., Wang, B., Chen, X. J., Zhang, J., Guo, B. L., et al. (2021). New steroidal glycosides from the roots of *Asparagus cochinchinensis*. *J. Asian Nat. Prod. Res.* 23 (3), 205–216. doi:10.1080/10286020.2021.1873956
- Papi, A., Brightling, C., Pedersen, S. E., and Reddel, H. K. (2018). Asthma. *Lancet (London, Engl.)* 391 (10122), 783–800. doi:10.1016/S0140-6736(17)33311-1
- Payne, A., Nahashon, S., Taka, E., Adinew, G. M., and Soliman, K. (2022). Epigallocatechin-3-Gallate (EGCG): New therapeutic perspectives for neuroprotection, aging, and neuroinflammation for the modern age. *Biomolecules* 12 (3), 371. doi:10.3390/biom12030371
- Pegiou, E., Mumm, R., Acharya, P., de Vos, R., and Hall, R. D. (2019). Green and white *Asparagus* (*Asparagus officinalis*): A source of developmental, chemical and urinary intrigue. *Metabolites* 10 (1), 17. doi:10.3390/metabo10010017
- Pillaiyar, T., Manickam, M., and Namasivayam, V. (2017). Skin whitening agents: Medicinal chemistry perspective of tyrosinase inhibitors. *J. Enzyme Inhib. Med. Chem.* 32 (1), 403–425. doi:10.1080/14756366.2016.1256882
- Ren, Y., Elkington, B. G., Henkin, J. M., Sydara, K., Kinghorn, A. D., and Soejarto, D. D. (2021). Bioactive small-molecule constituents of Lao plants. *J. Med. Plant Res.* 15 (12), 540–559. doi:10.5897/jmpr2021.7137
- Safriani, N., Zakaria, F. R., Prangdimurti, E., SuwartiVerpoorte, R., and Yuliana, N. D. (2022). Using metabolomics to discover the immunomodulator activity of food plants. *Heliyon* 8 (5), e09507. doi:10.1016/j.heliyon.2022.e09507
- Sakuma, K., Ogawa, M., Sugibayashi, K., Yamada, K., and Yamamoto, K. (1999). Relationship between tyrosinase inhibitory action and oxidation-reduction potential of cosmetic whitening ingredients and phenol derivatives. *Arch. Pharm. Res.* 22 (4), 335–339. doi:10.1007/BF02979054
- Schoettler, N., and Strek, M. E. (2020). Recent advances in severe asthma: From phenotypes to personalized medicine. *Chest* 157 (3), 516–528. doi:10.1016/j.chest.2019.10.009
- Shen, Y., Xu, C. L., Xuan, W. D., Li, H. L., Liu, R. H., Xu, X. K., et al. (2011). A new furostanol saponin from *Asparagus cochinchinensis*. *Arch. Pharm. Res.* 34 (10), 1587–1591. doi:10.1007/s12272-011-1001-7
- Sheng, W. (2022a). The complete chloroplast genome of two traditional medical plants: *Asparagus cochinchinensis* Lour. Merr. And *Asparagus dauricus* Fisch. Ex link. *Mitochondrial DNA. B Resour* 7 (5), 725–726. doi:10.1080/23802359.2022.2068976
- Sheng, W. (2022b). The entire chloroplast genome sequence of *Asparagus cochinchinensis* and genetic comparison to *Asparagus* species. *Open Life Sci* 17 (1), 893–906. doi:10.1515/biol-2022-0098
- Shi, J. G., Li, G. Q., Huang, S. Y., Mo, S. Y., Wang, Y., Yang, Y. C., et al. (2004). Furostanol oligoglycosides from *Asparagus cochinchinensis*. *J. Asian Nat. Prod. Res.* 6 (2), 99–105. doi:10.1080/1028602031000135576
- Shi, Z., Zhang, H., and Zhao, X. (2009). Ultrasonic-assisted precolumn derivatization-HPLC determination of acrylamide formed in *Radix Asparagi* during heating process. *J. Pharm. Biomed. Anal.* 49 (4), 1045–1047. doi:10.1016/j.jpba.2008.12.019
- Siand, G., Kris-Etherton, P., and Boulos, N. M. (2015). Impact of functional foods on prevention of cardiovascular disease and diabetes. *Curr. Cardiol. Rep.* 17 (6), 39. doi:10.1007/s11886-015-0593-9
- Sommer, F., Anderson, J. M., Bharti, R., Raes, J., and Rosenstiel, P. (2017). The resilience of the intestinal microbiota influences health and disease. *Nat. Rev. Microbiol.* 15 (10), 630–638. doi:10.1038/nrmicro.2017.58
- Sun, Q., Zhu, L., Li, Y., Cui, Y., Jiang, S., Tao, N., et al. (2020). A novel inulin-type fructan from *Asparagus cochinchinensis* and its beneficial impact on human intestinal microbiota. *Carbohydr. Polym.* 247, 116761. doi:10.1016/j.carbpol.2020.116761
- Sung, J. E., Choi, J. Y., Kim, J. E., Lee, H. A., Yun, W. B., Park, J. J., et al. (2017a). Hepatotoxicity and nephrotoxicity of saponin-enriched extract of *Asparagus cochinchinensis* in ICR mice. *Lab. Anim. Res.* 33 (2), 57–67. doi:10.5625/lar.2017.33.2.57
- Sung, J. E., Lee, H. A., Kim, J. E., Go, J., Seo, E. J., Yun, W. B., et al. (2016). Therapeutic effect of ethyl acetate extract from *Asparagus cochinchinensis* on phthalic anhydride-induced skin inflammation. *Lab. Anim. Res.* 32 (1), 34–45. doi:10.5625/lar.2016.32.1.34
- Sung, J. E., Lee, H. A., Kim, J. E., Yun, W. B., An, B. S., Yang, S. Y., et al. (2017). Saponin-enriched extract of *Asparagus cochinchinensis* alleviates airway inflammation and remodeling in ovalbumin-induced asthma model. *Int. J. Mol. Med.* 40 (5), 1365–1376. doi:10.3892/ijmm.2017.3147
- Tabatabai, L. S., and Sellmeyer, D. E. (2021). Nutritional supplements and skeletal health. *Curr. Osteoporos. Rep.* 19 (1), 23–33. doi:10.1007/s11914-020-00651-x
- Tao, C., Zeng, W., Zhang, Q., Liu, G., Wu, F., Shen, H., et al. (2021). Effects of the prebiotic inulin-type fructans on post-antibiotic reconstitution of the gut microbiome. *J. Appl. Microbiol.* 130 (3), 634–649. doi:10.1111/jam.14827
- Topolska, K., Florkiewicz, A., and Filipiak-Florkiewicz, A. (2021). Functional food-consumer motivations and expectations. *Int. J. Environ. Res. Public Health* 18 (10), 5327. doi:10.3390/ijerph18105327
- Vandeputte, D., Falony, G., Vieira-Silva, S., Wang, J., Sailer, M., Theis, S., et al. (2017). Prebiotic inulin-type fructans induce specific changes in the human gut microbiota. *Gut* 66 (11), 1968–1974. doi:10.1136/gutjnl-2016-313271
- Wang, G. H., Lin, Y. M., Kuo, J. T., Lin, C. P., Chang, C. F., Hsieh, M. C., et al. (2019). Comparison of biofunctional activity of *Asparagus cochinchinensis* (Lour.)

- Merr. Extract before and after fermentation with *Aspergillus oryzae*. *J. Biosci. Bioeng.* 127 (1), 59–65. doi:10.1016/j.jbiosc.2018.06.015
- Wang, T., Liu, J., Luo, X., Hu, L., and Lu, H. (2021). Functional metabolomics innovates therapeutic discovery of traditional Chinese medicine derived functional compounds. *Pharmacol. Ther.* 224, 107824. doi:10.1016/j.pharmthera.2021.107824
- Weijing, L., Yuanjiang, D., and Baolian, L. (2006). Treatment of the localized neurodermatitis by plum-blossom needle tapping and with the modified yangxue dingfeng tang—a clinical observation of 47 cases. *J. traditional Chin. Med. = Chung i tsa chih ying wen pan* 26 (3), 181–183.
- Wong, K. H., Kong, B. L., Siu, T. Y., Wu, H. Y., But, G. W., Shaw, P. C., et al. (2022). Complete chloroplast genomes of *asparagus aethiopicus* L., *a. densiflorus* (kunth) jessop 'myers', and *a. cochinchinensis* (lour.) merr.: comparative and phylogenetic analysis with congeners. *PloS one* 17 (4), e0266376. doi:10.1371/journal.pone.0266376
- Wuyts, S., Van Beeck, W., Allonsius, C. N., van den Broek, M. F., and Lebeer, S. (2020). Applications of plant-based fermented foods and their microbes. *Curr. Opin. Biotechnol.* 61, 45–52. doi:10.1016/j.copbio.2019.09.023
- Xiong, D., Yu, L. X., Yan, X., Guo, C., and Xiong, Y. (2011). Effects of root and stem extracts of *Asparagus cochinchinensis* on biochemical indicators related to aging in the brain and liver of mice. *Am. J. Chin. Med.* 39 (4), 719–726. doi:10.1142/S0192415X11009159
- Xiong, W., Zhao, X., Xu, Q., Wei, G., Zhang, L., Fan, Y., et al. (2022). Qisheng Wan formula ameliorates cognitive impairment of Alzheimer's disease rat via inflammation inhibition and intestinal microbiota regulation. *J. Ethnopharmacol.* 282, 114598. doi:10.1016/j.jep.2021.114598
- Yeung, Y. T., Aziz, F., Guerrero-Castilla, A., and Arguelles, S. (2018). Signaling pathways in inflammation and anti-inflammatory therapies. *Curr. Pharm. Des.* 24 (14), 1449–1484. doi:10.2174/1381612824666180327165604
- Zhang, H. J., Sydara, K., Tan, G. T., Ma, C., Southavong, B., Soejarto, D. D., et al. (2004). Bioactive constituents from *Asparagus cochinchinensis*. *J. Nat. Prod.* 67 (2), 194–200. doi:10.1021/np030370b
- Zhang, L., He, F., Gao, L., Cong, M., Sun, J., Xu, J., et al. (2021a). Engineering exosome-like nanovesicles derived from *Asparagus cochinchinensis* can inhibit the proliferation of hepatocellular carcinoma cells with better safety profile. *Int. J. Nanomedicine* 16, 1575–1586. doi:10.2147/IJN.S293067
- Zhang, R. S., Liu, Y. Y., Zhu, P. F., Jin, Q., Dai, Z., and Luo, X. D. (2021b). Furostanol saponins from *Asparagus cochinchinensis* and their cytotoxicity. *Nat. Prod. Bioprospect.* 11 (6), 651–658. doi:10.1007/s13659-021-00321-0
- Zhang, W., and Jin, L. H. (2016). *Asparagus cochinchinensis* extract alleviates metal ion-induced gut injury in drosophila: an in silico analysis of potential active constituents. *Evidence-Based complementary and alternative medicine*. 2016, 7603746. doi:10.1155/2016/7603746
- Zhang, X., Qiu, H., Li, C., Cai, P., and Qi, F. (2021c). The positive role of traditional Chinese medicine as an adjunctive therapy for cancer. *Biosci. Trends* 15 (5), 283–298. doi:10.5582/bst.2021.01318
- Zhu, G. L., Hao, Q., Li, R. T., and Li, H. Z. (2014). Steroidal saponins from the roots of *Asparagus cochinchinensis*. *Chin. J. Nat. Med.* 12 (3), 213–217. doi:10.1016/S1875-5364(14)60035-2
- Zhu, G. L., Hao, Q., Xing, L., Yang, X. Q., Xie, S. D., Zhao, P., et al. (2021). C21, C22 pregnane glycosides and cytotoxic C27 spirostanol steroids from *Asparagus cochinchinensis*. *Steroids* 172, 108874. doi:10.1016/j.steroids.2021.108874

Glossary

ACNP *Asparagus cochinchinensis* neutral polysaccharide

ACNVs *Asparagus cochinchinensis*-derived nanovesicles

Ara Arabinose

BDNF Brain-derived neurotrophic factor

CAT Catalase

COX-2 Cyclooxygenase-2

CZE Capillary zone electrophoresis

DPPH 1,1-diphenyl-2-picrylhydrazyl radical 2,2-diphenyl-1-(2,4,6-trinitrophenyl) hydrazyl

Fru Fructose

Gal Galactose

GalUA Galacturonic acid

Glc Glucose

GlcUA Glucuronic acid

GPX Glutathione peroxidase

Ig E Immunoglobulin E

IL-4 Interleukin 4

IL-13 Interleukin 13

IL-1 β Interleukin-1 beta

iNOS Inducible nitric oxide synthase

LPS Lipopolysaccharide

Man Mannose

MDA Malondialdehyde

MPO Myeloperoxidase

NGF Nerve growth factor

NO Nitric oxide

NOS Nitric oxide synthase

OVA Ovalbumin

PA Phthalic anhydride

ROS Reactive oxygen species

Rha Rhamnose

SOD Superoxide dismutase

SP Substance P

TCM Traditional Chinese medicines

Tg Transgenic

TNF- α Tumor necrosis factor- α

TPA 12-O-tetradecanoyl-phorbol-13-acetate

TrkB Tropomyosin receptor kinase B

Xyl Xylose



OPEN ACCESS

EDITED BY

Zheng Xiang,
Liaoning University, China

REVIEWED BY

Arabinda Mahanty,
National Rice Research Institute (ICAR),
India
Jozsef Dudas,
Innsbruck Medical University, Austria

*CORRESPONDENCE

Mohd Farooq Shaikh,
farooq.shaikh@monash.edu

SPECIALTY SECTION

This article was submitted to
Ethnopharmacology,
a section of the journal
Frontiers in Pharmacology

RECEIVED 21 October 2022

ACCEPTED 16 November 2022

PUBLISHED 05 December 2022

CITATION

Lee VLL, Choo BKM, Norazit A, Noor SM
and Shaikh MF (2022), *Channa striatus* in
inflammatory conditions: A
systematic review.
Front. Pharmacol. 13:1076143.
doi: 10.3389/fphar.2022.1076143

COPYRIGHT

© 2022 Lee, Choo, Norazit, Noor and
Shaikh. This is an open-access article
distributed under the terms of the
[Creative Commons Attribution License](#)
(CC BY). The use, distribution or
reproduction in other forums is
permitted, provided the original
author(s) and the copyright owner(s) are
credited and that the original
publication in this journal is cited, in
accordance with accepted academic
practice. No use, distribution or
reproduction is permitted which does
not comply with these terms.

Channa striatus in inflammatory conditions: A systematic review

Vanessa Lin Lin Lee¹, Brandon Kar Meng Choo¹, Anwar Norazit²,
Suzita Mohd Noor² and Mohd Farooq Shaikh^{1*}

¹Neuropharmacology Research Laboratory, Jeffrey Cheah School of Medicine and Health Sciences, Monash University Malaysia, Bandar Sunway, Selangor, Malaysia, ²Department of Biomedical Science, Faculty of Medicine, University of Malaya, Kuala Lumpur, Malaysia

Channa striatus (CS), or snakehead murrel, is an obligate air-breathing freshwater fish. Besides its wound healing properties, CS has also been reported to exhibit anti-inflammatory effects in multiple studies. While there are anti-inflammatory medications such as nonsteroidal anti-inflammatory drugs (NSAIDs), their long-term use is associated with an increased risk of peptic ulcers, acute renal failure, stroke, and myocardial infarction. Thus, it is essential to look at natural methods such as CS extract. While there is an abundant number of investigative studies on the inflammatory properties of CS, the quality of these studies has not been evaluated effectively. Thus, this review aims to summarise, evaluate, and critically appraise currently available literature regarding the anti-inflammatory properties of CS extract. This is done by performing a search using four databases, namely Google Scholar, Embase via Elsevier, Scopus, and Web of Science, with the following terms: *Channa striatus* AND inflammation. From our review, CS has been experimentally shown to positively affect inflammatory conditions such as gastric ulcers, dermatitis, osteoarthritis, and allergic rhinitis. Beneficial effects were also found on inflammation in the presence of tuberculosis and in situations that involve inflammation, such as wound healing. While CS clearly has potential for treating inflammatory conditions, much work needs to be done on identifying and isolating the active constituents before exact mechanisms of action can be worked out to develop future anti-inflammatory medications.

KEYWORDS

traditional medicine, *Channa striatus*, inflammation, anti-inflammatory, natural product

Introduction

Channa striatus (CS), or snakehead murrel, is an obligate air-breathing freshwater fish that inhabits all types of water bodies from small ditches to rice fields, rivers, and lakes (Figure 1). It can be found across tropical and subtropical Asian countries from Pakistan and India to Southeast Asia and Southern China (Hossain et al, 2008; Shafri and Abdul Manan, 2012). It belongs to the Channidae family, which has been around since 50 million years ago, with an origin purportedly from the ancient Himalayan Valley (Madeleine, 2004).

Besides its wound healing properties, CS has also been reported to exhibit anti-inflammatory, anti-nociceptive, anti-microbial, and wound healing effects in multiple pre-clinical studies (Jais, 2007; Jais, 2007; Raju et al., 2020; Zakaria, Mat). These pharmacological properties may be contributed by the fact that CS extract contains high levels of major amino acids such as glycine, alanine, lysine, aspartic acid, and proline, as well as fatty acids such as docosahexaenoic acid (DHA), palmitic acid, oleic acid, stearic acid and arachidonic acid (Shafri and Abdul Manan, 2012; Zakaria et al., 2007; Zuraini et al., 2006). Glycine makes up human skin collagen and can also be a polypeptide involved in wound healing together with other amino acids such as alanine, leucine, and phenylalanine, all of which are found in CS extract (Zakaria et al., 2007). Most of these are found in the fillet, but some are found in CS fish roe as well. Roe protein concentrates prepared from CS were also reported to have high antioxidant activity, thus warranting its selection as a functional ingredient in preparing specialty food products (Galla et al, 2012).

Traditionally, CS or more locally known as 'Haruan' fish, is encouraged to be consumed as part of a post-partum diet, especially for women who underwent a cesarean section, because it is believed that CS enhances wound healing as well as improves pain and trauma (Poh et al, 2005; Haniffa et al, 2014). In Malaysia, CS is commonly prepared by frying, roasting, or cooking with curry among the Malay community. Broth or fish tonic made from CS extract are also quite popular as an "energy-restoring" diet (Shafri and Abdul Manan, 2012).

Inflammation is a tissue response to injury caused by hazardous chemicals, physical trauma, or pathological threats (Suhendi et al, 2019). Inflammation is a cascade of events promoted by inflammatory mediators such as histamine, serotonin, kinins, prostaglandins, and interferons (Larsen and Henson, 1983; Weissmann, 2013). Chronic inflammation is universally associated with various diseases such as obesity, cancer, cardiovascular, and neurological disorders (Okin and Medzhitov, 2012). The prevalence of such diseases varies, with symptomatic osteoarthritis occurring in around 10%–13% of Americans older than 60 (Zhang and Jordan, 2010) and allergic rhinitis afflicting an average of 23% of adults in several European countries (Bauchau and Durham, 2004). While there are anti-inflammatory medications such as nonsteroidal anti-inflammatory drugs (NSAIDs), their long-term use is associated with an increased risk of peptic ulcers, acute renal failure, stroke, and myocardial infarction (Marcum and Hanlon, 2010). Anti-inflammatory drugs also interfere with essential cellular pathways (Ghosh et al., 2016). Combined with the risks associated with their chronic use, they are ineffective for treating chronic inflammatory diseases. Thus, it is essential to look at natural methods such as CS extract. While there is an abundant number of investigative studies on the inflammatory properties of CS, the quality of these studies has not been evaluated effectively. Thus, this review aims to summarise,

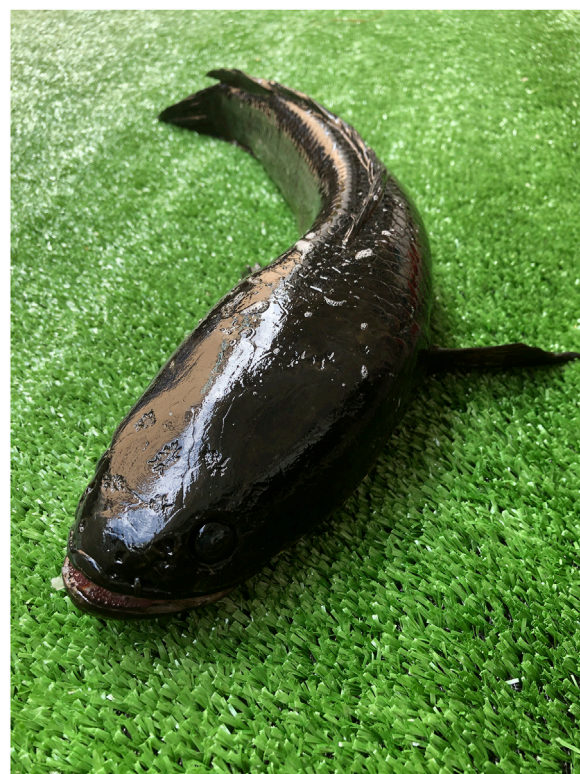


FIGURE 1
A picture of *Channa striatus*.

evaluate, and critically appraise currently available literature regarding the anti-inflammatory properties of CS extract. To our knowledge, this is the first review to evaluate the highly beneficial characteristic of CS extract, therefore establishing this review as a timely topic that may propagate the development of effective future anti-inflammatory interventions for a growing number of debilitating inflammatory diseases, with minimal consequences.

Materials and methods

Search strategy

A literature search was performed on *Channa striatus* extract in relation to inflammation for inclusion in this systematic review. Articles published from January 2010 until March 2020 were identified and retrieved using four databases: Google Scholar, Embase via Elsevier, Scopus, and Web of Science. The following terms were used for the literature search: *Channa striatus* AND inflammation. The Boolean operator AND was used to connect both search terms on all four databases.

TABLE 1 Characteristics and significant findings of the selected pre-clinical studies.

Subjects/Disease model	Inflammatory parameters	Treatment	Significant findings	References
Albino Wistar rats ($n = N/A$) inflammation model	Edema volume	CS powder (150 mg/kg)	The CS extract significantly reduced edema volume in the treatment groups compared to the negative controls The anti-inflammation power of CS extract is comparable to the positive control, diclofenac sodium	Suhendi et al. (2019)
Male Sprague Dawley rats ($n = 30$) gastritis model	Ulcer area and index Histopathological evaluation Gastric juice parameters Gastric wall mucus	Chloroform extract of CS extract (500 mg/kg)-oral	Significant reduction in gastric ulcer formation and ulcer area in a dose-dependent manner, similar to the positive control, 100 mg/kg ranitidine Mild to moderate hemorrhaging and edema to almost normal mucosa architecture in the treated groups compared to severe hemorrhagic erosion, edema, necrosis, and leucocyte infiltration in the vehicle controls CS extract did not cause significant change to the volume of gastric juice but significantly reduced the total acidity of the gastric juice in a dose-dependent manner	Azemi et al. (2018)
Male ICR Rats ($n = 30$) dermatitis model	Edema- ear thickness Histological analysis TNF α and GADPH gene expression	CS cream 1%, 5%, and 10%	Significant reduction in mouse ear thickness Suppression of inflammatory cell infiltration and epidermal hyperplasia was observed All concentrations produced comparable effects to H-cort 1% (positive control) A significant reduction in the expression of TNF α levels was observed	Isa et al. (2016)
Male Wistar Kiyoto rats ($n = 48$) laparotomy wound healing model	Tensile strength Histological analysis	CS extract (100 mg/100 g)- oral	The tensile strength for the malnourished group treated with oral CS was significantly higher than the untreated control group There was no significant difference in epithelisation count between the two groups CS treatment produced a significantly higher fibroblast count compared with the untreated control group The hydroxyproline measurement for the CS treated group was significantly higher than the untreated control group	Hassan et al. (2020)
Male Sprague-Dawley rats ($n = 72$), female Sprague-Dawley Rats ($n = 24$), mice and rabbits wound healing model	Irritation test Tensile strength test Burn wound closure	CS spray	The ability of CS spray to irritate the skin of rabbits was found to be very small Intracutaneous and systemic injection showed that the response from rabbits to CS extracts from four different media were similar to those of the control, indicating that CS spray is safe and non-irritant to the skin of rabbits CS spray promotes proliferation of fibroblast cells, increases collagen production and tensile strength	Laila et al. (2011)
Male Galur Wistar rats ($n = 128$) wound healing model	Histological analysis	CS extract 25%, 50% and 100% 2.5 ml/250 g	CS extract supplementation increased epithelial thickness at a post-incision area on the rats' buccal mucosa	Tamales et al. (2016)
Adult male ICR rats ($n = 42$) edema model	Ear thickness MPO assay	CS cream 1%, 5% and 10%	A significant reduction of ear edema in the treatment group was observed Edema reduction was as effective as 1% hydrocortisone cream (positive control) The CS creams significantly reduced myeloperoxidase concentration	Abedi et al. (2012)
Adult male New Zealand white rabbits ($n = 33$) osteoarthritis model	Histological grading	CS extract (51.4 mg/kg)- dry spray	A marked reduction was observed in the macroscopic score compared to the control group in all joint compartments	Abdul Kadir et al. (2019)

(Continued on following page)

TABLE 1 (Continued) Characteristics and significant findings of the selected pre-clinical studies.

Subjects/Disease model	Inflammatory parameters	Treatment	Significant findings	References
	COMP, COX-2, and PGE ₂ serum levels		CS treatment reduced the severity of cartilage lesions compared to the control group Histomorphometrically, CS treated groups demonstrated higher cartilage surface area than the control group The serum level of COMP, a cartilage degradation biomarker, was significantly higher in the control group compared to CS and 77.5 mg/kg glucosamine (positive control) groups No significant difference was observed between all the treatment groups in serum COX-2 and PGE ₂ levels	
PC12 cells	Neurite outgrowth	CS extract (100, 200, 300, and 400 µl)	Notable neurite outgrowth were observed in CS treated groups compared to negative control, but the growth pattern was different from the cells treated with 1 ml dibutyryl cAMP (positive control)	[M. A. M. Shafri et al., (2011)]

CS, *Channa striatus*; H-cort, Hydrocortisone; TNF-α, Tumor Necrosis Factor-alpha; GADPH, Glyceraldehyde 3-phosphate dehydrogenase; MPO, Myeloperoxidase; COMP, Cartilage oligomeric matrix protein; COX-2, cyclooxygenase-2; PGE₂, prostaglandin E.

Study selection and exclusion/inclusion criteria

The search was limited to articles published in the English language only and original research articles investigating *Channa striatus* in the context of inflammation. Duplicated articles from the literature search were excluded from this review. Reviews, abstracts, book chapters, patents, symposiums, oral and poster presentations in conferences were also excluded due to inadequate data for assessment and comparison with other studies. Finally, articles that were irrelevant to the aim of the review, did not investigate *Channa striatus* in relation to inflammation or inflammatory diseases, and had no full text were also excluded.

Results

A total of 1,217 articles were identified from the initial database literature search, which was then reduced to 1,100 articles after the removal of duplicates. These 1,100 articles were manually screened according to the aforementioned inclusion and exclusion criteria, and 1,083 articles were excluded as they did not meet the aim of this review or were not full-text original research articles. Thus, based on the PRISMA guidelines, a total of 17 articles were eligible for critical evaluation and appraisal in this study (Figure 2). Among the 16 articles selected, there were seven clinical studies and nine animal studies. These selected articles' significant findings and characteristics were summarised in Table 1 (animal studies) and Table 2 (clinical studies).

Inflammation model

In a study by Suhendi et al. (2019), an inflammation Wistar rat model was induced using carrageenan 2%. Prior to the induction of inflammation, the groups were treated with either CS powder, *Nephelium lappaceum* fruit peel extract (NPLE), or a combination of both. Diclofenac sodium was also given as a positive control. From the results, it could be concluded that the CS extract affects reducing edema volume. Based on statistical tests, diclofenac sodium, CS Powder (CSP), *Nephelium lappaceum* fruit peel extract (NPLE), and a combination of CSP and NPLE showed significantly different results ($p < 0.05$) compared with the negative controls. Interestingly, the combination treatment consisting of CSP and NPLE extract did not show a stronger anti-inflammatory effect than the single extract treatment. (Suhendi et al., 2019).

However, we did find some discrepancies in the information given by this journal article. It is unclear if the study was done on rats or mice because these two words seemed to be used interchangeably. The authors also mentioned that diabetes was also induced in this study, but it is unclear if the diabetes was induced in the same animals. Thus it was unclear if the inflammation was measured in a diabetic condition or not.

Tuberculosis

A randomized, placebo-controlled, double-blind pilot study was conducted on pulmonary tuberculosis (TB) patients to study the effects of CS capsules on cytokine conversion in pulmonary TB patients when given in conjunction with standard anti-TB

TABLE 2 Characteristics and significant findings of the selected clinical studies.

Type of study	Treatment	Inflammatory markers	Findings	References
Randomized double-blind, placebo-controlled study- Post Lower Segment Caesarean Section (LSCS) pain study. <i>n</i> = 60.	500 mg (2 capsules) of freeze-dried CS extract	C-reactive protein (CRP) Total white cell counts Platelet count	No significant difference in inflammatory markers between CS and control group	Shafii et al. (2017)
Randomized, double-blind, two-arm parallel comparative study- post LSCS study. <i>n</i> = 73.	500 mg freeze-dried CS extract daily for 6 weeks	Serum IL-6 Serum vascular endothelial growth factor (VEGF) Serum matrix metalloproteinase 9 (MMP-9)	CS consumption significantly increased the wound healing biomarkers, IL-6, MMP-9, and VEGF compared to the placebo group Findings from this study suggested that CS extract increased the cytokines and growth factors in response to tissue injury	Omar et al. (2020)
Randomized, double-blind, two-arm parallel comparative study- post-LSCS pain study. <i>n</i> = 76.	500 mg/day freeze-dried CS extract for 6 weeks	NRS for pain analysis WES for wound healing VAS for wound appearance PSS for overall patient satisfaction with wound appearance	The VAS and PSS scores were significantly elevated in the CS group than in the placebo group The CS group showed an insignificant decrease in pain score over time than the placebo group WES scores were higher in the CS group compared with the placebo group	Ab Wahab et al. (2015)
Randomized, double-blind, placebo-controlled 3-arm trial- knee osteoarthritis. <i>n</i> = 120.	500 mg/day and 1,000 mg/day of CS extract	Pain score Stiffness score Physical function score Analgesic score Serum cartilage oligomeric matrix protein (COMP)	Significant reductions were found in the pain score in the CS 1000 mg (52.5%) and CS 500 mg (49.2%) individuals as compared to the placebo (30.4%) group CS 1000 mg/day (<i>p</i> < 0.05) and CS 500 mg/day had significantly higher stiffness and physical score value compared to the placebo group No significant difference in analgesic scores and serum COMP between the treatment groups were detected	Azidah et al. (2017)
Randomized, double-blind, placebo-controlled pilot study- pulmonary tuberculosis. <i>n</i> = 36.	Antituberculosis drug supplemented with 2 g CS extract capsule, three times per day for 12 weeks	TNF- α IFN- γ IL-10	Supplementation of CS capsules significantly decreased TNF- α , IFN- γ , and IL-10 levels compared to the baseline	Paliliewu et al. (2013)
Randomized, double-blind, placebo-controlled, parallel-group comparative study- allergic rhinitis. <i>n</i> = 46.	500 mg/day oral CS extract for 6 weeks	Total nasal symptoms score (TNSS) Serum eosinophil Serum IL-4	There was no significant difference in TNSS, serum eosinophil, and IL-4 in the CS group compared to the placebo group at week 4 In patients with moderate and severe symptoms scores, there were significant differences in TNSS, serum eosinophil, and IL-4 levels between the CS and placebo groups Supplementation of CS significantly decreased serum eosinophil count, IL-4 levels, and TNSS at week six compared to the baseline There were no side effects of CS treatment reported in this study	Bakar, (2015)
Randomized, double-blind, placebo-controlled trial- allergic rhinitis. <i>n</i> = 70.	500 mg/day CS extract for 6 weeks	Nasal symptom score	Significant reduction of blockage and itchiness symptoms in the treatment group compared to subjects of the placebo group	Susibalan et al. (2018)

(Continued on following page)

TABLE 2 (Continued) Characteristics and significant findings of the selected clinical studies.

Type of study	Treatment	Inflammatory markers	Findings	References
		Non-nasal symptom score	Insignificant reduction of sneezing symptoms in the CS group compared to the placebo group was observed	
		Serum IgE	Subjects of the CS group had significant improvement of non-nasal symptoms score in terms of eye itchiness, general symptoms, and serum IgE compared to the placebo group subjects There were no serious adverse events reported in this trial. No significant differences in the laboratory parameters (LFT, RP, and FBC) were observed	

CS, *Channa striatus*; TNF- α , Tumor Necrosis Factor-alpha; IFN- γ , Interferon-gamma; IL-10, Interleukin-10; IgE, Immunoglobulin E; LFT, liver function test; RP, renal profile; FBC, full blood Count; NRS, numeric pain rating scale; WES, Wound Evaluation scale; VAS, Visual Analogue scale; PSS, patient satisfaction score.

drugs. The levels of the inflammatory cytokines, TNF- α , IFN- γ , and IL-10, were significantly reduced in the CS group compared to the baseline. This was seen in the control group, except for the IL-10 level, which was not significant. The conclusion was that adjunctive supplementation of CS capsules accelerated the beneficial therapeutic effect of TB chemotherapy, possibly by improving cytokine response (Paliliewu et al, 2013).

Gastritis

The antiulcer profile of CS extract, given orally at the doses of 50, 350, and 500 mg/kg, was assessed using ethanol- and indomethacin-induced gastric ulcer models. The antiulcer mechanisms of CS extract were determined as follows: 1) anti-secretory activity of CS extract measured using the pyloric ligation rat model, and 2) the role of nitric oxide and sulfhydryl compounds in the modulation of CS extract antiulcer activity. It was found that CS extract exerted significant antiulcer activity in both models of gastric ulcer. CS extract did not change the volume and pH of gastric juice but reduced the total acidity of gastric juice at lower doses. The antiulcer activity by CS extract was reversed by N-methylamide (NEM) but not by N^G-omega-Nitro-L-arginine methyl ester (L-NAME).

Therefore, the antiulcer activity demonstrated by CS extract was modulated *via* its cytoprotective, but not anti-secretory effect, and in the presence of sulfhydryl compounds, but not nitric oxide (NO) (Azemi et al., 2018).

Dermatitis

Chronic-like dermatitis on the ears was induced in male ICR mice using 12-0-tetradecanoylphorbol 13-acetate (TPA).

Treatment with CS cream was carried out by applying 1%, 5%, and 10% cream two times a day for three consecutive days after TPA application. A significant reduction of mouse ear thickness by the CS creams was observed compared to TPA alone group (negative control). All concentrations of CS creams produced comparable effects to hydrocortisone (H-cort), the positive control.

Histological analysis revealed suppression of inflammatory cell infiltration and epidermal hyperplasia, noticeable under $\times 400$ magnification. The reduction of dermal edema can also be observed, which was more visible under $\times 100$ magnification. Gene expression analysis showed that all concentrations of CS cream downregulated the expression of TNF- α , with a significant reduction in a dose-dependent manner (Isa et al., 2016).

In another study by Abedi et al. (2012), the anti-inflammatory activity of CS-based cream on ear thickness and myeloperoxidase activity was studied using croton oil-induced ear edema. The effects were compared to hydrocortisone 1% cream as the positive control. It was found that all percentages of CS cream (1%, 5%, and 10%) significantly inhibited edema at 4 h and 24 h after croton oil application. Myeloperoxidase assays results showed that applications of these three dosages of CS cream blocked the migration of polymorphonuclear leukocytes to the dermis. The effect is as effective as hydrocortisone 1% cream in a dose-dependent manner (Abedi et al., 2012).

Osteoarthritis

The chondroprotective activity of CS was evaluated in an osteoarthritis (OA) rabbit model. OA was induced by performing anterior cruciate ligament transection in male New Zealand white rabbits. The articular cartilage was evaluated macroscopically and histologically using semiquantitative and



PRISMA 2009 Flow Diagram

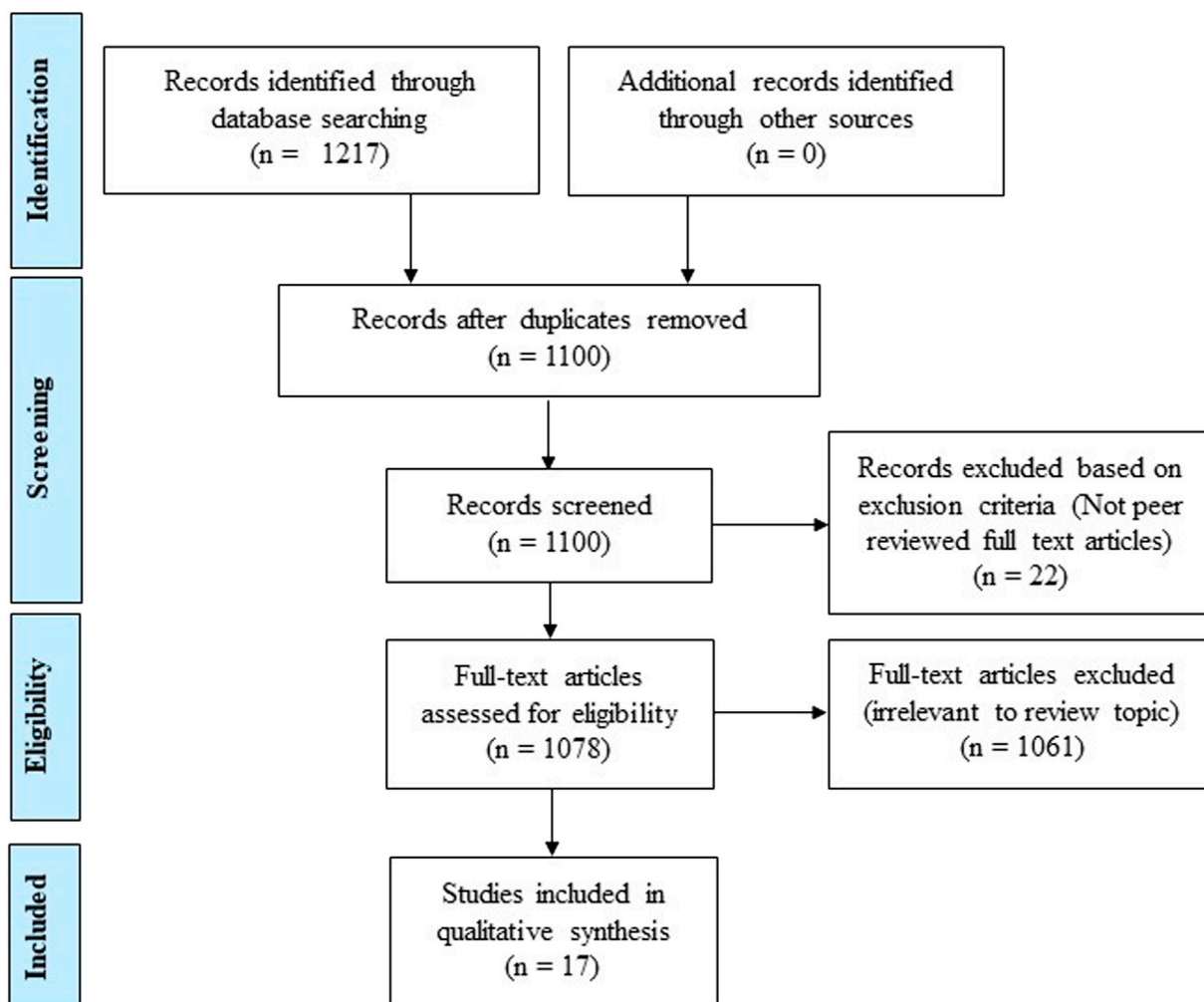


FIGURE 2

Flow chart showing the article selection and exclusion criteria based on the Preferred Reporting Items for Systematic Reviews and Meta-Analyses (PRISMA) guidelines.

quantitative methods. The levels of serum cartilage oligomeric matrix protein (COMP), cyclooxygenase 2 (COX-2) enzyme, and prostaglandin E2 (PGE2) were also determined. Macroscopic analysis revealed that CS administration significantly lowered the severity grade of the total macroscopic score compared to the control and glucosamine (positive control) groups.

The CS group had lower histopathological changes in the three compartments of the joint compared to the glucosamine group, which had lower histological scoring in two compartments only. The cartilage thickness, area, and

roughness of both CS and glucosamine groups were superior to the control group. Serum COMP levels were lower in both CS ($p < 0.05$) and glucosamine ($p < 0.05$) groups compared to the control group (Abdul Kadir et al., 2019).

A randomized, double-blind, placebo-controlled 3-arm trial was conducted comparing oral CS extract and placebo among knee OA patients for a 6-month intervention period. Significant reductions in Western Ontario and McMaster University Osteoarthritis Index (WOMAC) stiffness and function scores were achieved. However, no significant differences were found

between the groups regarding analgesic scores, serum cartilage oligomeric matrix protein (COMP) levels, and biochemical parameters. In conclusion, CS extract treatment was more effective than placebo in treating the symptoms of knee OA (Azidah et al., 2017).

Wound healing

The wound healing property of CS extract was studied on laparotomy wound healing in malnourished male Wistar Kyoto rats. The study evaluated the effects of CS on tensile strength, epithelialization, and fibroblastic proliferation. CS extract treatment groups demonstrated better tensile strength and significantly higher epithelial and fibroblast cell counts than placebo control (Hassan et al., 2020). A similar study also found that CS has similar positive effects on tensile strength and epithelial and fibroblast cell counts in malnourished male Wistar Kyoto rats when given orally in tablet form and applied topically as a cream (Pasha et al., 2015).

In a separate study, the wound healing effect of CS extract spray was studied in Sprague Dawley rats. Here, CS extract was formulated in an aerosol system, producing a film for wound dressing. CS spray increased the tensile strength of the incision wound and sped up the wound contraction process. This showed that the CS water spray is effective and safe for application to incision and burn injuries (Laila et al., 2011).

Another study by Tamales et al. (2016) was done to study the effect of CS extract on the reepithelization count in the wound healing process. An incision was made in the buccal mucosa area of Galur Wistar rats, and CS extract was administered orally. It was found that CS extract treatment increased epithelial thickness count compared to the negative control, but the difference was not significant (Tamales et al., 2016).

In a randomized, double-blinded study amongst post-Lower Segment Caesarean Section (LSCS) women, CS extract was found to have significant effects on IL-6, Vascular Endothelial Growth Factor (VEGF), and Matrix metalloproteinase 9 (MMP-9) levels between the CS treatment group and placebo group. These factors are involved in different wound healing phases, which suggests that CS extract has potential wound healing properties (Omar et al., 2020). Ab Wahab et al. (2015) found that CS extract significantly improved visual analog scale (VAS) and patient satisfaction score (PSS) in post-LSCS women in a separate study. Although there was no significant effect on postoperative pain and wound evaluation scale (WES), CS extract produced a marked difference in wound cosmetic appearance (Ab Wahab et al., 2015).

In a separate randomized, double-blinded, placebo-controlled study among post LSCS women, however, there were no significant differences in the inflammatory markers during wound healing between the CS extract group and the placebo group (Shafii et al., 2017).

Allergic rhinitis

A study conducted by Susibalan et al. (2018) on allergic rhinitis subjects revealed that CS treatment significantly improved nasal blockage, nasal itchiness, eye itchiness, and general symptoms compared to the placebo groups. Serum Immunoglobulin E (IgE) was also significantly lowered in the CS group compared to placebo. There were no significant differences between groups regarding nasal discharge, sneezing, palate itchiness, and smell score. This showed some beneficial role in improving nasal symptoms in allergic rhinitis subjects (Susibalan et al., 2018).

In a study by Bakar (2015), CS extract did not significantly reduce Total Nasal Symptoms Score (TNSS), serum eosinophil, and IL-4 in the CS group compared to the placebo group. However, a significant decrement of these parameters was found within the CS treatment group (Bakar, 2015).

Discussion

After analyzing the available literature on the use of *Channa striatus* derived treatments in inflammatory conditions, beneficial effects were found for several conditions. These conditions were gastric ulcers, dermatitis, osteoarthritis, and allergic rhinitis. Beneficial effects of CS were also found in wound healing as well as on inflammation in the presence of tuberculosis. All the studies in this review used some form of CS extract rather than working with isolated extract constituents. Nevertheless, the studies in the review pointed out several constituents which could be responsible for the beneficial effect of CS extract. These include albumin (Suhendi et al., 2019), the fatty acids linoleic acid, stearic acid, oleic acid, and N-arachidonylglycine, (Abedi et al., 2012), omega-6 polyunsaturated fatty acids, vitamins A, B, E, and D, and minerals such as calcium, sodium, magnesium, and zinc (Paliliewu et al., 2013), omega-3 fatty acids such as eicosapentaenoic acid and docosahexaenoic acid (Susibalan et al., 2018). Excluding the ubiquitous vitamins and minerals, albumin and fatty acids appear to be leading candidates for the anti-inflammatory action seen in CS extract. The two constituents are related as although albumin has antioxidant properties due to its ability to scavenge free radicals, it is also capable of binding fatty acids (Roche et al., 2008). Thus, not only is albumin anti-inflammatory, but by binding fatty acids and facilitating its transport around the body (van der Vusse, 2009), albumin could be enhancing the anti-inflammatory effects of fatty acids. Omega-3 and 6 polyunsaturated fatty acids (Wall et al., 2010), the omega-9 fatty acid, oleic acid (Santamarina et al., 2021), and stearic acid (Pan et al., 2010) are also known to be anti-inflammatory. Curiously, CS extract also contains arachidonic acid (Che Ku Daud et al., 2010), a known contributor to inflammation. It is possible that CS extract has

a net anti-inflammatory effect overall due to its other constituents, or it could be due to CS extract also containing N-arachidonylglycine (Abdul Kadir et al., 2019), which is derived from arachidonic acid but inhibits inflammation instead (Succar et al, 2007).

Knowing the possible active constituents of CS extract is only half the battle won as the mechanism by which it works is also essential. However, we found that a majority of the studies in the review attributed the positive effects of CS extract on the inflammatory conditions to its anti-inflammatory properties in general without identifying specific mechanisms. One of the rare studies in the review that did postulate a mechanism stated that CS extract has a cytoprotective effect by positively modulating the free radical scavenging action of non-protein sulfhydryl compounds (Azemi et al., 2018). Another study pointed to the inhibition of inflammatory cells due to a downregulation of TNF- α (Isa et al., 2016). Different research hypothesized the mechanism to be a downregulation of not only TNF- α but also IFN- γ and IL-10 (Paliliewu et al., 2013). The final study pointed towards a reduction in IgE levels and the chemokines, IL-5 and IL-8 (Susibalan et al., 2018). While an in-depth discussion regarding the mechanisms of anti-inflammatory action is outside the scope of this review, the previously postulated mechanisms of action point to the involvement of the JAK-STAT signaling pathway due to the participation of IL-10, IFN- γ , and IL-5 (Banerjee et al, 2017). Notably however, IL-10 is an anti-inflammatory cytokine (Iyer & Cheng, 2012), and therefore its apparent downregulation could be due to a lack of need because of the overall anti-inflammatory effect of the CS extract, rather than the extract directly suppressing it.

On the other hand, the involvement of TNF- α and IL-8 suggests an effect on the Nuclear Factor kappa-light-chain-enhancer of activated B cells (NF- κ B) and c-Jun N-terminal kinases (JNKs) (Bradley, 2008). In the case of allergic inflammatory responses, the reduction in IgE levels is likely a consequence of a reduction in IL-5 levels, possibly by interfering with its production by T-helper 2 cells. This review also included articles looking into wound healing. While the study on wound healing did not look into the anti-inflammatory effects of CS extract specifically, inflammation is a normal part of wound healing. However, wound healing becomes impaired when the inflammation becomes excessive or persistent (Eming et al, 2007). Thus, the wound healing properties of CS extract could also be related to its ability to dampen the inflammatory response.

Conclusion and future directions

From our review, CS has been experimentally shown to positively affect inflammatory conditions such as gastric ulcers, dermatitis, osteoarthritis, and allergic rhinitis. Beneficial effects were also found on inflammation in the presence of tuberculosis and in situations that involve

inflammation in some capacity, such as wound healing. While we were able to suggest several anti-inflammatory pathways that CS might act upon, the use of CS extract by all the studies in this review rather than isolated constituents somewhat clouded the exact mechanisms of action. CS extract is anti-inflammatory overall, even though it contains arachidonic acid, which is pro-inflammatory. While CS clearly has potential for treating inflammatory conditions, more work needs to be done on identifying and isolating the active constituents before exact mechanisms of action can be worked out. Priorities should lie in studying the active compounds which contributes to the pharmacological activities of CS extract. Future pre-clinical and clinical studies can be done using these compounds instead of the crude extract. The candidates for active constituents pointed out in this review will hopefully help in the search for future anti-inflammatory medications.

Data availability statement

The raw data supporting the conclusion of this article will be made available by the authors, without undue reservation.

Author contributions

All authors were involved in conception and literature review; VL took the lead in drafting and revising the manuscript; BC contributed to the discussion and proofread the final version of the manuscript; AN and SN provided critical questions and suggestions to the manuscripts; MS conceptualized the review, supervised all aspects of the study, and approved the final manuscript as submitted. All authors read and approved the final manuscript.

Conflict of interest

The authors declare that the research was conducted in the absence of any commercial or financial relationships that could be construed as a potential conflict of interest.

Publisher's note

All claims expressed in this article are solely those of the authors and do not necessarily represent those of their affiliated organizations, or those of the publisher, the editors and the reviewers. Any product that may be evaluated in this article, or claim that may be made by its manufacturer, is not guaranteed or endorsed by the publisher.

References

- Ab Wahab, S. Z., Abdul Kadir, A., Hussain, N., Hazlina, N., Omar, J., Yunus, R., et al. (2015). The effect of *Channa striatus* (Haruan) extract on pain and wound healing of post-lower segment caesarean section women. *Evidence-based Complementary Altern. Med.* 2015, 1–6. doi:10.1155/2015/849647
- Abdul Kadir, A., Abdul Kadir, A., Abd Hamid, R., Jais, M., Manan, A., Omar, J., et al. (2019). Evaluation of chondroprotective activity of *Channa striatus* in rabbit osteoarthritis model. *BioMed Res. Int.* 2019, 6979585. doi:10.1155/2019/6979585
- Abedi, S., Far, F. E., Hussain, M. K., and Ahmad, Z. (2012). Effects of haruan (*Channa striatus*) based cream on acute inflammation in Croton oil induced mice ear edema model. *Res. J. Biomed. Sci.* 7, 181–187. doi:10.3923/rjbsci.2012.181.187
- Azemi, A. K., Rahim, A., Hafiz, M., Mamat, S. S., Jais, M., Manan, A., et al. (2018). Antiulcer activity of methanol-chloroform extract of *Channa striatus* fillet. *Pak. J. Pharm. Sci.* 31, 143–151.
- Azidah, A. K., Arifah, A. K., Roslida, A. H., Jais, A. M. M., Omar, J., Sadagatullah, A. N., et al. (2017). A randomized, double-blind study comparing multiple doses of *Channa striatus* supplementation for knee osteoarthritis. *Orient. Pharm. Exp. Med.* 17 (4), 345–354. doi:10.1007/s13596-017-0293-7
- Bakar, M. N. A. (2015). *Effect of Channa striatus on inflammatory markers as an adjunct treatment in allergic rhinitis-a randomized double-blinded study*. Malaysia: universiti sains malaysia.
- Banerjee, S., Biehl, A., Gadina, M., Hasni, S., and Schwartz, D. M. (2017). JAK-STAT signaling as a target for inflammatory and autoimmune diseases: Current and future prospects. *Drugs* 77 (5), 521–546. doi:10.1007/s40265-017-0701-9
- Bauchau, V., and Durham, S. R. (2004). Prevalence and rate of diagnosis of allergic rhinitis in Europe. *Eur. Respir. J.* 24 (5), 758–764. doi:10.1183/09031936.04.00013904
- Bradley, J. R. (2008). TNF-mediated inflammatory disease. *J. Pathol.* 214 (2), 149–160. doi:10.1002/path.2287
- Che Ku Daud, C. K. D., Jais, A., Ahmad, Z., Md Akim, A., and Adam, A. (2010). Amino and fatty acid compositions in Haruan traditional extract (HTE). *Bol. Latinoam. del Caribe Plantas Med. Aromat.* 9, 414–429.
- Eming, S. A., Krieg, T., and Davidson, J. M. (2007). Inflammation in wound repair: Molecular and cellular mechanisms. *J. Invest. Dermatol.* 127 (3), 514–525. doi:10.1038/sj.jid.5700701
- Galla, N. R., Karakala, B., Akula, S., and Pamidighantam, P. R. (2012). Physico-chemical, amino acid composition, functional and antioxidant properties of roe protein concentrates obtained from *Channa striatus* and *Lates calcarifer*. *Food Chem.* 132 (3), 1171–1176. doi:10.1016/j.foodchem.2011.11.055
- Ghosh, N., Ali, A., Ghosh, R., Das, S., Mandal, S. C., and Pal, M. (2016). Chronic inflammatory diseases: Progress and prospect with herbal medicine. *Curr. Pharm. Des.* 22 (2), 247–264. doi:10.2174/138161282266615112151419
- Haniffa, M. A. K., Jeya Sheela, P. A., Kavitha, K., and Jais, A. M. M. (2014). Salutory value of haruan, the striped snakehead *Channa striatus* - a review. *Asian pac. J. Trop. Biomed.* 4, S8–S15. doi:10.12980/APJTB.4.2014C1015
- Hassan, S. A. S., Rosnelifaizur, R., Maya, Y. M., Samarendra, S. M., Saringat, B., Naing, N. N., et al. (2020). Effect of oral *Channa striatus* in laparotomy wound healing of malnourished rats. *Int. Med. J.* 27 (1), 67–70.
- Hossain, M., Latifa, G., and Rahman, M. (2008). Observations on induced breeding of snakehead murrel, *Channa striatus* (Bloch, 1793). *Int. J. Sustain. Crop Prod.* 3, 65–68.
- Isa, I. I. M., Abu Bakar, S., Tohid, S. F. M., and Jais, A. M. M. (2016). *Channa striatus* cream down-regulates tumour necrosis factor (TNF)-alpha gene expression and alleviates chronic-like dermatitis in mouse model. *J. Ethnopharmacol.* 194, 469–474. doi:10.1016/j.jep.2016.10.033
- Iyer, S. S., and Cheng, G. (2012). Role of interleukin 10 transcriptional regulation in inflammation and autoimmune disease. *Crit. Rev. Immunol.* 32 (1), 23–63. doi:10.1615/critrevimmunol.v32.i1.30
- Jais, A. M. M. (2007). Pharmacognosy and pharmacology of Haruan (*Channa striatus*), a medicinal fish with wound healing properties. *Bol. Latinoam. del Caribe Plantas Med. Aromat.* 6 (3), 52–60.
- Laila, L., Febriyenti, F., Salhimi, S. M., and Baie, S. (2011). Wound healing effect of Haruan (*Channa striatus*) spray. *Int. Wound J.* 8, 484–491. doi:10.1111/j.1742-481X.2011.00820.x
- Larsen, G. L., and Henson, P. M. (1983). Mediators of inflammation. *Annu. Rev. Immunol.* 1 (1), 335–359. doi:10.1146/annurev.iy.01.040183.002003
- Marcum, Z. A., and Hanlon, J. T. (2010). Recognizing the risks of chronic nonsteroidal anti-inflammatory drug use in older adults. *Ann. Longterm. Care.* 18 (9), 24–27.
- Okin, D., and Medzhitov, R. (2012). Evolution of inflammatory diseases. *Curr. Biol.* 22 (17), R733–R740. doi:10.1016/j.cub.2012.07.029
- Omar, J., Shafii, N., Zainan, A. E., Sirajudeen, K. N. S., and Abdullah, M. R. (2020). Evaluation of wound healing biomarkers of interleukin 6 (IL-6), vascular endothelial Growth factor (VEGF) and matrix metalloproteinases 9 (MMP-9) in post lower segment caesarean section (LSCS) patients consuming *Channa striatus* extract. *Bangladesh J. Med. Sci.* 19 (3), 520–526. doi:10.3329/bjms.v19i3.45870
- Paliliewu, N., Datau, E. A., Matheos, J. C., and Surachmanto, E. E. (2013). *Channa striatus* capsules induces cytokine conversion in pulmonary tuberculosis patients. *J. Exp. Integr. Med.* 3 (3), 237. doi:10.5455/jeim.230513.or.076
- Pan, P. H., Lin, S. Y., Ou, Y. C., Chen, W. Y., Chuang, Y. H., Yen, Y. J., et al. (2010). Stearic acid attenuates cholestasis-induced liver injury. *Biochem. Biophys. Res. Commun.* 391 (3), 1537–1542. doi:10.1016/j.bbrc.2009.12.119
- Pasha, M., Huin, R. A., and Hassan, S. (2015). The influence of oral and topical *Channa striatus* on laparotomy wound healing in malnourished Wistar Rats. *Int. J. Pharm. Sci. Invent.* 4 (5), 37–41.
- Poh, B. K., Wong, Y. P., and Karim, N. A. (2005). Postpartum dietary intakes and food taboos among Chinese women attending maternal and child health clinics and maternity hospital, Kuala Lumpur. *Malays. J. Nutr.* 11 (1), 1–21.
- Raju, V. S., Sarkar, P., Pachaiappan, R., Paray, B. A., Al-Sadoon, M. K., and Arockiaraj, J. (2020). Defense involvement of piscidin from striped murrel *Channa striatus* and its peptides CsRG12 and CsLC11 involvement in an antimicrobial and antibiofilm activity. *Fish. Shellfish Immunol.* 99, 368–378. doi:10.1016/j.fsi.2020.02.027
- Roche, M., Rondeau, P., Singh, N. R., Tarnus, E., and Bourdon, E. (2008). The antioxidant properties of serum albumin. *FEBS Lett.* 582 (13), 1783–1787. doi:10.1016/j.febslet.2008.04.057
- Santamarina, A. B., Pisani, L. P., Baker, E. J., Marat, A. D., Valenzuela, C. A., Miles, E. A., et al. (2021). Anti-inflammatory effects of oleic acid and the anthocyanin keracyanin alone and in combination: Effects on monocyte and macrophage responses and the NF-κB pathway. *Food Funct.* 12 (17), 7909–7922. doi:10.1039/D1FO01304A
- Shafii, N., Omar, J., Sirajudeen, K., and Kadir, A. A. (2017). Changes in the inflammatory markers with supplementation of *Channa striatus* extract in post lower segment caesarean section. *Int. Med. J.* 26, 268–271.
- Shafri, M., and Abdul Manan, M. (2012). Therapeutic potential of the haruan (*Channa striatus*): From food to medicinal uses. *Malays. J. Nutr.* 18, 125–136.
- Shafri, M. A. M., Jais, A. M. M., and Kyu, K. M. (2011). Neuroregenerative property of haruan (*Channa striatus* spp.) traditional extract. *J. Intelek* 6 (1).
- Succar, R., Mitchell, V. A., and Vaughan, C. W. (2007). Actions of N-arachidonylglycine in a rat inflammatory pain model. *Mol. Pain* 3, 24. doi:10.1186/1744-8069-3-24
- Suhendi, A., Muhtadi, M., and Sutrisna, E. (2019). Anti-inflammatory and antidiabetic of *Channa striata* powder and Nephelium lappaceum fruit peel ethanolic extracts on albino Wistar mice. *Drug Invent. Today* 12 (11), 2472–2476.
- Susibalan, B. D., Abdullah, B., Lazim, N. M., and Kadir, A. A. (2018). Efficacy of snakehead fish (*Channa striatus*) in subjects with allergic rhinitis: A randomized controlled trial. *Orient. Pharm. Exp. Med.* 18 (3), 209–215. doi:10.1007/s13596-018-0327-9
- Tamale, D., Dewi, N., and Rosida, L. (2016). Extract of haruan (*channa striata*) extract increasing reepithelialisation count in wound healing process on wistar rat's buccal mucosa. *J. Dentomaxillofac. Sci.* 1, 7–15. doi:10.22208/jdmfs.1.1.2016.7-10
- van der Vusse, G. J. (2009). Albumin as fatty acid transporter. *Drug Metab. Pharmacokinet.* 24 (4), 300–307. doi:10.2133/dmpk.24.300
- Wall, R., Ross, R. P., Fitzgerald, G. F., and Stanton, C. (2010). Fatty acids from fish: The anti-inflammatory potential of long-chain omega-3 fatty acids. *Nutr. Rev.* 68 (5), 280–289. doi:10.1111/j.1753-4887.2010.00287.x
- Weissmann, G. (2013). *Mediators of inflammation*. Berlin, Germany: Springer Science & Business Media.
- Zakaria, Z., Mat Jais, A., Goh, Y., Sulaiman, M., and Somchit, M. (2007). Amino acid and fatty acid composition of an aqueous extract of *Channa striatus* (Haruan) that exhibits antinociceptive activity. *Clin. Exp. Pharmacol. Physiol.* 34 (3), 198–204. doi:10.1111/j.1440-1681.2007.04572.x
- Zhang, Y., and Jordan, J. M. (2010). Epidemiology of osteoarthritis. *Clin. Geriatr. Med.* 26 (3), 355–369. doi:10.1016/j.cger.2010.03.001
- Zuraini, A., Somchit, M., Solihah, M., Goh, Y., Arifah, A., Zakaria, M., et al. (2006). Fatty acid and amino acid composition of three local Malaysian *Channa* spp. fish. *Food Chem.* 97 (4), 674–678. doi:10.1016/j.foodchem.2005.04.031



OPEN ACCESS

EDITED BY
Zheng Xiang,
Liaoning University, China

REVIEWED BY
YaJun Yang,
Chinese Academy of Medical Sciences
and Peking Union Medical College,
China
Hua Sun,
Tianjin University, China

*CORRESPONDENCE
Yong-Rui Bao,
✉ byr1026@163.com
Xian-Sheng Meng,
✉ mxswv@126.com

[†]These authors have contributed equally
to this work and share first authorship

SPECIALTY SECTION
This article was submitted to
Ethnopharmacology,
a section of the journal
Frontiers in Pharmacology

RECEIVED 05 November 2022
ACCEPTED 29 November 2022
PUBLISHED 15 December 2022

CITATION
Yang X-X, Wang S, Cui L-L, Li T-J, Bai G,
Bao Y-R and Meng X-S (2022),
Pharmacological effects of Bufeijianpi
granule on chronic obstructive
pulmonary disease and its metabolism
in rats.
Front. Pharmacol. 13:1090345.
doi: 10.3389/fphar.2022.1090345

COPYRIGHT
© 2022 Yang, Wang, Cui, Li, Bai, Bao and
Meng. This is an open-access article
distributed under the terms of the
Creative Commons Attribution License
(CC BY). The use, distribution or
reproduction in other forums is
permitted, provided the original
author(s) and the copyright owner(s) are
credited and that the original
publication in this journal is cited, in
accordance with accepted academic
practice. No use, distribution or
reproduction is permitted which does
not comply with these terms.

Pharmacological effects of Bufeijianpi granule on chronic obstructive pulmonary disease and its metabolism in rats

Xin-Xin Yang^{1,2,3†}, Shuai Wang^{1,2,3†}, Lin-Lin Cui¹, Tian-Jiao Li^{1,2,3},
Gang Bai⁴, Yong-Rui Bao^{1,2,3*} and Xian-Sheng Meng^{1,2,3*}

¹College of Pharmacy, Liaoning University of Traditional Chinese Medicine, Dalian, China, ²Liaoning Multi-Dimensional Analysis of Traditional Chinese Medicine Technical Innovation Center, Dalian, China, ³Liaoning Province Modern Chinese Medicine Research Engineering Laboratory, Dalian, China, ⁴State Key Laboratory of Medicinal Chemical Biology, College of Pharmacy and Tianjin Key Laboratory of Molecular Drug Research, Nankai University, Tianjin, China

This work was performed to determine the pharmacological effects of Bufeijianpi granules on chronic obstructive pulmonary disease and its metabolism in rats.

Chronic obstructive pulmonary disease (COPD), ranked as the third leading cause of death worldwide, is seriously endangering human health. At present, the pathogenesis of COPD is complex and unclear, and the drug treatment mainly aims to alleviate and improve symptoms; however, they cannot achieve the purpose of eradicating the disease. Bufeijianpi granule (BJG) is a Chinese medicine developed by the First Affiliated Hospital of Henan University of Traditional Chinese Medicine for treating COPD. This study focuses on the pharmacological effects of BJG on COPD and its metabolism in rats, aiming to provide a scientific basis for developing BJG against COPD. A total of 72 Sprague–Dawley (SD) rats were divided into the blank group, model group, positive control group, and BJG groups (2.36, 1.18, and 0.59 g/kg). Except for the blank group, rats in other groups were administered lipopolysaccharide (LPS) combined with smoking for 6 weeks to establish the COPD model. After another 6 weeks of treatment, the therapeutic effect of BJG on COPD rats was evaluated. In the BJG (2.36 g/kg) group, the cough condition of rats was significantly relieved and the body weight was close to that of the blank group. Compared with the mortality of 16.7% in the model group, no deaths occurred in the BJG (2.36 g/kg) and (1.18 g/kg) groups. The lung tissue damage in the BJG groups was less than that in the COPD

Abbreviations: AMINOPH, aminophylline; BALF, bronchoalveolar lavage fluid; BJG, Bufeijianpi granule; BJGH, Bufeijianpi granule high-dose group; BJGM, Bufeijianpi granule medium-dose group; BJGL, Bufeijianpi granule low-dose group; COPD, chronic obstructive pulmonary disease; EF50, expiratory flow rate at 50% ventilation; ESI, electrospray ion source; FRC, functional residual volume; IL-8, interleukin-8; IL-6, interleukin-6; LPS, lipopolysaccharide; MMP-9, matrix metalloproteinase-9; MV, minute ventilation volume; NO, nitric oxide; PEF, peak expiratory flow rate; PGE2, prostaglandin E2; PIF, peak inspiratory flow rate; Raw, airway resistance; SD, Sprague–Dawley; sRaw, special airway resistance; TCMS, traditional Chinese medicines; TIC, total ion-flow chromatogram; TNF- α , tumor necrosis factor α ; Vcap, capillary voltage.

group. Compared with the model group, MV, PIF, PEF, and EF50 in the BJG groups were observably increased in a dose-dependent manner, while sRaw, Raw, and FRC were obviously decreased. Also, the contents of IL-6, IL-8, TNF- α , PGE2, MMP-9, and NO in the serum and BALF were lowered dramatically in all BJG groups. All indicators present an obvious dose-effect relationship. On this basis, the UPLC-QTOF-MS/MS technology was used to analyze characteristic metabolites in rats under physiological and pathological conditions. A total of 17 prototype and 7 metabolite components were detected, and the concentration of most components was increased in the COPD pathologic state. It is suggested that BJG has a pharmacological effect in the treatment of COPD and the absorption and metabolism of chemical components of BJG in rats exhibited significant differences under physiological and pathological conditions.

KEYWORDS

Bufei Jianpi granule (BJG), chronic obstructive pulmonary disease (COPD), pharmacological effects, metabolites, UPLC-QTOF-MS/MS technology

1 Introduction

Chronic obstructive pulmonary disease (COPD) is a preventable and treatable lung disease characterized by continuous airflow restriction (Rong et al., 2020; Huang et al., 2022). Its airflow restriction mostly develops in a progressive manner, which is associated with the enhanced chronic inflammatory response of airways and lung tissue to harmful gases or particles such as tobacco smoke. It is a common and frequently occurring disease that seriously endangers human health (Ono et al., 2020). In 2020, it was ranked as the third leading cause of death in the world along with hypertension and diabetes, seriously endangering physical and mental health of humans (Song et al., 2021; Zou et al., 2022). The treatment of COPD mainly includes drug treatment and nondrug treatment, where the former is the key to improving the symptoms of COPD and reducing acute exacerbation (Li, 2020). Thus, long-term adherence to drug therapy and regular follow-up should be ensured. Furthermore, in terms of drug treatment, it mainly involves bronchodilators, glucocorticoids, and expectorants (Lin et al., 2020). However, due to the complex pathogenesis of COPD and incomplete understanding, drug treatment mainly aims to relieve and improve symptoms but is unable to achieve the goal of radical cure of the disease.

As an effective preparation commonly used in the First Affiliated Hospital of Henan University of Traditional Chinese Medicine for the treatment of COPD, the Bufei Jianpi granule (BJG) is composed of 12 traditional Chinese medicines (TCMs), including *Astragalus mongholicus* Bunge [Fabaceae; *Astragalus mongholicus* radix], *Codonopsis pilosula* (Franch.) Nannf [Campanulaceae; *Codonopsis pilosula* radix], *Polygonatum kingianum* Collett & Hemsl [Asparagaceae; *Polygonatum kingianum* rhizoma], *Atractylodes macrocephala* Koidz [Asteraceae; *Atractylodes macrocephala* rhizoma], *Poria cocos* (Schw.) Wolf [Poromycetidae; *Poria*], *Fritillaria thunbergii* Miq

[Liliaceae; *Fritillariae thunbergii* bulbus], *Pheretima aspergillum* (E. Perrier) [Lumbricidae; *Pheretima*], *Magnolia officinalis* Rehder & E. H. Wilson [Magnoliaceae; *Magnoliae officinalis* cortex], *Citrus reticulata* Blanco [Rutaceae; *Citri reticulatae* pericarpium], *Aster tataricus* L. f [Asteraceae; *Asteris* radix et rhizoma], *Epimedium brevicornu* Maxim [Berberidaceae; *Epimedii* folium], and *Ardisia japonica* (Thunb.) Blume [Primulaceae; *Ardisiae japonicae* herba] at a ratio of 12:6:12:9:9:6:9:6:9:6:6:15 (Li and Li, 2011). Clinical studies found that BJG can efficiently enhance the pulmonary function of patients with COPD in the stable stage, lower the number of acute exacerbations, and improve exercise endurance (Tang et al., 2019). However, at present, it is only used internally in the First Affiliated Hospital of Henan University of Traditional Chinese Medicine. In order to meet the needs of the majority of patients, it is urgently needed to develop BJG into a Chinese patent medicine preparation with a national brand for the treatment of COPD. For this purpose, systemic research has been carried out on the pharmacological effects, mechanism of action, and process and quality control of BJG in the treatment of COPD (Yu et al., 2019; Cui et al., 2020).

In this study, the commonly recognized pharmacological model of lipopolysaccharide (LPS) combined with the smoke-induced rat COPD model was used. The daily physiological state, lung function, lung tissue appearance and morphology, lung histopathological changes, and inflammatory factors in the serum and bronchoalveolar lavage fluid (BALF) were taken as the detection indicators to investigate the therapeutic effect of BJG at different doses on COPD from the perspective of pharmacological efficacy. On this basis, adopting the UPLC-QTOF-MS/MS technology combined with tandem mass spectrometry fragment ion information and comparison methods of the reference substance, the components of BJG absorbed into blood and their metabolites were analyzed under physiological and pathological conditions. The differences in

chemical component metabolism in rats were compared so as to explore the effective chemical components of the prescription and the law of disease treatment, which provide the experimental basis for the development of BJG as a new drug for the treatment of COPD.

2 Materials and methods

2.1 Chemicals and reagents

MS-grade methanol and acetonitrile were purchased from Merck (Germany). MS-grade formic acid was bought from Thermo Fisher Technology Co., Ltd. (United States). Mullein isoflavone glucoside, naringin, hesperidin, ononin, epimedeside A, icariin, nobiletin, and tangeretin (purities > 98%) were all purchased from Sichuan Vicky Biotechnology Co., Ltd. (Chengdu, China). Betaine, adenosine, magnoflorine, peimine, peiminine, vanillin, hesperetin, wogonin, honokiol, magnolol, and linoleic acid (purities > 98%) were all acquired from Chengdu Pufei De Biotech Co., Ltd. (Chengdu, China). Lipopolysaccharide (LPS) was offered by Shanghai Sulaibao Biotechnology Co., Ltd. (Shanghai, China). Interleukin-8 (IL-8), interleukin-6 (IL-6), tumor necrosis factor α (TNF- α), prostaglandin E2 (PGE2), matrix metalloproteinase-9 (MMP-9), and nitric oxide (NO) testing kits were purchased from Shanghai Langton Biotechnology Co., Ltd. (Shanghai, China).

2.2 Preparation process of Bufei Jianpi granule

BJG was provided by the First Affiliated Hospital of Henan University of Traditional Chinese Medicine and produced by Jiangyin Tianjiang Pharmaceutical Co., Ltd. (batch no. 1905301, China). The preparation process of BJG is an industrial production process amplified proportionally according to the following single feeding amount: *Astragalus mongholicus* Bunge [Fabaceae; *Astragalus mongholicus* radix] 12 g, *Codonopsis pilosula* (Franch.) Nannf [Campanulaceae; *Codonopsis pilosula* radix] 6 g, *Polygonatum kingianum* Collett & Hemsl [Asparagaceae; *Polygonatum kingianum* rhizoma] 12 g, *Atractylodes macrocephala* Koidz [Asteraceae; *Atractylodes macrocephala* rhizoma] 9 g, *Poria cocos* (Schw.) Wolf [Poromycetidae; *Poria*] 9 g, *Fritillaria thunbergii* Miq [Liliaceae; *Fritillaria thunbergii* bulb] 6 g, *Pheretima aspergillum* (E. Perrier) [Lumbricidae; *Pheretima*] 9 g, *Magnolia officinalis* Rehder & E. H. Wilson [Magnoliaceae; *Magnolia officinalis* cortex] 6 g, *Citrus reticulata* Blanco [Rutaceae; *Citri reticulatae* pericarpium] 9 g, *Aster tataricus* L. f [Asteraceae; *Asteris radix et rhizoma*] 6 g, *Epimedium brevicornu* Maxim [Berberidaceae; *Epimedii folium*] 6 g, and *Ardisia japonica* (Thunb.) Blume [Primulaceae; *Ardisia japonicae* herba] 15 g.

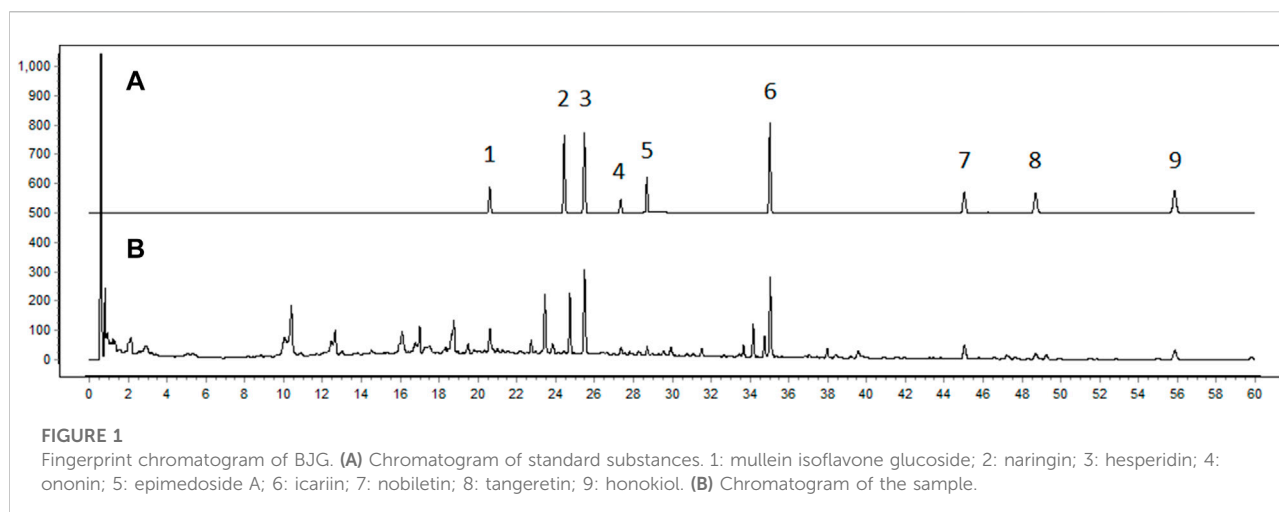
After being crushed, *Atractylodes macrocephala* rhizoma was combined with *Citri reticulatae* pericarpium, six times the volume of water was added, and the sample was hydrodistilled for 5 h. The volatile oil was collected. Then, the sample was filtered to get decoction (I), and the residue was collected for later use. Extract (I) was obtained as follows: *Magnolia officinalis* cortex, *Asteris radix et rhizoma*, and *Fritillariae thunbergii* bulb are taken, six times the volume of 70% ethanol is added, the extract is refluxed for 1.5 h, and the process is repeated three times. The filtrates of three repetitions are combined, the sample is decompressed to recover ethanol, and it is concentrated to a relative density of 1.15 at 50°C to obtain extract (I). The residue was collected for later use. Extract (II) was obtained as follows: we combine the aforementioned drug residues, add eight times the volume of water, and decoct the sample three times for 1 h. Then, we filter and mix the filtrates with decoction (I), decompress the sample, and concentrate it to a relative density of 1.15 at 50°C to obtain extract (II). Dry powder (I) was obtained as follows: we combine extract (I) with extract (II) to obtain the total extract, 20% dextrin is added, and after spray-drying, dry powder (I) is obtained. Dry powder (II) was obtained as follows: the volatile oil is mixed with 10 times its amount of β -cyclodextrin by the grinding method to obtain the inclusion complex; after vacuum-drying and crushing, dry powder (II) is obtained. We mix dry powder (I), dry powder (II), and 10% honey of the total powder weight uniformly and make granules; after drying, the granules are formed (Li and Li, 2011).

2.3 Bufei Jianpi granule qualification

The quality of BJG was verified by HPLC detection (Figure 1). Mullein isoflavone glucoside, naringin, hesperidin, ononin, epimedeside A, icariin, nobiletin, tangeretin, and honokiol were quantified for controlling the quality of the granule, and their contents in the batch 1905301 sample were 0.071 mg/g, 0.172 mg/g, 0.028 mg/g, 0.017 mg/g, 0.021 mg/g, 0.343 mg/g, 0.047 mg/g, 0.018 mg/g, and 0.042 mg/g, respectively. The chemical composition of BJG was described in our previous study by the HPLC-QTOF-MS technology (Cui et al., 2020). Based on this, the authenticity of these nine quality control indicators was confirmed by comparing the retention time, accurate mass number, isotope peak, and other information of these chemical components (please refer to the [Supplementary Material](#) for details of HPLC and HPLC-QTOF-MS).

2.4 Animals

Male Sprague–Dawley (SD) rats (200 \pm 20 g) were purchased from Liaoning Changsheng Biotechnology Co., Ltd. [number: SCXK (Liao) 2020-0001]. All rats were acclimated for 1 week after arrival and housed in a room under controlled temperature



($22 \pm 2^{\circ}\text{C}$) and humidity with a 12-h light/dark cycle and free access to water and food. Apart from that, all experiments were carried out following the approved animal protocols and guidelines established by the Medicine Ethics Review Committee for Animal Experiments of Liaoning University of Traditional Chinese Medicine with approval number 2020YS013(KT)-013-01.

2.5 Pharmacological efficacy of BJG on the COPD rat model

A total of 72 SD rats were randomly divided into six groups, namely, the blank group, COPD model group, AMINOPH (aminophylline) (0.0054 g/kg) positive control group, BJG high-dose (2.36 g/kg) group, medium-dose (1.18 g/kg) group, and low-dose (0.59 g/kg) group, with 12 rats in each group. The medium dose of BJG is determined according to the conversion of animal dose to human equivalent dose. For the high dose, we used two times the medium dose, and for low dose, we used two times below the medium dose, to investigate the dose–effect relationship. Except for the blank group, for rats in the other groups, the COPD model was established by administering LPS combined with smoking according to the method with minor modification (Shin et al., 2017; Mao et al., 2022; Pelgrim et al., 2022). The administration intervention was started in the 6th week, twice a day. The blank group and the model group were given distilled water of equal volume, and the whole process lasted for 6 weeks. During this period, the activity and behavior changes of the rats such as hair, mental state, activity ability, weight, death, and other physiological state indicators were observed and detected. After the drug intervention, the Buxco noninvasive animal airway detection system was used to measure the lung function of rats (Luo et al., 2021). The rats to be tested were placed into the

noninvasive animal airway detection cavity. After the rats' breathing was stable, the minute ventilation volume (MV), special airway resistance (sRaw), airway resistance (Raw), functional residual volume (FRC), peak inspiratory flow rate (PIF), peak expiratory flow rate (PEF), and expiratory flow rate at 50% ventilation (EF50) were measured continuously. In addition, the contents of IL-6, IL-8, TNF- α , PGE2, MMP-9, and NO in the serum and BALF were determined using ELISA kits.

2.6 Analysis of chemical components absorbed into the blood

A total of 24 SD rats were randomly classified into the blank group, blank administration group, model group, and model administration group. In the model groups, the rat model of COPD was established by administering LPS combined with the smoking method (Shin et al., 2017; Mao et al., 2022; Pelgrim et al., 2022), while in the administration groups, rats were gavaged with 2.36 g/kg solution of BJG, twice a day for 7 consecutive days. The blank group and the model group were given the same amount of normal saline. Then, 12 h before the last administration, fasting without water was performed, followed by 60 min after the last administration, blood being taken from the abdominal aorta into centrifuge tubes with heparin sodium, and 30 min later, it being centrifuged at 3,000 rpm for 15 min to separate the plasma. Afterward, the supernatant was taken and kept in a refrigerator at -80°C for later use.

2.7 Preparation of plasma samples

The plasma samples were thawed at room temperature, and 400 μl of plasma samples was accurately extracted, followed by protein removal with 1,200 μl of methanol. After that, by

vortexing for 3 min and centrifugation at 13,000 rpm (4°C) for 10 min, the supernatant was taken, cryogenic freeze-dried, redissolved in 50 µl of methanol, and vortexed for 3 min. Furthermore, the supernatant was centrifuged again at 13,000 rpm (4°C) for 10 min and was directly detected by LC-MS (Li et al., 2022; Wang et al., 2022).

2.8 Chromatography–mass spectrometry analysis conditions

The positive ion mode is adjusted as follows: Agilent Poroshell 120 SB-C18 (100 mm × 4.6 mm, 2.7 µm) is used; the mobile phase consists of 0.1% formic acid water (A)–acetonitrile (B); gradient elution conditions are 0–25 min, 5–40% B; 25–35 min, 40–75% B; 35–40 min, and 75–100% B; the flow rate is 0.8 ml min^{−1}; the column temperature is 30°C; the injection volume is 1 µl; the electrospray ion source (ESI) is detected in the positive ion mode; the drying gas flow is 13 L/min; the drying gas temperature is 350°C; the capillary voltage (Vcap) is 4,000 V; the neutralizer pressure is 45 psig; the fragmentor voltage is 125 V; the skimmer voltage is 65 V; the mass scanning range is 50–1,000 m/z; and the secondary MS collision voltage is 40 eV.

The negative ion mode is set as follows: Agilent Poroshell 120 SB-C18 (100 mm × 4.6 mm, 2.7 µm) is used; the mobile phase consists of water (A)–acetonitrile (B); gradient elution conditions are 0–30 min, 5–100% B; the flow rate is 0.8 ml min^{−1}; the column temperature is 30°C; the injection volume is 5 µl; the drying gas flow is 11 L/min; the drying gas temperature is 250°C; the Vcap is 3,500 V; the neutralizer pressure is 45 psig; the fragmentor voltage is 125 V; the skimmer voltage is 65 V; the mass scanning range is 50–1,000 m/z; and the secondary MS collision voltage is 40 eV (Wang et al., 2021).

2.9 Data analysis

SPSS 19.0 software was adopted for statistical analysis. The data were represented as mean ± standard deviation (mean ± SD). Statistical comparisons were analyzed by one-way analysis of variance (ANOVA). A value of $p < 0.05$ suggests a difference, and $p < 0.01$ represents a significant difference (Chen et al., 2019; Liu et al., 2021).

MS data processing was performed with MassHunter software and the PCDL database, which contained extracted ion chromatograms and calculations of elemental compositions with mass errors within 10 ppm. The chemical structures of all analytes were explained and verified based on their elemental compositions, accurately measured mass values, the elution order on a C18 column, retention time, fragmentation behavior, and the comparison with authentic standards and literature as far as possible (Lu et al., 2021).

3 Results

3.1 General state of rats in the pharmacodynamic experiment

The rats in the blank group featured normal hair color and luster, good mental state, flexible and frequent activities, stable exhalation, and normal diet and water intake, while those in the model group had dull and yellow hair, no luster, cough, phlegm in the throat, mental fatigue, slow movement, reduced diet, and weight loss. In the BJG high-dose group and the AMINOPH group, cough was significantly relieved and phlegm and sound in the larynx disappeared, with daily activities of rats being more frequent. There was no significant difference in drinking water compared with the blank group. Furthermore, compared to the model group, the cough condition of rats in the BJG medium- and low-dose groups was reduced and their mental state was improved, while their water intake was reduced compared with the blank group.

3.2 Body weight change and deaths of rats

Before the experiment, there existed no significant difference in the weight of rats in each group. After the experiment, a significant difference in the body weight existed between the blank group and the model group ($p < 0.01$). In comparison with the model group, the body weight in the BJG groups and the AMINOPH group was obviously higher ($p < 0.01$) (Figure 2A). Before and after the experiment, the weight of rats in each group increased linearly. The weight growth rate of the blank group was faster, and that of the model group was the slowest (Figure 2B). Furthermore, during the whole experiment, there was no death in the blank control group and BJG high-dose, medium-dose, and AMINOPH groups, while deaths occurred in the model and BJG low-dose groups, with mortality rates of 16.7% and 8.3%, respectively.

3.3 Evaluation of lung function in rats

In comparison with the blank group, MV, PIF, PEF, and EF50 in the model group were dramatically decreased, while sRaw, Raw, and FRC were significantly increased ($p < 0.01$). Compared with the model group, MV, PIF, PEF, and EF50 in the BJG groups and the AMINOPH group were observably increased, while sRaw, Raw, and FRC were obviously decreased ($p < 0.01$) (Figure 2C). According to the results, compared with the blank group, the model group had increased airway resistance, decreased lung compliance, restricted airflow, and airway obstruction. However, compared with the model group, the indexes of each treatment group, especially the BJG high-dose and AMINOPH groups, had

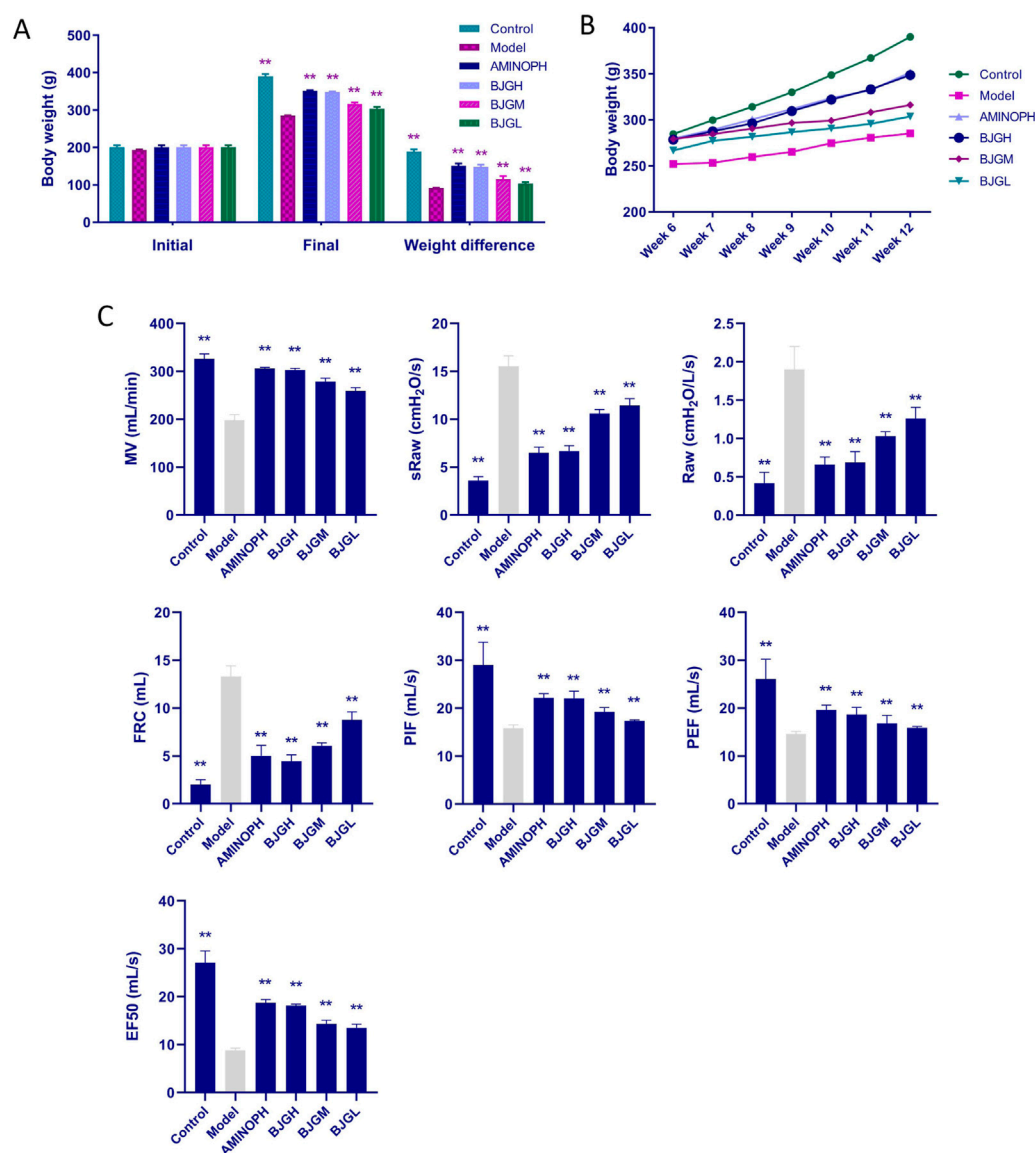


FIGURE 2

Changes in body weight and lung function of rats in each group. (A) Changes in body weight at the beginning and end of the experiment. (B) Changes in body weight of rats per week during treatment. (C) Changes in lung function indexes of rats in each group.

improved, indicating that BJG can ameliorate airway obstruction, enhance pulmonary ventilation, and exert a protective effect on the pulmonary function of COPD rats. In addition, a certain dose–effect relationship was observed.

3.4 Morphological changes in the lung tissue of rats

The lung tissues of the blank control group were smooth, shiny, soft, light red in color, and normal in size. In the

model group, the surface of lung tissue was rough, the whole lung was white, luster was lost, and lung swelling was obvious. Compared with the model group, the lung volume of rats in each administration group was significantly reduced, shiny, and soft. The color of the BJG high-dose group and the AMINOPH group was close to that of the normal group, and the volume was reduced compared with the model group to a great extent. Moreover, the color of the BJG medium- and low-dose groups was lighter, and the volume was larger than that of the blank group (Figure 3A).

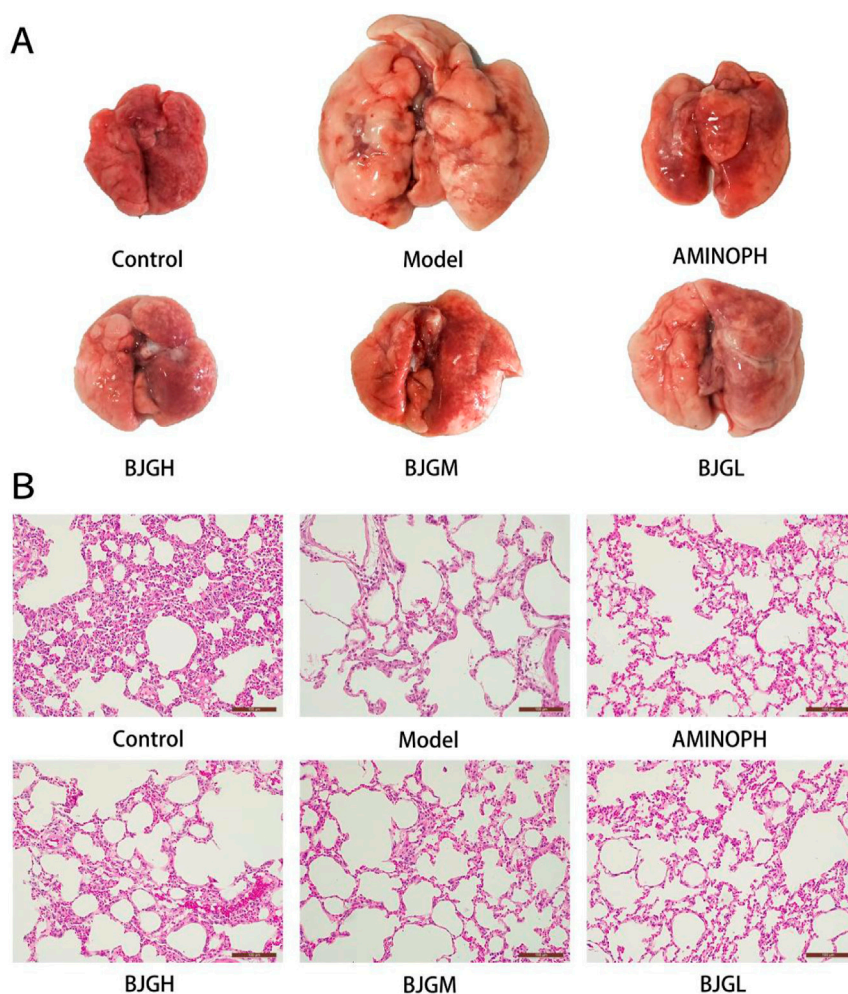


FIGURE 3
(A) Morphological changes in the lung tissue of rats. (B) Pathological changes in the lung tissue of rats [HE staining (magnification $\times 200$)].

3.5 Pathological changes in the lung tissue of rats

Under the light microscope, the lung tissue structure of the blank group was complete and the bronchial tube wall was not thickened; other than that, there was no exudate in the lumen, the cilia were arranged neatly, and no inflammatory cell infiltration occurred. The size of the alveoli was normal, and the structure of the alveolar septum was clear. Compared with the blank group, the bronchial smooth muscle in the model group was significantly thickened and the lumen was filled with a large number of neutrophils. The alveolar septum was severely broken, alveolar cells were fibrotic, neutrophils were denatured and necrotic, cellulose was dissolved, alveolar walls were thinner, alveolar cavities were significantly expanded, and some alveoli fused to form pulmonary bullae. The pathological changes of the abovementioned trachea and lung tissues were consistent with

those of COPD patients. Compared with the model group, the lung tissue damage in each drug intervention group was less than that in the COPD group and the lung tissue damage in the AMINOPH and BJG high-dose groups was the least (Figure 3B).

3.6 Changes in inflammatory factors in the rat serum and BALF

The contents of IL-6, IL-8, TNF- α , PGE2, MMP-9, and NO in the serum and BALF of rats in each group are shown in Figure 4. Compared to the blank group, the expression levels of IL-6, IL-8, and TNF- α were increased in the model group and all treatment groups, and compared to the model group, they were lowered dramatically in all treatment groups ($p < 0.01$), especially in the BJG high-dose group and the AMINOPH group. Compared with the blank group, the expression levels

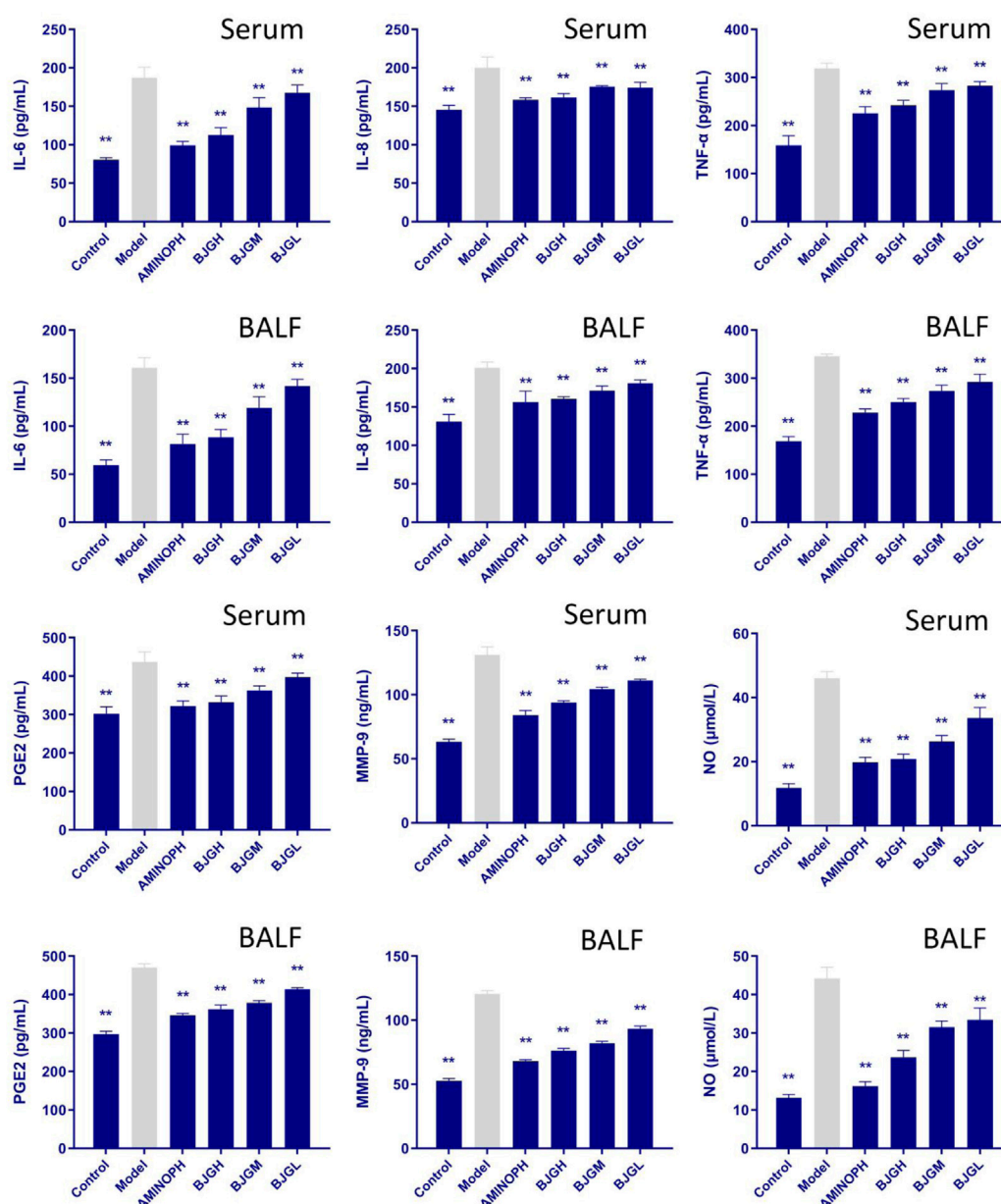


FIGURE 4

Changes in inflammatory factors in the rat serum and BALF.

of NO and MMP-9 factors in the model group and each treatment group were increased, while compared with the model group, they were decreased to a great extent in all treatment groups ($p < 0.01$), especially in the BJG high-dose group and the AMINOPH group. Moreover, compared with the blank group, the expression levels of PGE2 in the model group and each treatment group were increased, whereas compared with the model group, they were noticeably decreased in all treatment groups ($p < 0.01$), especially in the BJG high-dose group and the AMINOPH group. These findings suggest that all

treatment groups could improve the inflammatory response in COPD rats.

3.7 LC-MS analysis on plasma samples of BJG under physiological and pathological conditions

By comparing the profiles of positive and negative blank plasma and drug-containing plasma, 13 different compounds,

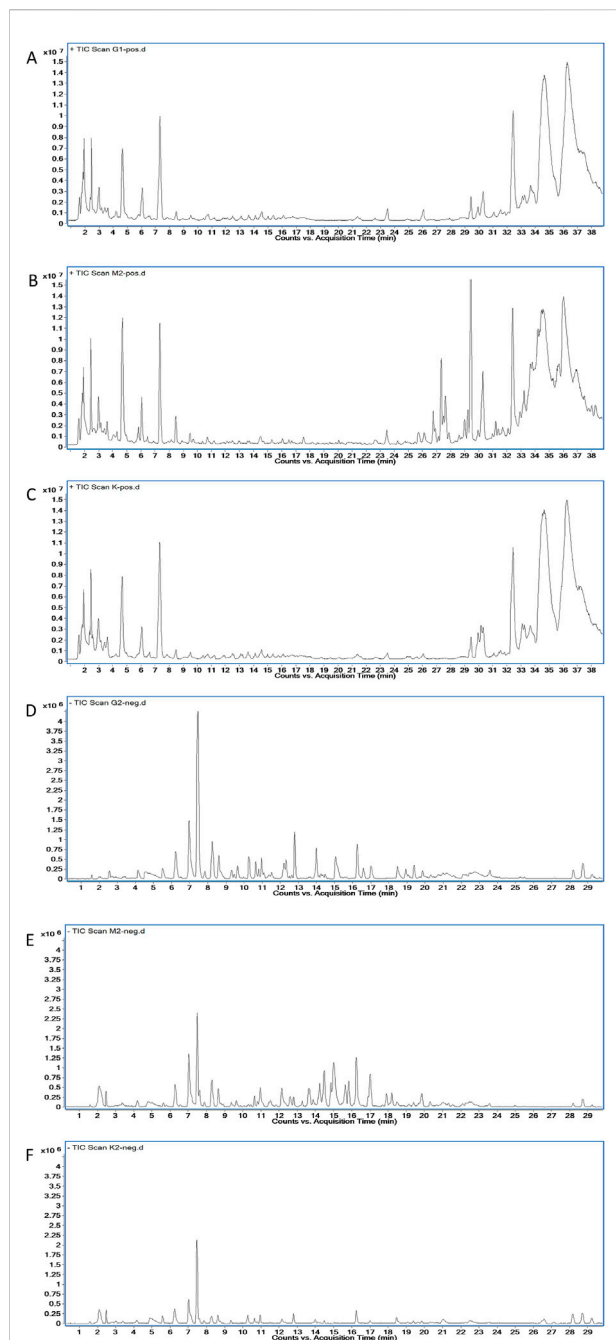


FIGURE 5

Plasma TIC of rats in each group. (A) Drug-containing plasma of healthy rats in the positive mode. (B) Drug-containing plasma of COPD rats in the positive mode. (C) Blank plasma of healthy rats in the positive mode. (D) Drug-containing plasma of healthy rats in the negative mode. (E) Drug-containing plasma of COPD rats in the negative mode. (F) Blank plasma of healthy rats in the negative mode.

including 10 prototype components and three metabolites, were found in the pathological plasma in the positive ion mode. In physiological plasma, it contains all pathological components,

but there is one prototypical component and one metabolite more than that in the pathological state. In the negative ion mode, eight different compounds, involving five prototypes and three metabolites, were discovered in the pathological plasma. In the physiological state, it contains all pathological components, but there is one more prototypical blood-entering component than that in the pathological state. The total ion-flow chromatogram (TIC) of each group is shown in Figure 5, while the retention time and molecular weight of each component are displayed in Table 1.

3.8 Identification of chemical components absorbed in rat plasma

In the positive ion mode, for compound P1 (1.829 min, m/z 118.0861) ($C_5H_{11}NO_2$, $M + H$)⁺, the secondary fragment ions were m/z 84.9595 ($M + H - 2OH$)⁺ and m/z 58.0650 ($M - C_2H_3O_2$)⁺. After comparison with the betaine reference substance, the fragment ion information was basically consistent with that of betaine and it was determined to be betaine. For compound P2 (3.022 min, m/z 268.1040) ($C_{10}H_{13}N_5O_4$, $M + H$)⁺, the secondary fragment ions were m/z 136.0616 ($M + H - C_5H_8O_4$)⁺, m/z 119.0349 ($M + H - C_5H_8O_4 - NH_3$)⁺, and m/z 94.0400 ($M - C_5H_8O_4 - NH_3 - CN$)⁺. After comparison with the adenosine control substance, the fragment ion information was in line with that of adenosine and, finally, it was identified as adenosine. For compound P3 (5.427 min, m/z 254.1387) ($C_{13}H_{19}NO_4 + H$)⁺, the secondary fragment ion was m/z 161.0580 ($M + H - H_2O - C_3H_9NO$)⁺. In addition, after comparison with the standard database information and references, the fragment ion information is roughly consistent with that of codonopsinol B. It was speculated to be codonopsinol B. For compound P4 (11.245 min, m/z 342.1695) ($C_{20}H_{24}NO_4 + H$)⁺, the secondary fragment ions were m/z 297.1130 ($C_{20}H_{24}NO_4 - CH_2O - CH_3$)⁺, m/z 282.0884 ($C_{20}H_{24}NO_4 - CH_2O - 2CH_3$)⁺, m/z 222.0670 ($C_{20}H_{24}NO_4 - CH_2O - 2CH_3 - C_2H_4O_2$)⁺, and m/z 191.0851 ($C_{20}H_{24}NO_4 - CH_2O - 2CH_3 - C_2H_4O_2 - CH_3O$)⁺. The fragment ion information was in accordance with that of magnoflorine, by comparison with that of magnoflorine, and it was detected as magnoflorine. For compound P5 (15.924 min, m/z 428.3139) ($C_{27}H_{41}NO_3 + H$)⁺, the secondary fragment ion was m/z 412.3205 ($C_{27}H_{41}NO_3 + H - O$)⁺. After comparison with the standard database information, the fragment ion information was roughly consistent with that of peimisine, so it was speculated that it might be peimisine. For compound P6 (16.551 min, m/z 432.3460) ($C_{27}H_{45}NO_3$)⁺, the main secondary fragment ions were m/z 414.3358 ($C_{27}H_{45}NO_3 - H_2O$)⁺, m/z 398.3054 ($C_{27}H_{45}NO_3 - H_2O - O$)⁺, and m/z 299.2351 ($C_{27}H_{45}NO_3 - H_2O - O - C_6H_{11}O$)⁺. After comparison with the control substance, the fragment ion information was basically in line with that of the control substance and the fragment ion

TABLE 1 Analysis on chemical components absorbed in healthy rat plasma.

Positive ion mode				Negative ion mode			
No.	t _R (min)	Excimer ion MS (m/z)	Source	No.	t _R (min)	Excimer ion MS (m/z)	Source
P1	1.829	118.0861	Prototype	N1	11.495	593.1872	Prototype
*P2	3.022	268.1040	Prototype	N2	14.287	301.0724	Prototype
P3	5.427	254.1387	Prototype	*N3	17.067	283.0619	Prototype
P4	11.245	342.1695	Prototype	N4	20.129	265.1250	Prototype
P5	15.924	428.3144	Prototype	N5	21.497	265.1248	Prototype
P6	16.551	432.3460	Prototype	N6	29.629	279.2328	Prototype
P7	16.934	430.3308	Prototype	NM1	2.537	167.0215	Metabolites
P8	17.553	430.3301	Prototype	NM2	6.666	273.0065	Metabolites
P9	19.934	432.3461	Prototype	NM3	15.175	259.1026	Metabolites
P10	21.570	414.3359	Prototype				
P11	22.379	414.3357	Prototype				
*PM1	3.820	169.0354	Metabolites				
PM2	8.417	349.1822	Metabolites				
PM3	11.981	565.2861	Metabolites				
PM4	15.796	461.1066	Metabolites				

*Components that were not detected in the pathological state.

information was determined to be peimine. In terms of compound P7 (16.934 min, m/z 430.3308) ($C_{27}H_{43}NO_3+H$)⁺, the secondary fragment ion was m/z 412.3199 ($C_{27}H_{43}NO_3+H-H_2O$)⁺. After comparison with standard database information, fragment ion information was roughly consistent with that of zhebeinone, so it was speculated to be zhebeinone. As for compound P8 (17.553 min, m/z 430.3301) ($C_{27}H_{43}NO_3+H$)⁺, the secondary fragment ions were m/z 412.3199 ($C_{27}H_{43}NO_3+H-H_2O$)⁺, m/z 396.2898 ($C_{27}H_{43}NO_3+H-H_2O-O$)⁺, and m/z 175.1474 ($C_{27}H_{43}NO_3+H-H_2O-O-C_{15}H_{27}N$)⁺. After comparison with the control substance, it was confirmed that it was peiminine. For compound P9 (19.934 min, m/z 432.3461) ($C_{27}H_{45}NO_3+H$)⁺, the main secondary fragment ion is m/z 414.3359 ($C_{27}H_{45}NO_3+H-H_2O$)⁺. After comparison of the fragment ion information with the standard database, it was speculated to be zhebeinine. For compounds P10 (21.570 min, m/z 414.3359) and P11 (22.379 min, m/z 414.3357), ($C_{27}H_{43}NO_2+H$)⁺ was compared with standard database information and fragment ion information, and it was speculated to be ebeidinone or zhebeirine. The specific association needs to be further confirmed by a reference substance. Compound PM1 with molecular ion peak m/z 169.0354 ($C_5H_4N_4O_3+H$)⁺, which is 32 Da more than the hypoxanthine excimer ion peak 137 ($C_5H_4N_4O + H$)⁺, prompted that O is added continuously and two oxygenation reactions occurred. Combined with the fragments m/z 152.0319

($C_5H_4N_4O_3+H-NH_3$)⁺, m/z 141.0669 ($C_5H_4N_4O_3+H-CO$)⁺, and m/z 125.9855 ($C_5H_4N_4O_3+H-CONH$)⁺, it is speculated to be hypoxanthine oxidation products. Compound PM2 m/z 349.1822 ($C_{16}H_{12}O_7S + H$)⁺, which was found to be 80 Da more than the formononetin excimer ion peak 269 ($C_{16}H_{12}O_4+H$)⁺, suggested that the compound is a sulfate metabolite. Combined with fragment m/z 269.1024 ($C_{16}H_{12}O_4+H$)⁺, which is the prototype component of formononetin, it was speculated that the combination is formononetin sulfate. Furthermore, for compound PM3 with the molecular ion peak of m/z 565.2861, the main secondary fragment ion is m/z 403.1357 ($C_{21}H_{22}O_8+H$)⁺, which is the excimer ion peak of nobiletin. The molecular weight of this substance in primary mass spectrometry is 162 Da more than that of nobiletin. It may be the product of glucuronidation and demethylation of nobiletin. Compound PM4 with m/z 461.1066, which is 176 Da more than that of calycosin excimer ion peak 285, demonstrated that the compound is a metabolite of glucoaldehyde acidification and the corresponding molecular formula is $C_{22}H_{20}O_{11}$. Combined with fragments m/z 285.0753 ($C_{16}H_{12}O_5+H$)⁺, m/z 270.0509 ($C_{16}H_{12}O_5+H-CH_3$)⁺, and m/z 125.9863 ($C_{16}H_{12}O_5+H-C_9H_4O_3$)⁺, m/z 285.0753 is the prototype component of the compound calycosin, so that the compound is speculated to be glucuronized calycosin.

In the negative ion mode, for compound N1 (11.495 min, m/z 593.1872) ($C_{28}H_{34}O_{14}-H$)⁻, the secondary fragment ions were m/z

510.2635 ($C_{28}H_{34}O_{14}-C_4H_4O_2$)⁻, m/z 285.0783 ($C_{28}H_{34}O_{14}-C_{12}H_{21}O_7$)⁻, and m/z 96.9587 ($C_{28}H_{34}O_{14}-C_{20}H_{25}O_{12}$)⁻. After comparison with vanillin, the fragment ion information was basically consistent and it was identified as vanillin. For compound N2 (14.287 min, m/z 301.0724) ($C_{28}H_{34}O_{14}-H$)⁻, the main secondary fragment ions were m/z 136.0171 ($C_{28}H_{34}O_{14}-C_{20}H_{26}O_{12}$)⁻, m/z 108.0223 ($C_{28}H_{34}O_{14}-C_{21}H_{26}O_{13}$)⁻, and m/z 65.0039 ($C_{28}H_{34}O_{14}-C_{23}H_{29}O_{14}$)⁻. After comparison with hesperetin, the fragment ion information was consistent with that of hesperetin. Therefore, it was identified as hesperetin. For compound N3 (17.067 min, m/z 283.0619) ($C_{16}H_{12}O_5$)⁻, the secondary fragment ions were m/z 239.0344 ($C_{16}H_{12}O_5-C_2H_5O$)⁻, m/z 163.0039 ($C_{16}H_{12}O_5-C_7H_5O_2$)⁻, m/z 135.0099 ($C_{16}H_{12}O_5-C_7H_5O_2-CO$)⁻, and m/z 110.0007 ($C_{16}H_{12}O_5-C_7H_5O_2-CO-C_2H_5$)⁻. After comparison with the control substance, the fragment ion information was in line with that of wogonin. It was finally determined to be wogonin. For compound N4 (20.129 min, m/z 265.1250) ($C_{18}H_{18}O_2-H$)⁻, the secondary fragment ions were m/z 249.0936 ($C_{18}H_{18}O_2-OH$)⁻, m/z 223.0771 ($C_{18}H_{18}O_2-C_3H_7O$)⁻, and m/z 197.0617 ($C_{18}H_{18}O_2-C_4H_5O_2$)⁻. After comparison with the honokiol control substance, fragment ion information was basically consistent with that of honokiol and it was identified as honokiol. For compound N5 (21.576 min, m/z 265.1248) ($C_{18}H_{18}O_2-H$)⁻, the main secondary fragment ions were m/z 223.0767 ($C_{18}H_{18}O_2-H-C_3H_5$)⁻, m/z 204.0577 ($C_{18}H_{18}O_2-H-C_3H_5-OH$)⁻, and m/z 119.0501 ($C_{18}H_{18}O_2-C_9H_7O_2$)⁻. After comparison with the reference substance, it was identified as magnolol. For compound N6 (29.296 min, m/z 279.2328) ($C_{18}H_{32}O_2-H$)⁻, no fragment ions were produced at 40 V. After comparison with the linoleic acid reference substance, it was determined to be linoleic acid. The molecular ion peak of compound NM1 was m/z 167.0215, which is the methyl group, 14 Da more than protocatechuic acid. When combined with the fragment m/z 122.4525 ($C_7H_6O_4-2O$)⁻ and according to the literature (Guo et al., 2019) as well as database comparison, it was speculated as a methylated product of protocatechuic acid. For compound NM2 with m/z 273.0065, which increased by 94 Da ($M + CH_2 + SO_3$) compared with caffeic acid ($C_9H_8O_4$), according to the comparison of literature studies and databases, it was speculated that the compound was 3-methoxy-caffeine-4-O-sulfate. Moreover, the basic ion peak of compound NM3 was m/z 259.1026, 80 Da more than that of caffeic acid 179, suggesting that $M + SO_3$ was increased. Beyond that, the corresponding molecular formula was $C_9H_8O_7S$, and in comparison with the characteristic ion of caffeic acid with m/z 179.0346, it was speculated to be caffeic acid-3-O-sulfate.

3.9 Difference of prototype components from BJG under physiological and COPD pathological conditions

According to Table 2 and Figure 6, betaine, codonopsinol B, magnoflorine, peimisine, peimine, zhebeinone, peiminine,

zhebeinine, ebeiedinone, zhebeirine, vanillin, hesperetin, honokiol, magnolol, and linoleic acid were all absorbed into the blood as the prototype under physiological and pathological conditions. Taking the variation of abundance greater than 1.5 times as the statistical standard, nine of the prototype components increased in the blood, five decreased, and one was not detected under the pathological state, while honokiol and linoleic acid did not change.

3.10 Difference of metabolites from BJG under physiological and COPD pathological conditions

It can be seen from Table 3 and Figure 7 that there are seven metabolic components that change under the pathological state compared with the physiological state. Among them, five components increase in the blood concentration under the pathological state, while one metabolite decreases in the blood concentration and hypoxanthine oxidation products are not detected under the pathological state, which may not affect the absorption of the aforementioned components under the pathological state.

4 Discussion

COPD is a preventable and treatable lung disease characterized by a persistent and progressive limitation of airflow (Rong et al., 2020; Huang et al., 2022). Its airflow restriction is associated with the enhanced chronic inflammatory response of the airways and lung tissue to harmful gases or particles such as tobacco smoke (Ono et al., 2020). COPD is a common and frequently occurring disease that poses a serious threat to human health (Li et al., 2020). The LPS combined with the smoke-induced rat COPD model is a classical and commonly used model to evaluate the drug treatment of COPD, based on which this study investigated the therapeutic effect of BJG on COPD from physiological, pathological, biochemical, and other aspects, providing better experimental data for its development into a new clinical drug for COPD.

The mental state directly reflects the physiological or physical state. In this study, the rats in the COPD model group were listless and sluggish, with dull and yellow hair and cough and throat phlegm sounds. Patients with advanced COPD tend to lose weight (Pershina et al., 2019), while rats in the model group presented an emaciated body type, and death occurs with a mortality rate of 16.7%. After the BJG treatment with different dosages, the state of the rats was improved by different degrees. In particular, the rats in the BJG high-dose group had more frequent daily activities, and the phlegm sounds between the larynx disappeared. There was no difference in

TABLE 2 Difference of prototype blood components.

No.	Compound	Physiological state	Relative abundance of the physiological state	Pathological state	Relative abundance of the pathological state
1	Betaine	√	1	√	↓
2	Adenosine	√	1	-	0
3	Codonopsinol B	√	1	√	↑
4	Magnoflorine	√	1	√	↑
5	Peimisine	√	1	√	↑
6	Peimine	√	1	√	↑
7	Zhebeinone	√	1	√	↑
8	Peiminine	√	1	√	↑
9	Zhebeinine	√	1	√	↑
10	Ebeiedinone/ zhebeirine	√	1	√	↑
11	Ebeiedinone/ zhebeirine	√	1	√	↑
12	Vanillin	√	1	√	↓
13	Hesperetin	√	1	√	↓
14	Wogonin	√	1	√	↓
15	Honokiol	√	1	√	-
16	Magnolol	√	1	√	↓
17	Linoleic acid	√	1	√	-

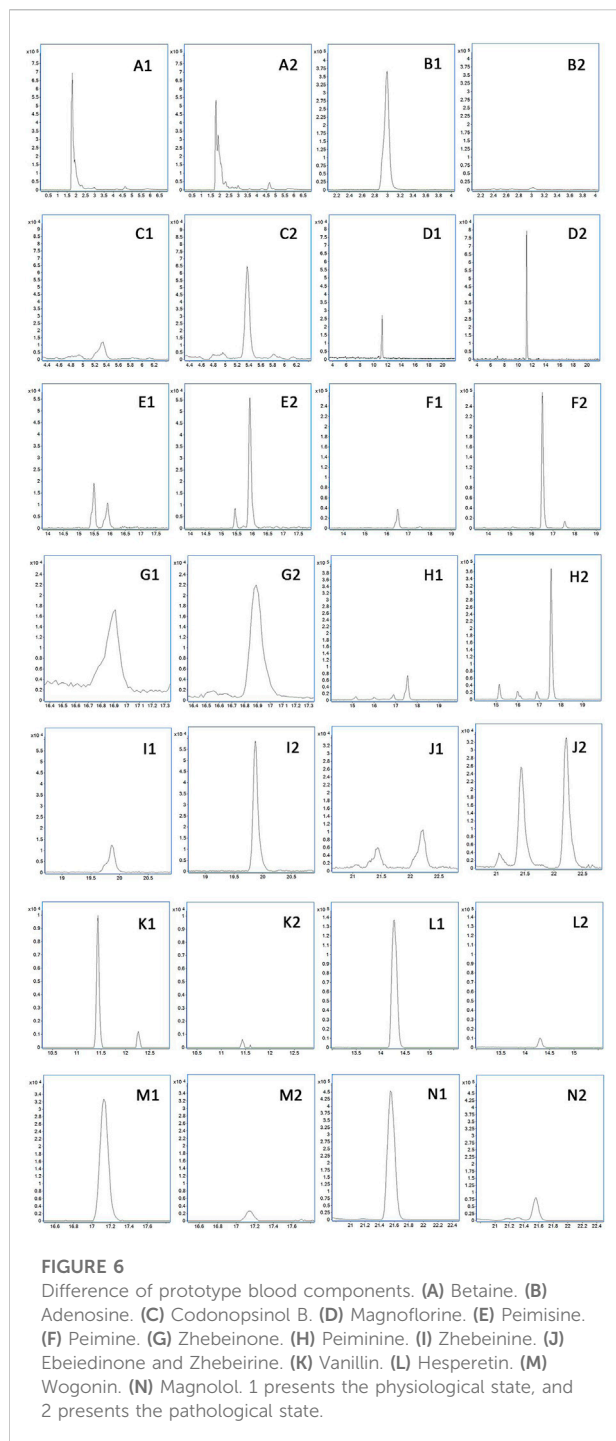
weight and water intake between the BJG high-dose and blank groups, and no deaths occurred.

Airway resistance refers to the viscous resistance generated by airflow, which is caused by the friction between airflow and the airway wall as well as by airflow itself when air flows through the airway during breathing. COPD is characterized by airflow restriction that is not completely reversible. Pulmonary function examination is the main objective index to judge airflow restriction, and it is an important index to diagnose COPD and evaluate the therapeutic effect (Kilk et al., 2018; Liu et al., 2018). Airway resistance is inversely related to the lung volume. In this study, sRaw, Raw, FRC, and other pulmonary function indicators reflecting airway resistance were significantly increased in the model group, while MV, PIF, PEF, and EF50 were significantly decreased, indicating that the COPD model was successfully established. The primary therapy for COPD is intended to reduce airway resistance (James et al., 2019). All doses of BJG treatment groups can significantly improve the phenomenon of increased airway resistance, decreased pulmonary compliance, airflow restriction, and airway obstruction in COPD rats, especially in the high-dose group. These results indicated

that BJG possesses protective effects on lung function in COPD rats and exerts a certain dose–effect relationship.

The main pathological changes of COPD are manifested by chronic bronchitis and emphysema (Jia et al., 2020). In this study, the lungs of rats in the model group showed obvious histopathological changes. Increased lung size, dark color, and scattered foci of necrosis were observed. Also, the number of pulmonary alveoli decreased significantly, with damaged structure, irregular expansion, and thinner walls. The alveolar space narrowed, and some of it broke and fused to form large vesicles, thus forming emphysema. In addition, there are a lot of inflammatory cells infiltrating the pulmonary interstitium, alveolar cavity, and vascular cavity and the lung tissue presents obvious pathological damage. The damage of lung tissue in each dose group of BJG was less severe than that in the COPD group. No emphysema was formed, only a few inflammatory cells were infiltrated, and the damage degree of lung tissue in the BJG high-dose group was the least.

The results of inflammatory factor detection in the serum and BALF of rats in each group showed that the levels of IL-6, IL-8, and TNF- α in the model group were significantly increased and the contents of NO and MMP-9 reflecting oxidative damage and tissue damage were also significantly increased as well as



those of PGE₂, reflecting vasodilatation and vascular permeability. The expression levels of the aforementioned factors were significantly reduced in different doses of BJG groups, manifesting that BJG can improve the vasodilation and vascular permeability of COPD rats, improve the inflammatory reaction, and reduce the oxidative damage and tissue damage of COPD rats in a dose–effect relationship.

For proving that BJG possesses an established therapeutic effect on COPD, the UPLC-QTOF-MS/MS technology was adopted to analyze the differences in chemical component metabolism in rats under physiological and pathological conditions so as to explore the effective chemical components of the prescription and the law of disease treatment. Based on the preliminary study on the chemical components of 95 monomers in BJG (Cui et al., 2020), 17 prototype monomers, namely, betaine, adenosine, codonopsinol B, magnoflorine, peimisine, peimine, zhebeinone, peiminine, zhebeinine, ebeiedinone, zhebeirine, vanillin, hesperetin, wogonin, honokiol, magnolol, and linoleic acid, were identified in the blood component of BJG. Among them, 11 were discovered in the comparison of reference materials and six in the secondary comparison; in addition, seven metabolites, namely, hypoxanthine oxidation products, sulfated formononetin, glucoaldehyde acidification and demethylation of citrine, glucoaldehyde acidification of calycosiflavone, protocathechuic acid methylation, 3-methoxy-caffeine-4-O-sulfate, and caffeine-3-O-sulfate, were confirmed in blood components. The products were derived from hypoxanthine, formononetin, citrine, calycosin, protocathechuic acid, and caffeic acid. Through this experiment, the research group found the tracks of 23 components in BJG in plasma and preliminarily clarified the blood transfer components and metabolism rules of the compound from *in vitro* to *in vivo*.

Through the comparative study on the blood components of BJG in physiological and COPD pathological states, it was found that 15 prototype components were detected in both physiological and pathological states. Among them, nine components increased in blood concentration in the pathological state and six prototype components decreased in blood concentration. Apart from that, seven metabolic components were detected under physiological and pathological conditions. Among them, five components increased in blood concentration and two components decreased in blood concentration. The aforementioned results show that the absorption of most chemical components is significantly enhanced when BJG is administered in the pathological state compared to that in the physiological state, and the structural types of these enhanced chemical components are mostly alkaloids and fatty acids, while the absorption of flavonoids and lignin is weakened. At the same time, it can be seen from the metabolites that the reason for the weakening of flavonoids and lignin components is related to the acceleration of compound metabolism in the pathological state, which leads to the decrease in peak time of components and the decrease in content at the same time. Furthermore, it is found that the physiological components include two more than the pathological prototype blood-entering components, namely, adenosine and wogonin, and the physiological components include one more than the pathological metabolites, which is hypoxanthine oxidation products. The reason is that, under pathological conditions, either the body performs poor

TABLE 3 Difference of metabolites in the blood.

No.	Compound	Physiological state	Relative abundance of the physiological state	Pathological state	Relative abundance of the pathological state
1	Hypoxanthine oxidation products	√	1	-	0
2	Formononetin sulfate	√	1	√	↑
3	Nobiletin glucuronidation and demethylation product	√	1	√	↓
4	Glucuronized calycosin	√	1	√	↑
5	Methylated product of protocatechuic acid	√	1	√	↑
6	3-Methoxy-caffeine-4-O-sulfate	√	1	√	↑
7	Caffeic acid-3-O-sulfate	√	1	√	↑

absorption of this compound or all of it is converted into related metabolites after absorption.

By comparing the differences in blood-entering components of the compound under pathological and physiological conditions, it is observed that there are significant differences in the metabolism of chemical components in BJG in rats under pathological and physiological models. The absorption of alkaloids and fatty acids in BJG under pathological conditions is enhanced, while the absorption of flavonoids and lignin is weakened. At the same time, it also objectively reflects the difference between taking drugs with disease and taking drugs without disease in traditional medicine. Thus, it provides data and theoretical support for the study on the metabolic mechanism of traditional Chinese medicine in different states.

Moreover, the chemical components absorbed in rat plasma are related to acute lung injury, asthma, and pulmonary fibrosis to varying degrees. There also exists a deeper relationship between these active components and pharmacodynamic indicators. Among the alkaloids, peimine and peiminine can alleviate LPS- or bleomycin-induced acute lung injury in rats. They can inhibit lung inflammation and pulmonary fibrosis, resulting in their apparent inhibition of inflammatory factors such as TNF- α , IL-6, IL-1 β , and IL-17 (Du et al., 2020; Liu et al., 2022). Betaine possesses anti-inflammatory activity, and it can reduce the inflammatory factors of TNF- α and IL-6 in the body (Detopoulou et al., 2008; Vinke et al., 2019). Ebeiedinone possesses a tracheobronchial relaxation effect (Wu et al., 2018). Most flavonoids possess potent anti-inflammatory activity, and some show antioxidant activity. For example, hesperetin can significantly reduce LPS-induced lung pathological injury and reduce the number of neutrophils and the levels of inflammatory cytokines TNF- α and IL-6 *in vivo* and *in vitro*. Also, the effect is related to regulating the TLR4-MyD88-NF- κ B signaling pathway, affecting the miR-410/SOX18 axis, and targeting the MD2 protein (Wang et al., 2019; Ye et al., 2019; Dong et al., 2020). Wogonin can prevent LPS-induced acute lung

injury and inflammation and inhibit the production of inflammatory cytokines such as TNF- α , IL-1 β , and IL-6. The mechanism is due to the regulation of the PPAR γ -involved NF- κ B pathway and the reduction of p38 MAPK and JNK phosphorylation (Yao et al., 2014; Wei et al., 2017). Formononetin has significant anti-inflammatory and antioxidant effects in a variety of diseases. In the study on treatment of asthma, it can diminish the expression of IL-4, IL-5, IL-13, IL-17A, IgE, CCL5, and CCL11, inhibit NF- κ B- and JNK-mediated inflammatory signaling, and reduce oxidative damage through decreasing the activity of ROS and increasing SOD (Yi et al., 2020). Calycosin has anti-inflammatory and antioxidant properties. It can obviously reduce the pathological damage to lung tissue and pulmonary edema in rats. The mechanism is through inactivating the HMGB1/MyD88/NF- κ B pathway and the NLRP3 inflammasome (Chen et al., 2021). Moreover, nobiletin and vanillin also exert anti-inflammatory activity (He et al., 2019; Costantini et al., 2021). Lignans are also related to anti-inflammatory and antioxidant properties. Honokiol can inhibit TGF- β /Smad signaling, matrix proteins, and the IL-6/CD44/STAT3 axis to reduce pulmonary fibrosis, which exerts anti-inflammatory and antioxidant effects (Pulivendala et al., 2020). Magnolol represents excellent protective effects on LPS-induced acute lung injury in rats. It can relieve lung tissue damage and downregulate the levels of proinflammatory factors such as TNF- α , IL-1 β and IL-6, which is related to PPAR- γ -dependent inhibition of NF- κ B activation (Ni et al., 2012; Lin et al., 2015). Furthermore, caffeic acid can decrease the suppression of TNF- α , NF- κ B, ERK1/2, STAT3, and JNK1/2 to play an anti-inflammatory role (Santos et al., 2019). Protocatechuic acid also possesses anti-inflammatory activity. Moreover, it can inhibit the inactivation of Smad2/3 proteins to exert the effect of inhibiting asthma airway remodeling (Lende et al., 2011; Liu et al., 2019).

In summary, as part of the research on the National Key R&D Program of China, this study proved that BJG is positively

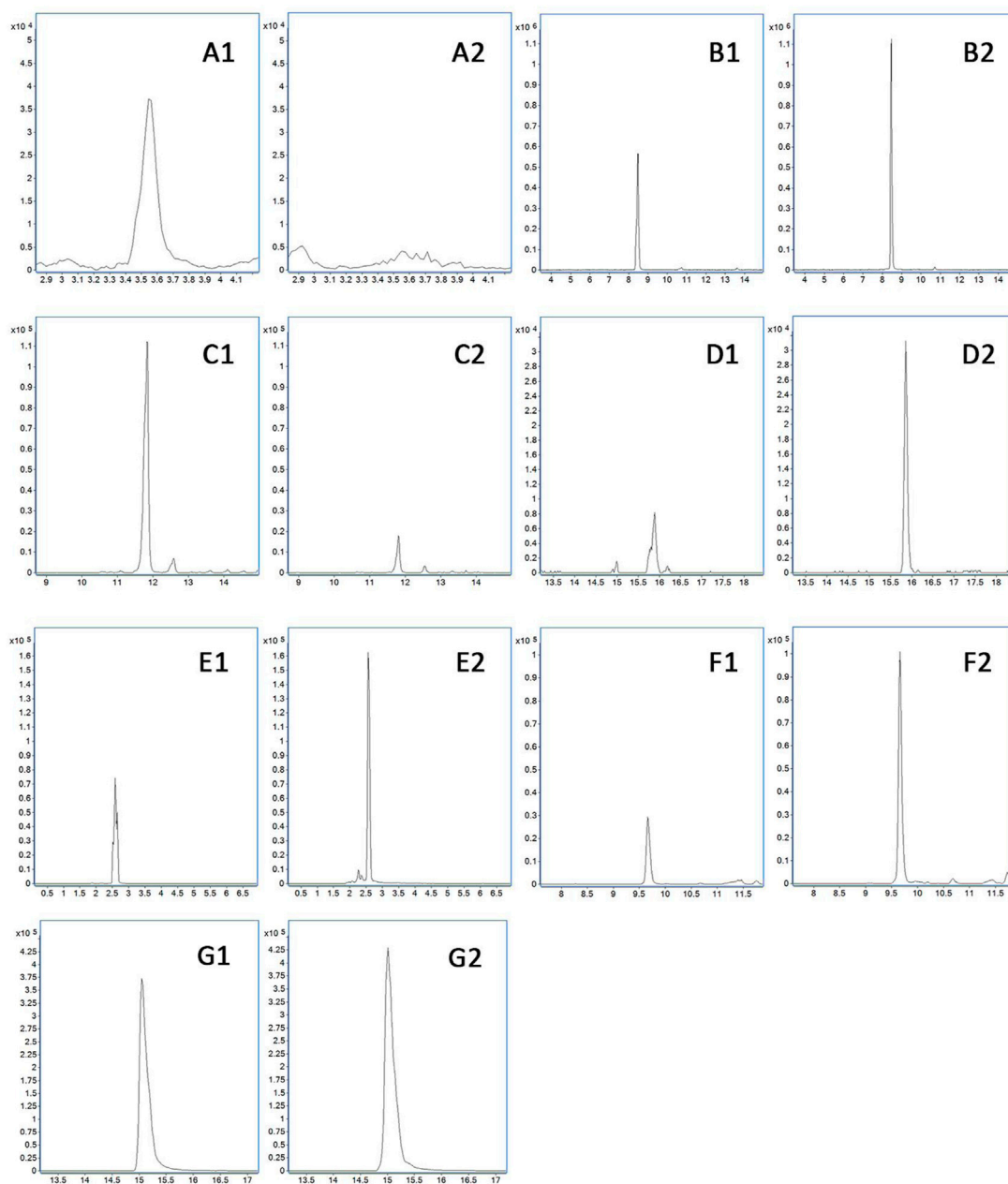


FIGURE 7

Difference of metabolites in the blood. (A) Hypoxanthine oxidation products. (B) Formononetin sulfate. (C) Nobiletin glucuronidation and demethylation product. (D) Glucuronized calycosin. (E) Methylated product of protocatechuic acid. (F) 3-Methoxy-caffeine-4-O-sulfate. (G) Caffeic acid-3-O-sulfate. 1 presents the physiological state, and 2 presents the pathological state.

effective for the treatment of COPD and revealed the active components and their metabolism, which provide reliable pharmacodynamic data for developing BJG into a Chinese patent medicine preparation with a national brand for the treatment of COPD. To achieve this, further research will be carried out around the mechanism of BJG curing COPD and evidence-based medicine.

5 Conclusion

BJG can improve the survival status of COPD rats, improve lung function, reduce lung injury, vasodilation, and vascular permeability, improve inflammatory reactions, reduce oxidative damage and tissue damage, and possess a superior protective effect on the lung function of COPD rats. There are

significant differences in the metabolism of chemical components of BJG in rats under pathological and COPD physiological states. Under pathological conditions, the absorption of alkaloids and fatty acids in BJG is enhanced, while the absorption of flavonoids and lignin is weakened. The aforementioned research provides a scientific basis for the development of BJG as a new clinical drug for the treatment of COPD.

Data availability statement

The original contributions presented in the study are included in the article/Supplementary Materials, further inquiries can be directed to the corresponding authors.

Ethics statement

The animal study was reviewed and approved by the Medicine Ethics Review Committee for Animal Experiments of Liaoning University of Traditional Chinese Medicine with approval number 2020YS013(KT)-013-01.

Author contributions

Study design: X-XY, SW, Y-RB, and X-SM; data collection: X-XY, L-LC, and T-JL; analysis and interpretation: X-XY, SW, and L-LC; statistical analysis: X-XY, SW, L-LC, and Y-RB; drafting the manuscript: X-XY and SW; manuscript revision:

SW, Y-RB, GB, and X-SM. All authors read and approved the final manuscript.

Funding

This study was supported by the National Key Research and Development Project (2018YFC1704805).

Conflict of interest

The authors declare that the research was conducted in the absence of any commercial or financial relationships that could be construed as a potential conflict of interest.

Publisher's note

All claims expressed in this article are solely those of the authors and do not necessarily represent those of their affiliated organizations, or those of the publisher, the editors, and the reviewers. Any product that may be evaluated in this article, or claim that may be made by its manufacturer, is not guaranteed or endorsed by the publisher.

Supplementary material

The Supplementary Material for this article can be found online at <https://www.frontiersin.org/articles/10.3389/fphar.2022.1090345/full#supplementary-material>

References

- Chen, C., Yao, X., Xu, Y., Zhang, Q., Wang, H., Zhao, L., et al. (2019). Dahuang Zhechong Pill suppresses colorectal cancer liver metastasis via ameliorating exosomal CCL2 primed pre-metastatic niche. *J. Ethnopharmacol.* 238, 111878. doi:10.1016/j.jep.2019.111878
- Chen, G. Y., Hou, Y., Li, X. G., Pan, R., and Zhao, D. C. (2021). Sepsis-induced acute lung injury in young rats is relieved by calyosin through inactivating the HMGB1/MyD88/NF- κ B pathway and NLRP3 inflammasome. *Int. Immunopharmacol.* 96, 107623. doi:10.1016/j.intimp.2021.107623
- Costantini, E., Sinjari, B., Falasca, K., Reale, M., Caputi, S., Jagarlapodii, S., et al. (2021). Assessment of the vanillin anti-inflammatory and regenerative potentials in inflamed primary human gingival fibroblast. *Mediat. Inflamm.* 2021, 5562340. doi:10.1155/2021/5562340
- Cui, L. L., Bao, Y. R., Wang, S., Li, T. J., and Meng, X. S. (2020). Identification of chemical constituents in Bufeijianpi formula by UPLC-Q-TOF-MS/MS. *Chin. J. Exp. Tradit. Med. Formulae* 26 (9), 184–193. doi:10.13422/j.cnki.syfx.20200547
- Detopoulou, P., Panagiotakos, D. B., Antonopoulou, S., Pitsavos, C., and Stefanadis, C. (2008). Dietary choline and betaine intakes in relation to concentrations of inflammatory markers in healthy adults: The ATTICA study. *Am. J. Clin. Nutr.* 87 (2), 424–430. doi:10.1093/ajcn/87.2.424
- Dong, J. Y., Zhou, H. Y., Zhao, H. Q., Zhao, Y. H., and Chang, C. (2020). Hesperetin ameliorates lipopolysaccharide-induced acute lung injury via the miR-410/SOX18 axis. *J. Biochem. Mol. Toxicol.* 34 (12), e22588. doi:10.1002/jbt.22588
- Du, B. X., Cao, L., Wang, K., Miu, J. J., Yao, L., Xu, Z. H., et al. (2020). Peiminine attenuates acute lung injury induced by LPS through inhibiting lipid rafts formation. *Inflammation* 43 (3), 1110–1119. doi:10.1007/s10753-020-01198-w
- He, P. P., Shen, Q. Q., Wen, M., Zou, J. Q., Wang, Y., Yang, J. X., et al. (2019). Nobiletin reduces LPL-mediated lipid accumulation and pro-inflammatory cytokine secretion through upregulation of miR-590 expression. *Biochem. Biophys. Res. Commun.* 508 (1), 97–101. doi:10.1016/j.bbrc.2018.11.075
- Huang, X., Guan, W. J., Xiang, B., Wang, W., Xie, Y. Q., and Zheng, J. P. (2022). MUC5B regulates goblet cell differentiation and reduces inflammation in a murine COPD model. *Respir. Res.* 23 (1), 11. doi:10.1186/s12931-021-01920-8
- James, P. H., Martin, L. M., Steve, D., and Philip, J. J. (2019). Physiologic and histopathologic effects of targeted lung denervation in an animal model. *J. Appl. Physiol.* 126 (1), 67–76. doi:10.1152/japplphysiol.00565.2018
- Jia, G. H., Yu, S. W., Sun, W. L., Yang, J., Wang, Y., Qi, Y. F., et al. (2020). Hydrogen sulfide attenuates particulate matter-induced emphysema and airway inflammation through nrf2-dependent manner. *Front. Pharmacol.* 11, 29. doi:10.3389/fphar.2020.00029
- Kilk, K., Aug, A., Ottas, A., Soomets, U., Altraja, S., and Altraja, A. (2018). Phenotyping of chronic obstructive pulmonary disease based on the integration of metabolomes and clinical characteristics. *Int. J. Mol. Sci.* 19 (3), 666. doi:10.3390/ijms19030666
- Lende, A. B., Kshirsagar, A. D., Deshpande, A. D., Muley, M. M., Patil, R. R., Bafna, P. A., et al. (2011). Anti-inflammatory and analgesic activity of protocatechuic acid in rats and mice. *Inflammopharmacology* 19 (5), 255–263. doi:10.1007/s10787-011-0086-4
- Li, J. S. (2020). International clinical practice guideline of Chinese medicine: Chronic obstructive pulmonary disease. *World J. Tradit. Chin. Med.* 6 (1), 39–50. doi:10.4103/wjtc.wjtc_9_20

- Li, J. S., and Li, S. Y. (2011). *China patent application No. 201110205234*. China: EPO.
- Li, J., Zhang, H., Ruan, H., Si, Y., Sun, Z., Liu, H., et al. (2020). Effects of Chinese herbal medicine on acute exacerbations of COPD: A randomized, placebo-controlled study. *Int. J. Chron. Obstruct. Pulmon. Dis.* 15, 2901–2912. doi:10.2147/COPD.S276082
- Li, W. X., Zhang, S. Q., Li, M. M., Zhang, H., Wang, X. Y., Niu, L., et al. (2022). Pharmacokinetic comparison of four major bio-active components of naoxintong capsule in normal and acute blood stasis rats using ultra-performance liquid chromatography coupled with triple-quadrupole mass spectrometry. *World J. Tradit. Chin. Med.* 8, 92–99. doi:10.4103/wjtcn.wjtcn_53_21
- Lin, J. G., Lyu, J., Sun, M. H., Liao, X., and Xie, Y. M. (2020). Systematic review and meta-analysis of shenfu injection on treating acute exacerbation of chronic obstructive pulmonary disease. *World J. Tradit. Chin. Med.* 6 (3), 276–283. doi:10.4103/wjtcn.wjtcn_30_20
- Lin, M. H., Chen, M. C., Chen, T. H., Chang, H. Y., and Chou, T. C. (2015). Magnolol ameliorates lipopolysaccharide-induced acute lung injury in rats through PPAR- γ -dependent inhibition of NF- κ B activation. *Int. Immunopharmacol.* 28 (1), 270–278. doi:10.1016/j.intimp.2015.05.051
- Liu, C. Y., Zhen, D., Du, H. H., Gong, G. H., Wu, Y., Ma, Q. Q., et al. (2022). Synergistic anti-inflammatory effects of peimine, peiminine, and forsythoside a combination on LPS-induced acute lung injury by inhibition of the IL-17-NF- κ B/ MAPK pathway activation. *J. Ethnopharmacol.* 295, 115343. doi:10.1016/j.jep.2022.115343
- Liu, W., Chen, Q., Liu, Z., Weng, Z., Nguyen, T. N., Feng, J., et al. (2021). Zihuai recipe alleviates cyclophosphamide-induced diminished ovarian reserve via suppressing PI3K/AKT-mediated apoptosis. *J. Ethnopharmacol.* 277, 113789. doi:10.1016/j.jep.2021.113789
- Liu, W., Liu, Z. G., Zhang, W. D., and Cai, S. X. (2018). Ulinastatin protects the lungs of COPD rats through the HMGB1/TLR4 signaling pathway. *Oncol. Lett.* 16 (3), 4057–4063. doi:10.3892/ol.2018.9123
- Liu, Y. D., Sun, X., Zhang, Y., Wu, H. J., Wang, H., and Yang, R. (2019). Protocatechuic acid inhibits TGF- β 1-induced proliferation and migration of human airway smooth muscle cells. *J. Pharmacol. Sci.* 139 (1), 9–14. doi:10.1016/j.jphs.2018.10.011
- Lu, E. Y., Pi, Z. F., Zheng, Z., Liu, S., Song, F. R., Li, N., et al. (2021). Rapid differentiation of Aconiti Kusnezoffii Radix from different geographic origins using ultra-performance liquid chromatography coupled with time-of-flight mass spectrometry. *World J. Tradit. Chin. Med.* 7, 71–77. doi:10.4103/wjtcn.wjtcn_52_20
- Luo, X. Q., Liu, J., Mo, L. H., Yang, G., Ma, F., Ning, Y., et al. (2021). Flagellin alleviates airway allergic response by stabilizing eosinophils through modulating oxidative stress. *J. Innate Immun.* 13 (6), 333–344. doi:10.1159/000515463
- Mao, J., Li, Y., Bian, Q., Xuan, Y., Li, J., Wang, Z., et al. (2022). The Bufeijianpi formula improves mucosal immune function by remodeling gut microbiota through the SCFAs/GPR43/NLRP3 pathway in chronic obstructive pulmonary disease rats. *Int. J. Chron. Obstruct. Pulmon. Dis.* 17, 1285–1298. doi:10.2147/COPD.S359428
- Ni, Y. F., Jiang, T., Cheng, Q. S., Gu, Z. P., Zhu, Y. F., Zhang, Z. P., et al. (2012). Protective effect of magnolol on lipopolysaccharide-induced acute lung injury in mice. *Inflammation* 35 (6), 1860–1866. doi:10.1007/s10753-012-9507-9
- Ono, M., Kobayashi, S., Hanagata, M., Ishida, M., Sato, H., Makiguchi, T., et al. (2020). Clinical characteristics of Japanese patients with chronic obstructive pulmonary disease (COPD) with comorbid interstitial lung abnormalities: A cross-sectional study. *PLoS One* 15 (11), e0239764. doi:10.1371/journal.pone.0239764
- Pelgrim, C. E., Wang, L., Peralta Marzal, L. N., Korver, S., Van Ark, I., Leusink-Muis, T., et al. (2022). Increased exploration and hyperlocomotion in a cigarette smoke and LPS-induced murine model of COPD: Linking pulmonary and systemic inflammation with the brain. *Am. J. Physiol. Lung Cell. Mol. Physiol.* 323 (3), L251–L265. doi:10.1152/ajplung.00485.2021
- Pershina, O. V., Pakhomova, A. V., Widera, D., Ermakova, N. N., Epanchintsev, A. A., Pan, E. S., et al. (2019). Gender differences in the pharmacological actions of pegylated glucagon-like peptide-1 on endothelial progenitor cells and angiogenic precursor cells in a combination of metabolic disorders and lung emphysema. *Int. J. Mol. Sci.* 20 (21), 5414. doi:10.3390/ijms20215414
- Pulivendala, G., Bale, S., and Godugu, C. (2020). Honokiol: A polyphenol neolignan ameliorates pulmonary fibrosis by inhibiting TGF- β /smad signaling, matrix proteins and IL-6/CD44/STAT3 axis both *in vitro* and *in vivo*. *Drug Deliv. Transl. Res.* 10 (2), 339–353. doi:10.1007/s13346-019-00690-7
- Rong, B. X., Fu, T., Rong, C. X., Liu, W., Li, K., and Liu, H. (2020). Association between serum CCL-18 and IL-23 concentrations and disease progression of chronic obstructive pulmonary disease. *Sci. Rep.* 10, 17756. doi:10.1038/s41598-020-73903-6
- Santos, E. S., de Moraes Oliveira, C. D., Menezes, I. R. A., do Nascimento, E. P., Correia, D. B., de Alencar, C. D. C., et al. (2019). Anti-inflammatory activity of herb products from *Licania rigida* Benth. *Complement. Ther. Med.* 45, 254–261. doi:10.1016/j.ctim.2019.06.001
- Shin, N. R., Kim, S. H., Ko, J. W., Park, S. H., Lee, I. C., Ryu, J. M., et al. (2017). HemoHIM, a herbal preparation, alleviates airway inflammation caused by cigarette smoke and lipopolysaccharide. *Lab. Anim. Res.* 33 (1), 40–47. doi:10.5625/lar.2017.33.1.40
- Song, X. Y., Hallensleben, C., Zhang, W. H., Jiang, Z. L., Shen, H. X., Gobbens, R. J. J., et al. (2021). Blended self-management interventions to reduce disease burden in patients with chronic obstructive pulmonary disease and asthma: Systematic review and meta-analysis. *J. Med. Internet Res.* 23 (3), e24602. doi:10.2196/24602
- Tang, S. H., Wang, Y. Q., Liao, Q., Jing, Y., and Zhang, H. C. (2019). Effects of Guben Zhike Recipe on pulmonary function and SIgA in model mice with chronic obstructive pulmonary disease. *Beijing J. Tradit. Chin. Med.* 38 (9), 893–897. doi:10.16025/j.1674-1307.2019.09.014
- Vinke, P., Bowen, T. S., Boekschoten, M. V., Witkamp, R. F., Adams, V., and van Norren, K. (2019). Anti-inflammatory nutrition with high protein attenuates cardiac and skeletal muscle alterations in a pulmonary arterial hypertension model. *Sci. Rep.* 9 (1), 10160. doi:10.1038/s41598-019-46331-4
- Wang, N. G., Geng, C. P., Sun, H. Y., Wang, X., Li, F. M., and Liu, X. C. (2019). Hesperetin ameliorates lipopolysaccharide-induced acute lung injury in mice through regulating the TLR4-MyD88-NF- κ B signaling pathway. *Arch. Pharm. Res.* 42 (12), 1063–1070. doi:10.1007/s12272-019-01200-6
- Wang, S., Yang, X. X., Li, T. J., Zhao, L., Bao, Y. R., and Meng, X. S. (2022). Analysis of the absorbed constituents and mechanism of liquidambaris fructus extract on hepatocellular carcinoma. *Front. Pharmacol.* 13, 999935. doi:10.3389/fphar.2022.999935
- Wang, S., Yang, X. X., Wang, W., Zhang, Y. K., Li, T. J., Zhao, L., et al. (2021). Interpretation of the absorbed constituents and pharmacological effect of Spica Schizonepetae extract on non-small cell lung cancer. *PLoS One* 16 (3), e0248700. doi:10.1371/journal.pone.0248700
- Wei, C. Y., Sun, H. L., Yang, M. L., Yang, C. P., Chen, L. Y., Li, Y. C., et al. (2017). Protective effect of wogonin on endotoxin-induced acute lung injury via reduction of p38 MAPK and JNK phosphorylation. *Environ. Toxicol.* 32 (2), 397–403. doi:10.1002/tox.22243
- Wu, X., Chan, S. W., Ma, J., Li, P., Shaw, P. C., and Lin, G. (2018). Investigation of association of chemical profiles with the tracheobronchial relaxant activity of Chinese medicinal herb Beimu derived from various *Fritillaria* species. *J. Ethnopharmacol.* 210, 39–46. doi:10.1016/j.jep.2017.08.027
- Yao, J., Pan, D., Zhao, Y., Zhao, L., Sun, J., Wang, Y., et al. (2014). Wogonin prevents lipopolysaccharide-induced acute lung injury and inflammation in mice via peroxisome proliferator-activated receptor gamma-mediated attenuation of the nuclear factor-kappaB pathway. *Immunology* 143 (2), 241–257. doi:10.1111/imm.12305
- Ye, J. Y., Guan, M. Q., Lu, Y., Zhang, D., Li, C. Y., Li, Y. P., et al. (2019). Protective effects of hesperetin on lipopolysaccharide-induced acute lung injury by targeting MD2. *Eur. J. Pharmacol.* 852, 151–158. doi:10.1016/j.ejphar.2019.02.042
- Yi, L., Cui, J., Wang, W. Q., Tang, W. F., Teng, F. Z., Zhu, X. Y., et al. (2020). Formononetin attenuates airway inflammation and oxidative stress in murine allergic asthma. *Front. Pharmacol.* 11, 533841. doi:10.3389/fphar.2020.533841
- Yu, X. Q., Wang, M. H., Li, J. S., Li, S. Y., Xie, Y., Bai, Y. P., et al. (2019). Effect of comprehensive therapy based on Chinese medicine patterns on self-efficacy and effectiveness satisfaction in chronic obstructive pulmonary disease patients. *Chin. J. Integr. Med.* 25 (10), 736–742. doi:10.1007/s11655-017-2417-9
- Zou, J. H., Sun, T., Song, X. H., Liu, Y. M., Lei, F., Chen, M. M., et al. (2022). Distributions and trends of the global burden of COPD attributable to risk factors by SDI, age, and sex from 1990 to 2019: A systematic analysis of GBD 2019 data. *Respir. Res.* 23 (1), 90. doi:10.1186/s12931-022-02011-y



OPEN ACCESS

EDITED BY
Zheng Xiang,
Liaoning University, China

REVIEWED BY
Li-Ping Bai,
Macao University of Science and
Technology, Macao SAR, China
Tao Liu,
China Medical University, China

*CORRESPONDENCE
Tie Qiao,
✉ qiao_0702@163.com

[†]These authors have contributed equally
to this work

SPECIALTY SECTION
This article was submitted to
Ethnopharmacology,
a section of the journal
Frontiers in Pharmacology

RECEIVED 10 November 2022
ACCEPTED 02 December 2022
PUBLISHED 21 December 2022

CITATION
Qiao T, Wang Y, Liang K, Zheng B, Ma J,
Li F, Liu C, Zhu M and Song M (2022),
Effects of the Radix Ginseng and Semen
Ziziphi Spinosae drug pair on the GLU/
GABA-GLN metabolic cycle and the
intestinal microflora of insomniac rats
based on the brain–gut axis.
Front. Pharmacol. 13:1094507.
doi: 10.3389/fphar.2022.1094507

COPYRIGHT
© 2022 Qiao, Wang, Liang, Zheng, Ma,
Li, Liu, Zhu and Song. This is an open-
access article distributed under the
terms of the [Creative Commons
Attribution License \(CC BY\)](https://creativecommons.org/licenses/by/4.0/). The use,
distribution or reproduction in other
forums is permitted, provided the
original author(s) and the copyright
owner(s) are credited and that the
original publication in this journal is
cited, in accordance with accepted
academic practice. No use, distribution
or reproduction is permitted which does
not comply with these terms.

Effects of the Radix Ginseng and Semen Ziziphi Spinosae drug pair on the GLU/GABA-GLN metabolic cycle and the intestinal microflora of insomniac rats based on the brain–gut axis

Tie Qiao^{1,2*†}, Yuan Wang^{1†}, Ke Liang¹, Bingyuan Zheng¹, Jin Ma³, Fangxiao Li¹, Chi Liu¹, Mingdan Zhu¹ and Meng Song¹

¹Liaoning Academy of Traditional Chinese Medicine Sciences, Liaoning University of Traditional Chinese Medicine, Shenyang, Liaoning, China, ²Guangdong Xin-Huangpu Joint Innovation Institute of Traditional Chinese Medicine, Guangzhou, Guangdong, China, ³The Second Affiliated Hospital of Liaoning University of Traditional Chinese Medicine, Shenyang, Liaoning, China

Introduction: To explore the mechanism of action of applying Radix Ginseng and Semen Ziziphi Spinosae Drug pair (R-S) in the treatment of insomnia by investigating the effect of R-S on GLU/GABA-GLN metabolic cycle and intestinal microflora of rats with insomnia.

Methods: Rats were intraperitoneally injected with 4-chloro-DL-phenylalanine (PCPA) to make sleep deprivation (SD) models. The rats were divided into 6 groups, with 8 rats in each group. The general status of the rats was observed and the pentobarbital sodium sleep synergy experiment was performed. The contents of GABA, GLU, GLN, GAD65, and GS in hippocampus of rats were determined by ELISA. The expressions of GABAAR α 1mRNA, mGluR5mRNA, NR1mRNA and GluR1mRNA in rats' hippocampal tissue were determined by Realtime PCR. 16SrRNA gene sequencing was used to analyze the intestinal microflora of insomnia rats.

Results: In PCPA-induced insomnia rats, the state of insomnia was relieved, the sleep rate was improved, the duration of sleep latency was shortened and the sleep duration was prolonged in each dose group of R-S ($p < 0.05$, $p < 0.01$) compared with the model group. The contents of GABA, GLN, GAD65 and GS were increased ($p < 0.05$, $p < 0.01$) while GLU content was decreased ($p < 0.01$) in both medium and high dose groups, especially in the high dose group. The expression of GABAAR α 1mRNA was increased ($p < 0.01$), and the expressions of mGluR5mRNA, NR1mRNA and GluR1mRNA were decreased ($p < 0.01$) in hippocampal tissue of rats in R-S groups, especially in the high dose group. At the same time, the various dose groups of R-S could improve the species diversity, microflora abundance of insomnia rats and regulate the KEGG metabolic pathway related to sleep.

Discussion: R-S can improve the sleep of PCPA-induced insomnia rats by regulating GLU/GABA-GLN metabolic cycle and intestinal microflora, which provides experimental basis for applying R-S in the treatment of insomnia.

KEYWORDS

Radix Ginseng–Semen Ziziphi Spinosae, drug pair, insomnia, GLU/GABA-GLN metabolic cycle, intestinal microflora

1 Introduction

Insomnia is a condition where patients have difficulty falling asleep, easily wake up, or cannot fall asleep after waking up. Traditional Chinese medicine (TCM) believes that the pathogenesis of insomnia is nothing more than the uneasiness aroused by a disorder of the body's function. Western medicine believes that the etiology of insomnia is complex, including physiology, psychology, age, and society; its pathogenesis is mainly believed to be related to the abnormal gamma-aminobutyric neuron system, central neurotransmitter disorder, and hypothalamic–pituitary–adrenal axis dysfunction (Chow and Cao, 2016; Vgontzas et al., 2020; Yang X. et al., 2021). Clinical drugs commonly used by Western medicine in the treatment of insomnia are divided into benzodiazepines (BZD) and non-BZD, with BZD being the first choice. However, both often induce drowsiness, dependence, withdrawal symptoms, and other side effects (Hua et al., 2021). TCM has a history of thousands of years in the treatment of insomnia and enjoys good clinical effects. It has a lower addiction tendency and fewer side effects. For instance, the Radix Ginseng and Semen Ziziphi Spinosae drug pair (R-S) is often used in the clinical treatment of insomnia. They are often combined in formulas such as Returning to Spleen Decoction (Gui Pi Tang), Heart-Nourishing Decoction (Yang Xin Tang), Celestial Emperor Heart-Tonifying Pill (Tian Wang Bu Xin Dan), and their compatibility can enhance the tranquilizing effect on the mind.

The brain–gut axis is a two-way information exchange system between the brain and intestine which is connected by the neuroendocrine, immune, and metabolic pathways. Intestinal microflora, an important link in the brain–gut axis, plays an important role in regulating digestion and absorption of the host, intestinal endocrine function, immune function, toxin clearance, and metabolism. Steady-state intestinal microflora maintains the integrity of the intestinal epithelial barrier and assists the host in resisting pathogen invasion. If the steady state between the intestinal microflora and the host is destroyed, then this flora will undermine the health of the host in, for example, the brain–gut axis, short-chain fatty acids, endotoxemia, energy absorption, choline, and the bile acid metabolism (Janssen and Kersten, 2015). Intestinal microflora plays an important role in the neuroendocrine pathway. By stimulating the afferent neurons of the intestinal nervous system, the intestinal

microflora generates synaptic connections between the intestinal and the vagus nerves, forming information transmission between the intestinal microflora and the brain (Li et al., 2018). Studies have shown that the disorder of intestinal microflora may be the mechanism leading to insomnia (Cryan John et al., 2019). For example, in the case of short-time sleep maintenance and fragmented sleep, the body breaks the balanced state of intestinal microflora by activating the HPA axis (Matenchuk Brittany et al., 2020), leading to the decline of beneficial bacteria and changing their metabolic function and level (Bowers et al., 2020).

Radix Ginseng is the dry root and rhizome of *Panax ginseng* C. A. Meyer. It has the effect of nourishing the heart and spleen, calming the mind, and intensifying intelligence. It is used for symptoms such as deficiency of the spleen and eating loss, palpitations, and insomnia. Semen Ziziphi Spinosae is the dry and mature seed of *Ziziphus jujube* (*Z. jujuba* Mill.var.*spinosa* (Bunge) HuexH.F.Chou), which has the effect of nourishing the heart, tonifying the liver, and calming the mind. It is suitable for symptoms such as irritation due to fatigue and insomnia, palpitations, and dreamfulness. According to the literature, ginsenoside Rg5/Rk1 can improve the GABA/GLU ratio and the expressions of the GABAA and GABAB receptors, thus improving sleep quality (Shao et al., 2020). Experimental studies have found that Semen Ziziphi Spinosae affects insomnia mainly by changing the contents of GABA and 5-HT, thus having a sedative and hypnotic effect (Yan J. et al., 2019). Studies have found that total saponins of Semen Ziziphi Spinosae can restore the intestinal microflora of insomniac rats to maintain the homeostatic flora (Cui, 2020). It was found that potential probiotics were up-regulated and the harmful bacterium TM7 was inhibited in the intestinal microflora of rats which were given ginseng extract (100 mg/kg) by long-term instillation (Sun et al., 2018). Li et al. (2020) found that R-S extracts (mass ratio 3:5) could significantly improve the relative abundance of Bacteroides and Firmicutes in insomniac rats, while the relative abundance of Actinobacteria decreased. Additionally, the extracts could significantly increase the relative abundance of beneficial bacteria in insomniac rats and reduce the relative abundance of *Bacillus coli*, Enterococcus, and other harmful bacteria.

It can be seen from the above that R-S can both relieve insomnia by affecting the level of neurotransmitters and expressions of receptors in the brain, and also regulate intestinal microflora. However, there has been no research on

the compatibility mechanism of the two in the treatment of insomnia. They two are often used together in clinical practice to nourish the spleen and calm the mind. Therefore, in this study, intraperitoneal PCPA injection was used to establish a rat model of insomnia. Based on the pharmacodynamics test of R-S, the mechanism of R-S in the treatment of insomnia was explored by studying the effect of R-S on the GLU/GABA-GLN metabolic cycle and the intestinal microflora of insomniac rats.

2 Materials and methods

2.1 Chemicals and reagents

Radix Ginseng and Semen Ziziphi Spinosae were sourced from Bozhou Sanfeng TCM decoction pieces Co., Ltd. (Hebei, China); both were authenticated by Professor Yanjun Zhai from Liaoning University of Traditional Chinese Medicine. 4-Chloro-DL-phenylalanine (PCPA) was purchased from Sigma-Aldrich Co., Ltd. (United States). GABA, GLU, GLN, GS, and GAD65 ELISA Kits were provided by AMEKO (Shanghai, China). Prime® Script RT Reagent Kit with gDNA Eraser, SYBR® Premix Ex Taq TMII (TliRNaseH Plus) were provided by Takara (Japan). Primer sequences were synthesized by Shanghai Sangong Bioengineering Co., Ltd. (Shanghai, China). Quant-iT PicoGreen dsDNA Assay Kit and TruSeq Nano DNA LT Library Prep Kit were purchased from Illumina (United States).

Following the Chinese pharmacopoeia, aqueous extraction was selected. R-S were soaked for 30 min in a 1:1 ratio of high, middle, and low dosage, respectively, and then boiled in 500 ml water for 30 min. The two decoctions were then mixed and concentrated into a crude drug containing R-S 0.216 g/ml, 0.163 g/ml, and 0.108 g/ml, respectively. After cold storage, the supernatant was centrifuged (15 min, 5,000 r/min). It was put into the material tank as the ultrafiltration material liquid, and the ultrafiltration pump was opened to extract and filter out a liquid of traditional Chinese medicine.

2.2 Animals and treatment

A total of 48 SPF male SD rats (180 ± 20 g) were purchased from Liaoning Changsheng Biotechnology Co., Ltd. (SCXK 2020-0001, Liaoning, China). These were randomly divided into six groups, including a control group (K), model group (M), diazepam group (DX), and G-Z groups with three R-S dosages (2.16 g/kg, 1.62 g/kg, 1.08 g/kg): a high-dose (G), medium-dose (Z), and low-dose (D) group ($n = 8$). All rats were fed in the Experimental Animal Center of Liaoning University of TCM (humidity 50%–65% at 18°C–24°C), with a 12-h light/dark cycle. Each group was allowed to eat and drink uncontrollably every day, and their bedding was changed every 2 days.

After a week of adaptive feeding, all rats were intraperitoneally injected with PCPA suspension (0.04 g/ml/d) according to method, with minor modifications (Lv et al., 2021; Guo et al., 2021) for 3 consecutive days; the same volume of saline was injected into the control group. Symptoms such as loss of circadian rhythm, shaggy hair or hair removal, reduced diet, and strong stress reaction were evidence of the model's success. From the 4th day on, the dose concentrations of the rats in each group were administered thus: high-dose R-S group 2.16 g/kg, medium-dose R-S group 1.62 g/kg, low-dose R-S group 1.08 g/kg, and diazepam group 0.001 g/ml. The rats of each group were intragastrically perfused with 2 ml every day. The model and control groups were given 2 ml distilled water every day for 15 consecutive days.

2.3 Sample collection

After an intragastric intervention, the rats were placed on the ultra-clean workbench and their lower abdomens were stimulated with a creep to defecate three to four particles. The feces were placed in a frozen tube and quickly transferred to a refrigerator at -80°C for storage. After the feces were collected, the rats were injected with 0.3 ml/100 g chloral hydrate to put them into a state of deep anesthesia. Their brains were taken out on the super-clean workbench and placed in the ice box. Their hippocampi were quickly separated according to the brain localization map, placed in EP tubes, preserved in liquid nitrogen, and quickly transferred to the refrigerator at -80°C .

2.4 Observation of rats' state

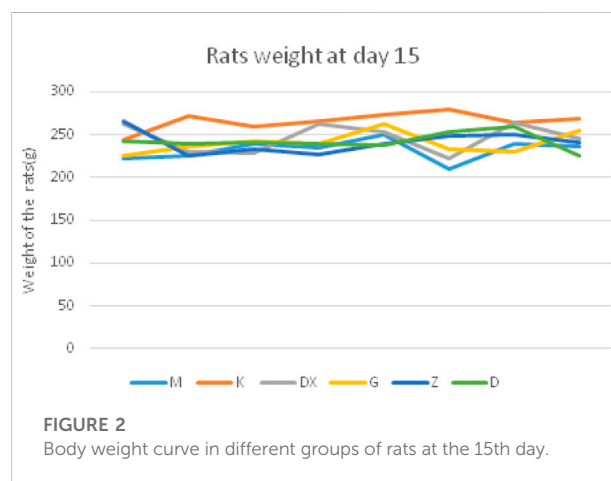
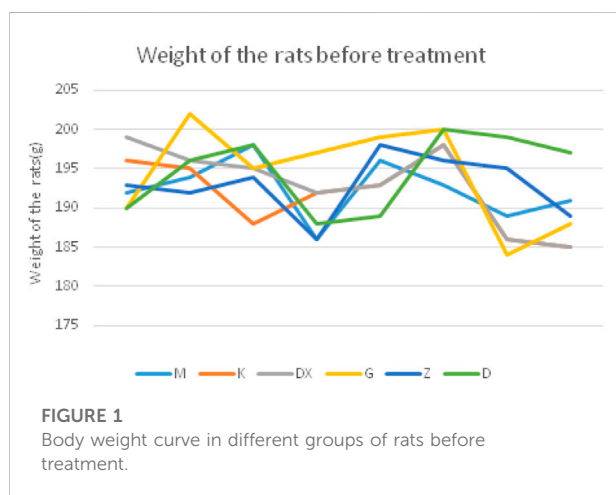
The rats' mental state (malaise or activity), diet (more, less, or normal), body weight (slow or normal weight gain), hair state (smooth or shaggy), and stress reaction (severe uncontrollable or controllable) were observed.

2.5 Pentobarbital sodium sleep synergistic experiment

Throughout the pre-experiment, the suprathreshold dose of pentobarbital sodium was 50 mg/kg and the subthreshold dose was 40 mg/kg. Six rats in each group were selected for the experiment. 1) Subthreshold dose experiment: pentobarbital sodium of 40 mg/kg was injected intraperitoneally in each group after intragastric administration, and the number of rats falling asleep in each group was observed and recorded. 2) Suprathreshold dose experiment: pentobarbital sodium of 50 mg/kg was injected after intragastric administration; the injection time, the disappearance time of righting reflex (with

TABLE 1 Table of primer sequences.

Gene name	Reference sequence	Primer sequences (5'-3')		Product size (bp)
GABAA α 1mRNA	NM_183,326	F	CGTGGTTCCAGAAAAGCCAA	79
		R	GCTGGTTGCTGTAGGAGCAT	
mGluR5mRNA	NM_017012	F	TGGGGAAACCCTAAGCTCCA	90
		R	GACAGTCGCTGCCACAAATG	
GluR1mRNA	NM_031608	F	GTCGAAGCGGATGAAGGGTT	70
		R	GGTCGATGTCCGTATGGCTT	
		R	CTCGGGAAGGCACAGCAATA	
β -actin	NM_031144	F	CGCGAGTACAACCTTCTTGC	70
		R	CGTCATCCATGGCGAACTGG	



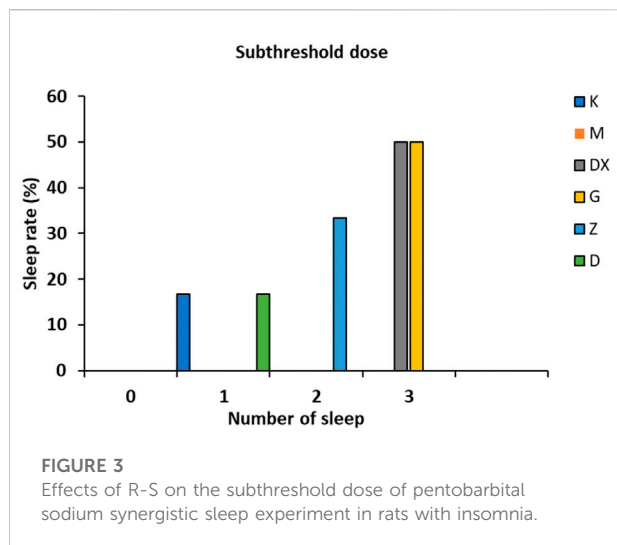
1 min as the standard), and the sleep duration (recovery of righting reflex as the standard) were observed and recorded for each group.

2.6 Analysis of the contents of GABA, GLU, GLN, GAD65, and GS in the hippocampi of the rats

Sodium chloride solution was added to 0.1 g hippocampal tissue and homogenized in a high-flux tissue grinder; 10% hippocampal homogenate was prepared. This was put into a centrifuge and centrifuged (at 4°C, 3000 r/min for 20 min) to obtain the supernatant. After treatment according to the instructions of the ELISA kit, the GABA, GLU, GLN, GS, and GAD65 content in the hippocampal tissue of rats was detected by an enzyme labeling instrument.

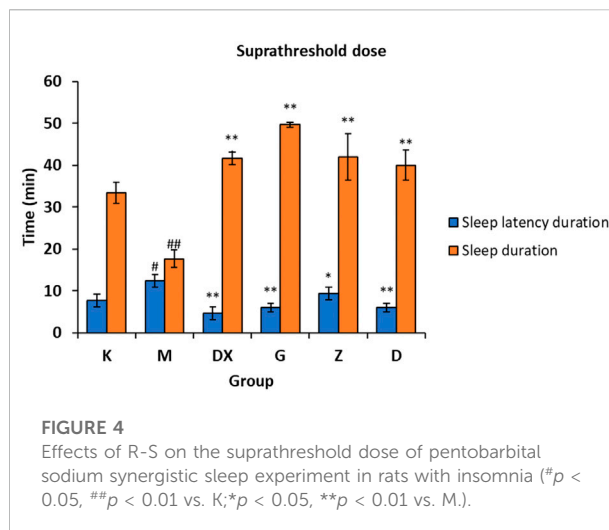
2.7 Expressions of GABAAR α 1mRNA, mGluR5mRNA, NR1mRNA, and GluR1mRNA in rat hippocampi

A quantity of 0.1 g hippocampal tissue was quickly ground in liquid nitrogen, and mRNA was extracted from the tissue using Trizol, chloroform, isopropanol, and DEPC water. The purity and concentration of RNA were then determined. We configured 10 μ L of DNA removal reaction solution, took a 1 μ L RNA sample, and added the reaction solution to 10 μ L, which was put into a PCR instrument to react (at 42°C for 2 min). The relative expressions of GABAAR α 1mRNA, mGluR5mRNA, NR1mRNA, and GluR1mRNA were calculated according to the 2-delta Ct (Livak) method. In the primer sequence, the primer design used Prime-BLAST (Table 1).



2.8 Analysis of intestinal microflora in rats with insomnia

The intestinal microflora of insomniac rats was analyzed by 16SrRNA gene sequencing technology. The above six groups of samples were delivered to Shanghai Paisenol Biotechnology Co., Ltd., and 16SrRNA gene sequencing technology was used to analyze the intestinal microflora. 1) The total DNA of the sample was extracted by a fecal DNA extraction kit and was quantified by NanoDrop. The extraction quality of DNA was detected by 1.2% agarose gel electrophoresis. 2) The corresponding primers were designed according to the conserved region of the sequence, and the variable region of the rRNA gene was amplified by PCR. 3) The PCR amplification products were purified by magnetic beads and quantified by fluorescence. 4) The TruSeq Nano DNA LT Library Prep Kit of Illumina was used to prepare the sequencing library. 5) MSeq sequencer (Illumina) was used for double-terminal sequencing; the corresponding reagent was MiSeq reagent Kit V3 (600cycles). The optimal sequencing length of the target fragment was 200-450bp. 6) Using QIIME software, high-quality sequences were obtained by quality control, denoising, splicing, and de-chimerism, and then classified according to 97% sequence similarity and operational taxonomic unit (OTU). 7) The most abundant sequence in each OTU was compared with the template sequence in the Greengenes database (Release13.8), obtaining the microflora of all OTUs at the classification levels of microbiology—including phylum, family, and genus. The fecal intestinal microflora was thus analyzed by species composition analysis, diversity analysis, and KEGG metabolic pathway prediction analysis.



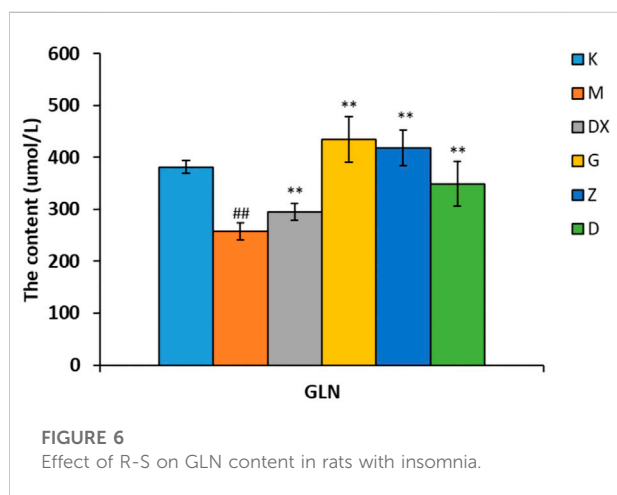
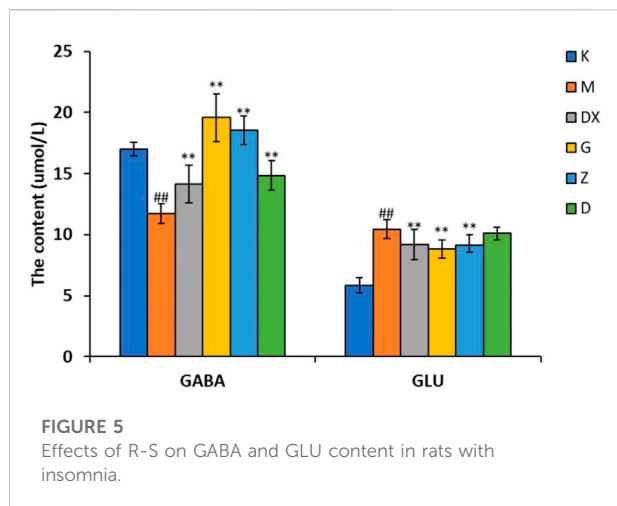
3 Results

3.1 Effects of R-S on the general state of insomniac rats

The rats in the control group were in a good mental state, having eaten an acceptable diet, gradually increased body weight, had smooth hair, and a slightly controllable stress response. Compared with the control group, rats in the model group were in low spirits, having eaten less food, gaining weight slowly, having dull and shaggy hair, and a strong stress response. Compared with the model group, the mental state, diet, weight, and other general states of the rats in the R-S administration groups were significantly improved, while the rats in the diazepam group were in a state of not resisting handling and being lethargic. The body weight curve of rats is described in Figure 1 and Figure 2.

3.2 Effects on the number of rats falling asleep induced by the subthreshold dose of pentobarbital sodium

As shown in Figure 3, no sleeping rats appeared in the model group. There were three sleeping rats in the diazepam group and the positive rate was up to 50.00%. There were three, two, and one sleeping rat in the high-, medium-, and low-dose groups, respectively, and the positive rates were 50.00%, 33.33%, and 16.66%, respectively, which all increased significantly.

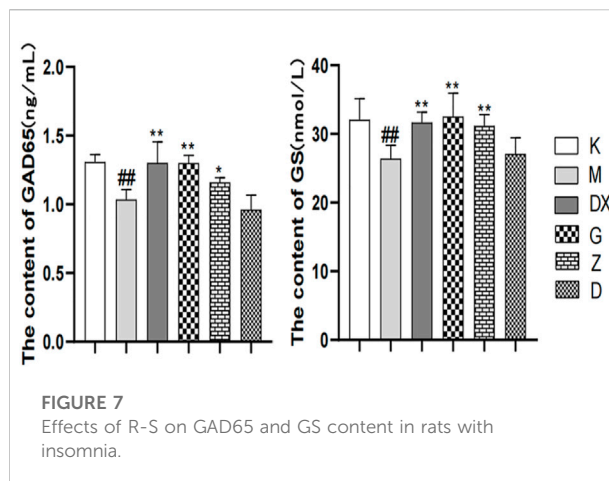


3.3 Effects on sleep latency and sleep duration induced by the suprathreshold dose of pentobarbital sodium in rats

As shown in Figure 4, compared with the control group, the sleep latency of the model group was significantly prolonged ($p < 0.05$) and the sleep duration was significantly shortened ($p < 0.01$) after administration. Compared with the model group, the sleep latency of the diazepam group and the high, medium, and low-dose R-S groups was shortened ($p < 0.05$, $p < 0.01$), and the sleep duration was significantly prolonged ($p < 0.01$).

3.4 Effects of R-S on the contents of GABA, GLU, GLN, GAD65, and GS in the hippocampi of insomniac rats

As shown in Figures 5–7, compared with the control group, the contents of GABA and GLN in the hippocampi of the rat

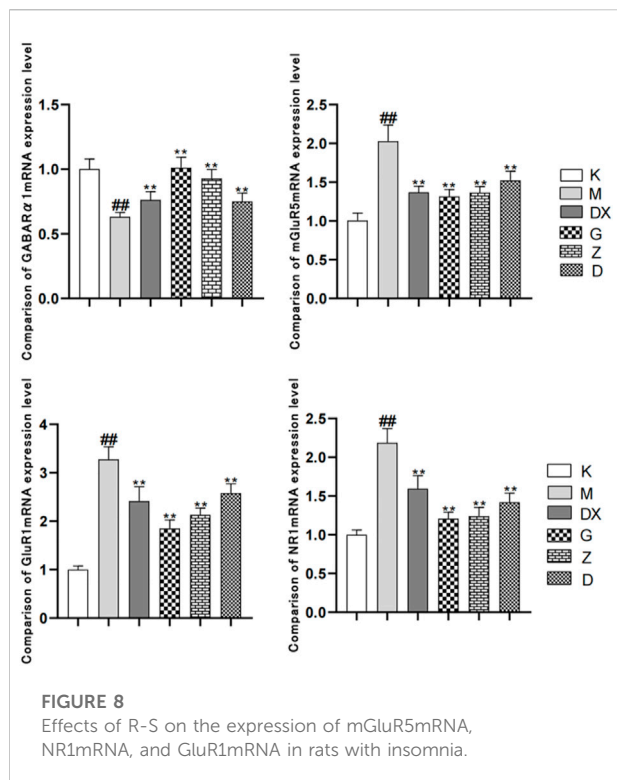


model group were significantly decreased ($p < 0.01$). Compared with the model group, the contents of GABA and GLN in the hippocampi of rats of the diazepam and the high-, medium- and low-dose R-S groups showed significant increase ($p < 0.01$). Compared with the control group, the GLU content of hippocampi in the model group significantly increased ($p < 0.01$). The GLU content of hippocampi in diazepam and the medium and high-dose R-S groups significantly decreased compared with the model group ($p < 0.01$). The low-dose R-S group had no significant difference to the model group. Compared with the control group, the contents of GAD65 and GS in the hippocampi of the model group were significantly decreased ($p < 0.01$), and the contents of GAD65 and GS in the hippocampi of the diazepam and the medium- and high-dose R-S groups were significantly increased compared with the model group ($p < 0.01$, $p < 0.05$). However, there was no significant difference between the low-dose group and the model group.

Insomniac rats were as described in the experiment. They were given medication or distilled water orally every day from the first day of insomnia. On the 16th day of insomnia, the expressions of GABA and GLU in the hippocampi of rats were detected by ELISA ($n = 8$ for each group). The results are expressed as the mean \pm SD, $^*p < 0.05$, $^{**}p < 0.01$ vs. K; $^*p < 0.05$, $^{**}p < 0.01$ vs. M.

Insomniac rats were as described in the experiment. They were given medication or distilled water orally every day from the first day of insomnia. On the 16th day of insomnia, the expressions of GLN in the hippocampi of rats were detected by ELISA ($n = 8$ for each group). The results are expressed as the mean \pm SD, $^*p < 0.05$, $^{**}p < 0.01$ vs. K; $^*p < 0.05$, $^{**}p < 0.01$ vs. M.

The effects of Radix Ginseng–Semen Ziziphi Spinosae on GAD65 and GS contents of the hippocampi of insomniac rats were regulated, as the insomniac rats described in the experiment were given medication or distilled water orally every day from the first day of insomnia. On the 16th day of insomnia, the expressions



of GAD65 and GS in the hippocampi of rats were detected by ELISA ($n = 8$ for each group). * $p < 0.05$, ** $p < 0.01$ vs. K; * $p < 0.05$, ** $p < 0.01$ vs. M.

3.5 Effects of R-S on the expressions of GABAAR α 1mRNA, mGluR-5mRNA, NMDA-NR1mRNA, and GluR1mRNA in the hippocampi of insomniac rats

As shown in Figure 8, compared with the control group, the GABAAR α 1mRNA level in the hippocampi of the model group was significantly decreased ($p < 0.01$). Compared with the model group, the levels of GABAAR α 1mRNA in the hippocampi of the diazepam and the high-, medium- and low-dose R-S groups were significantly increased, and the difference was statistically significant ($p < 0.01$). Compared with the control group, the expressions of mGluR5mRNA, NR1mRNA, and GluR1mRNA in the hippocampi of the model group were significantly increased ($p < 0.01$). Compared with the model group, the expressions of mGluR5mRNA, NR1mRNA, and GluR1mRNA in the diazepam, high-, medium- and low-dose R-S groups were significantly decreased and the difference was statistically significant ($p < 0.01$).

As shown in Figure 9A, the species accumulation curve showed that when the sample size was between 40 and 50, the species abundance in the community gradually stabilized, which confirms that the sample size was sufficient. As shown in Figure 9B, principal coordinate analysis (PCoA) showed that the composition of

intestinal microflora in the model group significantly differed from the control group ($p < 0.01$). The composition of intestinal microflora in the R-S groups significantly differed from the model group ($p < 0.01$) but was similar to the control group. The intestinal microflora of the diazepam group deviated from the model group with a significant difference ($p < 0.05$).

3.6 Effects of R-S on the species classification composition of intestinal microflora in insomniac rats

As shown in Table 2 and Figure 10, the intestinal microflora phyla mainly comprised Firmicutes, Bacteroidetes, Proteobacteria, and Actinobacteria. In this study, Firmicutes and Bacteroidetes were the most abundant in the intestinal tract of rats in each group. The proportions of Firmicutes, Bacteroidetes, Actinobacteria, and Proteobacteria in the intestinal microflora of rats in the control group were 36.65%, 60.95%, 1.25%, and 0.11%, respectively. The proportions of Firmicutes, Bacteroidetes, Proteobacteria, and Actinobacteria in the intestinal microflora of the model group were 49.68%, 38.42%, 1.49%, and 9.19%, respectively. Compared to the control group, the relative abundance of Bacteroidetes in the model group was lower ($p < 0.05$), and the relative abundance of Actinomycetes was significantly higher ($p < 0.01$). Compared with the model group, the relative abundance of Bacteroidetes in the intestinal tract of the diazepam group was higher ($p < 0.05$), the relative abundance of Bacteroidetes in the R-S groups was higher, while the relative abundance of Actinobacteria in the diazepam group was lower ($p < 0.01$). Meanwhile, the relative abundance of Actinobacteria in the R-S groups was significantly lower ($p < 0.01$). The F/B value of intestinal microflora (Firmicutes/Bacteroidetes) in the model group was higher than that in the control group, and the F/B value significantly decreased after RS intervention.

Figure 11 displays, at the family level, the top 30 abundant intestinal microflora in the intestinal tract of rats in each group, indicating that the intestinal microflora structure of rats in the model group was significantly different from that in the control group. Compared with the control group, the relative abundance of Paraprevotellaceae, Bacteroidaceae, Mogibacteriaceae, Rikenellaceae, Porphyromonadaceae, and Peptococcaceae were lower ($p < 0.05$, $p < 0.01$), while the relative abundance of Ruminococcaceae and Lachnospiraceae was lower, but there was no significant difference. The relative abundance of Peptostreptococcaceae, Alcaligenaceae, Streptococcaceae, Bacillaceae, Erysipelotrichaceae, Clostridiaceae, Turicibacteraceae, Staphylococcaceae, Corynebaccillaceae, and Coriobacteriaceae showed an upward trend ($p < 0.05$, $p < 0.01$). Compared with the model group, the relative abundance of Paraprevotellaceae was higher ($p < 0.05$), while the relative abundance of Coriobacteriaceae and

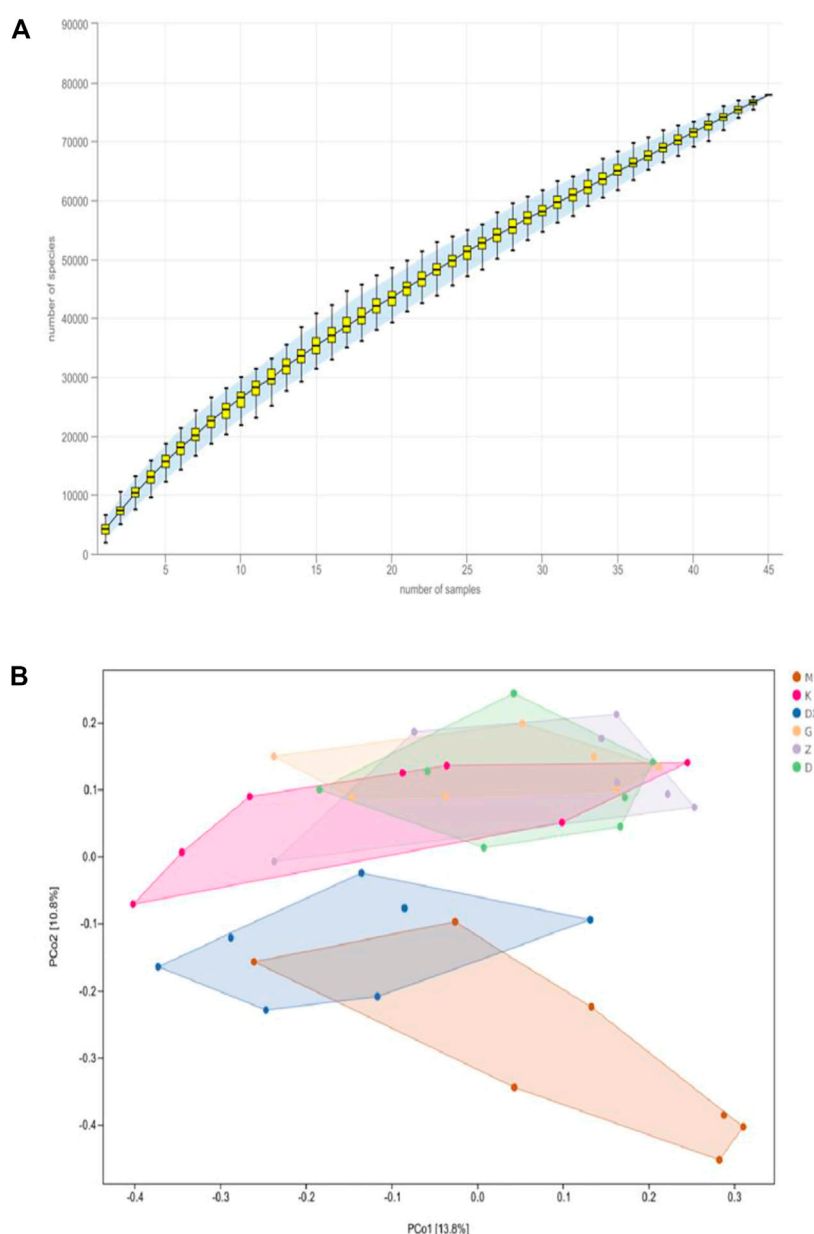


FIGURE 9
Effects of R-S on species accumulation curve (A) and principal coordinate analysis (B) of intestinal microflora in rats with insomnia ($n = 7$).

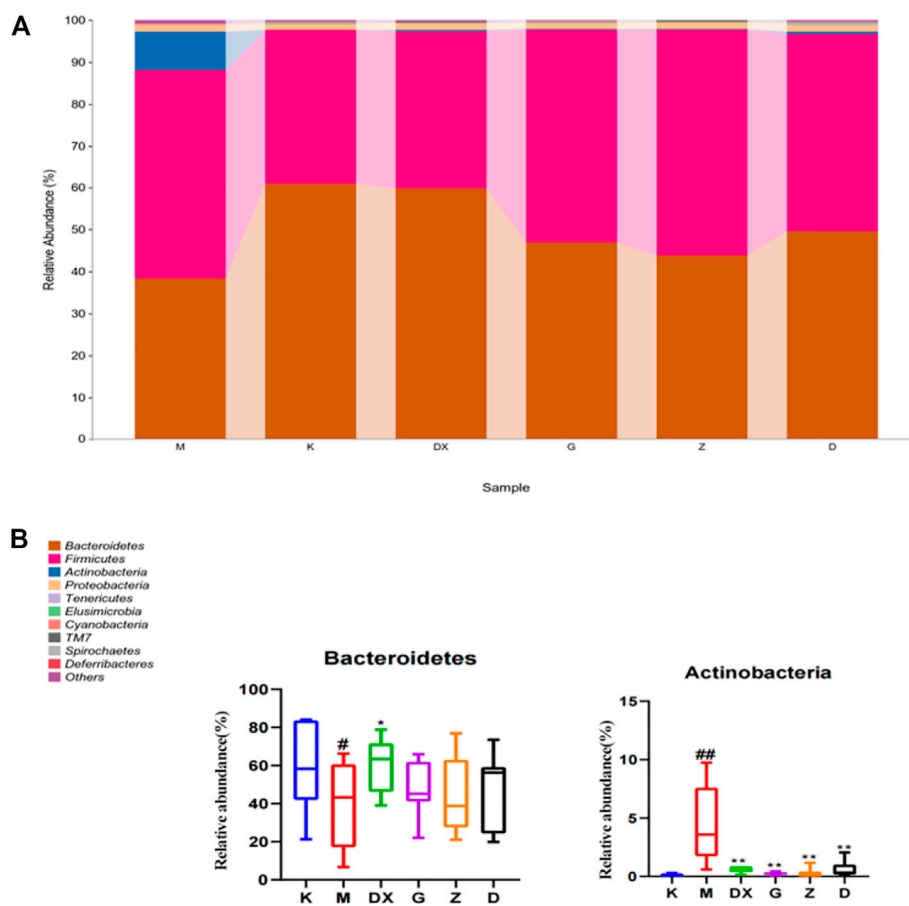
Staphylococcaceae was lower in the intestinal tract of rats in the diazepam group ($p < 0.05$, $p < 0.01$). The relative abundance of Paraprevotellaceae in the intestinal tract of rats in the R-S groups was up-regulated without significant difference, and the relative abundance of Bacteroidaceae was up-regulated, especially in the intestinal tract of rats in the high-dose group ($p < 0.01$). The relative abundance of Ruminococcaceae and Lachnospiraceae was up-regulated ($p < 0.05$, $p < 0.01$) and there was a significant difference in the intestinal tract of rats in the high- and medium-dose groups ($p < 0.05$, $p < 0.01$). The relative abundance of

Mogibacteriaceae, Porphyromonadaceae, and Peptococcaceae was higher ($p < 0.05$, $p < 0.01$). The relative abundance of Erysipelotrichaceae, Peptostreptococcaceae, Clostridiaceae, and Bacillaceae in the intestinal tract of rats in each dose group was lower ($p < 0.05$, $p < 0.01$). The relative abundance of Coriobacteriaceae, Alcaligenaceae, and Streptococcaceae in the intestinal tract of rats in the high- and medium-dose groups also showed a downward trend ($p < 0.05$, $p < 0.01$), while the relative abundance of Rikenellaceae in the intestinal tract of rats in the high- and low-dose groups decreased ($p < 0.01$). The relative

TABLE 2 Effects of R-S on species composition of the intestinal microflora of insomniac rats in phylum.

Phylum	K	M	DX	G	Z	D
Firmicutes	36.65%	49.68%	37.35%	50.80%	54.00%	46.97%
Bacteroidetes	60.95%	38.42% [#]	59.85% [*]	46.89%	43.71%	49.62%
Proteobacteria	1.25%	1.49%	1.40%	1.26%	1.34%	1.55%
Actinobacteria	0.11%	9.19% ^{##}	0.55% ^{**}	0.26% ^{**}	0.30% ^{**}	0.61% ^{**}
F/B	0.60	1.29	0.62	1.08	1.23	0.94

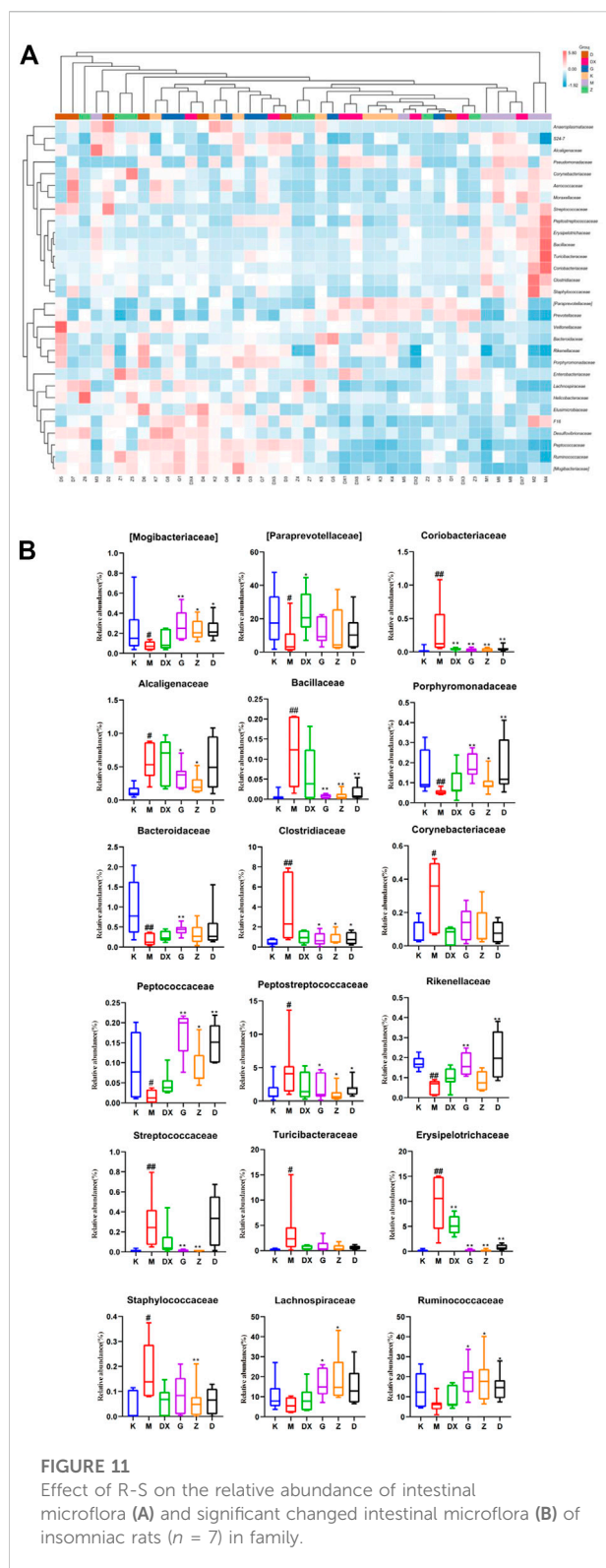
[#] $p < 0.05$, ^{##} $p < 0.01$ vs. K; ^{*} $p < 0.05$, ^{**} $p < 0.01$ vs. M.

**FIGURE 10**

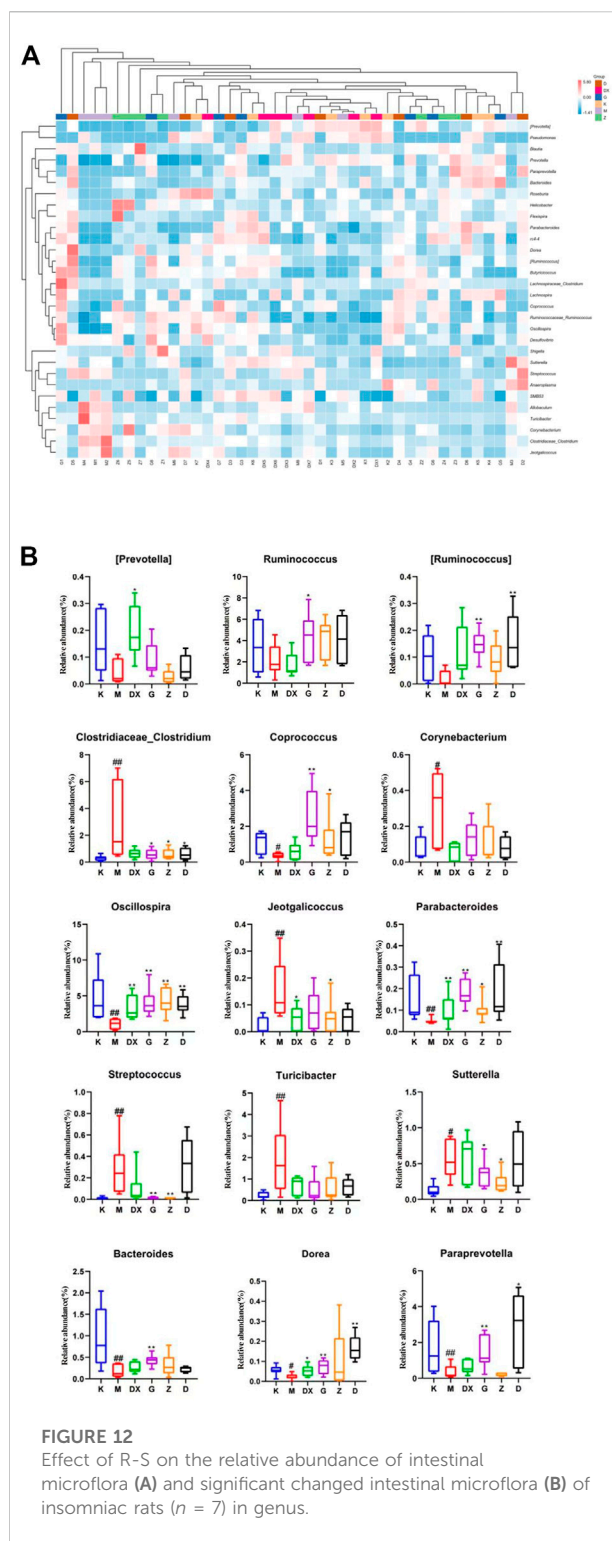
Effect of R-S on relative abundance of intestinal microflora (A) and significant changed intestinal microflora (B) of insomniac rats ($n = 7$) in phylum.

abundance of Staphylococcaceae decreased, which was most obvious in the intestinal tract of rats in the medium-dose group ($p < 0.01$), while the relative abundance of Turicibacteraceae and Corynebacteriaceae showed a decreasing trend without significant difference.

Figure 12 displays, at the genus level, the most abundant 30 intestinal microflora in the feces of rats in each group. Compared with the control group, the relative abundance of Paraprevotella, Bacteroides, Parabacteroides, Oscillospira, Coprococcus, Ruminococcus, and Dorea ($p <$



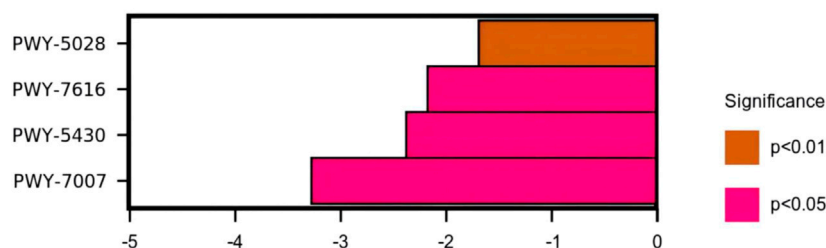
0.05, $p < 0.01$) in intestinal tract of rats in the model group was lower ($p < 0.05$, $p < 0.01$), and so was the relative abundance of Prevotella and Ruminococcus. However, there was no significant



difference. The relative abundance of Clostridium, Turicibacter, Jeotgalicoccus, Corynebacterium, Allobaculum, Sutterella, and Streptococcus was higher ($p < 0.05$, $p < 0.01$). Compared with the model group, the relative abundance of Prevotella, Paraprevotella,

TABLE 3 Analysis of metabolic pathway differences of intestinal microflora.

ID of pathway	Name of pathway	logFC	SD	P
PWY-5028	L-histidine degradation II	-1.682	0.3994	0.009858
PWY-7616	methanol oxidation to carbon dioxide	-2.167	0.5769	0.02222
PWY-5430	meta cleavage pathway of aromatic compounds	-2.369	0.6573	0.03025
PWY-7007	methyl ketone biosynthesis	-3.268	0.8135	0.01137

**FIGURE 13**
Differential analysis of the KEGG metabolic pathways.

Oscillospira, and Dorea in the intestinal tract of rats in the diazepam group was higher ($p < 0.05$, $p < 0.01$). The relative abundance of Oscillospira and Parabacteroides was higher in the intestinal tract of rats in the R-S groups ($p < 0.01$). The abundance of Prevotella was higher in the high- and medium-dose groups but there was no significant difference. The relative abundance of Ruminococcus, Paraprevotella, and Dorea in intestinal tract of rats in the R-S groups was significantly higher ($p < 0.01$), and the relative abundance of Coprococcus in the intestinal tract of rats in the high- and medium-dose group was higher ($p < 0.05$, $p < 0.01$). The relative abundance of Ruminococcus and Bacteroides in the intestinal tract of rats in the high-dose group was significantly increased ($p < 0.05$). The relative abundance of intestinal Allobaculum and Clostridium was significantly lower ($p < 0.05$, $p < 0.01$) in the intestinal tract of the rats in the R-S groups, and the relative abundance of intestinal Sutterella and Streptococcus was significantly lower ($p < 0.05$, $p < 0.01$) in the intestinal tract of the rats in the high- and medium-dose groups. The relative abundance of Jeotgalicoccus decreased most significantly in the medium-dose group ($p < 0.05$), while the relative abundance of Turicibacter and Corynebacterium in the R-S groups decreased without significant difference.

3.7 Effect of R-S on the metabolic pathway of insomniac rats

The use of the KEGG database and metagenomeSeq method identified metabolic pathways with significant differences between groups (Table 3 and Figure 13). Compared with the model group,

there were significant differences in the metabolic pathways of L-histidine degradation II ($p < 0.01$), methanol oxidation to carbon dioxide ($p < 0.05$), meta cleavage pathway of aromatic compounds ($p < 0.05$), and methyl ketone biosynthesis ($p < 0.05$) in the intestinal microflora of rats in the high-dose R-S group.

4 Discussion

Insomnia is closely related to the disorder of neurotransmitter levels in the metabolic cycle of GLU/GABA-GLN (Liu et al., 2021). This cycle is the main pathway for the metabolic regulation of GLU and GABA, which is very important for maintaining GLU and GABA levels in the brain, which maintain its dynamic balance of excitation and inhibition system (Guo, 2019). GABA is an inhibitory neurotransmitter in the central nervous system, which is decarboxylated by GLU under the action of glutamate decarboxylase (GAD). The isoenzyme GAD65 of GAD is mainly responsible for synthesizing synaptically released GABA. GABA binds to receptors (GABAA, GABAB, GABAC) in the synaptic space (Lang and Chen, 2015). The GABAA receptor is commonly used in the study of insomnia, and the A receptors play further roles as the GABAARα1 receptors (Liu et al., 2011). Studies have shown that the content of GABA can be reduced in the hypothalamus and cerebral cortex, as can the expression of GABAARα1 positive cells in PCPA insomniac rats (Zhong et al., 2021). Shen et al.

(2020) found that the content of GAD65 can be reduced in the brain of PCPA insomniac rats. GLU is an excitatory neurotransmitter in the central nervous system which is produced by glutamine (GLN) under the action of glutaminase. GLU is released in the synaptic space to bind to the receptor, having an excitatory role. About 20% of the neurons in the human brain are GLU neurons. GLU has an excitatory effect on neurons, but excessive GLU will produce neurotoxicity, leading to neuronal death and nervous system diseases (Machado-Vieira et al., 2012). Therefore, the remaining GLU in the synaptic space is transported by glutamate transporter to glial cells, where it is transformed into GLN by tricarboxylic acid cycle and under the action of glutamine synthetase (GS). It then enters the next cycle to avoid neurotoxicity caused by GLU accumulation.

The results showed that the level of GLU in the hypothalamus and brainstem of insomniac rats increased and the relative expression of GS protein decreased (Guo, 2019; Xing et al., 2021). GLU receptors are ion channel receptors (N-methyl aspartate receptor (NMDAR), α -amino-3-hydroxy-4-isooxy-propionic acid receptor (AMPA), kainic acid receptor (KAR)), which are coupled with ion channels to form receptor channel complexes for rapid signal transduction. The other is a metabolic receptor (mGluRs) which is activated by coupling with G-protein in the membrane to produce slow physiological effects through the signal transduction system. mGluR5mRNA is widely distributed in the brain, playing a very important role in the regulation of the normal physiological functioning of the brain nervous system with its downstream signals. It participates in physiological processes such as the plastic changes of learning, memorizing, and synaptic transmission efficiency (Francesconi et al., 2004). Studies have found that mGluR5mRNA is associated with schizophrenia (Matosin et al., 2018), depression (Cosson et al., 2018), autism (D'Antoni et al., 2014), Parkinson's (Vallano et al., 2013), Alzheimer's (Zhang et al., 2019), and many other neurological diseases. There are three subtypes of NMDAR—NR1, NR2, and NR3—among which NR1 plays a more extensive role (Zhao et al., 2012). It was found that sleep demand was positively correlated with the transcriptional level of NMDAR1 in the brain area of the ventrolateral preoptic nucleus. The transcriptional level of NMDAR1 was lower when sleep pressure was low, and the transcription of NMDAR1 increased when sleep pressure was high (Wang, 2021). The AMPA receptor is a tetramer, composed of four sub-units (GluR1-4), which mediates rapid excitatory synaptic transmission in the central nervous system. McDermott et al. (2006) found that the expression of GluR1 (sub-unit of AMPAR) in the cortex and hippocampus increased after complete sleep deprivation.

The results showed that the GABA and GAD65 content and the expression of GABAAR α 1 mRNA in the hippocampal tissue of the model group decreased. Compared with the model group, the GABA and GAD65 content in the hippocampus of the diazepam group and high- and

medium-dose R-S groups increased while the expression of GABAAR α 1 mRNA decreased, which was close to that of the control group—especially the high-dose group. The GLU content in the hippocampus of rats in the model group increased, while the GLN and GS contents decreased. Compared with the model group, the GLU content in the hippocampus of rats in the diazepam group and the high- and medium-dose R-S groups decreased, while the GLN and GS contents increased, which was close to those of the control group—especially the high-dose group. The expressions of mGluR5mRNA, NR1mRNA, and GluR1mRNA in the hippocampus of rats in the model group all increased ($p < 0.01$). Compared with the model group, the expressions of mGluR5mRNA, NR1mRNA and GluR1mRNA in the hippocampus of rats in each group decreased, which was close to those in the control group.

The intestinal microflora plays an important role in human physiology and metabolic homeostasis. Under physiological conditions, the amount of Firmicutes and Bacteroidetes parasitic on the large intestine account for about 90% of the intestinal microflora, and the ratio between them is closely related to susceptibility to some diseases. Research demonstrates that the value of F/B is significantly increased after sleep deprivation (Benedict et al., 2016). Actinobacteria can produce bio-active substances in animal intestines, but they are conditional pathogens. For example, *Corynebacterium*, *Mycobacteria*, etc. can cause disease (Zhao et al., 2020). At the phylum level, this study found that Firmicutes increased, Bacteroidetes significantly decreased, and the F/B ratio increased significantly in insomniac rats. At the same time, it was found that the number of Actinobacteria in the intestinal tract of rats in the model group was significantly higher than in the control group. The diazepam and R-S groups could adjust the relative abundance of Firmicutes, Bacteroidetes, and Actinobacteria to make them close to those of the control group in order to maintain the homeostasis of intestinal microflora to regulate sleep.

At the family level, it was found that the relative abundance of Paraprevotellaceae, Bacteroidaceae, Mogibacteriaceae, Rikenellaceae, Porphyromonadaceae, and Peptococcaceae in the intestinal tract of insomniac rats decreased significantly, as did the relative abundance of Ruminococcaceae and Lachnospiraceae. However, there was no significant difference. On the other hand, the relative abundance of Peptostreptococcaceae, Alcaligenaceae, Streptococcaceae, Bacillaceae, Erysipelotrichaceae, Clostridiaceae, Turicibacteraceae, Staphylococcaceae, Corynebacteriaceae, and Coriobacteriaceae increased significantly. The relative abundance of beneficial bacteria such as Bacteroidaceae, Paraprevotellaceae, Ruminococcaceae, Lachnospiraceae, Rikenellaceae, and Porphyromonadaceae in the intestines of insomniac rats was all down-regulated. Tianwang Buxin Granule can play a role in calming the nerves by regulating the disordered intestinal flora of perimenopausal female insomniac patients, which is manifested by the decrease in the detection of *Barriella rosenbergii*, rumen

coccus, *Platyclusus*, and *Clostridium saccharose* in feces. The proportion of *Clostridium praecox*, *Bacteroides*, *Bacteroides faecalis*, *Bifidobacterium* and *Lactobacillus* increased (Yang et al., 2020). The acetic acid and lactic acid produced by beneficial bacteria can reduce intestinal Eh and PH values, improve the micro-environment of the intestine, protect the intestinal tract, and inhibit the growth of pathogenic bacteria. In addition, its metabolites have certain nutritional effects. The relative abundance of pathogenic or conditional pathogenic bacteria such as *Peptostreptococcaceae*, *Alcaligenaceae*, *Streptococcaceae*, *Erysipelotrichaceae*, *Turicibacteraceae*, *Staphylococcaceae*, *Corynebacteriaceae*, and *Coriobacteriaceae* increase in the intestinal tract of insomniac rats, which destroys the intestinal mucosal barrier, secretes a large amount of endotoxin, and increases intestinal permeability—further persecuting intestinal epithelial cells and causing intestinal inflammation. Zhao showed that Buzhong Yiqi Decoction can reduce the intestinal pathogenic bacteria of insomniac patients, increase the flora which maintains intestinal homeostasis, and improve the sleep state of insomniac patients with spleen deficiency (Zhao, 2020).

This study found that the relative abundance of beneficial bacteria such as *Paraprevotellaceae*, *Bacteroidaceae*, *Rikenellaceae*, and *Porphyromonadaceae* were up-regulated in each R-S group, especially in the high-dose group ($p < 0.05$, $p < 0.01$). However, the relative abundance of *Peptostreptococcaceae*, *Alcaligenaceae*, *Streptococcaceae*, *Erysipelotrichaceae*, *Turicibacteraceae*, *Staphylococcaceae*, *Corynebacteriaceae*, and *Coriobacteriaceae* decreased, which was close to those of the control group. The effect of high-dose R-S on pathogenic bacteria was particularly obvious ($p < 0.05$, $p < 0.01$). Although the relative abundance of beneficial bacteria in the intestinal tract of rats in the diazepam group showed an upward trend and the relative abundance of pathogenic bacteria decreased, there was no significant difference compared to the model group. All groups can thus promote the intestinal microflora of insomniac rats to return to a steady state, increasing the relative abundance of beneficial bacteria and reducing the relative abundance of pathogenic bacteria. However, the high-dose R-S group showed the best effect.

It was found that the relative abundance of *Paraprevotella*, *Bacteroides*, *Parabacteroides*, *Oscillospira*, *Coprococcus*, *Ruminococcus*, and *Dorea* decreased significantly in the intestinal tract of insomniac rats. The relative abundance of *Prevotella* and *Ruminococcus* decreased, but there was no significant difference. The relative abundance of *Clostridium*, *Turicibacter*, *Jeotgalicoccus*, *Corynebacterium*, *Allobaculum*, *Sutterella*, and *Streptococcus* increased significantly. The relative abundance of *Prevotella* in the intestines of patients with spleen deficiency and insomnia decreased significantly, while the relative abundance of *Sutterella* increased (Zhao, 2020). The relative abundance of *Ruminococcus* in the intestinal tract of insomniac patients with spleen-stomach disharmony decreased (Huang et al., 2019), which was consistent with the results of this experiment. A variety of

neurotransmitters are produced in the intestinal tract, and intestinal microflora is the main producer of neurotransmitters (Huang et al., 2019). Strandwitz P et al. (2019) found that *Bacteroides* can produce a large amount of GABA. Liu Shujun et al. (2020) found that *Bacteroides* can secrete GAD and metabolize GLU to produce GABA. Olson et al. (2018) found that epilepsy can be treated by up-regulating the abundance of *Parabacteroides* and thus increasing the ratio of GABA/GLU. There is thus a positive correlation between *Parabacteroides* and the content of GABA.

In addition, it was found that the relative abundance of *Bacteroides* in the intestines of peri-menopausal insomniac patients decreased (Yang Y. W. et al., 2021). Thompson Robert S et al. (2021) found that an intake of probiotics for rats could increase the relative abundance of healthy microorganisms such as *Parabacteroides*, improve the intestinal micro-environment, and promote the recovery of sleep and a circadian rhythm. It can be inferred that *Parabacteroides* are closely related to sleep.

Chen Yiran et al. (2020) identified a positive correlation between *Oscillospira* and amount of sleep. Zhang et al. (2021) identified a negative correlation between *Coprococcus*, *Dorea*, and PSQI in the intestinal microflora of patients with severe depression associated with sleep disorder, demonstrating that *Coprococcus* and *Dorea* could promote sleep. *Clostridium* is a strict anaerobic bacillus containing *Clostridium botulinum*, *C. tetanus* and *C. perfringens*. Yu ShuYan et al. (2008) found that the application of *C. tetanus* neurotoxin could increase the expression of AMPAR on the cell surface. Animal experiments showed that the relative abundance of *C. perfringens* in the intestine of intermittent sleep-deprived mice increased significantly (Li et al., 2016), as did *perfringens* in the intestinal tract of sleep-deprived rats (Wang et al., 2017). Cui Xiaofang's study found that the relative abundance of *Clostridium* and *Turicibacter* in insomniac patients increased significantly. *Corynebacterium* is a genus of *Actinobacteria*. *Corynebacterium* glutamate can be used to produce GLU (Long et al., 2019). As a central excitatory neurotransmitter, glutamate often leads to insomnia. In this study, it was found that the content of GABA in the hippocampi of insomniac rats decreased significantly, as did the relative abundance of *Bacteroides* and *Parabacteroides* in their intestinal tracts, further suggesting that the brain and intestine must be related and that intestinal microflora can affect sleep through neuroendocrine pathways. It was found that the relative abundance of *Oscillospira* in the model group decreased, which was consistent with the results of Chen Yiran et al. (2020).

The relative abundance of *Coprococcus* and *Dorea* decreased in the insomniac rats in the model group, which was consistent with Zhang Qi's study. In this experiment, it was found that the relative abundance of *Clostridium* in the intestinal tract of the model group rats increased significantly, as did the expression of *GluR1mRNA* (sub-unit of AMPA receptor) in their hippocampi. Thus, the intestinal microflora can affect sleep by regulating the expression of neurotransmitter receptors. This experiment found

that the relative abundance of *Clostridium* and *Turicibacter* increased significantly in insomniac rats, which was consistent with Cui Xiaofang's study. In addition, the GLU content in the hippocampi of insomniac rats increased significantly, as did the relative abundance of *Corynebacterium* in the intestinal tract. The experiment found that, compared with the model group, all the treatment groups could adjust the abundance of bacteria to restore the intestinal microecological environment. It was found that the relative abundance of *Prevotella*, *Paraprevotella*, *Oscillospira*, and *Dorea* in the intestinal tract of rats in the diazepam group was significantly up-regulated, while *Bacteroides*, *Parabacteroides*, *Ruminococcus*, and *Coprococcus* were up-regulated with no significant difference. The relative abundance of *Clostridium*, *Turicibacter*, *Jeotgalicoccus*, *Corynebacterium*, *Allobaculum*, *Sutterella*, and *Streptococcus* decreased, but there was no statistical significance. The relative abundance of *Oscillospira* and *Parabacteroides* in the intestines of rats in the R-S groups increased significantly, and the relative abundance of *Prevotella* in the high- and low-dose groups increased, but not significantly. However, the relative abundance of *Ruminococcus*, *Paraprevotella*, and *Dorea* increased significantly, as did the relative abundance of *Coprococcus*, *Ruminococcus* and *Bacteroides* in the high-dose group. The relative abundance of *Corynebacterium* and *Clostridium* in each R-S group decreased significantly, the relative abundance of *Sutterella* and *Streptococcus* decreased significantly in the high- and medium-dose groups, and the relative abundance of *Jeotgalicoccus* decreased most significantly in the medium-dose group. The relative abundance of *Turicibacteraceae* and *Corynebacterium* decreased but not significantly. It can be seen from the above that the R-S groups had a better regulatory effect on the intestinal microflora of insomniac rats—especially the high-dose group. Consequently, applying R-S to improve the sleep condition of insomniac rats is closely related to the regulation of their intestinal microflora.

Through analysis of the KEGG functional metabolic pathway, it can be shown that high-dose R-S mainly affects the pathways of L-histidine degradation II, methanol oxidation to carbon dioxide, the meta cleavage pathway of aromatic compounds, and methyl ketone biosynthesis, in which the metabolic pathway of L-histidine degradation II may be related to the reduction of the relative abundance of histidine-producing bacteria in the intestinal tract of insomniac rats. As an important substance to promote awakening, histidine can excite the central nervous system to provoke insomnia. Yang Yuhan et al. (2020) found that one of the main ways that insomnia is caused by a heart–kidney imbalance is by unbalancing the body's histidine metabolism. Studies have found that methanol can damage the central nervous system of humans, resulting in insomnia, dreamfulness, and blurred vision (Feng et al., 2004). Yan Jiao et al. (2019) found that methanol inhalation causes

neurotoxicity and significant nerve cell apoptosis in rats. Therefore, the metabolic pathway of methanol oxidation to carbon dioxide may be related to high-dose R-S to reduce the relative abundance of methanol-producing bacteria. Both aromatic compounds and methyl ketones easily cause neurotoxicity and can harm the central nervous system of humans. This study found that the relative abundance of intestinal microflora involved in the meta cleavage pathway of aromatic compounds and methyl ketone biosynthesis metabolic pathways in insomniac rats in the high-dose R-S group was significantly lower than that in the model group.

Radix Ginseng and *Semen Ziziphi Spinosae* could affect the amount of GABA, GLN, GAD65, and GS and the expressions of mGluR5mRNA, NR1mRNA, and GluR1mRNA in the hippocampal tissue in rats induced by PCPA to insomnia through the GLU/GABA-GLN metabolic cycle. R-S can regulate the flora structure in the intestine of insomniac rats, increase beneficial intestinal bacteria, and reduce pathogenic bacteria to restore the homeostasis of the intestinal micro-environment. Therefore, the effect of R-S on the sleep of insomniac rats is closely related to the regulation of intestinal microflora. This experiment provides an experimental basis for potential action targets of insomnia treatment and the use of R-S in the treatment of insomnia.

Data availability statement

The original contributions presented in the study are included in the article/Supplementary Material; further inquiries can be directed to the corresponding author.

Ethics statement

The animal study was reviewed and approved by the Experimental Animal Ethics Committee of Liaoning University of TCM.

Author contributions

TQ: research design, conducted experiments, collected data, and contributed to manuscript writing. YW: conducted experiments, collected data, and contributed to manuscript writing. KL, BZ, and JM: conducted experiments and contributed to manuscript writing. FL, CL, and MZ: conducted experiment and performed data analysis. MS: manuscript writing.

Funding

This study was supported by grants from the innovative talents in colleges and universities of Liaoning Province (No. LR2019039).

and the platform construction of Liaoning University of traditional Chinese Medicine (No. 2019JH6/10100002).

Acknowledgments

This is a short text to acknowledge the contributions of specific colleagues, institutions, or agencies that aided the efforts of the authors.

Conflict of interest

The authors declare that the research was conducted in the absence of any commercial or financial relationships that could be construed as a potential conflict of interest.

References

- Benedict, C., Vogel, H., Jonas, W., Woting, A., Blaut, M., Schurmann, A., et al. (2016). Gut microbiota and glucometabolic alterations in response to recurrent partial sleep deprivation in normal-weight young individuals. *Mol. Metab.* 5 (12), 1175–1186. doi:10.1016/j.molmet.2016.10.003
- Bowers, S. J., Vargas, F., González, A., He, S., Jiang, P., Dorrestein, P. C., et al. (2020). Repeated sleep disruption in mice leads to persistent shifts in the fecal microbiome and metabolome. *PLoS one* 15 (2), e0229001. doi:10.1371/journal.pone.0229001
- Chen, Y. R., Zheng, H. M., Zhang, G. X., Chen, F. L., Chen, L. D., and Yang, Z. C. (2020). High Oscillospira abundance indicates constipation and low BMI in the guangdong gut microbiome project. *Sci. Rep.* 10 (1), 9364. doi:10.1038/s41598-020-66369-z
- Chinese Pharmacopoeia Commission (2020a). “Radix ginseng,” in *Chinese pharmacopoeia* (Beijing: China Medical Science and Technology Press), 8.
- Chinese Pharmacopoeia Commission (2020b). “Semen Ziziphi Spinosae,” in *Chinese pharmacopoeia* (Beijing: China Medical Science and Technology Press), 382.
- Chow, M., and Cao, M. (2016). The hypocretin/orexin system in sleep disorders: Preclinical insights and clinical progress. *Nat. Sci. Sleep.* 8, 81–86. doi:10.2147/NSS.576111
- Cosson, V., Schaedeli-Stark, F., Arab-Alameddine, M., Chavanne, C., Guerini, E., Derks, M., et al. (2018). Population pharmacokinetic and exposure-dizziness modeling for a metabotropic glutamate receptor subtype 5 negative allosteric modulator in major depressive disorder patients. *Clin. Transl. Sci.* 11 (5), 523–531. doi:10.1111/cts.12566
- Cryan John, F., O’Riordan Kenneth, J., Cowan Caitlin, S. M., Sandhu Kiran, V., Bastiaanssen Thomaz, F. S., Boehme, M., et al. (2019). The microbiota-gut-brain Axis. *Physiol. Rev.* 99 (4), 1877–2013. doi:10.1152/physrev.00018.2018
- Cui, X. F. (2020). “Study on metabolic transformation of Ziziphi Spinosae Semen saponins by intestinal microflora in vitro,” (Taiyuan, China: Shanxi University of Traditional Chinese Medicine). Master thesis. doi:10.27820/d.cnki.gszy.2020.000204
- D’Antoni, S., Spatuzza, M., Bonaccorso, C. M., Musumeci, S. A., Ciranna, L., Nicoletti, F., et al. (2014). Dysregulation of group-I metabotropic glutamate(mGlu) receptor mediated signalling in disorders associated with Intellectual Disability and Autism. *Neurosci. Biobehav. Rev.* 46 (2), 228–241. doi:10.1016/j.neubiorev.2014.02.003
- Feng, S. W., Kong, X. J., Wang, X. F., and Yu, L. L. (2004). Investigation and analysis of low concentration of methanol on optic nerve damage. *Chin. Occup. Med.* (03), 68–69. doi:10.3969/j.issn.1000-6486.2004.03.033
- Francesconi, W., Cammalleri, M., and Sanna, P. P. (2004). The metabotropic glutamate receptor 5 is necessary for late-phase long-term potentiation in the hippocampal CA1 region. *Brain Res.* 1022 (1–2), 12–18. doi:10.1016/j.brainres.2004.06.060
- Guo, B. J. (2019). “The effect of Per2 Clock gene and Glu/GABA-Gln metabolic loop in insomnia rats by acupuncture of “Qiao” meridian theory,” (Chengdu, China: Chengdu University of Traditional Chinese Medicine). phd dissertation. doi:10.26988/d.cnki.gcdzu.2019.000003
- Guo, J. L., Zhong, Q. M., JiYang, H. J. L., Song, M. Q., Tong, L., Niu, Y., et al. (2021). Regulation of hypnotic active components of cnidii fructus on melatonin synthesis rate-limiting enzyme AANAT in rats with PCPA-induced insomnia. *Chin. J. Exp. Traditional Med. Formulae* 27 (14), 47–52. doi:10.13422/j.cnki.sy-fjx.20211309
- Guo, X., Guo, R., Xing, J., Wang, J. L., and Yuan, Q. J. (2017). Mechanism of Ningxin Anshen Fang in regulation of unbalanced Glu/GABA-Gln metabolic loop in insomnia rats. *J. Beijing Univ. Traditional Chin. Med.* 40 (5), 413–419. doi:10.3969/j.issn.1006-2157.2017.05.010
- Hua, Y., Guo, S., Xie, H., Zhu, Y., Yan, H., Tao, W., et al. (2021). Ziziphus jujuba mill.var.spinosa(bunge) hu ex H.F.chou seed ameliorates insomnia in rats by regulating metabolomics and intestinal flora composition. *Front. Pharmacol.* 12, 653767. doi:10.3389/fphar.2021.653767
- Huang, T. T., Lai, J. B., Du, Y. L., Xu, Y., Ruan, L. M., and Hu, S. H. (2019). Current understanding of gut microbiota in mood disorders:an update of human studies. *Front. Genet.* 10, 98. doi:10.3389/fgene.2019.00098
- Janssen, A. W., and Kersten, S. (2015). The role of the gut microbiota in metabolic health. *FASEB journal:official Publ. Fed. Am. Soc. Exp. Biol.* 29 (8), 3111–3123. doi:10.1096/fj.14-269514
- Lang, C., and Chen, Z. (2015). Research and application status on physiologic functions of Y-aminobutyric acid and its receptors. *Prog. Veterinary Med.* 36 (04), 108–112. doi:10.16437/j.cnki.1007-5038.2015.04.025
- Li, F. T., Yang, D., Song, F. Y., Liu, M., Dai, Y. L., Zheng, F., et al. (2020). In vitro effects of ginseng and the seed of zizyphus jujuba var.spinosa on gut microbiota of rats with spleen deficiency. *Chem. Biodivers.* 17 (9), e2000199. doi:10.1002/cbdv.202000199
- Li, Y., Hao, Y., Fan, F., and Zhang, B. (2018). The role of microbiome in insomnia, circadian disturbance and depression. *Front. Psychiatry* 9, 669. doi:10.3389/fpsy.2018.00669
- Li, Y., Zhou, M. M., Gou, X. J., Zhao, L., Shi, X. W., Jia, W., et al. (2016). Effects of curcumin on gut microbiota of interval sleep deprivation rats. *Chin. Traditional Herb. Drug* 47 (05), 794–798. doi:10.7501/j.issn.0253-2670.2016.05.018
- Liu, L. S., Dong, B. Q., Liu, X. L., Yu, B. X., and Su, Z. (2021). Mechanism of acupuncture at Sanyinjiao, Shenmen and Neiguan on hypothalamic 5-HT content and imbalance of Glu/GABA Gln metabolic pathway in insomnia rats. *Chin. Archives Traditional Chin. Med.* 40 (03), 65–68. doi:10.13193/j.issn.1673-7717.2022.03.016
- Liu, S. J., ChenWang, M. F. Z., Bao, Y. M., Xin, F. J., Wen, B., Bao, Y., et al. (2020). Vitro fermentation of monosodium glutamate with human gut microbes. *Biotechnol. Bull.* 36 (12), 104–112. doi:10.13560/j.cnki.biotech.bull.1985.2020-0600

Publisher’s note

All claims expressed in this article are solely those of the authors and do not necessarily represent those of their affiliated organizations, or those of the publisher, the editors, and the reviewers. Any product that may be evaluated in this article, or claim that may be made by its manufacturer, is not guaranteed or endorsed by the publisher.

Supplementary material

The Supplementary Material for this article can be found online at: <https://www.frontiersin.org/articles/10.3389/fphar.2022.1094507/full#supplementary-material>

- Liu, Z. L., Tang, C. L., Yu, M., Hou, Y. X., and Liu, R. J. (2011). Effect of different intensities of electroacupuncture on the expression of GABA and GABRA1. doi:10.16605/j.cnki.1007-7847.2011.03.003
- Long, M. F., Xu, M. J., Zhang, X., Yang, T. W., Shao, M. L., Xu, Z., et al. (2019). Synthetic biology and metabolic engineering for amino acid production in *Corynebacterium glutamicum*. *Sci. Sin. - Vitae*. 49, 541–552. doi:10.1360/N052018-00248
- Lv, Y. B., Zhou, Q., Yan, J. X., Luo, L. S., and Zhang, J. L. (2021). Enzymolysis peptides from *Mauremys mutica* plastron improve the disorder of neurotransmitter system and facilitate sleep-promoting in the PCPA-induced insomnia mice. *J. Ethnopharmacol.* 274, 114047. doi:10.1016/j.jep.2021.114047
- Machado-Vieira, R., Ibrahim, L., Henter, I. D., and Zarate, C. A. (2012). Novel glutamatergic agents for major depressive disorder and bipolar disorder. *Pharmacol. Biochem. Behav.* 100 (4), 678–687. doi:10.1016/j.pbb.2011.09.010
- Matenchuk Brittany, A., Mandhane Piush, J., and Kozyrskyj Anita, L. (2020). Sleep, circadian rhythm, and gut microbiota. *Sleep. Med. Rev.* 53, 101340. doi:10.1016/j.smrv.2020.101340
- Matosin, N., Newell, K. A., Quidé, Y., Andrews, J. L., Teroganova, N., Green, M. J., et al. (2018). Effects of common GRM5 genetic variants on cognition, hippocampal volume and mGluR5 protein levels in schizophrenia. *Brain Imaging Behav.* 12 (2), 509–517. doi:10.1007/s11682-017-9712-0
- McDermott, C. M., Hardy, M. N., Bazan, N. G., and Magee, J. C. (2006). Sleep deprivation-induced alterations in excitatory synaptic transmission in the CA1 region of the rat hippocampus. *J. Physiol.* 570 (3), 553–565. doi:10.1113/jphysiol.2005.093781
- Olson, C. A., Vuong, H. E., Yano, J. M., Liang, Q. Y., Nusbaum, D. J., and Hsiao, E. Y. (2018). The gut microbiota mediates the anti-seizure effects of the ketogenic diet. *Cell* 173 (7), 1728–1741. e13. doi:10.1016/j.cell.2018.04.027
- Shao, J. J., Zheng, X. Y., Qu, L. L., Zhang, H., Yuan, H. F., Hui, J., et al. (2020). Ginsenoside Rg5/Rk1 ameliorated sleep via regulating the GABAergic/serotonergic signaling pathway in a rodent model. *Food Funct.* 11 (2), 1245–1257. doi:10.1039/c9fo02248a
- Shen, C. Y., Wan, L., Zhu, J. J., and Jiang, J. G. (2020). Targets and underlying mechanisms related to the sedative and hypnotic activities of saponin extracts from *Ziziphus jujube*. *Food Funct.* 11 (5), 3895–3903. doi:10.1039/d0fo00098a
- Strandwitz, P., Kim, K. H., Terekhova, D., Liu, J. K., Sharma, A., Levering, J., et al. (2019). GABA-modulating bacteria of the human gut microbiota. *Nat. Microbiol.* 4 (3), 396–403. doi:10.1038/s41564-018-0307-3
- Sun, Y. F., Chen, S. Q., Wei, R. M., Xie, X., Wang, Fan, S., et al. (2018). Metabolome and gut microbiota variation with long-term intake of *Panax ginseng* extracts on rats. *Food Funct.* 9 (6), 3547–3556. doi:10.1039/c8fo00025e
- Thompson, R. S., Gaffney, M., Hopkins, S., Kelley, T., Gonzalez, A., Bowers, S. J., et al. (2021). *Ruminiclostridium 5*, *Parabacteroides distasonis*, and bile acid profile are modulated by prebiotic diet and associate with facilitated sleep/clock realignment after chronic disruption of rhythms. *Brain Behav. Immun.* 97, 150–166. doi:10.1016/j.bbi.2021.07.006
- Vallano, A., Fernandez-Duenas, V., Garcia-Negredo, G., Quijada, M. A., Simon, C. P., Cuffi, M. L., et al. (2013). Targeting striatal metabotropic glutamate receptor type 5 in Parkinson's disease: bridging molecular studies and clinical trials. *CNS Neurol. Disord. Drug Targets* 12 (8), 1128–1142.
- Vgontzas, A. N., Puzino, K., Fernandez-Mendoza, J., Krishnamurthy, V. B., Basta, M., and Bixler, E. O. (2020). Effects of trazodone versus cognitive behavioral therapy in the insomnia with short sleep duration phenotype: a preliminary study. *J. Clin. Sleep. Med.* 16 (12), 2009–2019. doi:10.5664/jcsm.8740
- Wang, H., Zhang, Y. H., Yang, J. K., and Liang, B. H. (2017). Berberine regulates gut microbiota and Th17/Treg balance in sleep deprived rats. *Basic & Clinical Med.* 37 (06), 860–864. doi:10.16352/j.issn.1001-6325.2017.06.022
- Wang, Q. (2021). "Melatonin recovers the period length prolonged by mk-801 in Constant darkness condition through the sleep homeostatic system and the underlying mechanism analysis," (Jinan, China: Shandong University). phd dissertation. doi:10.27272/d.cnki.gshdu.2021.000458
- Xing, C. R., Chen, Y. Q., Sun, Z., and Liu, Y. L. (2021). Improvement of symptoms and spontaneous activity of insomniac rats by regulating GABA-Gln metabolism. *Chin. J. Comp. Med.* 31 (05), 47–52. doi:10.3969/j.issn.1671-7856.2021.05.008
- Yan, J., Chen, N., Li, Y. N., Hao, L. L., Liu, H. R., and Hui, S. (2019). Role of p25-CDK5-p53 signaling pathway in methanol-induced apoptosis of human neuroblastoma cells. *J. Environ. Occup. Med.* 36 (12), 1150–1155. doi:10.13213/j.cnki.jeom.2019.19353
- Yan, Y., Li, Q., Du, H. Z., Shen, C. X., Li, A. P., Pei, X. P., et al. (2019). Determination of five neurotransmitters in the rat brain for the study of the hypnotic effects of *Ziziphi Spinosae Semen* aqueous extract on insomnia rat model by UPLC-MS/MS. *Chin. J. Nat. Med.* 17 (7), 551–560. doi:10.1016/S1875-5364(19)30077-9
- Yang, X., Xiao, H., Zeng, Y., Huang, L., Ji, K., Deng, D., et al. (2021). Tianwang buxin granules influence the intestinal flora in perimenopausal insomnia. *Biomed. Res. Int.* 2021, 9979511. doi:10.1155/2021/9979511
- Yang, Y. H., Sun, Y., Wang, J., Jiang, H. Q., Cui, N., Su, B. Z., et al. (2020). [Establishment of rat heart-kidney insomnia model consistent with traditional Chinese medicine syndrome and its serum metabolomics]. *Zhongguo Zhong yao za zhi=Zhongguo zhongyao zazhi=China J. Chin. materia medica* 45 (2), 383–390. doi:10.19540/j.cnki.cjcmm.20190524.502
- Yang, Y. W., Y. W., Wu, Y., Xu, P. Q., Guo, F., Guo, F., and Yang, B. (2021). Nictinastic herbs decoction improves para-chlorophenylalanine-induced insomnia by regulating the expression level of neurotransmitters. *Ann. Transl. Med.* 9 (20), 1524. doi:10.21037/atm-21-4462
- Yu, S. Y., Wu, D. C., Liu, L., Ge, Y., and Wang, Y. T. (2008). Role of AMPA receptor trafficking in NMDA receptor-dependent synaptic plasticity in the rat lateral amygdala. *J. Neurochem.* 106 (2), 889–899. doi:10.1111/j.1471-4159.2008.05461.x
- Zhang, Q., Yun, Y., An, H., Zhao, W., Ma, T., Wang, Z., et al. (2021). Gut microbiome composition associated with major depressive disorder and sleep quality. *Front. Psychiatry* 12, 645045. doi:10.3389/fpsy.2021.645045
- Zhang, X., Lao, K., Qiu, Z., Rahman, M. S., Zhang, Y., and Gou, X. (2019). Potential astrocytic receptors and transporters in the pathogenesis of alzheimer's disease. *J. Alzheimers Dis.* 67 (4), 1109–1122. doi:10.3233/JAD-181084
- Zhao, C. Y. (2020). "Explore the characteristics of intestinal flora of spleen and stomach diarrhea yinhuoshengyang decoction in treating spleen deficiency and stomach heat insomnia," (Guangzhou, China: Guangzhou University of Chinese Medicine). Master thesis. doi:10.27044/d.cnki.ggz.2020.000650
- Zhao, R. Z., Tang, Q. S., Tian, Q., and Li, X. L. (2012). Expressions of brain NR1 and NR2B of NMDA receptor in depressive rats and interference effect of phoxinus lagowskii. *J. Beijing Univ. Traditional Chin. Med.* 35 (06), 383390–384385.
- Zhao, Y. L., Ye, Y. M., Wang, J. Q., Yu, T., and Zhang, D. M. (2020). Effects of fermented feed on growth, immunity, antioxidant capacity and intestinal flora of phoxinus lagowskii. *Chin. J. Animal Sci.* (08), 172–176. doi:10.19556/j.0258-7033.20190912-03
- Zhong, Y., Zheng, Q., Hu, P., Huang, X., Yang, M., Ren, G., et al. (2021). Sedative and hypnotic effects of *Perilla frutescens* essential oil through GABAergic system pathway. *J. Ethnopharmacol.* 279, 113627. doi:10.1016/j.jep.2020.113627



OPEN ACCESS

EDITED BY
Zheng Xiang,
Liaoning University, China

REVIEWED BY
Xuan Lu,
Dalian University, China
Hong-Hua Wu,
Tianjin University of Traditional Chinese
Medicine, China

*CORRESPONDENCE
Mo-Fei Wang,
✉ wangm1228@sina.com

SPECIALTY SECTION
This article was submitted to
Ethnopharmacology,
a section of the journal
Frontiers in Pharmacology

RECEIVED 08 December 2022
ACCEPTED 28 December 2022
PUBLISHED 09 January 2023

CITATION
Wang M-F, Li H, Cui J, Chen Y-H and Cui Y
(2023), Effects of *Kalimeris indica* (L.) Sch
Bip on colitis-associated
colorectal cancer.
Front. Pharmacol. 13:1119091.
doi: 10.3389/fphar.2022.1119091

COPYRIGHT
© 2023 Wang, Li, Cui, Chen and Cui. This is
an open-access article distributed under
the terms of the [Creative Commons
Attribution License \(CC BY\)](#). The use,
distribution or reproduction in other
forums is permitted, provided the original
author(s) and the copyright owner(s) are
credited and that the original publication in
this journal is cited, in accordance with
accepted academic practice. No use,
distribution or reproduction is permitted
which does not comply with these terms.

Effects of *Kalimeris indica* (L.) Sch Bip on colitis-associated colorectal cancer

Mo-Fei Wang^{1*}, Hao Li¹, Jian Cui¹, Yu-Han Chen² and Yong Cui³

¹The Department of General Surgery, The Affiliated Hospital of Inner Mongolia University for the Nationalities, Tongliao, Inner Mongolia Autonomous Region, China, ²School of Traditional Chinese Materia Medica, Shenyang Pharmaceutical University, Shenyang, China, ³School of Medical Device, Shenyang Pharmaceutical University, Shenyang, China

Kalimeris indica (L.) Sch Bip (*K. indica*) is a plant of the genus *Kalimeris* in Asteraceae, and its whole herb can be used as medicine for the treatment of intestinal inflammatory diseases. But the mechanism is not clear. Therefore, this study was designed to explore the mechanism of *K. indica* (KI) in colitis-associated colorectal cancer. The expression levels of miR-31-5p and proinflammatory factors were detected using THP-1 and Caco2 cells *in vitro*. KI could rescue the upregulation of miR-31-5p induced by IL-6 and TNF- α in Caco2 and THP-1 cells. In LPS-stimulated PMA-differentiated THP-1 cells, KI restored miR-31-5p expression by downregulating the expression of IL-6 and TNF- α . C57BL/6 mice were used to construct CAC model through the induction of azoxymethane/dextran sulfate sodium. The successfully established CAC mice were treated with water extract of KI through intragastric administration for 5 weeks. The result showed that KI could significantly reduce the atypical hyperplasia in colon tissue, and inhibit the expression of proinflammatory factors such as IL-6, TNF, IL-11, IL-7, etc. At the same time, KI could restore the level of miR-31-5p in mice, and therefore the downstream LATS2 to inhibit the development of CAC. These above results indicate that KI is a potentially effective herb medicine to prevent CAC.

KEYWORDS

colitis associated cancer, microRNA, miR-31-5p, *Kalimeris indica* (L.) Sch Bip, colorectal cancer

1 Introduction

Colorectal cancer (CRC) is one of the most common malignant tumors of the digestive system in clinic, and its incidence rate and mortality rate are among the top three in all cancers (Bray et al., 2018). According to the etiological classification, CRC can be divided into hereditary, sporadic, and colitis-associated colorectal cancer (CAC). The incidence of colorectal cancer in patients with inflammatory bowel disease such as ulcerative colitis is higher than that in the general population (Dugum et al., 2017; Limidi and Farraze, 2018; Samadder et al., 2019; Olén et al., 2020). The epidemiological investigation found that the occurrence of various tumors is related to inflammation, and chronic inflammation of intestinal mucosa is an important risk factor for CRC. No clear adenoma is formed during the development of CAC, and its pathogenesis was mainly attributed to the repeated cycle of the intestinal epithelial cell (IECs) injury and healing process (Rajamäki et al., 2021). Therefore, the pathogenic factors of CAC include the degree and duration of chronic inflammation, genetic susceptibility, symbiotic microbiota, etc. Sporadic CRC often develops from adenomatous polyps to cancer, and its pathogenesis is an adenoma-cancer process, while the pathogenesis of CAC goes through the sequence evolution of inflammation-atypical hyperplasia-cancer (Baker

K T et al., 2018). Because the lesion boundary of CAC is not clear, it is difficult to diagnose it by the ordinary electronic endoscopy (Buchner and Lichtenstein, 2016; Hata et al., 2016; Baker A M et al., 2018; Mark-Christensen et al., 2018; Gui et al., 2020).

With the application of genome and epigenome methods and gene-modified mouse models, the molecular mechanism of CAC has been greatly promoted, but the exact molecular mechanism of the transformation from inflammation to cancer is still unclear. Chronic inflammation can cause intestinal mucosa damage, mutation, and epigenetic changes of cell proliferation-related genes, and finally lead to atypical hyperplasia and oncogenesis (Romano et al., 2016; Kameyama et al., 2018; Fantini and Guadagni, 2021). There are two main forms of oncogenesis in colitis, including villous process oncogenesis and flat mucosa oncogenesis. CAC is usually asymptomatic in the early stage. With the progress of the disease, the focus gradually increases, and the local and systemic effects on the body gradually increase, resulting in a series of symptoms, such as changes in stool characteristics and defecation habits, abdominal masses, acute and chronic intestinal obstruction, intestinal perforation, peritonitis, and other manifestations. Due to the different nature, location, and course of the tumor, its clinical manifestations differ to some extent (Okayasu et al., 1996; Liu et al., 2021). Chemotherapy and surgery are the main treatment for CAC clinically. Fluorouracil and molecular targeted drugs are clinical drugs but with many adverse reactions (Fiala et al., 2019; Ginghină et al., 2021). At the same time, there is a possibility of complications in the above treatments, and long-term medication will also reduce the compliance of patients. With the increasing number of CAC patients in China, traditional Chinese medicine (TCM) plays a very important role in the treatment of CAC. Many research experiments on the treatment of CAC with TCMs have been carried out, and many prescriptions have begun to be used in clinical practice.

Kalimeris indica (L.) Sch Bip (*K. indica*) is a plant of the genus *Kalimeris* in Asteraceae, and its whole herb can be used as a folk medicine (Wang G K et al., 2019). *K. indica* (KI) is rich in plant resources and widely distributed (Wang L et al., 2019). It is mainly grown in low-altitude humid environments such as roadsides and hillsides. Because of its large resource stock and low development cost, *K. indica* has the basis for large-scale development and application. As a common folk medicine, it has a long medicinal history (Maoa et al., 2015) with its application recorded firstly in the *Bencao Shiyi* (741 AD). Chinese Pharmacopoeia records that *K. indica* has the effect of regulating the flow of vital energy, digesting food, and clearing away dampness and heat, and can be used to treat epigastric pain, dysentery, enteritis, urinary tract infection, etc., (Wang et al., 2010; Wang et al., 2015; Wang et al., 2017). *K. indica* mainly contains phenolic acids, flavonoids, alkaloids, phytosterols, triterpenoids, volatile oils, polysaccharides, et al. (Lin et al., 2006; Ji et al., 2014; Ueda et al., 2014; Wang et al., 2017; Huang, et al., 2020). Pharmacological studies showed that it has anti-inflammatory and analgesic, anti-tumor, anti-virus, blood coagulation improving, and other pharmacological effects. At present, *K. indica* is not only a folk medicine but also the main component of various Chinese commercial medicines. The therapeutic effect of *K. indica* on intestinal inflammatory diseases has been practiced, but its pharmacological effect on tumors needs to be clarified. In this study, the therapeutic effect of *K. indica* on CAC mice was evaluated for the first time, and its related mechanism of alleviating colitis-associated colorectal cancer was explored.

2 Materials and methods

2.1 Cells culture

Thp-1 and Caco2 cells were purchased from ATCC. The two cell lines were cultured in the medium of MEM supplemented with 10% fetal bovine serum (v/v) and 100U/mL penicillin and streptomycin (Solarbio Life Sciences Co., Ltd.) at 5% CO₂ at 37°C. Cells were subcultured using trypsin when reaching 80% confluency.

2.2 Animals and treatment

C57BL/6 mice were obtained from Liaoning Changsheng Biotechnology Co., Ltd. All experiments were performed in Liaoning Changsheng Biotechnology Co., Ltd. The study protocol was approved by the Ethics Committee for Animal Experiments of Liaoning Changsheng Biotechnology Co., Ltd. Azoxymethane (AOM) was prepared at the concentration of 10 µg/µl. Dextran sulfate sodium (DSS) was prepared to 3.0% DSS in dH₂O when needed. The experimental procedure was according to the method with modification (Chen et al., 2019). Briefly, mice were divided into four groups including the control group, AOM/DSS group, and KI groups (15 and 30 mg/kg daily). In AOM/DSS group, and KI groups, AOM of 12.5 mg/kg was administrated, i. p., respectively. After 7 days, 2.5% DSS (v/v) was prepared to drink for 7 consecutive days, followed by 14 days of regular water and normal feed, which constitutes the first 21-day cycle. Then the 21-day cycle was repeated twice. KI extract was orally administrated at dosages of 15 and 30 mg/kg from the fourth to the eighth week. Mice were sacrificed at the end of the tenth week. Serum and colon tissues were obtained and stored at -80°C for analysis.

2.3 Preparation of *K. indica* extract

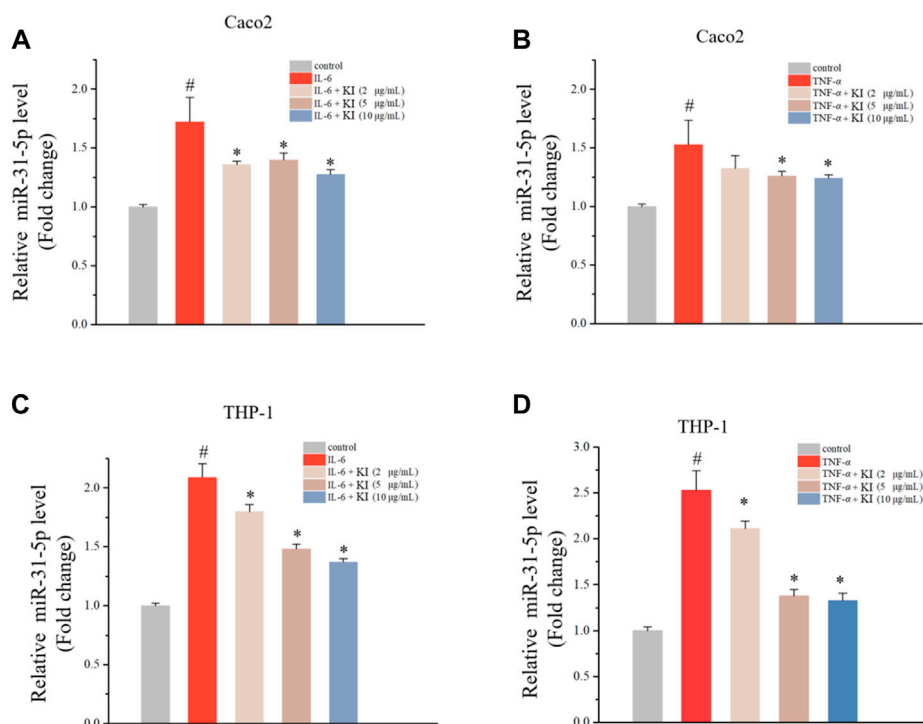
K. indica was obtained from Anguo Herb Material Co., Ltd. (Anguo, China). And the herb sample was deposited with voucher specimen No. 19KI0516. The dried herb of *K. indica* (2.5 kg) was soaked in water for 60 min, and then refluxed with water (10 L) for 3 times, 1.5 h each time. After combining the KI extraction, 0.43 kg of the extract was obtained under vacuum.

2.4 Western blot assay

The whole cell lysis suspension was prepared and centrifuged at 4°C at a rate of 15,000 G for 15 min. Take the centrifuged supernatant and boil it for 5 min. The obtained samples were separated by SDS/PAGE gel containing 10% acrylamide. Add primary antibodies recognizing P-p65, p65, IκB, GPADH and LATS2 and incubate at room temperature for 120 min. After washing, continue to add secondary antibody, incubate again at room temperature for 60 min, and detect the results through chemiluminescence.

2.5 Bio-plex assay and ELISA assay

Bio-Rad Bio-Plex Assay specific kits were used to test the concentrations of G-CSF, and MIP-1β concentrations in serum

**FIGURE 1**

Levels of miR-31-5p in Caco2 and THP-1 cells treated with IL-6 or TNF- α . (A–B) RT-qPCR results of miR-31-5p in Caco2 cells stimulated by IL-6 (A) or TNF- α (B) for 48 h (C–D) RT-qPCR results of miR-31-5p in THP-1 cells stimulated by IL-6 (A) or TNF- α (B) for 48 h. Values are means \pm SD from three separate experiments. [#] $p < 0.05$ compared with the control group; ^{*} $p < 0.05$ compared with the IL-6 (A) and (C) or TNF- α (B) and (D) groups.

following the manufacturer's instructions. Contents of interleukins including IL-6, IL-11, IL-17A, IL-22, and IL-23 in serum were examined with ELISA method following the manufacturer's instructions.

2.6 RT-PCR analysis

Total RNA was isolated by using the RNeasy mini kit (Qiagen) and used in RT and PCR amplification and the reverse transcription was used with the Master Mix kit (Takara, Shiga, Japan) following the standard protocol to make cDNA. For miRNA quantification: Bulge-loop miRNA qRT-PCR Primer Sets specific for miR-31-5p was designed by RiboBio. Mouse U6 was used as an endogenous control to normalize for total RNA loaded. RT-PCR and subsequent calculations were performed by the Step One Plus Real-time PCR system, which detected the signal emitted from fluorogenic probes during PCR.

2.7 Statistics

The data were analyzed by the statistics software of SPSS and all the data were expressed as means and standard deviations (Mean \pm SD). The significance of data differences compared between groups by ANOVA. $p < 0.05$ means the difference is statistically significant.

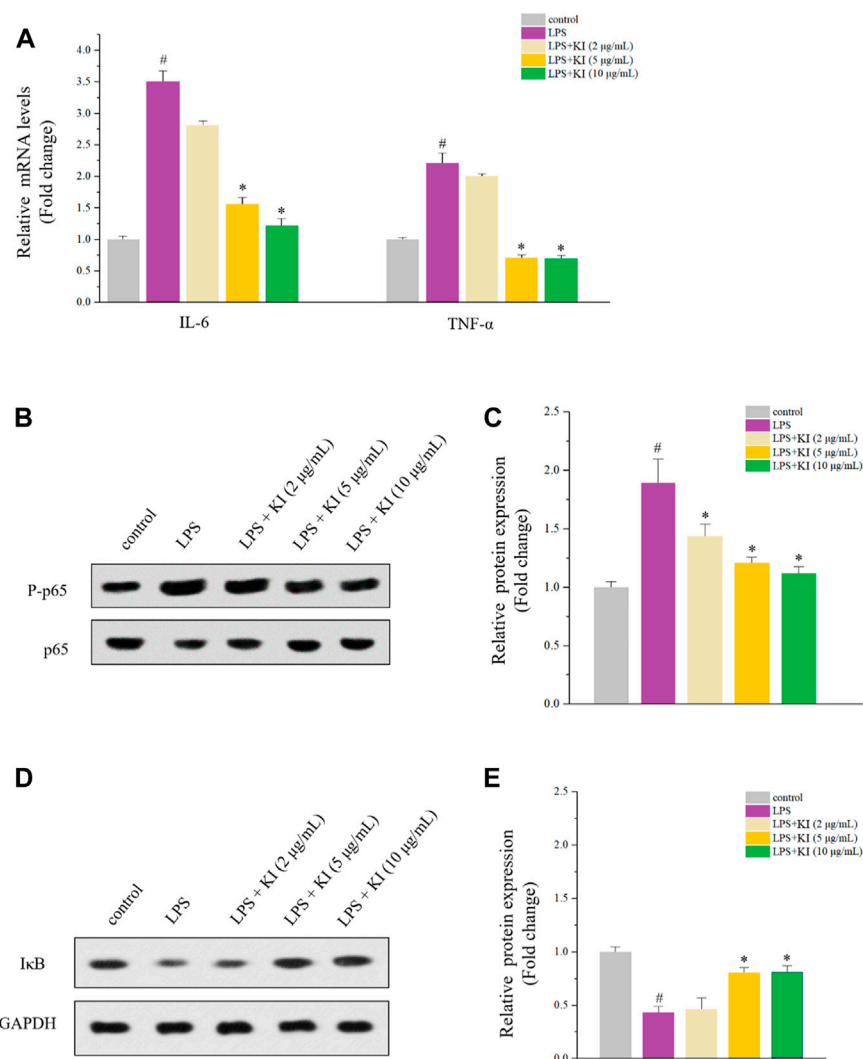
3 Results

3.1 Effects of KI on miR-31-5p levels in cells treated with IL-6/TNF- α

MiR-31 is ectopically expressed in CAC by modulating Wnt signaling pathway (Liu et al., 2017; Song et al., 2020; Bocchetti et al., 2021). Therefore, the level of miR-31-5p was assessed in THP-1 and Caco2 cells stimulated by IL-6 and TNF- α indicating that IL-6 and TNF- α could elevate miR-31-5p levels (Figure 1). Subsequently, the effect of KI on the IL-6/TNF- α -driven miR-31-5p upregulation was examined. As a result, KI (5 and 10 μ M) potently reversed the overexpression of miR-31-5p both in THP-1 and Caco2 cells stimulated by IL-6 and TNF- α (Figure 1). All these results implied KI might be able to prevent CAC through anti-inflammatory effects.

3.2 Effect of KI on NF- κ B signaling

The anti-inflammatory activity of KI was evaluated, and PMA-differentiated THP-1 macrophage model was used. After the treatment of LPS, levels of IL-6 and TNF- α were increased while KI (5 and 10 μ M) significantly reversed the overexpression of both TNF- α and IL-1 β (Figure 2A). Similarly, KI (5 and 10 μ M) also attenuated P-p65 expression and inhibited the degradation of I κ B as indicated by the western blot experiment (Figures 2B–E). These data

**FIGURE 2**

Effects of KI on LPS-stimulated THP-1 cells. **(A)** RT-qPCR results of IL-6 and TNF-α. PMA was used to differentiate THP-1 cells for 72 h and then the fresh PMA-free medium was used before the 24-h treatment of LPS or various concentrations of KI. Values are means ± SD from three separate experiments. [#]*p* < 0.05 compared with the control group; ^{*}*p* < 0.05 compared with LPS group. **(B)** Western blot results of P-p65/p65 of cells described in **(A)**. **(C)** Quantitative results of **(B)**. **(D)** Western blot results of P-p65/p65 of cells described in **(A)**. **(E)** Quantitative results of **(D)**. For **(D)** and **(E)**, values are means ± SD from three separate experiments. [#]*p* < 0.05 compared with the control group; ^{*}*p* < 0.05 compared with LPS group.

suggested that KI could restore miR-31-5p levels by inhibiting TNF-α and IL-6 expression in the NF-κB-dependent pathway.

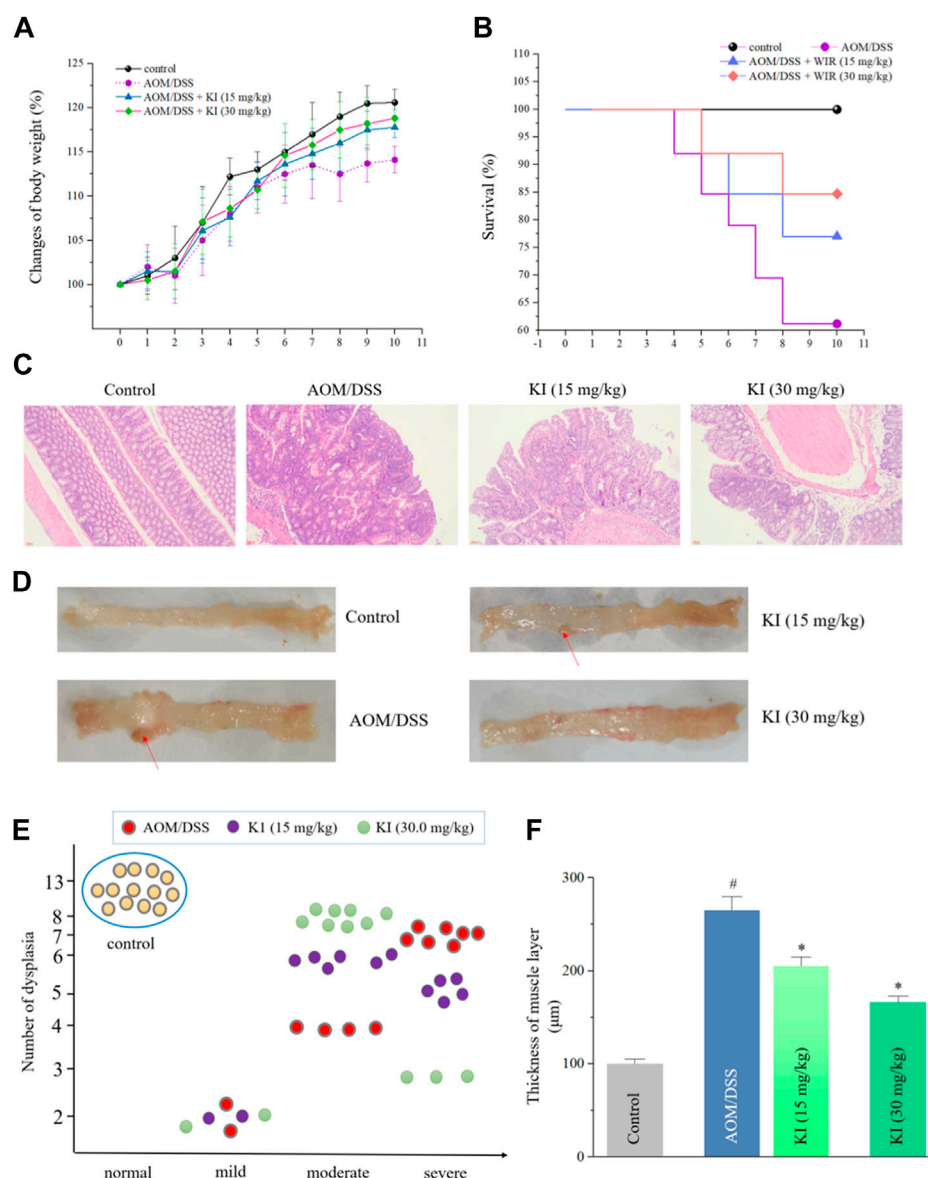
3.3 KI on CAC induced by AOM/DSS

The AOM/DSS-induced CAC model was established to evaluate the *in vivo* preventive effect of KI (Zhang et al., 2021). There was no evident disparity in the mean body weight among each group except for the AOM/DSS group, indicating the toxic-free property of KI (Figure 3A). After treatment of KI (15 and 30 mg/kg) for five weeks, the CAC-induced mortality was decreased (survival rate: 84.6% for 30.0 mg/kg and 76.9% for 15 mg/kg in KI groups compared with 61.5% in AOM/DSS group) (Figure 3B). The AOM/DSS induced severe dysplasia and even tumors in the intestinal tissues after 10 weeks. KI (30.0 mg/kg) elicited an evident preventive effect on the intestine resulting in a reduction in the extent of

intestinal injury and dysplasia (Figures 3C–E). Furthermore, increased thickness of the muscle layer was observed in the AOM/DSS group, which was to a large extent attenuated by the treatment of KI (30.0 mg/kg) (Figure 3F). All these preventive effect of KI (15.0 mg/kg) was much less significant than that of the KI (30.0 mg/kg) group (Figures 3C–F).

3.4 KI inhibited the expression of inflammatory cytokine in AOM/DSS-treated mice

Due to the result that KI at the dose of 30.0 mg/kg showed a more potent therapeutic effect in mice, we, therefore, tested the profile of *in vivo* inflammatory cytokines in the serum of KI (30.0 mg/kg) group. As a result, AOM/DSS increased the level of IL-6, IL-11, IL-17, IL-22, IL-23, MIP-1β, and G-CSF in serum, which was partially

**FIGURE 3**

In vivo effects of KI on AOM/DSS-induced CAC. (A) Mean body weight (percentage) for each group (n = 13). Values are means \pm SD from three separate experiments. (B) The survival rate for each group. (C) Histological changes for each group (x 200). (D) Representative macroscopic features of colon tissues for each group. Red arrows for the dysplasia. (E) Degrees of dysplasia event number (total = 13) for each group. (F) Thickness of muscle layer for each group. Values are means \pm SD from three separate experiments. [#] $p < 0.05$ compared with the control group; ^{*} $p < 0.05$ compared with AOM/DSS group.

reversed by the KI (30.0 mg/kg) treatment (Figure 4A). In the colon tissue, mRNA expression of TNF- α , IL-1 β , and COX-2 was elevated in the AOM/DSS group and KI group. KI lowered the overexpression of these genes in the colon tissue compared with the AOM/DSS group (Figure 4B).

3.5 KI decreases miR-31-5p expression and restores LATS2 level in colon tissues

The *in vivo* level of miR-31-5p was examined to reveal if KI prevented CAC through a miR-31-5p-related mechanism as implied by *in vitro* experiments (Figure 1). The result indicated that miR-31-5p was overexpressed in the mice of AOM/DSS group compared with that

of the control group and KI (30.0 mg/kg) significantly rescued the ectopic miR-31-5p overexpression caused by AOM/DSS (Figure 5A), suggesting miR-31-5p was involved in the KI-elicited preventive effect on CAC. To further confirm this notion, a western blot experiment was performed to assess the downstream LATS2 gene level of miR-31-5p. The protein level of LATS2 was attenuated in the AOM/DSS group due to the up-regulation of miR-31-5p and KI (30.0 mg/kg) partially restored the level of LATS2 of CAC mice (Figure 5B).

4 Discussion

MicroRNA, a kind of endogenous small RNAs with a length of about 20–24 nucleotides, can construct a regulatory network to

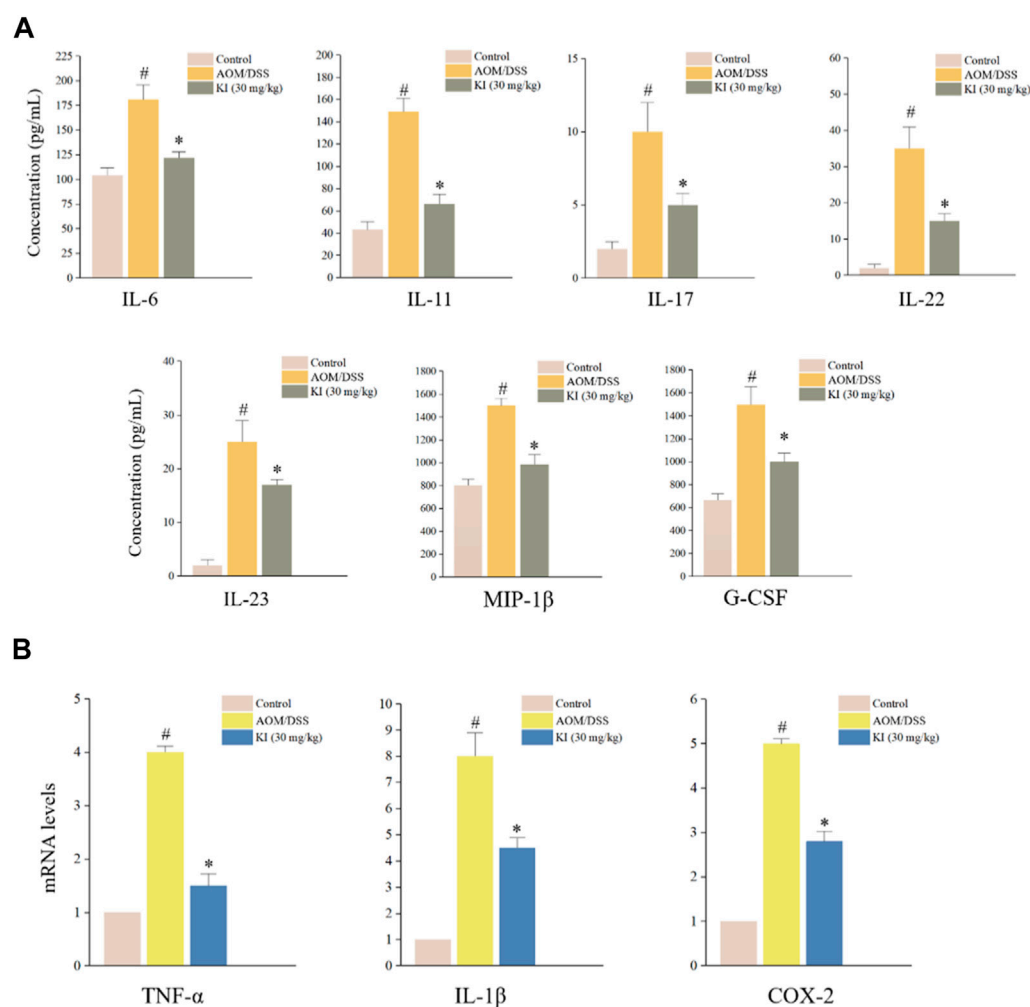


FIGURE 4

In vivo levels of inflammatory cytokines in CAC mice. (A) Results of Bio-Plex Assay or ELISA for indicated gene serum levels in mice at the 10th week (n = 6). (B) Relative levels of TNF-α, IL-1β, and COX-2 levels in mouse colons at 10th weeks (n = 6) assessed by RT-qPCR. Values are means ± SD from three separate experiments. [#]*p* < 0.05 compared with the control group; ^{*}*p* < 0.05 compared with AOM/DSS group.

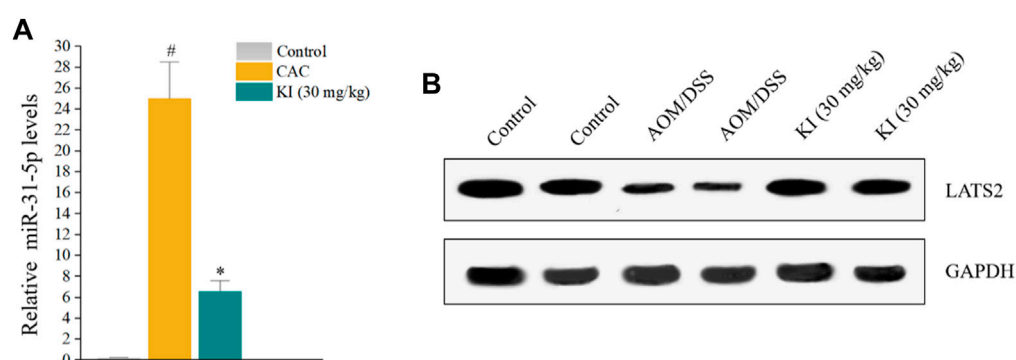


FIGURE 5

Effects of KI on miR-31-5p expression in CAC mice. (A) Rt-qPCR results of miR-31-5p in colon tissue at 10th week. Values are means ± SD from three separate experiments. [#]*p* < 0.05 compared with the control group; ^{*}*p* < 0.05 compared with AOM/DSS group. (B) Representative immunoblots of LATS2.

modulate the expression of multiple genes. Through this complex network, miRNA with abnormal expression is always related to the high occurrence of diseases (Jin et al., 2018; Kang, 2018; Pheiffer et al., 2018). MiRNAs play an important role in the pathogenesis of CAC (Jaslin et al., 2020; Bocchetti et al., 2021), and this study explored the role of KI in regulating the miR-31-5p to prevent the development of CAC.

The results showed that the expression level of miR-31-5p was significantly up-regulated in CAC model mice. In addition, it was reported that mice with miR-31 knocked out would suffer from more serious CAC than wild-type mice (Liu et al., 2017). Based on these results, it can be concluded that the expression level of miR-31-5p will contribute to the occurrence and development of CAC in mice. Therefore, it can be considered that maintaining the stable and normal expression of miR-31-5p in mice plays a crucial role in preventing the occurrence of CAC. This experiment also investigated the mechanism of miR-31-5p upregulation in CAC and the results showed that proinflammatory cytokines IL-6 and TNF- α could enhance the expression of miR-31-5p. IL-6 and TNF- α in immune cells were overexpressed during CAC, and excessive IL-6 and TNF- α will stimulate the increase of expression level of miR-31-5p in intestinal epithelial cells. LATS2 is a downstream gene of miR-31-5p in the Wnt signaling pathway in intestinal epithelial cells. The decrease of LATS2 caused by the upregulation of miR-31-5p will lead to the blockage of YAP phosphorylation, the decrease in P-YAP entering the cytoplasm, and the relative increase of YAP in the nucleus, which will ultimately inhibit YAP repairing the damaged intestinal tissue cells in a short period of time during intestinal inflammation. Although the rapid increase of YAP can immediately start the repair of damaged intestinal tissue, there are still other risks of repeated damage and excessive repair because YAP also has a carcinogenic effect, increasing the risk of cancer. The possible pathway is that YAP accumulated in the nucleus will form YAP/TAZ complex and further trigger the transcription process of many downstream oncogenes. However, KI significantly reduced the level of YAP in CAC mice, suggesting that it could prevent the occurrence and development of CAC by regulating the cumulative amount of YAP, at least partially by restoring the normal level of miR-31-5p.

Data availability statement

The original contributions presented in the study are included in the article/supplementary material, further inquiries can be directed to the corresponding author.

References

- Baker, A. M., Cross, W., Curtius, K., Al Bakir, I., Choi, C. R., Davis, H. L., et al. (2018). Evolutionary history of human colitis-associated colorectal cancer. *Gut* 68 (6), 985–995. doi:10.1136/gutjnl-2018-316191
- Baker, K. T., Salk, J. J., Brentnall, T. A., and Risques, R. A. (2018). Precancer in ulcerative colitis: The role of the field effect and its clinical implications. *Carcinogenesis* 39 (1), 11–20. doi:10.1093/carcin/bgx117
- Bocchetti, M., Ferraro, M. G., Ricciardiello, F., Ottaiano, A., Luce, A., Cossu, A. M., et al. (2021). The role of microRNAs in development of colitis-associated colorectal cancer. *Int. J. Mol. Sci.* 22 (8), 3967. doi:10.3390/ijms22083967
- Bray, F., Ferlay, J., Soerjomataram, I., Siegel, R. L., Torre, L. A., and Jemal, A. (2018). Global cancer statistics 2018: GLOBOCAN estimates of incidence and mortality

Ethics statement

The animal study was reviewed and approved by Ethics Committee for Animal Experiments of Liaoning Changsheng Biotechnology Co., Ltd.

Author contributions

Study design: MW and YC; Data collection: JC and Y-HC; Analysis and interpretation: Y-HC and YC; Statistical analysis: HL; Drafting manuscript: YC; Revision manuscript: MW.

Funding

Scientific Research Projects for Higher Education in Inner Mongolia Autonomous Region (No. NJZZ21027); Support Plan for the Innovation and Entrepreneurship Initiation Plan for Overseas Students in Inner Mongolia Autonomous Region (No. MOHRSS2020122); Doctoral Start-up Fund of the Affiliated Hospital of Inner Mongolia University for the Nationalities (No. MDFY2020001).

Acknowledgments

The authors thanks Yueqing Han from Shenyang Pharmaceutical University for his kind help in the design of the experiments.

Conflict of interest

The authors declare that the research was conducted in the absence of any commercial or financial relationships that could be construed as a potential conflict of interest.

Publisher's note

All claims expressed in this article are solely those of the authors and do not necessarily represent those of their affiliated organizations, or those of the publisher, the editors and the reviewers. Any product that may be evaluated in this article, or claim that may be made by its manufacturer, is not guaranteed or endorsed by the publisher.

worldwide for 36 cancers in 185 countries. *CA Cancer J. Clin.* 68 (6), 394–424. doi:10.3322/caac.21492

Buchner, A. M., and Lichtenstein, G. R. (2016). Evaluation and detection of dysplasia in IBD: The role of chromoendoscopy and enhanced imaging techniques. *Curr. Treat. Options Gastroenterol.* 14 (1), 73–82. doi:10.1007/s11938-016-0078-y

Chen, G., Han, Y. Q., Feng, Y., Wang, A. P., Li, X. Z., Deng, S., et al. (2019). Extract of *Ilex rotunda* Thunb alleviates experimental colitis-associated cancer via suppressing inflammation-induced miR-31-5p/YAP overexpression. *Phytomedicine* 62, 152941. doi:10.1016/j.phymed.2019.152941

Dugum, M., Lin, J., Lopez, R., Estfan, B., Manilich, E., Stocchi, L., et al. (2017). Recurrence and survival rates of inflammatory bowel disease-associated colorectal

- cancer following postoperative chemotherapy: A comparative study. *Gastroenterol. Rep. (Oxf)* 5 (1), 57–61. doi:10.1093/gastro/gow016
- Fantini, M. C., and Guadagni, I. (2021). From inflammation to colitis-associated colorectal cancer in inflammatory bowel disease: Pathogenesis and impact of current therapies. *Dig. Liver Dis.* 53 (5), 558–565. doi:10.1016/j.dld.2021.01.012
- Fiala, O., Ostasov, P., Hosek, P., Sorejs, O., Liska, V., Buchler, T., et al. (2019). The predictive role of primary tumour sidedness in metastatic colorectal cancer treated with targeted agents. *Anticancer Res.* 39 (10), 5645–5652. doi:10.21873/anticancer.13761
- Ginghină, O., Hudiță, A., Zaharia, C., Tsatsakis, A., Mezhev, Y., Costache, M., et al. (2021). Current landscape in organic nanosized materials advances for improved management of colorectal cancer patients. *Mater. (Basel)* 14 (9), 2440. doi:10.3390/ma14092440
- Gui, X., Köbel, M., Ferraz, J. G., Iacucci, M., Ghosh, S., Liu, S., et al. (2020). Histological and molecular diversity and heterogeneity of precancerous lesions associated with inflammatory bowel diseases. *J. Clin. Pathol.* 73 (7), 391–402. doi:10.1136/jclinpath-2019-206247
- Hata, K., Kishikawa, J., Anzai, H., Shinagawa, T., Kazama, S., Ishii, H., et al. (2016). Surveillance colonoscopy for colitis-associated dysplasia and cancer in ulcerative colitis patients. *Dig. Endosc.* 28 (3), 260–265. doi:10.1111/den.12505
- Huang, W. P., Wen, Z. Q., Wang, Q., Chen, R. H., Li, Z. F., Feng, Y. L., et al. (2020). The chemical profile of active fraction of *Kalimeris indica* and its quantitative analysis. *Biomed. Chromatogr.* 34 (7), e4828. doi:10.1002/bmc.4828
- Jaslin, P. J., Riis, L. B., Malham, M., Hogdall, E., Langholz, E., and Nielsen, B. S. (2020). MicroRNA biomarkers in IBD-differential diagnosis and prediction of colitis-associated cancer. *Int. J. Mol. Sci.* 21 (21), 7893. doi:10.3390/ijms21217893
- Ji, P., Wang, G. K., Liu, J. S., Luo, Z. H., Liu, J. K., and Wang, G. (2014). Five phenols from *Kalimeris indica*. *Nat. Prod. Res. Dev.* 26, 212–214. doi:10.16333/j.1001-6880.2014.02.019
- Jin, D., Wu, X., Yu, H., Jiang, L., Zhou, P., Yao, X., et al. (2018). Systematic analysis of lncRNAs, mRNAs, circRNAs and miRNAs in patients with postmenopausal osteoporosis. *Am. J. Transl. Res.* 10, 1498–1510.
- Kameyama, H., Nagahashi, M., Shimada, Y., Tajima, Y., Ichikawa, H., Nakano, M., et al. (2018). Genomic characterization of colitis-associated colorectal cancer. *World J. Surg. Oncol.* 16 (1), 121. doi:10.1186/s12957-018-1428-0
- Kang, P. (2018). Clinical diagnostic value of circulating serum miR-509-3p in pulmonary arterial hypertension with congenital heart disease. *Hell. J. Cardiol.* 61, 26–30. doi:10.1016/j.hjc.2018.06.004
- Limdi, J. K., and Farraye, F. A. (2018). An update on surveillance in ulcerative colitis. *Curr. Gastroenterol. Rep.* 20 (2), 7. doi:10.1007/s11894-018-0612-2
- Lin, C., Cao, P. X., and Liang, G. Y. (2006). Studies on chemical constituents of *Kalimeris indica*. *Chin. Pharm.* 41, 251–252. doi:1001-2494(2006)04-0251-03
- Liu, W., Zhang, X., Xu, H., Li, S., Lau, H. C., Chen, Q., et al. (2021). Microbial community heterogeneity within colorectal neoplasia and its correlation with colorectal carcinogenesis. *Gastroenterology* 160 (7), 2395–2408. doi:10.1053/j.gastro.2021.02.020
- Liu, Z., Bai, J., Zhang, L., Lou, F., Ke, F., Cai, W., et al. (2017). Conditional knockout of microRNA-31 promotes the development of colitis associated cancer. *Biochem. Biophys. Res. Commun.* 490 (1), 62–68. doi:10.1016/j.bbrc.2017.06.012
- Mao, R., Zou, F., Yang, L., Lin, S., Li, Y., Ma, M., et al. (2015). The loss of MiR-139-5p promotes colitis-associated tumorigenesis by mediating PI3K/AKT/Wnt signaling. *Int. J. Biochem. Cell. Biol.* 69, 153–161. doi:10.1016/j.biocel.2015.10.008
- Mark-Christensen, A., Laurberg, S., and Haboubi, N. (2018). Dysplasia in inflammatory bowel disease: Historical review, critical histopathological analysis, and clinical implications. *Inflamm. Bowel. Dis.* 24 (9), 1895–1903. doi:10.1093/ibd/izy075
- Okayasu, I., Ohkusa, T., Kajiura, K., Kanno, J., and Sakamoto, S. (1996). Promotion of colorectal neoplasia in experimental murine ulcerative colitis. *Gut* 39 (1), 87–92. doi:10.1136/gut.39.1.87
- Olén, O., Erichsen, R., Sachs, M. C., Pedersen, L., Halfvarson, J., Askling, J., et al. (2020). Colorectal cancer in crohn's disease: A scandinavian population-based cohort study. *Lancet Gastroenterol. Hepatol.* 5 (5), 475–484. doi:10.1016/S2468-1253(20)30005-4
- Pheiffer, C., Dias, S., Willmer, T., Pace, R., Aagaard, K., and Louw, J. (2018). Altered microRNA expression during impaired glucose tolerance and high-fat diet feeding. *Exp. Clin. Endocrinol. Diabetes.* 127, 524–532. doi:10.1055/a-0619-4576
- Rajamäki, K., Taira, A., Katainen, R., Välimäki, N., Kuosmanen, A., Plaketti, R. M., et al. (2021). Genetic and epigenetic characteristics of inflammatory bowel disease-associated colorectal cancer. *Gastroenterology* 161 (2), 592–607. doi:10.1053/j.gastro.2021.04.042
- Romano, M., Francesco, F. D. E., Zarbonello, L., Ruffolo, C., Ferraro, G. A., Zanus, G., et al. (2016). From inflammation to cancer in inflammatory bowel disease: Molecular perspectives. *Anticancer Res.* 36 (4), 1447–1460.
- Samadder, N. J., Valentine, J. F., Guthery, S., Singh, H., Bernstein, C. N., Leighton, J. A., et al. (2019). Family history associates with increased risk of colorectal cancer in patients with inflammatory bowel diseases. *Clin. Gastroenterol. Hepatol.* 17 (9), 1807–1813. doi:10.1016/j.cgh.2018.09.038
- Song, Y., Jiang, K., Wang, B. M., Liu, W. T., and Lin, R. (2020). miR-31 promotes tumorigenesis in ulcerative colitis associated neoplasia via downregulation of SATB2. *Mol. Med. Rep.* 22 (6), 4801–4809. doi:10.3892/mmr.2020.11573
- Ueda, Y., Ando, T., Nanjo, S., Ushijima, T., and Sugiyama, T. (2014). DNA methylation of microRNA-124a is a potential risk marker of colitis-associated cancer in patients with ulcerative colitis. *Dig. Dis. Sci.* 59, 2444–2451. doi:10.1007/s10620-014-3193-4
- Wang, G. K., Liu, J. S., Zhang, C. E., Wang, Z., Cai, B. X., and Wang, G. (2015). Study on chemical constituents of *Kalimeris indica*. *Zhong Yao Cai* 38 (1), 81–84.
- Wang, G. K., Yu, Y., Wang, Z., Cai, B. X., Zhou, Z. Y., Wang, G., et al. (2017). Two new terpenoids from *Kalimeris indica*. *Nat. Prod. Res.* 31 (20), 2348–2353. doi:10.1080/14786419.2017.1306700
- Wang, G. K., Zhang, N., Wang, Y., Liu, J. S., Wang, G., Zhou, Z. Y., et al. (2019). The hepatoprotective activities of *Kalimeris indica* ethanol extract against liver injury *in vivo*. *Food Sci. Nutr.* 7 (11), 3797–3807. doi:10.1002/fsn3.1241
- Wang, G., Wang, G. K., Liu, J. S., Yu, B., Wang, F., and Liu, J. K. (2010). Studies on the chemical constituents of *Kalimeris indica*. *Zhong Yao Cai* 33 (4), 551–554.
- Wang, L., Shen, J., Xu, L., Gao, J., Zhang, C., Wang, Y., et al. (2019). A metabolite of endophytic fungus *Cadophora orchidicola* from *Kalimeris indica* serves as a potential fungicide and TLR4 agonist. *J. Appl. Microbiol.* 126 (5), 1383–1390. doi:10.1111/jam.14239
- Zhang, Y., Pu, W., Bousquenaud, M., Cattin, S., Zaric, J., Sun, L. K., et al. (2021). Emodin inhibits inflammation, carcinogenesis, and cancer progression in the AOM/DSS model of colitis-associated intestinal tumorigenesis. *Front. Oncol.* 10, 564674. doi:10.3389/fonc.2020.564674



OPEN ACCESS

EDITED BY
Zheng Xiang,
Liaoning University, China

REVIEWED BY
Jiang Pi,
Guangdong medical University, China
Xiqing Bian,
Macau University of Science and
Technology, Macao SAR, China

*CORRESPONDENCE
Li-Ping Cao,
✉ caoliping006@163.com
Zhong-Wen Yuan,
✉ zhwyuan1985@163.com

[†]These authors have contributed equally to
this work

SPECIALTY SECTION
This article was submitted to
Ethnopharmacology,
a section of the journal
Frontiers in Pharmacology

RECEIVED 05 December 2022
ACCEPTED 28 December 2022
PUBLISHED 09 January 2023

CITATION
Jin H-L, Liu X-J, Feng X-Y, Zhu W-T,
Feng S-L, Cao L-P and Yuan Z-W (2023),
Quercetin 7-rhamnoside protects against
alpha-naphthylisothiocyanate (ANIT)-
induced in cholestatic hepatitis rats by
improving biliary excretion and inhibiting
inflammatory responses.
Front. Pharmacol. 13:1116257.
doi: 10.3389/fphar.2022.1116257

COPYRIGHT
© 2023 Jin, Liu, Feng, Zhu, Feng, Cao and
Yuan. This is an open-access article
distributed under the terms of the [Creative
Commons Attribution License \(CC BY\)](#).
The use, distribution or reproduction in
other forums is permitted, provided the
original author(s) and the copyright
owner(s) are credited and that the original
publication in this journal is cited, in
accordance with accepted academic
practice. No use, distribution or
reproduction is permitted which does not
comply with these terms.

Quercetin 7-rhamnoside protects against alpha-naphthylisothiocyanate (ANIT)-induced in cholestatic hepatitis rats by improving biliary excretion and inhibiting inflammatory responses

Hong-Liu Jin^{1,2,3†}, Xiao-Jia Liu^{4†}, Xiao-Ying Feng^{1,2,3},
Wen-Ting Zhu^{1,2,3}, Sen-Ling Feng^{1,2,3}, Li-Ping Cao^{5*} and
Zhong-Wen Yuan^{1,2,3*}

¹Department of Pharmacy, The Third Affiliated Hospital of Guangzhou Medical University, Guangzhou, China, ²School of Pharmaceutical Sciences, Guangzhou Medical University, Guangzhou, China, ³Guangdong Provincial Key Laboratory of Major Obstetric Diseases, Guangzhou Medical University, Guangzhou, China, ⁴School of Pharmaceutical Sciences, Guangzhou University of Chinese Medicine, Guangzhou, China, ⁵Department of Pharmacy, Shenzhen Bao'an Traditional Chinese Medicine Hospital Group, Guangzhou University of Chinese Medicine, Shenzhen, China

Objective: To explore the pharmacological effects and molecular mechanism of quercetin 7-rhamnoside (Q7R) in the treatment of cholestatic hepatitis induced by alpha-naphthylisothiocyanate (ANIT).

Methods: ANIT-induced cholestatic hepatitis rat model was used to investigate the hepatoprotective effects of three different doses of Q7R (1.25 mg/kg; 2.5 mg/kg; 5 mg/kg). Serum biochemical indices were detected using commercial kits. H&E and masson staining were used to observe hepatic tissue damage and collagen deposition in hepatocytes. The metabolism of bile acid-related substances was detected via HPLC-MS/MS by 5-(diisopropylamino) amylamine (DIAAA) derivative method. Hepatocyte injury, cholestasis, and inflammation were detected at the mRNA and protein levels using reverse transcription-polymerase chain reaction (RT-PCR) and western blotting, respectively.

Results: Q7R can decrease the level of CYP7A1, and increase FXR, CYP27A1 so then improving abnormal bile acid secretion. Furthermore, Q7R can also ameliorating inflammation by reduce TNF- α , IL-1 β , PTGS1, PTGS2, NCOA2, NF- κ B level. Therefore, Q7R had an effective therapeutic effect on ANIT-induced cholestatic hepatitis, improving abnormal bile acid secretion, and inhibiting inflammatory responses.

Conclusion: The results demonstrated that Q7R treat cholestatic hepatitis by regulating bile acid secretion and alleviating inflammation.

KEYWORDS

quercetin 7-rhamnoside, cholestatic hepatitis, inflammation, bile acid, traditional Chinese medicine

1 Introduction

The liver is the most important organ for the excretion of cholesterol from the body. Cholestasis is a common clinical disorder of intrahepatic cholesterol metabolism and bile acid metabolism that causes serious damage to the liver. A large amount of cholesterol is first converted into bile acids in the liver before being discharged from the body (Wang et al., 2018). Bile acid has important physiological functions that can reduce the risk for cardiovascular diseases caused by high cholesterol, fatty liver, and cirrhosis. Therefore, bile acid synthesis is vital for maintaining normal cholesterol levels (Wagner et al., 2009). Alpha-naphthylisothiocyanate (ANIT) is a hepatotoxic agent that causes cholestatic hepatitis. It mainly damages intrahepatic bile duct epithelial cells and causes capillary bile duct hyperplasia and inflammation around the interlobular bile duct, resulting in bile duct obstruction and cholestasis. Moreover, it is accompanied by spotty necrosis of the liver and parenchymal cell damage, resulting in cholestatic jaundice, hyperbilirubinemia, and decreased bile secretion. Therefore, it is widely used to induce cholestatic hepatitis in related research (Roth and Dahm, 1997; Chen et al., 2021).

Traditional Chinese medicine (TCM) are used for treatment of cholestatic hepatitis with a long history. There have been many pharmacology and molecular mechanism researches on Chinese herbal medicine treat cholestatic hepatitis. Wang et al. (Wang et al., 2022) explored the therapeutic effect of Da-Huang-Xiao-Shi Decoction on cholestasis; Wu et al. (Wu et al., 2022) explored the therapeutic effect of combination of resveratrol and luteolin on cholestasis by regulating bile acid homeostasis and inhibiting oxidative stress to improve disease occurrence. *Hypericum japonicum* is a dried whole plant of *Hypericum japonicum* Thunb., and has been widely applied to cure infectious hepatitis, acute and chronic hepatitis in traditional medicine. In addition, flavonoids, phloroglucinols, phenolic acids and xanthenes and trimethylated acylphloroglucinol meroterpenoids isolated from *Hypericum japonicum* Thunb. have already been proved the hepatoprotective, anti-tumor, antibacterial, antiviral, and antioxidant activities (Liu et al., 2014; Peron et al., 2019; Deng et al., 2022).

Our previous research also proved that *Hypericum japonicum* has the effect of improving cholestatic hepatitis (Feng et al., 2021). The quercetin 7-rhamnoside (Q7R) is main flavonoid component of *Hypericum japonicum*, which has strong hepatoprotective, antioxidant, and antiviral activity (Choi et al., 2009; Song et al., 2011). Awaad et al. (Awaad et al., 2006) found that Q7R has therapeutic effect on CCl₄ induced liver fibrosis, and Li et al. (Liang et al., 2013) also explored the effect of Q7R on the apoptosis of L-O₂ cells induced by glycodeoxycholic acid, and confirmed that Q7R can inhibit the excessive production of ROS and GSH depletion, decrease the production of malonaldehyde and increased catalase activities, and then reducing the apoptosis of normal hepatocytes (Huang et al., 2018).

In this research, we used a rat model of ANIT-induced cholestatic hepatitis to investigate the effects of Q7R on bile acid metabolism and inflammation. The therapeutic effect of Q7R on cholestatic hepatitis was verified using pharmacological experiments of pathological evaluation and molecular mechanism.

2 Materials and methods

2.1 Materials and chemicals

Quercetin 7-rhamnoside was purchased from Biopurify (Chengdu Biopurify Phytochemicals Ltd.). Kits for detecting albumin (ALB), aspartate aminotransferase (AST), and alanine aminotransferase (ALT) were purchased from Nanjing Jiancheng (Nanjing Jiancheng Bioengineering Institute). Ursodeoxycholic acid (>98%, J0324A), Chenodeoxycholic acid (>98%, D1217A), Cholic acid (>98%, M0412AS), Hyodeoxycholic acid (>98%, D1017AS), Deoxycholic acid (>98%, J0602AS) were purchased from meilunbio (Dalian Meilun Biotech Co., Ltd.). d4-glycochenodeoxycholate (>99.5%, ZZS19022701) was purchased from ZZBIO (Shanghai ZZBIO Co., Ltd.). 5-(Diisopropylamino) amylamine (DIAAA, B02669513), 1-[Bis(dimethylamino) methylene]-1H-1,2,3-triazolo [4,5-b] pyridinium 3-oxid hexafluorophosphate (HATU, ≥98.0%, 102409029), 1-Hydroxybenzotriazole hydrate (HOBt, ≥97.0%, BCCF3867), Triethylamine (TEA, ≥99.5%) were purchased from Sigma (Sigma-Aldrich (Shanghai) Trading Co. Ltd.). Primary anti-FXR antibodies were purchased from Abcam (Abcam Plc.). anti-CYP7A1 antibodies were purchased from Boster (Boster Biological Technology Co., Ltd.), and anti-CYP27A1 antibodies were purchased from Affinity Biosciences (Affinity Biosciences Co., Ltd.). Secondary antibodies such as goat anti-mouse IgG (H + L) and goat anti-rabbit IgG (H + L) were purchased from CWBIO (Beijing Kangwei Century Biotechnology Co., Ltd.).

2.2 Animals

Male Sprague-Dawley rats (SD) rats (200–220 g) were purchased from Guangzhou Ruige Biological Technology Co., Ltd. (medical experimental animal number: SCXK [YUE] 2021-0059; animal certification number: 44827200001399). All animals were acclimatized and kept in a well-ventilated environment at 22–25°C and 50%–60% relative humidity under a 12/12 h light/dark cycle for 1 week. Rats were allowed free access to food and water and were fasted for 1 day prior to the experiments. All animal care and experimental protocols were performed according to the guidelines for the Institutional Animal Care and Use of Laboratory Animals at Guangzhou Medical University (Ethical approval: 2018-051).

2.3 Experimental design

To evaluate the therapeutic effects of Q7R, thirty-six rats were randomly divided into six groups ($n = 6$ rats each group): 1) control group and 2) model group: blank solvent, intragastrical administration (i.g.); (3) positive control group: ursodeoxycholic acid (UDCA) 50 mg/kg, i.g.; 4) high-dose group (Q7RH): 5 mg/kg Q7R, i.p.; 5) medium-dose group (Q7RM): 2.5 mg/kg Q7R, i.p.; and 6) low-dose group (Q7RL) 1.25 mg/kg, i.p. ANIT was administered 1 week later in all groups (Figure 1).

2.4 Sample collection and liver index calculation

Animals were fasted for 24 h after the last administration. Before the rats in each group were anesthetized with pentobarbital sodium

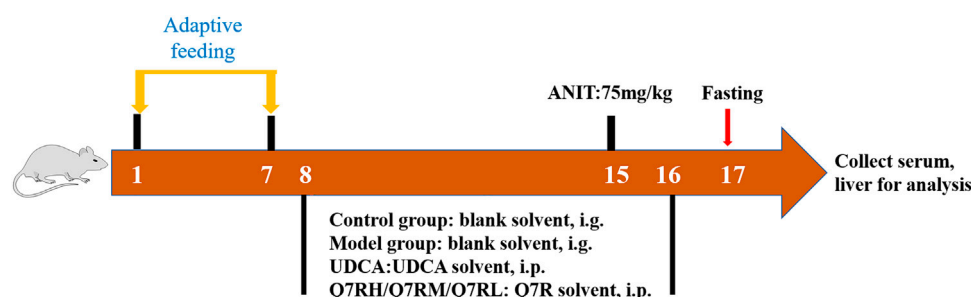


FIGURE 1

Diagrammatic sketch of the experimental design of the effect of Q7R on rat cholestatic hepatitis.

TABLE 1 Primers for real-time reverse transcription-polymerase chain reaction (RT-PCR).

Gene	Primer sequences (5'-3')	Fragment length (bp)
PTGS1	GGTCTGATGCTCTCTCCACG	135
	GATGGTTTCCCCTATAAGGATGA	
FXR	CCATTTACAAGCCACGGACG	180
	CCCAGGTTGGAATAATAGGACG	
NCOA2	AACCAGCCAAACCACTGAGAC	270
	GGTCATATTCAACCCCTGTCTCTCT	
PTGS2	GTGTTGACGTCCAGATCACATTTG	132
	GCAGTCATCAGCCACAGGAG	
TNF- α	CCAGGTTCTCTTCAAGGGACAA	80
	GGTATGAAATGGCAAATCGGCT	
IL-1 β	GAACAACAAAAATGCCTCGTGC	264
	GACAAACCGCTTTTCCATCTTCT	
NF- κ B	GGCCCATACCTTCAAATACTAGAGC	130
	CCTGCGGGTAAGATTCTTGTTTC	
GAPDH	CTGGAGAAACCTGCCAAGTATG	138
	GGTGGAAGAATGGGAGTTTGCT	

(60 mg/kg) and sacrificed, their body weights were recorded. Subsequently, blood was collected from the abdominal aorta for biochemical assessment, and livers were isolated and accurately weighed after the remaining blood on their surface was washed with PBS and wiped clean with filter paper. The formula for calculating the relative liver index was as follows: Liver index = Liver weight/Rat body weight \times 100%.

2.5 Histopathology and biochemical analysis

The isolated rat livers were fixed with 4% paraformaldehyde, embedded in paraffin, and sliced. Slices were stained with hematoxylin and eosin (H&E), and masson-stained. Histological changes were evaluated by randomly selecting visual fields using an upright microscope (Nikon, Japan). The levels of alanine transaminase

(ALT), aspartate transaminase (AST), gamma-glutamyl transferase (γ -GGT), total bilirubin (TBIL) and direct bilirubin (DBIL) were measured using a Chemray 240 Automatic Biochemical Analyzer (Rayto Life and Analytical Sciences Co., Ltd., Shenzhen, China). Albumin (ALB) was evaluated using commercial kits, according to the manufacturer's instructions.

2.6 Reverse transcription-polymerase chain reaction (RT-PCR)

Total RNA was extracted from liver tissue using an RNA extraction solution (Wuhan Servicebio Biotechnology Co., Ltd. Wuhan, China) according to the manufacturer's instructions. The primer sequences used for PCR are listed in Table 1. Briefly, total RNA (10 μ L) was reverse transcribed into cDNA. Each PCR reaction (20 μ L) for prostaglandin G/H synthase 1 (PTGS1), prostaglandin G/H synthase 2 (PTGS2), nuclear receptor coactivator 2 (NCOA2), interleukin-1 β (IL-1 β), nuclear factor kappa-B (NF- κ B), farnesoid X receptor (FXR), and tumor necrosis factor- α (TNF- α) included 2 μ L cDNA, 1.5 μ L of each primer (2.5 μ M), 7.5 μ L of 2 \times qPCR Mix, and 4 μ L nuclease-free water. RT-PCR was performed as follows: pre-denaturation at 95°C for 30 s, followed by 40 cycles of denaturation at 95°C for 15 s, and annealing at 60°C for 30 s. The melting curve was obtained from 65°C to 95°C, and fluorescence signals were acquired for every .5°C increase in temperature. The expression of *PTGS1*, *PTGS2*, *NCOA2*, *IL-1 β* , *NF- κ B*, *FXR*, and *TNF- α* mRNAs relative to *GAPDH* mRNA expression was detected using the $2^{-\Delta\Delta CT}$ method.

2.7 Western blotting

The proteins in liver tissue of rats in each group were extracted and quantified using the BCA method. The protein samples were then subjected to electrophoresis, membrane transfer, blocking, and incubation with anti-FXR (1:1000), anti-CYP7A1 (1:1000), anti-CYP27A1 (1:1000) antibodies. The membranes were washed three times with TBST and incubated with the corresponding horseradish peroxidase-labeled secondary antibodies (1:3000) for 1 h. After washing three times with TBST, the proteins were detected using an ECL chemiluminescence reagent. After exposure scanning (Bio-Rad Laboratories, Hercules, CA, United States), ImageJ software was used for analysis.

TABLE 2 Mass spectrometric characteristics of CA-DIAAA, CDCA-DIAAA, DCA-DIAAA, UDCA-DIAAA, HDCA-DIAAA, and IS-DIAAA (D4-GCA-DIAAA).

Compound	Q1 Mass (Da)	Q3 Mass (Da)	DP (volts)	EP(Volts)	CE (volts)	CXP (volts)
CA-DIAAA	577.50	577.50	138.00	10.00	33.04	5.38
CDCA-DIAAA	561.30	561.30	107.76	10.62	32.52	5.43
DCA-DIAAA	561.40	561.40	105.50	9.81	32.52	5.80
UDCA-DIAAA	561.40	561.30	103.20	10.28	32.52	5.07
HDCA-DIAAA	561.40	561.40	107.43	11.20	32.52	5.56
(D4-GCA-DIAAA) IS	622.50	622.50	121.76	11.35	34.5	5.89

Note: CA-DIAAA, derivatization of cholic acid; CDCA-DIAAA, derivatization of chenodeoxycholic acid; DCA-DIAAA, derivatization of deoxycholic acid; UDCA-DIAAA, derivatization of ursodeoxycholic; HDCA-DIAAA, derivatization of hyodeoxycholic acid; IS, internal standard; D4-GCA-DIAAA, derivatization of D4-glycocholic acid.

2.8 Detection of bile acid metabolites (BAs) in Serum by high-performance liquid chromatography-mass spectrometry (HPLC-MS/MS)

Serum (100 μ L) was added to 400 μ L of cold methanol (100 ng/mL of D4-GCA), vortexing for 1 min, the precipitated protein was centrifuged (5804R, Eppendorf, Hamburg, Germany) at 21380 g at 4°C for 15 min, and 400 μ L supernatant was collected and repeated three times. The 1200 μ L supernatant was combined and vacuum dried. 5 μ L HOBt, 5 μ L DIAAA-TEA, 5 μ L HATU were successively added to the dried product, vortexed for 1 min, then incubated at room temperature for 2 min, add 35 μ L acetonitrile, vortexed, centrifuged at 21,380 g for 15 min at 4°C, and collected 40 μ L of the supernatant for analysis (Bian et al., 2018).

Serum extracts were analyzed on a Sciex 4000 Triple Quadrupole HPLC-MS/MS system (AB Sciex, Massachusetts, United States) using a Symmetry C18 analytical column (3.5 μ m, 2.1 \times 50 mm; Waters Co., Milford, MA, United States). The mobile phase containing 1% formic acid aqueous solution (solvent A) and methanol solution (solvent B) was provided according to the following procedure: 0–8 min (5%–40% B); 8–15 min (40%–60% B); 15–18 min (60%–80% B); 18–20 min (80%–98% B); 20–25 min (98%–60% B); 25–30 min (60%–40% B). The injection volume and flow rate were 10 μ L and 25 mL/min, respectively. The multiple reaction monitoring parameters were listed in Table 2.

The following MS parameters were used: curtain gas = 35 psi; ion spray voltage = +4500 V; temperature = 450°C; ion source gas 1 = 45 psi; ion source gas 2 = 45 psi; interface heater = on; collision gas = medium. The multiple reaction monitoring parameters are listed in Table 2. All of the HPLC-MS/MS data were obtained using Analyst software (v1.6.2).

2.9 Statistical analysis

All experimental data are expressed as the mean \pm standard error (SEM). Statistical analyses were performed using GraphPad Prism 9.0 software. Mean comparisons between two data sets were performed using the *t*-test, and mean comparisons between three or more treatments were performed using one-way analysis of variance. *p* < .05 was considered statistically significant.

3 Results

3.1 Protective effect of Q7R on cholestatic hepatitis in rats

The liver index of the model group was higher than that of the control group. The liver indices of the positive control, Q7RM, and Q7R H groups were all significantly decreased (*p* < .05) compared to that of the model group (Supplementary Figure S1).

Biochemical analysis was conducted to evaluate the therapeutic effects of Q7R. Results showed that the levels of AST, ALT, ALP, γ -GGT, TBIL, and DBIL in the model group were significantly increased (*p* < .05) (Figure 2). In contrast, the levels of these parameters were decreased significantly (*p* < .05) in the positive control group and the different Q7R-treatment groups.

3.2 Q7R alleviates cholestatic hepatitis

The results of H&E staining (Figure 3A) showed that the structure of the hepatocytes in the blank control group is normal, and the hepatic lobules was complete, the cells sizes were uniform, their nucleus were clearly visible, without cell necrosis or the infiltration of inflammatory cell. In contrast, the sizes of the hepatocytes in the model group were different, and their cytoplasm were loose. The liver cells also showed focal necrosis, eosinophilic changes, and punctate necrosis. Inflammatory factor infiltration was also observed in the liver tissue. The positive control and high-dose groups were significantly lighter than the model group, and the low-dose group also improved. This finding showed that the drug effectively improved liver tissue cell damage.

Masson staining (Figure 3B) showed that the cell structure of liver tissue sections in the blank control group was complete, and no obvious blue collagen fiber deposition was observed. However, in the liver tissue sections of the model group, abnormal structural hepatic lobules and hepatocyte degeneration and necrosis were observed. The appearance of a large amount of blue collagen fiber deposition in the liver indicates serious fibrosis. The Area of collage fibers in liver according to masson stain was shown in Supplementary Figure S2.

Q7R treatment significantly attenuated the degree of hepatic putrescence, fibrosis, and inflammatory cell infiltration. These results revealed that Q7R protected against ANIT-induced liver fibrosis in cholestatic hepatitis rats.

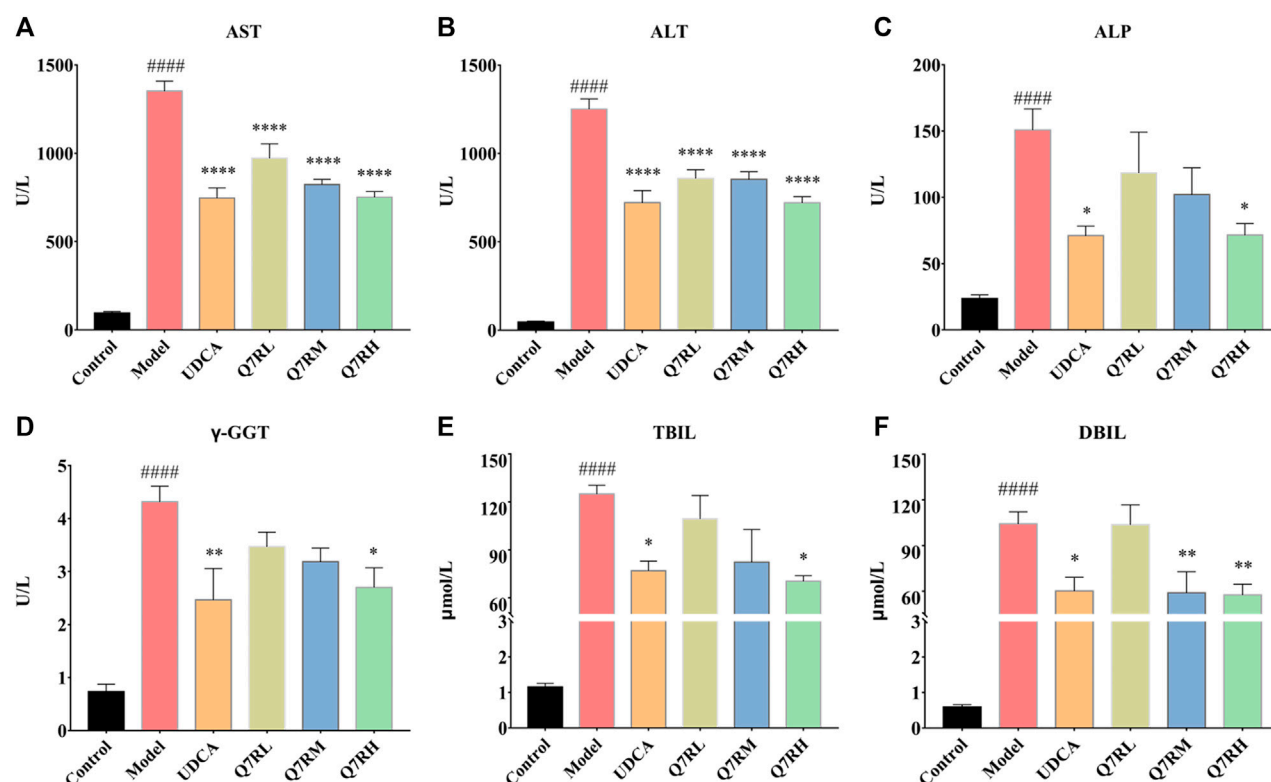


FIGURE 2

Effect of Q7R treatment on the levels of serum biochemical indices in model rats ($n = 6$). (A) Serum AST; (B) Serum ALT; (C) Serum ALP; (D) Serum γ -GGT; (E) Serum TBIL; (F) Serum DBIL; Values are presented as mean \pm SEM for three biological replicates per group. * $p < .05$, ** $p < .01$, *** $p < .001$ vs. the model group, #### $p < .001$ vs. the control group.

3.3 Effect of Q7R on inflammation and bile acid secretion

To evaluate the effect of Q7R treatment on bile acid secretion and inflammation, mRNA levels of *TNF- α* , *IL-1 β* , *PTGS1*, *PTGS2*, *NCOA2*, *FXR*, and *NF- κ B* were measured. The results showed that the mRNA expression of *TNF- α* , *IL-1 β* , *PTGS1*, *PTGS2*, *NCOA2*, and *NF- κ B* were upregulated in the model group but were downregulated after administration Q7R treatment (Figure 4). This result indicates that Q7R could effectively improve inflammation caused by the disease and alleviate the symptoms of the cholestasis. On the other hand, *FXR* mRNA expression was downregulated in the model group and upregulated after Q7R administration. These results suggest that Q7R could regulate the secretion of bile acids, maintain the mitochondrial membrane potential of hepatocytes by promoting the excretion and transport of bile acids, and play a protective role for hepatocytes.

3.4 Q7R administration improves inflammation and cholestasis

To further evaluate the improvement in inflammation and cholestasis after Q7R treatment, western blotting was performed to detect the protein expression of *FXR*, *CYP7A1*, and *CYP27A1*. The results showed that the protein expression of *FXR* and *CYP27A1* were downregulated in the model group, but were upregulated after Q7R

administration (Figure 5), indicating that Q7R can effectively alleviate the bile acid synthesis disorder caused by the disease, alleviating the cholestasis-induced damage to hepatocytes. In addition, *CYP7A1* protein expression was upregulated in the model group but downregulated after Q7R administration. This result indicates that Q7R could alleviate inflammation caused by cholestasis.

3.5 Q7R regulated to the bile acid metabolism

Bile acid synthesis and decomposition play a crucial role in the process of disease, the bile acid levels reflect the degree of liver injury caused by hepatotoxicity and cholestasis. In order to improve detection sensitivity of BAs and evaluate the effect of Q7R on bile acid metabolism, in this research, DIAA was applied to establish a highly sensitive derivatization HPLC-MS/MS approach that achieved the simultaneous determination of 5 CAs in serum. The results of method validation are shown in the supplementary material (Supplementary Tables S1, S2). The correlation coefficients of the calibration curves exceeded .9990, proclaiming an excellent linearity over the concentration range employed. The accuracy varied between 95.34% and 107.30% (within-run), and 94.58% and 102.10% (between-run). The relative standard deviations (RSDs) of within- and between-run precision were below 7.47% and 7.22%, respectively. The detection results (Figure 6) showed that serum CA increased, while CDCA, DCA, UDCA and HDCA decreased in cholestatic hepatitis model rats. Notably, Q7R treatment reduced CA level,

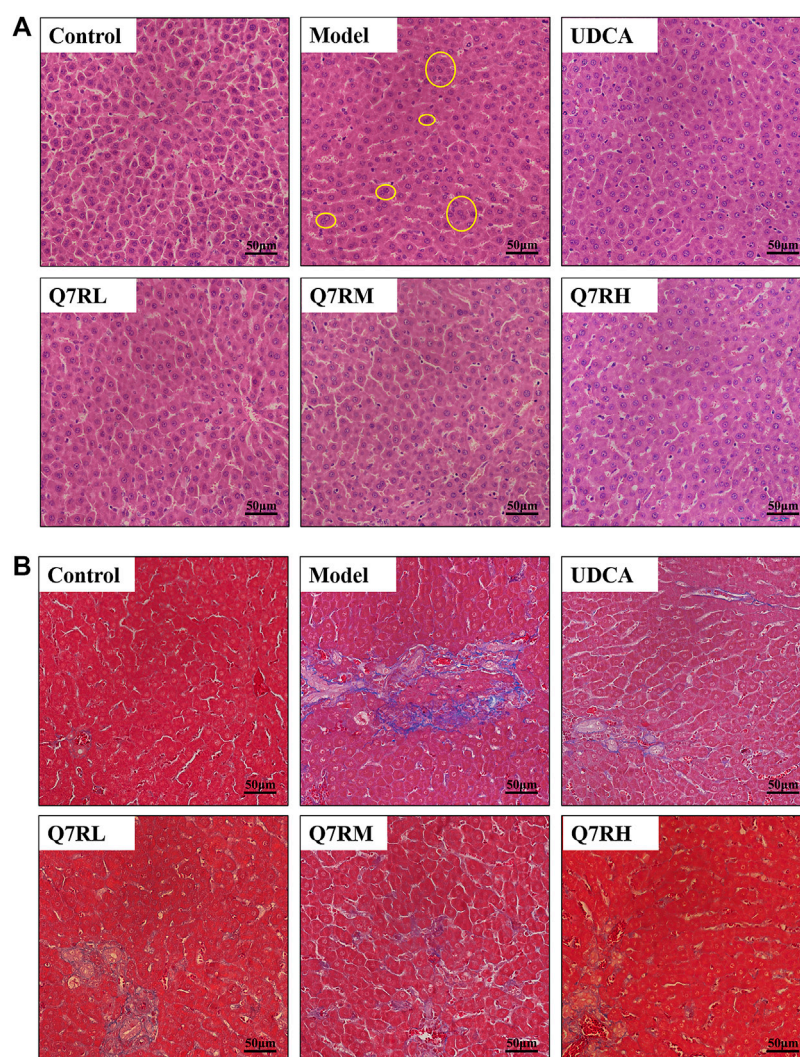


FIGURE 3
Histological analysis. **(A)** Hematoxylin and eosin (H&E)-stained sections of the liver. Original magnification $\times 40$. **(B)** Masson-stained sections of the liver. Original magnification $\times 40$. The part circled by yellow circle is inflammatory cell infiltration.

and raised the CDCA, DCA, UDCA and HDCA levels, indicating that Q7R can improve bile excretion and liver damage.

4 Discussion

Cholestatic hepatitis is a common liver disease with a characterized that retention and accumulation of bile acids in the liver (Zhou et al., 2017). Many factors leading to cholestasis hepatitis disease including infections, drugs toxicity, metabolic disorder, genetic disorders, or liver transplantation. cholestatic hepatitis may progress hepatic fibrosis, cirrhosis or liver failure without appropriate treatments. Therefore, early effective intervention and potential drugs -screening for cholestatic hepatitis is extremely urgent. ANIT is a characterized cholestatic toxic agent for rats, and has widespread influence on liver basolateral and canalicular transporters. ANIT can be conjugated with GSH in hepatocytes and transported into the bile by multidrug resistance-associated protein 2, and the ANIT-GSH conjugate dissociated into free GSH and ANIT in the

bile lead to damage and necrosis of bile duct cells and liver cells. Oxidative injury and inflammation likely plays a large role in ANIT-induced cholestatic hepatitis (Wang et al., 2014).

In a sense, serum biochemical indicators reflect liver injury. The liver is the only organ that synthesizes ALB, which is required by the body and is not excreted. Therefore, the ALB level reflects the synthesis, metabolism, and reserve function of the liver. It is also an indicator to evaluate the severity and prognosis of cirrhosis, as decreased ALB levels indicate liver function damage. Liver injury leads to edema, degeneration, necrosis, and cell membrane damage in hepatocytes (Xiao et al., 2020). In this study, intracellular ALT and AST were secreted, causing serum levels to increase, reflecting the degree of liver injury (Cai et al., 2019; Liu et al., 2019). The experimental results showed that Q7R treatment could reduce ALT and AST levels and thus alleviate liver injury. Moreover, Q7R can also improve cholestasis, which can be seen from the reduction in ALT, γ -GGT, TBIL, and DBIL levels.

Bile acid is an endogenous ligand of the farnesoid X receptor (FXR), a member of the nuclear receptor (NR) superfamily, and a

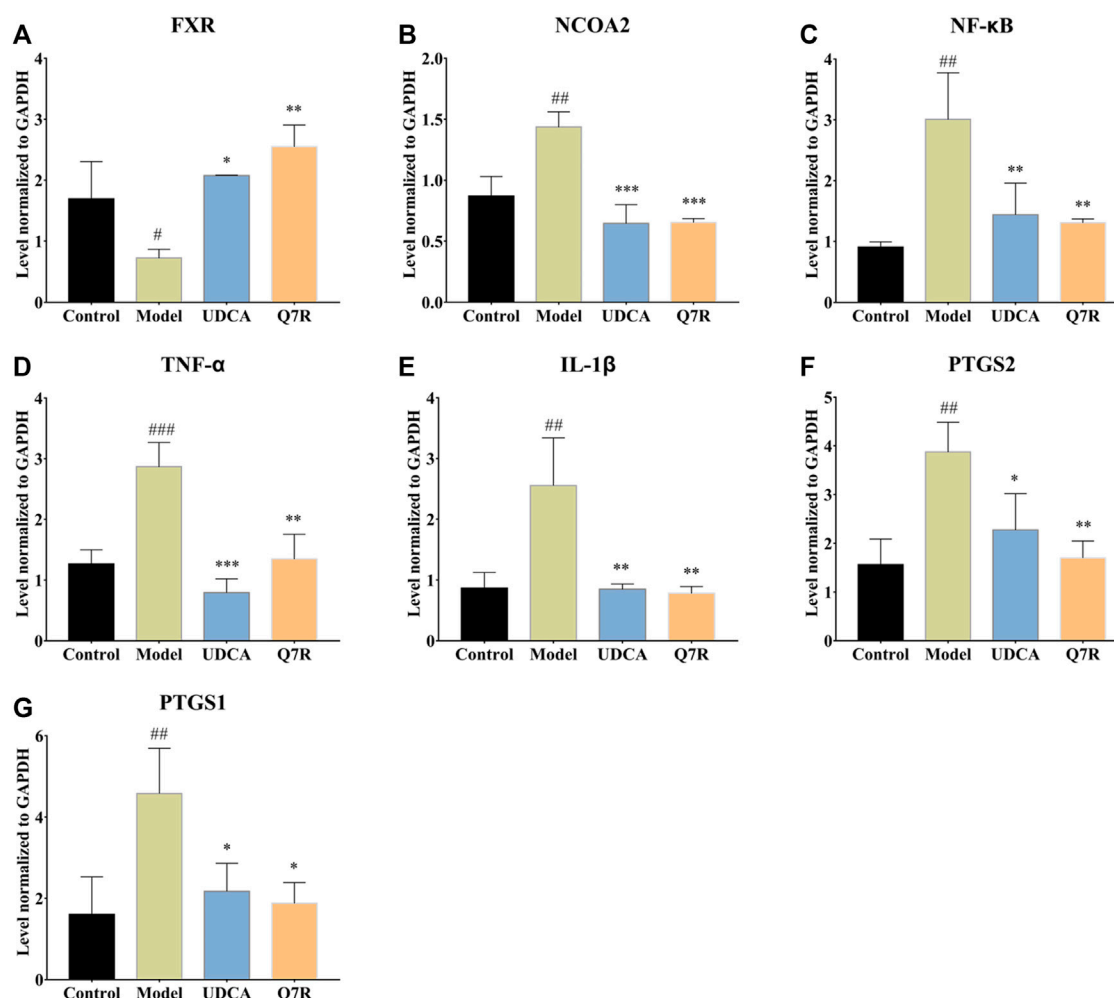


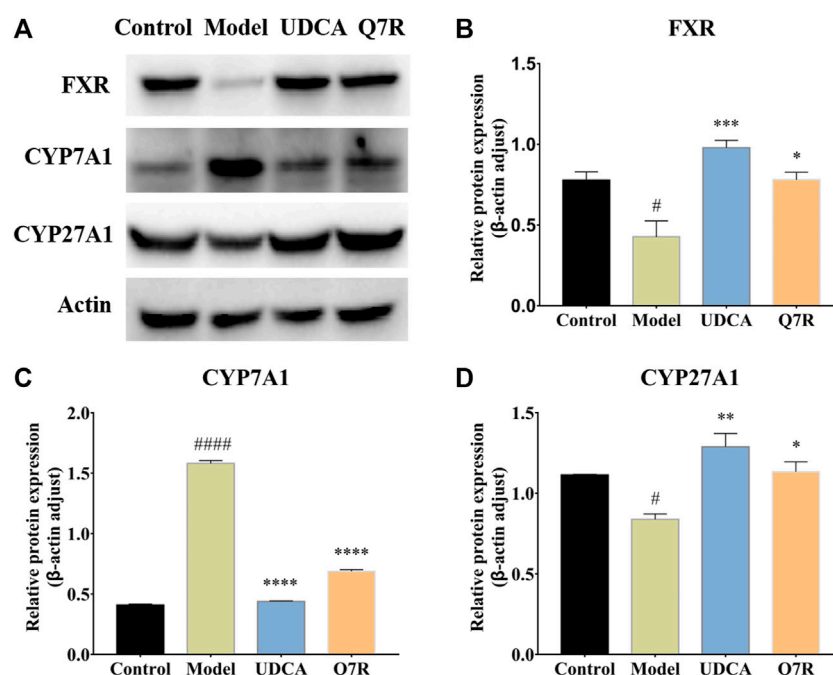
FIGURE 4

RT-PCR analysis for FXR, NCOA2, NF-κB, TNF-α, IL-1β, PTGS2, PTGS1 mRNA levels in the liver of model rats ($n = 3$). (A) FXR; (B) NCOA2; (C) NF-κB; (D) TNF-α; (E) IL-1β; (F) PTGS2; (G) PTGS1; Values are presented as mean \pm SEM for three biological replicates per group. * $p < .05$, ** $p < .01$, *** $p < .005$ vs. the model group, # $p < .05$, ## $p < .01$, ### $p < .005$ vs. the control group.

major regulator of bile acid biosynthesis and enterohepatic circulation. Under normal physiological conditions, liver FXR activity regulates bile acid levels while limiting bile acid accumulation (Keitel et al., 2019; Li et al., 2020). When the cholestasis occurs, the expression of FXR is inhibited; however, FXR expression was upregulated after Q7R administration. The activation of FXR inhibits the activity of CYP7A1, a key enzyme that catalyzes the *de novo* synthesis of bile acids from cholesterol. CYP7A1 inhibition reduces bile acid synthesis, bile acid accumulation in the liver tissue, and cholestasis (Zhao et al., 2017).

On the other hand, CYP27A1 is a key enzyme in the alternative pathway of bile acid synthesis. The inhibition of CYP7A1 leads to an increase in the expression of CYP27A1, which converts cholesterol into 27-hydroxycholesterol (27-HC). The molecule 27-HC is an important component of the negative feedback loop that regulates cholesterol biosynthesis. Thus, when CYP27A1 expression is elevated by pharmacological intervention, 27-HC production and cholesterol efflux are increased, and cholesterol accumulation is reduced, thereby alleviating the symptoms of the disease (Alfaqih et al., 2017).

Liver is the only organ that has all the enzymes required for bile acid synthesis. In the liver, CYP7A1 initiates the classical bile acid synthesis pathway by hydroxylating the steroid ring to form 7 α -Hydroxycholesterol. Then, CA and CDCA are generated by the catalyzed of CYP8B1, and CA continues to react to generate GCA and TCA. Next, GCA and TCA are transported out of the liver. In the intestine, GCA and TCA are hydrolyzed into CA by the bile salt hydrolase (BSH), CA at 7 α -Dehydroxylase acts to biotransformed DCA. Meanwhile, in the bile acid alternative pathway, cholesterol is biotransformed to 27-HC by the action of CYP27A1 and then to CDCA by the action of CYP7B1. Similarly to the classical pathway, after a series of biotransformation, CDCA is transformed into tauro- β -Muricholic acid (T β -MCA), which is transported out of the liver and then hydrolyzed into β -MCA in the intestine. β -MCA biotransformation HDCA through 6 β -epimerization and additional 7 β -dehydroxylation (Fiorucci et al., 2004; Wahlstrom et al., 2016). According to our experimental results, the increase of CA and the decrease of CDCA are consistent with the results of protein (Tang et al., 2016). The bile acid metabolism process can be seen in Figure 7. Furthermore, DIAAA—derivatization method can

**FIGURE 5**

Western blot analysis for FXR, CYP7A1 and CYP27A1 protein levels in the liver of model rats ($n = 3$). (A) Western blot analysis of FXR, CYP7A1 and CYP27A1 protein levels; (B) Relative protein of FXR was quantitatively expressed by densitometric analysis, β -Actin was served as an internal control; (C) Relative protein of CYP7A1; (D) Relative protein of CYP27A1. Values are presented as mean \pm SEM for three biological replicates per group. * $p < .05$, ** $p < .01$, *** $p < .001$, **** $p < .0001$ vs. the model group, # $p < .05$, #### $p < .0001$ vs. the control group.

improve the detection sensitivity of bile acid compounds which with carboxyl group but the disadvantage is not applicable to the all bile acid compounds. In particular, the derivative method is not suitable for taurocholic acid, tauroursodeoxycholic acid, taurochenodeoxycholic acid et al., which the chemical structure with sulfonyl group. It is necessary to cooperate with other detection methods to detect all bile acids, we will continue to explore the most suitable detection technology in future research.

An inflammatory response can be induced in the early stage of cholestasis, producing many inflammatory mediators, such as cytokines and chemokines, which induce the activation of neutrophils and their infiltration and aggregation in liver tissue (Liew and Kubes, 2019). Bile acid-induced liver inflammation induces pro-inflammatory cytokines to activate NF- κ B (Liu et al., 2017), which inhibits the transcription of FXR in the liver and prevents the subsequent activation of the small heterodimer chaperone (SHP). SHP activation inhibits the synthesis of the bile-producing rate-limiting enzyme CYP7A1 via the activated SHP pathway (Shaik et al., 2015). Furthermore, NCAO2, also known as steroid receptor coactivator 2 (SRC2), is a member of the p160 steroid receptor coactivator family (Suresh et al., 2017), whose target gene is SHP.

Therefore, the role of NCAO2 in liver bile acid homeostasis has been widely studied.

On the other hand, TNF- α is a pro-inflammatory cytokine involved in normal inflammatory and immune responses and is mainly produced by activated monocytes and macrophages (Idriss and Naismith, 2000). TNF- α production is thought to occur primarily through signals that activate NF- κ B. IL-1 β is another pro-inflammatory cytokine that plays a key role in acute and chronic inflammation. Inflammasomes can promote the maturation of IL-1 β (Kaneko et al., 2019). As a target gene of NF- κ B, it regulates the recruitment and activation of other immune cells after activation to amplify the inflammatory response.

PTGS2, also known as COX2, is an enzyme capable of initiating inflammation and promoting prostaglandin synthesis upon stimulation by various inflammatory factors, such as cytokines and bacteria. Prostaglandins can alter hepatic bile flow and may be related to the release and action of some cholelithogenic hormones. It is also involved in gallbladder contraction and water absorption and is closely related to the occurrence of cholecystitis and gallstones (Wang et al., 2021). Similarly, PTGS1 is an enzyme that constitutes prostaglandins, and its expression is closely related to inflammation.

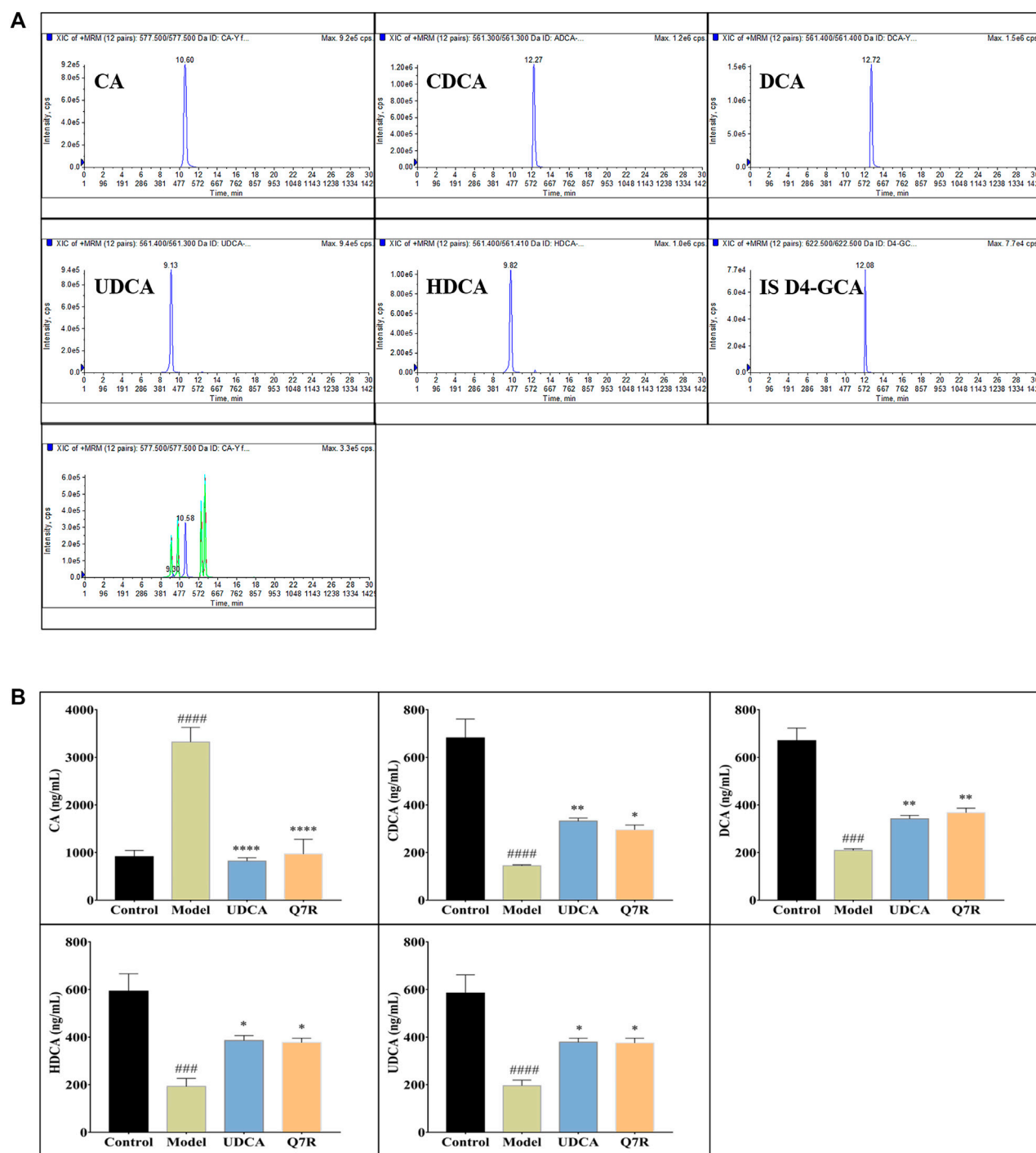
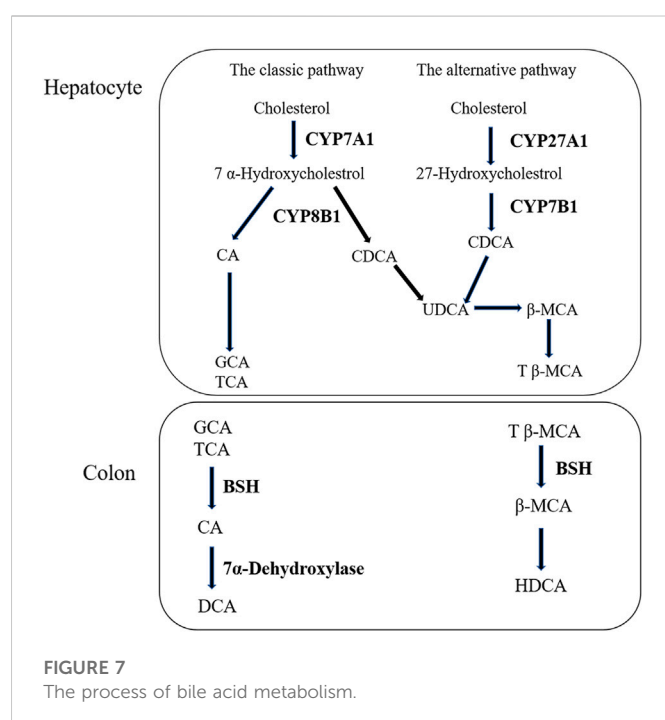


FIGURE 6

HPLC-MS/MS analysis for serum CA, CDCA, DCA, HDCA and UDCA levels in model rats ($n = 6$). **(A)** Typical chromatograms of CA, CDCA, DCA, HDCA, UDCA and internal standard (D4-GCA); **(B)** Serum CA, CDCA, DCA, HDCA and UDCA levels. Values are presented as mean \pm SEM for three biological replicates per group. * $p < .05$, ** $p < .01$, **** $p < .001$ vs. the model group, ### $p < .005$, ##### $p < .001$ vs. the control group.



5 Conclusion

In conclusion, this study demonstrated that Q7R could activate FXR, CYP7A1, and CYP27A1, effectively regulate bile acid synthesis disorders, and ameliorate hepatocyte membrane damage. Moreover, Q7R can also reduce TNF- α , IL-1 β , PTGS1, PTGS2, NCOA2, and NF- κ B levels and alleviate the inflammatory response caused by cholestasis. Additionally, Q7R plays a hepatoprotective role. Taken together, the results of this study may provide support for further research and clinical application of Q7R in cholestatic hepatitis.

Data availability statement

The original contributions presented in the study are included in the article/Supplementary Material, further inquiries can be directed to the corresponding authors.

Ethics statement

The animal study was reviewed and approved by the Institutional Animal Care and Use of Laboratory Animals at Guangzhou Medical University.

References

- Alfaqih, M. A., Nelson, E. R., Liu, W., Safi, R., Jasper, J. S., Macias, E., et al. (2017). CYP27A1 loss dysregulates cholesterol homeostasis in prostate cancer. *Cancer Res.* 77, 1662–1673. doi:10.1158/0008-5472.CAN-16-2738
- Awaad, A. S., Maitland, D. J., and Soliman, G. A. (2006). Hepatoprotective activity of *Schouwia thebaica* webb. *Bioorg Med. Chem. Lett.* 16, 4624–4628. doi:10.1016/j.bmcl.2006.06.011
- Bian, X., Li, N., Tan, B., Sun, B., Guo, M. Q., Huang, G., et al. (2018). Polarity-tuning derivatization-LC-MS approach for probing global carboxyl-containing metabolites in colorectal cancer. *Anal. Chem.* 90, 11210–11215. doi:10.1021/acs.analchem.8b01873
- Cai, M., Liang, X., Sun, X., Chen, H., Dong, Y., Wu, L., et al. (2019). Nuclear receptor coactivator 2 promotes human breast cancer cell growth by positively regulating the MAPK/ERK pathway. *Front. Oncol.* 9, 164. doi:10.3389/fonc.2019.00164

Author contributions

H-LJ: Investigation, methodology, writing—original draft, writing—review, and editing. X-JL: Investigation, methodology, writing—original draft, writing—review, and editing. X-YF: Writing—original draft, and methodology. W-TZ: Conceptualization, investigation, and methodology. S-LF: Writing—original draft, writing—review, and editing. L-PC: Funding acquisition, writing—original draft, writing—review, and editing. Z-WY: Conceptualization, mechanism analysis, funding acquisition, investigation, methodology, writing—original draft, writing—review, and editing. All authors contributed to the article and approved the submitted version.

Funding

This work was supported by the National Natural Science Foundation of China (Grant Number. 81803689); the Natural Science Foundation of Guangdong Province (Grant Number. 2018A030310292); Administration of Traditional Chinese Medicine of Guangdong Province (Grant Number. 20211341) and the YIWEN Talent Project of The Third Affiliated Hospital of Guangzhou Medical University (Grant Number. 2021#9), The Research Fund for Lin He Academician New Medicine (Grant Number. 2021HLKY10).

Conflict of interest

The authors declare that the research was conducted in the absence of any commercial or financial relationships that could be construed as a potential conflict of interest.

Publisher's note

All claims expressed in this article are solely those of the authors and do not necessarily represent those of their affiliated organizations, or those of the publisher, the editors and the reviewers. Any product that may be evaluated in this article, or claim that may be made by its manufacturer, is not guaranteed or endorsed by the publisher.

Supplementary material

The Supplementary Material for this article can be found online at: <https://www.frontiersin.org/articles/10.3389/fphar.2022.1116257/full#supplementary-material>

- Chen, Z., Wu, Y., Wang, B., Fang, J., Gan, C., Sang, C., et al. (2021). Intrahepatic cholestasis induced by alpha-naphthylisothiocyanate can cause gut-liver axis disorders. *Environ. Toxicol. Pharmacol.* 86, 103672. doi:10.1016/j.etap.2021.103672
- Choi, H. J., Kim, J. H., Lee, C. H., Ahn, Y. J., Song, J. H., Baek, S. H., et al. (2009). Antiviral activity of quercetin 7-rhamnoside against porcine epidemic diarrhea virus. *Antivir. Res.* 81, 77–81. doi:10.1016/j.antiviral.2008.10.002
- Deng, X., Xia, J., Hu, B., Hou, X. C., Pu, X. D., and Wu, L. (2022). Hyjaones A-D, trimethylated acyphloroglucinol meroterpenoids from *Hypericum japonicum* thunb. With anti-inflammatory activity. *Phytochemistry* 202, 113308. doi:10.1016/j.phytochem.2022.113308
- Feng, S. L., Zhang, J., Jin, H., Zhu, W. T., and Yuan, Z. (2021). A network pharmacology study of the molecular mechanisms of *Hypericum japonicum* in the treatment of cholestatic hepatitis with validation in an alpha-naphthylisothiocyanate (ANIT) hepatotoxicity rat model. *Med. Sci. Monit.* 27, e928402. doi:10.12659/MSM.928402
- Fiorucci, S., Antonelli, E., Rizzo, G., Renga, B., Mencarelli, A., Riccardi, L., et al. (2004). The nuclear receptor SHP mediates inhibition of hepatic stellate cells by FXR and protects against liver fibrosis. *Gastroenterology* 127, 1497–1512. doi:10.1053/j.gastro.2004.08.001
- Huang, Z. Q., Chen, P., Su, W. W., Wang, Y. G., Wu, H., Peng, W., et al. (2018). Antioxidant activity and hepatoprotective potential of quercetin 7-rhamnoside *in vitro* and *in vivo*. *Molecules* 23, 1188. doi:10.3390/molecules23051188
- Idriss, H. T., and Naismith, J. H. (2000). TNF alpha and the TNF receptor superfamily: Structure-function relationship(s). *Microsc. Res. Tech.* 50, 184–195. doi:10.1002/1097-0029(20000801)50:3<184::AID-JEMT2>3.0.CO;2-H
- Kaneko, N., Kurata, M., Yamamoto, T., Morikawa, S., and Masumoto, J. (2019). The role of interleukin-1 in general pathology. *Inflamm. Regen.* 39, 12. doi:10.1186/s41232-019-0101-5
- Keitel, V., Droge, C., and Haussinger, D. (2019). Targeting FXR in cholestasis. *Handb. Exp. Pharmacol.* 256, 299–324. doi:10.1007/164_2019_231
- Li, T., Xu, L., Zheng, R., Wang, X., Li, L., Ji, H., et al. (2020). Picroside II protects against cholestatic liver injury possibly through activation of farnesoid X receptor. *Phytomedicine* 68, 153153. doi:10.1016/j.phymed.2019.153153
- Liang, S., Su, W. W., Wang, Y. G., Peng, W., Nie, Y. C., and Li, P. B. (2013). Effect of quercetin 7-rhamnoside on glycochenodeoxycholic acid-induced L-02 human normal liver cell apoptosis. *Int. J. Mol. Med.* 32, 323–330. doi:10.3892/ijmm.2013.1414
- Liew, P. X., and Kubes, P. (2019). The neutrophil's role during health and disease. *Physiol. Rev.* 99, 1223–1248. doi:10.1152/physrev.00012.2018
- Liu, L. S., Liu, M. H., and He, J. Y. (2014). *Hypericum japonicum* thunb. Ex murray: Phytochemistry, pharmacology, quality control and pharmacokinetics of an important herbal medicine. *Molecules* 19, 10733–10754. doi:10.3390/molecules190810733
- Liu, N., Feng, J., Lu, X., Yao, Z., Liu, Q., Lv, Y., et al. (2019). Isorhamnetin inhibits liver fibrosis by reducing autophagy and inhibiting extracellular matrix formation via the TGF- β 1/smad3 and TGF- β 1/p38 MAPK pathways. *Mediat. Inflamm.* 2019, 6175091. doi:10.1155/2019/6175091
- Liu, T., Zhang, L., Joo, D., and Sun, S. C. (2017). NF- κ B signaling in inflammation. *Signal Transduct. Target Ther.* 2, 17023. doi:10.1038/sigtrans.2017.23
- Peron, G., Hošek, J., Rajbhandary, S., Pant, D. R., and Dall'Acqua, S. (2019). LC-MS(n) and HR-MS characterization of secondary metabolites from *Hypericum japonicum* Thunb. ex Murray from Nepalese Himalayan region and assessment of cytotoxic effect and inhibition of NF- κ B and AP-1 transcription factors *in vitro*. *J. Pharm. Biomed. analysis* 174, 663–673. doi:10.1016/j.jpba.2019.06.042
- Roth, R. A., and Dahm, L. J. (1997). Neutrophil- and glutathione-mediated hepatotoxicity of alpha-naphthylisothiocyanate. *Drug Metab. Rev.* 29, 153–165. doi:10.3109/03602539709037578
- Shaik, F. B., Prasad, D. V., and Narala, V. R. (2015). Role of farnesoid X receptor in inflammation and resolution. *Inflamm. Res.* 64, 9–20. doi:10.1007/s00011-014-0780-y
- Song, J. H., Shim, J. K., and Choi, H. J. (2011). Quercetin 7-rhamnoside reduces porcine epidemic diarrhea virus replication via independent pathway of viral induced reactive oxygen species. *Virol. J.* 8, 460. doi:10.1186/1743-422X-8-460
- Suresh, S., Durakoglugil, D., Zhou, X., Zhu, B., Comerford, S. A., Xing, C., et al. (2017). SRC-2-mediated coactivation of anti-tumorigenic target genes suppresses MYC-induced liver cancer. *PLoS Genet.* 13, e1006650. doi:10.1371/journal.pgen.1006650
- Tang, X., Yang, Q., Yang, F., Gong, J., Han, H., Yang, L., et al. (2016). Target profiling analyses of bile acids in the evaluation of hepatoprotective effect of gentiopicroside on ANIT-induced cholestatic liver injury in mice. *J. Ethnopharmacol.* 194, 63–71. doi:10.1016/j.jep.2016.08.049
- Wagner, M., Zollner, G., and Trauner, M. (2009). New molecular insights into the mechanisms of cholestasis. *J. Hepatol.* 51, 565–580. doi:10.1016/j.jhep.2009.05.012
- Wahlstrom, A., Sayin, S. I., Marschall, H. U., and Backhed, F. (2016). Intestinal crosstalk between bile acids and microbiota and its impact on host metabolism. *Cell Metab.* 24, 41–50. doi:10.1016/j.cmet.2016.05.005
- Wang, B., Wu, L., Chen, J., Dong, L., Chen, C., Wen, Z., et al. (2021). Metabolism pathways of arachidonic acids: Mechanisms and potential therapeutic targets. *Signal Transduct. Target Ther.* 6, 94. doi:10.1038/s41392-020-00443-w
- Wang, T., Zhou, Z. X., Sun, L. X., Li, X., Xu, Z. M., Chen, M., et al. (2014). Resveratrol effectively attenuates α -naphthyl-isothiocyanate-induced acute cholestasis and liver injury through choleretic and anti-inflammatory mechanisms. *Acta Pharmacol. Sin.* 35, 1527–1536. doi:10.1038/aps.2014.119
- Wang, W., Jiang, S., Xu, C., Tang, L., Liang, Y., Zhao, Y., et al. (2022). Transcriptome and gut microbiota profiling analysis of ANIT-induced cholestasis and the effects of da-huang-xiao-shi decoction intervention. *Microbiol. Spectr.* 10, e0324222. doi:10.1128/spectrum.03242-22
- Wang, Y., Ding, W. X., and Li, T. (2018). Cholesterol and bile acid-mediated regulation of autophagy in fatty liver diseases and atherosclerosis. *Biochim. Biophys. Acta Mol. Cell Biol. Lipids* 1863, 726–733. doi:10.1016/j.bbalip.2018.04.005
- Wu, W., Li, K., Ran, X., Wang, W., Xu, X., Zhang, Y., et al. (2022). Combination of resveratrol and luteolin ameliorates α -naphthylisothiocyanate-induced cholestasis by regulating the bile acid homeostasis and suppressing oxidative stress. *Food & Funct.* 13, 7098–7111. doi:10.1039/d2fo00521b
- Xiao, Q., Zhang, S., Ren, H., Du, R., Li, J., Zhao, J., et al. (2020). Ginsenoside Rg1 alleviates ANIT-induced intrahepatic cholestasis in rats via activating farnesoid X receptor and regulating transporters and metabolic enzymes. *Chem. Biol. Interact.* 324, 109062. doi:10.1016/j.cbi.2020.109062
- Zhao, Y., He, X., Ma, X., Wen, J., Li, P., Wang, J., et al. (2017). Paeoniflorin ameliorates cholestasis via regulating hepatic transporters and suppressing inflammation in ANIT-fed rats. *Biomed. Pharmacother.* 89, 61–68. doi:10.1016/j.biopha.2017.02.025
- Zhou, H. Q., Liu, W., Wang, J., Huang, Y. Q., Li, P. Y., Zhu, Y., et al. (2017). Paeoniflorin attenuates ANIT-induced cholestasis by inhibiting apoptosis *in vivo* via mitochondria-dependent pathway. *Biomed. Pharmacother.* 89, 696–704. doi:10.1016/j.biopha.2017.02.084



OPEN ACCESS

EDITED BY
Zheng Xiang,
Liaoning University, China

REVIEWED BY
Hongxun Tao,
Jiangsu University, China
Huijun Wang,
Shanghai University of Traditional
Chinese Medicine, China

*CORRESPONDENCE
Xiao-Bo Wang,
✉ wxbbenson0653@ sina.com

SPECIALTY SECTION
This article was submitted to
Ethnopharmacology,
a section of the journal
Frontiers in Pharmacology

RECEIVED 11 November 2022
ACCEPTED 12 December 2022
PUBLISHED 09 January 2023

CITATION
Xu B-L, Wang Y-Y, Jiang L-L, Liu Z,
Liu D-R, Zhao H, Li S-L and Wang X-B
(2023), Inhibitory effect of main
phenolic acid components of *Jacobaea
cannabifolia* (Less.) on inflammation
caused by PM_{2.5}.
Front. Pharmacol. 13:1096137.
doi: 10.3389/fphar.2022.1096137

COPYRIGHT
© 2023 Xu, Wang, Jiang, Liu, Liu, Zhao,
Li and Wang. This is an open-access
article distributed under the terms of the
[Creative Commons Attribution License
\(CC BY\)](https://creativecommons.org/licenses/by/4.0/). The use, distribution or
reproduction in other forums is
permitted, provided the original
author(s) and the copyright owner(s) are
credited and that the original
publication in this journal is cited, in
accordance with accepted academic
practice. No use, distribution or
reproduction is permitted which does
not comply with these terms.

Inhibitory effect of main phenolic acid components of *Jacobaea cannabifolia* (Less.) on inflammation caused by PM_{2.5}

Bao-Li Xu^{1,2}, Yuan-Yuan Wang², Ling-Ling Jiang², Zhen Liu²,
Ding-Rui Liu², He Zhao², Shi-Liang Li² and Xiao-Bo Wang^{1*}

¹967th Hospital of People's Liberation Army, Dalian, China, ²Department of Pharmacy, Affiliated Zhongshan Hospital of Dalian University, Dalian, China

PM_{2.5} is an important environmental problem threatening human health at present, which poses serious harm to human body after inhalation. *J. cannabifolia* is a traditional Chinese medicine which exhibits anti-inflammatory effect. This study aimed to investigate the inhibitory effect of main phenolic acid components of *J. cannabifolia* on inflammation caused by PM_{2.5}. Effect of PM_{2.5} on cell activity and apoptosis were determined by MTT, flow cytometry and calcein AM/PI staining. PHBA, PHPAA, and mixture of PHBA and PHPAA of different concentrations were given to RAW264.7 cells pretreated with PM_{2.5}. The effect of drugs on cellular inflammatory factors was detected by ELISA. The expressions of TLRs related signal pathway at protein and gene levels were detected by western blot and qRT-PCR. The results showed that PM_{2.5} had no effect on cell activity and apoptosis within the determined concentration range. PHBA and PHPAA could markedly inhibit the level of IL-1 β , IL-6, and TNF- α in RAW264.7 cells. Furthermore, the expressions of TLR2, TLR4, MyD88, IRAK1, TRAF6, TAK1, IKK β , and NF- κ B induced by PM_{2.5} were markedly inhibited by PHBA and PHPAA at protein and gene levels. This study demonstrated that PHBA and PHPAA could attenuated inflammation caused by PM_{2.5} through suppressing TLRs related signal pathway.

KEYWORDS

PM_{2.5}, *Jacobaea cannabifolia* (Less.), PHBA, PHPAA, toll-like receptors

1 Introduction

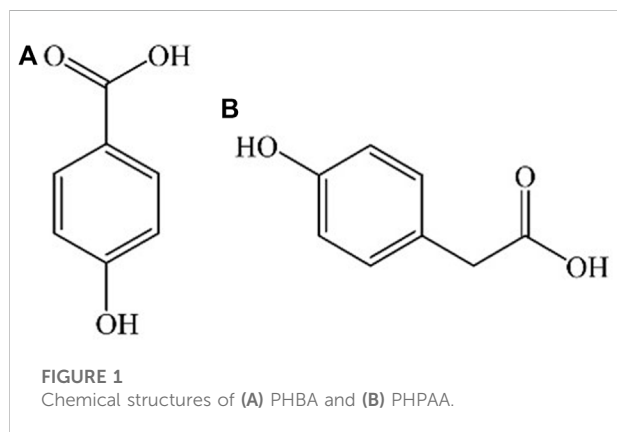
In recent years, some cities in China have experienced haze weather with particulate matter as the main pollution feature, and the ambient air quality is facing a severe test, which is extremely adverse to the national health and socio-economic development (Lin et al., 2018). PM₁₀ (diameter of inhalable particles which are less than 10 μ m) and PM_{2.5} (diameter of inhalable particles which are less than

2.5 μm and can enter the lung) are the main pollutant (Huang et al., 2014). The particle size of $\text{PM}_{2.5}$ is smaller, resulting in a larger surface area, which makes it easy to be absorbed. At the same time, $\text{PM}_{2.5}$ can stay in the atmosphere for a long time, and can travel a long distance (Han et al., 2015; Ji and Zhao., 2015). Therefore, $\text{PM}_{2.5}$ has a great impact on people's health and air quality.

The sources of $\text{PM}_{2.5}$ are very complex, mainly including emissions of combustibles, particles generated in chemical processes, human activities, equipment operation, cleaning and cooking (Ji and Zhao., 2015; Li et al., 2016; Zhou et al., 2016). $\text{PM}_{2.5}$ is a major threat to human health and can affect many systems of the body, including the central nervous system, blood system, metabolic immune system, urogenital system, digestive system and skin (Boothe et al., 2014; Park and Wang., 2014; Piao et al., 2018; Geng et al., 2019; Jeong et al., 2019; Shaffer et al., 2019). Therefore, it is very important for human health to develop new drugs to treat $\text{PM}_{2.5}$.

Jacobaea cannabifolia (Less.) E.Wiebe is a plant of *Senecio* genus, which is a genuine medicinal material in Northeast China. *J. cannabifolia* has anti-inflammatory, bacteriostatic, anti-virus, immune regulation, anti-tumor, and other effects (Li et al., 2005; Chen et al., 2015). It is clinically used to treat acute and chronic bronchitis, asthmatic bronchitis and acute respiratory tract infection. The main metabolites of the herb are flavonoids, phenolic acids, alkaloids, volatile oils, glycosides, and tannins. P-hydroxybenzoic acid (PHBA) and p-hydroxyphenylacetic acid (PHPAA) (Figure 1) are the main phenolic acids in *J. cannabifolia* and they have anti-inflammatory and other activities (Zhao et al., 2013; Sun et al., 2014).

This study aimed to explore the effect of PHBA and PHPAA on inflammation induced by $\text{PM}_{2.5}$ and its possible mechanism, to provide an experimental basis for PHBA and PHPAA to become clinical therapeutic drugs for lung injury caused by $\text{PM}_{2.5}$.



2 Materials and methods

2.1 Chemicals and reagents

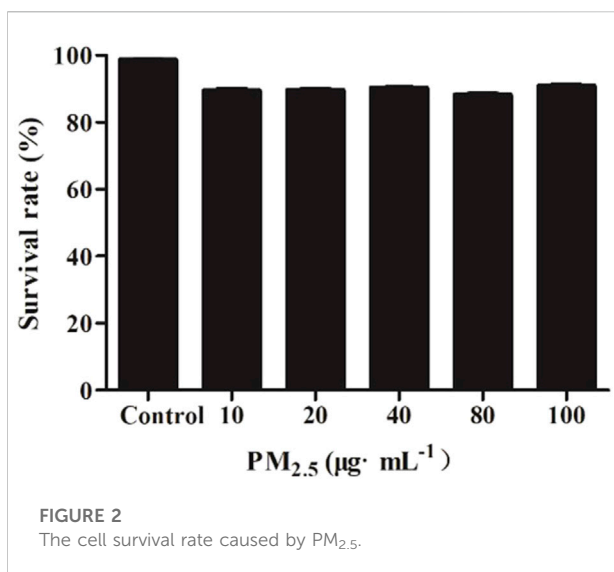
PHBA ($\geq 99\%$) and PHPAA (98%) were provided by Sigma Chemical Co. (St. Louis, MO, United States). $\text{PM}_{2.5}$ particles were provided by Hong-Hai Yu, senior engineer of Huadian Electric Power Research Institute Co., Ltd. Northeast Branch. Mouse tumor necrosis factor- α (TNF- α), interleukin-6 (IL-6) and interleukin-1 β (IL-1 β) ELISA kits were purchased from Biyuntian Biotechnology Research Institute. TLR4, TLR2, TRAF6, NF- κB , MyD88, IRAK1, TAK1, and IKK β polyclonal antibody IgG were obtained from Proteintech Group Inc (Chicago, IL, United States).

2.2 Cell culture

RAW264.7 murine macrophage cells were purchased from cell bank of Chinese Academy of Science, Shanghai. Cells were maintained in Dulbecco's modified Eagle's medium (Hyclone,

TABLE 1 Sequences of primers used for qRT-PCR.

Gene	Strand	The sequence of the primer (5'-3')	bp
TLR2	Forward	GAGCATCCGAATTGCATCACC	174
	Reverse	CCCAGAAGCATCATGACAGAG	
TLR4	Forward	CATGGATCAGAACTCAGCAA AGTC	179
	Reverse	CATGCCATGCCTTGTCTTCA	
NF- κB	Forward	GAAGCCGCTGACCATGGAA	103
	Reverse	GATCAGAGCAAGTGAGTGGA	
MyD88	Forward	TACAGGTGGCCAGAGTGGAA	119
	Reverse	GCAGTAGCAGATAAAGGC ATCGAA	
IRAK1	Forward	CGGACTTCCACAGTTCGAGGTA	125
	Reverse	TGACCAGCAAGGGTCTCCAG	
TRAF6	Forward	TCATTATGATCTGGACTGCCCAAC	150
	Reverse	TTATGAACAGCCTGGGCCAAC	
TAK1	Forward	AGCAGAGTAGCTGCGGT	134
	Reverse	GAGGAGCTTGCTGCAGAT	
IKK β	Forward	CAGAATCATCCATCGAGA CCTGAA	122
	Reverse	TGCACAGACTGCCCTGATCC	
GAPDH	Forward	TGTGTCCGTCGTGGATCTGA	150
	Reverse	TTGCTGTTGAAGTCGAGGAG	



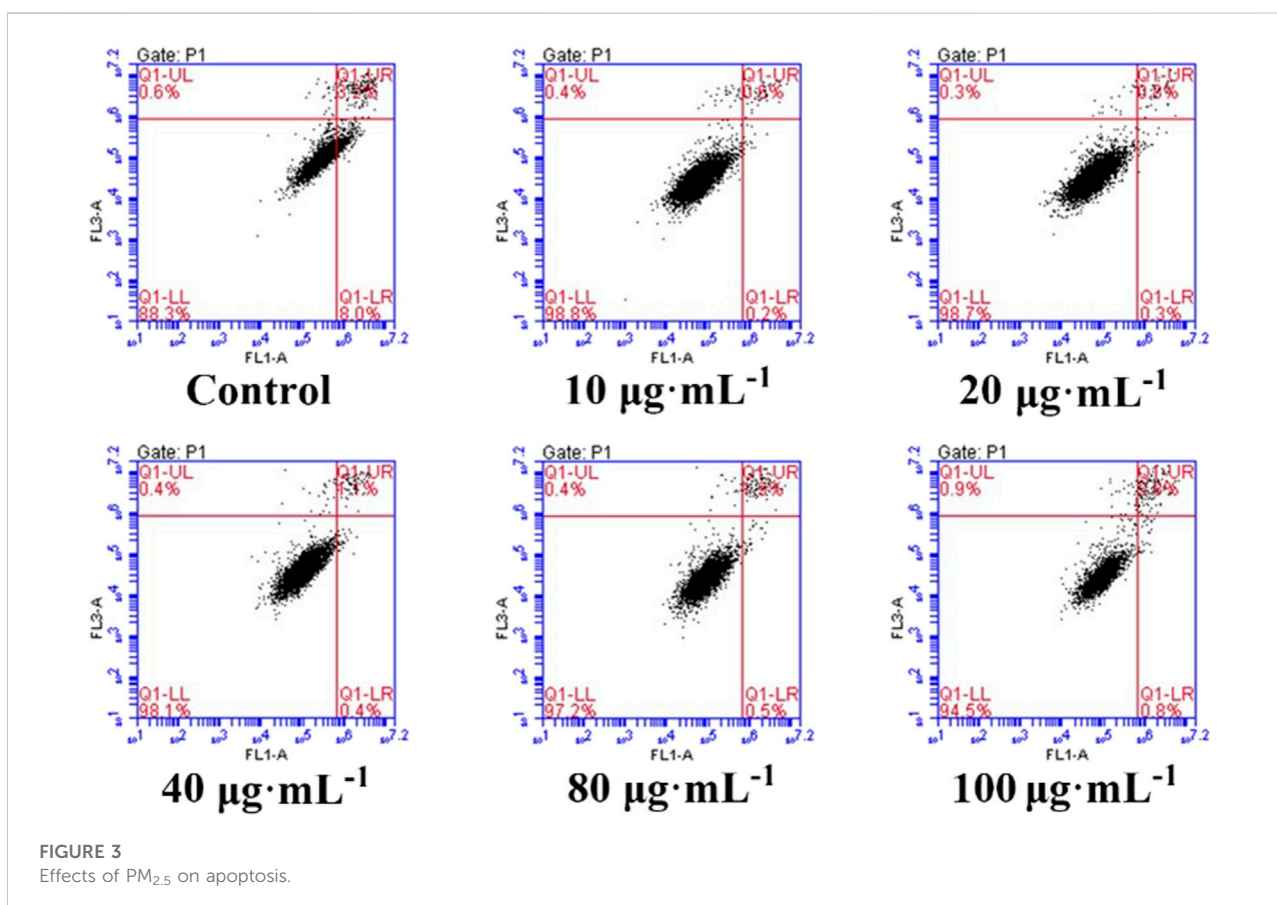
2.3 Determination of cell viability

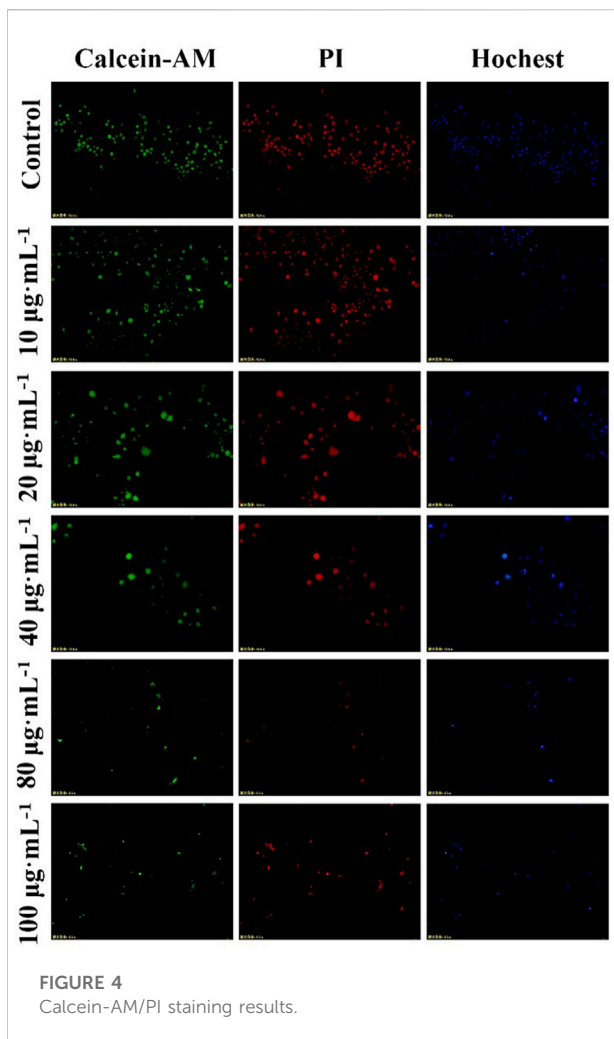
The cell viability was determined by MTT method after treating with PM_{2.5}. Collect RAW264.7 cells growing in logarithmic phase, add culture medium to make cell suspension, adjust cell concentration, and add 100 µl cell suspension to each well, and adjust the cell density to 1.0×10^4 /well. The cells were incubated in an environment of 5% CO₂ and 37°C. When the cells covered the bottom of 96 wells, a series of concentrations of PM_{2.5} were added. After incubation for 48 h, add 10 µl MTT to each hole, culture the cells for 4 h, discard the culture medium, and carefully rinse it out with PBS for 2–3 times, then add 100 µl DMSO to each hole. Vibrate the shaking table at a low speed for 10 min, set the OD value to 490 nm on the microplate reader and conduct a light absorption measurement for each test hole, and calculate the cell survival rate. Survival % = (A_{490 nm} for treated cells/A_{490 nm} for control cells) × 100%, where A_{490 nm} represents the absorbance value.

2.4 Annexin V-FITC/PI apoptosis assay

Logan, UT) supplemented with 5% FBS (Gibco, United States), 1% streptomycin and penicillin (Hyclone) at 37°C in 5% CO₂ in a humidified atmosphere incubator.

RAW264.7 cells were pretreated with PM_{2.5} (0, 10, 20, 40, 80, 100 µg/ml) for 48 h. Cells were digest with trypsin,





collected by centrifugation and washed twice with PBS. 1×10^6 cells were suspended in 500 μ l binding buffer followed by the addition of 10 μ l Annexin V-FITC. After incubation at room

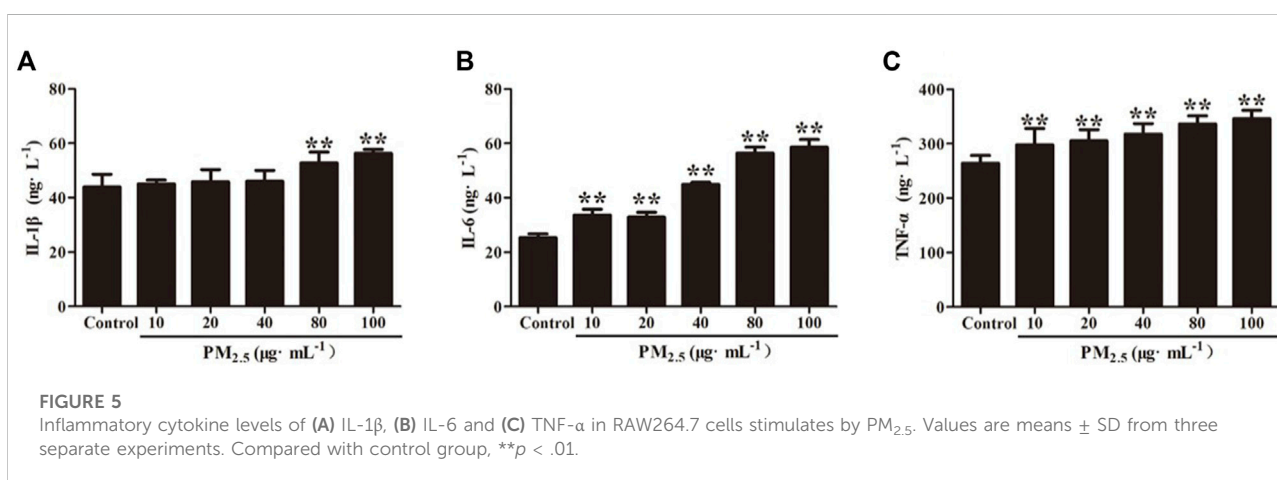
temperature in dark for 15 min, add 5 μ l PI and the cells were then analyzed using a flow cytometer (BD Accuri, US).

2.5 Calcein AM/PI staining

RAW264.7 cells were seeded in a 6-well plate at a density of 1×10^6 cells/well and cultured overnight in a 5% CO_2 incubator at 37°C to adhere. The cells were incubated with different concentrations of $\text{PM}_{2.5}$ for 48 h. According to the instructions, the cells were gently washed with PBS twice. A small amount of about 200 μ l suspension was added to the test tube, and then an appropriate amount of 100 μ l dye solution was added. Incubate the cell suspension at 37°C for 15 min and then the fluorescence microscope was used to observe the cell staining.

2.6 Determination of cytokines by ELISA

Determination of the effect of $\text{PM}_{2.5}$ on the production of inflammatory factors in RAW264.7 cells by ELISA. RAW264.7 cells were seeded in a 96-well plate at a density of 1×10^4 cells/well and cultured overnight in a 5% CO_2 incubator at 37°C . After cell adhesion, different concentrations of $\text{PM}_{2.5}$ (0, 10, 20, 40, 80, and 100 $\mu\text{g}/\text{ml}$) were added into the culture medium and the cells were continued to culture for 48 h. Then, the concentration of IL-1 β , IL-6, and TNF- α in each was measured according to the ELISA instruction with a microplate reader at 450 nm. The effects of PHBA and PHPAA on inflammatory cytokines induced by $\text{PM}_{2.5}$ were also determined using ELISA method and the duration of drugs was 24 h. The concentrations of PHBA or PHPAA were 10, 100, and 1,000 μM . In the mixture of PHBA and PHPAA, the molar ratio was 1:1.



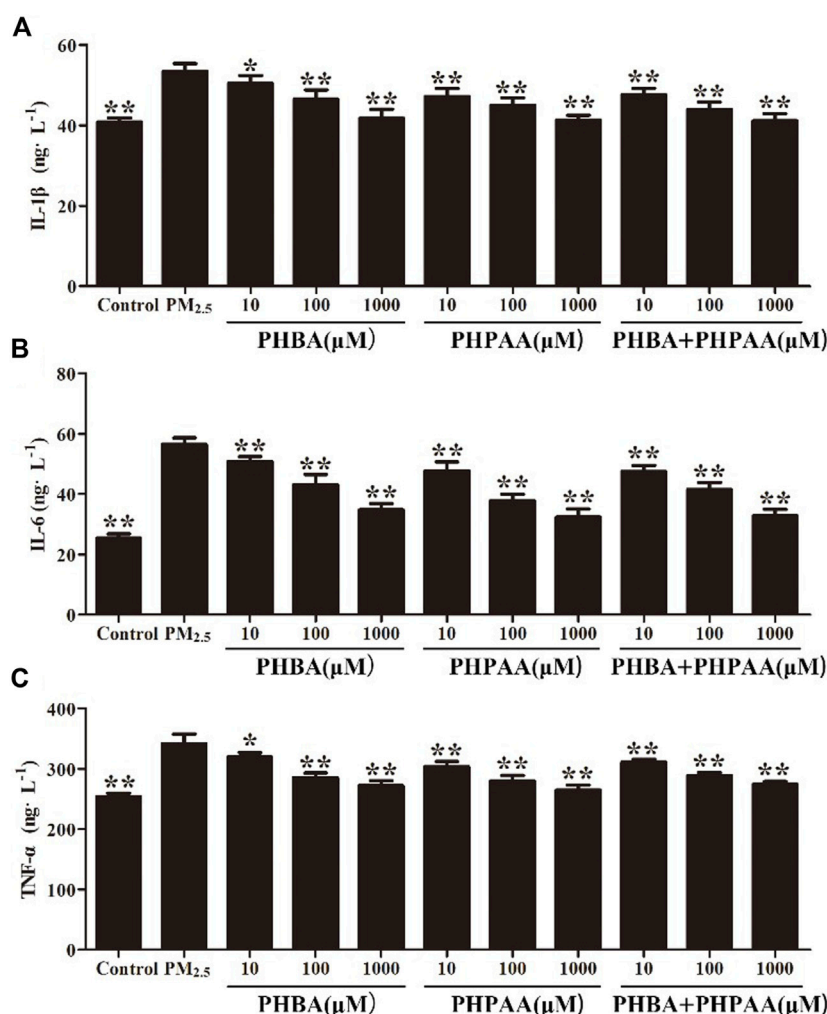


FIGURE 6

Inhibition of PHBA and PHPAA on inflammatory cytokines produced by PM_{2.5}. (A–C), Relative levels of IL-1β, IL-6, and TNF-α levels at 48 h assessed by ELISA. Values are means ± SD from three separate experiments. Compared with PM_{2.5} stimulation group, **p* < .05, ***p* < .01.

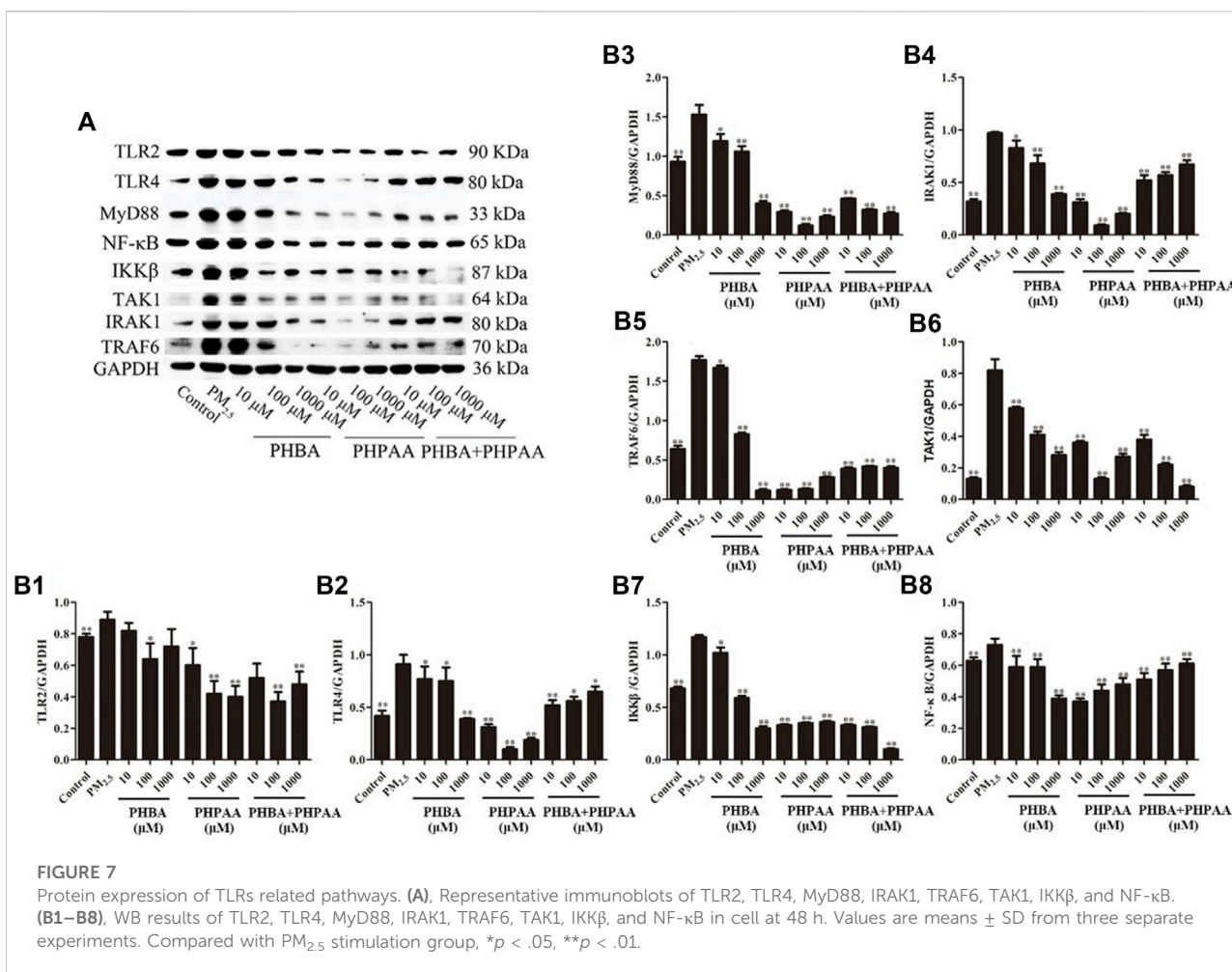
2.7 Quantitative real-time PCR

RAW264.7 cells (2×10^6 cells/well) were seeded in a 6-well plate, pretreated with PM_{2.5} (80 μg/L) for 48 h, and then treated with PHBA, PHPAA or mixture of PHBA and PHPAA for 24 h. Trizol reagent (Invitrogen Life Technologies, Carlsbad, CA, United States) was used to extract the total RNA of the cells pretreated with PM_{2.5}. Detection of mRNA expression with Applied Biosystems ViiATM 7 Real-Time PCR system. cDNA synthesis was performed using a PrimeScript™ RT Reagent Kit according to the manufacturer's instructions. After reverse transcription, the cDNA was amplified using SYBR-Green Premix (Takara, Otsu, Japan). Level of TLR2, TLR4, MyD88, IRAK1, TRAF6, TAK1, IKKβ, and NF-κB mRNA expressions were examined, and GAPDH was used as an internal control.

Data were analyzed by the $2^{-\Delta\Delta CT}$ method. Sequences of primers used for qRT-PCR are list in Table 1.

2.8 Western blot

After overnight culture in a 6-well plate (2×10^6 cells/well, 3 ml medium/plate), the cells were pre-treated with PM_{2.5} for 48 h and drugs for an additional 24 h, cells were harvested and lysed in lysis buffer for 15 min on ice. After incubation, lysates were centrifuged and supernatant was collected. The protein concentration was measured by the bicinchoninic acid (BCA) method. 20 μg protein sample was separated on 10% SDS-PAGE and transferred to PVDF membranes. At room temperature, the membrane was sealed with 5% skimmed



milk powder dissolved in triple buffered saline containing .1% Tween-20 (TBST) for 1 h. Then incubate the membrane with the primary antibody that recognized TLR2, TLR4, MyD88, IRAK1, TRAF6, TAK1, IKK β , NF- κ B, and GAPDH in a shaking incubator at 4°C overnight, wash it with TBST three times, and incubate it with the secondary antibody conjugated with peroxidase diluted in the closed solution at room temperature for 1 h. After washing, proteins of interest were detected using ECL detection reagent.

2.9 Statistical analysis

Statistical analyses were performed using the SPSS 24.0 software. The data were expressed as the Mean \pm SD. Multiple comparisons were evaluated by one-way analysis of variance (ANOVA) with Dunnett's posttest. Statistical significance was accepted at p < .05 or p < .01.

3 Results

3.1 Effect of PM_{2.5} on RAW264.7 cells

After administration of PM_{2.5} at different concentrations, the survival rate of RAW264.7 cells decreased, but there was no statistical difference compared with the control group, indicating that PM_{2.5} within the measurement range could not inhibit the growth of RAW264.7 cells (Figure 2). It was found by flow cytometry that compared with the control group, PM_{2.5} of all concentrations did not induce apoptosis (Figure 3). Fluorescence staining results showed that the number of dead cells (red fluorescence) did not increase significantly after the action of PM_{2.5} of various concentrations. Hoechst staining results showed that the nuclear morphology of each PM_{2.5} group did not change significantly, and no apoptotic cells were observed (Figure 4).

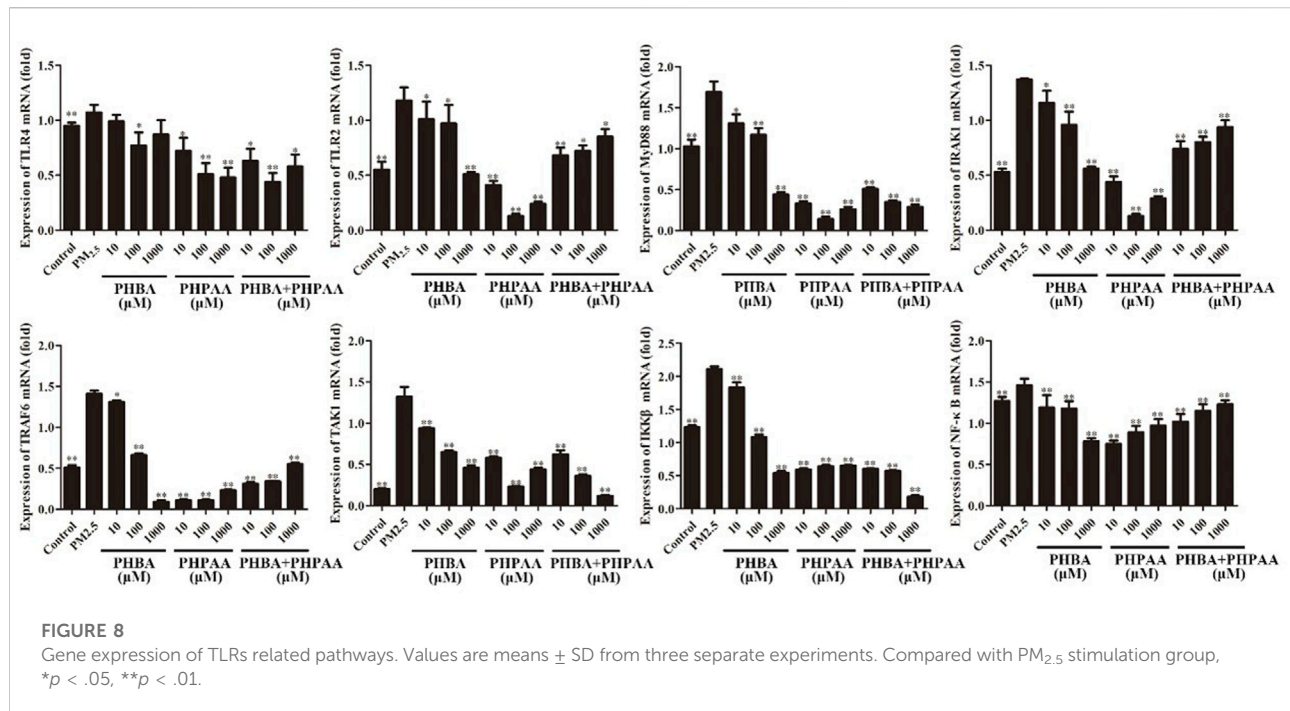


TABLE 2 Effects of PHBA on gene expression in TLRs related pathways.

Name	Control	PM _{2.5}	PHBA(μ M)		
			10	100	1,000
TLR2	.95 \pm .03**	1.07 \pm .07	.99 \pm .06	.77 \pm .12*	.87 \pm .13
TLR4	.55 \pm .073**	1.18 \pm .12	1.01 \pm .16*	.97 \pm .17*	.51 \pm .02**
MyD88	1.03 \pm .08**	1.69 \pm .13	1.31 \pm .11*	1.17 \pm .08**	.44 \pm .03**
IRAK1	.53 \pm .03**	1.37 \pm .01	1.16 \pm .11*	.96 \pm .12**	.56 \pm .02**
TRAF6	.51 \pm .03**	1.41 \pm .04	1.34 \pm .02*	.66 \pm .02**	.09 \pm .02**
TAK1	.20 \pm .01**	1.32 \pm .12	.94 \pm .01**	.65 \pm .02**	.46 \pm .03**
IKK β	1.23 \pm .03**	2.11 \pm .04	1.83 \pm .08*	1.08 \pm .04**	.54 \pm .03**
NF- κ B	1.27 \pm .05**	1.46 \pm .08	1.19 \pm .15**	1.18 \pm .09**	.78 \pm .04**

Note: Compared with PM_{2.5} stimulation group, * $p < .05$, ** $p < .01$.

3.2 Effect of PM_{2.5} on inflammatory cytokines produced by RAW264.7 cells

The inflammatory factors produced by RAW264.7 cells stimulated by PM_{2.5} were detected by ELISA, and the results showed that 80 μ g/ml and 100 μ g/mL PM_{2.5} produced significantly higher IL-1 β , IL-6, and TNF- α than that of the control group ($p < .01$). Compared with the control group, there was no difference of IL-1 β concentration produced by RAW264.7 cells that stimulated by 10, 20 or 40 μ g/mL PM_{2.5} ($p > .05$) (Figure 5). Through microscopic

observation, high concentration of PM_{2.5} will cause unclear observation field of vision, so 80 μ g/ml of PM_{2.5} was applied in subsequent experiments.

3.3 Inhibitory effect of PHBA and PHPAA on inflammatory factors produced by PM_{2.5}

Compared with the control group, PM_{2.5} significantly increased the production of inflammatory factors ($p < .01$).

TABLE 3 Effects of PHPAA on gene expression in TLRs related pathways.

Name	Control	PM _{2.5}	PHPAA (μM)		
			10	100	1,000
TLR2	.95 ± .03**	1.07 ± .07	.72 ± .12*	.51 ± .1**	.48 ± .09**
TLR4	.55 ± .073**	1.18 ± .12	.41 ± .04**	.13 ± .02**	.24 ± .02**
MyD88	1.03 ± .08**	1.69 ± .13	.33 ± .03**	.14 ± .03**	.26 ± .03**
IRAK1	.53 ± .03**	1.37 ± .01	.44 ± .05**	.13 ± .02**	.29 ± .02**
TRAF6	.51 ± .03**	1.41 ± .04	.11 ± .01**	.11 ± .01**	.23 ± .01**
TAK1	.20 ± .01**	1.32 ± .12	.58 ± .02**	.23 ± .01**	.44 ± .02**
IKKβ	1.23 ± .03**	2.11 ± .04	.59 ± .02**	.64 ± .02**	.65 ± .01**
NF-κB	1.27 ± .05**	1.46 ± .08	.75 ± .04**	.89 ± .08**	.97 ± .08**

Note: Compared with PM_{2.5} stimulation group, * $p < .05$, ** $p < .01$.

TABLE 4 Effects of PHBA combined with PHPAA on gene expression in TLRs related pathways.

Name	Control	PM _{2.5}	PHBA + PHPAA (μM)		
			10	100	1,000
TLR2	.95 ± .03**	1.07 ± .07	.63 ± .11*	.44 ± .08**	.58 ± .11*
TLR4	.55 ± .07**	1.18 ± .12	.68 ± .07**	.72 ± .05*	.85 ± .07*
MyD88	1.03 ± .08**	1.69 ± .13	.51 ± .02**	.35 ± .02**	.29 ± .03**
IRAK1	.53 ± .03**	1.37 ± .01	.74 ± .07**	.8 ± .05**	.94 ± .06**
TRAF6	.51 ± .03**	1.41 ± .04	.31 ± .02**	.34 ± .01**	.55 ± .02**
TAK1	.20 ± .01**	1.32 ± .12	.62 ± .05**	.36 ± .02**	.12 ± .01**
IKKβ	1.23 ± .03**	2.11 ± .04	.60 ± .01**	.57 ± .01**	.18 ± .02**
NF-κB	1.27 ± .05**	1.46 ± .08	1.02 ± .09**	1.15 ± .08**	1.23 ± .05**

Note: Compared with PM_{2.5} stimulation group, * $p < .05$, ** $p < .01$.

After different concentrations of PHBA or PHPAA (10, 100, 1,000 μM) treatment, the content of IL-1 β, IL-6, and TNF- α significantly decreased ($p < .01$). After combined treatment of PHBA and PHPAA (the molar ratio of PHBA and PHPAA was 1:1), the content of IL-1 β, IL-6, and TNF- α significantly decreased ($p < .01$) (Figure 6).

3.4 Effect of PHBA and PHPAA on TLRs related signal pathway protein expression

Compared with the control group, the protein expression of TLRs (TLR2 and TLR4) and related receptors MyD88, IRAK1, TRAF6, TAK1, IKKβ, and NF-κB increased significantly after PM_{2.5} stimulation ($p < .01$) (Figure 7). After treating RAW264.7 cells stimulated by PM_{2.5} with different

concentrations of PHBA, the expressions of TLR2, TLR4, MyD88, IRAK1, TRAF6, TAK1, IKKβ, and NF-κB decreased, and the changes showed a dose-effect relationship. However, when treated with a high concentration of PHBA (1,000 μM), the protein expression of TLR2 increased (Figure 7). Treating RAW264.7 cells stimulated by PM_{2.5} with different concentrations of PHPAA (10, 100, 1,000 μM) could make the protein expression of TLR2, TLR4, MyD88, IRAK1, TRAF6, TAK1, IKKβ, and NF-κB significantly decreased ($p < .01$). The protein expressions of TLR4, MyD88, IRAK1, TRAF6, TAK1, IKKβ, and NF-κB were increased when PHPAA was treated with high concentration (1,000 μM) (Figure 7). The combination of PHBA and PHPAA (1:1) also significantly decreased the expression of TLRs pathway proteins ($p < .01$), but increased the expression of TLR2, TLR4, IRAK1 and NF-κB proteins at high concentrations (1000 μM) (Figure 7).

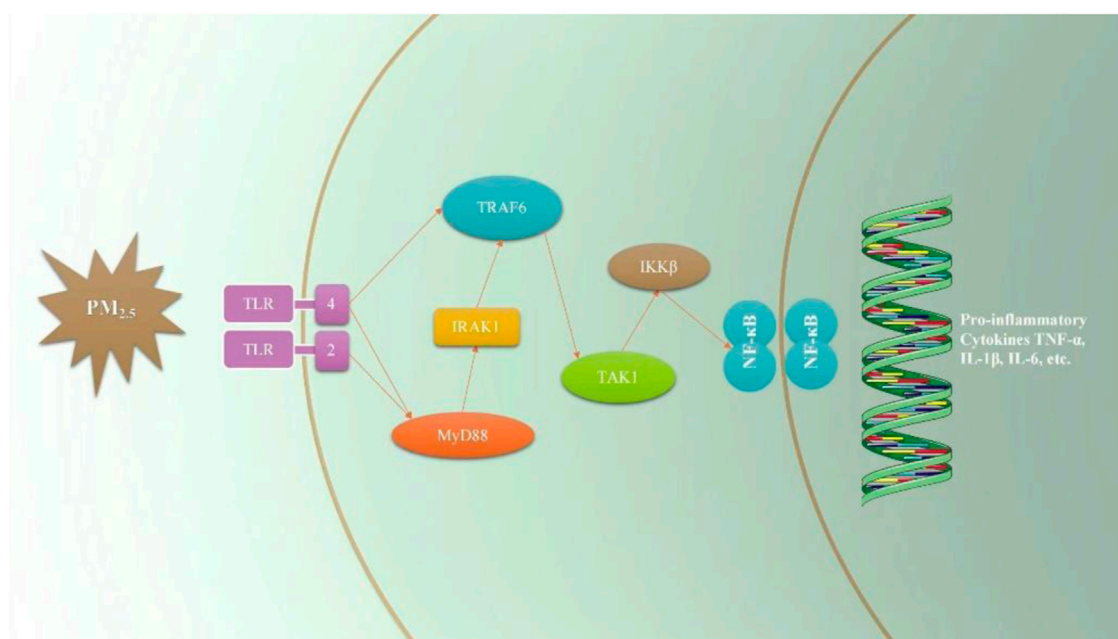


FIGURE 9
Sketch of the effect of PM_{2.5} on TLRs signal pathway.

3.5 Effects of PHBA and PHPAA on TLRs signal pathway gene expression

The gene expressions of TLRs and its downstream related pathway were determined by RT-qPCR. PM_{2.5} can significantly up-regulate the gene expression of TLR2, TLR4, MyD88, IRAK1, TRAF6, TAK1, IKK β and NF- κ B ($p < .01$) (Figure 8, Table2). After treating RAW264.7 cells stimulated by PM_{2.5} with drugs for 24 h, the TLRs and its downstream pathway related genes were detected. The results showed that PHBA could significantly down regulate the TLRs related pathway genes in a dose effect relationship ($p < .01$) (Figure 8; Table2). After the cells stimulated by PM_{2.5} were treated with PHPAA, the gene expression of TLRs pathway was significantly decreased ($p < .01$). When PHPAA concentration is high (1,000 μ M), the expression of related genes TLR4, MyD88, IRAK1, TRAF6, TAK1, IKK β , and NF- κ B increased (Figure 8; Table3). When the mixture of PHBA and PHPAA (1:1) was used, the gene expression of TLRs pathway was significantly decreased ($p < .01$). When the mixture is at high concentration (1,000 μ M), the expression of TLR2, TLR4, IRAK1 and NF- κ B significantly increased (Figure 8; Table4).

4 Discussion

PM_{2.5} has a great impact on the central nervous system, blood system, metabolic immune system, digestive system, skin

and other human bodies, and may lead to a variety of diseases. PM_{2.5} can destroy the integrity of the blood brain barrier (BBB) and make it easy for peripheral systemic inflammation to pass through the BBB to reach the central nervous system (Shou et al., 2019). The study found that the concentration of PM_{2.5} had a certain toxic effect on children's bone marrow stromal cells, which affected the hematopoietic microenvironment of bone marrow. PM_{2.5} may activate PINK1/Parkin pathway signal and induce mitochondrial autophagy by increasing ROS, and further activate HSCs (hepatic stellate cells) to cause liver fibrosis (Qiu et al., 2019). Cholesterol and squalene are key substances that affect the skin barrier function. PM_{2.5} can cause barrier disorder by increasing cholesterol synthesis, leading to the temporary accumulation of epidermal cholesterol and the reduction of squalene (Liao et al., 2019). It can be seen that PM_{2.5} is harmful to human health. It is very important to find effective drugs to treat PM_{2.5} as soon as possible.

It has been reported that PM_{2.5} can activate the inflammatory axis of vascular endothelial cell COX-2/PGES/PGE2, and promote cell apoptosis and inflammatory response (Yin et al., 2017). PM_{2.5} may induce apoptosis by increasing lipid accumulation, ROS level and activating mitochondrial pathway of macrophages. However, the results of MTT, flow cytometry and Calcein AM/PI staining showed that PM_{2.5} used in our study had no cytotoxicity to RAW264.7 and had no effect on apoptosis. The experimental results obtained in this study are different from those in related papers, which may be related to

the physical and chemical properties of PM_{2.5} collected, processing and preservation methods of PM_{2.5}.

It is reported that PM_{2.5} can cause airway inflammation and lung injury in mice, and can also produce cellular inflammation and secrete inflammatory factors from RAW264.7 cells (He et al., 2017; Ogino et al., 2018). In this study, PM_{2.5} was used to stimulate RAW264.7 cells, and the related inflammatory factor IL-1 β , IL-6, and TNF- α secreted by cells significantly increased. However, when PHBA, PHPAA, the mixture of PHBA and PHPAA (1:1) were given in advance, the detection results of inflammatory factors secreted by cells were significantly reduced. It suggests that PHBA and PHPAA can repair the damage caused by PM_{2.5} through inhibiting inflammatory factors.

In the induction of inflammatory response, TLRs play a role mainly through MyD88 and TRIF mediated pathways (Deguine and Barton, 2014). When sensing external stimuli, TLRs allow MyD88 to dock with MAL (MyD88 adapter-like). MAL is a bridging linker, often involved in TLR4 signal pathway, while TLR2 signal pathway is less involved, and interacts with MyD88 through TIR. In addition to the TIR domain, MyD88 also contains a dead domain, which can help it interact with IRAK4 (Janssens and Beyaert, 2003; Lim and Staudt, 2013). The interaction between these domains produces a large polymer, and the nitration of this polymer leads to the activation and dimerization of TRAF6 (Lin et al., 2010). TRAF6 mediates the ubiquitination of TAK1. The lack of TAK1 reduces the inflammatory signal of TLRs, but this phenomenon is not observed when TAB protein is lacking. TAK1 signal then activate NF- κ B and MAPK, respectively. NF- κ B is a molecular center of inflammation signal, and activated by phosphorylated IKK α and IKK β (Kawai and Akira, 2007). TRF signal is a separate branch of TLR signal, which can only be continued through TLR3 and TLR4, where TRIF interacts with TRAF3 and TRAF6 (Akira et al., 2006). In this study, the protein and gene of TLR pathway related factors were determined. It was found that PM_{2.5} can increase the expression of TLR2/4 \rightarrow MyD88 \rightarrow IRAK1 (TRAF6) \rightarrow TAK1 \rightarrow IKK β \rightarrow NF- κ B protein and gene in TLR pathway and eventually lead to inflammation (Figure 9). When PHBA, PHPAA and the mixture of PHBA and PHPAA (1:1) were added to PM_{2.5}-stimulated RAW264.7 cells, the above three factors could reduce the expression of TLRs related pathway proteins and genes. These results indicate that PHBA and PHPAA can reduce inflammation caused by PM_{2.5} by regulating TLRs and their related pathway signal transduction factors.

In this study, we measured the protein and gene of TLR pathway related factors and found that PM_{2.5} can increase the protein and gene expression of TLR pathway and eventually lead to inflammation. PHBA, PHPAA and the mixture of PHBA and PHPAA (1:1) can reduce the expression of TLRs related pathway proteins and genes of RAW264.7 cells stimulated by PM_{2.5}, indicating that PHBA and PHPAA can reduce the inflammation produced by PM_{2.5} by regulating TLRs and its related pathway signal transduction factors.

5 Conclusion

PM_{2.5} can produce inflammatory reaction and secrete inflammatory cytokines. The molecular mechanism of inflammation produced by PM_{2.5} is related to TLRs and its related pathways, and TLRs pathway can become a potential new target for treating inflammation produced by PM_{2.5}. PHBA, PHPAA and their combination can reduce the inflammatory reaction produced by PM_{2.5}. The mechanism of action is related to the inhibition of TLRs and its related pathways, indicating that TLRs signal pathway may be a potential pathway for PHBA and PHPAA to treat inflammation induced by PM_{2.5}.

Data availability statement

The original contributions presented in the study are included in the article/Supplementary Material, further inquiries can be directed to the corresponding author.

Author contributions

Study design: B-LX and X-BW; data collection: B-LX, Y-YW, L-LJ, and ZL, D-RL, HZ, and S-LL; Analysis and interpretation: B-LX, Y-YW, and L-LJ; Statistical analysis: Y-YW; Drafting manuscript: B-LX; Revision manuscript: X-BW.

Acknowledgments

The authors thanks Hong-Hai YU from Huadian Electric Power Research Institute Co., LTD. Northeast Branch provided PM_{2.5} in the experiment.

Conflict of interest

The authors declare that the research was conducted in the absence of any commercial or financial relationships that could be construed as a potential conflict of interest.

Publisher's note

All claims expressed in this article are solely those of the authors and do not necessarily represent those of their affiliated organizations, or those of the publisher, the editors and the reviewers. Any product that may be evaluated in this article, or claim that may be made by its manufacturer, is not guaranteed or endorsed by the publisher.

References

- Akira, S., Uematsu, S., and Takeuchi, O. (2006). Pathogen recognition and innate immunity. *Cell* 124 (4), 783–801. doi:10.1016/j.cell.2006.02.015
- Boothe, V. L., Boehmer, T. K., Wendel, A. M., and Yip, F. Y. (2014). Residential traffic exposure and childhood leukemia: A systematic review and meta-analysis. *Am. J. Prev. Med.* 46 (4), 413–422. doi:10.1016/j.amepre.2013.11.004
- Chen, P., Wang, Y., Chen, L., Jiang, W., Niu, Y., Shao, Q., et al. (2015). Comparison of the anti-inflammatory active constituents and hepatotoxic pyrrolizidine alkaloids in two *Senecio* plants and their preparations by LC-UV and LC-MS. *J. Pharm. Biomed. Anal.* 10 (115), 260–271. doi:10.1016/j.jpba.2015.07.014
- Deguine, J., and Barton, G. M. (2014). MyD88: A central player in innate immune signaling. *F1000Prime Rep.* 4, 697. doi:10.12703/P6-97
- Geng, J., Liu, H., Ge, P., Hu, T., Zhang, Y., Zhang, X., et al. (2019). PM2.5 promotes plaque vulnerability at different stages of atherosclerosis and the formation of foam cells via TLR4/MyD88/NFκB pathway. *Ecotoxicol. Environ. Saf.* 30 (176), 76–84. doi:10.1016/j.ecoenv.2019.03.068
- Han, Y., Qi, M., Chen, Y., Shen, H., Liu, J., Huang, Y., et al. (2015). Influences of ambient air PM- concentration and meteorological condition on the indoor PM_{2.5} concentrations in a residential apartment in Beijing using a new approach. *Environ. Pollut.* 205, 307–314. doi:10.1016/j.envpol.2015.04.026
- He, M., Ichinose, T., Yoshida, S., Ito, T., He, C., Yoshida, Y., et al. (2017). PM2.5-induced lung inflammation in mice: Differences of inflammatory response in macrophages and type II alveolar cells. *J. Appl. Toxicol.* 37 (10), 1203–1218. doi:10.1002/jat.3482
- Huang, X. F., Yun, H., Gong, Z. H., Li, X., He, L. Y., Zhang, Y. H., et al. (2014). Source apportionment and secondary organic aerosol estimation of PM2.5 in an urban atmosphere in China. *Sci. China(Earth Sci.)* 57 (06), 1352–1362. doi:10.1007/s11430-013-4686-2
- Janssens, S., and Beyaert, R. (2003). Functional diversity and regulation of different interleukin-1 receptor-associated kinase (IRAK) family members. *Mol. Cell* 11 (2), 293–302. doi:10.1016/s1097-2765(03)00053-4
- Jeong, S., Park, S. A., Park, I., Kim, P., Cho, N. H., Hyun, J. W., et al. (2019). PM2.5 exposure in the respiratory system induces distinct inflammatory signaling in the lung and the liver of mice. *J. Immunol. Res.* 1, 3486841. doi:10.1155/2019/3486841
- Ji, W., and Zhao, B. (2015). Contribution of outdoor-originating particles, indoor-emitted particles and indoor secondary organic aerosol (soa) to residential indoor PM2.5 concentration: A model-based estimation. *Build. Environ.* 90, 196–205. doi:10.1016/j.buildenv.2015.04.006
- Kawai, T., and Akira, S. (2007). Signaling to NF-κB by toll-like receptors. *Trends Mol. Med.* 13 (11), 460–469. doi:10.1016/j.molmed.2007.09.002
- Li, L. J., Wang, J. Y., Wang, Y., Wang, L. J., Wang, H. Y., and Wang, B. X. (2005). Anti-virus activities of the extract and effective components isolated from *Senecio cannabifolius* less. *China J. Basic Med. TCM.* 11 (8), 585–587.
- Li, T., Cao, S., Fan, D., Zhang, Y., Wang, B., Zhao, X., et al. (2016). Household concentrations and personal exposure of PM2.5 among urban residents using different cooking fuels. *Sci. Total Environ.* 1, 548–549. doi:10.1016/j.scitotenv.2016.01.038
- Liao, Z., Nie, J., and Sun, P. (2019). The impact of particulate matter (PM2.5) on skin barrier revealed by transcriptome analysis: Focusing on cholesterol metabolism. *Toxicol. Rep.* 25 (7), 1–9. doi:10.1016/j.toxrep.2019.11.014
- Lim, K. H., and Staudt, L. M. (2013). Toll-like receptor signaling. *Cold Spring Harb. Perspect. Biol.* 5 (1), a011247. doi:10.1101/cshperspect.a011247
- Lin, S. C., Lo, Y. C., and Wu, H. (2010). Helical assembly in the MyD88-IRAK4-IRAK2 complex in TLR/IL-1R signalling. *Nature* 17 (7300), 465885–465890. doi:10.1038/nature09121
- Lin, Y., Zou, J., Yang, W., and Li, C. Q. (2018). A review of recent advances in research on PM_{2.5} in China. *Int. J. Environ. Res. Public Health* 15 (3), 438. doi:10.3390/ijerph15030438
- Ogino, K., Nagaoka, K., Ito, T., Takemoto, K., Okuda, T., Nakayama, S. F., et al. (2018). Involvement of PM2.5-bound protein and metals in PM2.5-induced allergic airway inflammation in mice. *Inhal. Toxicol.* 30 (13-14), 498–508. doi:10.1080/08958378.2018.1561769
- Park, S. K., and Wang, W. (2014). Ambient air pollution and type 2 diabetes: A systematic review of epidemiologic research. *Curr. Environ. Health Rep.* 1 (3), 275–286. doi:10.1007/s40572-014-0017-9
- Piao, M. J., Ahn, M. J., Kang, K. A., Ryu, Y. S., Hyun, Y. J., Shilnikova, K., et al. (2018). Particulate matter 2.5 damages skin cells by inducing oxidative stress, subcellular organelle dysfunction, and apoptosis. *Arch. Toxicol.* 92 (6), 2077–2091. doi:10.1007/s00204-018-2197-9
- Qiu, Y. N., Wang, G. H., Zhou, F., Hao, J. J., Tian, L., Guan, L. F., et al. (2019). PM2.5 induces liver fibrosis via triggering ROS-mediated mitophagy. *Ecotoxicol. Environ. Saf.* 167, 178–187. doi:10.1016/j.ecoenv.2018.08.050
- Shaffer, R. M., Sheppard, L., Peskind, E. R., Zhang, J., Adar, S. D., and Li, G. (2019). Fine particulate matter exposure and cerebrospinal fluid markers of vascular injury. *J. Alzheimers Dis.* 71 (3), 1015–1025. doi:10.3233/JAD-190563
- Shou, Y., Huang, Y., Zhu, X., Liu, C., Hu, Y., and Wang, H. (2019). A review of the possible associations between ambient PM2.5 exposures and the development of Alzheimer's disease. *Ecotoxicol. Environ. Saf.* 15 (174), 344–352. doi:10.1016/j.ecoenv.2019.02.086
- Sun, J. D., Wang, X. B., Jiang, S., Xi, R. G., and Tian, Y. (2014). Preventive effect of *Senecio cannabifolius* Less. on perfluoroisobutylene inhalation-induced acute lung injury in rats. *J. Int. Pharm. Res.* 41 (4), 444. doi:10.13220/j.cnki.jipr.2014.04.01
- Yin, J., Xia, W., Li, Y., Guo, C., Zhang, Y., Huang, S., et al. (2017). COX-2 mediates PM2.5-induced apoptosis and inflammation in vascular endothelial cells. *Am. J. Transl. Res.* 9 (9), 3967–3976.
- Zhao, G. Y., Wang, X. B., Xi, R. G., Jiang, S., and Wu, L. J. (2013). Protective effect of *Senecio cannabifolius* less. On acute lung injury induced by perfluoroisobutylene on mice. *Pharm. J. Chin. People's Lib. Army.* 29 (01), 13–16.
- Zhou, Z. H., Liu, Y. L., Yuan, J. J., Zuo, J., Chen, G. Y., Xu, L. Y., et al. (2016). Indoor PM2.5 concentrations in residential buildings during a severely polluted winter: A case study in tianjin, China. *Renew. Sustain. Energy Rev.* 64, 372–381. doi:10.1016/j.rser.2016.06.018



OPEN ACCESS

EDITED BY
Zheng Xiang,
Liaoning University, China

REVIEWED BY
Yuhui Yan,
Jiangsu Food and Pharmaceutical
Science College, China
Zhongwen Yuan,
Guangzhou Medical University, China

*CORRESPONDENCE
Yusheng Han,
✉ hysh1973@126.com
Guijun Liu,
✉ liuguojun9626@163.com
Hao Li,
✉ lihaostudy@sina.com

SPECIALTY SECTION
This article was submitted to
Ethnopharmacology,
a section of the journal
Frontiers in Pharmacology

RECEIVED 06 November 2022
ACCEPTED 14 December 2022
PUBLISHED 10 January 2023

CITATION
Han X, Ma T, Wang Q, Jin C, Han Y, Liu G
and Li H (2023), The mechanism of
oxymatrine on atopic dermatitis in mice
based on SOCS1/JAK-STAT3 pathway.
Front. Pharmacol. 13:1091090.
doi: 10.3389/fphar.2022.1091090

COPYRIGHT
© 2023 Han, Ma, Wang, Jin, Han, Liu and
Li. This is an open-access article
distributed under the terms of the
[Creative Commons Attribution License](https://creativecommons.org/licenses/by/4.0/)
(CC BY). The use, distribution or
reproduction in other forums is
permitted, provided the original
author(s) and the copyright owner(s) are
credited and that the original
publication in this journal is cited, in
accordance with accepted academic
practice. No use, distribution or
reproduction is permitted which does
not comply with these terms.

The mechanism of oxymatrine on atopic dermatitis in mice based on SOCS1/JAK-STAT3 pathway

Xianwei Han¹, Tianming Ma², Qiang Wang¹, Chunlin Jin¹,
Yusheng Han^{3*}, Guijun Liu^{3*} and Hao Li^{4*}

¹Department of Dermatology, The Seventh People's Hospital of Shenyang, Shenyang, China, ²The Second Hospital of Heilongjiang University of Chinese Medicine, Harbin, China, ³Heilongjiang University of Chinese Medicine, Harbin, China, ⁴Shenzhen University General Hospital, Shenzhen, China

Based on the suppressor of cytokine signaling 1 (SOCS1)/Janus kinase (JAK)/signal transducer and activator of transcription 3 (STAT3) pathway, the mechanism of oxymatrine in the treatment of atopic dermatitis (AD) was preliminarily explored in this study. C57BL/6 mice were induced to establish AD model by smearing carbatriol (MC903) on their back. The AD mice were randomly divided into model group, oxymatrine groups with three dosages (25, 50 and 100 mg/kg), ($n = 10$). Oxymatrine groups were intragastric administered once daily for 14 days. The same volume of saline was given in the normal control group and model group once daily for 14 days. Subsequently, HE staining was used to observe the pathological changes of skin tissue, ELISA was used to detect the levels of serum inflammatory factors including interleukin-4, 6 and 17 (IL-4, IL-6, and IL-17), tumor necrosis factor- α (TNF- α) and immunoglobulin E (IgE). Immunohistochemistry was used to detect the expression of suppressor of cytokine signaling 1 and CD3 in skin tissue, and Western blotting was used to detect the proteins in suppressor of cytokine signaling 1/JAK-STAT3 pathway. Compared with the normal control group, the pathological damage of mice in the model group, such as skin hyperplasia, edema, congestion and inflammatory infiltration, aggravated increased significantly. And the expression of serum inflammatory factors, CD3 positive expression and JAK-STAT3 pathway protein in the model group were increased ($p < .05$), and the expression of suppressor of cytokine signaling 1 protein ($p < .05$) was decreased. Compared with the model group, the above pathological damage of the mice was reduced, and the serum inflammatory factors, JAK-STAT3 pathway protein, and CD3 positive expression were decreased as a dose-dependant manner ($p < .05$), and the expression of suppressor of cytokine signaling 1 protein was increased as a dose-dependent manner ($p < .05$). Oxymatrine can improve the skin inflammation symptoms of AD mice by up regulating the expression of suppressor of cytokine signaling 1, inhibiting the activation of JAK-STAT3 pathway and blocking the activation of T lymphocytes.

KEYWORDS

oxymatrine, SOCS1, janus kinase, JAK-STAT3, atopic dermatitis

1 Introduction

Atopic dermatitis (AD) is a chronic inflammatory skin disease that was related to autoimmunity (Kim et al., 2019). AD could cause some complications, such as metabolic disorders, cardiovascular diseases, and emotional disorders, which seriously affect the quality of life of patients (Robert et al., 2018; Tsakok et al., 2019). At present, the etiology and pathogenesis of AD are still unclear. It is generally believed that it was caused by the interaction of multiple complex factors such as genetics, immune disorders, epidermal gene mutations, and environment and microorganisms, and is highly correlated with the helper T cell 2 (Th2) and helper T cell 22 (Th22) cell response drive (Liang et al., 2021).

Clinical treatment of AD is to relieve or eliminate clinical symptoms, eliminate inducing factors, reduce and prevent recurrence, and improve the quality of life of patients (Boothe et al., 2017; Tiago et al., 2019). So, external drugs such as glucocorticoids, phosphodiesterase 4 (PDE-4) inhibitors, and systemic drugs such as oral antihistamines, immunosuppressive agents, biological agents, Janus kinase inhibitors are the main clinical drugs in the treatment of AD (Liu et al., 2022).

Due to the chronic and recurrent characteristics of AD, patients need to receive long-term treatment, looking for good efficacy and less adverse reactions of drugs has been of concern. Oxymatrine (OMT), a common matrine-type alkaloid with quinolizidine structure, was the main active ingredient in the herb of *Sophora flavescens* Alt., *Sophora tonkinensis* Gagnep and *Sophora alopecuroides* L. OMT and the pharmaceutical preparation with OMT have been widely used in the clinical treatment of a variety of diseases, and showed a certain therapeutic effect (Lan et al., 2020; Lan et al., 2021). Clinically, OMT injection has been used in the treatment of chronic hepatitis B and C, herpes zoster, liver fibrosis and other diseases (Song et al., 2016). The therapeutic effect is obvious and the related symptoms are effectively alleviated. OMT has a variety of pharmacological effects, such as anti-infection, anti-virus, sedative and hypnotic, antipyretic and analgesic, and immune regulation (Wu and Gao, 2015; Clarissa et al., 2019; Wang et al., 2021). It has been reported that OMT has a certain therapeutic effect on atopic dermatitis (AD) model mice, and its mechanism is related to inhibiting the infiltration of mast cells in the dermis and reducing the expression of Th2 cytokines (Sun et al., 2021).

Suppressor of cytokine signaling 1 (SOCS1) can effectively avoid excessive immune response and prevent the development of chronic inflammatory diseases by negatively regulating Janus kinase (JAK)/signal transducer and activator of transcription 3 (STAT3) (Ho et al., 2020). Therefore, this study established an AD model in mice to explore the therapeutic mechanism of oxymatrine on AD from

the perspective of SOCS1/JAK-STAT3 pathway, in order to find specific and effective drugs for the treatment of AD.

2 Materials and methods

2.1 Reagents

Oxymatrine (Y30S6-Y17043, HPLC grade, purity $\geq 98\%$) was purchased from Shanghai Yuanye Bio-Technology Co., Ltd. Interleukin-4 (IL-4) ELISA kit (EK0405), interleukin-6 (IL-6) ELISA kit (EK0411), interleukin-17 (IL-17) ELISA kit (EK0431) and tumor necrosis factor- α (TNF- α) ELISA kit (EK0527) were purchased from Wuhan Boster Biological Engineering Co., Ltd. Immunoglobulin E (IgE) ELISA kit (bsk12030) was purchased from Beijing Bioss Biotechnology Co., Ltd. Rabbit anti-mouse antibodies such as SOCS1 (ab280886), T lymphocyte surface marker CD3 (ab5690), JAK1 (ab125051), STAT3 (ab68153), and phosphorylated JAK1 (p-JAK1) (ab1380056) were purchased from the Abcam Co., Ltd.

2.2 Animals and treatment

50 healthy male C57BL/6 mice, the weight range of which was 18–22 g, were purchased from Beijing Vital River Laboratory Animal Technology Co., Ltd. with the certificate number of SCXK (Jing) 2021-006. The AD model was established with applying 20 μ l carbوترiol (MC903) solution (2 nmol/L) to the dorsum for 10 days according to the method with minor modification (Chang et al., 2020). AD model was successful when the ear skin of mice has the phenomena of scratches, erosion, erythema bleeding, and scab. 40 AD mice were randomly divided into model group, oxymatrine group (25 mg/kg, OMT-L), oxymatrine group (50 mg/kg, OMT-M), and oxymatrine group (100 mg/kg, OMT-H) ($n = 10$). Oxymatrine groups were intragastric administered once daily for 14 consecutive days, and the same volume of saline was given in the normal control group and model group once daily for 14 consecutive days. All the mice were anesthetized 2 h after administration on the 14th day. Serum was obtained after the blood samples were collected and centrifugated at 3000 rpm for 15 min at 4°C.

2.3 Detection of TNF- α , IgE, IL-4, IL-6, and IL-17 by ELISA

After the end of the last administration, blood was taken from the abdominal aorta of the mice after anesthesia to obtain the serum, and the contents of TNF- α , IgE, IL-4, IL-6, and IL-17 in the serum were detected according to the instructions of the ELISA kit.

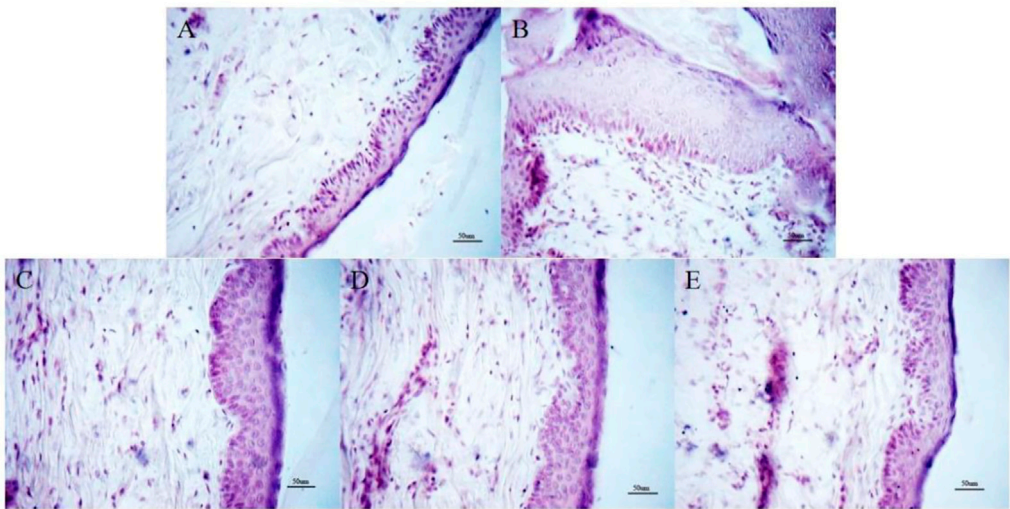


FIGURE 1
Histopathological changes of skin tissue (HE staining, $\times 200$). (A) Control group; (B) Model group. (C) OMT-H group. (D) OMT-M group. (E) OMT-L group.

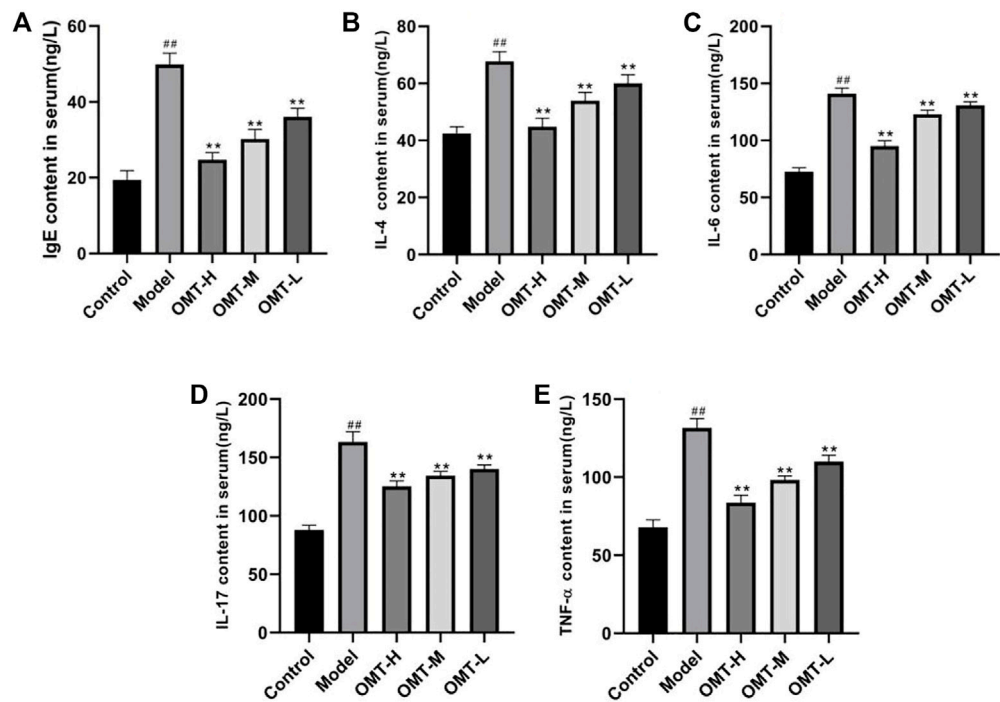
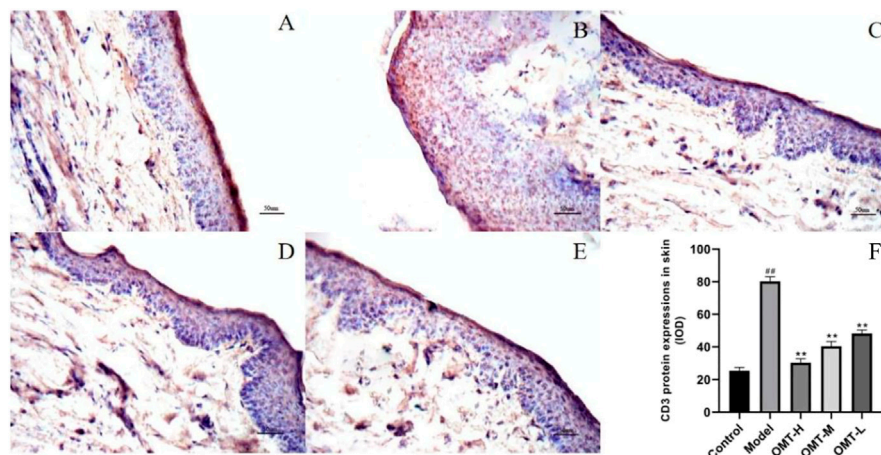
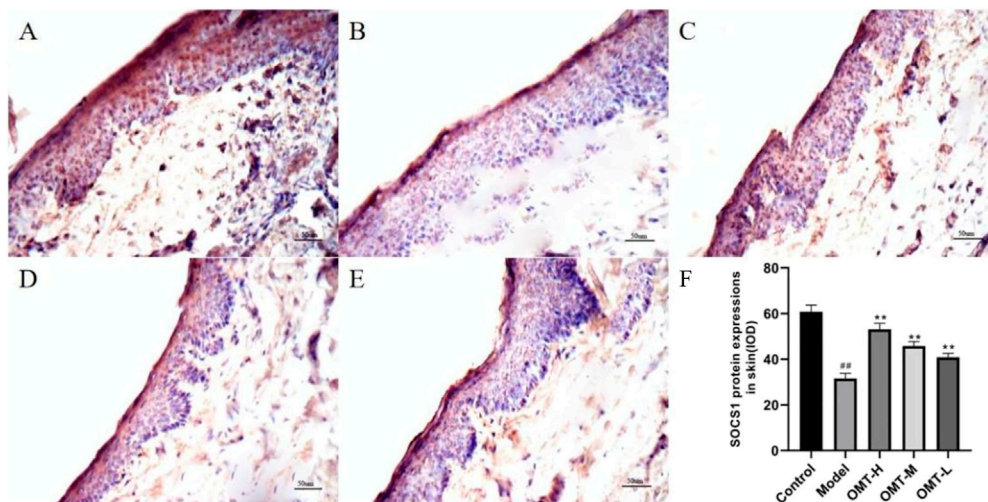


FIGURE 2
Comparison of (A) IgE, (B) IL-4, (C) IL-6, (D) IL-17 and (E) TNF- α levels in serum. (^{##}, $p < .01$, vs. Control group; ^{**}, $p < .01$, vs. model group).

**FIGURE 3**

Positive expression of CD3 in skin tissue (immunohistochemical staining, $\times 200$). (A) Normal control group; (B) Model group. (C) OMT-H group. (D) OMT-M group. (E) OMT-L group. (F) Statistical data of positive expression of CD3 in each group. (^{##}, $p < .01$, vs. Control group; ^{**}, $p < .01$, vs. model group).

**FIGURE 4**

Positive expression of SOCS1 in skin tissue (immunohistochemical staining, $\times 200$). (A) Normal control group; (B) Model group. (C) OMT-H group. (D) OMT-M group. (E) OMT-L group. (F) Statistical data of positive expression of SOCS1 in each group. (^{##}, $p < .01$, vs. Control group; ^{**}, $p < .01$, vs. model group).

2.4 Histopathological observation of skin

The dorsum tissue of mice was cut and separated. Some of the samples were quickly stored in liquid nitrogen for standby, and the other part was fixed in 4% paraformaldehyde for 24 h. The sections with a size of 5 μm were made after conventional paraffin embedding, and the histopathological changes of skin in each group were observed under microscope after HE staining.

2.5 Detection of SOCS1 and T lymphocyte surface marker CD3 positive expression by immunohistochemical

The paraffin sections of skin tissue were dewaxed and antigen repaired, then the SOCS1 and CD3 rabbit anti mouse antibodies with the ratio of 1:200 were dripped and incubated overnight at 4°C. After the biotin labeled IgG antibody was dripped and

incubated at room temperature for 2 h, DAB staining and hematoxylin re-staining were performed, and then observed and photographed under the microscope. Image-Pro Plus 6.0 software was used to analyze the average optical density value of positive staining under each field of vision.

2.6 Detection of SOCS1/JAK-STAT3 pathway protein by western blotting

Skin tissue was weighted and the protein of the tissue was extracted after grinding with liquid nitrogen. BCA method was used to detect the protein concentration. 50 µg of protein was subjected to electrophoresis and membrane transfer reaction, and the primary antibodies of SOCS1, JAK1, p-JAK1, STAT3, p-STAT3 with the ratio of 1:1,000 and the antibody of β-actin with the ratio of 1:2,000 were dropped for incubating overnight at 4°C. HRP goat anti rabbit secondary antibody with the ratio of 1:3,000 was dropped and incubated at room temperature for 2 h. After enhanced chemiluminescence color exposure, the relative expression of the bands was analyzed by ImageJ software.

2.7 Statistical methods

SPSS 24.0 software was used for statistical analysis. The measurement data conforming to the normal distribution was expressed by mean ± standard deviation ($\bar{x} \pm s$). Single factor analysis of variance was used for comparison between groups, and *t*-test was used for pairwise comparison between groups.

3 Results

3.1 Effect of OMT on histopathological damage of skin tissue

The skin texture of mice in the control group was clear and normal without pathological symptoms. In the model group, the pathological symptoms such as hyperplasia of epidermis, thickening of acanthocyte layer, tissue edema and congestion, telangiectasia, and infiltration of inflammatory cells were obvious; The above pathological damage of OMT-H, OMT-M and OMT-L groups were significantly reduced compared with that of model group (Figure 1).

3.2 Effect of OMT on TNF-α, IgE, IL-4, IL-6 and IL-17 levels in serum

Compared with the normal control group, the TNF-α, IgE, IL-4, IL-6 and IL-17 levels in serum of the mice in model group

increased ($p < .05$). Compared with the model group, the TNF-α, IgE, IL-4, IL-6, and IL-17 levels in serum of the mice in OMT-H, OMT-M and OMT-L groups decreased as a dose-dependent manner ($p < .05$) (Figure 2).

3.3 Effect of OMT on T lymphocyte infiltration in skin tissue

The positive expression of CD3 can reflect the infiltration of T lymphocytes. Compared with the normal control group, the positive expression of CD3 in the skin tissue of the model group increased ($p < .05$). Compared with the model group, the positive expression of CD3 in the skin tissue of mice in the OMT-H, OMT-M, and OMT-L groups decreased as a dose-dependent manner ($p < .05$) (Figure 3).

3.4 Effect of OMT on the expression of SOCS1 in skin tissue

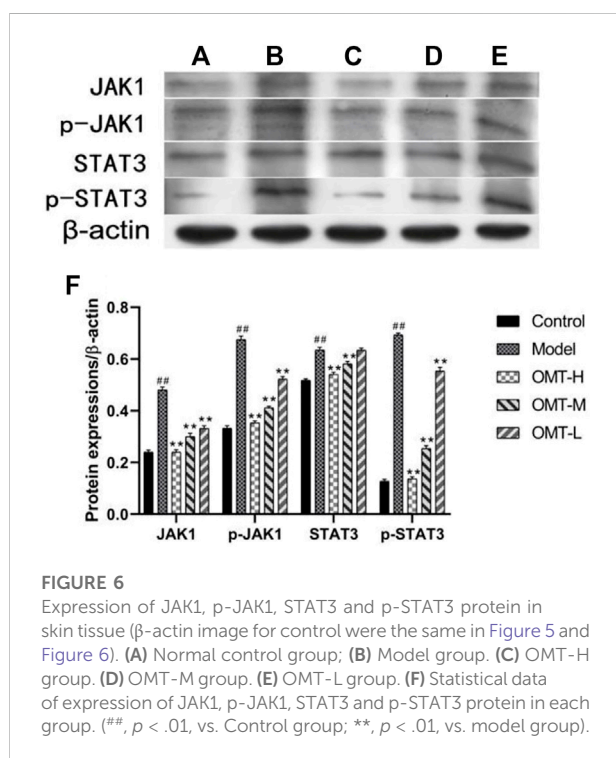
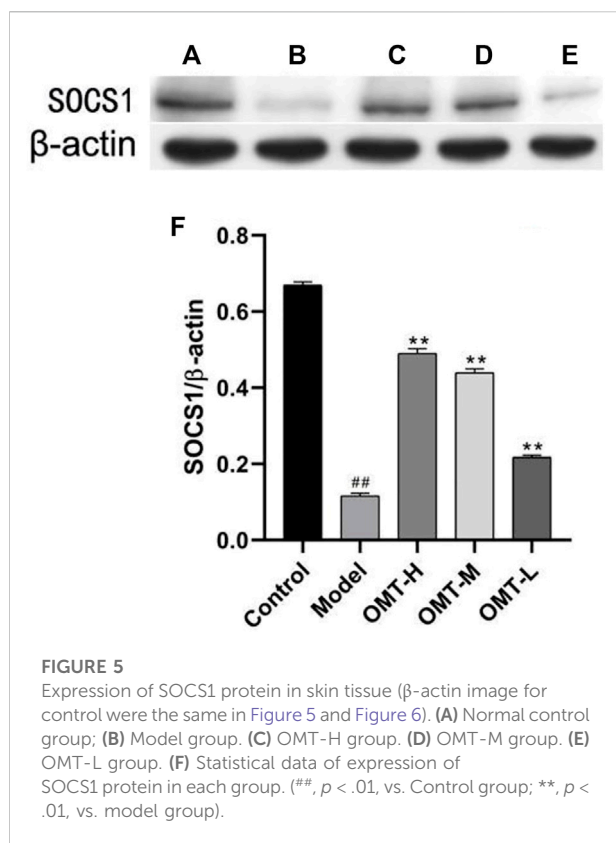
The positive expression of SOCS1 was brownish yellow granules. Compared with the normal control group, the brownish yellow particles in the skin tissue of the model group decreased, and the positive expression of SOCS1 and protein expression decreased ($p < .05$); Compared with the model group, the positive expression of SOCS1 and protein expression in skin tissue of mice in the OMT-H, OMT-M, and OMT-L groups increased as a dose-dependent manner ($p < .05$) (Figures 4, 5).

3.5 Effect of OMT on expression of JAK-STAT3 pathway protein in ear tissue

Compared with the normal control group, the expression of p-JAK1, JAK1, p-STAT3, and STAT3 protein in the skin tissue of mice in the model group increased ($p < .05$). Compared with the model group, the expression of p-JAK1, JAK1, p-STAT3 protein in skin tissue of mice in OMT-H and OMT-L groups decreased as a dose-dependent manner ($p < .05$), and the expression of STAT3 protein in skin tissue of mice in OMT-H and OMT-M groups decreased ($p < .05$). The expression of STAT3 protein in OMT-L group was not statistically significant (Figure 6).

4 Discussion

The cure rate of AD is low, and the incidence rate of AD is high in children. At present, studies have found that the activation of inflammatory reaction mediated by the interaction of activated T lymphocytes, eosinophils and mast cells is the key mechanisms of AD skin damage (Demeyer et al., 2019). After allergen contacts with skin to



form complex, it can induce antigen presenting cells in skin to activate and present allergen to T lymphocytes, stimulate T lymphocytes to activate and transform into Th2 cell subsets and release IL-4, IL-17 and other inflammatory factors to aggravate skin damage (Wu et al., 2021). In addition, the expansion of T lymphocytes to Th2 cell subsets will also promote the conversion of B cells and recognize IgE antibodies of specific environmental allergens, thus causing type I hypersensitivity. The levels of IgE, TNF- α , IL-4, IL-7 and other inflammatory factors in the serum of AD patients are abnormal and higher than that of normal people. The higher the level of IgE, TNF- α , IL-4 and IL-7, the more serious the condition of AD patients (Pei et al., 2020). Inhibiting skin inflammatory damage and regulating immune response are currently widely accepted therapeutic strategies for AD (Hu and Zhang, 2019). In this study, it was found that at the same time as the levels of IgE, TNF- α , IL-4 and IL-7 in serum of mice in the model group increased, the positive expression of CD3, the surface marker of T lymphocytes in skin tissue, was also increased, and the pathological manifestations such as skin epidermal hyperplasia, congestion, edema, and inflammatory cell infiltration were significantly aggravated, suggesting that mice had T lymphocyte activation and inflammatory damage, indicating that the model was established successfully.

OMT is one of the active ingredients in *S. flavescens* Alt., *S. tonkinensis* and *S. alopecuroides* L. Modern clinical studies have found that it has a variety of pharmacological effects such as anti-virus, anti-inflammatory, anti-fibrosis, immune regulation, etc. Studies have shown that OMT can inhibit the contact dermatitis and lymphocyte proliferation induced by dinitrofluorobenzene in mice, improve the symptoms of skin lesions, and significantly reduce the inflammatory reaction (Wu et al., 2005; Wu et al., 2006), indicating that OMT may be a potential drug for the treatment of AD.

In this study, after the intervention treatment with different doses of OMT in mice, it was found that the serum inflammatory factors IgE, TNF- α , IL-4 and IL-7 decreased, the positive expression of CD3 in skin tissue decreased, and the pathological damage such as skin epidermal hyperplasia and inflammatory cell infiltration also eased significantly, indicating that OMT has potential application value in the treatment of AD.

SOCS1/JAK-STAT3 pathway is one of the important pathways that mediate the body's immune inflammatory response. A large number of studies have found that the kinase inhibition region sequence of SOCS1 can inhibit the activation of STAT3 by JAK2 kinase, prevent the production of IL-23 and IL-17, and reduce the inflammatory damage of tissues (Oh et al., 2019). In addition, immunogens and allergens stimulate the body to secrete inflammatory factors such as IL-6 or IL-23, stimulate JAK-STAT pathway, and generate activated p-STAT3 to promote the expression of Th17 transcription factor-ROR γ T in T-lymphoid subsets,

which can promote the expression of inflammatory factors such as IL-17, aggravate the occurrence of immune diseases (Dhanushkodi et al., 2020), inhibit the activation of JAK-STAT3 pathway, and improve the symptoms of AD lesions (Li et al., 2021). The generation of SOCS1 can combine with JAKs to inhibit the over activation of JAK-STAT signal cascade reaction generated by IL-4, IL-6 and other stimuli, thus alleviating tissue damage (Luan et al., 2020). This study found that in the AD model group, the expression of SOCS1 in the ear skin tissue was decreased, the expression of its downstream JAK-STAT3 pathway and T lymphoid activation related promoters IL-6 and IL-17 were increased, and the AD-like pathological damage of skin was aggravated, suggesting that the decreased expression of SOCS1 and the continued activation of JAK-STAT3 might be one of the reasons for aggravation of skin inflammatory damage mediated the activation of T lymphocytes in AD mice. The expression of SOCS1 in the ear skin of mice in the OMT-H, OMT-M and OMT-L groups increased, and the expression of JAK-STAT3 pathway and T lymphoid activation related promoters decreased, suggesting that OMT could improve AD skin inflammation symptoms, which may be related to the up regulation of SOCS1 expression, inhibition of JAK-STAT3 pathway and T lymphoid activation.

To sum up, OMT can up regulate the expression of SOCS1, inhibit the activation of JAK-STAT3 pathway, block the activation of T lymphocytes, improve the skin inflammatory symptoms of AD mice. This study provided some theoretical basis in the field of the treatment on AD by OMT.

Data availability statement

The original contributions presented in the study are included in the article/Supplementary Material, further inquiries can be directed to the corresponding authors.

Ethics statement

The animal study was reviewed and approved by Institutional Animal Ethics Committee of Heilongjiang University of Chinese Medicine.

References

- Boothe, W. D., Tarbox, J. A., and Tarbox, M. B. (2017). Atopic dermatitis: Pathophysiology. *Adv. Exp. Med. Biol.* 1027, 21–37. doi:10.1007/978-3-319-64804-0_3
- Chang, J., Yao, Z. F., Zhang, D., and Wang, L. (2020). Study on mechanism of compound glycyrrhizin in treatment of atopic dermatitis in mice based on miR-155/SOCS1 axis. *Chin. J. Immunol.* 36 (13), 1583–1588. doi:10.3969/j.issn.1000-484X.2020.13.009
- Clarissa, E. H., Xinjing, S. L., Fan, L., Bailey Vitarbo, J., Arfuso, F., Tan, C. H., et al. (2019). Anti-cancer effects of oxymatrine are mediated through multiple molecular mechanism(s) in tumor models. *Pharmacol. Res.* 147, 104327. doi:10.1016/j.phrs.2019.104327
- Demeyer, A., Nuffel, E. V., Baudelet, G., Driege, Y., Kreike, M., Muylleert, D., et al. (2019). MALT1-Deficient mice develop atopic-like dermatitis upon aging. *Front. Immunol.* 10, 2330. doi:10.3389/fimmu.2019.02330

Author contributions

XH and YH were contributed to the conception of the study. XH and TM were performed the experiment. XH, HL, and CJ were contributed significantly to analysis and manuscript preparation. TM and GL were performed the data analyses and wrote the manuscript. All authors read and approved the final manuscript.

Funding

This study was supported by the Natural Science Foundation of Liaoning Province, China (2021-MS-368), the Fund of Public Health Research and Development Project of Shenyang Bureau of Science and Technology (20-205-4-037) and the Scientific Research Project of Health Commission of Shenyang, Liaoning Province (2021047).

Conflict of interest

The authors declare that the research was conducted in the absence of any commercial or financial relationships that could be construed as a potential conflict of interest.

Publisher's note

All claims expressed in this article are solely those of the authors and do not necessarily represent those of their affiliated organizations, or those of the publisher, the editors and the reviewers. Any product that may be evaluated in this article, or claim that may be made by its manufacturer, is not guaranteed or endorsed by the publisher.

Supplementary material

The Supplementary Material for this article can be found online at: <https://www.frontiersin.org/articles/10.3389/fphar.2022.1091090/full#supplementary-material>

- Dhanushkodi, N., Srivastava, R., Prakash, S., Roy, S., Coulon, P. G. A., Vahed, H., et al. (2020). High frequency of gamma interferon-producing PLZF^{hi}RORγ^{hi} invariant natural killer 1 cells infiltrating herpes simplex virus 1-infected corneas is associated with asymptomatic ocular herpesvirus infection. *J. Virol.* 94 (9), 001400. doi:10.1128/JVI.00140-20
- Ho, C. H., Lu, Y. C., Fan, C. K., Yu, H. J., Liu, H. T., Wu, C. C., et al. (2020). Testosterone regulates the intracellular bacterial community formation of uropathogenic *Escherichia coli* in prostate cells via STAT3. *Int. J. Med. Microbiol.* 310 (7), 151450. doi:10.1016/j.ijmm.2020.151450
- Hu, Y. Q., and Zhang, J. Z. (2019). Medications for atopic dermatitis. *Chin. J. Dermatol.* 52 (1), 57–60. doi:10.3760/cma.j.issn.0412-4030.2019.01.019
- Kim, J. H., Kim, B. E., and Leung, D. Y. M. (2019). Pathophysiology of atopic dermatitis: Clinical implications. *Allergy Asthma Proc.* 40 (2), 84–92. doi:10.2500/aap.2019.40.4202
- Lan, X., Hu, Y. H., Li, X., Kong, D. J., Qin, Y. F., and Wang, H. (2021). Oxymatrine protects cardiac allografts by regulating immunotolerant cells. *Int. Immunopharmacol.* 100, 108080. doi:10.1016/j.intimp.2021.108080
- Lan, X., Zhao, J., Zhang, Y., Chen, Y., Liu, Y., and Xu, F. (2020). Oxymatrine exerts organ- and tissue-protective effects by regulating inflammation, oxidative stress, apoptosis, and fibrosis: From bench to bedside. *Pharmacol. Res.* 151, 104541. doi:10.1016/j.phrs.2019.104541
- Li, Y. Y., Pan, X. F., and Chi, L. Q. (2021). Mechanism of isoliquiritigenin in the treatment of atopic dermatitis in mice through JAK-STAT pathway. *Hebei Med.* 27 (5), 710–715. doi:10.3969/j.issn.1006-6233.2021.05.03
- Liang, X. D., Tan, G. Q., Li, C. H., Deng, X. H., and Zang, X. B. (2021). Advances in the influence of IL-33 on ST2-ILC2s axis and skin barrier in atopic dermatitis. *J. Diagn. Ther. Dermatol-Venereol.* 28 (3), 237–240+244. doi:10.3969/j.issn.1674-8468.2021.03.020
- Liu, L. X., Yang, G. Y., and Wu, R. N. (2022). Research progress in the pathogenesis of atopic dermatitis. *Beijing Med. J.* 35 (5), 377–379. doi:10.15932/j.0253-9713.2013.05.032
- Luan, J., Fu, J., Wang, D., Jiao, C., Cui, X., Chen, C., et al. (2020). miR-150-Based RNA interference attenuates tubulointerstitial fibrosis through the SOCS1/JAK/STAT pathway *in vivo* and *in vitro*. *Mol. Ther. Nucleic Acids.* 22, 871–884. doi:10.1016/j.omtn.2020.10.008
- Oh, H., Park, S. H., Kang, M. K., Kim, Y. H., Lee, E. J., Kim, K. Y., et al. (2019). Asaronic acid attenuates macrophage activation toward M1 phenotype through inhibition of NF-κB pathway and JAK-STAT signaling in glucose-loaded murine macrophages. *J. Agric. Food Chem.* 67 (36), 10069–10078. doi:10.1021/acs.jafc.9b03926
- Pei, X. P., Gu, M., Chen, W. J., and Chen, Y. F. (2020). The correlation between severity of atopic dermatitis and serum levels of 25-hydroxyvitamin D, total IgE and IL-4 in children. *J. Diagn. Ther. Dermatol-Venereol.* 27 (4), 227–231. doi:10.3969/j.issn.1674-8468.2020.04.003
- Robert, S., Kodama, S., and Samantha, K. (2018). Atopic dermatitis guidelines: Diagnosis, systemic therapy, and adjunctive care. *Clin. Dermatol* 36 (5), 648–652. doi:10.1016/j.clindermatol.2018.05.008
- Song, W. J., Luo, J., Wu, T., and Yao, S. K. (2016). Oral oxymatrine preparation for chronic Hepatitis B: A systematic review of randomized controlled trials. *Chin. J. Integr. Med.* 22 (2), 141–149. doi:10.1007/s11655-015-2143-0
- Sun, Y., Chen, G. F., Gao, J., Zhang, L. J., Zhang, Y., and Wang, R. R. (2021). Protective effects of oxymatrine on atopic dermatitis model mice. *Chin. J. Comp. Med.* 31 (9), 10–15. doi:10.3969/j.issn.1671-7856.2021.09.002
- Tiago, T., Goncalo, M., Mendes-Bastos, P., Selores, M., Filipe, P., and Eduarda, O. F. (2019). Update on atopic dermatitis. *Acta Med. Port.* 32 (9), 606–613. doi:10.20344/amp.11963
- Tsakok, T., Woolf, R., Smith, C. H., Weidinger, S., and Flohr, C. (2019). Atopic dermatitis: The skin barrier and beyond. *Br. J. Dermatol.* 180 (3), 464–474. doi:10.1111/bjd.16934
- Wang, J., Chen, F., Shi, H., Zhang, M., Yan, L., Pei, X. Y., et al. (2021). Oxymatrine inhibits neuroinflammation byRegulating M1/M2 polarization in N9 microglia through the TLR4/NF-κB pathway. *Int. Immunopharmacol.* 100, 108139. doi:10.1016/j.intimp.2021.108139
- Wu, B., Cai, X. E., Zeng, Y. Y., Shi, J., Wang, T., Zhao, J. X., et al. (2005). Effect of oxymatrine on mouse allergic contact dermatitis induced by DNFB and lymphocyte proliferation stimulated by Con A. *Chin. J. Pathophysiol.* 21 (5), 931–935.
- Wu, B., Ren, X. Q., Xie, H. F., Zhang, J. L., Chen, M. L., Du, Q. J., et al. (2006). Effects of oxymatrine on allergic contact dermatitis in mice. *J. Zhengzhou Univ. Med. Sci.* 41 (4), 643–645. doi:10.13705/j.issn.1671-6825.2006.04.015
- Wu, Q., and Gao, Y. (2015). Research advances in molecular mechanism of pharmacological actions of oxymatrine. *Chin. Pharmacol. Bull.* 31 (06), 759–762. doi:10.3969/j.issn.1001-1978.2015.06.005
- Wu, S., Pang, Y., He, Y., Zhang, X., Peng, L., Guo, J., et al. (2021). A comprehensive review of natural products against atopic dermatitis: Flavonoids, alkaloids, terpenes, glycosides and other compounds. *Biomed. Pharmacother.* 140, 111741. doi:10.1016/j.biopha.2021.111741



OPEN ACCESS

EDITED BY

Haitao Wang,
National Cancer Institute (NIH),
United States

REVIEWED BY

Jian Li,
National Institutes of Health (NIH),
United States
Zhiyong Liu,
The Rockefeller University, United States
Yan-Jin Liu,
University of California San Francisco,
United States
Li Duan,
Shenzhen University, China

*CORRESPONDENCE

Jing Han,
✉ hanjing@njucm.edu.cn
Jianning Zhao,
✉ zhaojianning.0207@163.com
Dongsheng Wang,
✉ wdssmmu@163.com

[†]These authors have contributed equally to
this work

SPECIALTY SECTION

This article was submitted to
Ethnopharmacology,
a section of the journal
Frontiers in Pharmacology

RECEIVED 21 November 2022

ACCEPTED 18 January 2023

PUBLISHED 26 January 2023

CITATION

Han J, Wang J, Wang Y, Zhu Z, Zhang S,
Wu B, Meng M, Zhao J and Wang D (2023),
Sesquiterpene lactones-enriched fractions
from *Xanthium mongolicum* Kitag alleviate
RA by regulating M1 macrophage
polarization via NF- κ B and MAPK
signaling pathway.
Front. Pharmacol. 14:1104153.
doi: 10.3389/fphar.2023.1104153

COPYRIGHT

© 2023 Han, Wang, Wang, Zhu, Zhang, Wu,
Meng, Zhao and Wang. This is an open-
access article distributed under the terms
of the [Creative Commons Attribution
License \(CC BY\)](https://creativecommons.org/licenses/by/4.0/). The use, distribution or
reproduction in other forums is permitted,
provided the original author(s) and the
copyright owner(s) are credited and that
the original publication in this journal is
cited, in accordance with accepted
academic practice. No use, distribution or
reproduction is permitted which does not
comply with these terms.

Sesquiterpene lactones-enriched fractions from *Xanthium mongolicum* Kitag alleviate RA by regulating M1 macrophage polarization via NF- κ B and MAPK signaling pathway

Jing Han^{1*†}, Jingwen Wang^{2†}, Yicun Wang^{3†}, Zhiqi Zhu¹,
Siwang Zhang¹, Bingrong Wu¹, Mingsong Meng¹, Jianning Zhao^{3*}
and Dongsheng Wang^{3*}

¹School of Pharmacy, Nanjing University of Chinese Medicine, Nanjing, China, ²Department of TCMs
Pharmaceuticals, School of Traditional Chinese Pharmacy, China Pharmaceutical University, Nanjing, China,
³Department of Orthopedics, Jinling Hospital, School of Medicine, Nanjing University, Nanjing, China

Introduction: Rheumatoid arthritis (RA) is a chronic autoimmune disease, characterized by activated M1-like macrophage in the joint. *Xanthium mongolicum* Kitag (*X. mongolicum*) is a traditional medicinal plant that has long been used to treat RA and other immune diseases in China.

Methods: Fractions of *X. mongolicum* were separated based on polarity. Anti-RA activity of the fractions were screened by LPS-stimulated RAW264.7 macrophage *in vitro*. The major active compounds were identified by UPLC-MS and quantified by HPLC. The anti-RA effects of the active fraction was evaluated in complete freund's adjuvant (CFA)-induced arthritis and collagen-induced arthritis (CIA) mouse models *in vivo* and LPS-stimulated macrophage *in vitro*.

Results: Sesquiterpene lactones-enriched fraction from *X. mongolicum* (SL-XM) exhibited the strongest anti-RA activity among all components *in vitro*. Five major constituents i.e., Xanthinosin (1), Xanthatin (2), Mogolide D (3), Mogolide E (4), and Mogolide A (5) were identified as major compounds of SL-XM. SL-XM ameliorated symptoms of CFA and CIA induced arthritis mice model. Furthermore, SL-XM treatment inhibited LPS-induced M1 macrophages polarization. In addition, SL-XM inhibited the phosphorylation of NF- κ B and MAPK signaling pathways in LPS-induced macrophage and CIA-challenged mice.

Discussion: The main anti-RA active fraction of *X. mongolicum* may be the Sesquiterpene lactones, which includes five key compounds. SL-XM may exert its anti-RA effect by suppressing M1 macrophage polarization via the NF- κ B and MAPK signaling pathway.

KEYWORDS

rheumatoid arthritis, *Xanthium mongolicum* kitag, sesquiterpene lactone, macrophage, traditional Chinese medicine

1 Introduction

Rheumatoid arthritis (RA) is an autoimmune inflammatory disease that affect about 1% of the world's population and is more common in women than in men (Chen et al., 2019). With the progression of the disease, more than 90% of RA patients will showed some degree of disability within 20 years of onset, which seriously affects their quality of life. The treatment of early RA is particularly important (Emery et al., 2002). To cope with RA, the main treatments are medication, physical therapy, and lifestyle modification. In terms of drug treatment, which generally include NSAIDs, glucocorticoids (GCs) and DMARDs. Which can effectively relieve the symptoms of RA, but chronic and high dose use of these drugs may cause serious side effects (Ramiro et al., 2017; Mazhar et al., 2018). Biological reagents such as tofacitinib (JAK inhibitor) and anti-TNF- α monoclonal antibodies have proven effective, but have significant side effects and high treatment costs (Puxeddu et al., 2016). Therefore, it is urgent to develop safer, more effective and lower-priced new therapeutic agents to treat RA.

Xanthium mongolicum Kitag (*X. mongolicum*) is a common traditional Chinese medicine, which belongs to the genus *Xanthium* (Family Compositae) (Han et al., 2007; Han et al., 2009). According to the Compendium of Materia Medica (Ben Cao Gang Mu, pinyin in Chinese) record, *Xanthium* can be used to treat RA. In addition, Chinese Materia Medica (Zhong Hua Ben Cao, pinyin in Chinese) records that *Xanthium* commonly used in the treatment of inflammatory and immune-related diseases, especially RA (Editorial Committee of Zhonghua Bencao National Traditional Chinese Herb Administration, 1999). Chemical studies have revealed more than 170 chemicals ingredients in *Xanthium* species, including sesquiterpenoids, caffeoylquinic acids, lignans, steroids, thiazinodiones, and flavonoids (Fan et al., 2019). However, to the best of our knowledge, the main anti-RA component of *X. mongolicum* remains unclear.

RA is mainly characterized by chronic inflammation of the synovial joints, ultimately damaging the cartilage and bone (Schett, 2019). Adaptive and innate immune cells participate in persistence and expansion of chronic inflammation in the synovial joints (Calabresi et al., 2018). Among this, macrophages have a dramatic effect on the pathophysiological response to RA, which can polarized into M1/M2 phenotype depending on the microenvironment. M1 macrophages induce early inflammatory responses by secreting pro-inflammatory cytokines, including TNF- α , IL-1 β , and IL-6. In contrast, M2 macrophages produce anti-inflammatory cytokines, such as IL-4, IL-10, and IL-13, which are associated with inflammation resolution. Studies have shown that the macrophage in RA joints are predominantly M1 phenotype, which promote RA progression by releasing multiple inflammatory factors. Therefore, targeting macrophages in RA joints has become a promising strategy for its treatment.

In this study, different fractions of the *X. mongolicum* extractions were separated through polarity; Fraction enriched with sesquiterpene lactones from *X. mongolicum* (SL-XM) exhibited the strongest anti-RA activity through *in vivo* experiment. Furthermore, the anti-RA activity of SL-XM was evaluated in CFA and CIA mouse models *in vivo*. Moreover, the possible anti-RA mechanisms of SL-XM was also explored. These results provide experimental evidence for the development of novel anti-RA drugs.

2 Materials and methods

2.1 Chemicals and reagents

Acetonitrile (34998) and formic acid (00940) for LC-MS were obtained from Merck (WGK, Germany). Incomplete Freund's adjuvant (IFA), Complete Freund's adjuvant (CFA), and bovine type II collagen were obtained from Chondrex, Inc. (Redmond, Wash.). ELISA kits for detections of IL-1 β (10 \times 96t, 88-7013-88), IL-6 (2 \times 96t, 88-7064-86), TNF- α (2 \times 96t, 88-7324-22), IL-4 (2 \times 96t, 88-7044-22) and IL-10 (2 \times 96t, 88-7105-22) were purchased from Invitrogen (Karlsruhe, Germany). Anti-IKK α (ab32041, 1:1000), Anti-IKK β (ab124957, 1/1000), anti-IKK α/β (ab194528, 1:1000), anti-NF- κ B p65 antibody (ab16502, 1:1000), anti-P-NF- κ B p65 (phospho S536) antibody (ab76302, 1:1000), anti-P38 (ab122517, 1:1000) antibody, anti-P-P38 (phospho Y182) antibody (ab47363, 1:1000), anti-Histone H3 antibody (ab1791, 1:1000) and secondary antibodies were obtained from Abcam (Cambridge, United Kingdom). Anti-I κ B α , anti-P-I κ B α (phospho S36/32), anti-P-ERK (Thr202/Tyr204), Anti-ERK, anti-JNK, anti-P-JNK (Thr183/Tyr185), anti-STAT6 and anti-P-STAT6 antibodies were obtained from cell signaling technology (Boston, United States). All other reagents and chemicals used were of standard biochemical quality.

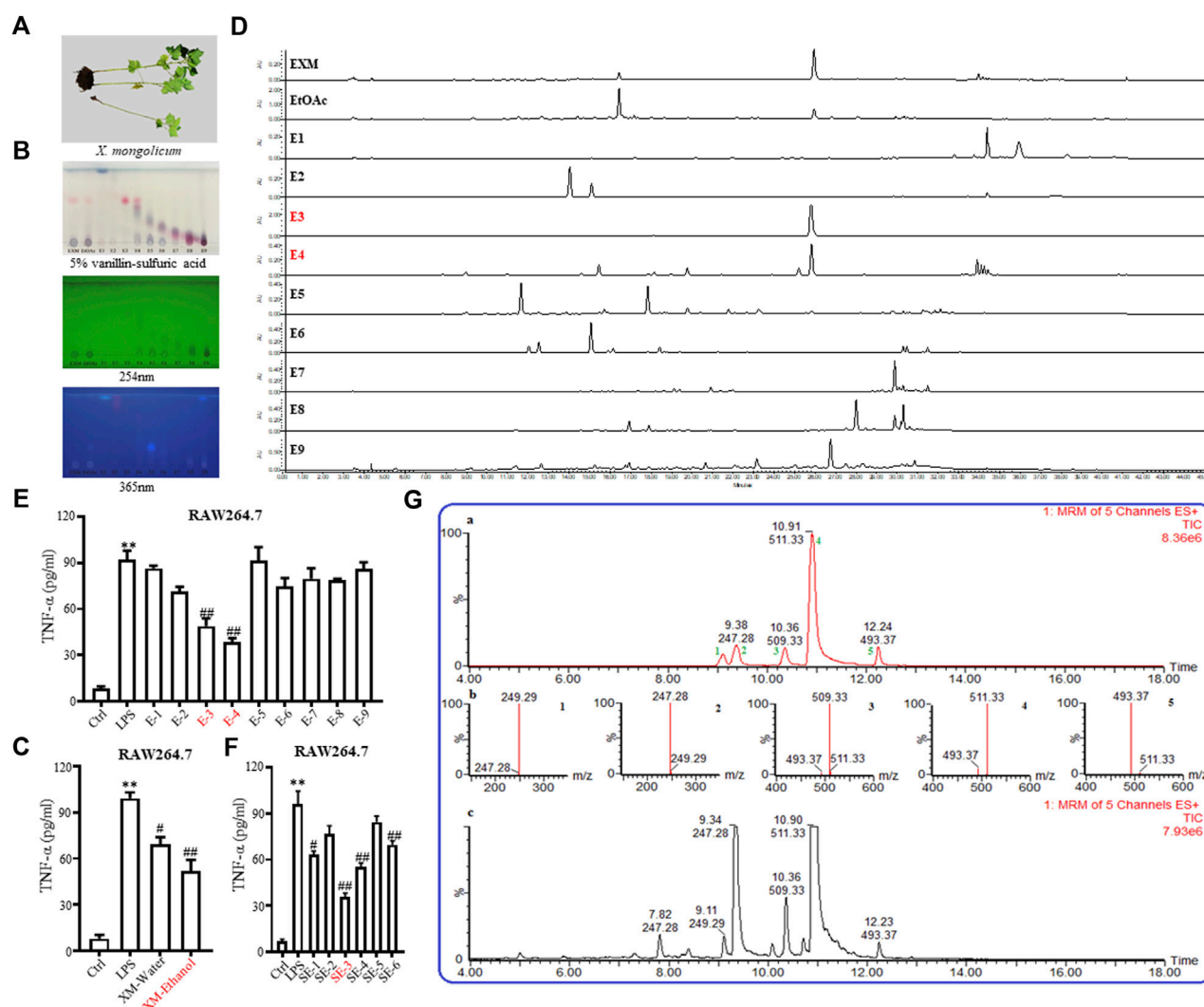
2.2 General experimental procedures

1D NMR spectra were run on a Bruker DRX-400 spectrometer with TMS as internal standard. LC-MS spectra were run on a Waters Xevo TQD mass spectrometer with Waters ACQUITY UPLC[®] BEH C18 column and Waters Acquity Arc system equipped with a 2998 PDA detector with Xbridge-C18. Semi-preparative HPLC was performed on an Agilent 1100 with the YMC AA12S05-C18. Column chromatography was performed on silica gel, Sephadex LH-20, or Lichroprep RP-18. Fractions were monitored by thin-layer chromatography (TLC), and spots were detected by spraying with 5% vanillin-sulphuric acid reagent for sesquiterpenes.

2.3 Plant material and extraction

The aerial parts (stems and leaves without seeds, floral bud and flower) of *X. mongolicum* were harvested at the roadside in Qiqihar (47°41'31.93" N, 123°93'32.76" E), Heilongjiang Province, China, in August 2018 (Figure 1A). The specimens were identified by Lingyun Chen, PhD. The voucher specimen (No. JH0002) is stored in Jiangsu Museum of Traditional Chinese Medicine (Nanjing, China).

A total of 10.00 kg of the aerial parts of *X. mongolicum* (without seeds) were collected. After being heated and refluxed, the sample was extracted with 70% ethanol (60 L \times 3, for 3, 3, and 2 h) and concentrated by decompression to obtain the crude extract (approximately 0.81 kg). The extract was partitioned successively with ethyl acetate (EtOAc). The EtOAc fraction (0.48 kg) was subjected to silica gel column chromatography eluting with polar petroleum-EtOAc to acquire nine fractions (E1~E9) (Supplementary Table S3). According to the anti-inflammatory, TLC and HPLC data (Figures 1B, D, E), which showed that fractions E3 and E4 (113.81 g) were enriched in sesquiterpene lactones and that both fractions showed strong anti-inflammatory activity. The fractions E3 and E4 were merged and subjected to silica gel column to obtain six



sub-fractions (SE1~SE6) (Supplementary Table S4). According to the anti-inflammatory data (Figure 1F), the SE3 (16.52 g, SL-XM) was subjected to RP-18 (MeOH-H₂O, 10:90-100:0), then to Sephadex LH-20 (MeOH-CHCl₃, 1:1), further purified by MPLC (YMC XDB-C18, 90 μ M, 9.4 mm \times 250 mm, 1.8 mL/min, UV detection at 254 and 280 nm) eluting with 50%–60% CH₃CN, which contained 1.0‰ formic acid to get 1 (1.33 g), 2 (2.79 g), 3 (0.585 g), 4 (0.98 g) and 5 (26.3 mg) (Figure 1G). Compounds were identified by ¹H NMR (Supplementary Figures S1–5).

Xanthinosin (1): Purity 98.5%; C₁₅H₂₀O₃, yellow oil, ¹H NMR (CDCl₃, 400 MHz) spectroscopic data see Supplementary Table S1. Positive ESI-MS m/z 249.2 [M + H]⁺ (Shi et al., 2015).

Xanthatin (2): Purity 98.3%; C₁₅H₁₈O₃, yellow oil, ¹H NMR (CDCl₃, 400 MHz) spectroscopic data see Supplementary Table S1. Positive ESI-MS m/z 247.35 [M + H]⁺ (Yuan et al., 2018).

Mogolide D (3): Purity 97.5%; C₃₀H₃₅O₇, white powder, ¹H NMR (CDCl₃, 400 MHz) spectroscopic data see Supplementary Table S2. Positive ESI-MS m/z 509.25 [M + H]⁺ (Xu et al., 2017).

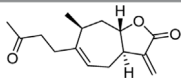
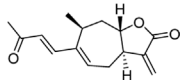
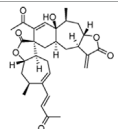
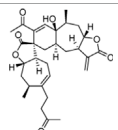
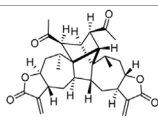
Mogolide E (4): Purity 96.4%; C₃₀H₃₇O₇, white powder, ¹H NMR (CDCl₃, 400 MHz) spectroscopic data see Supplementary Table S2. Positive ESI-MS m/z 509.25 [M + H]⁺ (Xu et al., 2017).

Mogolide A (5): Purity 98.2%; C₃₀H₃₇O₆, white powder, ¹H NMR (CDCl₃, 400 MHz) spectroscopic data see Supplementary Table S2. Positive ESI-MS m/z 493.25 [M + H]⁺. (Shang et al., 2014).

2.4 Analysis SL-XM by UPLC-MS

The identification analysis of subfraction SE3 was carried with a Waters Xevo-TQD MS spectrometer. Each compound was dissolved in the concentration range of 0.01–0.1 μ g/mL (in triplicate). The peak areas at 280 nm were plotted against the concentration. The LC conditions: the injection volume of Waters ACQUITY UPLC[®] BEH C18 column was 2 μ L with flow rate of 0.3 mL/min. The mobile phase composed of Pump A (0.1% formic acid in water) and Pump B (acetonitrile). The gradient program

TABLE 1 Identification and qualification of sesquiterpene lactone constituents in SL-XM by UPLC.

Peak no Figure 1D	SL-XM component	Mol. formula	Chemical structure	Retention time (min)	Content (‰)
1	Xanthinosin	C ₁₅ H ₂₀ O ₃		25.409	0.133
2	Xanthatin	C ₁₅ H ₁₈ O ₃		26.012	0.279
3	Mogolide D	C ₃₀ H ₃₆ O ₇		26.841	0.0585
4	Mogolide E	C ₃₀ H ₃₈ O ₇		27.603	0.0981
5	Mogolide A	C ₃₀ H ₃₆ O ₆		28.133	0.00263

started from 10% B, increased to 50% B for 8 min, increased to 100% B for 2 min, kept at 100% B for 2 min, returned to 10% B for 4 min, and kept at 10% B for 2 min. The mass spectrum conditions: Capillary voltage 2.5 kV; nitrogen gas flow rate 800 L/h; dissociation temperature 500 °C; and multiple reaction monitoring ESI positive mode.

2.5 Analysis SL-XM by HPLC

The quantitative analysis of the compounds from SL-XM were confirmed by HPLC analysis on the standard compounds, and the ethanolic extract of *X. mongolicum* was dissolved in methanol. The injection volume on Waters X-Bridge C18 column was 10 µL. The wavelengths were detected at 254 and 280 nm. The gradient elution in mobile phase was composed of 0.1% formic acid (solvent A) and acetonitrile (solvent B), with the flow rate set to 0.8 mL/min. The gradient elution program started from 5% B, increased to 50% B for 25 min, increased to 100% B for 5 min, kept at 100% B for 6 min, returned to 5% B for 4 min, and kept under 5% B for 5 min. The results showed that the concentrations of the compounds in SL-XM were 0.133‰ (xanthinosin), 0.279‰ (xanthatin), 0.0585‰ (mogolide D), 0.0981‰ (mogolide E), and 0.00263‰ (mogolide A) respectively as shown in [Table 1](#).

2.6 Animals

Male C57/BL6 and DBA/1 mice (8–10 weeks, 20–25 g) were adapted to a 12-hour light-dark cycle in a 23°C ± 2°C environment for a week before use. Mice were raised in a pathogen-free

environment with free access to food and water. All experiments were permissioned by the animal ethics committee of Nanjing University of Chinese Medicine (Nanjing, China).

2.7 Induction and assessment of CFA

The CFA model was established by subcutaneous injection CFA (Sigma-Aldrich, United States) into the left hind-paw of C57/BL mice as previously reported ([Quintao et al., 2019](#)). The control animals received equal amount of saline. Dexamethasone (DXM) is a classic drug for the treatment of RA, so we choose oral administrated DXM as a positive control drug for CFA-challenge mice ([Quintao et al., 2019](#)). Han et al. reported effects of *Xanthium strumarium* on acetic acid-induced writhing responses in mice, the doses of chloroform fraction, ethyl acetate fraction, aqueous fraction, and n-Butanol fraction of *Xanthium strumarium* L used were 100, 200, and 400 mg/kg/day in mice ([Han et al., 2007](#)). A previous study of ethanolic leaves extract of *X. strumarium* for anti-plasmodial activity used doses of 150, 250, 350 and 500 mg/kg/day in BALB/c mice ([Chandel et al., 2012](#)). Muhammad et al. reported effects of methanol extract of the aerial parts of *X. strumarium* on HCl/EtOH-induced mouse model of gastritis, which used doses of 50 and 200 mg/kg/day in mice ([Hossen et al., 2016](#)). Based on above studies, we chose 200, 400 mg/kg of SL-XM for mice in our experiments. Mice in SL-XM groups orally received SL-XM (200, 400 mg/kg) daily from day 1 to day 6, and mice in the control and CFA groups received same volume of solvent (*n* = 6 per group). An electronic caliper was used to measure the left hind paw thickness and ankle thickness. Animals were weighed with an electronic scale. In each cases, a

trained observer blinded to the experimental groups performed the severity analysis.

2.8 Induction and assessment of CIA

CIA model was established in DBA/1 mice as previously reported (Wang et al., 2021). The experimental process is detailed in Figure 6A. Briefly, CFA and bovine type II collagen were fully mixed at a 1:1 ratio. The mice in CIA, SL-XM and DXM groups received an injection of 100 µg emulsified reagent subcutaneously at the root of the tail. 21 days later, the same mice were injected intraperitoneal with 100 µg bovine type II collagen. The control mice received same amount of saline. From day 21 to day 45 after the initial immunization, mice in SL-XM and DXM groups received oral SL-XM (200, 400 mg/kg) or DXM (1 mg/kg) daily. While the control and CIA mice received the same volume of vehicle ($n = 8$ per group). In addition, the arthritis of the mice was evaluated every other day. Paw arthritis was scored 0-4 based on previous report (Atkinson et al., 2012); the scores of the four paws were added to get the mouse arthritis score. The occurrence of arthritis was defined as inflammation of the four paws with an arthritis score of 2 or higher, the incidence of arthritis was the percentage of the diseased mice in all mice. An electronic caliper was used to measure the left hind paw thickness. Animals were weighed with an electronic scale. In each cases, a trained observer blinded to the experimental groups performed the severity analysis.

2.9 X rays and Micro-CT

Ankle joint destruction was analyzed by X-ray, radiographs were evaluated on a 0-3 scale as previously reported (Wang et al., 2021). Three-dimensional (3D) image of the mice paws was performed by micro-CT (NFR Polaris-G90).

2.10 Histopathological evaluation

The mouse hind paws were harvested at the end of experiment. After immersed in 4% paraformaldehyde for up to 3 days. The tissues were immersed in 17% EDTA at 4°C for 14 days. The paws were paraffin-embedded, cut into 5-µm sections, and stained with H&E using standard protocol. Histopathological images were taken under a Leica DM 4000B photomicroscope. Synovial inflammation, cartilage erosion, and bone erosion were estimated on a 0–3 scale as previously reported (Brenner et al., 2005).

2.11 ELISA

Mice blood was taken from the eye socket, and serum was obtained after centrifugation. The concentrations of TNF-α, IL-1β, IL-6, IL-10 and IL-4 were measured with the indicate ELISA kits following the manufacturer's protocols. After RAW264.7 cells were stimulated with Extracts, Fractions, Sub-fractions of *X. mongolicum* for 4 h and then incubated with LPS for additional 24 h. The culture supernatants were collected for TNF-α ELISA assay kits following the manufacturer's protocols.

2.12 Cell culture

The RAW264.7 macrophages and THP-1 cells were obtained from the Cell bank of the Chinese Academy of Medical Sciences (Shanghai, China). Cells were cultured in RPMI-1640 medium (supplemented with 10% FBS and 1% penicillin-streptomycin) at 37°C in an atmosphere of 95% O₂ and 5% CO₂.

2.13 Cell viability analysis

RAW264.7 cells were seeded at 10,000 per well in 96-well plates. Plant extract, SL-XM were dissolved in DMSO, and DMSO was used as a control in all experiments at a maximum concentration of 0.1%. After addition of the drug, cells were further incubated for 24 h. Cell viability was detected using the CCK8 kit according to the reagent instructions.

2.14 Macrophage polarization toward M1 or M2 phenotype

To explore the effect of SL-XM on the polarization of macrophage towards M1, RAW264.7 or THP-1 cells were stimulated to polarization toward M1 phenotype with LPS (100 ng/mL) for 24 h. At the same time cells were treated with SL-XM. To assess the effect of SL-XM on the polarization of macrophage toward M2, RAW264.7 or THP-1 cells were treated with IL-4 (20 ng/mL) for 24 h, during polarization, macrophages were administrated with SL-XM.

2.15 qRT-PCR

Total RNA was extracted from macrophage or ankle tissue using TRIzol reagent, and transcription-PCR was performed by real-time PCR with a standard procedure as previous reported (Wang et al., 2021). Values were normalized to *Gapdh* mRNA levels and calculated by $2^{-\Delta\Delta Ct}$. The primers used are listed in Supplementary Table S3.

2.16 Western blot analysis

RAW264.7 cells were planted in a 6-well plate and cultured for 24 h, incubated with SL-XM for 1 h and then added LPS (100 ng/mL) for 30 min, then the cells were harvested. At the end of animal experiment, ankle tissues of different groups were harvested. Proteins were extracted from cells and tissues, and the protein concentration was measured with a BCA kit. Western blot was analysis using the standard protocol as previous reported (Wang et al., 2018).

2.17 Immunofluorescence staining

RAW264.7 cells were seeded and cultured on 12 mm glass coverslips, and then cells were fixed with 4% PFA for 10min, permeabilized with Triton-X 100 and blockaded with BSA. After incubated with primary antibody at 4°C overnight, the indicate

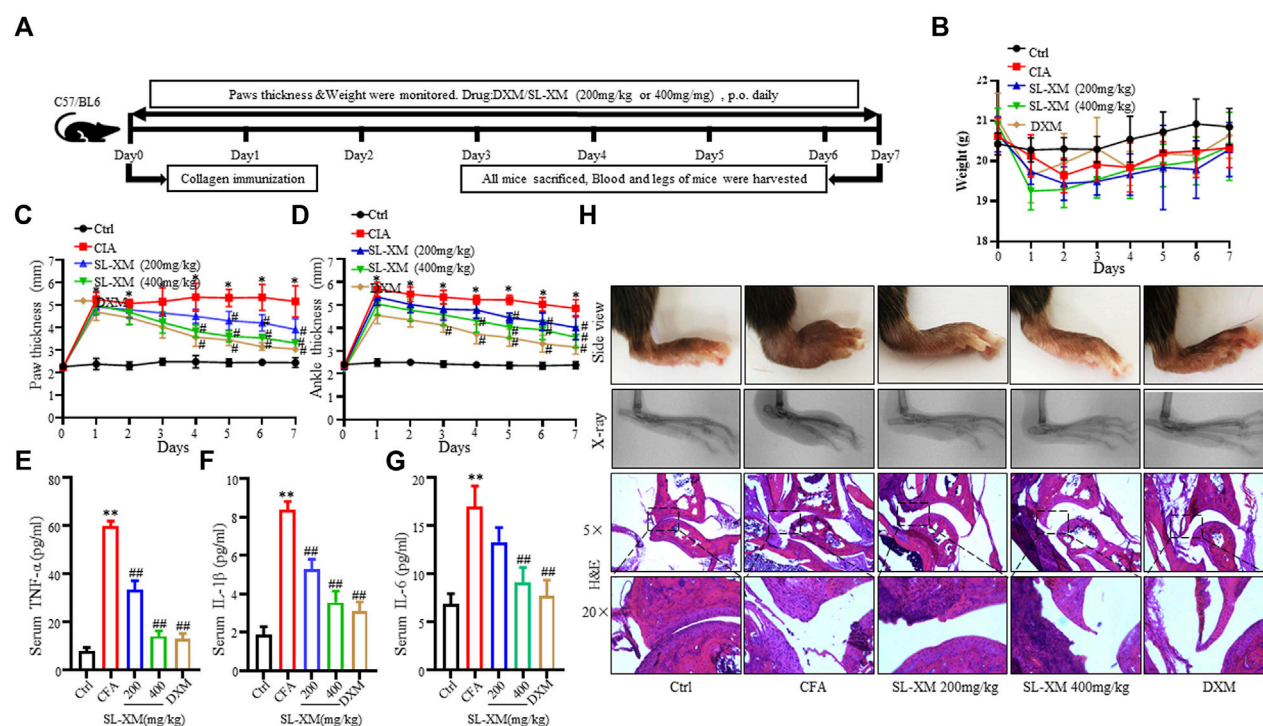


FIGURE 2

SL-XM dose-dependently attenuates CFA-induced RA in mice. The mice were orally administrated with SL-XM (200, 400 mg/kg) or DXM (1 mg/kg) daily after CFA injection. (A) Schematic depiction of the experimental schedule; the body weight (B), Hind paw thickness (C), Ankle thickness (D) were measured daily during experiment procedure. Serum levels of TNF- α (E), IL-6 (F), and IL-1 β (G) were measured 6 days after CFA challenged. (H) Representative image of the general features, X-ray and H&E histological graphs of the ankle joint at the end of experiment. $n = 6$ in each group, * $p < 0.05$, ** $p < 0.01$ vs. Ctrl group. # $p < 0.05$, ## $p < 0.01$ vs. CFA group.

secondary antibody for additional 2 h, and DAPI for the next 5 min, the samples were transferred onto glass slides and analyzed by fluorescence microscopy analysis.

2.18 Flow cytometry

RAW264.7 cells were planted in a 6-well plate and stimulated with IL-4 (20 ng/mL) or LPS (100 ng/mL) for 24h, meanwhile, cells were treated with SL-XM (160 μ g/mL). After the cells were prepared into single cell suspension with the density of 10^6 cells in 100 μ L volume in PBS, the cells were incubated with corresponding flow cytometry antibodies on ice for 30 min in dark. After filtration, the stained cells were analyzed with an Attune[®] NxT Acoustic Focusing Cytometer (Thermo Fisher Scientific, Waltham, MA, United States). The data were further analyzed using FlowJo software version 10.6.2 (Tree Star Inc., Ashland, Or, United States). Antibodies for flow cytometry including BV421-conjugated F4/80, PE-Cy7-conjugated CD86, Alexa 647-conjugated CD206 (San Diego, CA, United States).

2.19 Statistical analysis

Statistical analysis was performed using GraphPad Prism 5.01 software. Unless otherwise stated, data are expressed as

mean \pm standard deviation (SD). Statistical comparative analysis of results between groups were performed using Student's t -test, one-way ANOVA, and two-way ANOVA. Statistically significant was considered when $p < 0.05$.

3 Results

3.1 Identified the major anti-inflammatory compounds from *X. mongolicum*

To investigate the anti-inflammatory activities of the aerial parts of *X. mongolicum* (Figure 1A), the aerial part of the plant was extracted by water or 70% ethanol. The anti-inflammatory activities of the extract was evaluated by LPS-stimulated macrophages, the result showed the ethanol extract (80 μ g/mL) inhibited the secretion of TNF- α in LPS-stimulated macrophages significantly compared with the water extract (80 μ g/mL) (Figure 1C). Then, the ethanol extract was isolated by silica gel chromatography to obtain nine fractions (E1-9). TLC and HPLC were applied for analysing sesquiterpene lactones from *X. mongolicum*. After sprayed with 5% vanillin-sulfuric acid reagent, the pink spots on TLC visibly appeared in fraction E3 and E4 (Figure 1B), which showed the main sesquiterpene lactones were enriched in fraction E3 and E4 (Figures 1B, D). At the same time, anti-inflammatory experiments found that fraction

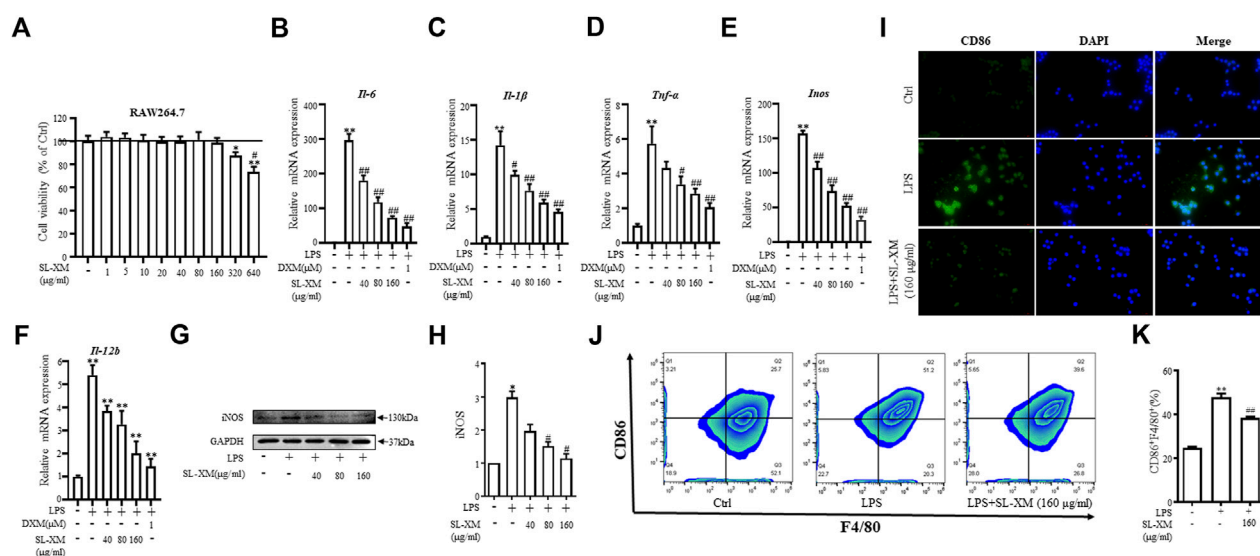


FIGURE 3

Inhibitory effects of SL-XM on M1 macrophages polarization. (A) RAW264.7 cells were stimulated with various concentration of SL-XM for 24 h, and cell viability was measured by CCK8 kit. After RAW264.7 cells were stimulated with LPS (100 ng/mL) and different concentration of SL-XM for 24h, mRNA levels of *IL-6* (B), *IL-1β* (C), *Tnf-α* (D), *Inos* (E), *IL-12b* (F) were determined by qRT-PCR; protein level of iNOS (G,H) was determined by Western blot analysis; protein level of CD86 (I) was determined by immunofluorescence; percentage of CD86-positive cells (J,K) was determined by flow cytometry. **p* < 0.05, ***p* < 0.01 vs. Ctrl group. #*p* < 0.05, ##*p* < 0.01 vs. LPS group.

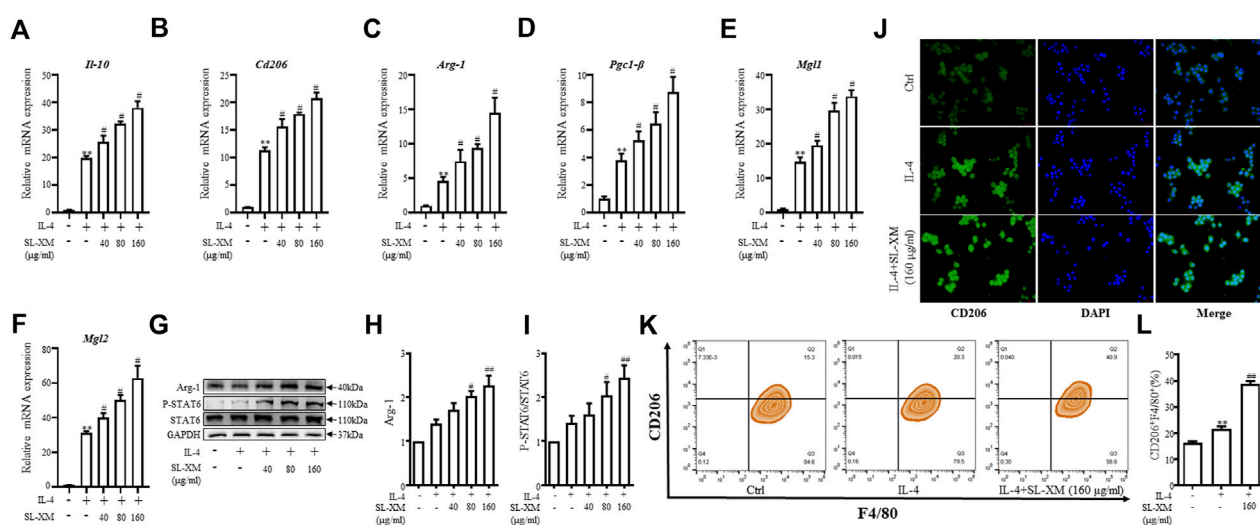


FIGURE 4

Promotional effect of SL-XM on the polarization of M2 macrophages. After RAW264.7 cells were stimulated with IL-4 (20 ng/mL) and different concentration of SL-XM for 24h, mRNA levels of *IL-10* (A), *Cd206* (B), *Arg-1* (C), *Pgc1-β* (D), *Mgl1* (E), *Mgl2* (F) were determined by qRT-PCR; protein level of Arg-1 (G,H), P-STAT6 and STAT6 (G,I) was determined by Western blot analysis; protein level of CD206 (J) was determined by immunofluorescence; percentage of CD206-positive cells (K,L) was determined by flow cytometry. **p* < 0.05, ***p* < 0.01 vs. Ctrl group. #*p* < 0.05, ##*p* < 0.01 vs. LPS group.

E3 and E4 (80 μg/mL) significantly inhibit the secretion of TNF-α in LPS-stimulated macrophages (Figure 1E). Then, fractions E3 and E4 were merged and isolated by silica gel to get six sub-fractions (SE1~SE6). While the sub-fraction (80 μg/mL) of SE-3 (which depicted as SL-XM later) showed a significant anti-

inflammatory activity in LPS-stimulated macrophages (Figure 1F). Then, sub-fraction SE3 was isolated and purified. Five sesquiterpene lactones (Figure 1G) were identified by UPLC-MS as the major constituents. All compounds were isolated using available spectrum data compared with published data. Xanthinosin (1) (Shi et al.,

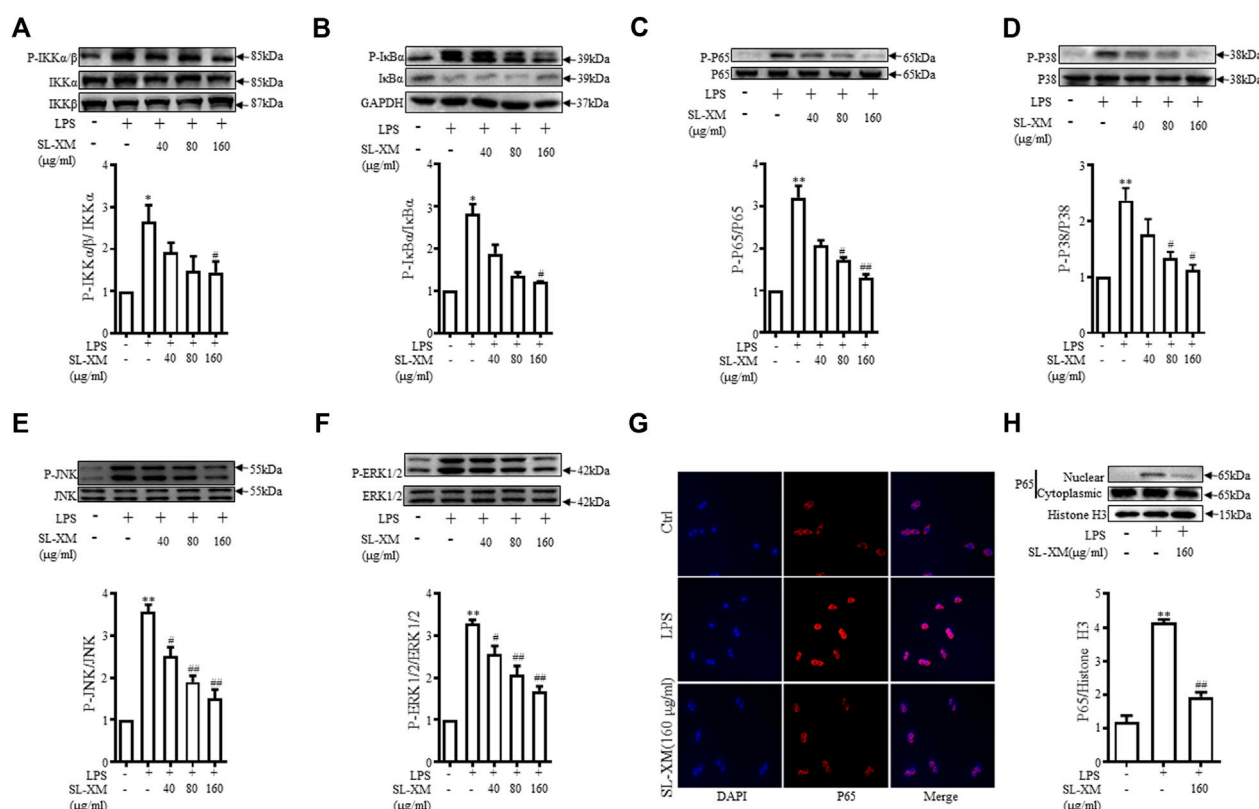


FIGURE 5

SL-XM regulated LPS-stimulated NF-κB and MAPK signaling pathways in RAW264.7 cells. After RAW264.7 cells incubated with SL-XM for 1 h and then stimulated with LPS (100 ng/mL) for 30 min, protein levels of P-IKKα/β, IKKα, IKKβ (A), P-IκBα, IκBα (B), P-P65, P65 (C), P-P38, P38 (D), P-JNK, JNK (E), P-ERK and ERK (F) were determined by Western blot analysis. In addition, NF-κB p65 nuclear translocation was determined by immunofluorescence (G) and western blot (H). * $p < 0.05$, ** $p < 0.01$ vs. Ctrl group. # $p < 0.05$, ## $p < 0.01$ vs. LPS group.

2015), Xanthatin (2) (Yuan et al., 2018), Mogolide D (3) (Xu et al., 2017), Mogolide E (4) (Xu et al., 2017), and Mogolide A (5) (Shang et al., 2014). The compounds 1–5 were quantified by HPLC (Table 1). In addition, the extracts, fractions and sub-fractions of *X. mongolicum* were lyophilized and configured as a solution, and the solution of extracts, fractions and sub-fractions of *X. mongolicum* showed little cytotoxicity at a concentration of 80 μg/mL (data not shown). In addition, RAW264.7 cells were treated with or without different solutions, and the ELSIA results showed the component showed little effect on the production of TNF-α (Supplementary Figures S6).

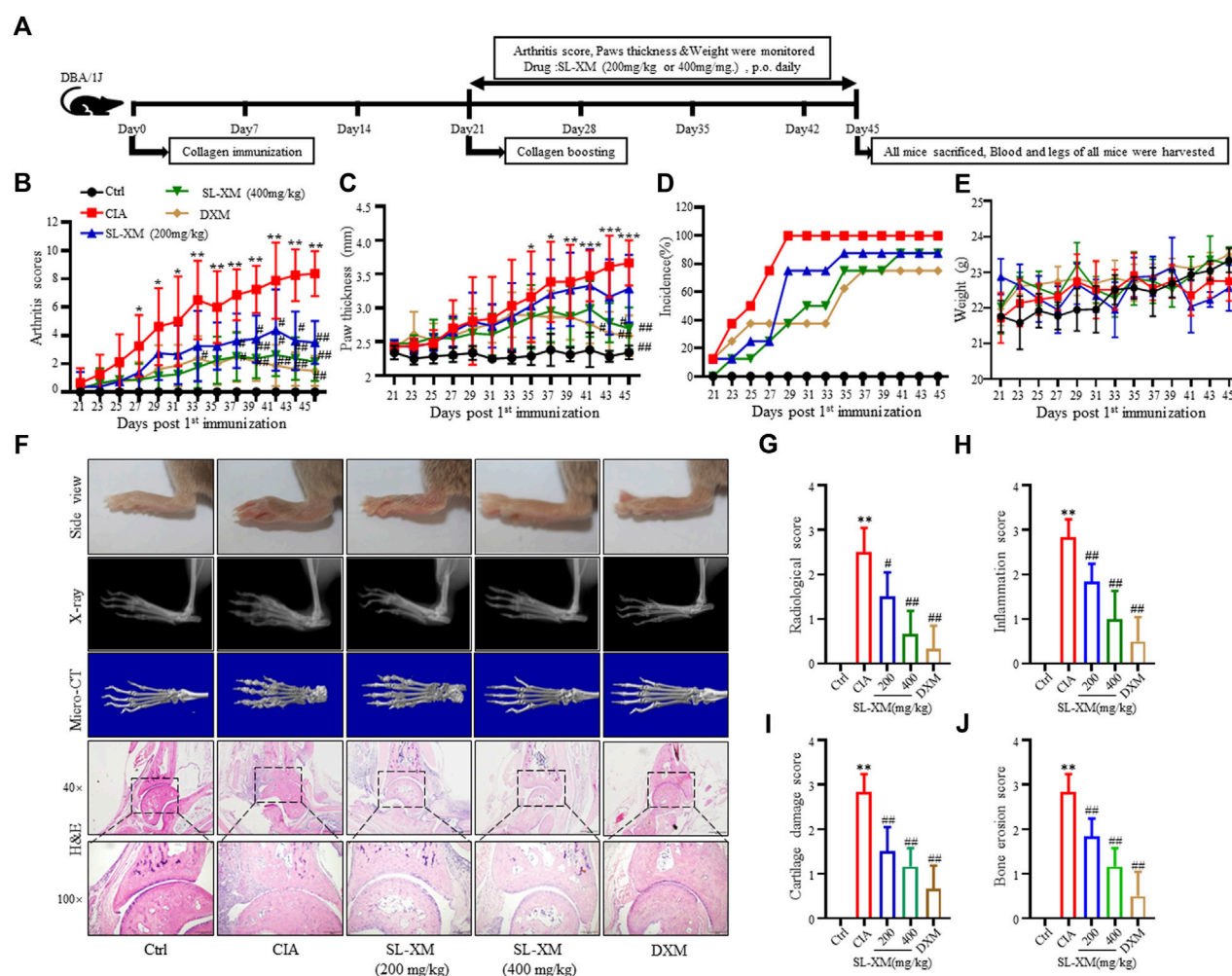
3.2 SL-XM attenuates symptoms of CFA in C57/BL mice

CFA-induced arthritis in mice is widely used to screen RA therapeutics. The effect of SL-XM on the symptoms of CFA mice ($n = 6$ per group) was investigated (Figure 2A). The results showed that oral (p.o.) administration of SL-XM (200 and 400 mg/kg) daily reduced paw thickness (Figure 2C); ankle thickness (Figure 2D) and symptom (Figure 2H) in CFA in a dose-dependent manner compared to mice receiving vehicle treatment. X-ray analysis showed that SL-XM attenuates paws bone damage of CFA mice (Figure 2H). H&E analysis showed that SL-XM alleviated paws

inflammatory infiltration of CFA mice (Figure 2H). In addition, SL-XM decreased the serum levels of M1 cytokines (IL-1β, IL-6, and TNF-α) in CFA mice (Figures 2E–G). While high-dose SL-XM (400 mg/kg) exhibit similar effect to DXM. During the experiment, there was no significant difference in the weight change of mice in each group (Figure 2B).

3.3 SL-XM inhibits M1 macrophage polarization

To determine the optimal concentration and cytotoxicity of SL-XM, a range of concentrations (1, 5, 10, 20, 40, 80, 160, 320, and 640 μg/mL) were selected for the cytotoxicity tests. As shown in Figure 3A, SL-XM treatments showed no significant toxic effect on macrophage viability below the concentration of 160 μg/mL. qRT-PCR analysis showed SL-XM dose dependently decrease the expression of M1-related genes *Il-6*, *Il-1β*, *Tnf-α*, *Inos* and *Il-12b* in LPS-stimulated RAW264.7 cells (Figures 3B–F). In addition, SL-XM also attenuated the upregulation of *Il-6*, *Il-1β*, *Tnf-α* and *Inos* in LPS-stimulated THP-1 cells (Supplementary Figures S7A–D). Western blot analysis showed that SL-XM dose dependently decreased the LPS stimulated iNOS (Figures 3G, H). Immunofluorescence and flow cytometry demonstrated that SL-XM suppressed CD86 positive cells (M1 macrophages) (Figures



3I–K). These data showed SL-XM inhibited M1 polarization in a dose-dependent manner.

3.4 SL-XM promotes M2 macrophage polarization

To explore the effect of SL-XM on the M2 macrophage polarization, macrophage was stimulated with IL-4, followed by treatment with SL-XM. qRT-PCR analysis showed that SL-XM slightly increased the expression of M2-related genes *Il-10*, *Cd206*, *Arg-1*, *Pcg1-β*, *Mgl1* and *Mgl2* (Figures 4A–F). In addition, SL-XM also slightly increased the expression of *Il-10* and *Cd206* in LPS-stimulated THP-1 cells (Supplementary Figures S7A–D). Western blot analysis showed that SL-XM increased the Arg-1 levels in a dose-dependent manner (Figures 4G, H). Immunofluorescence (Figure 4J) and flow cytometry (Figures 4K, L) demonstrated that

SL-XM increased CD206 positive cells (M2 macrophages). Subsequently, we examined the molecular expression of M2-related STAT6 pathway (Yang et al., 2017), western blot analysis showed a higher proportion of P-STAT6/STAT6 (Figures 4G, I) in SL-XM-treated macrophages. Which may explain the effect of SL-XM on M2 polarization. These data showed SL-XM slightly increased M2 polarization.

3.5 SL-XM negatively regulates LPS-induced M1 macrophage polarization through NF-κB and MAPK signal pathways

NF-κB and MAPKs signaling pathways are classic signaling pathways involved in regulating M1 macrophage polarization. RAW264.7 cells were treated with SL-XM for 1 h, followed by treatment with LPS for 30 min. Western blot analysis showed the

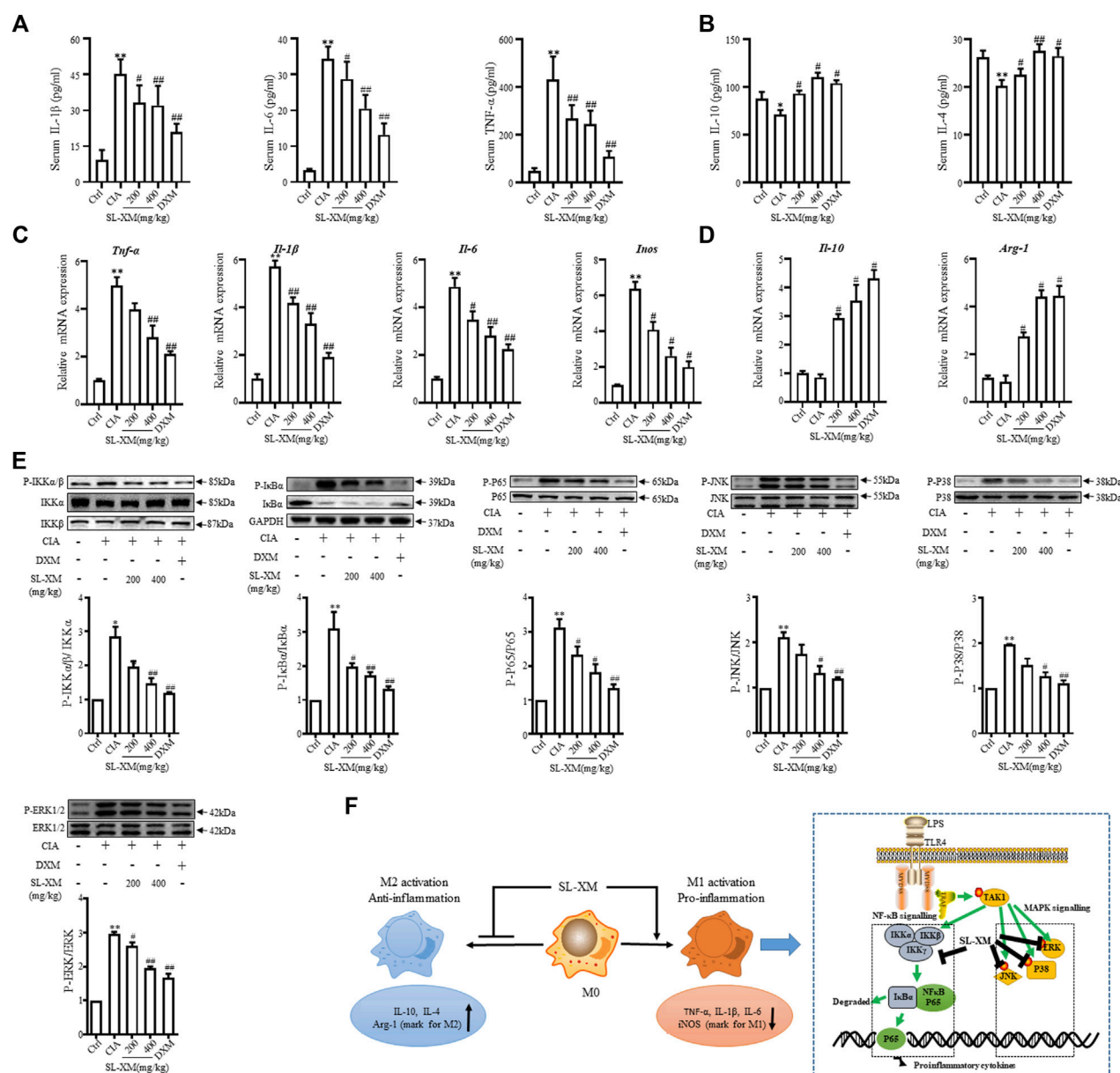


FIGURE 7

SL-XM reduces M1 cytokines, while increasing M2 cytokines in serum and ankle tissue of CIA mice. At the end of experiment serum level of M1 cytokines (IL-1 β , IL-6, and TNF- α) (A) and M2 cytokines (IL-10 and IL-4) (B) were measured by indicated ELISA kits. At the end of experiment mRNA level of M1 cytokines (*Il-1 β* , *Il-6*, *Tnf- α* , and *Inos*) (C) and M2 cytokines (*Il-10* and *Arg-1*) (D) in the ankle tissue of CIA mice were determined by qRT-PCR. Protein levels of NF- κ B and MAPK signaling pathway components in the ankle tissue were determined by Western blot analysis (E). (F) Schematic illustration of SL-XM regulates the M1 macrophage polarization through NF- κ B to attenuate experimental RA mouse model symptoms. * p < 0.05, ** p < 0.01 vs. Ctrl group. # p < 0.05, ## p < 0.01 vs. CIA group.

phosphorylation of IKK α / β , IkB α , P65, JNK1/2, P38, and ERK in Raw264.7 cells were markedly increased after LPS stimulation. While treated with SL-XM dose dependently inhibited LPS-stimulated phosphorylated IKK α / β , IkB α , P65, JNK, P38, and ERK (Figures 5A–F). In addition, an immunofluorescence assay revealed that SL-XM significantly reduced the nuclear level of P65 in RAW264.7 cells induced by LPS (Figure 5G). We also investigated the abundance of nuclear NF- κ B P65 protein by Western blot analysis, the result showed SL-XM significantly reduced the upregulated nuclear level of P65 in RAW264.7 cells induced by LPS (Figure 5H).

3.6 SL-XM alleviates symptoms of CIA in DBA/1 mice

The CIA mouse model display synovial hyperplasia, cellular infiltration, and cartilage degeneration in the ankle, which are hallmark of RA pathology. The functional role of SL-XM on CIA mice were investigated (Figure 6A). The results showed that p.o. administration of SL-XM (200 and 400 mg/kg) dose-dependently reduced the arthritis score (Figure 6B), paw thickness (Figure 6C), and disease onset (Figure 6D) of CIA mice. In addition, X-ray (Figures

6F, G) and Micro-CT (Figure 6F) analysis showed that oral administration of SL-XM attenuated paws bone damage of CIA mice. H&E staining showed that SL-XM alleviated inflammatory cell infiltration in the paws of CIA mice (Figures 6F, H–J). During the experiment, there was no significant difference in the weight change of mice in each group (Figure 6E). ELISA analysis showed SL-XM treatment attenuated the upregulation of M1 cytokines (IL-1 β , IL-6, and TNF- α) (Figure 7A) and the downregulation of M2 cytokines (IL-4 and IL-10) (Figure 7B) in serum. qRT-PCR analysis showed SL-XM treatment reversed the upregulation of M1 cytokines (*Tnf- α* , *Il-1 β* , *Il-6* and *Inos*) (Figure 7C) while upregulated M2 cytokine (*Il-10* and *Arg-1*) (Figure 7D) in the ankle tissues. Western blot analysis showed SL-XM treatment attenuated the upregulation of phosphorylation of IKK α / β , I κ B α , P65, JNK1/2, P38 and ERK in the ankle tissues of CIA mice (Figure 7E).

4 Discussion

In our study, the most potent anti-inflammatory sub-fractions enriched with sesquiterpene lactones was isolated and identified from *X. mongolicum* (SL-XM), and five major sesquiterpene lactones were identified from SL-XM. Furthermore, oral administration of SL-XM significantly reduced arthritis symptoms in CFA and CIA model mice. Regarding the mechanism, in RAW264.7 cells and a CIA-induced RA mouse model, SL-XM significantly relieved the upregulated of M1 related cytokines, while slightly restoring the reduction of M2 related cytokines. Suggesting SL-XM relieved RA progression by regulating M1/M2 balance, especially by inhibiting M1 macrophage polarization. In addition, SL-XM blocked the upregulation of phosphorylation of IKK α / β , I κ B α , P65, JNK, ERK and P38 in LPS-stimulated RAW264.7 cells and the ankle tissue of CIA mouse model, suggesting SL-XM may exert its anti-RA effect by inhibits M1 macrophage polarization through NF- κ B and MAPK signaling pathway.

Xanthium is an annual herb that has long been used clinically to treat a range of inflammatory diseases, with many researchers focusing on anti-inflammatory properties. Yeom et al. reported *Xanthii fructus* inhibits inflammatory responses in LPS-stimulated RAW264.7 macrophages through suppressing NF- κ B and JNK/P38 MAPK (Yeom et al., 2015). Hossen et al. reported the anti-inflammatory activity of *X. strumarium* methanolic extract (Hossen et al., 2016). *X. mongolicum* is the most widely distributed *Xanthium* species in the north area of China (Han et al., 2009). However, as far as we know, there are few laboratory studies on the phytochemical and pharmacological properties of *X. mongolicum* for its anti-inflammatory, especially anti-RA efficacy. In our study, the ethanol extract of the aerial part of *X. mongolicum* showed stronger anti-inflammatory activity versus water extract. Then the ethanol extract was separated to get nine fractions based on the polarity, the active anti-inflammatory fractions were merged and separated to obtain the most active anti-inflammatory sub-fraction (SL-XM). Our study found sesquiterpene lactones were the main anti-inflammatory active ingredient of *X. mongolicum*. This is consistent with previous findings that sesquiterpene lactones were the characteristic and major active metabolites of *Xanthium* species (Merfort, 2011; Schomburg et al., 2013). In terms of the composition of SL-XM, five major sesquiterpene lactones including Xanthinosin, Xanthatin, Mogolide D, Mogolide E and Mogolide A were isolated. As the

main compounds in SL-XM, Xanthinosin inhibits iNOS and COX-2 expression and NF- κ B activity by inhibiting LPS-induced degradation of I κ B α in microglia (Yoon et al., 2008), and Xanthatin alleviated airway inflammation in asthmatic mice by regulating STAT3/NF- κ B signaling pathway (Chang et al., 2020), which partially indicates the anti-RA activity of SL-XM.

The imbalance of M1/M2 macrophages in the synovium is related to the inflammation and destruction of RA joints. Previous studies have reported active M1 macrophages express CD86, CD80, and CD64 on their surface and secrete a substantial number of cytokines (such as IL-1 β , IL-6, and TNF- α), which promote the onset and progression of RA (Gu et al., 2017). Since LPS is common inducers of M1 macrophage initiation and development, we used LPS to stimulate macrophage to mimic M1 macrophage polarization in the RA. Our study showed that SL-XM significantly reduced M1-related cytokine production, as well as the number of CD86-positive cells in LPS-induced macrophages. Furthermore, M2 macrophages are dominate in promoting tissue remodeling, eliminating inflammatory response and restoring imbalance. As IL-4 plays a key role in the polarization of uncommitted M0 cells into M2 cells (Zhong et al., 2022), it was delighting to find that SL-XM slightly upregulated IL-4 induced M2 macrophage markers, as well as IL-4-induced CD206 positive cells. CFA-induced arthritis is a reliable model to evaluate chronic and acute inflammation leading to joint damage (Quintao et al., 2019), and SL-XM was found dose-dependently alleviate arthritis symptoms in CFA mice. CIA is the most common animal model and its histological features are similar to RA (Miyoshi and Liu, 2018). In the CIA mouse model, SL-XM administered reduced arthritis score and arthritis onset in a dose-dependent manner. In addition, SL-XM treatment reduced immune cell infiltration, cartilage and bone damage in the paw of CIA mice. While high dose of SL-XM showed a similar effect to the treatment of DXM in CIA mice. Moreover, no death or other serious adverse effects were observed in the SL-XM treated mice. These results demonstrate for the first time the significant therapeutic effect of SL-XM on experimental animal model of RA. Macrophage-associated cytokines are primarily produced by macrophages in the inflamed joints and then released into blood, this study found SL-XM strongly inhibited the serum levels of M1-associated cytokines (IL-1 β , IL-6 and TNF- α) in CFA and CIA mouse models. We also found SL-XM treatment reversed the upregulation of M1 cytokines (*Tnf- α* , *Il-1 β* , *Il-6*, and *Inos*) and the downregulation of M2 cytokine (*Il-10* and *Arg-1*) in the ankle tissues of CIA mouse. These results suggest that SL-XM has a protective effect on RA pathology by regulating macrophage M1/M2 balance, particularly by inhibiting macrophage polarization toward M1.

LPS, as an outer membrane polysaccharide of Gram-negative bacteria, can activate downstream NF- κ B and MAPK signaling pathways by binding to the cell surface TLR4 receptor, thereby stimulating cells to produce inflammatory cytokines, chemokines and mediators (Abdollahi-Roodsaz et al., 2007; Yeung et al., 2018). In addition, blocking the NF- κ B and MAPK pathways is the key strategy to control the inflammatory response in RA (Fearon et al., 2016). It was found in our study that SL-XM suppressed the LPS-stimulate phosphorylation of IKK α / β , I κ B α , P65, P38, ERK and JNK in macrophages *in vitro*. In addition, SL-XM reduced P65 nuclear translocation in LPS stimulated macrophage. These results suggest the protective role of SL-XM in RA may achieved by inhibiting NF- κ B and MAPK pathways. Which partially indicate SL-XM inhibits M1 macrophage polarization through NF- κ B and MAPK signaling pathway, thereby reducing inflammation and alleviating RA symptoms (Figure 7F).

In our study, we isolated the most potent anti-inflammatory sub-fractions from *X. mongolicum* (SL-XM). The anti-RA effect of SL-XM was evaluated and possible mechanism was explored. For the first time, the anti-RA material base of *X. mongolicum* was explored. We also isolated five major sesquiterpene lactones from SL-XM that have the potential to be developed as anti-RA drug. Nevertheless, more experiments are needed to isolate more active compound from SL-XM, identify key anti-RA compound, and elucidate the anti-RA effects of each compound in the future studies.

Our study offered experimental evidence for the potential therapeutic effects of SL-XM on RA and isolates five major sesquiterpene lactones from SL-XM. The anti-RA effect of SL-XM is related to the regulation of M1/M2 macrophage homeostasis, especially M1 macrophage polarization. In addition, the anti-RA effect of SL-XM by inhibiting M1 macrophage polarization is closely related to the NF- κ B and MAPK signaling pathway. These findings showed that SL-XM has a significant therapeutic effect on RA, and provide an experimental basis for the development of new anti-RA drugs from *X. mongolicum*.

Data availability statement

The original contributions presented in the study are included in the article/Supplementary Material, further inquiries can be directed to the corresponding authors.

Ethics statement

The animal study was reviewed and approved by the Ethics Committee of Jinling hospital (protocol code 2020DZGKJDWLS-00131 and approval on 12/3/2020).

Author contributions

DW and JZ designed the study. JH, ZZ, JW, MM, BW, and YW performed the experiments. SZ was in charge of statistical analysis.

References

- Abdollahi-Roodsaz, S., Joosten, L. A., Roelofs, M. F., Radstake, T. R., Matera, G., Popa, C., et al. (2007). Inhibition of Toll-like receptor 4 breaks the inflammatory loop in autoimmune destructive arthritis. *Arthritis Rheum.* 56 (9), 2957–2967. doi:10.1002/art.22848
- Atkinson, S. M., Usher, P. A., Kvist, P. H., Markholst, H., Haase, C., and Nansen, A. (2012). Establishment and characterization of a sustained delayed-type hypersensitivity model with arthritic manifestations in C57BL/6J mice. *Arthritis Res. Ther.* 14 (3), R134. doi:10.1186/ar3867
- Brenner, M., Meng, H. C., Yarlett, N. C., Griffiths, M. M., Remmers, E. F., Wilder, R. L., et al. (2005). The non-major histocompatibility complex quantitative trait locus Cia10 contains a major arthritis gene and regulates disease severity, pannus formation, and joint damage. *Arthritis Rheum.* 52 (1), 322–332. doi:10.1002/art.20782
- Calabresi, E., Petrelli, F., Bonifacio, A. F., Puxeddu, I., and Alunno, A. (2018). One year in review 2018: Pathogenesis of rheumatoid arthritis. *Clin. Exp. Rheumatol.* 36 (2), 175–184.
- Chandel, S., Bagai, U., and Vashishat, N. (2012). Antiplasmodial activity of *Xanthium strumarium* against Plasmodium berghei-infected BALB/c mice. *Parasitol. Res.* 110 (3), 1179–1183. doi:10.1007/s00436-011-2611-1
- Chang, J., Gao, J., Lou, L., Chu, H., Li, P., Chen, T., et al. (2020). Xanthatin alleviates airway inflammation in asthmatic mice by regulating the STAT3/NF- κ B signaling pathway. *Respir. Physiol. Neurobiol.* 281, 103491. doi:10.1016/j.resp.2020.103491
- Chen, Z., Bozec, A., Rammig, A., and Schett, G. (2019). Anti-inflammatory and immune-regulatory cytokines in rheumatoid arthritis. *Nat. Rev. Rheumatol.* 15 (1), 9–17. doi:10.1038/s41584-018-0109-2
- Editorial Committee of Zhonghua Bencao National Traditional Chinese Herb Administration (1999). *Zhonghua Bencao*. Shang Hai: Shanghai Scientific and Technical Publishing House.
- Emery, P., Breedveld, F. C., Dougados, M., Kalden, J. R., Schiff, M. H., and Smolen, J. S. (2002). Early referral recommendation for newly diagnosed rheumatoid arthritis: Evidence based development of a clinical guide. *Ann. Rheum. Dis.* 61 (4), 290–297. doi:10.1136/ard.61.4.290
- Fan, W., Fan, L., Peng, C., Zhang, Q., Wang, L., Li, L., et al. (2019). Traditional uses, botany, phytochemistry, Pharmacology, pharmacokinetics and toxicology of *Xanthium strumarium* L.: A review. *Molecules* 24 (2), 359. doi:10.3390/molecules24020359
- Fearon, U., Canavan, M., Biniecka, M., and Veale, D. J. (2016). Hypoxia, mitochondrial dysfunction and synovial invasiveness in rheumatoid arthritis. *Nat. Rev. Rheumatol.* 12 (7), 385–397. doi:10.1038/nrrheum.2016.69
- Gu, Q., Yang, H., and Shi, Q. (2017). Macrophages and bone inflammation. *J. Orthop. Transl.* 10, 86–93. doi:10.1016/j.jot.2017.05.002
- Han, T., Li, H. L., Zhang, Q. Y., Han, P., Zheng, H. C., Rahman, K., et al. (2007). Bioactivity-guided fractionation for anti-inflammatory and analgesic properties and

DW and JH wrote the manuscript. All the authors approved the final version of the manuscript.

Funding

This work was supported by the National Natural Science Foundation of China (No. 31900283 to JH); the Natural Science Foundation of Nanjing University of Chinese Medicine (No. NZY31900283 to JH); the China Postdoctoral Science Foundation (2021T140786 to DW); the Nanjing Postdoctoral Science Foundation (48289 to DW); Natural Science Foundation of Jiangsu province (No. BK20221556 to DW); the Jinling Hospital Postdoctoral Science Foundation (48289 to DW); and the Jinling Hospital Science Foundation (YYQN2021075 to DW).

Conflict of interest

The authors declare that the research was conducted in the absence of any commercial or financial relationships that could be construed as a potential conflict of interest.

Publisher's note

All claims expressed in this article are solely those of the authors and do not necessarily represent those of their affiliated organizations, or those of the publisher, the editors and the reviewers. Any product that may be evaluated in this article, or claim that may be made by its manufacturer, is not guaranteed or endorsed by the publisher.

Supplementary material

The Supplementary Material for this article can be found online at: <https://www.frontiersin.org/articles/10.3389/fphar.2023.1104153/full#supplementary-material>

- constituents of *Xanthium strumarium* L. *Phytomedicine* 14 (12), 825–829. doi:10.1016/j.phymed.2007.01.010
- Han, T., Zhang, Q. Y., Zhang, H., Wen, J., Wang, Y., Huang, B. K., et al. (2009). Authentication and quantitative analysis on the chemical profile of *Xanthium* fruit (Cang-Er-Zi) by high-performance liquid chromatography-diode-array detection tandem mass spectrometry method. *Anal. Chim. Acta* 634 (2), 272–278. doi:10.1016/j.aca.2008.12.027
- Hossen, M. J., Cho, J. Y., and Kim, D. (2016). PDK1 in NF- κ B signaling is a target of *Xanthium strumarium* methanolic extract-mediated anti-inflammatory activities. *J. Ethnopharmacol.* 190, 251–260. doi:10.1016/j.jep.2016.06.019
- Mazhar, F., Haider, N., Sultana, J., Akram, S., and Ahmed, Y. (2018). Prospective study of NSAIDs prescribing in Saudi Arabia: Cardiovascular and gastrointestinal risk in patients with diabetes mellitus. *Int. J. Clin. Pharmacol. Ther.* 56 (2), 64–71. doi:10.5414/CP203071
- Merfort, I. (2011). Perspectives on sesquiterpene lactones in inflammation and cancer. *Curr. Drug Targets* 12 (11), 1560–1573. doi:10.2174/138945011798109437
- Miyoshi, M., and Liu, S. (2018). Collagen-induced arthritis models. *Methods Mol. Biol.* 1868, 3–7. doi:10.1007/978-1-4939-8802-0_1
- Puxeddu, I., Caltran, E., Rocchi, V., Del Corso, I., Tavoni, A., and Migliorini, P. (2016). Hypersensitivity reactions during treatment with biological agents. *Clin. Exp. Rheumatol.* 34 (1), 129–132.
- Quintao, N. L. M., Pastor, M. V. D., Antonialli, C. D., da Silva, G. F., Rocha, L. W., Berte, T. E., et al. (2019). Aleurites moluccanus and its main active constituent, the flavonoid 2'-O-rhamnosylswertisin, in experimental model of rheumatoid arthritis. *J. Ethnopharmacol.* 235, 248–254. doi:10.1016/j.jep.2019.02.014
- Ramiro, S., Sepriano, A., Chatzidionysiou, K., Nam, J. L., Smolen, J. S., van der Heijde, D., et al. (2017). Safety of synthetic and biological DMARDs: A systematic literature review informing the 2016 update of the EULAR recommendations for management of rheumatoid arthritis. *Ann. Rheum. Dis.* 76 (6), 1101–1136. doi:10.1136/annrheumdis-2016-210708
- Schett, G. (2019). Resolution of inflammation in arthritis. *Semin. Immunopathol.* 41 (6), 675–679. doi:10.1007/s00281-019-00768-x
- Schomburg, C., Schuehly, W., Da Costa, F. B., Klempnauer, K. H., and Schmidt, T. J. (2013). Natural sesquiterpene lactones as inhibitors of myb-dependent gene expression: Structure-activity relationships. *Eur. J. Med. Chem.* 63, 313–320. doi:10.1016/j.ejmech.2013.02.018
- Shang, H., Liu, J., Bao, R., Cao, Y., Zhao, K., Xiao, C., et al. (2014). Biomimetic synthesis: Discovery of xanthanolide dimers. *Angew. Chem. Int. Ed. Engl.* 53 (52), 14494–14498. doi:10.1002/anie.201406461
- Shi, Y. S., Liu, Y. B., Ma, S. G., Li, Y., Qu, J., Li, L., et al. (2015). Bioactive sesquiterpenes and lignans from the fruits of *Xanthium sibiricum*. *J. Nat. Prod.* 78 (7), 1526–1535. doi:10.1021/np500951s
- Wang, D., Wu, Z., Zhao, C., Yang, X., Wei, H., Liu, M., et al. (2021). KP-10/Gpr54 attenuates rheumatic arthritis through inactivating NF- κ B and MAPK signaling in macrophages. *Pharmacol. Res.* 171, 105496. doi:10.1016/j.phrs.2021.105496
- Wang, D., Zhao, C., Gao, L., Wang, Y., Gao, X., Tang, L., et al. (2018). NPNT promotes early-stage bone metastases in breast cancer by regulation of the osteogenic niche. *J. Bone Oncol.* 13, 91–96. doi:10.1016/j.jbo.2018.09.006
- Xu, F. W., Xiao, C. Q., Lv, X., Lei, M., and Hu, L. H. (2017). Two new dimmeric xanthanolides isolated from *Xanthium mogolium* Kitag plant. *Tetrahedron Lett.* 58 (13), 1312–1315. doi:10.1016/j.tetlet.2017.02.044
- Yang, X., Xu, S., Qian, Y., and Xiao, Q. (2017). Resveratrol regulates microglia M1/M2 polarization via PGC-1 α in conditions of neuroinflammatory injury. *Brain Behav. Immun.* 64, 162–172. doi:10.1016/j.bbi.2017.03.003
- Yeom, M., Kim, J. H., Min, J. H., Hwang, M. K., Jung, H. S., and Sohn, Y. (2015). *Xanthium fructus* inhibits inflammatory responses in LPS-stimulated RAW 264.7 macrophages through suppressing NF- κ B and JNK/p38 MAPK. *J. Ethnopharmacol.* 176, 394–401. doi:10.1016/j.jep.2015.11.020
- Yeung, Y. T., Aziz, F., Guerrero-Castilla, A., and Arguelles, S. (2018). Signaling pathways in inflammation and anti-inflammatory therapies. *Curr. Pharm. Des.* 24 (14), 1449–1484. doi:10.2174/1381612824666180327165604
- Yoon, J. H., Lim, H. J., Lee, H. J., Kim, H. D., Jeon, R., and Ryu, J. H. (2008). Inhibition of lipopolysaccharide-induced inducible nitric oxide synthase and cyclooxygenase-2 expression by xanthanolides isolated from *Xanthium strumarium*. *Bioorg. Med. Chem. Lett.* 18 (6), 2179–2182. doi:10.1016/j.bmcl.2007.12.076
- Yuan, Z., Zheng, X., Zhao, Y., Liu, Y., Zhou, S., Wei, C., et al. (2018). Phytotoxic compounds isolated from leaves of the invasive weed *Xanthium spinosum*. *Molecules* 23 (11), 2840. doi:10.3390/molecules23112840
- Zhong, Y. M., Zhang, L. L., Lu, W. T., Shang, Y. N., and Zhou, H. Y. (2022). Moxibustion regulates the polarization of macrophages through the IL-4/STAT6 pathway in rheumatoid arthritis. *Cytokine* 152, 155835. doi:10.1016/j.cyt.2022.155835

Frontiers in Pharmacology

Explores the interactions between chemicals and living beings

The most cited journal in its field, which advances access to pharmacological discoveries to prevent and treat human disease.

Discover the latest Research Topics

[See more →](#)

Frontiers

Avenue du Tribunal-Fédéral 34
1005 Lausanne, Switzerland
frontiersin.org

Contact us

+41 (0)21 510 17 00
frontiersin.org/about/contact



Frontiers in Pharmacology

